Functional characterisation of putative Plasmodium falciparum invasion ligands and their homologues

Juan Miguel Balbin

Bachelor of Science (Advanced)

Research Centre for Infectious Diseases

Department of Molecular and Biomedical Sciences

School of Biological Sciences

The University of Adelaide

October 2021

THE UNIVERSITY of ADELAIDE

A thesis submitted by

Juan Miguel Balbin

Bachelor of Science (Advanced)

To

The University of Adelaide,

For total fulfilment of the requirements for the degree of

Doctor of Philosophy, in the Biological Sciences

in the Department of Molecular and Biomedical Sciences,

School of Biological Sciences.

Table of contents

List of figures

List of tables

Abbreviations

ACT	artemisinin-combinational therapies
ACβ	adenylate/adenylyl cyclase beta
AIP	armadillo/ARO-interacting protein
ALBA	acetylation lowers binding affinity domain
AMA1	apocal membrane antigen 1
AmBic	ammonium bicarbonate
ARE	AU-rich region
ARE	AU-rich element
ARO	armadillo repeats only
ART	artemisinin chemical derivatives
ATP	adenosine triphosphate
BAM	Binary Alignment Map file
BirA	bifunctional ligase/repressor (biotinylator protein)
BSA	bovine serum albumin
BSD	blasticidin deaminase
C-RIP	cytosolically exposed rhoptry interacting proteins
C1	compound 1
C2H2	Cys-X_2-His-X_2-Cys-X_2-His zinc finger domain
C3H1	Cys-X_8-Cys-X_5-Cys-X_3-His zinc finger domain
C3H1 ZnF	C3H1-type zinc finger protein
CA_RP	carbonic anhydrase-related protein
CA1	carbonic anhydrase 1
cAMP	cyclic adenosine monophosphate
CD8+	cluster of differentiation 8 positive
cDNA	complementary DNA
CDPK	calcium-dependent protein kinase
CERLI	cytosolically exposed rhoptry leaflet interacting protein
CITH	CAR-I and Trailer Hitch
CLIPseq	cross-linking immunoprecipitation sequencing
CRISPR	clustered regularly interspaced short palindromic repeats
CSA	chondroitin sulphate A
CSP	circumsporozoite protein
CyRPA	cysteine-rich protective antigen
CZIF	C3H1 zinc finger protein
DAPI	diamidino-2-pheylindole dihydrochloride
DDT	dichlorodiphenyltrichloroethane
DHFR	dihydrofolate reductase
DHHC	aspartate-histidine-histidine-cysteine palmitoylation domain
DiQ-BioID	dimerisation induced quantitative proximity-dependent biotin identification
DNA	deoxyribonucleic acid

DTT	dithiothreitol
EBA	erythrocyte binding antigen
EDTA	ethylenediaminetetraacetic acid
EMP1	erythrocyte membrane protein 1
ERC	endoplasmic reticulum-located calcium-binding protein
ERD2	ER lumen protein-retaining receptor 2
EtBr	ethidium bromide
EtOH	ethanol
EXP2	exported protein 2
FC	fold change
FDR	false discovery rate
Fer2	ferlin 2
FIB-SEM	focussed-ion beam scanning electron microscopy
FKBP	FK binding protein
FRB	FKBP rapamycin binding protein domain
G418	geneticin
G6PD	glucose-6-phosphate dehydrogenase
GAP45	glideosome-associated protein 45
GAPDH	glyceraldehyde 3-phosphate dehydrogenase
gDNA	genomic DNA
GFF	general feature format file
GFP	green fluorescent protein
GlcN	glucosamine
***glm*S**	Gene encoding the glucosamine-inducible ribozyme
GLURP	glutamate-rich protein
GO	gene ontology
GOI	gene of interest
GPI	glycosylphosphatidylinositol
GTF	Gene Transfer Format file
HA	haemagglutinin
HEPES	4-(2-hydroxyethyl)-1-piperazineethanesulfonic acid)
HPC	High Performance Computing
HRP2	histidine rich protein 2
IFA	immunofluorescence assay
IFNγ	interferon gamma
IGV	Integrative Genomics Viewer
IMC	inner membrane complex
iRBC	infected (parasitised) red blood cell
IRS	indoor residual sprays
ITN	insecticide treated nets
K13	Kelch13
KAHRP	knob-associated histidine rich protein
KO	knockout

L	litres
LB	Lennox broth media
LDH	lactate dehydrogenase
M	molar (concentration)
MAb	monoclonal antibody
MAC	membrane attack complex
MACS	magnet-activated cell sorting
MAg-1	ag-1 blood-stage membranr protein homologue
MDS	multidimensional scaling
MeOH	methanol
MES	2-(N-morpholino)ethanesulfonic acid
mg	milligram
MHC	major histocompatibility complex class
min	minute
mL	millilitres
mRBP	mRNA-binding protein
mRNA	messenger ribonucleic acid
MSP	merozoite surface protein
MyoA	myosin A
MyoF	myosin F
NAB	NGFI-A-binding protein
NABP	nucleic acid binding proteins
ncRNA	non-coding RNA
NeoR	neomycin resistance cassette
NHE	Na+/H+ exchanger
nM	nanomolar
NPP	new permeability pathway
PAM	pregnancy-associated malaria
PAM	protospacer adjacent motif
PAMP	pathogen-associated molecular pattern
PBS	phosphate buffered saline
PBS-T	phosphate buffered saline with Tween20 detergent
PCR	polymerase chain reaction
PFA	paraformaldehyde
pH	potential of hydrogen
PH	Pleckstrin homology domain
PHD	plant homeodomain (zinc finger class)
PhiL1	photosensitised INA-labelled protein 1
PIC1	PhiL1-interacting candidate 1
PMSF	phenylmethylsulfonyl fluoride
PPM	parasite plasma membrane
PTEX	*P. falciparum* translocon of exported proteins
PV	parasitophorous vacuole

PVM	parasitophorous vacuole membrane
RALP1	rhoptry-associated leucine zipper-like protein 1
RAP1	rhoptry-associated protein
RASP	rhoptry apical surface protein
RBC	red blood cell
RBP	RNA-binding protein
rcf	relative centrifugal force
RDT	rapid diagnostic test
RESA	ring-infected erythrocyte surface antigen
RFP	RING finger protein
RH	reticulocyte-binding protein homologue
RING	really interesting new gene (zinc finger class)
RIPR	RH5-interacting protein
RMD	R Markdown file
RNA	ribonucleic acid
RNA-EMSA	RNA electrophoretic mobility shift assay
RNAi	RNA interference
RNAseq	RNA sequencing
RON	rhoptry neck protein
ROP	rhoptry protein (protein family)
RPKM	Reads Per Kilobase of Transcript
rpm	rotations per minute
RPMI	Roswell Park Memorial Institute Medium
RUF	RNA of unknown function
SBF-SEM	surface block face-scanning electron microscopy
SDS-PAGE	sodium dodecyl sulphate-polyacrylamide gel electrophoresis
SERA5	serine-repeat antigen protein 5
sgRNA	single guide RNA
SILAC	Stable Isotype Labeling with Amino Acids in Cell Culture
SLI	selection linked integration
SLI-TGD	selection linked integration targeted gene disruption
SLURM	Simple Linux Utility for Resource Management
SNARE	snap receptor
SOC	super optimal broth with catabolite repressor
SOTE	sorbitol-Tris-EDTA
SP	signal peptide
SUB	subtilisin
TBS	Tris-buffered saline
TE	Tris-ethylenediaminetetraacetic acid
TEM	transmission electron microscopy
TFIIIA	transcription factor IIIA
TNF- α	tumour necrosis factor alpha
TRF	telomere repeat-binding factor zinc finger protein

Tris	tris(hydroxymethyl)aminomethane
TRZ	telomere repeat-binding factor zinc finger protein
TTP	tristetraprolin
TX-100	Triton X-100
uRBC	uninfected red blood cell
UTR	untranslated region
v/v	volume/volume
w/v	weight/volume
WHO	World Health Organization
WR	WR99210
WT	wild-type
ZFN	zinc finger nuclease
Zfp	*(P. berghei*) zinc finger protein
ZnF	zinc finger
µg	microgram
µl	microlitre
µM	micromolar

Abstract

The apicomplexan parasite *Plasmodium falciparum* is a major threat to global health, accounting for the majority of malaria-related morbidities and mortalities, totalling to cause ~400,000 deaths per year of which the lives of children under the age of 5 are the most impacted (WHO 2020). This is exacerbated by the onset of resistance against our frontline antimalarials and the lack of an effective licensed vaccine against malaria. Studies which investigate novel interventions against *P. falciparum* host infection are critical in order produce clinically relevant outcomes.

In this thesis, I focussed my studies on the blood stage lifecycle of *P. falciparum* which is responsible for all clinical symptoms of malaria. More specifically, I examined the molecular mechanisms by which the invasive form of the parasite, the merozoite, uses to invade host red blood cells. The point in time in which merozoites invade red blood cells is defined as a vital crux for the blood stage lifecycle to proceed, whereby blocking invasion prevents further downstream parasite growth and the resulting pathologies. Uncovering the proteins which govern merozoite invasion will aid in informing effective vaccine and antimalarial design in the field. As such, we have identified several conserved genes in *P. falciparum* which encode proteins with a potential function in merozoites for functional characterisation.

We first undertook a study on cytosolically-exposed rhoptry leaflet interacting protein 2 (PfCERLI2), expressed from a duplicated gene of its paralogue PfCERLI1 which is essential for merozoite invasion. Using super-resolution microscopy platforms and Western blot-based membrane assays, we discerned that PfCERLI2 localises to the cytosolic face of the rhoptry, a key invasion organelle, and is more specifically attached to the rhoptry bulb membrane. Our attempts to knock out *Pfcerli2* have failed, suggesting it as essential for blood stage growth. To investigate its function, we generated glucosamine-inducible knockdown parasite lines for PfCERLI2 which revealed it as essential for merozoite invasion. Moreover PfCERLI2 appears to be important for establishing proper rhoptry organellar development. Lastly, to determine which proteins may be working in tandem with

both PfCERLI1 and PfCERLI2, we utilised dimerization induced quantitative proximity-dependent biotin identification (DiQ-BioID) and quantitative mass spectrometry. The results of this study have revealed the new unexplored biology linked to PfCERLI1 and PfCERLI2's function in merozoites.

Concurrently, we performed a functional characteirsation of *P. falciparum* C3H1 zinc finger proteins 1 and 2 (PfCZIF1 (Pf3D7_1468400), PfCZIF2 (Pf3D7_0818100)). Our studies have shown PfCZIF1 and PfCZIF2 to be peripherally-attached to a membrane facing the cytosol, with peak expression in schizonts at the point of merozoite development. Functional data in protein truncation and knockout parasite lines have revealed that neither protein in isolation is essential for blood-stage growth, however both cannot be knocked out in tandem suggesting that they fulfil compensatory roles. PfCZIF2 has revealed potential links with the protein PfKAHRP, which is involved in host cell modification. This study has provided the first insights into the functional interplay between PfCZIF1 and PfCZIF2.

Declaration

I certify that this work contains no material which has been accepted for the award of any other degree or diploma in my name, in any university or other tertiary institution and, to the best of my knowledge and belief, contains no material previously published or written by another person, except where due reference has been made in the text. In addition, I certify that no part of this work will, in the future, be used in a submission in my name, for any other degree or diploma in any university or other tertiary institution without the prior approval of the University of Adelaide and where applicable, any partner institution responsible for the joint-award of this degree.

I acknowledge that copyright of published works contained within this thesis resides with the copyright holder(s) of those works.

I also give permission for the digital version of my thesis to be made available on the web, via the University's digital research repository, the Library Search and also through web search engines, unless permission has been granted by the University to restrict access for a period of time.

I acknowledge the support I have received for my research through the provision of an Australian Government Research Training Program Scholarship.

Signed,

Juan Miguel Balbin

October 1st 2021

Publications

Research manuscripts in preparation to support this thesis.

1. Liffner B*, **Balbin JM***, Shami, GJ, Siddiqui G, Strauss J, Frölich S, Heinemann GK, Edwards EM, Alder A, Wichers JS, Creek DJ, Tilley L, Dixon MWA, Gilberger T, Wilson DW. Pfcerli2, a duplicated gene in the malaria parasite Plasmodium falciparum essential for invasion of erythrocytes as revealed by phylogenetic and cell biological analysis. ***equal contribution**

2. **Balbin JM**, Heinemann GK, Yeoh L, Armstrong M, Duffy M, Gilson P, Wilson DW. Characterisation of PfCZIF1 and PfCZIF2 in *Plasmodium falciparum* asexual stages.

Peer-reviewed review papers

1. Burns AL, **Dans MG***, **Balbin JM***, de Koning-Ward TF, Gilson PR, Beeson JG, Boyle MJ, Wilson DW. (2019) Targeting malaria parasite invasion of red blood cells as an antimalarial strategy. *FEMS Microbiol Rev.* ***equal contribution**

2. Liffner B, **Balbin JM**, Wichers JS, Gilberger T, Wilson DW. (2021) The Ins and Outs of Plasmodium Rhoptries, Focusing on the Cytosolic Side. *Trends in Parasitology*.

Communications

Results in this thesis were presented at the following scientific conferences.

1. **Balbin JM**, Liffner B, Gilson P, Wilson DW. Functional characterisation of a stage-specific *Plasmodium falciparum* protein and its role in erythrocyte invasion. Lorne Infection & Immunity 2019, Lorne, Australia. Poster presentation.

2. **Balbin JM**, Liffner B, Gilson P, Wilson DW. Functional characterisation of a stage-specific *Plasmodium falciparum* protein and its role in erythrocyte invasion. University of Adelaide School of Biological Sciences 2019 Symposium, Adelaide, Australia. Poster presentation.

3. **Balbin JM**, Liffner B, Gilson P, Wilson DW. Functional characterisation of a stage-specific *Plasmodium falciparum* protein and its role in erythrocyte invasion. Adelaide Protein Group 2019 Student Awards Night, Adelaide, Australia. Poster presentation. **Awarded best poster.**

4. **Balbin JM**, Gilson P, Paton J, Wilson DW. Functional characterisation of a stage-specific *Plasmodium falciparum* protein and its role in erythrocyte invasion. Australian Society for Parasitology Conference 2019, Adelaide, Australia. Oral presentation. **Awarded best 5 minute talk.**

5. **Balbin JM**, Liffner B, Heinemann G, Liu B, Dixon M, Gilberger T, Wilson DW. PfCERLI2 is a potential mediator of rhoptry biogenesis. Malaria in Melbourne 2019, Melbourne, Australia. Poster presentation.

6. **Balbin JM**, Liffner B, Heinemann G, Liu B, Dixon M, Gilberger T, Wilson DW. PfCERLI2 is a potential mediator of rhoptry biogenesis. Molecular Approaches to Malaria 2020, Melbourne, Australia. Poster presentation.

7. **Balbin JM**, Liffner B, Heinemann G, Liu B, Dixon M, Gilberger T, Wilson DW. (2019) PfCERLI2 is a potential mediator of rhoptry biogenesis. Biology and Pathology of the Malaria Parasite XVI 2020 (online), Heidelberg, Germany. Poster presentation.

8. Edwards E, **Balbin JM**, Wilson DW. Biting back: Developing tools to explore functional properties of essential invasion proteins in the malaria parasite. Principles and Practices of Science III Symposium 2020, Adelaide, Australia. Poster presentation.

Collaborative communications

Research projects undertaken with collaborators which are not featured in this thesis were presented at the following scientific conferences.

1. Chan J, **Balbin JM**, Barber R, Gooley A, Breadmore MC, Arrua D, Wilson D, Hilder EF. Isolation of Malaria Parasites using Polymer Monoliths. Australasian Polymer Symposium 2019, Sunshine Coast, Australia. Poster presentation.

Acknowledgements

My PhD was a journey like no other that I've experienced so far in life. A journey of every human emotion. A journey of both scientific and self-discovery. A journey that led me to understand what I wanted out of my time at university. If you were to ask me what my aspirations were at the beginning of my PhD, my overly excitable and naïve self would simply answer with "I want to do science". If you were to ask me now, I can proudly say "I want to do science with a purpose I firmly believe in". And that purpose was only made clear to me in the mere months before writing these very words – I want to communicate how amazing science can be and that there are innumerable paths on the road of science.

To Danny, I feel extremely lucky to have been originally assigned as your PPR2 mentee. Meeting you has opened so many doors for me and has continued to pave the path for me in science from a summer scholarship, volunteer and finally as your student. Thank you for being an understanding and caring supervisor who showed me the ropes and allowed me to develop my own interests, albeit on a tangent from simply getting you your Nobel Prize to warrant your (hopefully) much-coveted early retirement. Words on paper can't describe how thankful I am to have been part of your team these past 3 and ¾ years. I promise that if you're ever interested, that in return I'll coach you on aesthetically pleasing fish tanks or maybe on making graphics for your next grant. Sadly, no mates rates on the real stuff though.

To Ben, you were my rolemodel all the way and you continue to be. I've never met someone more curious and passionate about their trade than you in literally every aspect of science thinkable. Working beside you was an absolute blast – even the stuff that didn't work was more fun than it should have, because I knew we could work past the hurdles together. I am so happy that you're fulfilling your dreams of becoming a big-shot scientist – I hope to hear more from you even beyond my time in research. Bring on the jellyfish facts!

To Amy, Issy, Jill, Sonja, Ornella, Xinli, Maria, Helin, Ella, Quinn and Max – what a dream team! A literal set of all-stars and legends. I feel so lucky to have

had such an enjoyable working culture and this is without a doubt owed to having all of you as great friends and colleagues. From twinning pictures, on-the-dot optimal lunch times, a respect for 4:20 pm, bakery runs, Korean schnitzel and Friday afternoon drinks – oh and work too, that's important. Thank you for being an incredible team. Amy, thanks for being that one nerdy person I could talk about games with, it assured me I wasn't the only weird one. Issy, our mutual motivation for each of us to get some sort of workable phenotype was the thing that kept me going, I hope your future endeavours have more statistical significance! Jill, thank you for dealing with my love for elevator music and showering me with pictures of your cats (and memes of cats), I will forever wish them well. Sonja, I am grateful that you made sure Danny's new ideas for experiments were tame and manageable (and made use of cool microscopy) – a moderator is important! Ornella, thanks for literally providing the best vibes, down-to-earth chats and ensuring our ice cream was cheaper thanks to your incredible coupon deals. Thanks for naming Trevor! Xinli, thank you for visiting our lab and introducing us to your wonderful family. Your ability to calculate a dilution in your head in a split second always impressed me. Maria, thank you for allowing me to hang out with you on the other side of the office at 5 pm to make cardboard Christmas trees. Helin, you graced us with your dog Bella and now she is forever a Slack emoji – no regrets. Thanks for showing me how to network over email to convince potential employers for a coffee chat! Ella, thank you for being an incredibly engaged student and a CERLI team player! I hope you continue to discover what you enjoy in science. Quinn and Max, in the short time I've known you both I've felt an incredible sense of ease when talking to you – thanks for helping take some weight off my shoulders. To every summer or winter student I've had under my wing – Ashley, Erin, Shamit and Malachi, thank you for giving me a chance to teach you all a little something about life on the bench. One Western blot wash at a time.

To the RCID and friends on Level 3 and 4 MLS, thank you for your continued friendship over the years. I have enjoyed our chats in the tearoom about the quality of our microwave, new eating spots on campus and highly exclusive gossip. I wish the department a successful future ahead, and someday maybe an official logo might be used.

To my friends from science undergrad – Tim, Ruth, Sarah, Tom, Nathan, Claudia, Khalia, Ethan, Katherine, Seb, Eugene, Mia and Chelsea. Thank you for being along on the journey with me despite the many different paths we've taken. I am so happy to have had such an incredible support network who pushed for the success of every individual. I wish all of you a very bright future ahead!

To my closest friends from non-science undergrad – David, Adam, Jesse, Lydia, Ryoga, Yen, Lachlan, Trang, Kiyo and Julia. We all studied different things but were united in our love of studying Japanese and travel. I can't express how thankful I am to have you all as my closest friends who believed that I could shoot for the stars if I tried hard enough. Once we're able, that promised trip to the hot springs is a must!

To my family, Mom and Dad. When I was six years old, I knew it was a tough decision for us to make the move. You had such a firm belief that Australia would provide the best opportunities for me, and I am happy to show the fruits of our labour as a family. Thank you for being incredibly understanding parents and for allowing me to make my own choices. I chose to pursue a doctorate, not just as a degree for my career, but to say that your sacrifices could amount to your son achieving the best he could. I'm going to make use of it to make the world a better place in my own way. I hope I've made you both proud and I hope I've made everyone else back home proud too.

To my loving partner, Paulo, who I have kept mostly a secret from the world. I can't imagine having done all this without you. Keeping a secret is difficult and pretending to be someone I wasn't was even harder. Thank you for giving me a safe haven to be myself, and to be by your side when I felt lost in my work or had a really rough time. Seeing you by the crossing seats every night, being able to talk to you about our days, sneaking in a snack or two before going home – I wouldn't trade these short exchanges for anything. I'm here because of you, and words can't begin to describe the joy I feel to be your partner in hand. You and I know what finishing my PhD means, thank you for your many years of patience. Thank you so much for giving me all the time I needed.

To my “favourite” duo Pf3D7_1468400 and Pf3D7_0818100, whom I named at the very last minute as PfCZIF1 and PfCZIF2, it’s time that I let you sleep. I hope one day someone discovers something great about you two that I wasn’t able to. Somehow, despite what the science was telling me, I feel as though there are so many things we have yet to know. I willingly pass on the baton, without a single hint of hesitation, to the next brave soul who finds you both on PlasmoDB.

To my actual favourite duo Pf3D7_0210600 and Pf3D7_0405200, the amazing PfCERLI1 and PfCERLI2, thank you for turning my PhD upside down and back onto the right track. Your baton, plated in gold, awaits for the next curious Wilson lab mind to pick you up.

Chapter 1

Introduction

Introduction

Plasmodium spp. parasites are the causative agents of malaria

Malaria is a mosquito-borne parasitic disease caused by small unicellular eukaryotic Apicomplexan parasites belonging to the genus *Plasmodium*. Malaria has existed far before the dawn of humans, with the first malaria parasites having evolved 165 million years ago (Carter & Mendis 2002). In the present day, highly specialised *Plasmodium* species are capable of infecting humans, where they continue to rapidly adapt to present-day interventions, with which we are at a constant arms race. Approximately half of the global human population is at risk of malaria infection, highlighting *Plasmodium* parasites as major human pathogens of our time. Globally, malaria continues to inflict an overwhelming burden on the public health and socioeconomic standing of affected endemic countries (WHO 2020), prompting the World Health Organization to pursue the goal of complete malaria eradication.

Malaria in humans

Several *Plasmodium* species are capable of infecting humans including *P. falciparum P. vivax*, *P. ovale curtisi*, *P. ovale wallikeri* and *P. malariae* (White *et al.* 2014, Cowman & Healer *et al.* 2016). Emerging primate-human zoonoses of *P. knowlesi* (Kantele & Jokiranta *et al.* 2011), *P. simium* (Brasil *et al.* 2017) and *P. cynomolgi* (Hartmeyer & Stensvold *et al.* 2019) from South-East Asian macaques and howler monkeys have also been identified and studied. All malaria parasites are transmitted to humans through the bite of an infected *Anopheles* mosquito.

Epidemiology and global health

In 2019 there were an estimated 229 million cases of malaria across 87 endemic countries, most of which are in tropical or sub-tropical regions of the world (Figure 1). Of these regions, the burden of malaria mortality is predominant to Sub-Saharan Africa, attributing to 94% of malaria-related deaths (WHO 2020). Of the *Plasmodium* spp. known to cause malaria in humans, *P. falciparum* by far is the largest contributor towards the current rates of morbidity and mortality and is thought to cause 99.7% of malaria-associated deaths (WHO 2020). *P. vivax*, which causes the second highest malaria burden, is more geographically widespread

outside Africa with >50% of cases occurring in Asia and Latin America (WHO 2020). Reassessment of *P. vivax*'s contribution to the global burden of malaria has revealed that *P. vivax*-related morbidity and mortality have been historically underestimated due to its unique ability to enter dormancy and cause relapsed infections (Naing *et al.* 2014). *P. ovale curtisi*, *P. ovale wallikeri* and *P. malariae* contribute to a substantially lower burden (Mueller *et al.* 2007). The zoonotic malaria species *P. knowlesi* has a localised prevalence in parts of South-East Asia while *P. simium* is found in Brazil, though they are considered to be the primary causative agents of malaria in their local regions. Human infection with *P. cynomolgi* has only been recently reported in a small number of individuals, with its geographic spread yet to be determined (Grignard *et al.* 2019).

In regions where malaria is endemic with high transmission rates, several rounds of childhood infections are likely to occur before children become clinically immune. For this reason, should an individual survive into adulthood, they are likely to have acquired non-sterilising immunity against malaria and consequently mortality in adults is relatively uncommon (Doolan *et al.* 2009). Non-sterile immune individuals in a community still harbour parasites while remaining asymptomatic, acting as a large reservoir for community transmission (Chaumeau *et al.* 2018). In comparison, populations in areas of lower transmission have fewer infections over a longer time period and do not acquire immunity. Therefore, adults can be equally as susceptible as children for infection and the resulting pathologies (Pinkevych *et al.* 2012). Immunity also wanes with time and dissipates should an individual leave an endemic region for a significant period (Chaumeau *et al.* 2019).

In this thesis, I focus specifically on *P. falciparum* in the interest of its global disease impact and its tractability to gene-editing techniques and *in vitro* culture.

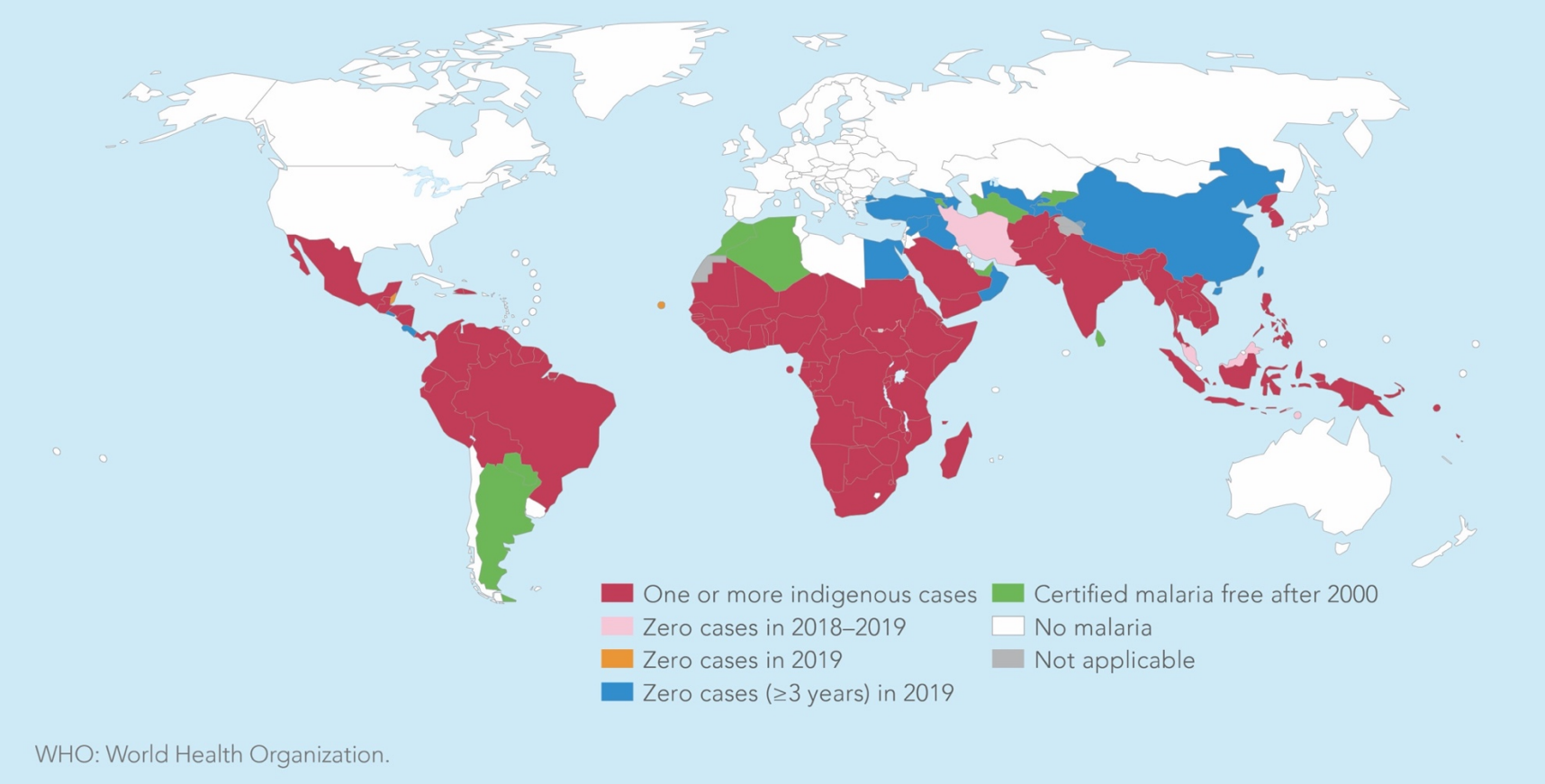

Figure 1. Countries with endemic cases of malaria (WHO 2020). Colour key indicates historical malaria presence.

The lifecycle of *P. falciparum*

Transmission of the parasite first occurs when an infected female *Anopheles* mosquito takes a blood meal from the human host, which provides an access point between the mosquito's saliva and the human bloodstream. During this initial stage, motile sporozoites are injected subcutaneously into the blood, which proceed to travel towards the liver to invade host hepatocytes. In this new environment, the parasite grows and replicates between 5-15 days to form a hepatic schizont containing thousands of merozoites, which then ruptures to release them into the bloodstream.

Free merozoites proceed to invade red blood cells (RBCs), where they grow over the next 48 hours. Morphologically, within the RBC the parasite transitions from a ring-stage trophozoite, then into mature trophozoites which begin to fill the volume of the host cell, coinciding with DNA replication. For the parasite to replicate itself, it develops into a schizont containing 16-32 daughter merozoites which rupture the host cell and are released into the blood to infect neighbouring RBCs. This cyclic invasion and rupture of RBCs is termed the blood stage lifecycle (synonymous with the term asexual lifecycle) and is the cause of all symptoms of malaria.

For the parasite to be re-transmitted, a small subset of blood stage parasites commit to form male and female gametocytes which can be taken up by a feeding *Anopheles* mosquito during a blood meal, then differentiate into gametes in response to changes in the surrounding chemical environment. Male and female gametes then fuse to form a zygote for sexual reproduction, which then differentiates into a motile ookinete that crosses the midgut boundary to form an oocyst. The oocyst replicates asexually to form thousands of motile transmissible sporozoites which travel to the mosquito salivary glands, stockpiled until injected into a new host. An illustrated overview of the lifecycle is shown in Figure 2. Although *P. falciparum* exhibits a complex, multi-host and multi-cell lifecycle (White *et al.* 2014, Maier *et al.* 2019), in this thesis I focus on the disease-causing blood stage.

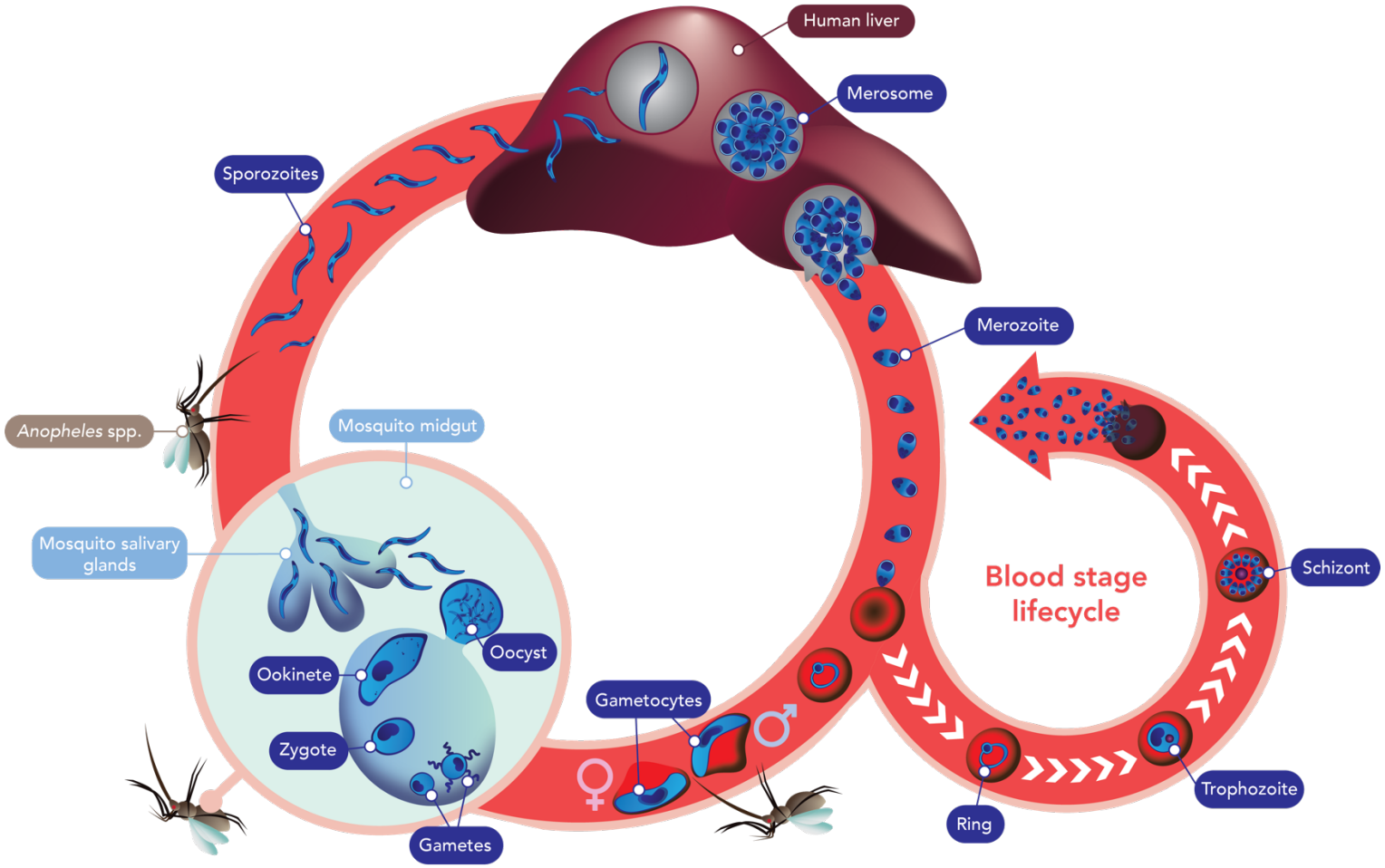

Figure 2. The lifecycle of *P. falciparum*. Key morphological stages and anatomical niches for the parasite in the mosquito vector and human host are highlighted. Lifecycle stages are described in the main text.

Clinical presentation of malaria infection

The blood stage is the disease-causing stage of the parasite lifecycle. Most cases of clinical malaria are presented as an uncomplicated febrile illness characterised by irregular, sporadic peaks of fever, headaches or muscular pain which can be resolved through effective antimalarial medications and by the immune response (Bartoloni & Zammarchi 2012). Generally, if malaria is treated early with effective drugs during this uncomplicated stage, prognostic outcomes are often positive. Individuals may also remain asymptomatic in spite of detectable parasites in the peripheral blood (Naeem *et al.* 2018).

Though the majority of cases of malaria are uncomplicated and readily treatable with effective antimalarials, approximately 1% of these cases progress into significant complications which are termed as severe malaria and can be fatal (Marsh *et al.* 1995). Severe malaria is attributed to ~400,000 deaths per year – a large majority of which have taken the lives of children under the age of five. Moreover, malaria causes a major health burden on women in pregnancy, contributing to ~800,000 low birthweight babies being born every year which leads to raised infant mortality (WHO 2020).

Severe malaria is characterised by the manifestation of several complicated pathologies which are summarised in Table 1, and can be influenced by the differences in *Plasmodium* species, age demographics, sex and blood parasitaemia. Of these listed, the most well-understood pathologies involve the manifestation of severe anaemia, metabolic acidosis and cerebral malaria, summarised in Figure 3. If an individual presents with more than one of these clinical manifestations, then medical prognoses are drastically poorer than if they present with just one (Marsh *et al.* 1995). Downstream complications involving multiple organ failure, though poorly understood, are hypothesised to be a direct or indirect outcome of these three main pathologies (Viriyavejakul *et al.* 2014).

Anaemia

Anaemia caused by malaria is represented by three main mechanisms: destruction of infected RBCs by blood stage parasites, enhanced splenic clearance of uninfected RBCs and downregulated levels of erythropoiesis (White *et al.* 2018). Though the destruction of infected RBCs (iRBCs) by the parasite contributes a

substantial amount to blood loss, clinical models have shown that more uninfected RBCs (uRBCs) are destroyed compared to infected RBCs (Jakeman *et al.* 1999, Price *et al.* 2001). Moreover, uRBC destruction by phagocytosis or splenic clearance is thought to occur as uRBCs co-circulating with parasite material become coated in pathogen-associated molecular patterns (PAMPs) (Jakeman *et al.* 1999). Lowered RBC count is further complicated by the inhibition of erythropoietin, a renally secreted hormone required for the induction of erythropoiesis and replenishment of RBCs (Chang *et al.* 2004). Lowered RBC counts in severe anaemia, defined as a haematocrit <15% or haemoglobin <50 g/L (WHO, 2000), is linked to the onset of several downstream pathologies.

Interestingly, the ancient presence of malaria in endemic regions has had a major impact on enriching genetic traits in the population of modern times which confer protective RBC polymorphisms to protect against infection, including sickle cell anaemia (Casanova *et al.* 2015). Though it was originally thought that sickle cells possessed biophysical properties that were more resistant to merozoite invasion, this protection is now thought to be conferred by hypoxia which stalls blood stage growth post-invasion (Archer *et al.* 2018). Indeed, at the cost of a lower oxygen carrying capacity, increased RBC autolysis, increased sickle cell blockages in the microvasculature, there remains a selective advantage to maintain sickle cell anaemia that reduces parasite proliferation in the human host. Additionally, glucose-6-phosphate dehygrogenase (G6PD) which is a key enzyme required to maintain RBC structural integrity, is often deficient in malaria endemic populations and is sex-linked to males. As such, G6PD-deficient individuals are naturally more susceptible to anaemia unrelated to infection by malaria parasites (Mbanefo *et al.* 2017, Beutler *et al.* 2008). Selection of these genetic modifications over time has shown the sheer impact of malaria to enrich for traits which prevent malaria infection but can also cause other impacts on human health.

Metabolic acidosis

The complex pathology of metabolic acidosis is thought to be caused by an increase in lactic acid production as a by-product of anaerobic glycolysis. Increased levels of anaerobic metabolism is caused in part by lowered RBC counts due to anaemia and decreased blood flow from sequestered infected and uninfected RBCs

(Sasi et al. 2007). Consequently, this results in a drastically lowered oxygen delivery capacity to host tissues. Moreover, a low pH environment is also known to directly inhibit oxygen transfer, and prevents the metabolic conversion of lactic acid to readily cleared waste products that would normally be processed through gluconeogenesis. Patients presenting with metabolic acidosis suffer from severe respiratory distress – a strong correlate of malaria-related mortality (Day *et al.* 2000).

Cerebral malaria

The clinical manifestation of cerebral malaria is usually characterised by a coma with concurrent detection of parasites in peripheral blood samples, though other characteristics include seizures and loss of consciousness. The pathophysiology of cerebral malaria is thought to be caused by the accumulation of infected RBCs in the endothelium of the brain microvasculature, impairing blood flow and inducing local tissue inflammation (Idro *et al.* 2011). Additionally, it is suggested that this would produce a similar fatal microenvironment as seen observed in metabolic acidosis (Zougbédé *et al.* 2011). While individuals who manifest cerebral malaria often recover from coma, they are at risk of developing long-term neurological and cognitive pathologies that are not well characterised. The sequestration of infected RBCs is not exclusive to the brain, they can also accumulate in other major organs which contributes to malaria pathology. Cerebral malaria contributes to ~10% of hospital submissions in Sub-Saharan Africa and between 15-25% of mortalities in the case of *P. falciparum* infection (Marsh *et al.* 1995).

Pregnancy-associated malaria

Malaria during pregnancy, commonly abbreviated as pregnancy-associated malaria (PAM), has severe outcomes for both the mother and developing foetus, resulting in low birthweights of < 2500 g, miscarriages, premature deliveries or still births. Most fatalities occur during the first and second pregnancies in immune naïve mothers, with latter pregnancies presenting with milder pathologies thought to be attributed to the development of immunity from repeated infections (Desai *et al.* 2007)

In *P. falciparum*, the pathophysiology underlying PAM is due to the sequestration of parasites which cytoadhere to the microvasculature of the placenta. Placenta-specific cytoadherence is mediated largely by the VAR2CSA variant of *P. falciparum* erythrocyte membrane protein 1 (PfEMP1) which binds the chondroitin sulphate A (CSA) and hyaluronic acid receptors on syncytiotrophoblasts (Rogerson *et al.* 1995, Fried & Duffy 1996, Beeson *et al.* 2000, Salanti *et al.* 2003). While parasites persist, they also effectively occupy and grow within the nutrient-rich environment of the placenta, sequestering resources away from the developing foetus. Blockages within the placental microvasculature also inhibits oxygen delivery to the foetus, further exacerbating the outcomes. The persistence of parasites in the placenta induces the recruitment of immune cells to the site, causing an inflammatory response which can result in foetal fatality (Menendez *et al.* 2000, Shulman *et al.* 2001).

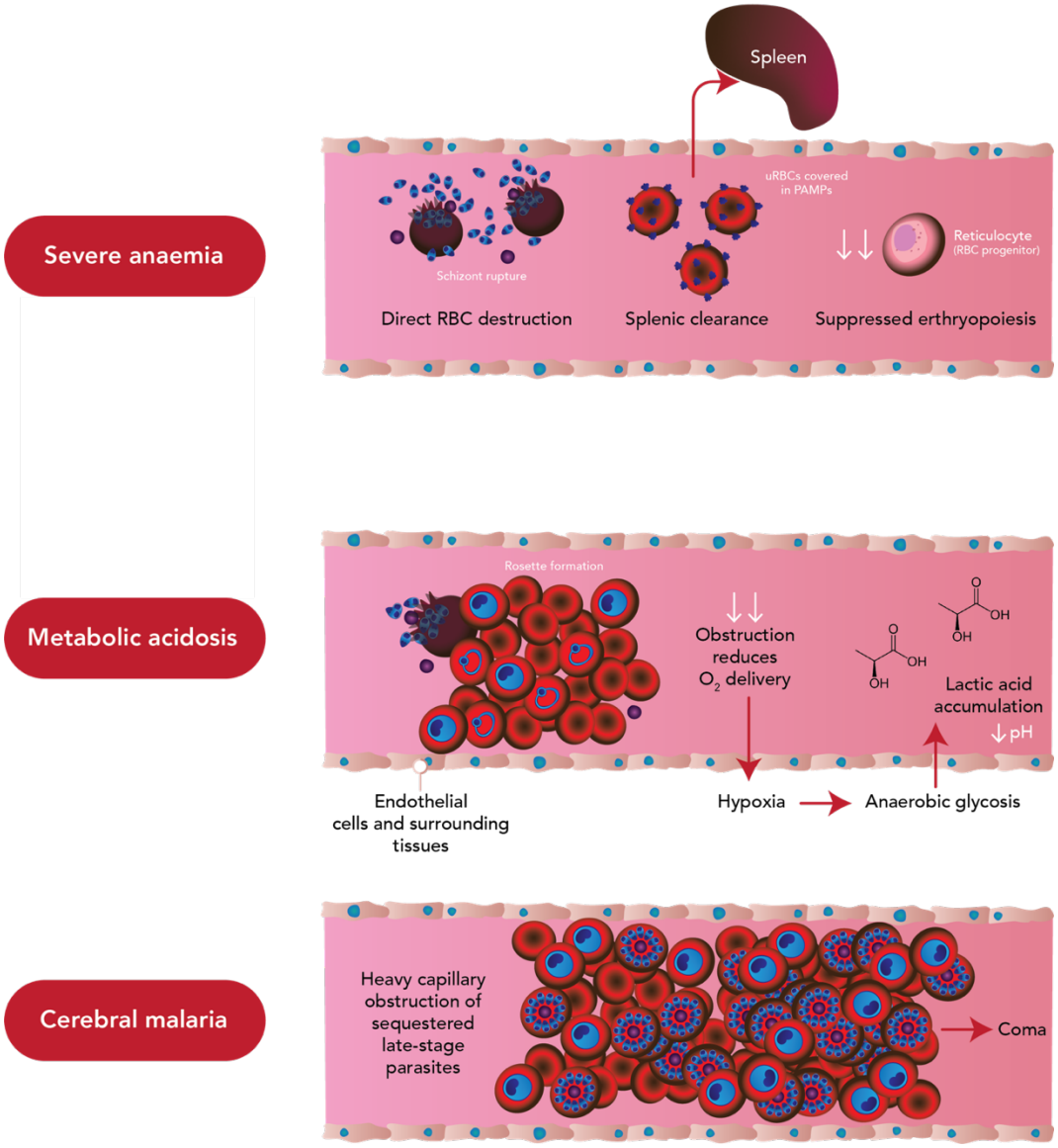

Figure 3. Mechanisms of pathogenesis in the human host for cases of severe malaria. Abbreviations: uninfected red blood cells (uRBCS), pathogen-associated molecular patterns (PAMPs).

Table 1. Syndromes associated with severe malaria, clinical features and pathogenic mechanisms (Ayimba *et al.* 2011, Pongponratn *et al.* 2003, Jakka *et al.* 2006, Day *et al.* 2000, Maguire *et al.* 2005, Yeo *et al.* 2009, Calis *et al.* 2008, Nguansangiam *et al.* 2007, Barcus *et al.* 2002, Desai *et al.* 2007).

Syndrome	***Clinical symptom(s)***	***Parameter(s) of choice for detection***	***Proposed disease mechanism(s)***
Severe anaemia	Shock, poor breathing	Low blood haemoglobin concentration (< 50 g/L)	Parasite-derived haemolysis, low erythropoiesis rates
Metabolic acidosis	Hyperlactatemia, hypoxia	High blood plasma lactate concentration (> 4 mmol/L), high blood lactate: pyruvate ratio	High anaerobic glycolysis rates from parasitized RBC cytoadherence
Cerebral malaria	Neurological impairment, comatose state	Ratio of cerebrospinal fluid constituents, post-mortem histology/immunohistochemistry	Parasitized RBC cytoadherence obstructs blood flow to the brain
Acute kidney injury	Hypoglycaemia	(see metabolic acidosis)	Parasitized RBC cytoadherence in kidney capillaries, tubular necrosis
Pulmonary oedema	Poor breathing, coughing blood	Lung function by spirometry	Inflammation of pulmonary endothelium, endothelial damage
Jaundice	Yellowed eyes and skin	High blood bilirubin	Co-infection with hepatitis B, hepatocyte injury, parasite-derived haemolysis
Malaria in pregnancy	Loss of foetus, low birthweight	Low birthweight (< 2500g), (see severe anaemia)	Inflammation of the placenta, cytoadherence in placental capillaries

Vector control

It was first demonstrated in 1897 that *Anopheles* mosquito vectors were capable of transmitting malaria parasites, paving the way for developing new means of vector control over the next century (Martinez-de la Puente *et al.* 2020). Initially, antilarval measures were taken to minimise hatching using chemical larvicides and draining breeding sites, with much success in the early 1900s in developed countries of lower malaria prevalence including the United States. In contrast in endemic countries in Asia, Latin America and Africa, these measures were insufficient given poor strategy implementation and lower overall socioeconomic settings (Rieckmann *et al.* 2006). Moreover, breeding patterns in times of high rainfall could not be easily intervened against due to the uncontrolled abundance of water bodies for mosquitos to lay eggs in (Abiodun *et al.* 2016)

Concurrent with antilarval countermeasures, interventions against adult mosquito bites were also developed. The long-lasting insecticide dichlorodiphenyltrichloroethane (DDT) was implemented in indoor residual spray (IRS) strategies across households in endemic countries, providing a high level of protection in communities (Rieckmann *et al.* 2006). This would then be implemented for use in insecticide treated nets (ITN) as bed nets, given that *Anopheles* mosquitoes mostly feed at night, though newer studies have shown that continued use of ITNs have influenced mosquito behaviours such that they bite earlier in the day (Milali *et al.* 2017). Household vector control strategies are cost-effective for reducing malaria cases in a community (Barnes *et al.* 2005). Unfortunately, these measures are now countered by the onset of insecticide resistance and lack of regular use. The WHO set out with a target to have at least 80% of households possessing an ITN, though this was not met in any endemic country. Moreover, in households with at least one ITN, only 46% of children under five and 52% of pregnant women, which are the two main at-risk demographics, are reported to regularly use it during sleep (WHO 2020). Stronger health promotion strategies, and the discovery and licensing of new classes of insecticides is essential for preventing the induction of malaria.

Current therapeutic strategies and diagnostics

Though malaria continues to retain a high global disease burden, there has been a significant decrease in malaria-related mortality since the year 2000, with up to 663 million clinical cases averted due to the successful implementation of ITNs, IRSs and our frontline antimalarial artemisinin and artemisinin-combinational therapies (ACTs) being available (Bhatt *et al.* 2015).

The value of antimalarial interventions is reliant on treatment availability, removing counterfeit drugs from the market, and compliance to treatment regimes in malaria endemic countries (Rieckmann *et al.* 2006). Though prophylactic drugs are available for travellers, they are of significantly reduced value proposition for people living in endemic areas given their additional expense, known side effects, long-term adherence and the likelihood of drug resistance developing with long-term use (Johnson & Kalra *et al.* 2012).

Frontline antimalarials

Artemisinin and its chemical derivatives (ARTs) are our frontline antimalarial treatments for non-severe and severe infections of malaria, and are administered as artemisinin combination therapies (ACTs) with a synergistic partner drug (Nosten & White 2007). Between 2010-2019, 3.1 billion treatment courses of ACTs have been administered across the world (WHO 2020). Though ACTs have been highly effective in decreasing the burden of malaria, resistance has begun to spread from South East Asia, emphasising the urgency for new antimalarials to be developed alongside a highly protective vaccine. Documented resistance to artemisinin and ARTs, including artesunate and artemether, is linked to parasite mutations in the *Pfkelch13* gene which is now frequently used as a trackable biomarker in molecular surveillance studies (Tilley *et al.* 2016, Khammanee *et al.* 2019)

Rapid diagnostic tests

Quickly identifying individuals infected by malaria, to inform appropriate medical prognoses and treatments, was made possible by the implementation of rapid diagnostic tests (RDT) in the early 1990s. RDTs are portable

immunochromatographic lateral flow devices which detect the presence of *Plasmodium* antigens in a droplet of patient blood, including *P. falciparum* histidine rich protein 2 (PfHRP2). Though highly sensitive, the recent emergence of *Pfhrp2* gene deleted-parasites has hampered the efficacy of *P. falciparum*-specific RDTs (Gatton *et al.* 2020), requiring *Plasmodium* lactate dehydrogenase (PLDH)-based diagnostics as an alternative which is not species-specific and detects all human *Plasmodium* species (Cunningham *et al.* 2019).

The immune response against *P. falciparum*

Repeat infections of *P. falciparum* in childhood gives rise to non-sterilising immunity in adults, due to the induction of an effective adaptive immune response which protects from the clinical manifestations of malaria. Therefore, it is possible to mount an effective immune response against the parasite. It was initially demonstrated that passively transferring gamma-globulins from immune adults could induce protection when administered to children (Cohen *et al.* 1961). This proof of concept shows that vaccines can be developed for malaria. However, the key mechanisms and antigenic targets that lead to a mounted adaptive immune response is poorly understood, and significant hurdles remain to identify safe and efficacious vaccine targets. An immune response can be mounted across all stages of the parasite lifecycle that is exposed to the bloodstream, with the following summary detailing the immune mechanisms at various time points.

The immune response in liver stages

Hepatocytes which have been parasitised by sporozoites are targetable by sporozoite antigen-specific cluster of differentiation 8 positive ($CD8^+$) T cells and the interferon gamma (IFNγ) response (Schofield *et al.* 1987). However, this process must be able to clear most if not all sporozoites, as even a single sporozoite can give rise to thousands of merozoites that will go on and establish the disease-causing blood stage infection.

Vaccine strategies for liver stages

In the past, it was demonstrated that irradiated (inactivated) *P. falciparum* sporozoites could be used as a whole-cell vaccine that could elicit immunity prior

to proper infection (Rieckmann *et al.* 1974, Hoffman *et al.* 2002). This was a proof of concept that sporozoites had immunogenic targets that could be accessed by antibodies, and remained the focus of several studies in early malaria vaccinology.

In the pursuit of a vaccine against liver stages, the RTS,S/AS01 vaccine was formulated. RTS,S is combined with the AS01 adjuvant (under the trade name Mosquirix) and is our only available licensed vaccine against malaria. RTS,S is a fusion protein that includes a region of the most highly abundant sporozoite protein, the circumsporozoite protein (CSP), with the aim to inhibit hepatocyte invasion and prevent the initial point of infection (Laurens 2020). Phase III trials reported varied efficacy levels of this vaccine against severe manifestations of malaria, preventing infection by 50% at first dose, declining in protection following two monthly boosters, resulting in a final efficacy of 36% at the 18 month final booster in malaria pre-exposed children 5-17 months old (RTS,S Clinical Trials Partnership 2015). Moreover, these trials have shown that protection from severe malaria is mostly induced in older children at 5-17 months of age, and is not protective in infants at 6-12 weeks of age. It was also reported that without the booster doses, no age group developed significant long-term immunity which highlights issues with continued vaccine expense, supply and compliance issues within a community. Overall this result leaves young children, which are the demographic of greatest mortality, at considerable risk of developing the pathologies of severe malaria.

However, in spite of RTS,S/AS01's limitations, it significantly reduced the number of clinical cases of malaria and hospital admissions. As an initial stepping stone, RTS,S/AS01 has demonstrated the viability of developing a vaccine against malaria and conversely illustrates the need for the development of alternative vaccines against other lifecycle stages.

The immune response in blood stages

During the blood-stage of infection, intracellular parasites are effectively hidden from the cell-mediated immune response as RBCs express neither major histocompatibility complex class I nor II (MHCI/MHCII) (Langhorne *et al.* 2008). As such, malaria antigens cannot be presented to T-cells in this scenario. The

humoral immune response instead plays a crucial role in targeting blood stage malaria parasites. The merozoite is a viable target against the antibody response, given that it is directly exposed to the bloodstream during invasion. Antibodies which target merozoites have three modes of action. First, antibodies can physically block essential receptor-ligand interactions during invasion. Second is by opsonisation of free merozoites, tagging them for phagocytosis by immune cells. Third is by recruitment of complement proteins to form of the membrane attack complex (MAC), destroying the merozoite. Though these mechanisms exist, inducing an effective antibody response against the merozoite is limited by high levels of functional redundancy, allelic variation, or antigenic polymorphism across key vaccine candidates (Beeson *et al.* 2016), or the employment of alternative invasion pathways (Tham *et al.* 2010, Duraisingh *et al.* 2003).

Blood stage parasites exert a range of immune evasion mechanisms which further complicates their targetability by the immune response. When *P. falciparum* establishes an infection within a host RBC, significant remodelling of the host occurs during growth. One such modification is the export of proteins onto the surface of infected RBCs, forming adhesive 'knobs'. The most highly studied and predominant proteins contributing to knob formation are encoded by the *var* gene family which express *Plasmodium falciparum* erythrocyte membrane protein 1 (PfEMP1). PfEMP1 has highly adhesive properties, allowing infected RBCs to clump together with adjacent RBCs, both infected and uninfected, in a process called rosetting. A rosette is capable of adhering to the host endothelium of the microvasculature, preventing transport of the parasite to the spleen for clearance. Moreover, these aggregates of rosettes exert virulent properties which can physically block whole capillaries. Further, the VAR2CSA variant of PfEMP1 is noted to be the key antigen responsible for cytoadherence to the maternal placenta microvasculature. While serological studies have suggested that PfEMP1 is highly immunogenic (Guillotte *et al.* 2016, Bull & Abdi 2016), *P. falciparum* evades clearance by the humoral immune response by epigenetically switching between 60 different *var* genes to encode a variable, functionally redundant PfEMP1 to escape from circulating antibodies (Duffy *et al.* 2017). Children continuously exposed to malaria and living in endemic areas do however raise effective antibodies against PfEMP1 leading to naturally acquired immunity against the parasite after repeated

exposure (Normark *et al.* 2007). Our understanding of PfEMP1 as an immunogen therefore highlights the difficulty in overcoming antigen redundancy for a malaria blood-stage vaccine and expresses the need for novel vaccines to have functionally non-redundant targets.

Vaccine strategies for blood stages

Vaccines which target blood stage parasite antigens, particularly those involved in RBC invasion, remain a vital research focus in the field. Proteins which localise to the merozoite surface and the major merozoite secretory organelles, the rhoptries and micronemes, are of most interest when considering new vaccine candidates. As of 2016, seven merozoite antigens in *P. falciparum* have been assessed in at least phase I human clinical trials, listed in Table 2. Of these, apical membrane antigen 1 (AMA1) is the most widely studied across a range of single-antigen, combined-antigen, and adjuvant formulated vaccines. Early trials for AMA1 vaccines suggested high immunogenicity in malaria-naïve adults and children (Dicko *et al.* 2007, Dicko *et al.* 2008). However, upon continued assessment in phase IIb clinical trials, the AMA1 vaccine failed to reduce parasitaemia in 2-3 year old children in Mali (Sagara *et al.* 2009). Vaccines targeting the merozoite surface proteins (MSPs), particularly MSP1, have also been a focus in clinical trials. However, it is understood that poor vaccine efficacy is caused by allelic variation and functional redundancies in MSP gene families.

More recently, there has been recent excitement in developing a vaccine against reticulocyte-binding protein homologue 5 (RH5). Rationale for an RH5-based vaccine stems from its essential role in invasion as an adhesin when coupled to its protein partners. The cysteine-rich protective antigen (CyRPA), RH5-interacting protein (RIPR) and RH5 form a complex to bind the RBC membrane receptor basigin (Richards *et al.* 2013, Volz *et al.* 2016). RH5 is highly conserved across strains of *P. falciparum* and has shown to be resistant to genetic deletion to illustrate that it is essential (Bustamante *et al.* 2013). Antibodies raised against RH5 have also shown cross-strain inhibitory properties across a range of lab-adapted isolates of *P. falciparum* (Chen *et al.* 2011, Douglas *et al.* 2011). Though promising, vaccines of merozoite antigens should be developed with a multivalent approach to

prevent vaccine resistance by incorporating a range of immunogens into the formulation.

Table 2. *P. falciparum* merozoite antigens which have been evaluated in at least phase I human vaccine trials. This table is adapted from Beeson *et al.* 2016.

Candidate	***Proposed primary function***
MSP1	Mediates initial attachment to heparin-like proteoglycans on host RBCs
MSP2	Unknown, putative essential function
MSP3	Unknown, forms a complex with MSP1, may interact with other proteins
AMA1	Mediates tight junction formation by binding RON2 (pre-translocated onto host RBCs)
EBA175	Mediates release of rhoptry proteins onto the merozoite surface by binding glycophorin A
GLURP	Unknown
SERA5	Unknown, putative protease function

Invasion biology of the merozoite

Invasion of host red blood cells is the critical first step in the disease-causing blood stage of the parasite lifecycle. Merozoites are known to search and recognise viable red blood cells for invasion within < 10 minutes (Boyle *et al.* 2010b), though the invasion process post-recognition occurs in a short span of ~ 30 seconds (Gilson & Crabb 2009). It is thought that this must occur rapidly to ensure minimal immune visibility of key ligands (Cowman & Crabb 2006). Understanding the mechanisms governing merozoite invasion requires a thorough investigation of this extremely short time window. The molecular events leading up to invasion of the host RBC have been studied extensively to show that invasion is a highly coordinated process involving both specific and redundant receptor-ligand interactions (Gaur *et al.* 2004). Merozoite invasion is often categorised into chronological phases based on discrete molecular and mechanical steps, as summarised in Figure 4 and discussed in further detail below.

Initial attachment

To initiate invasion requires a weak reversible attachment of the merozoite to the host cell membrane which is thought to be mediated by glycosylphosphatidylinositol (GPI) anchored merozoite surface proteins (MSPs), though the exact receptor-ligand interactions for the MSPs remain somewhat speculative or inconclusive. Of the MSPs, the most extensively studied is MSP1 which forms a large majority of the MSP coat (Gilson *et al.* 2006), and is complexed with MSP6 and MSP7 (Kauth *et al.* 2006). MSP1 exerts its function not only during invasion possibly by binding Band 3 or glycophorin A on the RBC cell surface (Goel *et al,*, 2003, Baldwin *et al.* 2015), but also during merozoite egress as a cleaved product by SUB1, to facilitate rupture of the host cell membranes (Glushakova *et al.* 2005, Yeoh *et al.* 2007, Das *et al.* 2015). Specific chemical inhibition of MSP1, in the presence of heparin-like molecules, also prevents merozoite attachment, further highlighting the importance of MSP1 during invasion (Boyle *et al.* 2010a). The role of other MSPs during merozoite invasion, including MSP2, 4, 5 and 10, remains largely uncharacterised (Beeson *et al.* 2016). Given that initial attachment is reversible and non-committing for the merozoite, the MSPs

may perform a generalised binding role across a range of host cell ligands, or by sheer number of intermolecular forces.

Reorientation

Shortly after attachment, the merozoite reorients itself to contact its apical tip onto the RBC to prime for invasion. The exact molecular force driving reorientation is thought to involve proteins which span the parasite plasma membrane (PPM) contacting the merozoite cytoskeleton to physically tilt the cell (Weiss *et al.* 2016). Once reorientation is achieved, its purpose is to position the apical invasion machinery, the rhoptries and micronemes, close to the host cell membrane and secrete invasion ligands (Riglar *et al.* 2011). The trigger for secretion is modulated by rapid changes in intracellular calcium levels and signalling cascades prompted by several kinases, including calcium-dependent protein kinases (CDPKs) (Gao *et al.* 2013, Holder *et al.* 2012). Key interactions early in *P. falciparum* merozoite invasion involve the reticulocyte binding homolog (RH) and erythrocyte binding antigen (EBA) protein families (Gaur *et al.* 2004). The RHs and EBAs are considered to be alternative pathway ligands with some degree of functional redundancy and overlapping function, as the merozoite can switch between multiple invasion pathways (Tham *et al.* 2010, Duraisingh *et al.* 2003). It is important to note that each protein family is not mutually exclusive and can function cooperatively (Lopaticki *et al.* 2011). Of the RHs, RH5 is unique in that it is absolutely required for invasion to proceed, where it complexes with RH5-interacting protein (RIPR) and cysteine-rich protective antigen (CyRPA) for binding the basigin receptor on the surface of the RBC (Volz *et al.* 2016).

Tight junction formation

A temporally distinct phase after reorientation was identified when inhibition of RH and EBA-specific binding was shown to prevent further secretion from the apical organelles (Singh *et al.* 2010), suggesting that there are prerequisites before the commitment point of invasion (Riglar *et al.* 2011). After establishment of the prerequisite interactions, a calcium flux occurs which triggers the secretion of rhoptry neck proteins (RON2, 4 and 5) from the rhoptry neck which are embedded as a small ring onto the RBC membrane (Richard *et al.* 2010), leaving

an exposed loop of RON2 visible on the extracellular surface (Weiss *et al.* 2015). Apical membrane antigen 1 (AMA1), which is microneme-derived, is pre-emptively secreted broadly across the merozoite surface before concentrating at the apical tip to bind the exposed loop of RON2 to form the irreversible tight junction. The merozoite therefore produces its own ligand and host receptor for RBC invasion (Alexander *et al.* 2005). Inhibition of this interaction results in significantly reduced invasion rates (Tonkin *et al.* 2011, Srinivasan *et al.* 2013).

Actin-myosin motility

The ring-like structure of the tight junction serves as a structure which primes the parasite to internalise into the host RBC. As the merozoite enters the RBC, the tight junction glides across the exterior length of the parasite towards its posterior. This movement is powered by an internal actin-myosin motor complex, with Myosin A as the primary motor which permits the parasite to pull itself through its mesh of F-actin in its cytoskeleton. It has been observed that several adhesins of micronemal origin, as well as AMA1, moves with the tight junction, highlighting the involvement of several proteins which serve as an intermediary link between the merozoite's motor and other host cell proteins (Baum *et al.* 2006, Riglar *et al* 2011). Concurrently, merozoite begins to form a double membrane by enveloping itself within the host RBC membrane to form the nascent parasitophorous vacuole membrane (PVM), which coincides with the timing of release of rhoptry bulb proteins including rhoptry-associated protein 1 (RAP1) (Baldi *et al.* 2000, Riglar *et al.* 2011). It is thought that bulb proteins play roles either late in invasion, during early establishment of the PVM, or in host cell remodelling during the initial stages of blood stage growth (Counihan *et al.* 2017, Suarez *et al.* 2019).

Internalisation

Nearing the completion of entry, the MSPs are shed from the merozoite surface which are hypothesised to have evolved to fulfil the role of an immunological smokescreen for the immune response to ensure successful entry (Ahlborg *et al.* 2002). As the tight junction reaches the posterior of the merozoite, AMA1 is thought to play a role in pinching the RBC membrane, simultaneously closing the mature PVM and fully encases the parasite. Shortly after internalisation,

the RBC can be temporarily distorted in a process called echinocytosis because of ion efflux during the invasion process (Gilson & Crabb 2009). A successfully invaded parasite then proceeds to grow over the next 48 hours until the next rupture event (Cowman *et al.* 2012).

Given that merozoite invasion is essential for parasite survival, and that the merozoites are in direct contact with the bloodstream and the immune system during this process, it presents itself as an attractive target for intervention. A detailed molecular understanding of the invasion process and how to inhibit it through protective antibodies or antimalarial drug-based approaches is of critical value to the field.

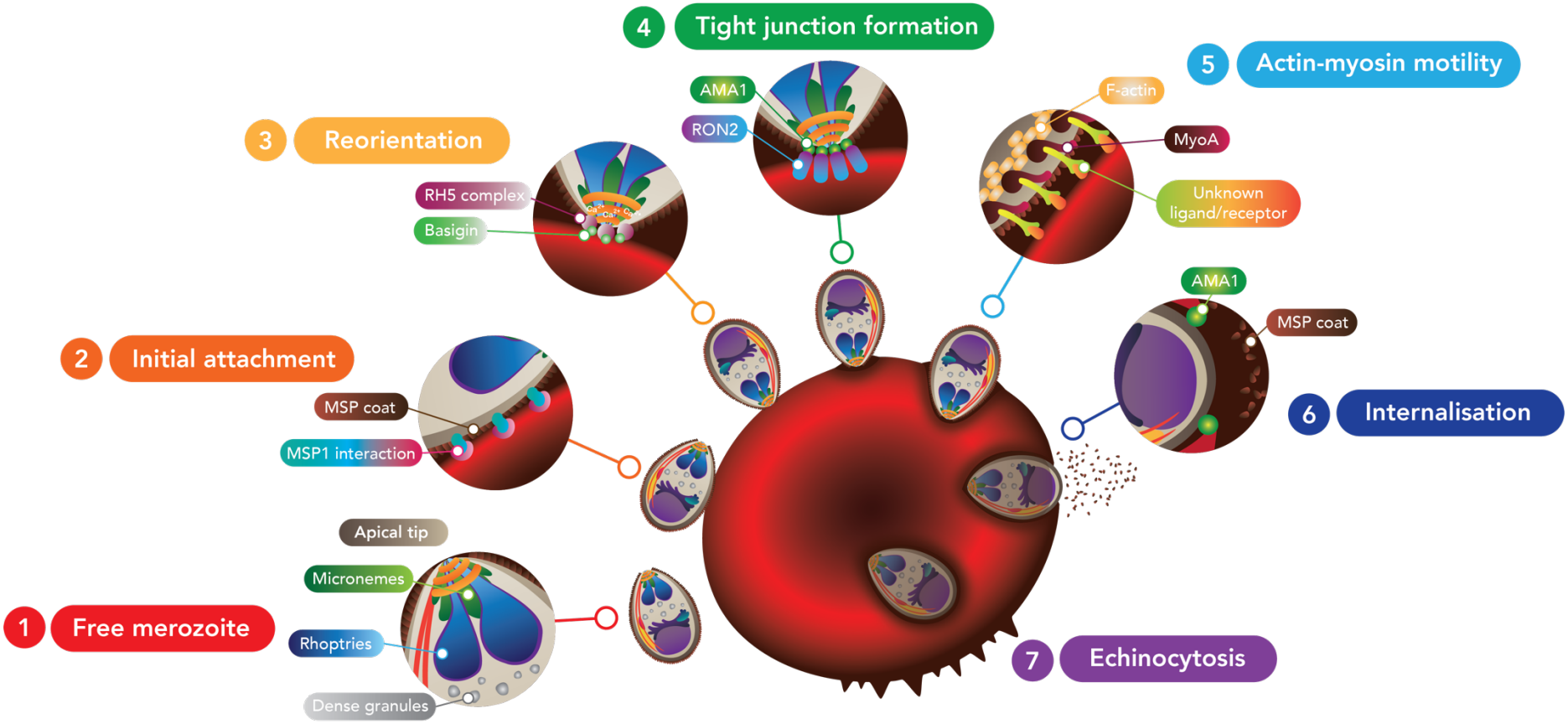

Figure 4. Merozoite invasion of the RBC. Key ligand-receptor interactions and the corresponding changes to parasite and host cell morphology are highlighted. Adapted from Burns *et al.* 2019. Abbreviations: merozoite surface protein (MSP), reticulocyte binding homologue (RH), apical membrane antigen (AMA), rhoptry neck protein (RON), myosin A (MyoA).

Invasion organelles

As preluded, Apicomplexans possess highly specialised secretory organelles called dense granules, micronemes, and rhoptries, which participate during invasion of a host cell. Being involved in invasion, they fulfil a function in invasive sporozoites and merozoites with many mechanisms remaining conserved between these two stages. For *P. falciparum* merozoites, these membranous organelles are, in a way, used to compartmentalise different components of the invasion proteome, or invadome, such that certain proteins are secreted or participate in the required order (Weiss *et al.* 2016). Though not strictly correlative, there is a general pattern which suggests the apical-most proteins within the micronemes and rhoptry neck are secreted first, followed by the rhoptry bulb (Liffner *et al.* 2021), and finally with the participation of the dense granules during the formation of the PVM (Mercier *et al.* 2005). The following provides an overview of the invasion machinery of *P. falciparum* merozoites, with a more expansive overview of rhoptry biology as per the scope of this thesis.

Dense granules

The dense granules have been described as membranous microspheres of varied diameter as large as 130 nm, occurring in quantities of up to ~ 50 spheres which localise freely in the cytosol of merozoites, though in close proximity to the remainder of the apical machinery (Culvenor *et al.* 1990, Blackman *et al.* 1998, Mercier *et al.* 2005). The known functions of dense granules are split between merozoite egress, the late stages of merozoite invasion, and early during the establishment of the newly invaded parasitised RBC, with all three processes requiring the secretion of dense granule-specific protein cargo via membrane fusion (Wirth & Pradel 2012). Prominent examples of protein cargo which participate during or after invasion are highlighted here. The most extensively studied protein cargo includes ring-infected erythrocyte surface antigen (RESA) which is linked to spectrin-based RBC membrane architectural maintenance after invasion (Pei *et al.* 2007, Diez-Silva *et al.* 2012), and subtilisin-like protease 2 (SUB2) which is a protease required for RBC membrane sealing (Collins *et al.* 2020). After invasion, dense granule cargo facilitates host cell remodelling. The most extensively studied of these are the components of the *P. falciparum* translocon of exported proteins

(PTEX), which is an essential protein trafficking machinery found on the PVM of intracellular parasite stages required for host cell remodelling (Bullen *et al.* 2012).

Micronemes and microneme-like organelles

Micronemes in merozoites are a collection of ~ 40 small bottle-shaped vesicles docked at the apical tip of merozoites, spanning 160 nm in length and 65 nm at their widest point (Bannister *et al.* 2003). Interestingly, merozoites have far fewer micronemes when compared to sporozoites and ookinetes, which is possibly correlated with the difference in cell size and therefore the amount of protein cargo required to be secreted (Dubois & Soldati-Favre 2019). Secretion from the micronemes via exocytosis is initially triggered by changes in intracellular calcium levels, prompting activation of calcium-dependent protein kinases (CDPKs) and phosphorylation of key substrates. It is currently not clear where calcium is stored inside of the cell to supply this process, though most of this takes place at the early points of invasion during or shortly after apical reorientation. Micronemal proteins are involved in specific receptor-ligand interactions which are essential axes for invasion, with the most extensively studied examples including CyRPA and RIPR which complex with the rhoptry neck protein RH5 for recognition of basigin, the EBAs which are involved in defining specific host-cell receptor invasion pathways, and AMA1 which is involved in the formation of the tight junction with RON2 (Weiss *et al.* 2015, Weiss *et al.* 2016).

Merozoites are unique from other invasive stages in that they also possess auxiliary microneme-like organelles called exonemes and mononemes which contain a variety of proteolytic enzymes. The function of these compartments is thought to be primarily limited to merozoite egress (Janse *et al.* 2007, Singh *et al.* 2007).

Rhoptries

Rhoptries in *P. falciparum* are large membrane-bound organelles found at the apical tip of the invasive lifecycle stages of the parasite. In merozoites, they are arranged as a pair of club-shaped vesicle-like organelles, spanning 500 nm in length each. They are morphologically divided into a “neck” which is proximal to the apical tip and “bulb” region on the distal end, with the latter being 200 nm wide

(Figure 5) (Hanssen *et al.* 2013). To current knowledge, there exists no physical scaffold or membrane between the neck and bulb, however the equivalent rhoptries in *T. gondii* tachyzoites suggests the presence of an intermediate region (Lemgruber *et al.* 2011), which may not be present or remains uncharacterised in *P. falciparum*. It is currently unknown whether possessing distinct neck and bulb regions exerts any physiological function, though it remains that the overall primary role of the rhoptries is to perform coordinated protein and lipid secretion during invasion which may be aided by having regions where distinct proteins are released from (Bannister *et al.* 1986). Certainly, evidence to date supports that there is a distinct neck or bulb distribution for a number of localised proteins in *P. falciparum* merozoites (Liffner *et al*. 2021).

The rhoptry proteome

As the largest secretory organelles, mature rhoptries contain a multitude of proteins within their luminal space, as well as having proteins embedded on its cytosolic-facing membrane. The rhoptry is the most proteinaceous organelle of the merozoite, as suggested by electron microscopy studies of relative protein density (Hanssen *et al.* 2013). Historically, proteins which localise to the neck have been called RONs while those that localise to the bulb have been called ROPs (Boothroyd & Dubremetz 2008). Though, over time this nomenclature has fallen out of use given that certain proteins do not definitively localise to one space or the other, possess different localisations between identically named homologues in different species, are capable of translocating across the rhoptry, or have been misnamed, for example RON3 which is reported to localise to the bulb (Zuccala *et al*. 2012, Sherling *et al*. 2019).

From start to finish: Rhoptry biogenesis, physiology, and disassembly

Rhoptries are thought to be synthesised *de novo* from Golgi-derived coated vesicles in early schizonts, though the initiator for this has not been elucidated. Early studies have suggested that at the beginning of rhoptry biogenesis, the nascent rhoptry appears as a spheroidal structure before separating into two regions with distinctly different protein masses. The less dense section, which is situated closer to the apical tip, elongates to form what is likely the rhoptry neck, while the distal

lipid-rich rounded base forms what is likely the rhoptry bulb. Rhoptry pairs do not necessarily form synchronously, and one may be larger than the other (Bannister *et al.* 2000). More recently, it has been shown that during rhoptry development, rhoptry proteins with signal peptides are packaged through the classical eukaryotic secretion pathway via clathrin-coated vesicles, and it is likely that the vesicles which form the rhoptries come pre-loaded with synthesised protein – suggesting that many rhoptry proteins are initially sorted in the Golgi (Figure 5) (Counihan *et al.* 2013).

Once rhoptries are fully matured and tethered to the apical tip in fully developed merozoites, they participate in protein secretion during invasion. To secrete proteins at the early stages of invasion during apical reorientation, the apical end of the rhoptry neck must fuse with the parasite plasma membrane (PPM) (Hanssen *et al.* 2013), which likely involves the snap receptor (SNARE) (Suarez *et al.* 2019) to form a channelling duct between the inside and the outside of the merozoite. This is followed by the rhoptry necks fusing to form a single duct to secrete proteins which interact with co-secreted micronemal proteins, such as the totalled RH5/RIPR/CyRPA complex. Then to prepare for tight junction formation, the RONs are secreted and embedded onto the host cell, for the upcoming interaction with the microneme-secreted AMA1. Functional interplay between the rhoptry neck and micronemal proteins are closely linked to the timing of their secretion. At the later points of invasion, the two rhoptry bulbs fuse which coincides with the timing of bulb protein secretion, such as RAP1 which is involved in PVM formation. A single rhoptry remains that is 75% smaller than its original size given that the majority of its contents have been secreted but maintains its distinct club-like morphology (Figure 5) (Hanssen *et al.* 2013, Riglar *et al.* 2011). Upon completion of invasion and formation of ring stages, the rhoptries are no longer visible and are thought to disassemble rapidly (Sachanonta *et al.* 2011), though the mechanism for disassembly has not been determined.

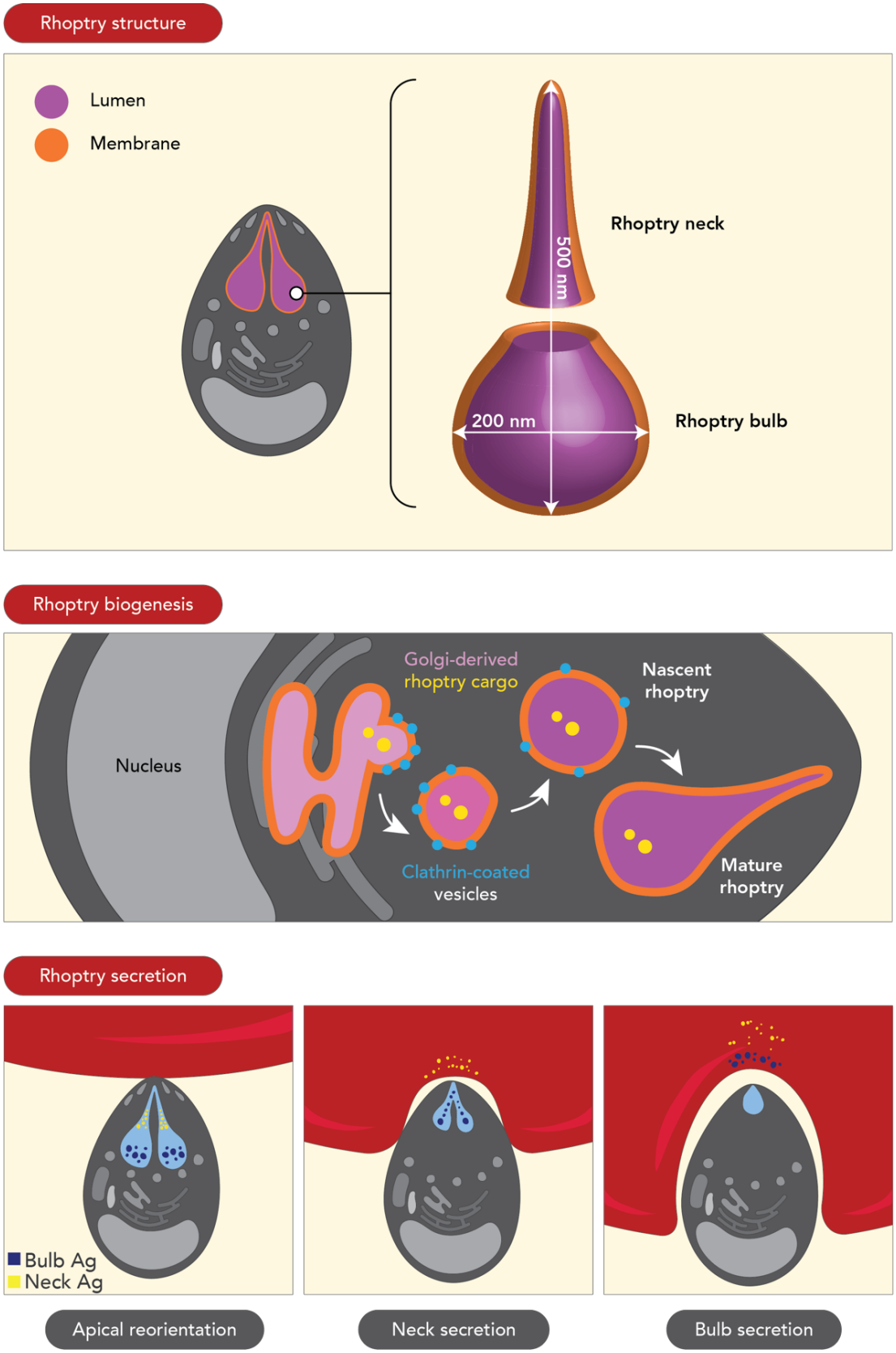

Figure 5. Structure, biogenesis and secretion of rhoptries of *P. falciparum* merozoites. Adapted from Liffner *et al*. 2021, Counihan *et al.* 2013. Ag = antigen.

Thesis theme I: Proteins involved in merozoite invasion and rhoptry biology

Preface - This thesis contains experimental studies which have focussed on two different aspects of *P. falciparum* biology. As such, the following introductory review has been split to provide the relevant background for each theme.

Cytosolically exposed rhoptry-interacting proteins

The primary motivation for studying rhoptry proteins has been to elucidate new vaccine candidates. This is because proteins secreted from the rhoptry lumen are, at a point during invasion, presented on the surface of the merozoite and therefore targetable by antibody responses. However comparatively little is known about the proteins which could be key facilitators for secretion, or whether there are proteins which are vital for rhoptry biogenesis and disassembly.

The cytosolically-exposed rhoptry interacting proteins (C-RIPs) are hypothesised to coordinate the mechanisms governing rhoptry function and biogenesis. As such, several C-RIPs perform their function during merozoite invasion and are essential to parasite growth, which has been determined either by gene knockdown or inducible knockout. To date, ten C-RIPs have been identified across apicomplexans, with only five having been directly characterised in *P. falciparum*. As per their naming, C-RIPs are defined by a distinct peripheral localisation on the cytosolic face of the rhoptry, or integrally spanning the rhoptry membrane on either the bulb or neck portion. This localisation places them in an ideal space for putative molecular contacts which occur outside of the rhoptry such as membrane fusion events and direct interaction with proteins from the cytosol, which are processes that are not likely to be facilitated by luminal proteins. However, this also dispels the suitability of C-RIPs as vaccine candidates as they are not presented onto the merozoite surface.

A thorough overview of currently characterised C-RIPs is provided in a co-authored review paper in the Appendix of this thesis (Liffner *et al.* 2021). For the following two sections, a detailed description of the initial discovery studies, either in *T. gondii* or *P. falciparum*, of C-RIPs is included.

C-RIPs of *P. falciparum*

CERLI1 (Pf3D7_0210600)

P. falciparum cytosolically-exposed rhoptry leaflet interacting protein 1 (PfCERLI1) was concurrently studied in *Toxoplasma gondii* under the suggested orthologue *T. gondii* rhoptry apical surface protein 2 (TgRASP2) (Suarez *et al.* 2019). PfCERLI1 is refractory to genetic ablation and was determined to be essential for blood stage parasite growth. To determine its direct effect on growth, inducible knockdown revealed its function to be specific to merozoite invasion (Liffner *et al.* 2020).

HA-tagged PfCERLI1 has been shown to localise to the cytosolic face of the rhoptry bulb in schizonts, as determined by super-resolution fluorescence microscopy, immuno-electron microscopy and biochemical protein assays. It was further elucidated that it is likely attached to the rhoptry membrane through a peripheral mechanism exhibited by its Pleckstrin homology (PH) and C2 domain which have been shown to target phosphatidic acid (PA) and phosphatidylinositol 4,5-bisphosphate ($PI(4,5)P_2$) lipids (Suarez *et al.* 2019). PfCERLI1 also exhibits an N-terminal signal peptide (SP) though it has been shown that the SP can be deleted and is not required for rhoptry membrane trafficking (Liffner *et al.* 2021).

Functional data has revealed that PfCERLI1 likely plays a role in coordinating rhoptry protein secretion, specifically shown for the neck proteins RON4 and RH4, and proteolytic processing of the bulb protein RAP1. This was further investigated to show that knockdown of PfCERLI1 alters rhoptry architecture, specifically in the spatial distribution of RON4 and RAP1 protein in the rhoptry neck and bulb respectively, but does not alter the shape or morphology of the organelle (Liffner *et al.* 2020). Interest is currently raised as to whether CERLI1 plays a regulatory role in the secretion, processing and distribution of other rhoptry proteins.

CERLI2 (Pf3D7_0405200)

A full characterisation of Pf3D7_0405200 (CERLI2), and its relationship to CERLI1, is presented in Chapter 2 of this thesis.

ARO (Pf3D7_0414900)

Armadillo repeats only (ARO) was initially studied in *T. gondii* as TgARO. Conditional knockout or deacylation of *Tgaro* has been shown to result in aberrant rhoptry positioning and anchoring at the apical tip of the tachyzoite (Mueller *et al.* 2013). It is thought that the most C-terminal of its ARM domains, of which it possesses six of, is specifically required for rhoptry anchoring to be successful (Mueller *et al.* 2016). Concurrently, this has shown that TgARO is essential for tachyzoite invasion, where rhoptry function during invasion has likely been severely abolished. It is thought that because TgARO interacts with myosin F, which is involved in actin polymerization, that the molecular basis for rhoptry targeting to the apical tip is an actomyosin-mediated process. TgARO also interacts with TgACβ, a key enzyme required for cAMP signalling (Mueller *et al.* 2013). Localisation of TgARO to the rhoptries, is mediated by the palmitoyltransferase TgDHHC7 (Beck *et al.* 2013), suggesting that its mode of membrane anchoring is by palmitoylation. Whether TgARO localises to the rhoptry neck or bulb is currently in debate, given its partial co-localisation by IFA to both neck and bulb antigens (Mueller *et al.* 2013).

PfARO's localisation has been determined more specifically to the cytosolic face of the rhoptry bulb (Cabrera *et al.* 2012, Sherling *et al.* 2019), though its precise membrane anchoring mechanics have not been directly studied. Functional studies of PfARO have primarily focussed on its role as a transient interacting partner for PfACβ and PfAIP. Its crystal structure has revealed that PfARO forms a bean-like structure (Geiger *et al.* 2020). Moreover, most of its most conserved residues are concentrated in its concave binding pocket with a highly polarised negative charge compared to the outer-facing surface of the bean shape. This pocket serves as a potential interface for protein-protein interactions (Mueller *et al.* 2016, Geiger *et al.* 2020).

AIP (Pf3D7_1136700)

Originally named armadillo-interacting protein (TgAIP), TgAIP was first shown as an interacting partner of TgARO (Mueller *et al.* 2013) and has since been renamed to ARO-interacting protein for *P. falciparum* (Geiger *et al.* 2020). Conditional knockout of TgAIP results in the intriguing loss of TgACβ from the rhoptries and from

whole parasites. Comparatively, conditional knockout of TgARO results in mislocalisation of both TgAIP and TgACβ, indicating that all three proteins are functionally linked and essential, leading to severe invasion defects (Mueller *et al.* 2016).

Bioinformatic analyses have identified a putative homologue of TgAIP in *P. falciparum* as PfAIP. The stark differences between TgAIP and PfAIP, which share 17.19% sequence identity, questioned whether it was a true homologue and whether it could interact similarly with PfARO. However, IFAs have shown that PfAIP localises in close proximity to PfARO, and validated further to show that it resides on the cytosolic face of the rhoptry neck. It has further been shown that the rhoptry localisation of PfAIP is dependent upon PfARO, where mutation of PfARO's putative protein-protein binding interface causes PfAIP to be mislocalised to the cytosol (Geiger *et al.* 2020).

Understanding that PfAIP and PfARO are functionally linked in *P. falciparum*, proteomic studies using DiQ-BioID were used to identify PfAIP's protein binding partners in mature schizonts. Interestingly, PfARO was not identified, though it remains to be determined if the two translocate to each other in free merozoites, to be more akin to their known interactions in tachyzoites of *T. gondii.* Instead, it was shown that PfAIP likely interacts or complexes with PfACβ which itself is linked to PfARO function, suggesting that PfACβ may spatially bridge PfAIP and PfARO (Geiger *et al.* 2020).

ACβ (Pf3D7_0802600)

P. falciparum adenylate cyclases alpha (PfACα) and beta (PfACβ) are enzymes which convert ATP to cAMP, an essential second messenger molecule required for many intracellular signalling pathways, however only the latter is expressed in blood stages (Salazar *et al.* 2012). As a key protein for cell signalling, PfACβ is refractory to deletion and is essential for blood stage growth. Furthermore, inducible knockdowns have revealed that it is required for merozoite invasion. HA-tagged PfACβ has been shown to localise to the cytosolic face of the rhoptry (Patel *et al.* 2019), though it remains inconclusive whether it is specific to the neck or the bulb.

The function of ACβ during invasion has not been completely elucidated, however it is suggested to be a potential signalling hub which involves the other known C-RIPs, as inducible knockdown results in inhibition of phosphorylation of PfARO, PfAIP and PfCERLI1 as shown in phosphoproteomic studies (Patel *et al.* 2019), as well as inhibiting phosphorylation of other rhoptry proteins including RON2. Additionally, ACβ knockdown surprisingly had no effect on rhoptry secretion mechanisms for neck proteins, though no evidence was presented for bulb proteins (Patel *et al.* 2019). ACβ may therefore have a coordinating role for the C-RIPs, though to what extent has not been investigated directly.

C-RIPs characterised exclusively in *T. gondii* with inferred functions in *P. falciparum*

Preface: The following proteins have only been studied in *T. gondii*. For each protein, the accession number for the corresponding predicted homologue in *P. falciparum* is included.

MyoF (Pf3D7_1329100)

The interaction between myosin F (TgMyoF) with TgARO has generated the hypothesis that TgARO targets the rhoptries to the apical tip via a putative actin polymerization mechanism (Mueller *et al.* 2013), however given that TgMyoF is not essential for invasion specifically, there are likely other proteins within TgARO's network which help fulfil its role. Nevertheless, their interaction suggests that TgMyoF must localise in proximity to TgARO on the cytosolic face of the rhoptries, though this may be transient as it is also dispersed across the tachyzoite cytosol. TgMyoF was initially characterised to instead be essential for centrosome positioning during tachyzoite endodyogeny – the mode of cell division in *T. gondii*, specifically mediating correct apicoplast inheritance in daughter cells through an actomyosin-based mechanism (Jacot *et al.* 2013). Given that TgMyoF plays a role in organellar segregation in daughter cells, it may play a part in rhoptry segregation as well.

Fer2 (Pf3D7_1455600)

Across eukaryotes, Ferlins are Ca^{2+}-responsive proteins that are important for fusion and trafficking events between membranous organelles (Lek *et al.* 2012). Interestingly, like PfCERLI1, all Ferlins possess a C2 domain, emphasizing a link between a canonical membrane fusion protein and proteins localising to the cytosolic face of the rhoptry bulb. Ferlin 2 (TgFer2) is the most highly conserved Ferlin across apicomplexans, has been shown to localise to two subcellular spaces in intracellular tachyzoites, including the cytosolic face of the rhoptry necks and the IMC. However, TgFer2 completely translocates to the former during tachyzoite invasion (Coleman *et al.* 2018), indicating a mechanistic interaction between the rhoptries and IMC at this point in time. Functional studies of TgFer2 have shown that when knocked down, tachyzoites fail to secrete rhoptry contents, leading to an invasion defect (Coleman *et al.* 2018).

NHE2 (Pf3D7_1303500)

The Na^+/H^+ exchangers (NHE) are involved in the carrier-mediated exchange of Na^+ and H^+ ions across membranes, and thus are membrane transport proteins in and of themselves. Specifically, TgNHE2, the first NHE to be characterised in apicomplexans, spans the rhoptry membrane integrally and ubiquitously without a specific bulb or neck localisation in *T. gondii*. It is thought that given the canonical role of NHEs, TgNHE2 may be involved in regulating osmotolerance of membranous organelles or maintaining structural turgidity of the rhoptries (Kasarov *et al.* 2005).

CA1 (Pf3D7_1140000)

Carbonic anhydrase 1 (TgCA1), also known as carbonic anhydrase-related protein (TgCA_RP), is a glycosylphophatidylinositol (GPI)-anchored protein found on the rhoptry bulb in *T. gondii* (Chasen *et al.* 2017). Across eukaryotes, carbonic anhydrases typically modulate intracellular bicarbonate levels through converting carbon dioxide and water into bicarbonate and H^+ ions. Because of this, TgCA1 may play an interactive role with TgACβ, of which adenylate cyclases in other species are

known to have a bicarbonate-sensitive activation mechanism (Supuran 2008). This highlights the possibility of identifying new cell signalling pathways with TgACβ as a central hub, and TgCA1 as a molecular trigger, which may have links to rhoptry function. TgCA1 can be knocked out, however resulting parasites exhibit an invasion defect which is likely due to a rhoptry biogenesis defect. Rhoptries in TgCA1 knockout tachyzoites have been described as dysmorphic and globular, without a distinct bulb and neck region (Chasen *et al.* 2017).

DHHC7 (Pf3D7_05282400)

Palmitoyltransferases and palmitoylacyltransferases are involved in protein lipidation by appending palmitic acid to cysteines residues in a process called *S*-palmitoylation (Tabaczar *et al.* 2017), and several are essential for growth in *T. gondii* (Frénal *et al.* 2013). The most extensively studied is the palmitoylacyltransferase TgDHHC7, named after its Asp-His-His-Cys (DHHC) palmitoylation enzymatic domain, which was identified as a rhoptry membrane protein. Knockdown of TgDHHC7 results in an invasion defect, thought to be caused by incorrect tethering of the rhoptries to the apical tip in tachyzoites, however with no change to overall rhoptry morphology. It has been shown that rhoptry tethering requires TgDHHC7 to have an intact C-terminal DHHC domain, which is required for palmitoylating protein substrates which include TgARO, which is dependent upon TgDHHC7 for correct localisation to the rhoptry bulb (Beck *et al.* 2013). Collectively, palmitoylation has been shown to be an essential process for rhoptry function overall.

Theme I: Aims and hypotheses

Molecular characterisation of C-RIPs is currently in its infancy in the field given their most recent discovery and classification. Therefore, studies directed towards identifying new C-RIPs are of valuable contribution for an increased functional understanding of rhoptry biology. For the first theme in this thesis, I have focussed on the molecular characterisation of PfCERLI2, in relation to PfCERLI1, with experimental insights on their roles for rhoptry function and merozoite invasion. Moreover, I have used PfCERLI1 and PfCERLI2 as platforms for identifying related C-RIPs through quantitative proteomics. These proteins are the topics of two results chapters, with two leading hypotheses:

Hypothesis I: PfCERLI2 is important for merozoite growth and invasion, and is functionally and phylogenetically related to PfCERLI1.

Hypothesis II: PfCERLI1 and PfCERLI2 are bound to other C-RIPs, inclusive of known and unknown proteins of this class.

Chapter 2 of this thesis is a first co-authored study, in manuscript style, written together with Benjamin Liffner (thesis submitted 2020, University of Adelaide), where we characterised PfCERLI2 with the following aims:

1. Perform a bioinformatic analysis to determine the phylogenetic ancestry of PfCERLI2 with respect to its homologue PfCERLI1, across related organisms.
2. Determine the subcellular localisation of PfCERLI2 in schizonts using immunofluorescence microscopy and other techniques.
3. Characterise the function of PfCERLI2 for merozoite invasion and rhoptry biology using a gene knockdown parasite line.
4. Develop the transgenic parasite lines required for dimerization-induced quantitative biotin identification (DiQ-BioID) for PfCERLI1 and PfCERLI2.

5. Identify the putative protein binding partners of PfCERLI1 and PfCERLI2 by mass spectrometry.

Combined, the expected primary outcomes of these studies are to assign PfCERLI2 with a specific role during merozoite invasion and to identify new C-RIPs for further investigation which are functionally related to both PfCERLI1 and PfCERLI2. It is in the authors' greatest wishes that these studies will form a firm foundation for understanding the biology occurring at the cytosolic face of the rhoptries in *P. falciparum*.

Thesis theme II: Schizont-expressed zinc finger proteins of *P. falciparum*

Novel protein domains in putative schizont proteins

With approximately two thirds of the *P. falciparum* proteome (3208 out of 5268 proteins) being unique to the species, many proteins do not have a comparable homologue in eukaryotes outside of apicomplexans (Gardner *et al.* 2002). This is largely due to the evolutionary divergence of *Plasmodium* from other currently sequenced eukaryotes. Gene ontologies (GO) of malaria proteins with keywords modelled from the prototypic eukaryotic model *Saccharomyces cerevisiae*, depict a distinct disparity between proteomes, with only key biological processes in cellular metabolism, nucleic acid synthesis and enzyme functions being reasonably conserved. As such, this has prevented the field from inferring protein function based on known models of proteins with domains of a canonical eukaryotic function. At best, proteins can be predicted to contain transmembrane domains, signal peptides or membrane anchors to a sufficient confidence (Gardner *et al.* 2002), though it is unknown whether certain domains with annotated functions across eukaryotes maintain a consistent function in *Plasmodium*.

Particularly for schizont and merozoite-expressed proteins, many functions involved during schizogony, which is a unique mode of mitosis, and merozoite invasion do not have equivalents in many model eukaryotes. Studies of proteins expressed at this stage often take insight from known homologues in closely related apicomplexans including *T. gondii*, if at all characterised. However, a large part of the schizont/merozoite proteome remains poorly characterised across all Apicomplexans and requires direct functional characterisation in order to determine their function.

As one of the two studies I took a lead on during my PhD, I investigated the function of proteins expressed late in the *P. falciparum* blood stage lifecycle which were predicted to possess zinc finger domains – a largely uncharacterised protein class in *P. falciparum*. Proteins with zinc finger domains have had few documented roles in schizogony or in merozoites so far (Ngwa *et al.* 2021), therefore warranting interest for investigation.

Zinc finger proteins

Zinc finger proteins (ZnFs) are a class of proteins which canonically bind nucleic acids in model eukaryotes. The ZnF domain structure is upheld by the coordination of a zinc ion to conserved cysteine and histidine residues, typically arranged as two β-sheets and a single α-helix (Zhang *et al.* 2011), exhibiting a unique fold for interacting with other macromolecules. Depending on the quantity and spatial arrangement of cysteines and histidines, ZnFs can be classed accordingly (Cassandri *et al.* 2017). Many ZnFs perform a downstream function related to nucleic acids, such as regulation of transcription or DNA repair, but some have also been shown to be involved in a plethora of other processes including signal transduction, cell migration, ubiquitination and much more (Cassandri *et al.* 2017). Gene editing technologies have also made use of ZnFs as zinc-finger nucleases (ZFNs), which bind DNA and induce a double-stranded break for targeted mutagenesis editing strategies (Carroll 2011).

P. falciparum is predicted to possess 170 ZnFs, which comprise 4% of all protein-encoding genes, and are primarily represented by the C2H2, RING, PHD and C3H1-type classes (Ngwa *et al.* 2021). Of all 170 ZnFs, approximately 90 are considered essential for blood stage growth, as verified by saturation mutagenesis studies (Zhang *et al.* 2018). ZnFs must therefore play an important role in blood stage parasites, though few ZnFs to date have been characterised with a specific function. Furthermore, our understanding of individual ZnF classes in *Plasmodium* is in its infancy, with the majority lacking homologues in other eukaryotic models.

C2H2 zinc fingers

The most well-characterised ZnF class in *P. falciparum* is the Cys-X_2-His-X_2-Cys-X_2-His (C2H2) configuration which can recognise and bind to both DNA and RNA. In eukaryotes, transcription factor IIIA (TFIIIA), which is an essential RNA polymerase, is the most well-studied of the C2H2 ZnFs and was originally discovered in *Xenopus laevis* oocytes (Picard & Wegnez 1979). *P. falciparum* possesses a functional homologue in the form of telomere repeat-binding factor zinc finger protein (PfTRZ), which is part of a superfamily of proteins called telomere repeat-binding factors (TRFs). The difference between PfTRZ and TFIIIA is that the former lacks a

key MYB domain that is needed for DNA-binding. Instead, it has been shown that PfTRZ employs its C2H2 ZnF to perform this interaction, which is key for proper cell growth and a myriad of other processes including the regulation of telomere length (Bertschi *et al.* 2017). PfTRZ demonstrates that despite the divergence of *Plasmodium* proteins from their eukaryotic counterparts, their functions can be compensated by employing alternative protein domains.

RING zinc fingers

The really interesting new gene (RING) finger class possesses a Cys-X_2-Cys-His-X_{9-39}-Cys-X_{1-3}-His- X_{2-3}-Cys-X_2-Cys consensus sequence, where RING finger proteins (RFPs) in eukaryotes play highly diverse functions through protein-protein interactions (Deshaies & Joazeiro *et al.* 2009, Ngwa *et al.* 2021). Interestingly, the most well-documented role of RFPs in *P. falciparum* are as E3 ligases which are involved during ubiquitination for targeting proteins to the proteasome for degradation (Harbut *et al.* 2012 Chung *et al.* 2012, Ngwa *et al.* 2017). RFPs therefore present a diverse function for ZnFs outside of nucleic acid binding.

PHD zinc fingers

The plant homeodomain (PHD) is characterised by a Cys_4-His_3-Cys_3 consensus sequence, are involved in epigenetic gene regulation by histone protein acetylation in model eukaryotes. In *P. falciparum*, the most well-understood PHD ZnFs include PfPHD1 and PfPHD2, which complex together with several protein partners to collectively bind chromatin and histones (Hoeijmakers *et al.* 2019). PfPHD1 in particular associates directly to the histone H3K9ac, which is associated with *var* gene activation (Voss *et al.* 2014).

C3H1 zinc fingers

Of direct interest to the ZnF proteins I characterised is the Cys-X_8-Cys-X_5-Cys-X_3-His (C3H1, also known as CCCH) ZnF configuration. Most C3H1 ZnFs are known to exclusively bind RNA, with the prototypical C3H1 ZnF tristetraprolin (TTP) being

the first and most well-studied in eukaryotes (Lai *et al.* 1990, Hall 2005). Rationale for studying TTP was led by its yet-unclassed zinc fingers which were hypothesised to bind DNA as a transcription factor, though was later shown to function as an RNA-binding protein (RBP) involved in the regulated induction of tumour necrosis factor alpha (TNF- α) (Taylor *et al.* 1996). Specifically, TTP was shown to bind the AU-rich regions (AREs) in the 3' untranslated region (3' UTR) of the TNF-α mRNA molecule, and induced the degradation of transcripts to regulate protein expression. In humans, there are 57 known C3H1 ZnFs of which a large proportion have no known function (Fu & Blackshear 2017). Of the few characterised, they have been shown to exhibit functions in RNA splicing, formation of the poly-A tail, mRNA export, translation, and stabilisation or degradation of mRNA transcripts (Hajikhezri *et al.* 2020).

Of the 27 predicted C3H1 ZnFs in *P. falciparum*, many of these proteins possess speculative annotations based on comparable homology with human C3H1 ZnFs. Only three have been explored in any experimental capacity, revealing three highly distinct roles (Ngwa *et al.* 2021). The first is a predicted homologue of NGFI-A-binding protein 2 (PfNAB2), which binds both DNA and RNA through its PWI motif, where it remains unclear whether it also uses C3H1 ZnF domain for this purpose (Szymczyna et al. 2003). The second is YTH-domain like protein 1 (PfYTH1), which is involved in N^6-methyladenosine (m^6A) post-transcriptional modifications, targeting transcripts for degradation (Baumgarten *et al.* 2019). The third is PfD13, a schizont-expressed protein that was considered to be a viable blood stage merozoite vaccine candidate due to its reported surface exposure and peak expression in schizonts (Daubenberger *et al.* 2003). Given PfD13's involvement in blood stage parasites, I have chosen to investigate its function further in the context of blood stage growth and merozoite invasion.

Theme II: Aims and hypotheses

Proteins with peak expression at blood stage schizogony are often inferred to have roles during schizont development, egress or merozoite invasion as *P. falciparum* exhibits high temporal control over its own gene expression. To date, no proteins classified as zinc fingers have been linked to this lifecycle stage with the exception of PfD13. Therefore, the significance of a C3H1 ZnF protein proposed as a vaccine candidate being expressed at schizogony no less, is truly an enigma that remains to be further explored. Here I perform a functional characterisation of PfD13, which we re-designate as C3H1 zinc finger protein 1 (PfCZIF1), alongside a newly identified protein PfCZIF2, in blood stage growth with the following hypothesis:

Hypothesis: PfCZIF1 and PfCZIF2 are both essential for blood stage growth, and localise to the merozoite surface.

Chapter 3 of this thesis features a molecular characterisation of the proteins PfCZIF1 and PfCZIF2, written in manuscript-style, with the following aims:

1. Using gene truncation and knockout parasite lines, target specific domains in PfCZIF1 and PfCZIF2 to determine whether they are functionally linked and essential to blood stage growth.
2. Determine the subcellular localisation of PfCZIF1 and PfCZIF2 across the blood stage lifecycle using immunofluorescence microscopy and other techniques.
3. Observe the direct effect of PfCZIF1 and PfCZIF2 truncation on the schizont transcriptome by RNAseq.

The expected outcomes of this study are to have verified the localisation of PfCZIF1 and PfCZIF2 to assess their suitability as vaccine candidates, and to have understood their function in blood stage parasites. This work is intended to provide the foundation

for future studies which will more explicitly explore the function of the C3H1 ZnF class in blood stages.

Overall PhD outcomes

The research conducted during my PhD provides essential framework for further studies across two distinct themes of *P. falciparum* blood stage biology.

Through my studies of PfCERLI1 and PfCERLI2, I have highlighted their importance during merozoite invasion with particular insights on their roles in rhoptry organelle biogenesis and physiology. Moreover, I have revealed that these proteins possess novel protein-protein interactions which are likely to occur on the cytosolic face of the rhoptry membrane. These interactions are likely linked to rhoptry related processes and are strongly warranted for further investigation.

My investigation of PfCZIF1 and PfCZIF2 in schizonts will have provided a thorough molecular characterisation of each protein's expression pattern, membrane dynamics, subcellular localisation, and roles for transcript regulation. This work also serves to validate existing studies for PfCZIF proteins for fortifying current literature and to provide an incentive to study these proteins in the future with a specific focus on their unique C3H1 ZnF domains.

Chapter 2

Pfcerli2, a duplicated gene in the malaria parasite *Plasmodium falciparum* essential for invasion of erythrocytes as revealed by phylogenetic and cell biological analysis

Statement of Authorship

Title of Paper	*Pf*cent2, a duplicated gene in the malaria parasite *Plasmodium falciparum* essential for invasion of erythrocytes as revealed by phylogenetic and cell biological analysis.
Publication Status	☐ Published ☐ Accepted for Publication ☑ Submitted for Publication ☐ Unpublished and Unsubmitted work written in manuscript style
Publication Details	Preprint doi: https://doi.org/10.1101/2020.11.26.400549

Principal Author

Name of Principal Author (Candidate)	Juan Miguel Bafbin
Contribution to the Paper	Designed and planned the study, performed experiments, generated reagents and data, manuscript writing. Added significant experimental contributions since the original submission of this manuscript in response to reviewers' comments.
Overall percentage (%)	[redacted] 55%
Certification:	This paper reports on original research I conducted during the period of my Higher Degree by Research candidature and is not subject to any obligations or contractual agreements with a third party that would constrain its inclusion in this thesis. I am the primary author of this paper.
Signature	Date: 10 · 7 · 21

Co-Author Contributions

By signing the Statement of Authorship, each author certifies that:

i. the candidate's stated contribution to the publication is accurate (as detailed above);
ii. permission is granted for the candidate to include the publication in the thesis; and
iii. the sum of all co-author contributions is equal to 100% less the candidate's stated contribution.

Name of Co-Author	Benjamin Liffner
Contribution to the Paper	Designed and planned the study, performed experiments, generated reagents and data, wrote the manuscript.
Signature	Date: 10/09/2021

Name of Co-Author	Ella Edwards
Contribution to the Paper	Study design and planning, performed proteomics experiments.
Signature	Date: 9 · 9 · 2021

Please cut and paste additional co-author panels here as required.

Name of Co-Author	Ghizal Siddiqui
Contribution to the Paper	Generated and analysed proteomics data.
Signature	Date 30-09-21

Name of Co-Author	Gerald Shami
Contribution to the Paper	Performed transmission electron microscopy experiments.
Signature	Date 01/10/2021

Name of Co-Author	Jan Strauss
Contribution to the Paper	Assisted with and performed phylogenetic analyses.
Signature	Date 30.09.21

Name of Co-Author	Sonja Frolich
Contribution to the Paper	Assisted with microscopy data analysis.
Signature	Date 10/9/21

Name of Co-Author	Gary Heinemann
Contribution to the Paper	Generated transfectant parasite lines.
Signature	Date 22-9-21

Name of Co-Author	Arne Alder
Contribution to the Paper	Generated transfectant parasite lines.
Signature	Date 20 09 21

Name of Co-Author	Jan Stephan Wichers
Contribution to the Paper	Generated transfectant parasite lines.
Signature	Date 20/09/21

Name of Co-Author	Leanne Tilley
Contribution to the Paper	Study design and planning.
Signature	Date 30/09/21

Name of Co-Author	Matthew Dixon
Contribution to the Paper	Study design and planning.
Signature	Date 23/09/21

Name of Co-Author	Tim-Wolf Gilberger
Contribution to the Paper	Study design and planning.
Signature	Date 20/09/21

Name of Co-Author	Darren Creek
Contribution to the Paper	Study design and planning.
Signature	Date 30/9/2021

Name of Co-Author	Danny Wilson
Contribution to the Paper	Study design and planning, performed analysis and generated reagents, manuscript writing.
Signature	Date 9/9/2021

Pfcerli2, a duplicated gene in the malaria parasite *Plasmodium falciparum* essential for invasion of erythrocytes as revealed by phylogenetic and cell biological analysis

Preface

This study was completed as a co-first authored manuscript that was written together with Dr Benjamin Liffner, who submitted his doctoral thesis to the University of Adelaide in 2020. As such, in this preface I will be highlighting my key contributions to this study during my co-candidature with Benjamin, as well as any notable additions to the updated manuscript at the time of writing of this thesis.

In this chapter, we describe *P. falciparum* cytosolically exposed rhoptry leaflet interacting protein 2 (PfCERLI2) as a protein that is essential for merozoite invasion of the host RBC using transgenic parasite lines which express an HA-tagged PfCERLI2. Many of our platforms for studying PfCERLI2 were reliant on visualising HA-tagged protein using anti-HA antibodies by western blotting (WB) and immunofluorescence assays (IFA), however PfCERLI2 was particularly difficult to detect using these methods. Indeed, PfCERLI2 is a lowly expressed protein and as such our research group was unable to overcome this technical barrier of detectability for many years prior to the start of my candidature. Upon joining this project in 2018, I performed numerous optimisation projects to increase PfCERLI2 detectability at the level of cell culture (enriching for HA-expressing transfectants by extended drug selection), sample preparation (testing blocking reagents, commercial anti-HA antibodies, antibody titrations, parasite fixation) and detection (western blot imaging, confocal microscopy settings adjustments, Airyscan mode settings adjustments). As such all experiments requiring WBs and IFAs in this study were completed by myself and analysed together with Benjamin and co-authors. Of all the methods I had attempted for increasing PfCERLI2's detectability, the most significant was implementing a biotin-conjugated anti-HA primary antibody and a streptavidin-conjugated AlexaFluor for our IFAs, allowing us to deduce it as a novel rhoptry bulb protein in *P. falciparum* merozoites.

Having identified this, we were able to proceed with all downstream experiments which focussed on rhoptry biology; forming a large bulk of our functional data.

Since the original submission of this manuscript as a preprint in late 2020 and as the version presented in Benjamin's thesis, I have also continued our characterisation of PfCERLI2 in response to reviewers' comments from Communications Biology. The first significant addition was developing a quantitative IFA-based bound merozoite assay adjusted from a protocol presented in Riglar *et al.* 2011. This allowed us to determine that PfCERLI2 knockdown likely causes an invasion defect at or prior to the formation of the tight junction in fixed merozoites in conjunction with existing light microscopy data. The second significant addition was the ground-up generation of new transgenic parasite lines for identifying the protein binding partners of PfCERLI2 (and its paralogue PfCERLI1) using dimerization inducible quantitative biotin identification (DiQ-BioID) and mass spectrometry. These lines were used in this study to answer specific reviewers' comments and are the basis of all the data in Figure 8. Other additions to this study include adjustments to all figures, production of parasite material for SBF-SEM studies, replacements of preliminary western blot data with better standardised experiments and undertaking the experiments for more several supplementary figures (Supplementary Figures 10, 17, 18, 19, 20). All drawn schematics in this chapter were produced by myself. Thus, my contribution to this study is of equal significance to that of Dr. Liffner and my contribution easily consists of 35% or more of the manuscript's data.

As this manuscript has been submitted for review, Chapter 2 features its own references in the style requested by Communications Biology. Footnote numbers correspond to the references at the end of the chapter.

Chapter 3, which is an unsubmitted manuscript, will have its references summarised at the end of the thesis document.

Pfcerli2, a duplicated gene in the malaria parasite *Plasmodium falciparum* essential for invasion of erythrocytes as revealed by phylogenetic and cell biological analysis.

Benjamin Liffner[1¶], Juan Miguel Balbin[1¶], Gerald J. Shami[2], Ghizal Siddiqui[3], Jan Strauss[4,5,6‡], Sonja Frölich[1], Gary K. Heinemann[7], Ella May Edwards[1], Arne Alder[4,5], Jan Stephan Wichers[4,5], Darren J. Creek[3], Leann Tilley[2], Matthew W. A. Dixon[2], Tim-Wolf Gilberger[4,5,6] Danny W. Wilson[1,8*]

[1]Research Centre for Infectious Diseases, School of Biological Sciences, University of Adelaide, Adelaide 5005, Australia.

[2]Department of Biochemistry and Molecular Biology, Bio21 Molecular Science and Biotechnology Institute, The University of Melbourne, Melbourne 3010, Victoria, Australia.

[3]Monash Institute of Pharmaceutical Sciences, Monash University, Parkville, Victoria, 3052, Australia.

[4]Centre for Structural Systems Biology, 22607 Hamburg, Germany.

[5]Bernhard Nocht Institute for Tropical Medicine, 20359 Hamburg, Germany.

[6]Biology Department, University of Hamburg, 20146, Hamburg, Germany.

[7]Experimental Therapeutics Laboratory, School of Pharmacy & Medical Sciences, University of South Australia Cancer Research Institute, Adelaide 5005, Australia.

[8]Burnet Institute, 85 Commercial Road, Melbourne 3004, Victoria, Australia.

* Corresponding author

E-mail: danny.wilson@adelaide.edu.au

¶These authors contributed equally to this work.

‡Current address: GEOMAR Helmholtz Centre for Ocean Research Kiel, Kiel, Germany.

Abstract

Merozoite invasion of host red blood cells (RBCs) is essential for survival of the human malaria parasite *Plasmodium falciparum*. Proteins involved with RBC binding and invasion are secreted from dual-club shaped organelles at the apical tip of the merozoite called the rhoptries. Here we characterise *P. falciparum* Cytosolically Exposed Rhoptry Leaflet Interacting protein 2 (PfCERLI2), as a rhoptry bulb protein that is essential for merozoite invasion. Phylogenetic analyses show that *cerli2* arose through an ancestral gene duplication of *cerli1*, a related cytosolically exposed rhoptry bulb protein. We show that PfCERLI2 is essential for blood-stage growth and localises to the cytosolic face of the rhoptry bulb. Inducible knockdown of PfCERLI2 led to a proportion of merozoites failing to invade after formation of the tight junction. PfCERLI2 knockdown was associated with inhibition of rhoptry antigen processing and a significant elongation of the rhoptries, suggesting that the inability of merozoites to invade is caused by aberrant rhoptry function due to PfCERLI2 deficiency. These findings identify PfCERLI2 as a protein that has key roles in rhoptry biology during merozoite invasion.

Introduction

Plasmodium falciparum, a human malaria parasite, is the cause of ~400,000 deaths each year; predominantly in children under the age of five[1]. *P. falciparum* is transmitted from *Anopheles* mosquitoes, its definitive host, to humans through the blood meal of an infected mosquito where invasive sporozoites are injected subcutaneously and migrate to the liver. Following invasion of liver hepatocytes, the parasite develops into thousands of daughter merozoites inside a hepatic schizont, which ruptures and releases the daughter merozoites into the blood stream where they invade red blood cells (RBCs)[2]. Over the following ~48 hours, the parasite develops inside the RBC until it forms 16-32 new daughter merozoites inside of a schizont that ruptures, releasing the merozoites that go on to infect new RBCs[2]. Replication of *P. falciparum* in this asexual blood-stage of the lifecycle is the cause of all the clinical symptoms of malaria.

RBC invasion by merozoites occurs over a period of ~30 seconds and involves the attachment of the merozoite to the RBC, which then reorients so its apical tip contacts the RBC membrane[3]. Specialised invasion organelles, known as the rhoptries and micronemes, then secrete their contents to form an irreversible tight junction before the merozoite pulls the RBC plasma membrane around itself, forming a parasitophorous vacuole (PV) and completing invasion[4]. Each merozoite has two rhoptries, the largest of the invasion organelles, which are club-shaped and divided into a bulb and neck, with the neck positioned at the apical tip of the merozoite[5]. Rhoptry neck proteins are released early in the invasion process and mediate initial attachment to the RBC and formation of the tight junction[6]. Rhoptry bulb contents are secreted following junction formation and are typically involved in establishing the PV[7].

Most rhoptry luminal proteins exclusively localise to the rhoptry bulb or neck, with minimal overlap between the two[8]. During the process of RBC invasion, the neck of the rhoptries fuse to the parasite plasma membrane (PPM) to allow secretion of rhoptry contents. Additionally, the dual club-shaped rhoptries fuse from neck to bulb,

leaving a singular rhoptry that retains its neck and bulb structure[5]. What controls both PPM and rhoptry fusion has not been elucidated.

It is likely that rhoptry and PPM fusion are controlled by proteins that localise to the cytosolic face of the rhoptry membrane, as they can contact both membranes to facilitate their fusion. To date, however, only three proteins in *P. falciparum* have been shown to localise to the cytosolic face of the rhoptry membrane: Armadillo repeats only (ARO)[9], ARO interacting protein (AIP)[10], and Cytosolically exposed rhoptry leaflet interacting protein 1 (CERLI1; also known as Rhoptry apical surface protein (RASP) 2)[11,12]. Here we describe PfCERLI2 (Pf3D7_0405200), a paralogue of *Pfcerli1*, which localises to the cytosolic face of the rhoptry bulb membrane and is essential for merozoite invasion of RBCs.

Results

PfCERLI2 is conserved among Apicomplexa and arose from an ancestral gene duplication

Plasmodium falciparum Cytosolically Exposed Rhoptry Leaflet Interacting protein 2 (PfCERLI2) (Pf3D7_0405200) is a protein of 579 amino acids in *P. falciparum* isolate 3D7. PfCERLI2 contains a predicted lipid-calcium binding C2 domain towards its N-terminus and possesses a decapeptide tandem repeat (consensus sequence QTEIkNDhi; upper case = fixed amino acid, lower case = variable amino acid) at its C-terminus, with the number of repeats ranging from 10 to 20 between different *P. falciparum* isolates (Figure 1a; Supplementary Table 1). PfCERLI2 shares homology (~20% amino acid identity) (Supplementary Figure 1) with the recently characterised protein PfCERLI1[11,12], with PfCERLI2 being the most similar protein to PfCERLI1 in the *P. falciparum* 3D7 proteome on PlasmoDB[13]. Notably, PfCERLI1 and PfCERLI2 both possess a C2 domain towards their N-terminus as well as a short but highly conserved motif we have termed PHIS, which has the consensus sequence PHIS[-]xxP ([-] = negatively charged) in *P. falciparum*. PfCERLI2 is highly conserved amongst *Laverania*, a subgenus that comprises *P. falciparum* and its closest ape-

infecting relatives (>90% amino acid identity with *Laverania* homologues), and shares approximately 65% amino acid identity amongst more distantly related *Plasmodium* spp. (Figure 1b) (Supplementary Figure 2). Notably, PfCERLI2 shares high similarity with its homologues over the first ~420 amino acids of its sequence, but this similarity decreases significantly at the *Laverania*-specific C-terminal repeat region.

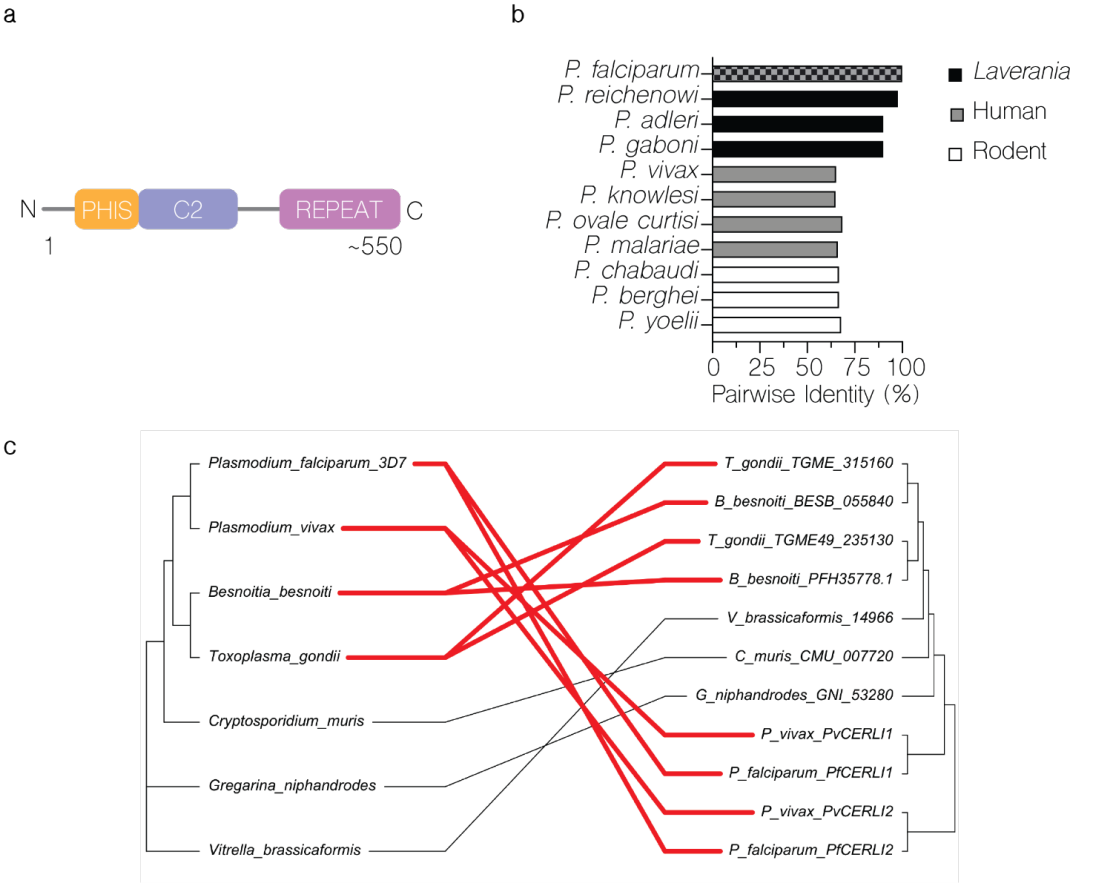

Figure 1: PfCERLI2 is conserved among Apicomplexa and may have evolved from an ancestral gene duplication.

(a) *PfCERLI2 is a protein of 579 amino acids in P. falciparum 3D7. Towards its N-terminus PfCERLI2 contains a motif with the consensus sequence PHIS[-]xxP we have termed PHIS, a C2 domain, and a decapeptide tandem repeat with the consensus sequence QTEIkNDhi at its C-terminus. Repeat number (10-20), and therefore PfCERLI2 amino acid length (559-659), is highly variable between P. falciparum isolates.* ***(b)*** *Amino acid sequence identity for Plasmodium spp. PfCERLI2 orthologues*

in Laverania, human-infecting, and rodent-infecting parasites was compared using multiple pairwise alignments. ***(c)*** *Tanglegram comparing general evolutionary relationships between selected Apicomplexa and Chromerids, as described in*[14] *(left), with phylogenetic tree constructed with PfCERLI1, PfCERLI2 and homologus sequences retrieved from EuPathDB using the unweighted pair group method with arithmetic mean (UPGMA) method (right). Branch length of UPGAM tree corresponds to amino acid substitutions per site. Taxa containing CERLI1 and CERLI2 homologues are joined by red edges, while taxa with a single CERLI are joined by black edges to visualise timing of ancestral gene duplication giving rise to CERLI2.*

All organisms that diverged from *Plasmodium* more recently than *Cryptosporidium* contain homologues of both *Pfcerli1* and *Pfcerli2*, while earlier diverging unicellular organisms, including the free-living alveolates *Gregarina niphandrodes* and Chromerid *Vitrella brassicaformis*, contain only a single identifiable homologue (Figure 1c) (Supplementary Figure 3); suggesting that *Pfcerli1* and *Pfcerli2* are paralogues that arose from an ancestral gene duplication event. As genomic DNA (14.6 %) and amino acid (22.9 %) sequence identities were low across Apicomplexa and Chromera, analysis of sequence conservation, outside of *Plasmodium*, was not able to identify the direct orthologues of either *Pfcerli1* or *Pfcerli2* outside the *Plasmodium* genus (Supplementary Figure 4a). Therefore, we compared the gene structure of *Pfcerli1* and *Pfcerli2*, along with homologous sequences in Apicomplexa and Chromerids (Supplementary Table 2) to identify the putative *cerli1* and *cerli2* orthologues across distantly related species. The comparison of *cerli1* and *cerli2* sequences across *Plasmodium spp.* indicated that *cerli1* orthologues have fewer introns and decreased exon length than the orthologues of *cerli2* (Supplementary Table 3). This gene structure pattern was also observed for homologues outside the *Plasmodium* genus, allowing for a classification of more divergent homologues as the direct orthologue of either *Pfcerli1* or *Pfcerli2.* Using this approach, we determined that the direct orthologue of *Pfcerli2* in *Toxoplasma gondii* is TGME49_315160 (TgRASP2), which was previously reported to be the direct orthologue of *Pfcerli1*[12]. Additionally, our classification suggests that the direct orthologue of *Pfcerli1* is TGME49_235130

(TgRASP1). As Apicomplexa and Chromerids that are distantly related to *P. falciparum* only possess a single homologue of *Pfcerli1* and *Pfcerli2*, we compared their gene structure to determine which gene is more similar to the conserved ancestral state and which one represents a more diverged duplicated copy. All *Cryptosporidium* spp. homologues have an intron number and exon length similar to the *cerli1* lineage, suggesting that *cerli1* represents the ancestral locus and *cerli2* the duplicated locus. There is no consistent trend in gene structure in more distantly related organisms (Gregarines or Chromerids), suggesting the gene structure may not have been conserved in more divergent organisms.

With our analysis supporting that *Pfcerli2* arose from a gene duplication event, we next assessed the selection pressure acting on the *Pfcerli1* and *Pfcerli2* sequences. To investigate this, we determined Ka/Ks ratios, which calculate the number of non-synonymous amino acid substitutions (Ka) relative to the number of synonymous substitutions (Ks). *Pfcerli1* and *Pfcerli2* across *Plasmodium* spp. had Ka/Ks of 0.091 and 0.29 respectively, indicating strong negative selection (favouring low sequence diversity), which is consistent with their essentiality for *P. falciparum*[11,12,15] and *P. berghei*[16] blood-stage survival. This negative selection in both lineages may be indicative of subfunctionalisation in Apicomplexa, where both paralogues have maintained a subset of the function of the ancestral gene.

Interestingly, homologues of PfCERLI2 within the *Plasmodium* genus no longer contain a Pleckstrin homology (PH) domain that is predicted for homologous sequences outside the *Plasmodium* genus (Supplementary Figure 5) and has been shown to be involved in rhoptry localisation and secretion for TgRASP2[12]. Analysis of predicted protein structures for PfCERLI1 and PfCERLI2 homologues outside the *Plasmodium* genus show that this PH domain is typically predicted to contain two sets of anti-parallel beta-sheets separated by a short alpha-helix, followed by a C-terminal helix (Supplementary Figure 6). By contrast, *Plasmodium* homologues of CERLI2 are predicted to have two beta-sheets in the region corresponding to the PH domain in CERLI2 of other species and PfCERLI1, but this region also has an expanded helix

and disordered region between the beta-sheets (Supplementary Figure 6). Additionally, PfCERLI2 is predicted to contain a shorter C-terminal helix (Supplementary Figure 6). The expansion between the beta-sheets is predicted to disrupt the interaction between them that is required for canonical PH domain formation. Therefore, although elements of the PH domain are predicted to remain (beta-sheets) structural predictions do not annotate a PH domain structure in this region and it is questionable whether this domain structure is functional in PfCERLI2.

While the overall sequence identity between PfCERLI1, PfCERLI2, and their homologues is low, all contain the highly conserved PHIS motif with the consensus sequence PHPSECxP (when comparing all apicomplexan/chromerid homologues; Supplementary Figure 4b) or PHIS[-]xxP (when comparing *P. falciparum* sequences; Supplementary Figure 7). Notably, the first proline is fully conserved across all analysed sequences, and the histidine residue is mutated only in *Gregarina niphandrodes*. A second proline lies at position 8 in all CERLI homologues in *Plasmodium* spp., while in all other apicomplexans outside *Plasmodium*, the second proline lies at position 3. Such high sequence conservation across highly divergent organisms suggests this motif is likely to be critical for the physiological function of PfCERLI1, PfCERLI2 and their homologues. Similar amino acid motifs exist in other *P. falciparum* proteins; including the ring-expressed surface antigens (RESA, RESA2, RESA3, and RESA-like), Iron superoxide dismutase (FeSoD) and ATP-dependent Clp protease proteolytic subunit (ClpR) (Supplementary Table 4; Supplementary Figure 7). Although the PHIS motif is a signature of PfCERLI1 and PfCERLI2, and their apicomplexan homologues, nothing is currently known about the function of this motif or whether it has a related role in the other *P. falciparum* PHIS-containing proteins.

PfCERLI2 contains a variable copy number decapeptide tandem repeat

All PfCERLI2 homologues in *Laverania* contain a C-terminal decapeptide tandem repeat, with the consensus sequence QTIEIkNDhi in *P. falciparum*, which is not present in any homologues outside the subgenus (Supplementary Table 1) [17]. The repeat number is variable both between *P. falciparum* isolates (e.g. 10 repeats in isolate

7G8 and 20 repeats in isolate Dd2), and between *Laverania* (9 repeats in *P. praefalciparum* and 4 repeats in *P. adleri*). It is not clear what the function of this repeat is, or what drives changes in its number. However, we noticed that *P. falciparum* has a higher number of repeats than other *Laverania*, with organisms more closely related to *P. falciparum* also displaying higher repeat numbers than those more distantly related (Supplementary Figure 8; Supplementary Table 1). The full sequence of *Pfcerli2* is under strong negative selection across *Laverania*, with a Ka/Ks ratio of 0.29. By contrast, the repeat region of *Pfcerli2* when comparing across *Laverania* has a Ka/Ks ratio of 1.43 indicating that positive selection (favouring sequence diversity) is occurring in the decapeptide repeat region of PfCERLI2 and Laveranian homologues.

PfCERLI2 is essential for blood-stage growth.

PfCERLI2 has previously been suggested to be essential by a saturation mutagenesis screen[15], and its homologue in *P. berghei* has also been shown to be essential for blood-stage growth[16]. To confirm this in *P. falciparum*, we targeted *Pfcerli2* by selection linked integration targeted gene disruption (SLI-TGD)[18]. Multiple attempts to knockout *Pfcerli2* failed confirming that *Pfcerli2* has an important role in blood-stage growth (Figure 2a). Next, we placed *Pfcerli2* under control of the glucosamine (GLCN) inducible *GlmS* ribozyme, whereby addition of GLCN leads to specific degradation of *Pfcerli2* mRNA (Figure 2 b&c). Additionally, we introduced a haemagglutinin (HA) tag onto the C-terminus of PfCERLI2, allowing detection using anti-HA antibodies. Using these PfCERLI2^{HAGlmS} parasites, we harvested parasites at either ring, trophozoite or schizont stages and probed for PfCERLI2 by Western blot (Figure 2d). Concordant with previously published transcriptomic data[19], PfCERLI2 was most highly expressed in schizonts. When PfCERLI2^{HAGlmS} parasites were treated from ring stages to schizonts with 2.5 mM GLCN, the expression of PfCERLI2 was reduced by 72% (± 3.8% SEM) relative to untreated controls (Figure 2e), showing that PfCERLI2 protein expression is tunable using the *GlmS* system.

To determine whether knockdown of PfCERLI2 altered parasite growth, we treated ring-stage PfCERLI2^{HAGlmS} and 3D7 WT parasites with increasing

concentrations of GLCN and measured trophozoite-stage parasitaemia by flow cytometry 72 hours later (Figure 2f). At 5 mM GLCN there was ~77% (± 5.1% SEM) decrease in the growth of PfCERLI2^{HAGlmS} parasites. However, at this high concentration of GLCN growth of 3D7 WT parasites was also affected. At a concentration of 2.5 mM GLCN, growth of PfCERLI2^{HAGlmS} parasites was inhibited by ~53% (± 6.0% SEM), with 3D7 WT parasites showing negligible off-target growth defects.

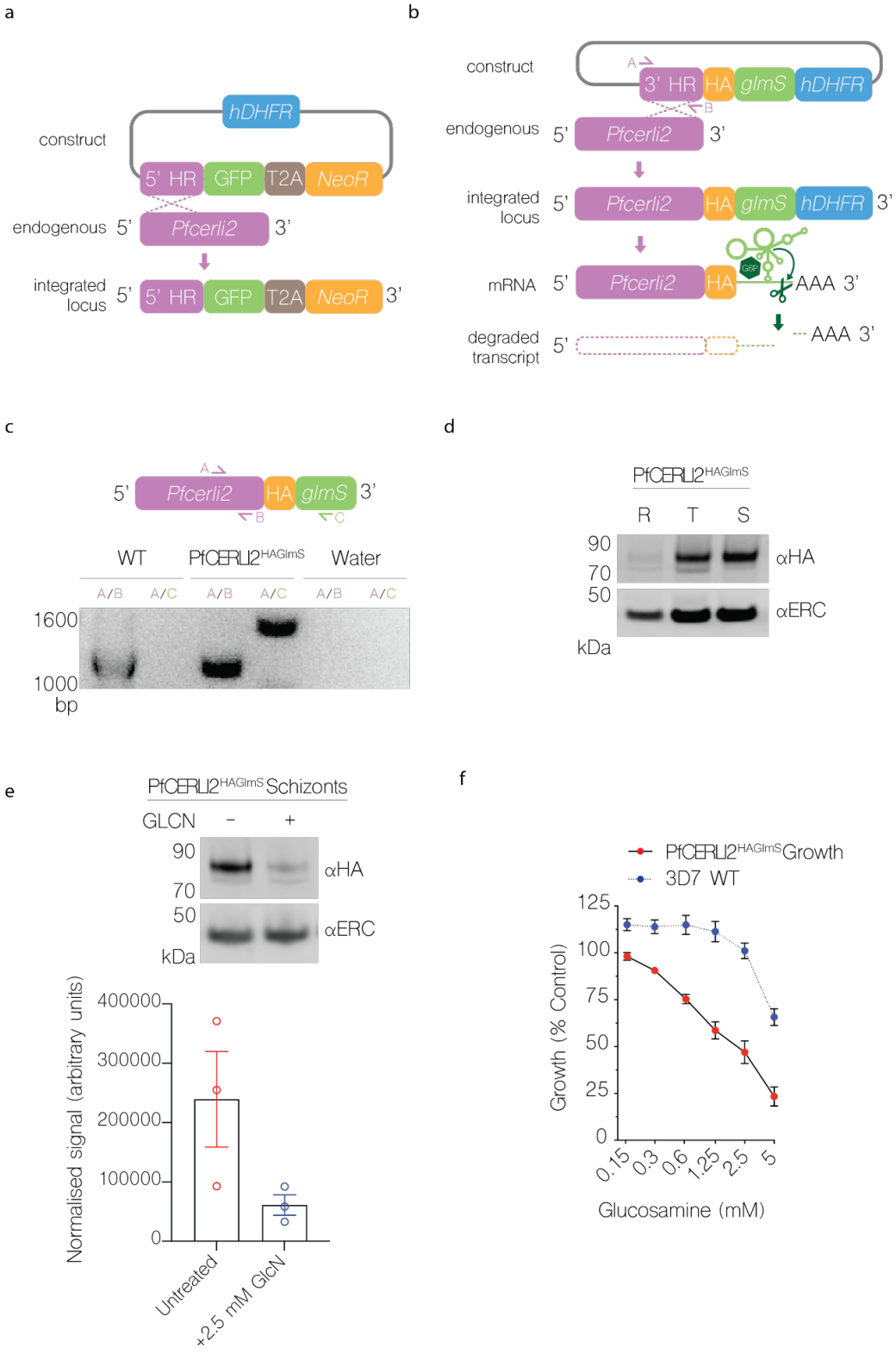

Figure 2: PfCERLI2 is essential for blood-stage growth.

(a) *Schematic representation of the selection linked integration targeted gene disruption (SLI-TGD) system used for the attempted gene knockout of Pfcerli2.* ***(b)*** *Schematic representation of the haemagglutinin (HA) tag, and GlmS ribozyme system used to identify and knockdown PfCERLI2. A plasmid that contained a 3' Pfcerli2 flank (2154bp-2912bp) with an HA-tag and GlmS ribyzome was transfected into 3D7 parasites by single crossover recombination. Following mRNA production, glucosamine-6-phosphate (G6P) binds to the GlmS ribozyme, leading to the cleavage of Pfcerli2 mRNA and subsequent protein knockdown.* ***(c)*** *To confirm integration of the Pfcerli2^{HAGlmS} plasmid, gDNA was harvested from transfected parasites. A Pfcerli2 specific forward primer A, which sits outside of the cloned 3' homology flank, with either a Pfcerli2 specific, B (WT), or GlmS specific, C (integrated), reverse primer was used to confirm WT DNA sequence or integration of the Pfcerli2^{HAGlmS} plasmid.* ***(d)*** *Western blot of ring, trophozoite, or schizont stage PfCERLI2^{HAGlmS} lysates probed with either anti-HA (PfCERLI2) or anti-ERC (loading control) antibodies. ERC is used given its uniform expression pattern throughout the blood stage lifecycle, and possesses comparable protein abundance to PfCERLI2. N=3 biological replicates.* ***(e)*** *Western blot of PfCERLI2^{HAGlmS} schizont lysates either GLCN treated (+) or untreated (-) and probed with anti-HA (PfCERLI2) normalised to ERC (loading control) antibodies. A graph quantifying the relative level of expression between treatments. N=3 biological replicates, error bars = SEM.* ***(f)*** *PfCERLI2^{HAGlmS} or 3D7 WT parasites were treated with increasing concentrations of GLCN for 72 hours, with the trophozoite-stage parasitaemia determined by flow cytometry. Growth is expressed as a percentage of an untreated media control. n=4, error bars = SEM. X-axis presented as a log 2 scale for viewing purposes.*

PfCERLI2 knockdown inhibits merozoite invasion

As PfCERLI2 was most highly expressed at schizont-stages, and its knockdown inhibited growth, we hypothesised that PfCERLI2 could be involved in schizont development, rupture, or merozoite invasion. To quantify invasion, we transfected PfCERLI2^{HAGlmS} parasites with a plasmid that expresses cytosolic GFP (PfCERLI2$^{HAGlmS/GFP}$), which allows reliable detection of newly invaded ring stages by

flow cytometry. Treating PfCERLI2$^{HAGlmS/GFP}$ parasites with increasing concentrations of GLCN from trophozoite-stages for 24 hours until early ring-stages the following cycle, we saw that PfCERLI2 knockdown inhibited invasion in a dose-dependent manner (Figure 3a). The extent of invasion inhibition caused by PfCERLI2 knockdown was lower than growth inhibition over 72 hours, however, it is likely that this difference is caused by the shorter GLCN treatment time used for assessing inhibition of invasion.

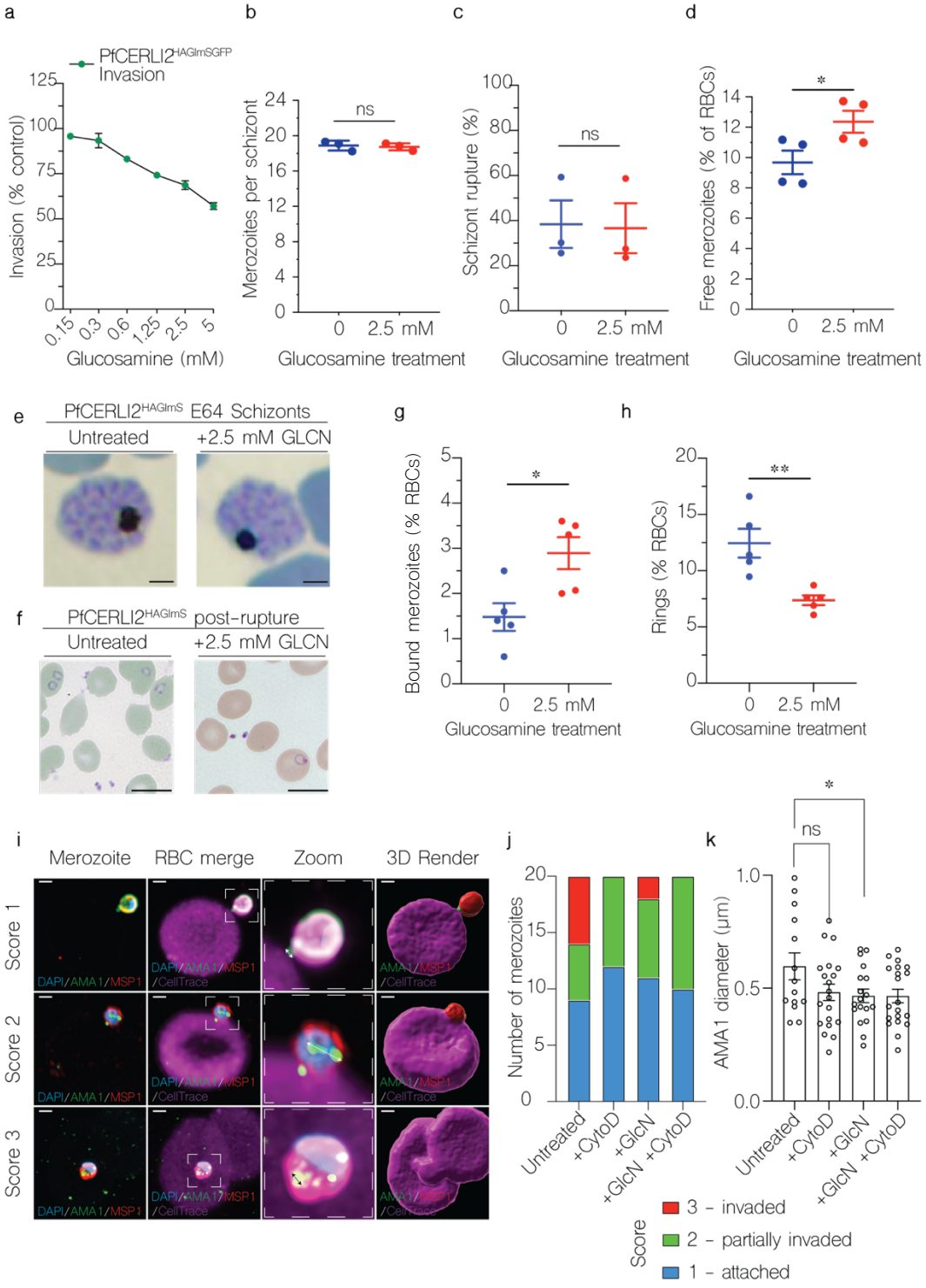

Figure 3: PfCERLI2 knockdown inhibits merozoite invasion.

(a) *GFP-expressing PfCERLI2$^{HAGlmS/GFP}$ parasites were treated with a range of concentrations of GLCN from early trophozoite stages until early rings the following cycle (~24 hours), with invasion assessed by flow cytometry as the number of newly*

invaded rings expressed as a percentage of an untreated media control. n=4, error bars = SEM. X-axis presented as log 2 scale for viewing purposes. ***(b)*** *PfCERLI2^{HAGlmS} parasites were either treated with GLCN from ring-stage to schizont-stage or left untreated. Early schizonts were treated with the egress inhibitor E64 for ~5 hours. Following treatment, cultures were smeared and the number of merozoites per schizont was determined by blinded microscopy analysis of Giemsa-stained blood smears. Each data point represents the mean number of merozoites per schizont from 20 schizonts. n=3, error bars = SEM, ns=p>0.05 by unpaired t-test.* ***(c)*** *Percentage of schizonts that ruptured over a 6-hour window in either the presence or absence of GLCN, as determined by flow cytometry. n=3, error bars = SEM, ns=p>0.05 by unpaired t-test.* ***(d)*** *During the invasion assay described in 3a, the number of free merozoites was also quantified by flow cytometry, with results presented as % of total RBCs. n=4, error bars = SEM, ns = p > 0.05, * = p = 0.0153 by unpaired t-test.* ***(e)*** *PfCERLI2^{HAGlmS} schizonts, either in the presence or absence of GLCN, were matured in the presence of the schizont rupture inhibitor E64 before being fixed, Giemsa-stained and imaged by light microscopy. Scale bar = 2 µm. PfCERLI2^{HAGlmS} parasites were treated with 2.5 mM GLCN or left untreated, with Giemsa smears made following schizont rupture* ***(f)*** *and the number of merozoites bound to RBCs* ***(g)*** *and newly-invaded rings* ***(h)*** *quantified, Scale bar = 5 µm, n=5, error bars =SEM, ns = p > 0.05, * = p = 0.0166, ** = p = 0.0054 by unpaired t-test.* ***(i)*** *Representative IFAs of merozoites, across three defined invasion stages scored 1-3, stained with DAPI, anti-AMA1 and anti-MSP1-19 antibodies invading CellTrace-stained RBCs. Scale bar = 1 µm.* ***(j)*** *Number of merozoites blind-assessed for each invasion score. n = 20 merozoites in a single biological replicate.* ***(k)*** *AMA1 signal diameter was measured under blinded assessment – measurements were taken as shown on the double arrows in (i). N = 20 merozoites in a single biological replicate, error bars = SEM, ns = p>0.05 * = p = 0.0446 by unpaired t-test.*

To determine if this invasion inhibition was specifically due to a defect in merozoite development, PfCERLI2^{HAGlmS} schizonts either GLCN treated or untreated, were matured in the presence of the schizont egress inhibitor E64. Knockdown of

PfCERLI2 did not result in a change in the morphological development of trophozoites (Supplementary Figure 10 a&b), nor in the number of fully formed merozoites per schizont (Figure 3b). The merozoites within the schizonts appeared morphologically normal (Figure 3e). To determine whether PfCERLI2 knockdown altered the rate of schizont rupture, the ability of both GLCN treated and untreated PfCERLI2^{HAGlmS} synchronised schizonts to rupture over a period of 6 hours was quantified. PfCERLI2 knockdown had no influence on the rate of schizont rupture (Figure 3c), suggesting knockdown has no influence on schizont development or egress. To test if PfCERLI2 knockdown directly inhibited the invasion of merozoites, we measured the number of free merozoites in the culture supernatant following invasion in both GLCN treated and untreated PfCERLI2$^{HAGlmS/GFP}$ parasites. PfCERLI2 knockdown lead to an increase in the number of free merozoites, suggesting that a direct defect in the ability of merozoites to invade is the cause of PfCERLI2 knockdown-mediated growth inhibition.

The flow cytometry-based assay does not allow discrimination between free merozoites inhibited prior to or after tight-junction formation. Therefore, we analysed Giemsa-stained thin smears of GLCN treated and untreated PfCERLI2^{HAGlmS} ring-stage parasites and quantified the number of bound merozoites following schizont rupture (Figure 3 f&g). PfCERLI2 knockdown led to a 49% (± 12% SEM) increase in the percentage of merozoites bound to RBCs, suggesting that knockdown inhibits invasion following tight-junction formation. Newly invaded ring-stage parasites (Figure 3h) were also quantified, with GLCN treatment leading to a 41% (± 5.9% SEM) reduction in newly invaded ring stages.

Although Giemsa smears demonstrated an increased in attached merozoites that had failed to invade with PfCERLI2 knockdown relative to control, they cannot accurately show whether the tight junction has formed. Therefore, we used a cytochalasin D-based strategy in fixed cells and analysed invading merozoites by Airyscan super-resolution microscopy (Figure 3i-k). Viable GLCN treated and untreated PfCERLI2^{HAGlmS} merozoites were purified and permitted to invade RBCs stained with CellTrace™ Far Red (Figure 3i), and treated with or without cytochalasin

D, a potent inhibitor of actin polymerisation which prevents completion of invasion[20]. CellTrace has been reported to not affect invasion and is a suitable stain to visualise the RBC[21]. Invasion scoring was performed and demonstrated that a large relative proportion of GLCN treated parasites were unable to fully invade the RBC (Figure 3j), consistent with earlier results. Following from our Giemsa-based observations, GLCN merozoites appeared to be able to successfully reorientate their apical tip to the RBC surface and thus we speculate that PfCERLI2 knockdown may inhibit invasion downstream of this step, for example at tight junction formation. To quantify this observation, the diameter of AMA1 staining was measured and used as a proxy to determine progression through the tight junction ring – where a larger ring indicates successful progression. However, as the tight junction ring ratchets itself behind the merozoite at the completion of invasion, potentially becoming smaller, we have excluded data points from merozoites with an invasion score = 3 (fully invaded) from all samples for this analysis (full data in Supplementary Figure 10c). Using this analysis, we found that PfCERLI2 knockdown parasites have a significantly smaller AMA1 diameter compared to untreated parasites (Figure 3k). As a control, cytochalasin D was used to inhibit the actin-myosin motor – the stage of invasion immediately after tight junction formation[4]. Though the AMA1 diameter in cytochalasin D-treated control parasites in comparison were not significantly different compared to untreated parasites, a similar data spread was observed when compared to knockdown parasites. Put together, these data indicate that GLCN inducible PfCERLI2 knockdown inhibits invasion at, or prior to, the formation of the tight junction.

PfCERLI2 localises to the rhoptry bulb

The homology to PfCERLI1 as well as its functional implications in RBC invasion suggested PfCERLI2 may have a rhoptry localisation. In our numerous attempts to localise PfCERLI2, we experienced that conventional antibody staining methods could not reliably visualise any foci directed to its HA-tag outside of background signal. After failing to obtain a consistent PfCERLI2 localisation, likely due to the low peak expression level of *Pfcerli2*[19], we investigated the cellular distribution of PfCERLI2 using a high affinity anti-HA biotin system to significantly

bolster the signal[22]. Despite its peak transcription late in schizont development, we observed that PfCERLI2 foci were brightest in early schizonts (~44 hrs post invasion) (Figure 4a), but largely absent in fully mature E64-treated schizonts (~48 hrs post invasion) (Supplementary Figure 11). Harvesting early schizonts (~44hr post invasion), we analysed subcellular organisation of CERLI2 by comparing it to known markers of the rhoptry bulb (RAP1), rhoptry neck (RON4), micronemes (AMA1), and merozoite surface (MSP1-19) (Figure 4 a&b). In these parasites, PfCERLI2 showed the strongest colocalisation with the rhoptry bulb marker RAP1, suggesting PfCERLI2 likely localises to the rhoptry bulb (Figure 4a&b). For a more detailed view of PfCERLI2 and its association with the rhoptry, we imaged double labelled parasites in three-dimensions using the super-resolution microscopy platform Airyscan, which showed that PfCERLI2 forms the donut shape characteristic of membrane associated rhoptry bulb proteins (Figure 4c).

Repeat immunofluorescence experiments consistently showed that mature schizonts had little PfCERLI2 staining. Parallel western blots, however, showed no significant decrease in PfCERLI2 detection between early and late schizonts (Supplementary Figure 12). Given the lack of change in detectability by Western blot, it is possible that the HA epitope is masked and therefore undetectable using anti-HA antibodies in microscopy with mature schizont stage parasites.

PfCERLI2 is peripherally associated with the cytosolic face of the rhoptry bulb membrane.

The absence of a signal peptide suggested that PfCERLI2 is a peripheral membrane protein that localises to the rhoptries but is exposed to the merozoite cytosol. To test this, we subjected PfCERLI2^{HAGlmS} schizont lysates to a proteinase protection assay. Following lysis with saponin and digitonin, which lyse the RBC membrane, PVM, and PPM, but not organellar membranes, PfCERLI2 was sensitive to proteinase K degradation (Figure 5a); suggesting it is exposed to the cytosol. To assess membrane association of PfCERLI2, we performed a solubility assay using lysates from PfCERLI2^{HAGlmS} schizonts (Figure 5b), whereby proteins are solubilised into cytosolic

(hypotonic lysis), peripheral membrane (carbonate treatment), integral membrane (triton-x-100 soluble), or covalently lipid-linked (triton-x-100 insoluble) fractions. PfCERLI2 predominantly solubilised in the carbonate fraction, a distinctive feature of peripheral membrane proteins[23]. Combining the localisation analyses with the proteinase protection and solubility assays suggest that PfCERLI2 localises to the cytosolic face of the rhoptry bulb membrane, a subcellular localisation akin to that reported for PfCERLI1[11].

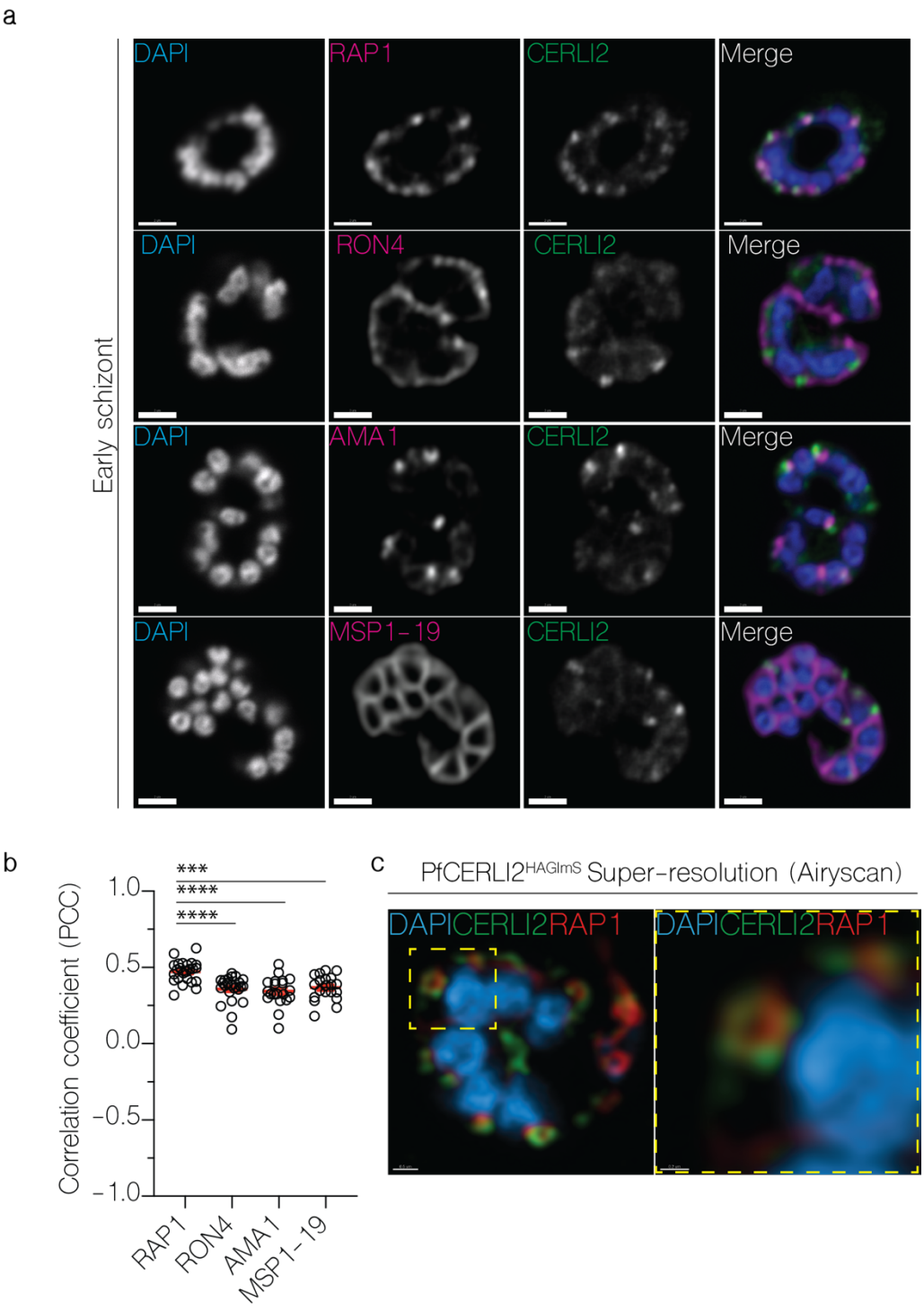

Figure 4: PfCERLI2 localises to the rhoptry bulb.

(a) *2D Confocal immunofluorescence microscopy of early PfCERLI2^{HAGlmS} schizonts stained with DAPI (nucleus) and anti-HA (PfCERLI2) antibodies, along with*

antibodies to either RAP1 (rhoptry bulb), RON4 (rhoptry neck), AMA1 (micronemes), or MSP1-19 (merozoite surface). Scale bar = 2 µm ***(b)*** *Quantification of colocalisation between PfCERLI2 and the merozoite organelle markers RAP1, RON4, AMA1 and MSP1-19. Colocalisation quantified as Pearson's correlation coefficient (PCC) when the PfCERLI2 signal was defined as the region of interest. n= 3 biological replicates, 6 schizonts per replicate. Error bars = SEM, *** = p<0.001, **** = p<0.0001.* ***(c)*** *Representative maximum-intensity projection of PfCERLI2^{HAGlmS} parasites stained with antibodies to RAP1 (rhoptry bulb) and HA (CERLI2) and imaged using the super-resolution microscopy platform Airyscan. Yellow box indicates the zoom area for the right-hand panel.*

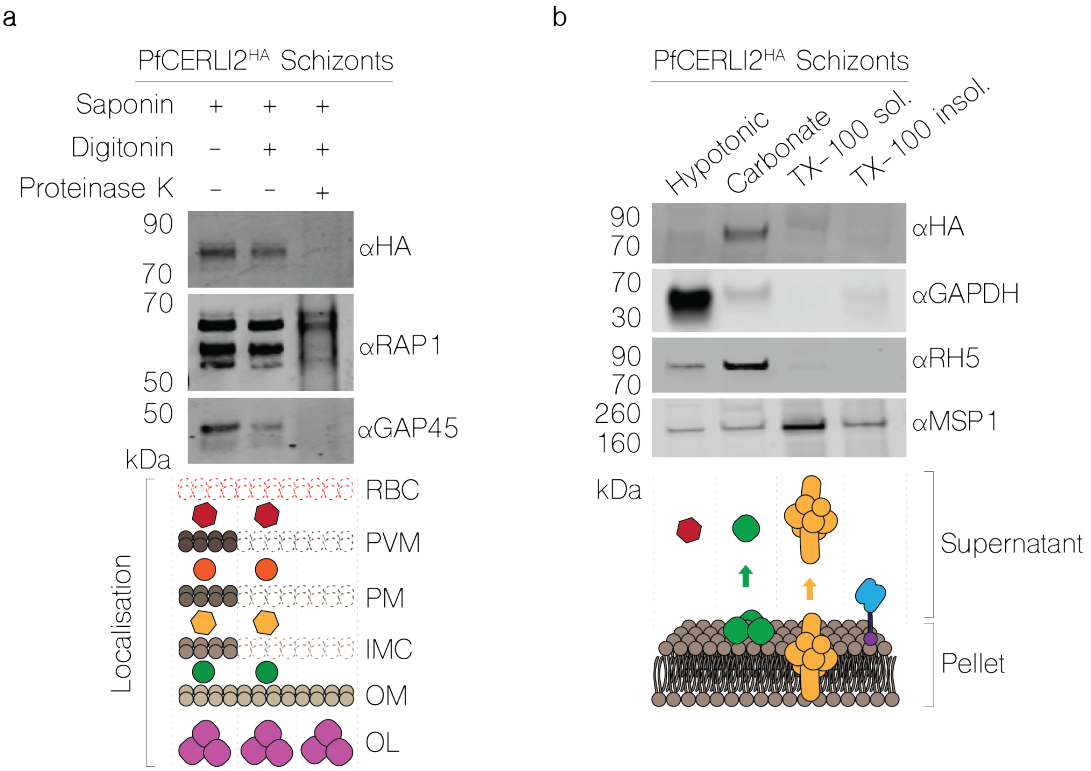

Figure 5: PfCERLI2 is peripherally associated with the cytosolic face of the rhoptry bulb membrane.

(a) *PfCERLI2^{HAGlmS} Schizont lysates were treated with either saponin alone, saponin and digitonin, or saponin, digitonin, and proteinase K. Saponin lyses the RBC membrane and PVM, while digitonin lyses the parasite plasma membrane but leaves the membrane of internal organelles intact. Treated lysates were then probed with anti-HA (PfCERLI2), anti-RAP1 (rhoptry bulb lumen), or anti-GAP45 (inner-membrane complex, exposed to cytosol) antibodies with RAP1 and GAP45 serving as negative and positive controls, respectively, for proteinase K digestion. The slight degradation observed for RAP1 is due to partial non-specific lysis of parasite material. Images representative of 3 independent experiments. RBC = RBC membrane, PVM = PV membrane, PM = parasite plasma membrane, IMC = inner-membrane complex, OM= organellar membrane, OL = organelle lumen.* ***(b)*** *PfCERLI2^{HAGlmS} schizont lysates were subjected to differential lysis and solubilisation to determine the membrane solubility of PfCERLI2. Lysates were first hypotonically lysed, before being treated sequentially with sodium carbonate and triton-x-100. The supernatant was collected following each treatment, along with a final triton-x-100 soluble fraction. Each*

fraction was then probed with anti-HA (PfCERLI2), anti-GAPDH (cytosolic), anti-RH5 (peripheral) and anti-MSP1 (GPI-anchored) antibodies. Images representative of 3 independent experiments.

PfCERLI2 knockdown inhibits rhoptry bulb antigen processing but not secretion of rhoptry neck proteins

PfCERLI1 has previously been shown to be involved with rhoptry secretion[11,12], and given the similarities between PfCERLI1 and PfCERLI2 we sought to determine whether PfCERLI2 was also involved in rhoptry secretion. To test the effect of PfCERLI2 knockdown on rhoptry secretion, ring-stage PfCERLI2^{HAGlmS} parasites were treated with 2.5 mM GLCN or left untreated. The RBCs of each culture had been treated with trypsin, chymotrypsin, and neuraminidase to prevent reinvasion. Parasites were cultured until schizont rupture when the supernatant was collected (containing secreted proteins) and a parasite lysate (containing merozoites that had failed to invade) were prepared for Western blot (Figure 6a). As expected, there was no change in secretion of the micronemal antigen erythrocyte binding antigen 175 (EBA-175) with knockdown of the rhoptry associated PfCERLI2 (Figure 6b). There was also no noticeable defect in the secretion of the rhoptry neck antigens reticulocyte binding homologue 4 (RH4) and rhoptry neck protein 4 (RON4). These data indicate that PfCERLI2 knockdown does not block secretion of rhoptry neck antigens in merozoites that fail to invade enzyme treated RBCs.

Parasite lysates from the secretion assay, containing free merozoites, were also probed with antibodies to the rhoptry bulb antigen rhoptry associated protein 1 (RAP1) (Figure 6a). RAP1 has previously been shown to be processed by Plasmepsin IX and subtilisin-like protease 1 (SUB1) from a predicted 84 kDa precursor in intact schizonts into a 67 kDa mature product in free merozoites[24-27]. Diminished PfCERLI2 expression leads to the inhibition of RAP1 processing, corresponding to an accumulation of the unprocessed form of the protein (Figure 6c). When PfCERLI2^{HAGlmS} schizonts either with, or without 2.5 mM GLCN were arrested prior to parasitophorous vacuole membrane (PVM) rupture with the protein kinase G inhibitor compound 1 (C1) [28] and

probed for RAP1 (Supplementary Figure 13a), both 2.5 mM GLCN treated and untreated cultures showed mostly unprocessed RAP1, supporting that the defect in RAP1 processing occurs only after schizont rupture and merozoite release (Supplementary Figure 13b). Collectively, this suggests that knockdown of PfCERLI2 interfers with the processing of RAP1 between PVM rupture and merozoite invasion, a phenotype previously demonstrated for PfCERLI1 knockdown[11].

PfCERLI2 knockdown alters rhoptry morphology

While PfCERLI2 knockdown schizonts showed no gross morphological defects, we aimed to determine if PfCERLI2 knockdown altered the morphology or biogenesis of the rhoptries. We matured GLCN treated or untreated 3D7 WT and PfCERLI2^{HAGlmS} schizonts in the presence of C1 and subsequently fixed and imaged these mature schizonts using thin-section transmission electron microscopy (TEM) (Figure 6d). PfCERLI2^{HAGlmS} schizonts that had not been treated with GLCN were morphologically indistinguishable to both GLCN treated and untreated 3D7 WT parasites. By contrast, GLCN treated PfCERLI2^{HAGlmS} parasites appeared to contain noticeably elongated rhoptry necks. We measured rhoptry length in randomly selected sections (38 untreated, 33 GLCN treated) and the measured rhoptry lengths were on average ~90 nm (± 3.4% SEM) longer in GLCN treated PfCERLI2^{HAGlmS} parasites than those of untreated controls (Figure 6e).

Dimensional analysis of organelles is partially compromised in thin section TEM, as XY measurements of an organelle are influenced by differences in sectioning. To overcome this, we performed serial block face scanning electron microscopy (SBF-SEM) array tomography of both GLCN treated and untreated PfCERLI2^{HAGlmS} schizonts (Figure 7a-f) to analyse changes in rhoptry morphology. Rhoptries of GLCN treated PfCERLI2^{HAGlmS} parasites (n = 100) were on average 130 nm (± 10 nm SEM) (Figure 7g) longer than rhoptries from untreated parasites (n = 100) representing a 24.17% rhoptry lengthening following PfCERLI2 knockdown. Additionally, rhoptries of GLCN treated PfCERLI2^{HAGlmS} parasites exhibited similar increases in surface area (Figure 7h) and volume (Supplementary Figure 14a) but no change in surface area to

volume ratio (Supplementary Figure 14b). By contrast to their lengthening, GLCN treated PfCERLI2^{HAGlmS} parasites showed a small decrease in rhoptry width (Supplementary Figure 14c) by an average of 12 nm (± 5.5 nm SEM), leading to overall longer and narrower rhoptries following PfCERLI2 knockdown (Supplementary Figure 14d).

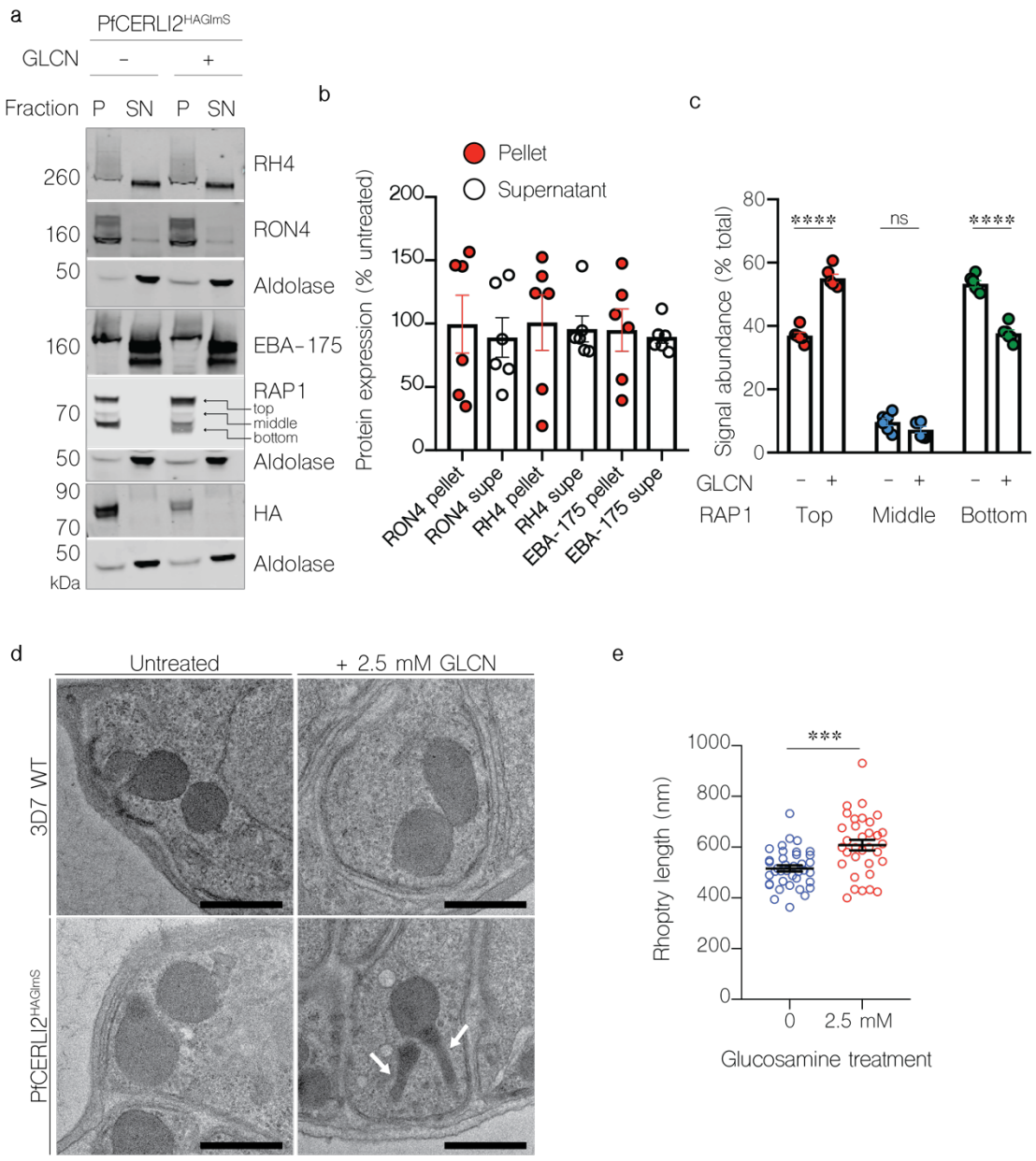

Figure 6: Knockdown of PfCERLI2 inhibits rhoptry antigen processing, but not secretion, and is associated with rhoptry malformation.

(a) *PfCERLI2^{HAGlmS} ring-stage parasites were GLCN treated (+) or left untreated (-), before enzyme treatment of RBCs to prevent reinvasion. Lysates (P) and culture supernatants (SN) were harvested following schizont rupture and probed with anti-RH4, anti-RON4 (rhoptry neck), anti-EBA-175 (microneme), anti-HA (PfCERLI2), anti-RAP1 (rhoptry bulb), or anti-aldolase (loading control) antibodies. Representative blots of 5 biological replicates shown.* ***(b)*** *Western blots were normalised to the loading control, aldolase, and quantified, with results displayed as protein expression in GLCN treated sample as a percentage of the untreated signal. Aldolase is used as a loading control as its abundance is not affected by glucosamine treatment, for both supernatant and pellet fractions. n=5 biological replicates.* ***(c)*** *Quantification of individual band intensities, as a percentage of the total signal, from RAP1 signals using the parasite lysates from the secretion assay. n=5 biological replicates. ns= p>0.05, **** = p<0.0001 by two-way ANOVA* ***(d)*** *Transmission electron microscopy of C1 schizont arrested PfCERLI2 and 3D7 WT parasites, either in the presence or absence of GLCN. Representative images from 3 biological replicates. Rhoptries appear as the dark dual clubs, with elongated necks indicated by arrows. Scale bar = 500 nm* ***(e)*** *Quantification of rhoptry length from PfCERLI2^{HAGlmS} TEM images. n=3 biological replicates. *** = p<0.001. All error bars = SEM.*

To further confirm the rhoptry morphological changes we observed by electron microscopy, we performed super-resolution (Airyscan) microscopy on either untreated or 2.5 mM GLCN treated PfCERLI2^{HAGlmS} parasites, probed with rhoptry bulb and neck markers RAP1 and RON4. We then measured the distance between the basal end of the nucleus and the centre of the RAP1 or RON4 (Supplementary Figure 15) foci, determining the average distance between nucleus and rhoptry. In GLCN treated parasites, we consistently observed a shorter distance between the nucleus and both RAP1 (Figure 7i) and RON4 (Figure 7j) foci (Supplementary Figure 16). This closer proximity of rhoptry markers to the nucleus supports the observation of rhoptry lengthening following PfCERLI2 knockdown.

To determine if distribution of these rhoptry markers changed following PfCERLI2 knockdown, we also quantified the area, volume, and sphericity of RAP1 and RON4 foci in both untreated and 2.5 mM GLCN treated PfCERLI2^{HAGlmS} parasites (Supplementary Figure 15). Consistent with the observation of an elongated rhoptry neck following PfCERLI2 knockdown, RON4 foci of GLCN treated parasites displayed a much larger surface area (Supplementary Figure 16a), larger volume (Supplementary Figure 16b) and were less spherical (Supplementary Figure 16c). Additionally, RAP1 foci in 2.5 mM GLCN treated parasites displayed a lower surface area and volume (Supplementary Figure 16d&e), although the magnitude of this change was small, but no change in sphericity (Supplementary Figure 16f). To determine if these minor changes in RAP1 foci shape following PfCERLI2 knockdown were indicative of a change to the size of the rhoptry bulb, RAP1 foci diameter was measured; but no change in rhoptry bulb diameter was observed in GLCN treated parasites (Supplementary Figure 16g). Thus, PfCERLI2 knockdown alters rhoptry morphology and is associated with incomplete processing of the rhoptry bulb protein RAP1, suggesting that PfCERLI2 plays an important role in normal rhoptry physiology.

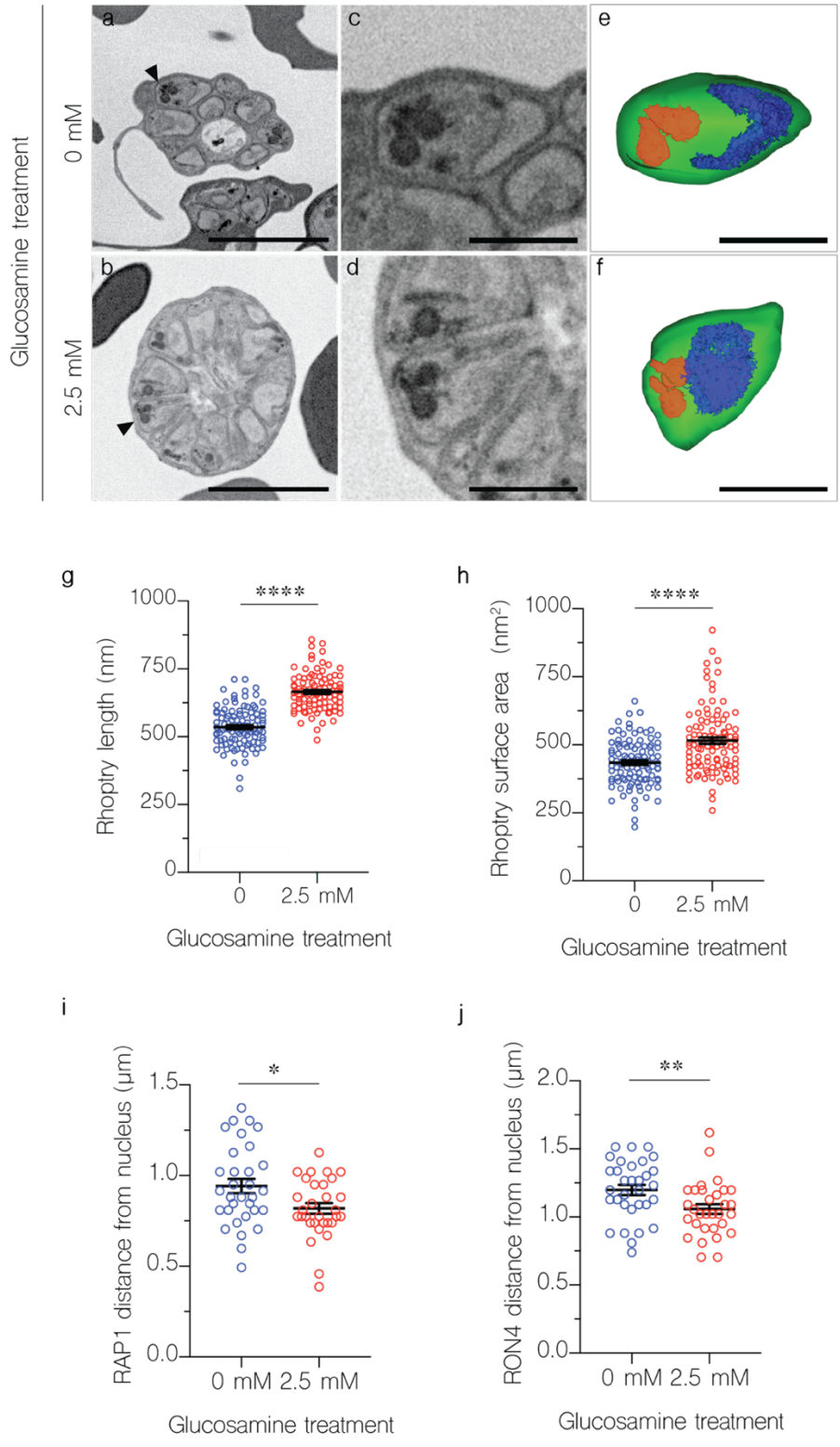

Figure 7: Knockdown of PfCERLI2 alters rhoptry length and positioning.

PfCERLI2^{HAGlmS} schizonts were matured in the presence of E64 and imaged using serial block face scanning electron microscopy (SBF-SEM) array tomography.

*Inverted backscattered images of untreated **(a)** and GLCN treated **(b)** PfCERLI2^{HAGlmS} schizonts. **(c&d)** Higher magnification images revealing individual merozoites and associated rhoptry pairs indicated by black arrow heads in a & b. **(e&f)** 3D renderings corresponding to the images in c & d. Colour legend: Merozoite plasma membrane, green; nucleus, blue; rhoptries, red. Scale bars: a & b = 4 µm; c-f = 1 µm. Using SBF-SEM array tomography, 100 rhoptries for each treatment were were analysed to determine their length **(g)** and surface area **(h)**. PfCERLI2^{HAGlmS} schizonts were matured in the presence of E64, stained with antibodies against RAP1 (rhoptry bulb) and RON4 (rhoptry neck), and imaged by Airyscan super-resolution microscopy. The fluorescence intensity from maximum-intensity projections of RAP1 **(i)** and RON4 **(j)** signals were then measured from the basal end of the nucleus. 32 merozoites for untreated and 31 merozoites for 2.5 mM GLCN treated were measured from a total of 12 schizont images across three biological replicates. Representative images corresponding to this data in Supplementary Figure 15. Error bars = SEM. * = p = 0.0152, ** = p = 0.0098, **** = p<0.0001 by unpaired t-test.*

Proximity dependent biotin interaction studies fail to show an interaction between PfCERLI1 and PfCERLI2

Given that both PfCERLI1 and PfCERLI2 share a localisation on the cytosolic face of the rhoptry bulb membrane and exhibit several similar knockdown phenotypes, we sought to determine whether the two proteins interacted as a complex in this niche. To assay for an interaction, we utilised dimerization induced quantitative proximity-dependent biotin identification (DiQ-BioID), a recently developed method in the field (Figure 8a) [29], and generated transgenic parasite lines, *Pfcerli1*$^{DiQ\text{-}BioID}$ and *Pfcerli2*$^{DiQ\text{-}BioID}$, which each separately express a bait PfCERLI1 and PfCERLI2 tagged with an FK binding protein (FKBP) and GFP. These lines are then co-transfected with an episomally-expressed BirA biotinylator ligase fused to an FKBP rapamycin-binding protein domain (FRB) and mCherry (Supplementary Figure 17a). Integration or episomal maintenance of these constructs were confirmed by PCR (Supplementary 17b).

Upon the addition of rapalog, the bait and biotinylator are able to dimerise, and the system can then be validated by live fluorescence of colocalising GFP/mCherry foci (Figure 8b). BirA, in the presence of excess biotin, then proceeds to biotinylate proteins in close proximity to the FKBP tagged bait protein, which we verified in fixed cell IFA using a streptavidin-conjugated fluorophore signal colocalising with RAP1 (Figure 8c). To prepare samples for proteomics, 36 hour-old parasites were double-treated with rapalog and biotin for 8 hours, including 4 hours on E64, before being processed for streptavidin-based pulldown and analysis by mass spectrometry.

To minimise the discovery of false positives from non-specific biotinylation, hits were first normalised against samples without rapalog treatment and then to a BirA-control line that has no FKBP tagged bait protein. A representative western blot for the extent of biotinylation between test and control samples are included in Supplementary Figure 18. In order to identify proteins that were reliably enriched, we only considered hits which were identified with at least 2 peptides with an overall peptide coverage of 10% or more across the library for all biological replicates. Applying these criteria generated an interactome of 23 proteins for PfCERLI1 (Figure 8d), and 26 proteins for PfCERLI2 (Figure 8e), which included the bait proteins themselves. PfCERLI2 was not identified as an interactor for PfCERLI1 and vice versa. Nevertheless, several rhoptry and schizont-expressed proteins were identified for both data sets to highlight the target specificity of DiQ-BioID. Of greatest interest includes RON11, ROP14 and the cAMP-dependent catalytic subunit of protein kinase A (PKAc) as potential interactors of PfCERLI1. Likewise, PfCERLI2 appears to interact with ROP14. Both lists display several uncharacterised proteins of unknown function that have peak expression at schizogony. The reproducibility between biological replicates was quantified using a linear correlation between the intensity values for the proteins identified in the interactome (Supplementary Figure 19).

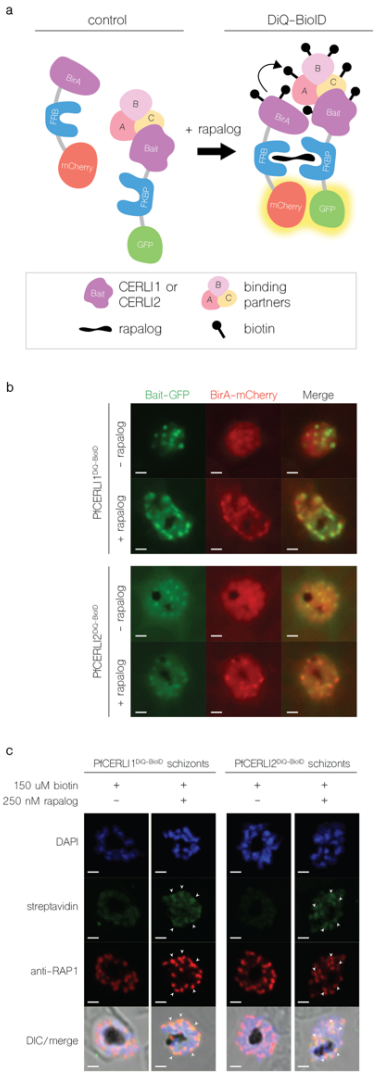

d

Accession number	PlasmoDB annotation	log2 average intensity	p-value*
PF3D7_1229300	conserved Plasmodium protein, unknown function	14.82686821	0.0294
PF3D7_0218200	SUZ domain-containing protein, putative	14.56513124	0.3585
PF3D7_0210600	CERLI1	14.52197456	0.0634
PF3D7_1012400	hypoxanthine-guanine phosphoribosyltransferase	13.80922149	0.0809
PF3D7_1133200	conserved Plasmodium protein, unknown function	13.75648127	0.2935
PF3D7_0517300	serine/arginine-rich splicing factor 1	13.68111869	0.0777
PF3D7_1407800	plasmepsin IV	13.31457758	0.0283
PF3D7_1463900	RON11	12.88910312	0.2547
PF3D7_0613300	rhoptry protein ROP14	12.75589904	0.0682
PF3D7_1359600	conserved Plasmodium protein, unknown function	12.7470907	0.0858
PF3D7_1208900	protein phosphatase PPM11, putative	12.66831417	0.1035
PF3D7_1019600	conserved Plasmodium protein, unknown function	12.28806291	0.0391
PF3D7_0519500	CCR4 domain-containing protein 1	12.0376777	0.0397
PF3D7_0730500	Plasmodium protein, unknown function	11.93831814	0.1004
PF3D7_1004400	RNA-binding protein, putative	11.91242495	0.0972
PF3D7_0310900	conserved Plasmodium protein, unknown function	11.76913202	0.0356
PF3D7_0716300	conserved Plasmodium protein, unknown function	11.75259557	0.0120
PF3D7_0934800	cAMP-dependent protein kinase catalytic subunit	11.72610063	0.0298
PF3D7_0302100	serine/threonine protein kinase	11.66306304	0.0163
PF3D7_1325900	conserved Plasmodium protein, unknown function	11.56915925	0.0352
PF3D7_1432900	SF-assemblin, putative	11.52130009	0.0832
PF3D7_1206300	conserved Plasmodium protein, unknown function	11.29526844	0.0009
PF3D7_1230200	vacuolar transporter chaperone	10.96498553	0.0000

e

Accession number	PlasmoDB annotation	log2 average intensity	p-value*
PF3D7_1138500	protein phosphatase PPM2	15.80786023	0.0020
PF3D7_0915400	ATP-dependent 6-phosphofructokinase	14.80140485	0.0001
PF3D7_0818200	14-3-3 protein	14.80113302	0.0032
PF3D7_0904800	replication protein A1, small fragment	14.79501828	0.0041
PF3D7_1426000	60S ribosomal protein L21	14.56332093	0.0479
PF3D7_0405200	CERLI2	14.40918375	0.0451
PF3D7_1016300	GBP130 protein	14.31198884	0.0119
PF3D7_0524000	karyopherin beta	14.23812028	0.0001
PF3D7_1239800	conserved Plasmodium protein, unknown function	13.96483209	0.0000
PF3D7_1018200	serine/threonine protein phosphatase 8, putative	13.75033765	0.0015
PF3D7_1206200	eukaryotic translation initiation factor 3 subunit C, putative	13.73307668	0.4449
PF3D7_1311900	V-type proton ATPase catalytic subunit A	13.24107114	0.1102
PF3D7_1406800	glideosome associated protein with multiple membrane spans 3	13.0784296	0.2058
PF3D7_1407100	rRNA 2'-O-methyltransferase fibrillarin, putative	13.07357315	0.2897
PF3D7_0607600	spindle assembly abnormal protein 6, putative	12.76712051	0.0015
PF3D7_0613300	rhoptry protein ROP14	12.66361043	0.2367
PF3D7_1025000	Eps15-like protein	12.58681299	0.0110
PF3D7_0627800	acetyl-CoA synthetase, putative	12.35378197	0.0010
PF3D7_1027700	centrin-3	12.22832579	0.0355
PF3D7_1303800	conserved Plasmodium protein, unknown function	11.64892929	0.1241
PF3D7_0218000	replication factor C subunit 2, putative	11.56293115	0.0835
PF3D7_1237700	conserved protein, unknown function	11.51724178	0.0577

Figure 8: DiQ-BioID of PfCERLI1 and PfCERLI2 reveals their protein interactome. *(a) A schematic of the DiQ-BioID system under control and test conditions. (b)* *Pfcerli1*$^{DiQ\text{-}BioID}$ and Pfcerli2^{DiQBioID} parasites were treated for 8 hours on rapalog to permit for dimerisation between the GFP-tagged bait construct and mCherry-tagged biotinylator, visualised by live fluorescence. *Scale bars = 2 µm. (c) Biotinylation at the rhoptry bulb was confirmed by co-localising foci between RAP1 staining and a streptavidin-conjugated AlexaFluor488 in fixed cells by IFA. Scale bars = 2 µm. (d) Interactors for PfCERLI1. N = 3 biological replicates. (e) Interactors for PfCERLI2. N = 3 biological replicates. (d-e) Colour code corresponds to: green (bait protein), yellow (peak schizont-expressed), pink (late trophozoite to schizont stage-expressed), blue (uniformly or ring stage-expressed). * P-value calculated by t-test between*

intensity values in double-treated parasites and no rapalog controls. For completion, statistical analyses were attempted for all hits based on their log2 average intensity values between control and test samples, where if a protein was not present in the controls it was assigned with an intensity value of 0. As a result, even the bait protein PfCERLI1 did not reach the p-value threshold of 0.05 due to this artificial calculation. These values in turn do not represent the true significance of a hit being real, but instead provide an indication of how much protein was present in the test samples compared to the controls. Therefore, a p-value near but greater than 0.05 suggests enrichment in the test samples.

Discussion

We and Suarez *et al*. had previously characterised the rhoptry bulb protein PfCERLI1 and determined that it played an essential role in merozoite invasion and rhoptry secretion[11,12]. Bioinformatic searches identified PfCERLI2 as a protein potentially related to PfCERLI1 based on their amino acid sequence homology. Here, we show that *cerli2* likely arose through ancestral gene duplication from *cerli1*. Furthermore, we show that like PfCERLI1, PfCERLI2 also localises to the cytosolic face of the rhoptry bulb, is essential for merozoite invasion and has important functions in rhoptry biology.

PfCERLI2 localised to the rhoptry bulb by immunofluorescence assays and solubilised mainly in the carbonate treatment, suggesting it is peripherally associated with the rhoptry bulb membrane. PfCERLI1 was present in both the carbonate and triton-x100 insoluble fractions, which we hypothesised may be a result of strong cooperative membrane association through its C2 domain, PH domain, and palmitoylation site[11]. By contrast, PfCERLI2 appears to lack a functional PH domain and the palmitoylation site possessed by PfCERLI1. In the most likely *Toxoplasma gondii* homologue of PfCERLI2 (TGME49_315160, also known as TgRASP2), the PH domain is involved in, but not essential for, rhoptry localisation and secretion[12]. Based on evidence from its *T. gondii* homologue and the lack of a canonical PH domain and palmitoylation site, we suggest that membrane attachment of PfCERLI2 is likely

mediated by its C2 domain, a structure involved in targeting many proteins to various membranes[30].

Knockdown of PfCERLI2 led to reduced parasite growth and merozoite invasion. Morphology and rate of schizont rupture in PfCERLI2 knockdown parasites were indistinguishable compared to the controls, indicating merozoite development and egress was not impacted by knockdown of PfCERLI2. Instead, we observed increased numbers of both free merozoites in the culture medium and merozoites bound to the RBC surface in PfCERLI2 knockdown parasites. Based on this evidence, the inducible growth inhibition seen with PfCERLI2 knockdown is most likely to be a result of merozoite invasion being interrupted at or before formation of the irreversible tight-junction with the RBC surface. This is further supported by a decrease in AMA1 diameter in merozoites bound to the RBC for PfCERLI2 knockdown parasites, suggesting that the invasion process had been halted at the early stages of host-cell entry and TJ formation. Indeed, a corresponding increase in RBC bound merozoites following PfCERLI2 knockdown suggests that rhoptry neck and micronemal protein contents were secreted for PfCERLI2 deficient merozoites, and the TJ formed for some of these, but these merozoites were then unable to proceed with invasion. The fact that we saw no reduction in secretion of the rhoptry neck proteins RON4 and RH4 following CERLI2 knockdown supports the idea that in many cases the glucosamine inducible ribozyme PfCERLI2 knockdown parasites can secrete enough protein to form the TJ, but these merozoites fail to invade due to a later-occurring defect.

The presence of a prominent decapeptide repeat region at the C-terminus of PfCERLI2 is a differentiating feature compared to PfCERLI1. Based on its differential evolution relative to the rest of the PfCERLI2 protein, and its exclusive presence in *Laverania*, we hypothesise that the decapeptide tandem repeat number may be under positive selection, whereas the rest of the protein is under negative selection that strongly favours amino acid conservation across *Plasmodium* spp. A previous study identified a growth inhibitory monoclonal antibody (known as M26-32[17]) that bound to PfCERLI2, as well as a number of other proteins[31], and was reported to localise this

protein to the merozoite surface. This study also reported that the decapeptide tandem repeat contained highly immunogenic antigens that bind malaria-exposed serum antibodies. It is possible that this is a result of MHC-processed PfCERLI2 of phagocytosed merozoites, presented by immune cells in the spleen or lymph nodes (Heide *et al.* 2019). Alternatively, a potential mechanism for the positive selection of the PfCERLI2 repeat could be classical antibody selection. However, our data using endogenously tagged PfCERLI2 shows that the protein localises to the cytosolic face of the rhoptry bulb membrane and has a role in the function of this organelle, making it unlikely that PfCERLI2 is significantly exposed to the host immune system and antibody selection. We therefore suggest that the PfCERLI2 repeat has a yet unidentified function in *P. falciparum* and its evolution is under positive selection based on its Ka/Ks value of 1.43 across *Laverania*. Amongst *P. falciparum* isolates, repeat number varies and it is currently unclear whether the same occurs among different isolates of all *Laverania*, or whether this is a unique property of PfCERLI2. Given the conservation of the repeat sequence in *P. falciparum*, but the variation in repeat number, this variation in repeat number may have an important role in this protein's function between isolates.

Due to the presence of two paralogous genes in all coccidians (e.g. *Toxoplasma gondii* and *Besnoitia* spp.) and haematozoa (e.g *Plasmodium* spp.), it is likely that an ancestral *cerli1* sequence was duplicated in the most recent common ancestor of these related parasite lineages. By contrast, all more divergent apicomplexans and Chromerids contain only a single *cerli* gene, suggesting that there was originally only a single *cerli* gene in the more distant ancestors of coccidia and haematozoa. *Cryptosporidium* is more divergent than coccidia and haematozoa and contains only a single CERLI homologue. As the gene structure of the *cerli* homologue of *Cryptosporidium* is highly similar to that of *cerli1* across other Apicomplexa, we suggest that *cerli1* is most similar to the ancestral gene that underwent duplication and gave rise to the more divergent *cerli2* gene. From studies of both PfCERLI1 and PfCERLI2, it is clear that both proteins have functional similarities due to their stage of expression and localisation, along with their knockout and knockdown

phenotypes[11,12,15]. Additionally, in *Toxoplasma gondii* it has been reported that TgRASP1 and TgRASP2 form a complex[12]. Our DiQ-BioID data for PfCERLI1 and PfCERLI2 currently does not support a direct interaction between these proteins in *P. falciparum*. However, it is still possible that the proteins interact via another protein or a complex that may not be detected by DiQ-BioID in intact cells but can immunoprecipitated in solubilised cells using a HA-tag. Low expression of PfCERLI2 is another possible explanation. For the coccidia and haematozoa containing *cerli* paralogues, it is likely that the duplicated *cerli2* locus that arose from gene duplication of an ancestral *cerli1* locus underwent subfunctionalisation. This is supported by shared characteristics of PfCERLI1 and PfCERLI2, along with the strong negative selection CERLI2 has been under across Apicomplexa and the presence of only a putative remnant of a PH domain.

Dimerization-induced proximity based biotinylation using either PfCERLI1 or PfCERLI2 as the bait delivered a list of putative interacting proteins. The most notable one is the multi-transmembrane domain containing ROP14, which appears in the interactomes for both proteins. Though the function of ROP14 remains largely unknown, it has been localised in *P. falciparum* schizonts by IFA and denoted to be slightly posterior to RON4[32] and therefore may possess a rhoptry bulb localisation. It is possible that ROP14, in complex with other proteins, forms either a bridge between PfCERLI1 and PfCERLI2 that was not detected within the biotinylation range of BirA, which can vary from 10-30 nm [33]. Alternatively, ROP14 may transiently interact with both proteins, but not simultaneously.

CERLI2 homologues in coccidia and haematozoa possess a PH domain towards their C-terminus that is under negative selection. The exception to this is the genus *Plasmodium*, where the region corresponding to the PH domain of PfCERLI1 in CERLI2 has undergone significant change in sequence and structure such that a PH domain is no longer predicted for, or likely functional in, this region of *Plasmodium* spp. CERLI2. Additionally, PfCERLI2 homologues in the *Laverania* subgenus of *Plasmodium* also have a decapeptide tandem repeat that is under positive selection.

While it is not clear what the function of this repeat region is, the likely absence of the PH domain's lipid-binding function [12] and presence of the decapeptide repeat region may indicate that CERLI2 in *Laverania* has undergone neosubfunctionalisation, where following subfunctionalisation one paralogue adopts a new function[34]. We can therefore speculate that CERLI2 homologues in *Laverania* may be evolving modified functions or different protein-protein/protein-lipid interactions compared to homologues outside this subgenus.

This study highlights that CERLI2, like its paralogue CERLI1, has an important role in *Plasmodium* invasion and rhoptry biology that is likely shared broadly across Apicomplexa. In *P. falciparum*, loss of PfCERLI2 led to elongated rhoptry structures that were evident in both 2D and 3D cell analysis and was associated with reduced merozoite invasion. The localisation of PfCERLI2 puts it in the right place at the right time to undertake overlapping functions with its paralogue PfCERLI1 on the cytosolic face of the rhoptry bulb, and this possibility may be resolved in future studies. The modified structure of CERLI2 in *Plasmodium* spp. suggests that the requirements of malaria parasite host cell invasion has led to further evolution of the protein, highlighting the ongoing specialisation of these proteins as the apicomplexan parasites diverged.

Methods

Bioinformatic analyses

PfCERLI2 (Pf3D7_0405200), PfCERLI1 (Pf3D7_0210600) and orthologous sequences used for comparison *of Pfcerli1* and *Pfcerli2* gene structure from *Babesia bigemina* (BBBOND_0209090, BBBOND_0311360), *B. bovis* (BBOV_IV005720, BBOV_III003780), *Cryptosporidium andersoni* (cand_006180), *C. hominis* (Chro.60252), *C. muris* (CMU_007720), *C. parvum* (cgd6_2143), *C. tyzzeri* (CTYZ_00001395), *C. ubiquitum* (cubi_02338), *Chromera Velia* (Cvel_21914), *Cyclospora Cayetanensis* (cyc_01372), *Cystoisopora Suis* (CSUI_005102), *Cytauxzoon Felis* (CF002482, CF003293), *Eimeria brunetti* (EBH_0041390), *G. niphandrodes* (GNI_053280), *N. caninum* (NCLIV_057920, NCLIV_049720), *P. reichenow*i (PRCDC_0402800, PRCDC_0209500), *P. malariae* (PmUG01_03015300, PmUG01_04021700), *P. ovale* (PocGH01_03012700, PocGH01_04019500), *P. knowlesi* (PKNH_0303300, PKNH_0410600), *P. vivax* (PVP01_0304600, PVP01_0414300), *P. berghei* (PBANKA_1002900, PBANKA_0307500), *P. yoelii* (PY17X_1004300, PY17X_0308100) and *P. chabaudi* (PCHAS_1003800, PCHAS_0309700), *S. neurona* (SN3_01800355, SN3_00600405), *T. annulata* (TA21020, TA12010), *T. equi* (BEWA_030720, BEWA_019330), *T. gondii* (TGME49_315160, TGME49_235130), *T. orientalis* (TOT_010000334, TOT_020000207), *V. brassicaformis* (Vbra_14966) were obtained by searching within the EuPathDB.org database[35]. Additionally, homologues of PfCERLI2 from the Laveranian parasites *P. adleri* (PADL01_0404800), *P. billcollinsi* (PBILCG01_0404100), *P. blacklocki* (PBLACG01_0402700), *P. gaboni* (PGABG01_0403400) *and P. praefalciparum* (PFRFG01_0404700) were obtained by searching within the PlasmoDB.org database[13].

Both pairwise and multiple sequence alignments were generated using Geneious 9.1.3 (Biomatters) using a Geneious global alignment with free end gaps (gap open penalty = 12, gap extension penalty = 3) algorithm with the Blosum62 cost matrix. Multiple sequence alignments were also constructed using Muscle[36] in an R

environment[37]. Phylogenetic trees were constructed from nucleotide and amino acid sequences using the Jukes-Cantor[38] DNA or LG[39] amino acid substitution models, respectively, genetic distance model and were built using the unweighted pair group method with arithmetic mean (UPGMA) tree build method using Geneious or the R package phangorn v. 2.5.5[40]. A tanglegram visualisation was generated using the cophyloplot function of the R package ape[41].

To identify *P. falciparum* proteins that contained a PHIS, or PHIS-like motif, the PHIS sequence from PfCERLI1, PfCERLI2, or the consensus sequence generated from their Apicomplexan homologues was used in a BLASTp search against the *P. falciparum* 3D7 proteome.

Ka/Ks ratios were calculated using the online Ka/Ks Calculation tool (http://services.cbu.uib.no/tools/kaks)[42,43] using the maximum likelihood tree method, discrete_Grantham submatrix, and a LI rate of moderate. Where Ka/Ks ratios are reported, they were generated using the same coding sequences as the corresponding phylogenetic tree.

Protein structure prediction

The protein structure of PfCERLI1, PfCERLI2, along with their homologues in *T. gondii* (TGME49_235130, TGME49_31516) and *C. muris* (CMU_007720) was predicted using the online protein structure prediction tool Phyre2 on intensive mode[44]. All predicted structures were visualised, presented and imaged using either Jmol[45] or EzMol[46].

Continuous culture of asexual stage *P. falciparum*

P. falciparum 3D7 parasites were cultured in O^+ red blood cells (Red Cross Blood Service Australia) as previously described[47]. Parasites were grown in RPMI-HEPES media (Sigma-Aldrich) supplemented with 0.5% v/v Albumax (Gibco), 52 mM gentamycin (Gibco), 367 mM hypoxanthine (Sigma-Aldrich), 2 mM L-Glutamax (Gibco) and 2 mM sodium bicarbonate (Thermo Fisher Scientific), adjusted to a pH of

7.4. Cultures were maintained at 37ºC in sealed acrylic boxes with the following gas composition: 1% O2, 5% CO2 and 94% N2.

Plasmid construction and transfection

List of genetic constructs in this study: *Pfcerli2*^{HAGlmS}, *Pfcerli2*$^{HAGlmS/GFP}$, *Pfcerli2*$^{SLI\text{-}TGD}$.

Pfcerli2^{HAGlmS} riboswitch transfection vectors were prepared from a PTEX150^{HAGlmS} plasmid backbone [48]. A 758 base pair homology region of *Pfcerli2* was PCR amplified from the 3' end of the genomic sequence of 3D7 gDNA using the primers *Pfcerli2* 5' F RBW (GGT**AGATCT**GAAGGAATCTTTTGGAGATGAGC) and *Pfcerli2* 3' R RBW (GGT**CTGCAGC**TATATTTTGTATGGTATTTTCTAATTGTGC). Each of the resulting PCR products were digested with the restriction enzymes BglII and PstI (indicated in bold in primer sequence) and cloned into the PTEX150^{HAGlmS} vector.
To generate the *Pfcerli2*$^{HAGlmS/GFP}$ parasite line, which expresses cytosolic GFP, the pHGBrHrBl-1/2 GFP plasmid was used, without modification[49].

For disruption of *Pfcerli2* using selection linked integration – targeted gene disruption (SLI-TGD) system, a source SLI-TGD vector (Pf3D7_1463000 SLI-TGD) was used[18]. A 772 bp homology region of *Pfcerli2* was PCR amplified using the primers *Pfcerli2* SLI-TGD F (GGT**GCGGCCGC**TCCACATATAAGTGATTTCGAGCC) and *Pfcerli2* SLI-TGD R (GGT**ACGCGT**CCTTGCACACTTCTTGTCC). Both PCR product, and the SLI-TGD vector were then digested with NotI and MluI (restriction sites in bold) and ligated together.

To generate the *Pfcerli1*$^{DiQ\text{-}BioID}$ and *Pfcerli2*$^{DiQ\text{-}BioID}$ lines, we utilized pBirA-7xGGGGS-FRB-mCherry and pSLI-2xFKBP-GFP plasmids, the latter of which was modified with a single homology flank for each gene [18,29]. Single homology flanks for each gene at their 3' end were PCR amplified from NF54 gDNA: 767 base pairs for *Pfcerli1* using the primers *Pfcerli1* DiQ-BioID F (GGT**GCGGCCGC**CATATCAAATTTGGTTCTTGAAG) and *Pfcerli1* DiQ-BioID

R (GGT**CCTAGG**CATCACTATAGTTGTACATATTTTTGC), and 758 base pairs for *Pfcerli2* using *Pfcerli2* DiQ-BioID F (GGT**GCGGCCG**GAAGGAATCTTTTGGAGATGAGC) and *Pfcerli2* DiQ-BioID R (GGT**CCTAGG**TATATTTTGTATGGTATTTTCTAATTGTGC). Each PCR product was digested with the restriction enzymes NotI and AvrII (sites indicated in bold) and cloned into pSLI-2xFKBP-GFP.

P. falciparum 3D7 or NF54 parasites were transfected by RBC loading[50] (*Pfcerli2*^{HAGlmS}, *Pfcerli2*$^{HAGlmS/GFP}$) or schizont transfection[51] (*Pfcerli2*$^{SLI\text{-}TGD}$, *Pfcerli1*$^{DiQ\text{-}BioID}$ and *Pfcerli2*$^{DiQ\text{-}BioID}$). For RBC loading, uninfected RBCs were centrifuged at 440 rcf for 1 min, washed in culture media and then washed in cytomix (0.895% KCl, 0.0017% CaCl2, 0.076% EGTA, 0.102% MgCl2, 0.0871% K2HPO4, 0.068% KH2PO4, 0.708% HEPES). Washed RBCs were then resuspended in cytomix containing 200 µg of the plasmid of interest. The combined RBCs and DNA were transferred to a 0.2 cm cuvette (Bio-Rad) to be electroporated (Bio-Rad) at 0.31 kV with a capacitance of 960 µF. Electroporated RBCs were rinsed from the cuvette with culture media, centrifuged at 440 rcf for 1 min, and washed twice before being introduced to cultures of gelatin-purified schizont stage parasites. Alternatively for schizont transfection, late stage schizont cultures were Percoll-purified[52] and resuspended in 90µl transfection buffer (90 mM Na_2HPO_4; 5 mM KCl; 50 mM HEPES; 0.15 mM $CaCl_2$; pH 7.3) plus 10 µl of TE containing 50 µg of the plasmid of interest, and electroporated using a 2D Nucleofector (Lonza) on program U-033. Electroporated parasites were transferred into 1.5 mL tubes with 1 mL culture media and 200 µL uninfected RBCs and shaken at 37°C for 30 min to promote merozoites to invade, before being placed back into culture. To generate *Pfcerli2*^{HAGlmS}, 5 nM WR99210 (Jacobus Pharmaceuticals) drug treatment was used to select for integration of the HA-*GlmS* construct over 3 cycles. For *Pfcerli2*$^{HAGlmS/GFP}$, the HA-*GlmS* line was transfected with the pHGBrHrBl-1/2 construct in order to episomally express cytosolic GFP then selected for using 5 µg/mL blasticidin-S-deaminase HCl (Merck Millipore). To generate *Pfcerli2*$^{SLI\text{-}TGD}$, *Pfcerli1*$^{DiQ\text{-}BioID}$ and *Pfcerli2*$^{DiQ\text{-}BioID}$, maintenance of the SLI-TGD construct was selected using 4 nM WR99210 and integrants were selected using

400 µg/mL G418 (geneticin, Sigma). *Pfcerli1*$^{DiQ\text{-}BioID}$ and *Pfcerli2*$^{DiQ\text{-}BioID}$ *lines were also selected on 5 µg/mL blasticidin-S-deaminase to select for episomal expression of pBirA-7xGGGGS-FRB-mCherry*[18]. *Pfcerli2*$^{SLI\text{-}TGD}$ plasmids were transfected twice into 3D7 parasite culture, which after they grew on WR99210 and were selected each four times independently with G418 for eight weeks.

Assessment of *in vitro* blood stage growth and invasion

To investigate the effects of *Pfcerli2* knockdown on parasite growth 3D7 and *Pfcerli2*^{HAGlmS} cultures were synchronised to ring-stages using sorbitol lysis and adjusted to 1% parasitaemia at 1% haematocrit in 96 well U-bottom plates (Corning) as previously described[53]. From this adjusted culture, 45 mL was then suspended in 5 mL of a 10 x stock of D-(+)-glucosamine hydrochloride (hereby referred to as GLCN, Sigma-Aldrich) or media to a final volume of 50 mL. Plates were then incubated in standard culture conditions for 72 hours, until trophozoite stages the following cycle. Completed assays were then stained in 10 mg/mL ethidium bromide (Bio-Rad) in PBS and the final parasitaemia was assessed using the BD Accuri^{TM} C6 Plus flow cytometer (PE-H, FSC-H filters for growth, PE-H, FITC-H for invasion to visualise GFP-fluorescent ring stages). All flow cytometry files were analysed using FlowJo Version 10 (Tree Star). Representative flow plots are included in Supplementary Figure 20 to show our gating strategies.

To investigate the effect of *Pfcerli2* knockdown on invasion, *Pfcerli2*^{HAGlmS} cultures were synchronised to early trophozoite stages using sorbitol lysis and adjusted to 1% parasitaemia at 1% haematocrit and placed in 96 well U-bottom plates and set up as described for growth assays. Plates were subsequently incubated in standard culture conditions for 24 hours, until early ring stages the following cycle. Completed assays were stained with ethidium bromide and analysed by flow cytometry as described for growth assays.

To observe whether PfCERLI2 knockdown had an impact on merozoite quantity per schizont or merozoite morphology, *Pfcerli2*^{HAGlmS} parasites were treated

with or without 2.5 mM GLCN at ring stages until matured into 40 hr schizonts. To ensure full merozoite development, schizonts were arrested with E64 for 5hrs to prevent rupture and then smeared as a thin blood film. Smears were fixed in 100% v/v methanol and stained in 10% v/v Giemsa (Merck Millipore) in water and then blindly assessed by light microscopy (n = 20 individual schizonts). To count free merozoites, *Pfcerli2*$^{HAGlmS/GFP}$ schizonts +/- 2.5 mM GLCN without E64 were permitted to incubate until rupture and gated for merozoites by flow cytometry as described above.

Schizont rupture assay

To observe whether PfCERLI2 knockdown affected schizont rupture and merozoite egress, synchronous *Pfcerli2*^{HAGlmS} ring stages were treated in duplicate with or without 2.5 mM GLCN in 96-well U bottom plates as described above. Parasites were permitted to grow into schizonts prior to rupture and the parasitaemia was recorded by flow cytometry. Plates were then incubated for an additional 6 hrs to allow for schizont rupture followed by a second round of parasitaemia measurement by flow cytometry. To calculate the percentage of schizont rupture within this time window, the following equation was used:

$$\% \text{ schizont rupture} = \left(\frac{post-rupture\ schizontaemia}{pre-rupture\ schizontaemia}\right) \times 100$$

Bound merozoite assay by light microscopy

To determine whether PfCERLI2 knockdown inhibited merozoite invasion prior to, or following, tight junction formation PfCERLI2^{HAGlmS} ring-stage parasites were either treated with 2.5 mM GLCN or left untreated and incubated until schizont rupture. Following schizont rupture, Giemsa-stained smears were made of these cultures without washing or removing the culture medium, blinded and counted to determine the number of bound merozoites and newly invaded rings in each treatment. For each treatment >1000 RBCs were counted per replicate.

Bound merozoite assay and invasion scoring by confocal microscopy

To determine whether PfCERLI2 knockdown inhibits invasion, prior, at or following tight junction formation, uninfected RBCs were stained in 1 mM CellTrace™ Far Red (Invitrogen) to allow for fluorescent visualisation and downstream 3D modelling of the RBC. Stained RBCs at 6% haematocrit were treated with 1 mM cytochalasin D (ThermoFisher Scientific) or left untreated, then distributed as 75 µL aliquots in a 96 well plate. PfCERLI2^{HAGlmS} ring-stages at 4-5% parasitaemia were treated with 2.5 mM GLCN or left untreated, incubated until young schizonts had formed at the point of chromatin segregation, Percoll-purified, then treated with E64 for 4 hours. Viable merozoites were purified as described previously with modifications[20]: Percoll-purified schizonts were resuspended in 2 mL culture media excluding Albumax and passed through a 1.2 mm Minisart® Syringe Filter, and 75 µL of flowthrough was immediately added to wells containing CellTrace-stained, cytochalasin D treated or untreated RBCs, now at a final haematocrit of 3%. The plate was shaken at 300 rpm at 37 ºC for 2 minutes to allow for a short invasion window, the cells were then fixed (final concentration 4% w/v paraformaldehyde (PFA, Sigma-Aldrich), 0.0075% v/v glutaraldehyde (Electron Microscopy Sciences), pH 7.4). Slides for confocal microscopy were prepared as described in a following section – stains included anti-AMA1 (mouse 1/500), anti-MSP1-19 (rabbit 1/1000) and DAPI. Slides were blinded shortly after sample preparation, and Z-stacks of 20 merozoites were taken per treatment group on an LSM800 (Zeiss) in Airyscan mode. Invasion was scored under three tiers: 1-attached, 2-partially invaded, 3-invaded, which could be determined by whether the merozoite appeared on the surface of, partway through the interface of, or enveloped inside the CellTrace fluorescently labelled RBC membrane respectively. The diameter of AMA1 of each merozoite was measured in Imaris (Bitplane). Samples were unblinded after statistical analyses were performed. Measurements for merozoites with an invasion score = 3 were excluded from the final data analysis as the tight junction closes behind the merozoite upon completion of invasion and becomes smaller. The full data set is provided in the supplementary material.

Saponin lysis and Western blot

To prepare protein samples, high parasitaemia cultures were lysed in 0.15% w/v saponin (ThermoFisher Scientific) on ice for 10 min, centrifuged at 16000 rcf, washed once in 0.075% w/v saponin and twice in PBS. All lysis reagents included protease inhibitors (CØmplete, Roche). Parasite lysates were DNase I treated (Qiagen) for 5 min at room temperature before being resuspended in reducing sample buffer (0.125 M Tris-HCl pH 7, 20% v/v glycerol, 4% v/v SDS, 10% v/v b-mercaptoethanol (Sigma-Aldrich), 0.002% w/v bromophenol blue (Sigma-Aldrich)). Protein lysates were separated by size on SDS-PAGE 4-12% Bis-tris Gels (Bolt, Invitrogen) at 110 V for 80 min then transferred onto a nitrocellulose membrane (iBlot, Invitrogen) at 20 V for 7 min. Membranes were blocked in 1% w/v skim milk 0.05% v/v Tween20 (Sigma-Aldrich) in PBS (hereby referred to as 1% milk PBS-T) for 1 hr at room temperature. Primary (mouse 12CA5 anti-HA (1:5000 Roche), rabbit anti-aldolase (1:5000 abcam), rabbit anti-GAP45 [54] (1:5000), mouse anti-RAP1[55] (1:10000), rabbit anti-RON4[56] (1:5000), rabbit anti-Rh4[57] (1:5000), rabbit anti-EBA175[58] (1:10000) and secondary (IRDye ® 800CW goat anti-mouse (1:4000, LI-COR Biosciences), IRDye® 680RD goat anti-rabbit (1:4000, LI-COR Biosciences) antibodies were prepared in 1% milk PBS-T and incubated on the membranes for 1 hr each at room temperature while rocking. Primary antibodies were washed three times in 0.05% v/v PBS-Tween20 (hereby referred to as PBS-T), while secondary antibodies were washed twice in PBS-T and once in PBS. Completed blots were dried on filter paper (Whatman) and visualised on the Odyssey Infrared Imaging System (LI-COR Biosciences). All band quantification was performed in Image Studio Lite 2.5 (LI-COR Biosciences).

Proteinase K protection assay

To determine whether PfCERLI2 was cytosolically exposed or compartmentalised in an organelle, a proteinase K protection assay modified from a previous study was performed[9,11]. Three 10 mL aliquots of high schizontaemia cultures were centrifuged at 440 rcf for 5 min, supernatant removed and lysed in 0.15% w/v saponin as described above. One set of schizonts were treated in SOTE (0.6 M sorbitol, 20 mM Tris HCl pH 7.5, 2 mM EDTA) alone, the second treated in SOTE with 0.02%

w/v digitonin (Sigma-Aldrich) left incubating for 10 min at 4ºC before being washed in SOTE, and the third digested with 0.1 mg/mL Proteinase K (Sigma-Aldrich) in SOTE for 30 min at 4ºC following the aforementioned digitonin treatment. Proteinase K was inactivated with 50 µL 100% v/v trichloroacetic acid followed by PBS. All samples were resuspended in 500 µL acetone to ensure full Proteinase K deactivation, centrifuged then washed twice in 500 µL MilliQ H_2O. The final pellets were used for Western blot analysis of PfCERLI2's sensitivity to Proteinase K.

Protein solubility assay

To biochemically determine whether PfCERLI2 was membrane-associated and by what mechanism of association, a protein solubility assay was performed as previously described[11]. Briefly, a high schizontaemia culture was saponin-lysed as described above, resuspended in 100 µL MilliQ H_2O, snap-frozen in dry ice four times, passed through a 29 gauge needle 5 times to disrupt parasite membranes, centrifuged at 16000 rcf for 10 min before reserving the water-soluble fraction containing cytosolic proteins. The remaining pellet was washed twice in MilliQ H_2O and once in PBS before being resuspended in 100 µL 0.1 M Na_2CO_3 for 30 min at 4ºC, centrifuged before reserving the carbonate-soluble fraction containing peripherally-associated proteins. The pellet was washed in the same manner above before being resuspended in 0.1% v/v Triton X-100 for 30 min at 4 ºC, centrifuged and the final supernatant reserved containing integral proteins. The remaining pellet was washed twice in PBS and was used to represent Triton X-100-insoluble proteins. All fractions were analysed by Western blot to determine PfCERLI2's membrane solubility profile.

Sample preparation for fixed-cell immunofluorescence microscopy

Pfcerli2^{HAGlmS} cultures of 3% E64 arrested schizonts were centrifuged at 440 rcf for 3 min, washed in PBS, resuspended in fixative (4% v/v paraformaldehyde (PFA, Sigma-Aldrich), 0.0075% v/v glutaraldehyde (Electron Microscopy Sciences), pH 7.4) and then left gently rocking for 30 min at room temperature. Samples were centrifuged at 440 rcf, fixative removed, washed twice in PBS, then adjusted to 1% haematocrit in PBS. #1.5H high-precision coverslips (Carl Zeiss, Oberkochen, Germany) were

soaked in methanol, airdried, coated in 0.01% v/v poly-L-lysine (Sigma-Aldrich) for 30 min at room temperature then washed in MilliQ H_2O. Fixed cells were then laid on top at room temperature for 30 min, with non-adherent cells being gently aspirated off. Cells were permeabilised with 0.1% v/v Triton X-100 for 10 minutes then incubated in 3% bovine serum albumin (BSA) in PBS-T for 1 hr. Primary antibodies (anti-HA biotin conjugate 1:1000 (Roche), mouse anti-RAP1[55] 1:500, mouse anti-AMA1[59]1:500, rabbit anti-RON4[56] 1:500, rabbit anti-MSP1-19[60] 1:500) were diluted in 1% w/v BSA in PBS-T as specified above and applied to the coverslips overnight at 4 ^{o}C. The next day, coverslips were washed three times in PBS-T, before being incubated with Alexa Fluor-conjugated secondary antibodies (streptavidin 488 nm, mouse 594 nm, rabbit 647 nm, Life Technologies) for 1 hour in the dark at room temperature. Coverslips were again washed three times in PBS-T before being dehydrated in ethanol (70% v/v 3 min, 90% v/v 3 min, 100 v/v 3 min), air dried and then mounted on glass slides with 20 mL Prolong® Gold antifade solution (refractive index 1.4) with 4', 6-diamidino-2-phenylindole dihydrochloride (DAPI, Thermofisher Scientific). The mountant was allowed to cure overnight and coverslips were analysed on an Olympus FV3000 confocal microscope.

Confocal microscopy and colocalisation analysis

Confocal microscopy was performed using an Olympus FV3000 fluorescence microscope (Olympus) equipped with a ×100 MPLAPON oil objective (NA 1.4) using the 405 nm, 488 nm, 561 nm, and 633 nm lasers. Colocalisation analysis was performed using Imaris Coloc Suite (v9.0, Bitplane Inc., Switzerland) as described in detail previously [11]. Briefly, images were exported from the Olympus FV3000 in .oir format, before conversion into .ims format. Following conversion, colocalisation analysis was performed whereby the image dataset was masked to the thresholded PfCERLI2 (anti-HA, 488nm laser) signal, defining the PfCERLI2 signal as the region of interest. Subsequently the other thresholded channels, corresponding to either RAP1, RON4, AMA1, or MSP1-19, were colocalised with the PfCERLI2 signal. Colocalisation statistics reported in this study are Pearson's correlation coefficient between the PfCERLI2 signal and the signal of the corresponding organelle marker, when

PfCERLI2 is defined as the region of interest. Colocalisation analyses were performed over three biological replicates. For each of these biological replicates, threshold values were determined for each of the channels used in the colocalisation analysis to differentiate between true signal and background. Threshold values were fixed across all channels for each image in that biological replicate.

Rhoptry and microneme ligand secretion assay

Secretion assays were modified from a previous protocol[11]. Briefly, *Pfcerli2*^{HAGlmS} synchronous ring stages at 15% haematocrit were grown in 6-well plates (Corning) with or without 2.5 mM GLCN for 24 hrs. Once trophozoite stages had formed, cultures were centrifuged at 440 rcf, supernatant removed and resuspended in an enzyme mix (0.067 U/mL neuraminidase (Sigma-Aldrich), 1 mg/mL chymotrypsin (Worthington Biochemical Corporation), 1 mg/mL trypsin (Sigma-Aldrich)) to be incubated at 37ºC for 45 minutes to cleave RBC surface receptors. Parasites were then washed twice in culture media and returned to culture for a further 24 hrs until schizont rupture. Once ruptured, cultures were centrifuged at 16000 rcf for 10 min at 4ºC to pellet uninvaded merozoites. Supernatants containing secreted protein was collected and kept on ice, and the pellet subject to saponin lysis to represent non-secreted protein. Each fraction was analysed by Western blot and quantified in Image Studio Lite 2.5 (LI-COR Biosciences).

Transmission electron microscopy

Pfcerli2^{HAGlmS} synchronous ring stage cultures were treated with or without 2.5 mM GLCN and grown until early schizonts had formed before being treated with 2 μM C1 for 4 hrs. Late schizonts were then enriched using Percoll then fixed in 2.5% v/v glutaraldehyde (Electron Microscopy Sciences) in PBS overnight at 4ºC. Fixed schizonts were post-fixed in 1% osmium tetroxide (v/v) and 1.5% potassium ferrocyanide (w/v) in 0.1 M Sorensen's phosphate buffer (PB) pH 7.4 for 30 min at room temperature. Cells were washed in 0.1 M PB (3 × 5 min) and incubated in 1% tannic acid (w/v) in 0.1 M PB for 30 min. Samples were washed in ultrapure water (3 × 5 min) and *en bloc* stained in 1% aqueous uranyl acetate (w/v) for 1 h at room

temperature. Cells were washed in ultrapure water (3 × 5 min) and incubated in Walton's Lead Aspartate for 30 min at 60ºC. Cells were then washed in ultrapure water (3 × 5 min), dehydrated in increasing concentrations of ethanol-H_2O and absolute acetone and finally embedded in medium-grade Procure 812 resin. 70 nm ultrathin sections were generated using a Leica EM UC7 ultramicrotome (Leica Microsystems) and attached to 100-mesh Cu formvar-carbon coated grids. Images were acquired using a Tecnai G2 F30 transmission electron microscope (Field Electron and Ion Company, FEI) operating at 200 kV.

Array tomography and rhoptry morphometric analysis

Array tomography[61] was performed in order to obtain 2-D and 3-D morphometric data. Blocks processed for TEM were sectioned on a Leica EM UC7 ultramicrotome (Leica Microsystems), generating 100 consecutive sections of 100 nm-thickness (depth sectioned = 10 µm/sample). Sections were collected on a hydrophilized silicon wafer and allowed to dry at room temperature. An aluminium stub was adhered to the underside of wafers using conductive double-sided adhesive carbon-tabs.

Inverted backscattered field emission scanning electron microscopy was performed using a FEI Teneo SEM (Field Electron and Ion Company, FEI) operating at 5 kV at a working distance of 7.3 mm. Images (6144 × 4096 pixel array, 8-bit, 9.76 × 9.76 × 100 nm voxel dimensions, pixel dwell time 2 µs) were acquired at 3,500× yielding a *XY* field of view of 59.97 × 39.98 µm).

Image histogram stack normalisation was performed, and images were aligned using the StackReg plugin for Fiji[62]. For 3-D modelling and visualisation, datasets were processed using 3dmod, a program bundled with the IMOD software package[61]. Rhoptries were segmented by means of manual tracing of high-contrast lines. 3-D information including surface area and volume was obtained using the "get info" command. Rhoptry length was quantified from SEM micrographs where rhoptry necks could be seen contacting the merozoite plasma membrane and the bottom of the bulb

could be clearly discerned. Using blinded assessment, a vector was drawn from the tip of the necks to the end of the rhoptry bulbs in 3dmod to provide a length in nm.

Quantitative analysis of rhoptry length in thin-section schizonts

Rhoptry length was quantified from transmission electron micrographs for rhoptries where necks could be seen contacting the merozoite plasma membrane and the bottom of the bulb could be clearly discerned. Using blinded assessment, a vector was drawn from the tip of the necks to the end of the rhoptry bulbs in ImageJ to provide a length in nm. Micrographs where the rhoptries had been cut sideways such that it removed part of the neck or bulb were excluded from this analysis.

Airyscan microscopy, merozoite measurement, and foci analysis

Airyscan microscopy was performed using a Zeiss LSM800 AxioObserver Z1 microscope (Carl Zeiss, Oberkochen, Germany) that had an Airyscan detector and a Plan-Apochromat 63x M27 oil objective (NA 1.4). Z-stacks were acquired using a 0.04 µm XY and 0.16 µm Z pixel resolution. Images were acquired sequentially as follows: Channel 1 (RON4) – 633 nm laser, channel 2 (RAP1) – 594 nm laser, channel 3 (HA) – 488 nm laser, channel 4 (DAPI) – 405 nm laser.

The distance between the basal end of the nucleus (DAPI signal) and the RAP1 or RON4 foci was measured as described previously[63]. Images were first blinded and then using the Plot Profile plugin on FIJI, a line was drawn from the basal extremity of the DAPI signal through the RAP1 and RON4 foci to generate intensity profiles for the three markers as a function of distance of the line. Data generated from these intensity plots was then exported, and graphed using GraphPad PRISM 7, with the distance corresponding to the highest RAP1 or RON4 signal intensity representing the distance of that signal from the basal end of the DAPI signal.

RON4 and RAP1 foci were analysed using an object analysis pipeline on Imaris (v9.8.0, BitPlane AG, Zurich, Switzerland) that had previously been established for

these markers[11]. RAP1 or RON4 signals were pre-processed to segment and split individual foci, and then thresholded to remove background signal. Threshold values for each marker were kept consistent across all replicates and treatments. Identified objects were then filtered on the basis of size, with only objects > 0.1 μm included in the analysis. This analysis was performed in batch mode, so all images were processed and quantified identically. Once the surfaces had been established, their surface area, volume, and sphericity values were exported as .csv files.

RAP1 diameter was measured using the line function on ImageJ. Briefly, images of PfCERLI2^{HAGlmS} parasites that had either been treated with 2.5 mM GLCN or left untreated and stained with anti-RAP1 antibodies were blinded. Rhoptry bulb diameters were then manually quantified by drawing a vector across the diameter of the RAP1 signal. Only rhoptries with visible 'donut-shapes' were measured, with the diameter measured on the Z-slice between the points with the greatest signal intensity. Merozoites that were densely packed inside the schizont, or RAP1 signals where it was unclear which merozoite they belong to, were excluded from the analysis.

Preparation of samples for DiQ-BioID

Early PfCERLI1$^{DiQ\text{-}BioID}$ PfCERLI2$^{DiQ\text{-}BioID}$ schizonts (36 hours old) were treated with 150 μM biotin (Sigma-Aldrich) and with or without rapalog A/C heterodimerizer (AP21967, Takara) for 8 hours total, where E64 was added at 4 hours into treatment. Once mature schizonts had formed, dimerisation between the bait protein and BirA was confirmed by live cell microscopy, and biotinylation confirmed by fixed cell IFA and western blot using a streptavidin-conjugated AlexaFluor488 and streptavidin-conjugated IRDye800 respectively. The remaining culture was centrifuged at 550 rcf, washed twice in PBS before being saponin lysed.

Saponin pellets were further lysed in 1.5 mL lysis buffer (50 mM Tris-HCl pH 7.5, 500 nM NaCl, 1% Triton X-100 (Sigma-Aldrich), 1 mM dithiothreitol (DTT, Sigma-Aldrich), 1 mM phenylmethylsulfonyl fluoride (PMSF, Sigma-Aldrich) with CØmplete EDTA-free protease inhibitor cocktail tablet (Roche)) and sonicated three times for 30 seconds at a time. Samples were centrifuged at max speed, and

supernatants were incubated with magnetic streptavidin beads (Pierce) at 4 ºC O/N to enrich for biotinylated proteins. The next day, the beads were separated on a magnetic separation rack, and flowthrough was discarded. Beads were washed three times in 1 mL lysis buffer, and six times in 50 mM ammonium bicarbonate (Sigma-Aldrich). Washed beads were then resuspended in 200 µL ammonium bicarbonate containing 1 µg equivalent of sequencing-grade trypsin (Promega) and incubated O/N at 37 ºC with gentle shaking. The following morning, an additional 0.5 µg of sequencing-grade trypsin was added to each sample, and incubated for another 4 hours at 37 ºC. Beads were magnetised, and supernatant containing peptides was collected. Residual peptides on the beads were collected with two rinses of 150 µL ddH_2O and supernatants were pooled. The pooled supernatant was centrifuged at max speed to remove any residual beads and collected in a new tube. The final supernatant was acidified to 0.5% v/v formic acid (Thermofisher) to inactivate trypsin, before being sent for LC-MS analysis.

Mass spectrometric instrumentation and data acquisition

Mass spectromtery acquisition and NanoLC-MS/MS was carried out as described previously [64,65], with minor modifications. Samples were loaded at a flow rate of 15 µl/min onto a reversed-phase trap column (100 µm × 2 cm), Acclaim PepMap media (Dionex) and maintained at a temperature of 40°C. Peptides were eluted from the trap column at a flow rate of 0.25 µl/min through a reversed-phase capillary column (75 µm × 50 cm) (LC Packings, Dionex). For acquisition by HPLC, a 158 min gradient was set using an incremental gradient that reached 30% ACN after 123 min, 34% ACN after 126 min, 79.2% ACN after 131 min and 2% ACN after 138 min for a further 20 min. The mass spectrometer was operated in a data-independent mode where a 43-fixed-window setup of 14 *m/z* effective precursor isolation over the *m/z* range of 376-967 Da was applied.

For analysis, raw files were processed using Spectronaut™ (version 13.0) against the in-house generated *P. falciparum* spectral library containing 44,449 peptides corresponding to 4,730 proteins. For processing, raw files were loaded in Spectronaut, the ideal mass tolerances for data extraction and scoring were calculated on its extensive mass calibration with a correction factor of 1. Both at precursor and fragment

level, the highest data-point within the selected *m/z* tolerance was chosen. Identification of peptides against the library was based on default Spectronaut settings (Manual for Spectronaut 13.0, available on Biognosis website). Briefly, precursor Qvalue Cut-off and Protein Qvalue Cut-off were as per default at 1% and therefore only those that passed this cut-off were considered as identified and used for subsequent processing. Retention time (RT) prediction type was set to dynamic indexed RT. Interference correction was performed at the MS2 level. For quantification, interference correction was activated and cross run normalisation was performed using the total peak area at a significance threshold of 0.01. Statistical analysis was performed in excel using relative protein and student t-test as described previously [65].

Statistical analysis

All graphs and statistical analyses were completed in Graphpad PRISM 7 (GraphPad Software Inc.). All figure legends note the type of statistical test, the definition of significance for various p-values, and the number of biological replicates (n) for each experiment.

Acknowledgements

We thank Prof. Alan Cowman for provision of RON4, EBA175 and GAP45 antibodies, A/Prof. Wai-Hong Tham for RH4 antibodies. We also thank Dr. Paul Gilson for the PTEX150^{HAGlmS} transfection vector. Electron microscopy was performed at the Ian Holmes Imaging Centre, Bio21, The University of Melbourne (www.microscopy.unimelb.edu.au). For provision of the SLI-TGD vector, we thank Dr. Tobias Spielmann. We thank Dr. Brad Sleebs for Compound 1. We thank the Australian Red Cross Blood Bank for the provision of human blood.

This work was supported by funding from the NHMRC (Project Grant APP1143974, DW), University of Adelaide Beacon Fellowship and Hospital Research Foundation Fellowship (DW), DAAD/Universities Australia joint research co-operation scheme (TG, DW, BL, JB), Australian Government Research Training Program Scholarship (BL, JB), South Australian Commonwealth Scholarship (BL), DFG BA5213/3-1 (JSW) and Jürgen Manchot-Stiftung fellowship (AA).

Author contributions

Study design and planning: D.W.W., B.L., J.B., M.W.A.D., L.T., and T.G. Performed experiments and generated reagents: B.L., J.B., E.M.E., D.W.W., G.J.S., J.S., G.K.H., A.A, and J.S.W. Data analysis: B.L., J.B., G.J.S., J.S., S.F., and D.W.W. Manuscript writing: B.L, J.B., and D.W.W. Manuscript was drafted with input from all authors.

Competing interests

The authors declare no competing interests.

References

1 World Health Organization. *World malaria report 2019*, <www.who.int/malaria/publications/world-malaria-report-2019/en/> (2019).

2 Cowman, A. F., Healer, J., Marapana, D. & Marsh, K. Malaria: Biology and Disease. *Cell* **167**, 610-624, doi:10.1016/j.cell.2016.07.055 (2016).

3 Cowman, A. F., Tonkin, C. J., Tham, W. H. & Duraisingh, M. T. The Molecular Basis of Erythrocyte Invasion by Malaria Parasites. *Cell Host and Microbe* **22**, 232-245, doi:10.1016/j.chom.2017.07.003 (2017).

4 Weiss, G. E., Crabb, B. S. & Gilson, P. R. Overlaying Molecular and Temporal Aspects of Malaria Parasite Invasion. *Trends Parasitol* **32**, 284-295, doi:10.1016/j.pt.2015.12.007 (2016).

5 Hanssen, E. *et al.* Electron tomography of *Plasmodium falciparum* merozoites reveals core cellular events that underpin erythrocyte invasion. *Cellular Microbiology* **15**, 1457-1472, doi:doi:10.1111/cmi.12132 (2013).

6 Weiss, G. E. *et al.* Revealing the Sequence and Resulting Cellular Morphology of Receptor-Ligand Interactions during *Plasmodium falciparum* Invasion of Erythrocytes. *PLOS Pathogens* **11**, e1004670, doi:10.1371/journal.ppat.1004670 (2015).

7 Riglar, D. T. *et al.* Super-Resolution Dissection of Coordinated Events during Malaria Parasite Invasion of the Human Erythrocyte. *Cell Host & Microbe* **9**, 9-20, doi:10.1016/j.chom.2010.12.003 (2011).

8 Counihan, N. A., Kalanon, M., Coppel, R. L. & de Koning-Ward, T. F. *Plasmodium* rhoptry proteins: why order is important. *Trends in Parasitology* **29**, 228-236, doi:10.1016/j.pt.2013.03.003 (2013).

9 Cabrera, A. *et al.* Dissection of Minimal Sequence Requirements for Rhoptry Membrane Targeting in the Malaria Parasite. *Traffic* **13**, 1335-1350, doi:10.1111/j.1600-0854.2012.01394.x (2012).

10 Geiger, M. *et al.* Structural Insights Into PfARO and Characterization of its Interaction With PfAIP. *Journal of Molecular Biology*, **432**, 878-896 doi:https://doi.org/10.1016/j.jmb.2019.12.024 (2019).

11 Liffner, B. *et al.* PfCERLI1 is a conserved rhoptry associated protein essential for *Plasmodium falciparum* merozoite invasion of erythrocytes. *Nature Communications* **11**, 1411, doi:10.1038/s41467-020-15127-w (2020).

12 Suarez, C. *et al.* A lipid-binding protein mediates rhoptry discharge and invasion in *Plasmodium falciparum* and *Toxoplasma gondii* parasites. *Nature Communications* **10**, 4041, doi:10.1038/s41467-019-11979-z (2019).

13 Aurrecoechea, C. *et al.* PlasmoDB: a functional genomic database for malaria parasites. *Nucleic Acids Research* **37**, D539-D543, (2008).

14 Woo, Y. H. *et al.* Chromerid genomes reveal the evolutionary path from photosynthetic algae to obligate intracellular parasites. *eLife* **4**, e06974, doi:10.7554/eLife.06974 (2015).

15 Zhang, M. *et al.* Uncovering the essential genes of the human malaria parasite *Plasmodium falciparum* by saturation mutagenesis. *Science* **360** (2018).

16 Bushell, E. *et al.* Functional Profiling of a *Plasmodium* Genome Reveals an Abundance of Essential Genes. *Cell* **170**, 260-272.e268, doi:10.1016/j.cell.2017.06.030 (2017).

17 Gao, Y. H. *et al.* Identification of a vaccine candidate antigen, PfMAg-1, from *Plasmodium falciparum* with monoclonal antibody M26-32. *Parasitology research* **105**, 1723-1732, doi:10.1007/s00436-009-1617-4 (2009).

18 Birnbaum, J. *et al.* A genetic system to study *Plasmodium falciparum* protein function. *Nature Methods* **14**, 450, doi:10.1038/nmeth.4223 (2017).

19 Lopez-Barragan, M. J. *et al.* Directional gene expression and antisense transcripts in sexual and asexual stages of *Plasmodium falciparum*. *BMC Genomics* (2011).

20 Boyle, M. J. *et al.* Isolation of viable *Plasmodium falciparum* merozoites to define erythrocyte invasion events and advance vaccine and drug development. *Proceedings of the National Academy of Sciences* **107**, 14378-14383, doi:10.1073/pnas.1009198107 (2010).

21 Thiam, L. G. *et al.* Cell trace far-red is a suitable erythrocyte dye for multi-color *Plasmodium falciparum* invasion phenotyping assays. *Experimental Biology and Medicine* **245**, 11-20, doi:10.1177/1535370219897393 (2020).

22 Yao, Z. *et al.* Improved targeting of radiolabeled streptavidin in tumors pretargeted with biotinylated monoclonal antibodies through an avidin chase. *J Nucl Med* **36**, 837-841 (1995).

23 Fujiki, Y., Hubbard, A. L., Fowler, S. & Lazarow, P. B. Isolation of intracellular membranes by means of sodium carbonate treatment: application to endoplasmic reticulum. *J Cell Biol* **93**, 97-102, doi:10.1083/jcb.93.1.97 (1982).

24 Silmon de Monerri, N. C. *et al.* Global identification of multiple substrates for *Plasmodium falciparum* SUB1, an essential malarial processing protease. *Infect Immun* **79**, 1086-1097, doi:10.1128/IAI.00902-10 (2011).

25 Howard, R. F., Narum, D. L., Blackman, M. & Thurman, J. Analysis of the processing of *Plasmodium falciparum* rhoptry-associated protein 1 and localization of Pr86 to schizont rhoptries and p67 to free merozoites. *Molecular and Biochemical Parasitology* **92**, 111-122, doi:10.1016/S0166-6851(97)00238-7 (1998).

26 Nasamu, A. S. *et al.* Plasmepsins IX and X are essential and druggable mediators of malaria parasite egress and invasion. *Science* **358**, 518, doi:10.1126/science.aan1478 (2017).

27 Favuzza, P. *et al.* Dual Plasmepsin-Targeting Antimalarial Agents Disrupt Multiple Stages of the Malaria Parasite Life Cycle. *Cell Host & Microbe*, doi:10.1016/j.chom.2020.02.005 (2020).

28 Taylor, H. M. *et al.* The Malaria Parasite Cyclic GMP-Dependent Protein Kinase Plays a Central Role in Blood-Stage Schizogony. *Eukaryotic Cell* **9**, 37, doi:10.1128/EC.00186-09 (2010).

29 Birnbaum, J. *et al.* A Kelch13-defined endocytosis pathway mediates artemisinin resistance in malaria parasites. *Science* **367**, 51-59, doi:doi:10.1126/science.aax4735 (2020).

30 Corbalan-Garcia, S. & Gómez-Fernández, J. C. Signaling through C2 domains: More than one lipid target. *Biochimica et Biophysica Acta (BBA) - Biomembranes* **1838**, 1536-1547, doi:10.1016/j.bbamem.2014.01.008 (2014).

31 Cheng, Q., Jones, G., Liu, E. X., Kidson, C. & Saul, A. Identification of a common *Plasmodium* epitope (CPE) recognised by a pan-specific inhibitory

monoclonal antibody. *Mol Biochem Parasitol* **49**, 73-82, doi:10.1016/0166-6851(91)90131-o (1991).

32 Zuccala, E. S. *et al.* Subcompartmentalisation of Proteins in the Rhoptries Correlates with Ordered Events of Erythrocyte Invasion by the Blood Stage Malaria Parasite. *PLOS ONE* **7**, e46160, doi:10.1371/journal.pone.0046160 (2012).

33 Varnaitė, R. & MacNeill, S. A. Meet the neighbors: Mapping local protein interactomes by proximity-dependent labeling with BioID. *Proteomics* **16**, 2503-2518, doi:10.1002/pmic.201600123 (2016).

34 Innan, H. & Kondrashov, F. The evolution of gene duplications: classifying and distinguishing between models. *Nature Reviews Genetics* **11**, 97-108, doi:10.1038/nrg2689 (2010).

35 Aurrecoechea, C. *et al.* EuPathDB: the eukaryotic pathogen genomics database resource. *Nucleic Acids Research*, **45**, D581-D591 (2016).

36 Edgar, R. C. MUSCLE: multiple sequence alignment with high accuracy and high throughput. *Nucleic Acids Research* **32**, 1792-1797, doi:10.1093/nar/gkh340 (2004).

37 R Core Team. *R: A language and environment for statistical computing*, <www.R-project.org/> (2020).

38 Jukes, T. H. & Cantor, C. R. in *Mammalian Protein Metabolism* (ed H.N. Munro) 21-132 (Academic Press, 1969).

39 Le, S. Q. & Gascuel, O. An Improved General Amino Acid Replacement Matrix. *Molecular Biology and Evolution* **25**, 1307-1320, doi:10.1093/molbev/msn067 (2008).

40 Schliep, K. P. phangorn: phylogenetic analysis in R. *Bioinformatics* **27**, 592-593, doi:10.1093/bioinformatics/btq706 (2010).

41 Paradis, E. & Schliep, K. ape 5.0: an environment for modern phylogenetics and evolutionary analyses in R. *Bioinformatics* **35**, 526-528, doi:10.1093/bioinformatics/bty633 (2019).

42 Liberles, D. A. Evaluation of Methods for Determination of a Reconstructed History of Gene Sequence Evolution. *Molecular Biology and Evolution* **18**, 2040-2047, doi:10.1093/oxfordjournals.molbev.a003745 (2001).

43 Siltberg, J. & Liberles, D. A. A simple covarion-based approach to analyse nucleotide substitution rates. *Journal of Evolutionary Biology* **15**, 588-594, doi:10.1046/j.1420-9101.2002.00416.x (2002).

44 Kelley, L. A., Mezulis, S., Yates, C. M., Wass, M. N. & Sternberg, M. J. E. The Phyre2 web portal for protein modeling, prediction and analysis. *Nature Protocols* **10**, 845, doi:10.1038/nprot.2015.053 (2015).

45 Jmol. *Jmol: an open-source Java viewer for chemical structures in 3D*, <http://www.jmol.org>

46 Reynolds, C. R., Islam, S. A. & Sternberg, M. J. E. EzMol: A Web Server Wizard for the Rapid Visualization and Image Production of Protein and Nucleic Acid Structures. *Journal of Molecular Biology* **430**, 2244-2248, doi:https://doi.org/10.1016/j.jmb.2018.01.013 (2018).

47 Trager, W. & Jensen, J. B. Human malaria parasites in continuous culture. *Science* **193**, 673 (1976).

48 Elsworth, B. *et al.* PTEX is an essential nexus for protein export in malaria parasites. *Nature* **511**, 587-591, doi:10.1038/nature13555 (2014).

49 Wilson, D. W., Crabb, B. S. & Beeson, J. G. Development of fluorescent *Plasmodium falciparum* for *in vitro* growth inhibition assays. *Malaria Journal* **9**, 152, doi:10.1186/1475-2875-9-152 (2010).

50 Deitsch, K., Driskill, C. & Wellems, T. Transformation of malaria parasites by the spontaneous uptake and expression of DNA from human erythrocytes. *Nucleic acids research* **29**, 850-853 (2001).

51 Moon, R. W. *et al.* Adaptation of the genetically tractable malaria pathogen *Plasmodium knowlesi* to continuous culture in human erythrocytes. *Proc Natl Acad Sci U S A* **110**, 531-536, doi:10.1073/pnas.1216457110 (2013).

52 Rivadeneira, E. M., Wasserman, M. & Espinal, C. T. Separation and concentration of schizonts of *Plasmodium falciparum* by Percoll gradients. *The Journal of protozoology* **30**, 367-370 (1983).

53 Wilson, D. W., Langer, C., Goodman, C. D., McFadden, G. I. & Beeson, J. G. Defining the timing of action of antimalarial drugs against *Plasmodium falciparum*. *Antimicrobial agents and chemotherapy* **57**, 1455-1467 (2013).

54 Baum, J. *et al.* A Conserved Molecular Motor Drives Cell Invasion and Gliding Motility across Malaria Life Cycle Stages and Other Apicomplexan Parasites. *Journal of Biological Chemistry* **281**, 5197-5208, doi:10.1074/jbc.M509807200 (2006).

55 Schofield, L. *et al.* A rhoptry antigen of *Plasmodium falciparum* contains conserved and variable epitopes recognized by inhibitory monoclonal antibodies. *Molecular and Biochemical Parasitology* **18**, 183-195, doi:10.1016/0166-6851(86)90037-X (1986).

56 Richard, D. *et al.* Interaction between *Plasmodium falciparum* Apical Membrane Antigen 1 and the Rhoptry Neck Protein Complex Defines a Key Step in the Erythrocyte Invasion Process of Malaria Parasites. *Journal of Biological Chemistry* **285**, 14815-14822, doi:10.1074/jbc.M109.080770 (2010).

57 Tham, W.-H. *et al.* Complement receptor 1 is the host erythrocyte receptor for *Plasmodium falciparum* PfRh4 invasion ligand. *Proceedings of the National Academy of Sciences* **107**, 17327, doi:10.1073/pnas.1008151107 (2010).

58 Lopaticki, S. *et al.* Reticulocyte and Erythrocyte Binding-Like Proteins Function Cooperatively in Invasion of Human Erythrocytes by Malaria Parasites. *Infect Immun* **79**, 1107, doi:10.1128/IAI.01021-10 (2011).

59 Coley, A. M. *et al.* The most polymorphic residue on *Plasmodium falciparum* apical membrane antigen 1 determines binding of an invasion-inhibitory antibody. *Infect Immun* **74**, 2628-2636, doi:10.1128/IAI.74.5.2628-2636.2006 (2006).

60 O'Donnell, R. A., Saul, A., Cowman, A. F. & Crabb, B. S. Functional conservation of the malaria vaccine antigen MSP-119 across distantly related *Plasmodium* species. *Nat Med* **6**, 91-95, doi:10.1038/71595 (2000).

61 Kremer, J. R., Mastronarde, D. N. & McIntosh, J. R. Computer Visualization of Three-Dimensional Image Data Using IMOD. *Journal of Structural Biology* **116**, 71-76, doi:https://doi.org/10.1006/jsbi.1996.0013 (1996).

62 Thevenaz, P., Ruttimann, U. E. & Unser, M. A pyramid approach to subpixel registration based on intensity. *IEEE Trans Image Process* **7**, 27-41, doi:10.1109/83.650848 (1998).

63 Ebrahimzadeh, Z. *et al.* A pan-apicomplexan phosphoinositide-binding protein acts in malarial microneme exocytosis. *EMBO reports* **20**, e47102, doi:10.15252/embr.201847102 (2019).

64 Siddiqui, G., Srivastava, A., Russell, A. S. & Creek, D. J. Multi-omics Based Identification of Specific Biochemical Changes Associated With PfKelch13-Mutant Artemisinin-Resistant *Plasmodium falciparum*. *J Infect Dis* **215**, 1435-1444, doi:10.1093/infdis/jix156 (2017).

65 Birrell, G. W. *et al.* Multi-omic Characterization of the Mode of Action of a Potent New Antimalarial Compound, JPC-3210, Against *Plasmodium falciparum*. *Mol Cell Proteomics* **19**, 308-325, doi:10.1074/mcp.RA119.001797 (2020).

Supplementary information

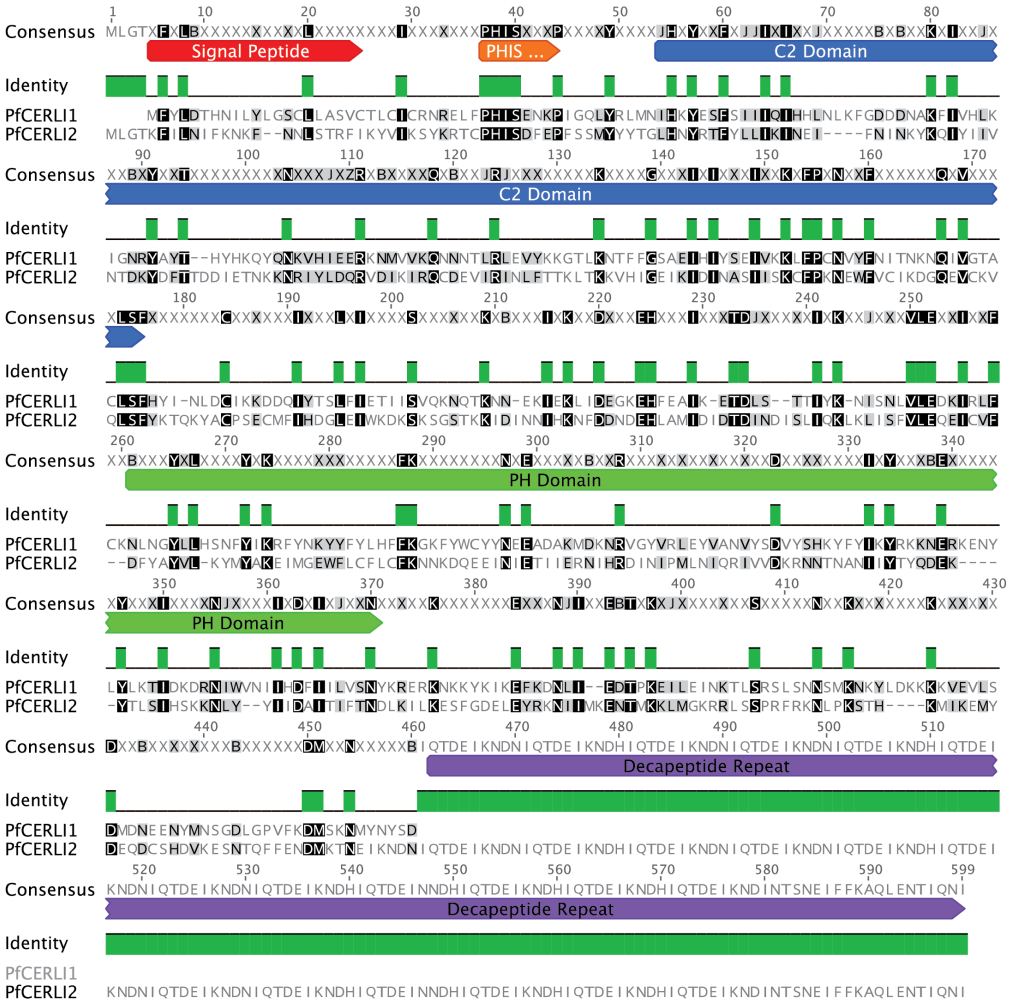

Supplementary Figure 1: Alignment of PfCERLI1 and PfCERLI2.

Geneious global alignment with free-end gaps between the amino acid sequences of PfCERLI1 (Pf3D7_0210600) and PfCERLI2 (Pf3D7_0405200). The signal peptide is predicted only for PfCERLI1 and is represented here as it is currently annotated on PlasmoDB. Removal of this signal peptide region does not affect localisation of PfCERLI1[1]. The PH domain is predicted only for PfCERLI1, and not PfCERLI2. The decapeptide repeat is present only in PfCERLI2, so shows 100% homology. Black shading indicates identities, grey similarities.

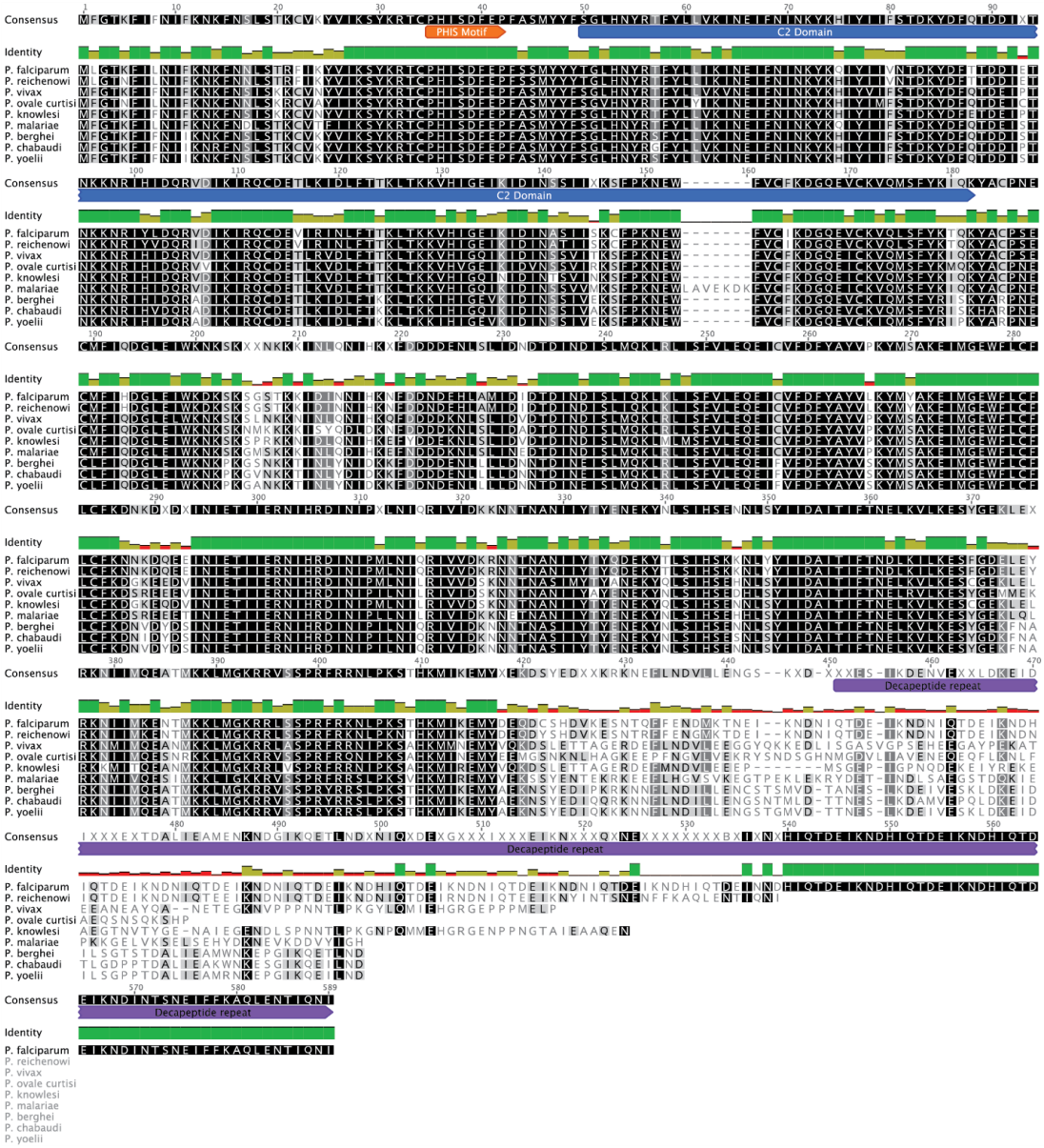

Supplementary Figure 2: Alignment of PfCERLI2 and its *Plasmodium* homologues. *Geneious global alignment with free-end gaps between the amino acid sequences of PfCERLI2 (Pf3D7_0405200) and its homologues in P. reichenowi (PRCDC_0402800), P. vivax (PVP01_0304600), P. ovale curtisi (PocGH01_030212700), P. knowlesi (PKNH_0303300) , P. malariae (PmUG01_03015300), P. berghei (PBANKA_1002900), P. chabaudi (PCHAS_1003800) , and P. yoelii (PY17X_1004300). The decapeptide repeat is present only in PfCERLI2, so shows 100% homology. Black shading indicates identities, grey similarities.*

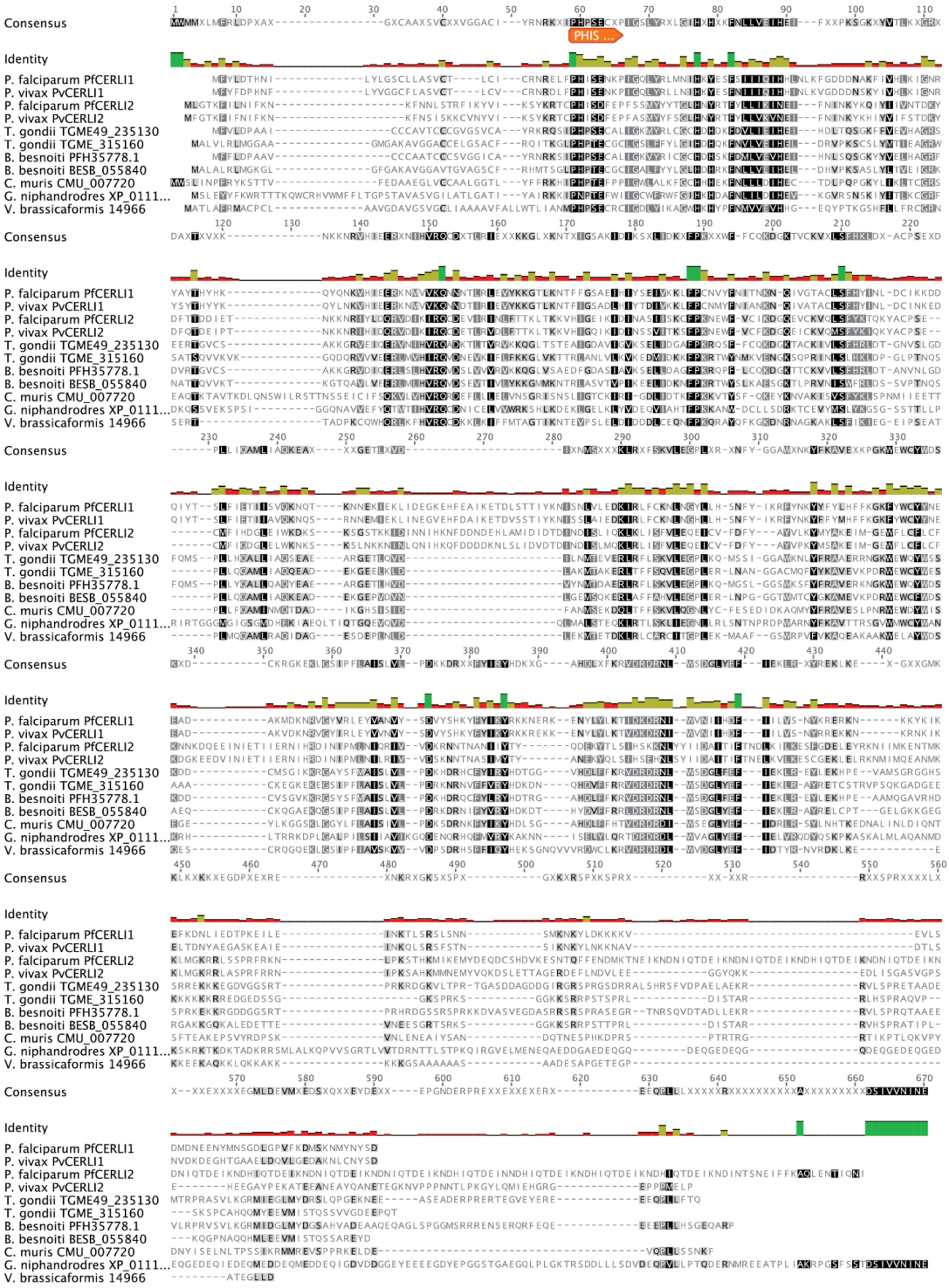

Supplementary Figure 3: Alignment of PfCERLI1, PfCERLI2, and their homologues.

Geneious global alignment with free-end gaps between the amino acid sequences of PfCERLI1 (Pf3D7_0210600), PfCERLI2 (Pf3D7_0405200) and their homologues in P. vivax (PVP01_0414300 & PVP01_0304600), Toxoplasma gondii (TGME49_235130 & TGME49_315160), Besnoitia besnoiti (PFH35778.1 & BESB_055840), Cryptosporidium muris (CMU_007720) , Gregarina niphandrodes (XP_011129839.1), and Vitrella brassicaformis (14966). Black shading indicates identities, grey similarities.

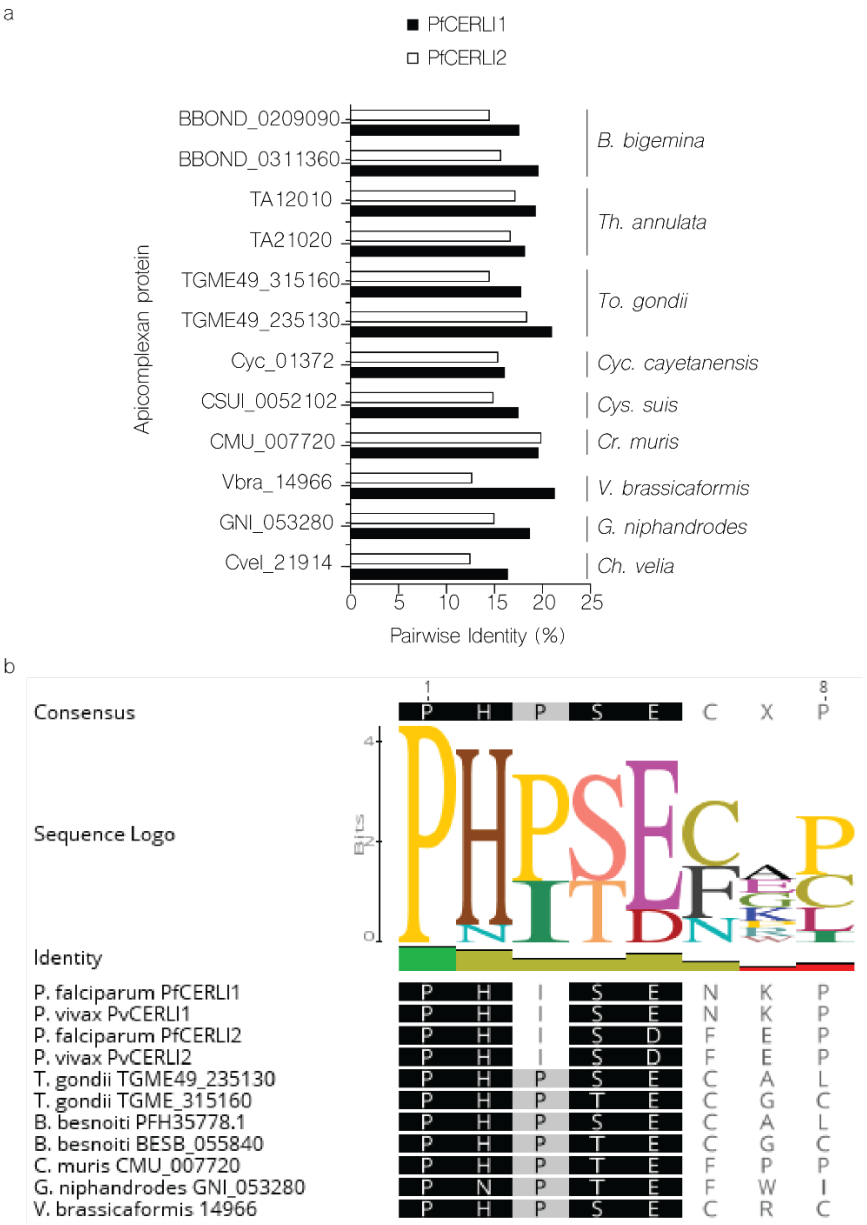

Supplementary Figure 4: Pairwise identity of PfCERLI1, PfCERLI2, and their Apicomplexan homologues.

(a) *Pairwise identities, as determined by Geneious global alignment with free-end gaps, of the amino acid sequence for either PfCERLI1 or PfCERLI2 and their homologues in Babesia bigemina (BBOND_0209090 & BBOND_0311360), Theileria annulata (TA12010 & TA21020), Toxoplasma gondii (TGME49_235130 & TGME49_315160), Cyclospora cayetanensis (Cyc_01372), Cystoisospora suis*

(CSUI_0052102), Cryptosporidium muris (CMU_007720), Vitrella brassicaformis (Vbra_14966), Gregarina niphandrodes (GNI_053280), and Chromera velia (Cvel_21914). ***(b)*** *Consensus sequence and conservation of the PHIS motif in PfCERLI1, PfCERLI2, and their apicomplexan homologues.*

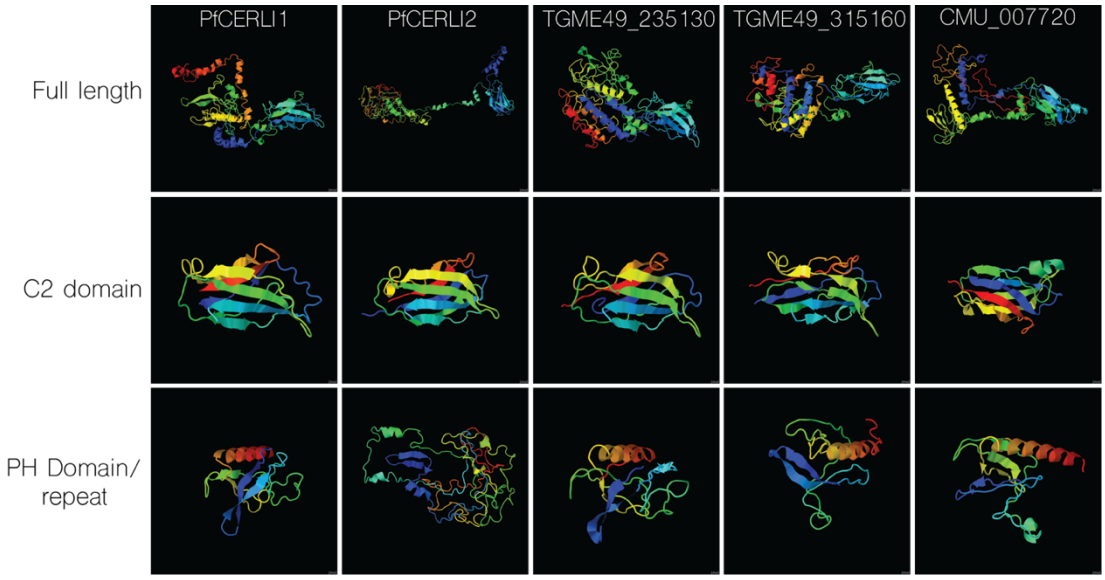

Supplementary Figure 5: Predicted protein structures of CERLI1, CERLI2 and their homologues.

Full length protein structure of PfCERLI1, PfCERLI2, their T. gondii homologues (TGME49_235130 and TGME49_315160), and their Cryptosporidium muris homologue (CMU_007720) was predicted using Phyre2. All proteins were predicted to have a C2 domain, and all proteins except PfCERLI2 were also predicted to contain a Pleckstrin homology (PH) domain. The N-termini are indicated in red, and progress in rainbow-order towards the C-termini in dark blue.

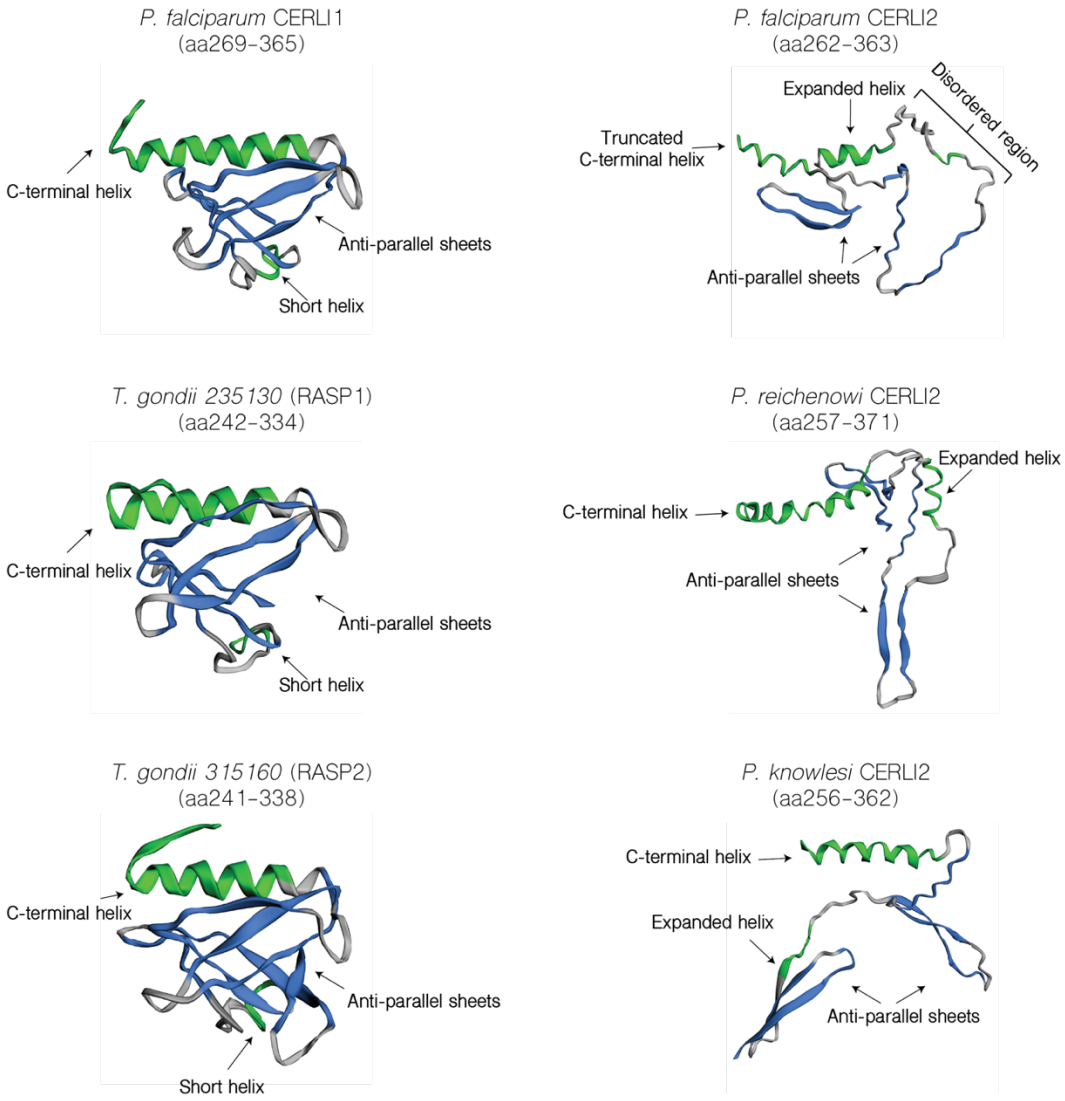

Supplementary Figure 6: Predicted structure of the PH domain region of PfCERLI2, PfCERLI1 and their homologues.

Full length protein sequences for PfCERLI1, PfCERLI2, along with both their homologues in Toxoplasma gondii, and the homologues of CERLI2 in Plasmodium reichenowi and Plasmodium knowlesi, were predicted using Phyre2. The PH domain region of those structures was visualised using EzMol. Region of each protein depicted are shown in brackets. Green = alpha-helix, blue = beta-strand, grey = coil.

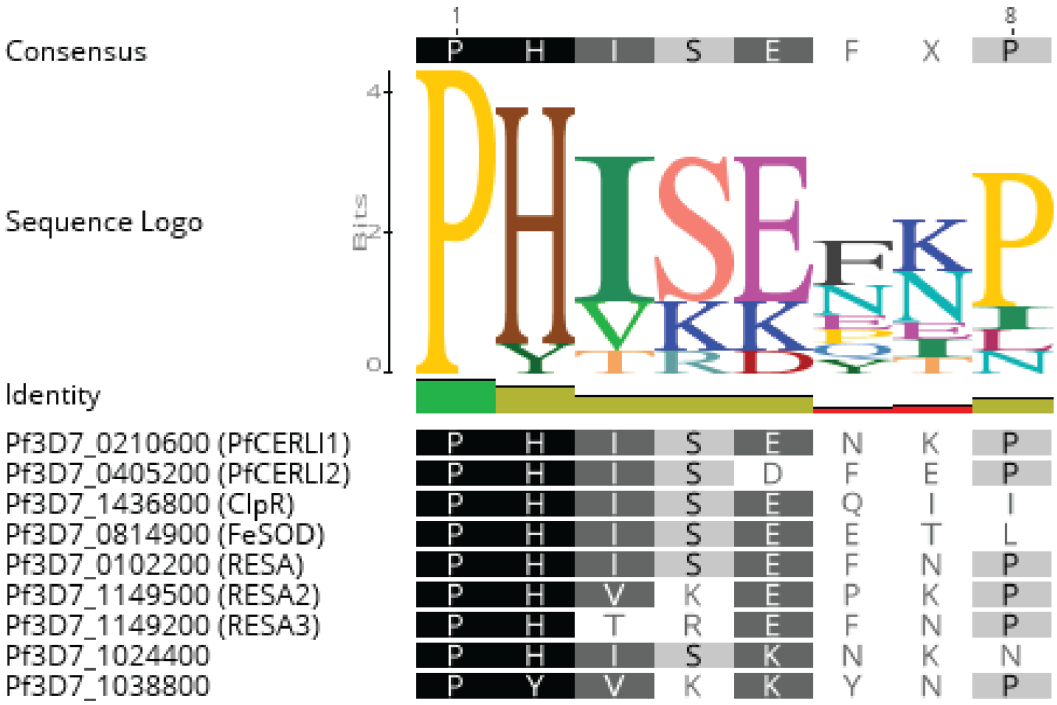

Supplementary Figure 7: PHIS consensus sequence of *P. falciparum* PHIS-containing proteins.

Consensus sequence and conservation of the PHIS motif for PHIS-containing proteins of P. falciparum.

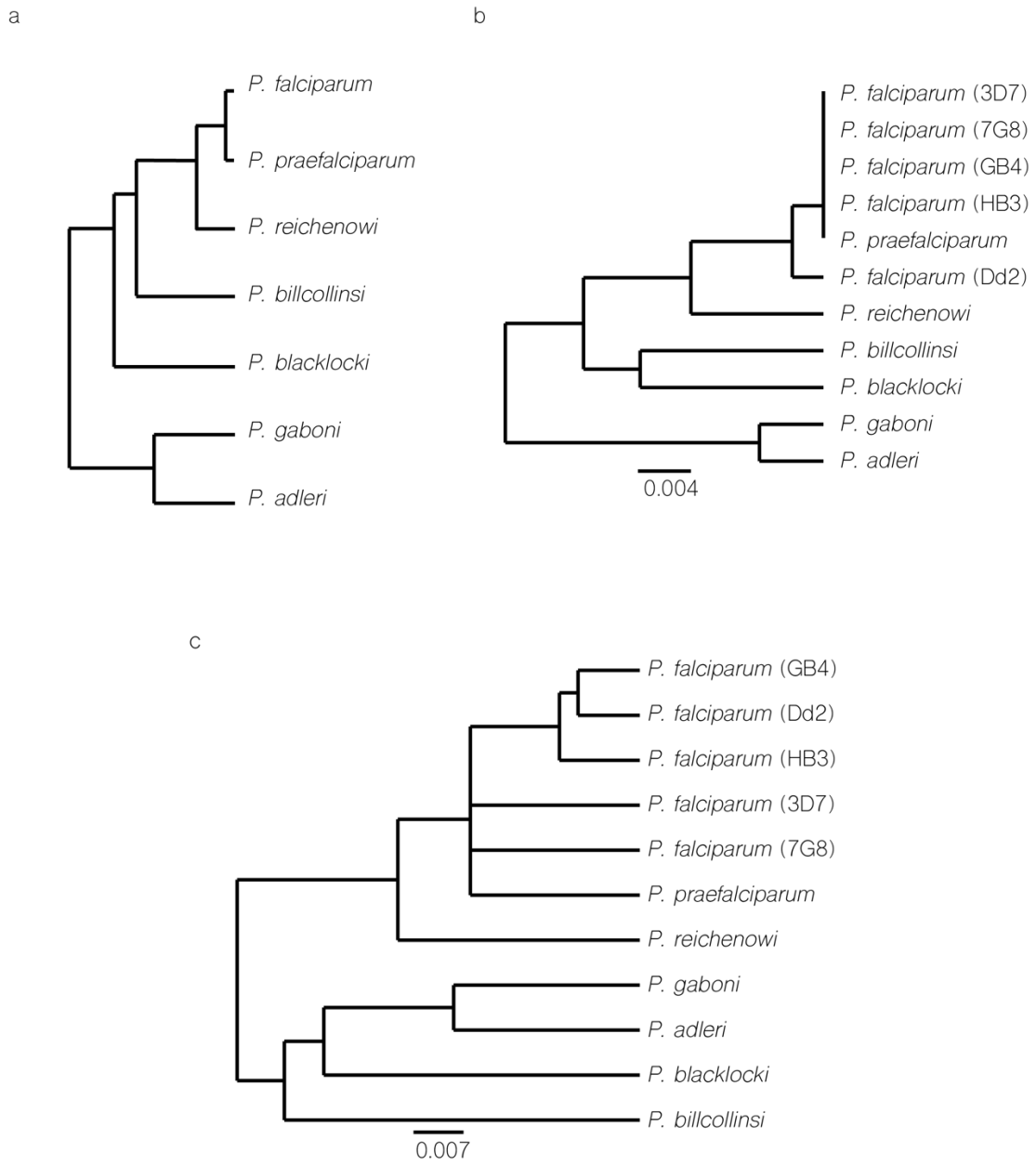

Supplementary Figure 8: The decapeptide repeat of PfCERLI2 is under differential selection in *Laverania*.

(a) *Cladogram of relationships between Laverania as determined by Otto et al., Nat. Microb. 2018.* ***(b)*** *Phylogenetic tree of PfCERLI2 and its homologues in Laverania and multiple P. falciparum isolates when the decapeptide repeat region of each protein has been removed.* ***(c)*** *Phylogenetic tree of full length PfCERLI2 and its homologues in Laverania and multiple P. falciparum. Scale bars = amino acid substitutions per site. Phylogenetic trees constructed using unweighted pair*

group method with arithmetic mean (UPGMA). Branch length corresponds to amino acids substitutions per site.

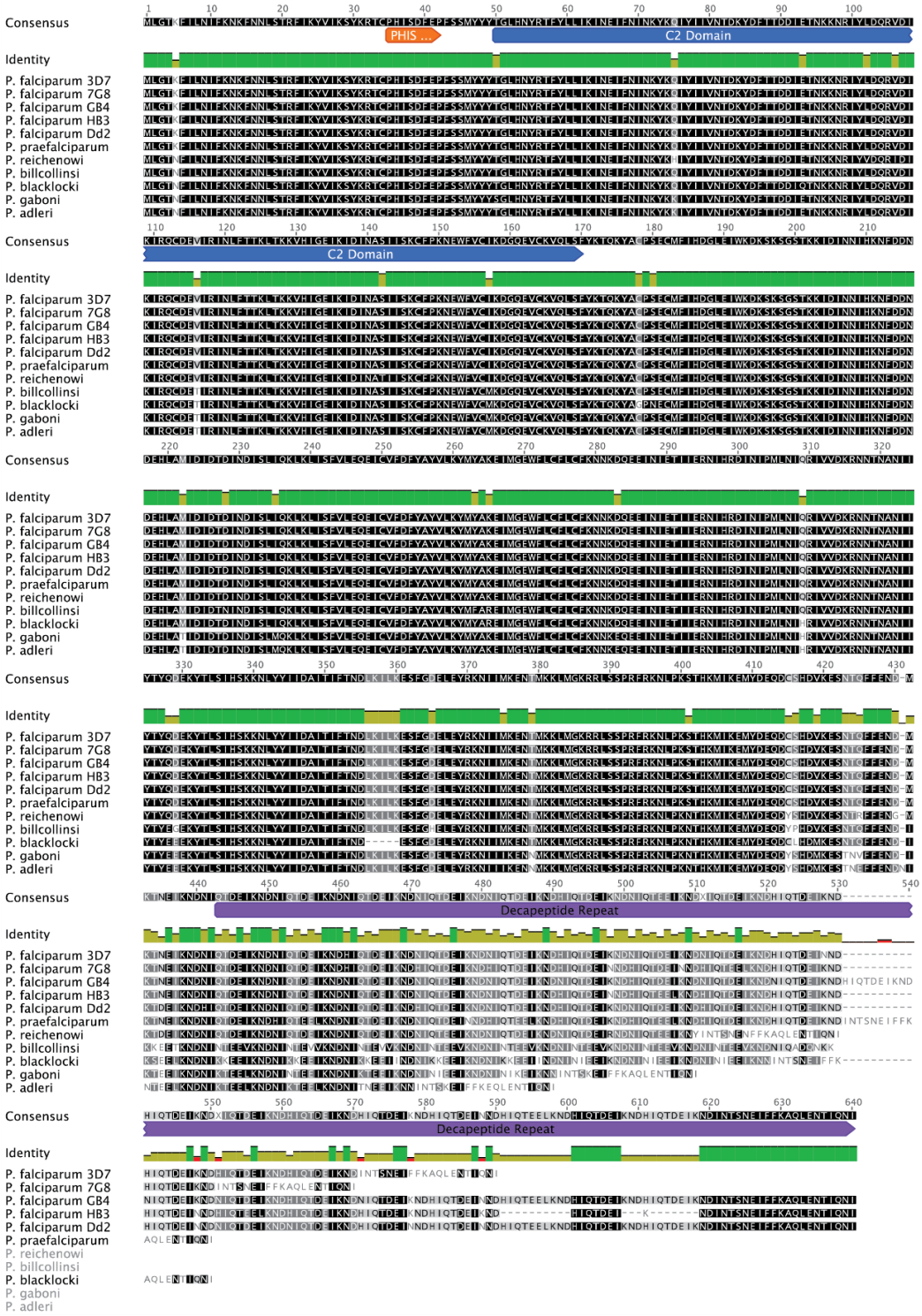

Supplementary Figure 9: Alignment of PfCERLI2 and its homologues in Laverania.

Geneious global alignment with free-end gaps between full length PfCERLI2 in Laverania and multiple P. falciparum isolates.

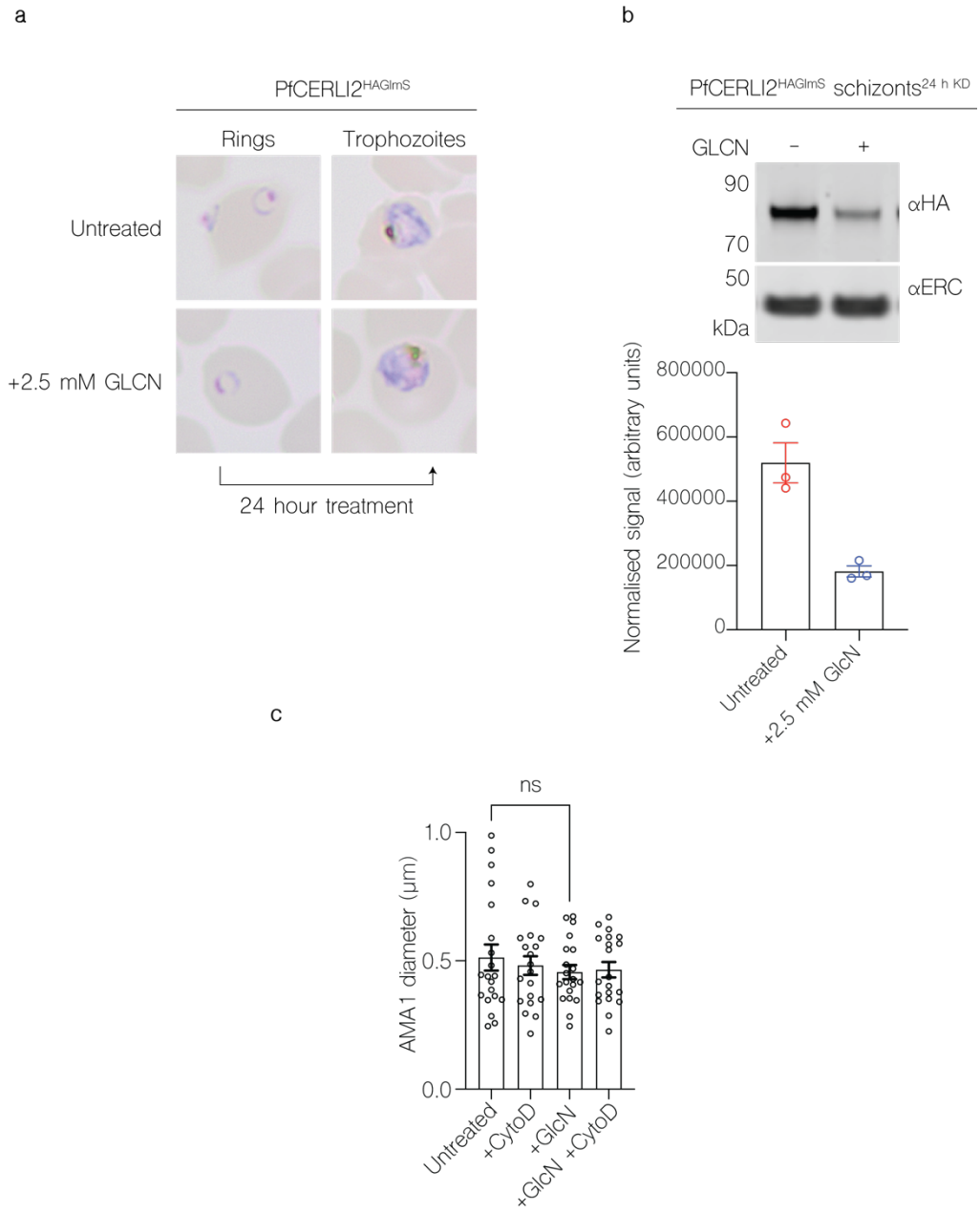

Supplementary Figure 10: Assessment of PfCERLI2^{HAGlmS} expression, growth and invasion under GLCN-inducible knockdown or inhibitive treatment.

(a) *PfCERLI2^{HAGlmS} ring stages (0-6 hrs) were treated with 2.5 mM GLCN or left untreated, and allowed to grow for 24 hours into trophozoites (24-30 hrs). Samples were smeared onto glass slides, blinded and imaged by light microscopy (n=5 images taken per condition, two biological replicates). Representative micrographs show no obvious defects in trophozoite morphology in response to GLCN treatment.* ***(b)*** *PfCERLI2^{HAGlmS} trophozoites (24 hrs) were treated with 2.5 mM GLCN or left untreated, allowed to grow until schizonts had fully developed to quantify PfCERLI2 GLCN-inducible knockdown over a 24 hour period. Densitometry shows a 65% reduction in PfCERLI2 signal (n=3 biological replicates).* ***(c)*** *PfCERLI2^{HAGlmS} ring stages were treated with 2.5 mM GLCN or left untreated, allowed to mature into schizonts in the presence of E64 and purified as free merozoites. Free merozoites, with or without GLCN-induced knockdown of PfCERLI2, were permitted to invade RBCs treated with or without 1 µM cytochalasin D. This graph represents the full data set presented in Figure 3 of the manuscript without exclusions. n=20 merozoites in a single biological replicate, ns=p>0.05 by unpaired t-test. Error bars = SEM.*

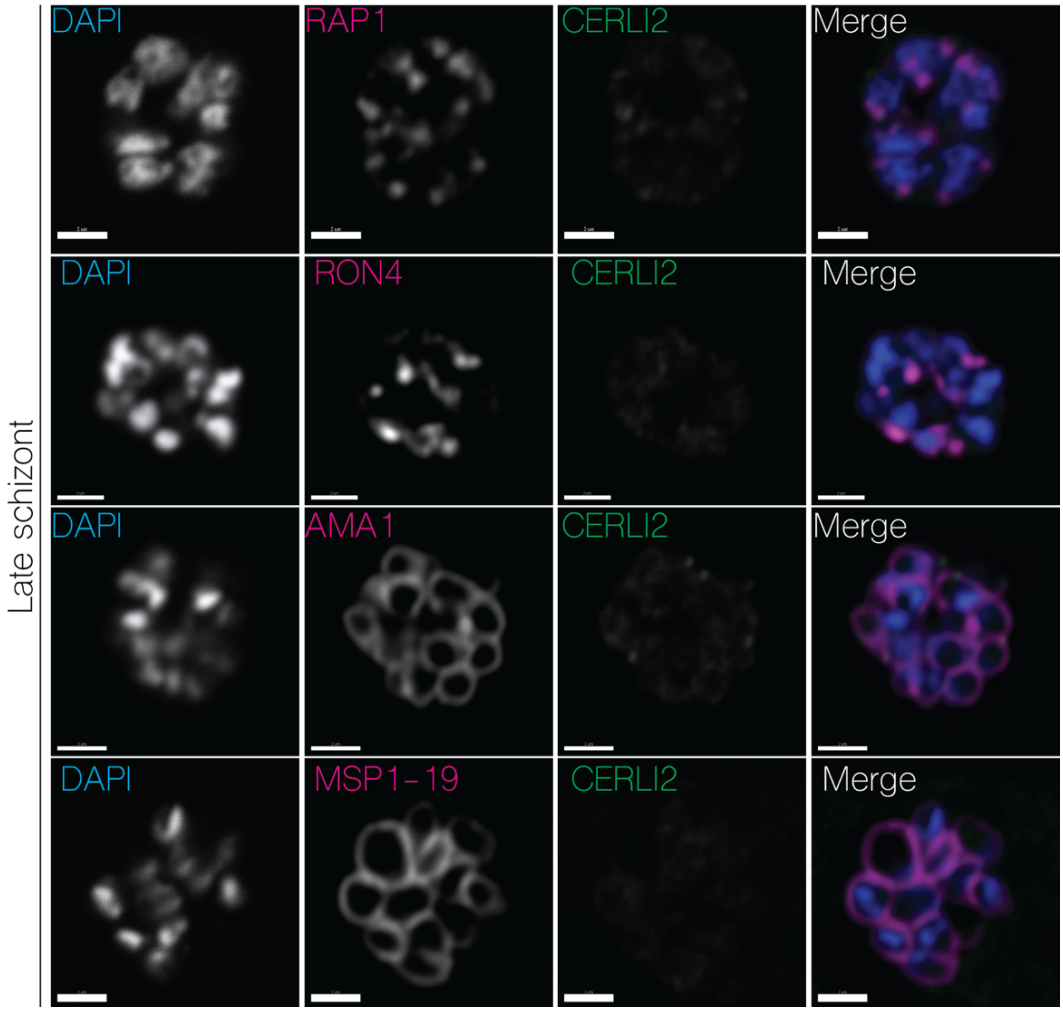

Supplementary Figure 11: Immunofluorescence microscopy of PfCERLI2 in late schizonts shows reduced CERLI2 signal.

Immunofluorescence microscopy of either late PfCERLI2^{HAGlmS} schizonts stained with DAPI (nucleus) and anti-HA (PfCERLI2) antibodies, along with antibodies to either RAP1 (rhoptry bulb, RON4 (rhoptry neck), AMA1 (micronemes), or MSP1-19 (merozoite surface). Scale bar = 2 µm

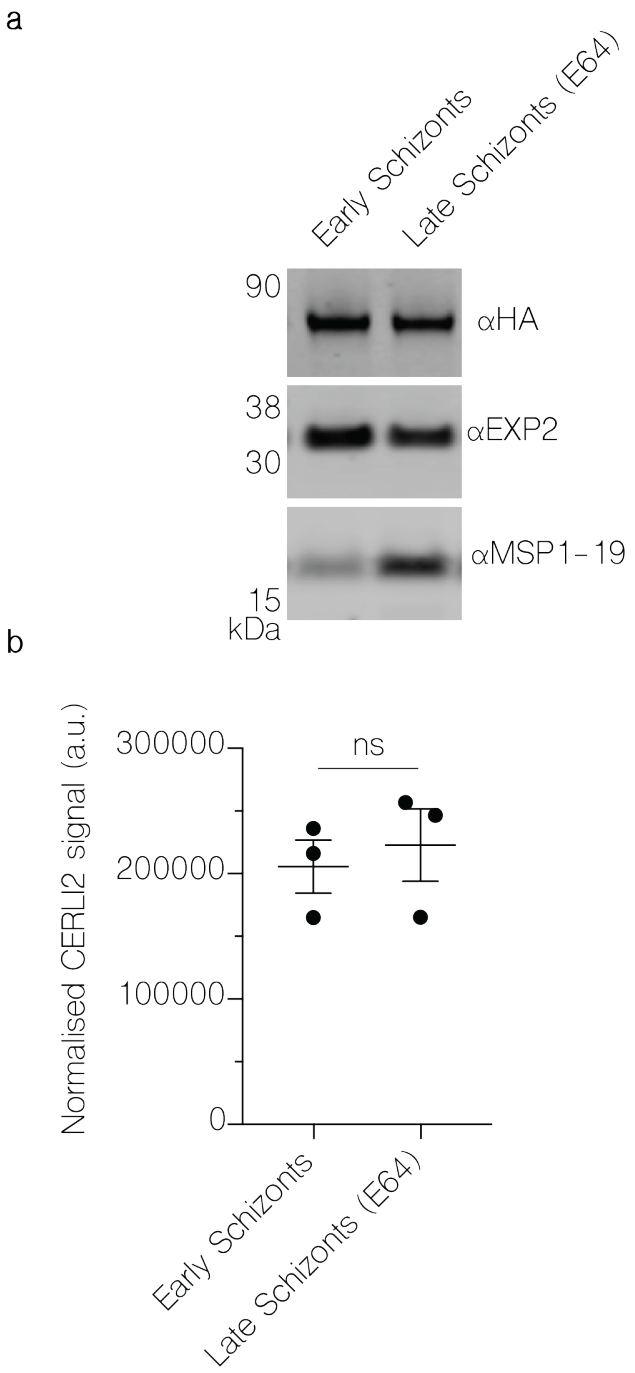

Supplementary Figure 12: Western blot of early and late PfCERLI2^{HAGlmS} schizonts.

(a) *PfCERLI2^{HAGlmS} parasite lysates were either harvested for Western blot as early schizonts (~44 hours post invasion), or matured in the presence of E64 and harvested as late schizonts (~48). Lysates were probed with either anti-HA (PfCERLI2), anti-EXP2 (loading control), or anti-MSP1-19 (schizont maturity*

control) antibodies. Image representative of 3 biological replicates. ***(b)*** *Quantification of PfCERLI2 signal, normalised to EXP2, for both early and late schizonts. n=3, ns=p>0.05 by unpaired t-test. Error bars = SEM.*

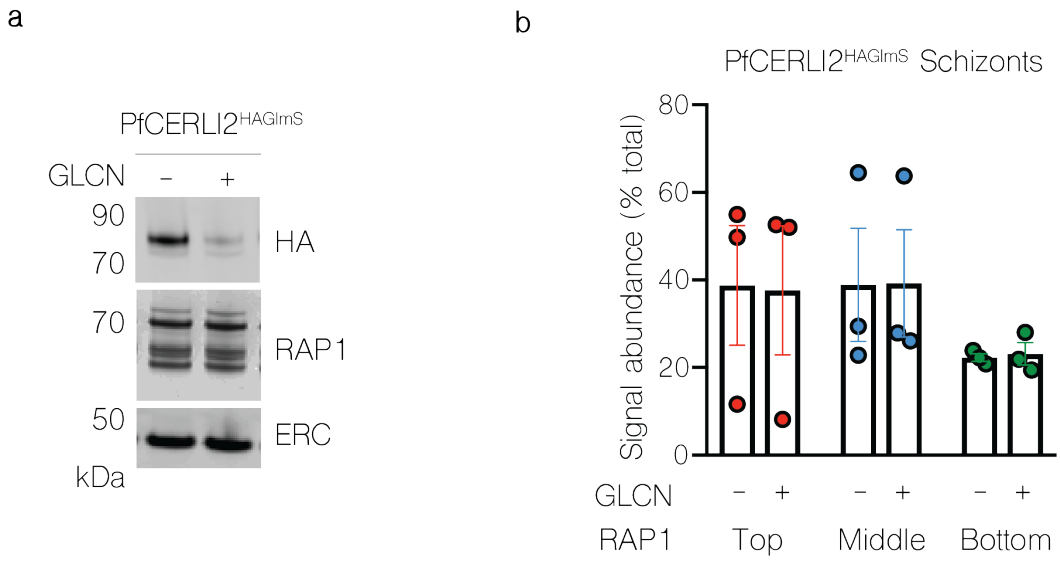

Supplementary Figure 13: PfCERLI2 knockdown does not alter RAP1 processing in C1 arrested schizonts.

(a) *PfCERLI2^{HAGlmS} parasites were either treated with 2.5 mM GLCN or left untreated, before being matured in the presence of C1 to prevent PVM rupture. Parasite lysates were then prepared and probed with anti-HA (PfCERLI2), anti-RAP1 (rhoptry bulb), and anti-ERC (loading control) antibodies. Images representative of 3 biological replicates.* ***(b)*** *Quantification of individiual band intensities, as a percentage of the total signal, from RAP1 signals using the parasite lysates from the secretion assay. n=3 biological replicates. Error bars = SEM.*

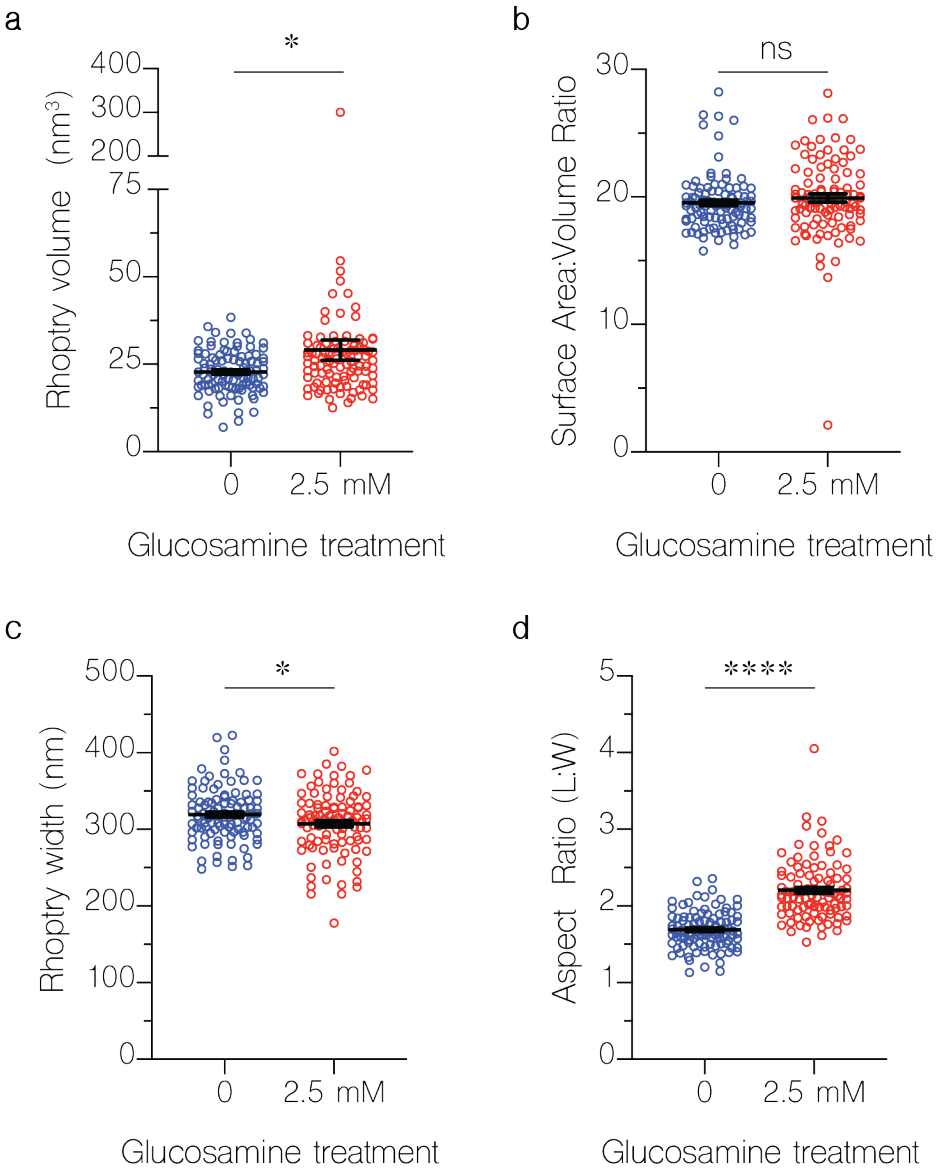

Supplementary Figure 14: PfCERLI2 knockdown grossly alters rhoptry morphology.

PfCERLI2^{HAGlmS} parasites were either treated with 2.5 mM GLCN, or left untreated, from ring-stages and arrested at schizont stages using C1. These parasites were then imaged by serial block face scanning electron microscopy (SBF-SEM) array tomography. 100 rhoptries for each treatment were segmented, with their volume ***(a)****, surface are to volume ratio* ***(b)****, width* ***(c)****, and length to width aspect ratio* ***(d)*** *calculated. Error bars = SEM. ns = p>0.05, *=p<0.05, ****=p<0.0001 by unpaired t-test.*

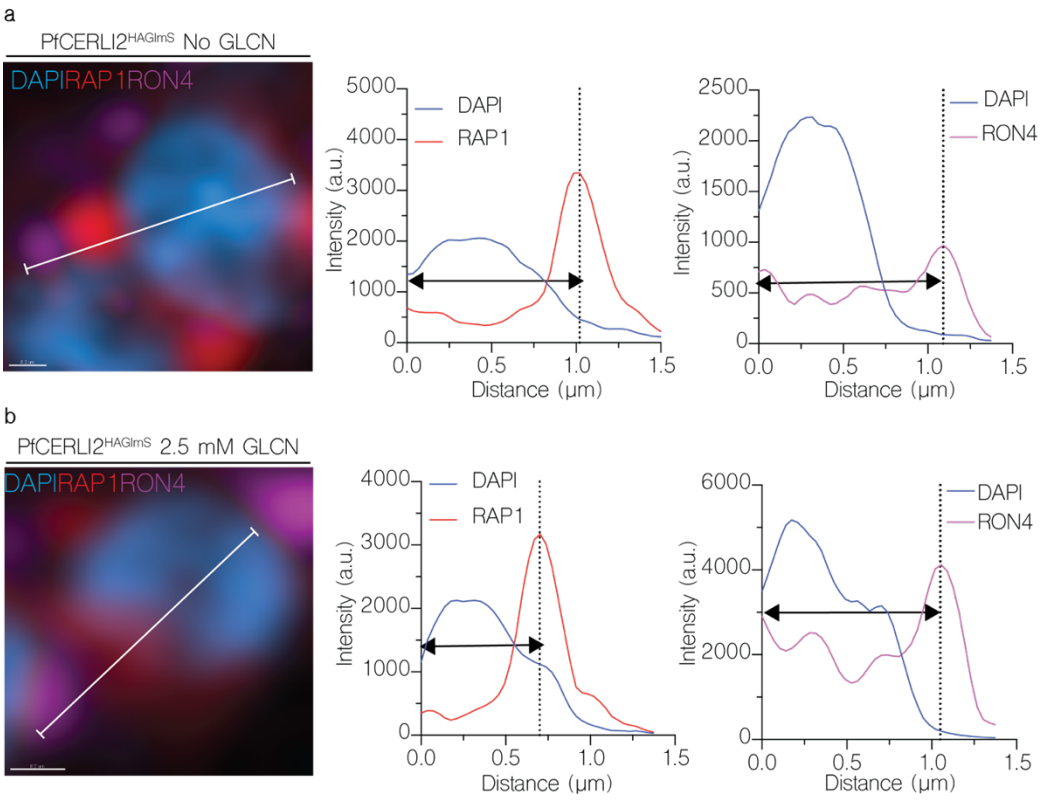

Supplementary Figure 15: Knockdown of PfCERLI2 alters rhoptry antigen positioning and distribution.

PfCERLI2^{HAGlmS} schizonts were matured in the presence of E64, stained with antibodies against RAP1 (rhoptry bulb) and RON4 (rhoptry neck), and imaged by Airyscan super-resolution microscopy. The flourescence intensity from maximum-intensity projections of RAP1 and RON4 signals were then measured from the basal end of the nucleus and plotted against merozoite length for parasites that were either left untreated ***(a)*** *or treated with 2.5 mM GLCN* ***(b)****. Dashed lines = RAP1/RON4 maximum fluorescence intensity.*

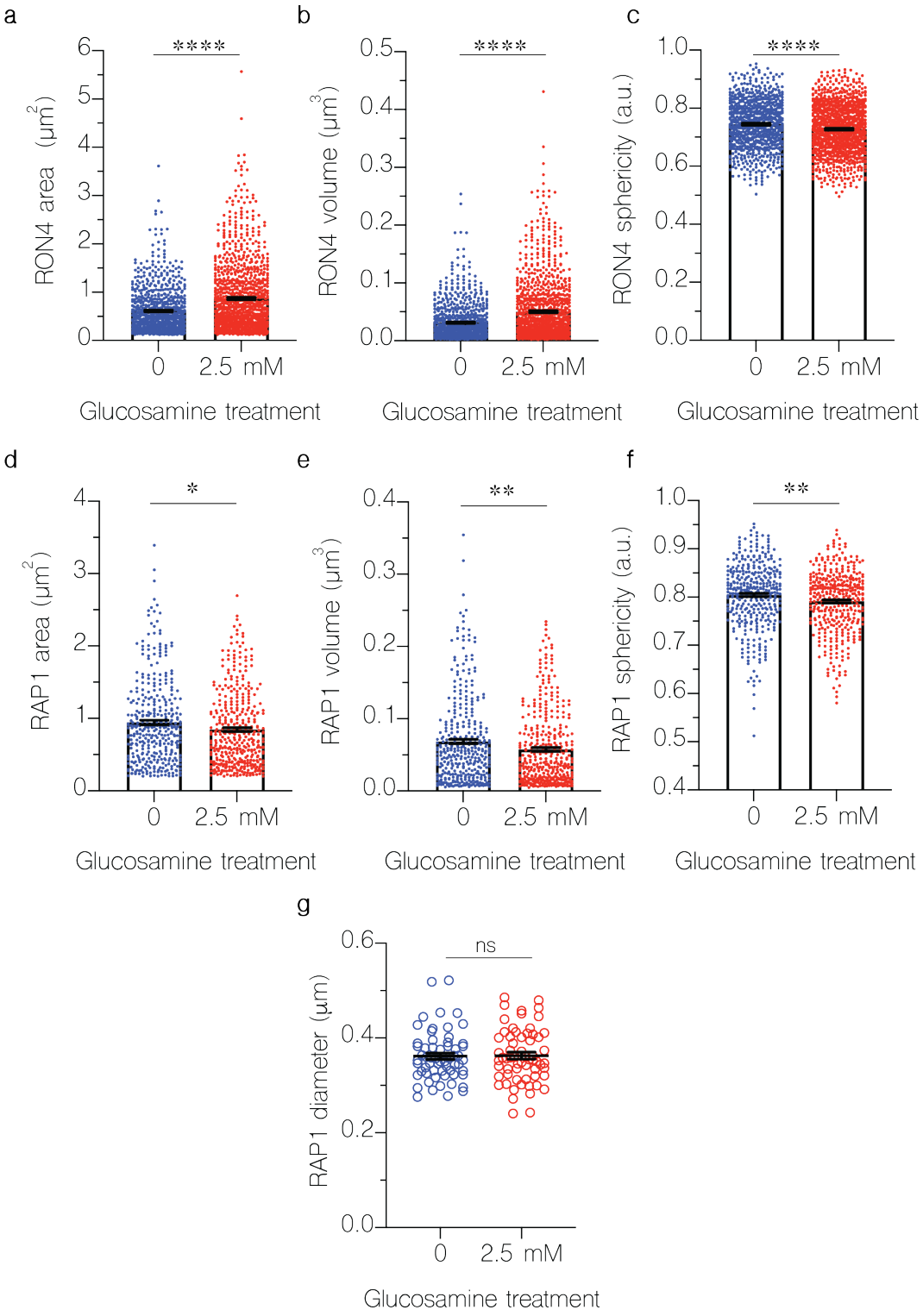

Supplementary Figure 16: PfCERLI2 knockdown alters the distribution of rhoptry markers.

PfCERLI2^{HAGlmS} parasites were either treated with 2.5 mM GLCN from ring-stages until schizont stages, or left untreated. Schizonts were then matured in the

presence of the egress inhibitor E64. Parasites were then stained with DAPI, anti-RAP1 (rhoptry bulb), and anti-RON4 (rhoptry neck) antibodies, and analysed by Airyscan super-resolution microscopy. RON4 foci area ***(a)****, volume* ***(b)*** *and sphericity* ***(c)****, along with RAP1 foci area* ***(d)****, volume* ***(e)****, and sphericity* ***(f)*** *were then quantified using an established automated image analysis pipeline for these markers*[1]*. 779 foci quantified for RON4 untreated, 1042 foci quantified for RON4 + 2.5 mM GLCN, 367 foci quantified for RAP1 untreated, 386 foci quantified for RAP1 + 2.5 mM GLCN.* ***(g)*** *Images of the same parasites were then blinded and the rhoptry bulb diameter (RAP1 signal) measured, with each datapoint representing a single rhoptry. 60 rhoptries were measured for untreated parasites, and 62 for + 2.5 mM GLCN parasites. N= 3 biological replicates, all error bars = SEM, ns = p>0.05, * = p<0.05, ** = p<0.01, **** = p<0.0001 by unpaired t-test.*

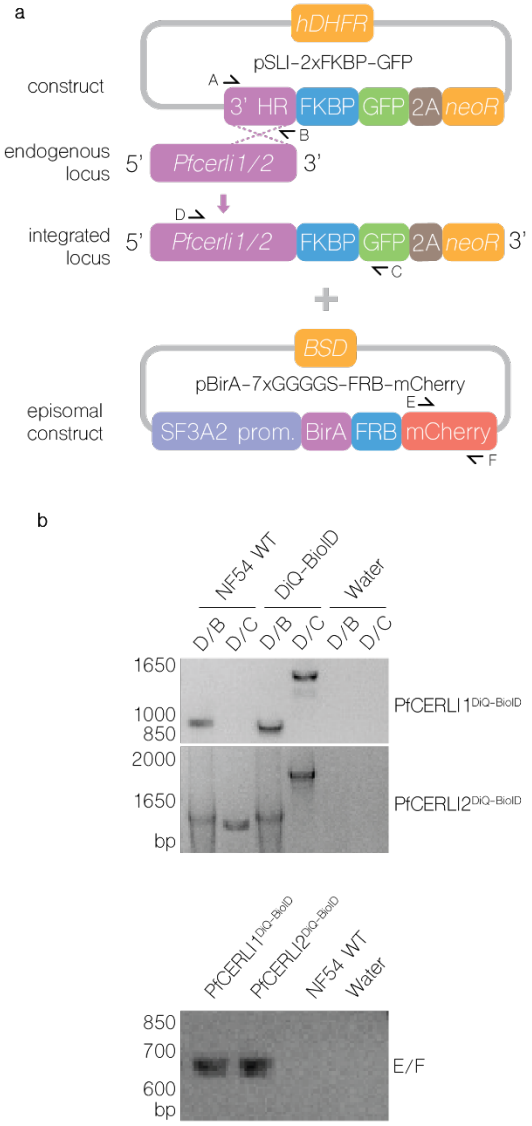

Supplementary Figure 17. Gene editing strategy for generating *Pfcerli1*$^{\text{DiQ-BioID}}$ and *Pfcerli2*$^{\text{DiQ-BioID}}$ parasite lines.

(a) PfNF54 parasites were first transfected with a selection-linked integration (SLI) construct used for endogenously integrating an FKBP-GFP tag onto the C-termini of PfCERLI1 and PfCERLI2. This was followed by transfection with an episomal construct expressing an FRB-mCherry tagged BirA biotinylator. (b) Confirmation of SLI construct integration and episomal maintenance of the biotinylator plasmid by PCR. Primer positions are denoted by arrows in (a).

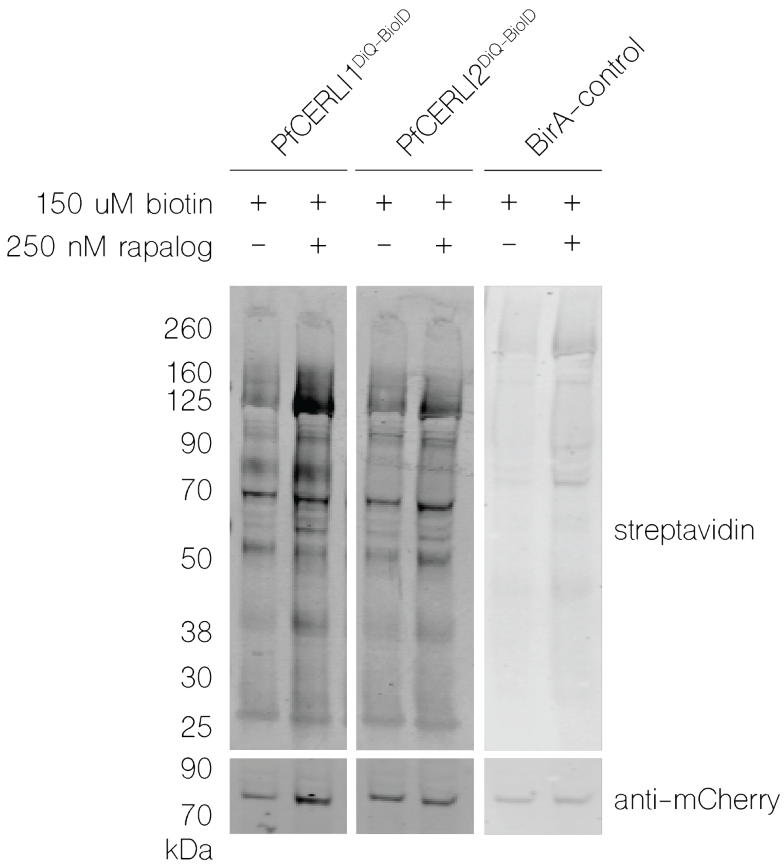

Supplementary Figure 18. Western blot of all test and control groups used for DiQ-BioID of PfCERLI1 and PfCERLI2.

Blot was probed with a streptavidin-conjugated IRDye800 to visualise biotinylated proteins, and an anti-mCherry antibody to visualise the BirA-FRB-mCherry fusion protein at approximately ~70 kDa.

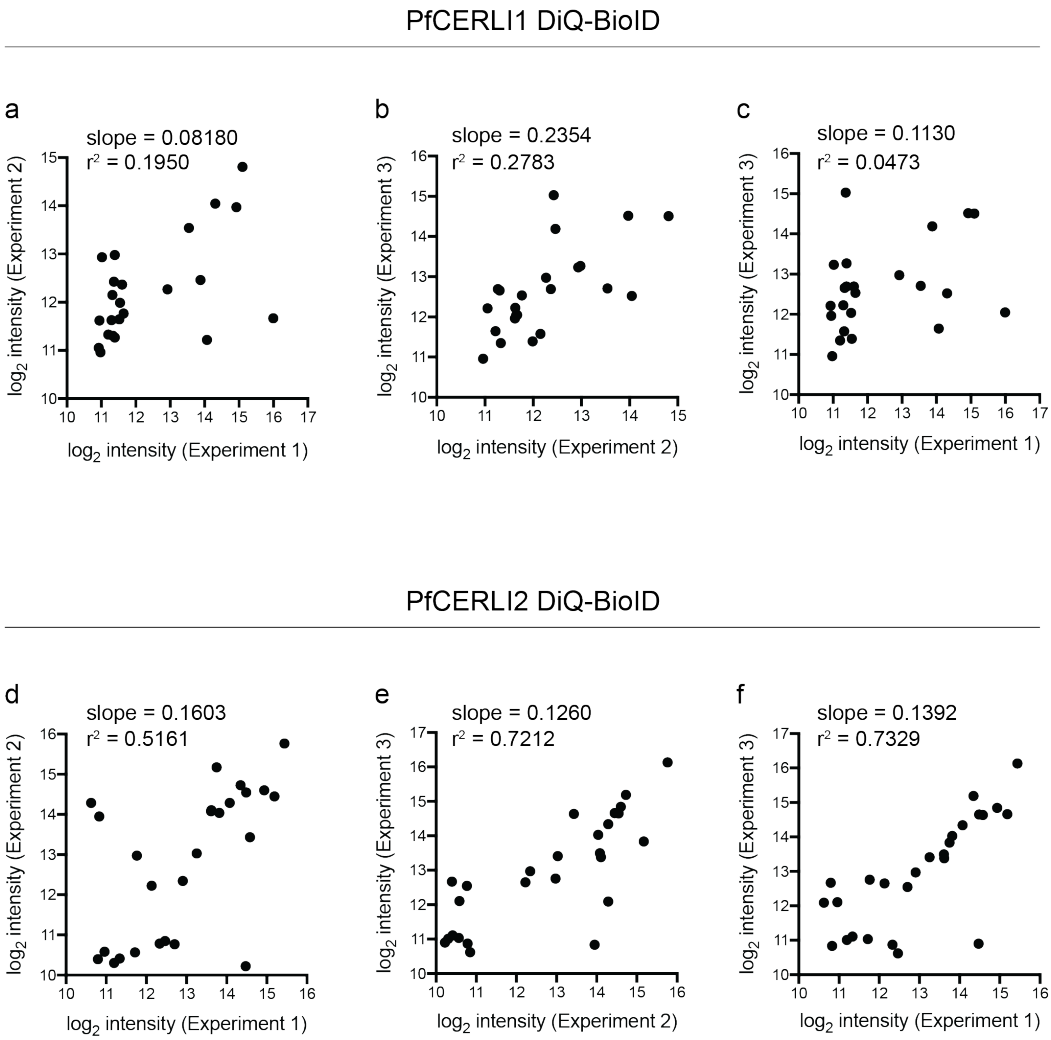

Supplementary Figure 19. Assessment of experimental reproducibility by linear correlation for dimerization inducible quantitative biotin identification (DiQ-BioID) intensity (abundance) values for: (a-c) PfCERLI1 and (d-f) PfCERLI2 for proteins identified with at least 2 peptides and 10% or greater library coverage, present in samples treated with both biotin and rapalog. Data represents all three biological replicates for each protein. Slopes and R^2 values calculated by linear regression. The slopes for each set of experiments were statistically different to a slope of zero by unpaired t-test: (a-c) $p = 0.0377$, (d-f) $p < 0.0001$.

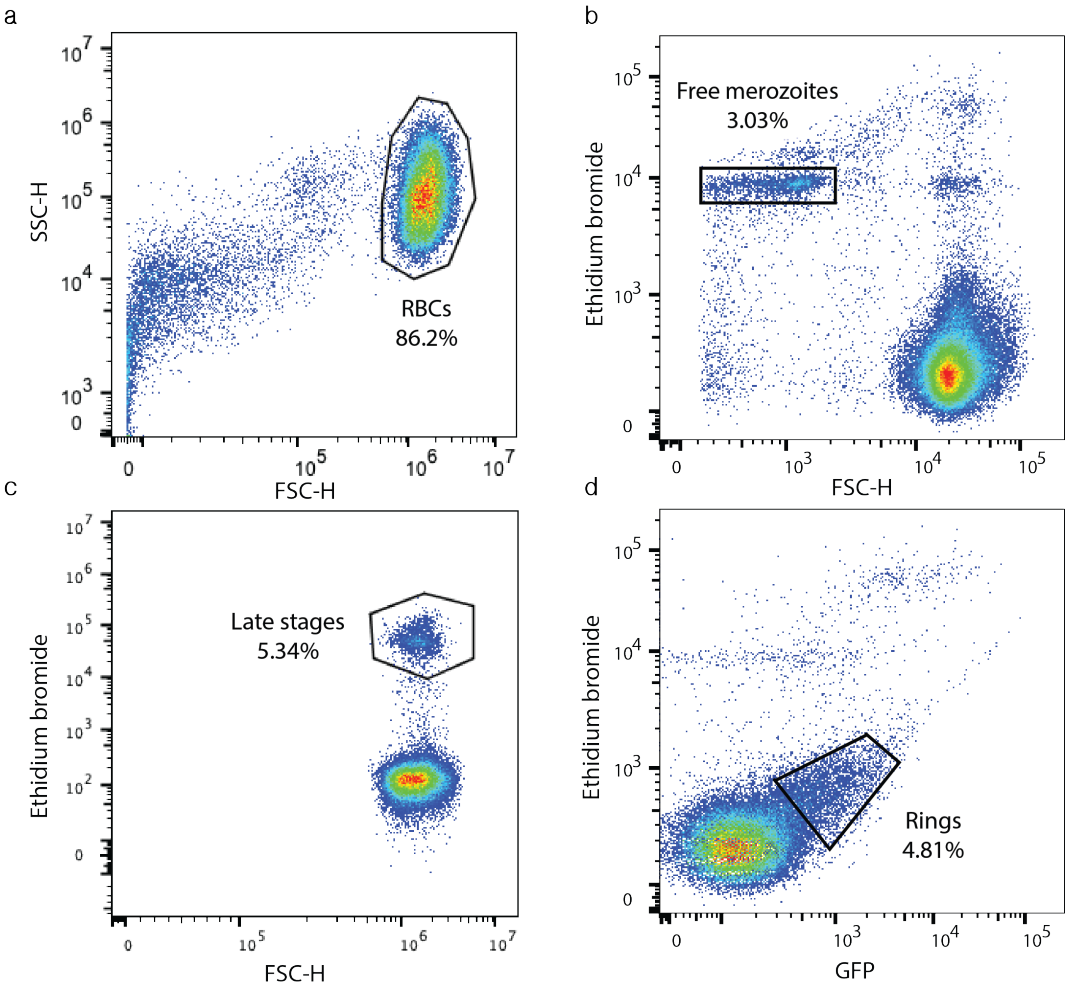

Supplementary Figure 20: Representative flow plots showing gating strategies for flow cytometry experiments performed in this study.

Plots were exported from FlowJo Version 10. (a), gating for red blood cells (RBCS) (b) free merozoites (c), late-stage parasites, including trophozoites and schizonts (d), GFP-fluorescent ring stage parasites.

Supplementary tables, which are in Excel format, are accessible at the following link:

https://www.biorxiv.org/content/10.1101/2020.11.26.400549v2.supplementary-material

Chapter 3

Characterisation of PfCZIF1 and PfCZIF2 in *Plasmodium falciparum* asexual stages

Statement of Authorship

Title of Paper	Characterisation of PfCZIF1 and PfCZIF2 in *Plasmodium falciparum* asexual stages
Publication Status	☐ Published ☐ Accepted for Publication ☐ Submitted for Publication ☑ Unpublished and Unsubmitted work written in manuscript style
Publication Details	

Principal Author

Name of Principal Author (Candidate)	Juan Miguel Balbin
Contribution to the Paper	Designed and planned the study, performed experiments, generated reagents and data, manuscript writing.
Overall percentage (%)	70%
Certification:	This paper reports on original research I conducted during the period of my Higher Degree by Research candidature and is not subject to any obligations or contractual agreements with a third party that would constrain its inclusion in this thesis. I am the primary author of this paper.
Signature	Date 10.9.21

Co-Author Contributions

By signing the Statement of Authorship, each author certifies that:

i. the candidate's stated contribution to the publication is accurate (as detailed above);

ii. permission is granted for the candidate in include the publication in the thesis; and

iii. the sum of all co-author contributions is equal to 100% less the candidate's stated contribution.

Name of Co-Author	Gary Heinemann
Contribution to the Paper	Generated transfectant parasite lines.
Signature	Date 22-9-21

Name of Co-Author	Lee Yeoh
Contribution to the Paper	Assisted with bioinformatic analyses for RNAseq.
Signature	Date 21/9/21

Please cut and paste additional co-author panels here as require

Name of Co-Author	Mark Armstrong		
Contribution to the Paper	Assisted with bioinformatic analyses for RNAseq.		
Signature		Date	22/09/21

Name of Co-Author	Paul Gilson		
Contribution to the Paper	Study design and planning.		
Signature		Date	10/09/21

Name of Co-Author	Danny Wilson		
Contribution to the Paper	Study design and planning, performed analysis and generated reagents, manuscript writing.		
Signature		Date	9/9/2021

Name of Co-Author	Michael Duffy		
Contribution to the Paper	Study design and planning.		
Signature		Date	20-9-2021

Name of Co-Author			
Contribution to the Paper			
Signature		Date	

Name of Co-Author			
Contribution to the Paper			
Signature		Date	

Characterisation of PfCZIF1 and PfCZIF2 in *Plasmodium falciparum* asexual stages

Juan M. Balbin[1], Gary K. Heinemann[2], Lee Yeoh[3], Mark Armstrong[4], Michael Duffy[3], Paul Gilson[5], Danny W. Wilson[1,5*]

[1]Research Centre for Infectious Diseases, School of Biological Sciences, University of Adelaide, Adelaide 5005, Australia.

[2]Experimental Therapeutics Laboratory, School of Pharmacy & Medical Sciences, University of South Australia Cancer Research Institute, Adelaide 5005, Australia.

[3]Department of Biochemistry and Molecular Biology, Bio21 Molecular Science and Biotechnology Institute, The University of Melbourne, Melbourne 3010, Victoria, Australia.

[4]University of South Australia, Adelaide 5005, Australia.

[5]Burnet Institute, Melbourne 3004, Victoria, Australia.

* Corresponding author

E-mail: danny.wilson@adelaide.edu.au

Abstract

Plasmodium falciparum exerts high temporal control of gene expression across its lifecycle. Proteins expressed exclusively during late schizogony of blood stages, for example, often have a role in facilitating merozoite invasion of the host red blood cell (RBC), through merozoite development, egress, invasion or early establishment of infection in the RBC. Here, we characterise the schizont expressed *P. falciparum* C3H1 zinc finger 1 (PfCZIF1, Pf3D7_1468400) and *P. falciparum* C3H1 zinc finger 2 (PfCZIF2, Pf3D7_0818100). Bioinformatic analyses have shown these to be the only C3H1-type zinc finger proteins with peak expression at schizogony and antibodies against PfCZIF1 have previously been reported to inhibit merozoite invasion, suggesting these proteins have a potential role during RBC invasion and may be exposed to inhibitory antibodies on the merozoite surface. C-terminal truncations and gene knockouts of each of *Pfczif1* and *Pfczif2* indicated that neither are essential for blood stage growth. However, they could not both be knocked out simultaneously, suggesting that at least one is needed for parasite growth *in vitro*. Immunofluorescence localisation of PfCZIF1 and PfCZIF2 indicated that both proteins occur in discrete foci on the periphery of the parasite's cytosol and biochemical assays suggest they are peripherally associated to a membrane. Transcriptomic analyses for the C-terminal truncation mutants reveal no significant expression perturbations with PfCZIF1 truncation. However, modification of PfCZIF2 appears to be linked with earlier and higher levels of expression for some exported proteins including PfKAHRP. This study does not support a role for PfCZIF1 or PfCZIF2 in merozoite invasion of the RBC and suggests that these proteins may help regulate the expression of proteins exported into the RBC cytosol after merozoite invasion.

Introduction

Plasmodium falciparum is a major threat to global health accounting for most malaria-related morbidities and the bulk of the ~400,000 malaria related deaths per year (WHO 2020). The parasite is transmitted to humans during a blood meal when infected *Anopheles* mosquitoes inoculate sporozoites which travel to the liver and infect hepatocytes (Matuschewski 2006). Within the hepatocyte, the parasite grows and divides into several thousand merozoites which are then released into the blood and invade red blood cells (RBCs) (reviewed in Cowman *et al.* 2016).

Disease causing blood stage parasites grow and divide over the next 48 hours to form a schizont containing 16-32 daughter merozoites, which ruptures to allow the merozoites to infect new RBCs (Wickham *et al.* 2003).

Merozoite invasion of the RBC is a rapid and dynamic process. It begins with a weak non-specific attachment of the merozoite to the RBC (Das *et al.* 2015, Cowman *et al.* 2017), followed by reorientation of its apical tip to interact with the RBC membrane (Riglar *et al.* 2011, Volz *et al.* 2016). Invasion proteins are then secreted from the apical organelles, the rhoptries and micronemes, leading to establishment of the irreversible tight junction that commits the merozoite to invading the host cell (Riglar *et al.* 2011). Invasion proceeds with the merozoite enveloping the RBC membrane around itself to form the parasitophorous vacuole within which the growing blood stage parasites resides (PV) (invasion reviewed in Cowman *et al.* 2012). Proteins essential for merozoite invasion are considered attractive targets for vaccines (Beeson *et al.* 2016) and drugs (Burns *et al*. 2019) that would stop multiplication of disease-causing blood stage parasites. Merozoite vaccine targets typically have two key defining characteristics. First, they are temporally controlled to be expressed at schizogony so that the parasite concentrates its resources towards assembling a proteome that is functionally focused towards merozoite invasion. Second, these proteins localise to an invasion-relevant space such as the merozoite surface, rhoptries or micronemes.

Pf3D7_1468400 (which we designate as *P. falciparum* C3H1 zinc finger 1 (PfCZIF1)), is a protein that is reported to broadly meet the characteristics of a merozoite vaccine candidate. Originally called D13, PfCZIF1 was reported to have peak expression at schizogony with a merozoite surface localisation using anti-D13 monoclonal antibodies (MAb), and parasite growth could be reduced by these antibodies *in vitro* (Daubenberger *et al.* 2003). For these reasons, Pf3D7_1468400 was reported to be exposed on the surface of the merozoite and proposed as a potential blood stage vaccine candidate (Daubenberger *et al.* 2003).

PfCZIF1 is annotated as a zinc finger domain-containing protein with three N-terminal C-x(8)-C-x(5)-C-x(3)-H (C3H1) zinc finger domains (ZnF, collectively herein referred to C3H1 ZnF). ZnFs are characterised by a conserved arrangement

of cysteines and histidines in a ~20 amino acid chain to coordinate a single zinc ion to form a stabilised structure capable of recognising and binding nucleic acids (Hall 2005). Across eukaryotes, the C3H1 class of ZnFs are canonically known to bind the AU-rich stretches in the 3' untranslated region (3'UTR) of messenger RNA (mRNA) (Hudson *et al.* 2004, Wells *et al.* 2015), and typically require tandem (two or more) C3H1 ZnFs to fulfil this function (Brown 2005), which are structural features exhibited by PfCZIF1. While the majority of ZnFs are involved in nucleic acid binding, several ZnFs in *P. falciparum* have been documented with atypical functions. These include RNF5 and HRD1 which are E3 ligases involved in ubiquitination, and PfPHD1 and PfPHD2 which form the SAGA complex to bind histones (reviewed in Ngwa *et al.* 2021). Although these examples are not C3H1 ZnFs, this still left open the possibility that PfCZIF1 itself possesses an atypical molecular role, and given its expression pattern, may be involved in merozoite invasion of RBCs. Here, we also identified a structurally related protein, PfCZIF2 (Pf3D7_0818100) with similar peak schizont stage of expression and investigated the function of both PfCZIF1 and PfCZIF2 in parasite growth. Using a range of genetically-modified *P. falciparum* lines, we characterise PfCZIF1 and PfCZIF2 stage-specific protein expression and localisation across the blood stage, domain-specific functions and their impact on the transcriptome at schizogony.

Results

Bioinformatic identification of *P. falciparum* C3H1-type ZnFs in schizonts

PfCZIF1 (Pf3D7_1468400), originally designated as D13, is an 862 amino acid, 99.7 kDa schizont-expressed protein with a central pentapeptide tandem repeat region with the repeat residues (K/R)(N/S)(D/E)N(I/M/T) of twelve repeat units in 3D7 (Daubenberger *et al.* 2003). To predict the presence of other unidentified protein domains in Pf3D7_1468400, we submitted its amino acid sequence to the ExPASY PROSITE web-based service (Sigrist *et al.* 2002), confirming that PfCZIF1 harboured three predicted tandem N-terminal C3H1 ZnFs, with no other distinct domain structures identified using this program. Additionally, a coiled-coil region was predicted in Pf3D7_1468400 in ExPASY COILS (Gasteiger *et al.* 2003) (Figure 1a).

In order to identify other potential C3H1 ZnFs expressed at schizogony, a bioinformatic approach was used to identify genes with a predicted consensus C-x(8)-C-x(5)-C-x(3)-H (C3H1) ZnF motif on PlasmoDB using a nested search strategy and gene ontology (GO) terms (Figure 1b). Genes were first filtered across the entire *P. falciparum* 3D7 genome for the text term "zinc finger" which searches for GO terms across all annotations before being subject to a second filter searching for the text term "C3H1" or the synonymous motif name "CCCH" – resulting in 25 C3H1-type zinc finger-encoding genes. These 25 were then enriched for genes with non-uniform peak transcriptional expression at schizogony using a blood stage expression exclusion filter. Briefly, the RNA-seq transcriptional profiles of (Otto *et al.* 2010) were applied to the 25 gene set to select genes with a ten-fold increase in expression from trophozoite stage (defined as 24-32 hours) to schizogony (defined as 40-48 hours) – the output resulting in two genes (Pf3D7_1468400, Pf3D7_0818100), which we now call *Pfczif1* and *Pfczif2* respectively. To ensure we did not miss any other C3H1 ZnF-expressing genes, we also executed this search strategy to identify proteins with a five-fold expression change from trophozoites to schizonts. This yielded two additional genes, Pf3D7_1210200 and Pf3D7_1220000. However, these genes had higher expression in ring stages than in schizonts and were subsequently excluded from further analysis.

PfCZIF2 is a 538 amino acid protein with a calculated molecular weight of 63.6 kDa. A BLAST search using PfCZIF1 as a reference revealed PfCZIF2 as the top hit, highlighting that PfCZIF2 shares the greatest level of sequence homology with PfCZIF1 across the *P. falciparum* proteome. Pairwise alignment of full-length PfCZIF1 with PfCZIF2 identified that they shared 20.1% amino acid identity. However, identity within the first 126 amino acids of PfCZIF1 and the first 162 amino acids of PfCZIF2, which covers the three C3H1 ZnF domains, reaches 50.6%, highlighting the high level of conservation at their N-termini. Analysing the amino acid sequence of PfCZIF2 on ExPASY PROSITE confirmed the likely presence of the three N-terminal C3H1 ZnFs, but the protein lacked any other notable domains, including the repeat region and coiled-coiled domains identified in PfCZIF1.

To compare the secondary and tertiary structures of each N-terminal region, the amino acid sequences for each protein were submitted to the Phyre2 web-based service in intensive mode (Kelley *et al.* 2015). *In silico* modelling predicted that the N-termini for each protein may fold similarly (Figure 1c). However, their whole protein structure could not be confidently predicted due to high levels of intrinsic sequence disorder, totalling 64% and 51% of PfCZIF1 and PfCZIF2's amino acids respectively (Supplementary Figure 1a, 1b). In mammalian systems, the secondary structures of C3H1 ZnFs canonically contain a short alpha-helix after the first cysteine and another short alpha-helix between the second and third cysteines (Hall 2005). Interestingly in PfCZIF2 one predicted alpha-helix is absent in the middle C3H1 ZnF. Pairwise alignment between the amino acid sequences for each gene identified a discrepancy in the C3H1 consensus in PfCZIF2 for the middle predicted C3H1 ZnF (relative to the other C3H1 ZnF domains of PfCZIF1) with a 37 amino acid insertion between the first and second cysteines. This discrepancy is arranged as a 25 amino acid insertion, followed by a short span of conserved residues, and an additional 12 amino acid insertion (Figure 1d). Put together, these data identify a second C3H1 ZnF containing protein with peak expression at schizogony, opening the possibility that both PfCZIF1 and PfCZIF2 have a role in merozoite development or invasion.

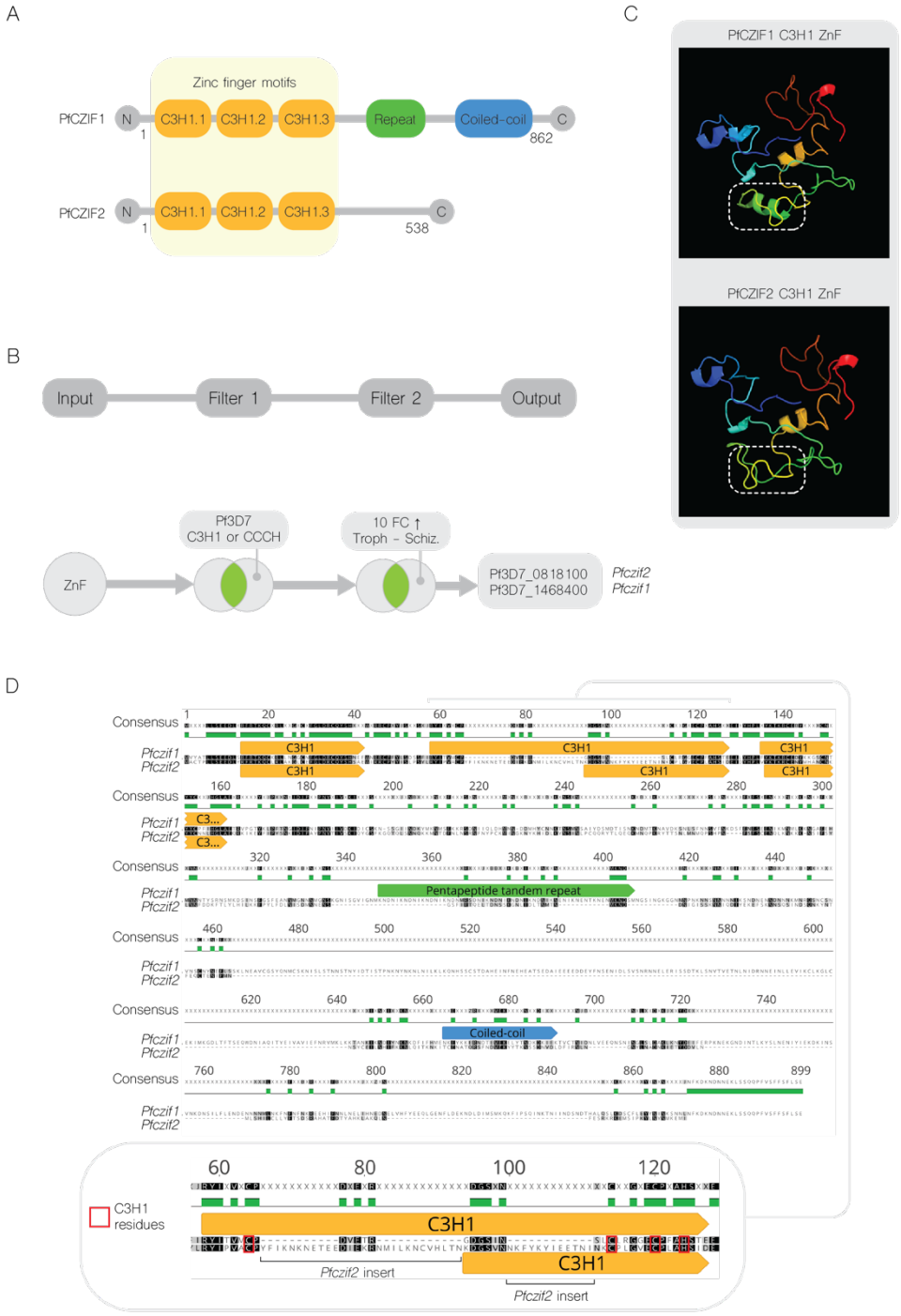

Figure 1. Bioinformatic identification of PfCZIF1 and PfCZIF2 as C3H1-type zinc finger proteins with sequence similarities at the protein level. (a) PfCZIF1 is 862 amino acids in length with three predicted tandem N-terminal C3H1-ZnF domains, a central pentapeptide repeat motif of (K/R)(N/S)(D/E)N(I/M/T) for twelve repeat units in 3D7 and a C-terminal coiled-coil region. PfCZIF2 is 538 amino acids in length, similarly with three predicted tandem N-terminal C3H1 ZnF

domains and no other identified motifs or regions. (b) Schematic of the PlasmoDB nested search strategy used to determine which C3H1 ZnFs were expressed at late schizogony, resulting in the identification of *Pfczif1* and *Pfczif2*. (c) Secondary protein structure predictions illustrating motif similarities in each of the tandem zinc fingers in PfCZIF1 and PfCZIF2 using Phyre2. Highlighted in the white dashed box is the PfCZIF1 helix which is predicted to be absent in PfCZIF2. (d) Amino acid sequences of PfCZIF1 and PfCZIF2 were compared using global pairwise alignment in Geneious revealing a 20.1% sequence similarity between the two proteins. Inset: sequence alignment revealed a 37 amino acid insert in the middle C3H1 ZnF for PfCZIF2 compared to PfCZIF1, resulting in the absence of the central helix. Black shading indicates identities, grey similarities.

The N-terminal regions of PfCZIF1 and PfCZIF2 are conserved amongst *Plasmodium* spp.

PfCZIF1 exhibits high sequence conservation, contributed mostly by its N-terminal C3H1 ZnFs, with other *Plasmodium* species, suggesting a tightly conserved function of these domains. Sequence comparison between 21 strains of *P. falciparum* showed 97% sequence identity across full length protein (Supplementary Figure 1e). When comparing the first 126 amino acids, which encompass the C3H1 ZnF domains in PfCZIF1, 92% of residues were identical between 11 analysed species (Supplementary Figure 1c). In comparison, residues beyond this which encompass the PfCZIF1 pentapeptide repeat region have relatively poor sequence homology (Supplementary Figure 1c). In the original characterisation of PfCZIF1, it was noted that the pentapeptide tandem repeat was absent in the predicted orthologues of *P. knowlesi* (PKNH_1213800) and *P. yoelii* (PY02869) (Daubenberger *et al.* 2003). We expand on this and show that it is also absent in predicted orthologues of *P. berghei* (PBANKA_1331700), *P. cynomolgi* (PCYB_124660), *P. gallinaceum* (PGAL8A_00227800), *P. inui* (C922_00098), *P. malariae* (PmUG01_12048500), *P. ovale curtisi* (PocGH01_12046400) and *P. vivax* (PVX_117045) (Supplementary Figure 2). Interestingly, this repeat, as well as the predicted coiled-coil domain, is present in the predicted orthologues of the chimpanzee-infective species *P. reichenowi* (PRCDC_1467600) and the gorilla-infective species *P. praefalciparum* (PPRFG01_1469000) which are both

phylogenetically close relatives of *P. falciparum*, suggesting a late evolutionary manifestation of this repeat region in *Laverania* parasites (Supplementary Figure 2).

PfCZIF2 exhibits a lower level of sequence conservation when compared to homologues of other *Plasmodium* species, with highest homology primarily located at the N-terminal C3H1 ZnFs. Like PfCZIF1, PfCZIF2 is conserved between strains of *P. falciparum* across its whole sequence, with 97% overall sequence identity across 21 strains (Supplementary Figure 1e). Sequence comparison by pairwise alignment of PfCZIF2 homologues in *P. berghei* (PBANKA_0712700), *P. cynomolgi* (PCYB_052360), *P. gallinaceum* (PGAL8A_00111100), *P. inui* (C922_02584), *P. knowlesi* (PKNH_0501900), *P. malariae* (PmUG01_05032900), *P. ovale curtisi* (PocGH01_05022800), *P. praefalciparum* (PPRFG01_0819600), *P. reichenowi* (PRCDC_0817400), *P. vivax* (PVX_089510) and *P. yoelii* (PY03958) (Supplementary Figure 1d) showed 60% identity across the first 162 amino acids, 32% lower than what was observed across the region compassing the C3H1 ZnF domains of PfCZIF1's homologues. This is largely owed to a lack of conservation in the region between the first two conserved cysteines of the C3H1 consensus as shown earlier with 37 additional amino acids in the middle C3H1 ZnF domain (Figure 1d). This region possesses a low pairwise identity of 63.7% across all CZIF2s (Supplementary Figure 3). Despite this, the cysteine and histidine residues that are coordinate zinc binding are completely conserved between species, as expected if they are required for C3H1 ZnF function (Supplementary Figure 3).

Put together, these analyses show that sequence conservation is primarily focused around the C3H1 ZnF domains of each protein, across strains of *P. falciparum* and between *Plasmodium* species, emphasising the importance of this region for PfCZIF1 and PfCZIF2.

PfCZIF1 and PfCZIF2 do not localise to the merozoite surface

Transcriptomic and protein expression evidence suggests that PfCZIF1 and PfCZIF2 are most highly expressed at schizogony, but protein expression data for PfCZIF1 indicates that protein remains detectable up until trophozoite stages in the next blood stage lifecycle (Otto *et al.* 2010, Daubenberger *et al.* 2003). To study the proteins' expression and localisation, we integrated a HA-tag to into the C-termini of PfCZIF1 and PfCZIF2 to generate the lines PfCZIF1^{HA} and PfCZIF2^{HA} and confirmed successful integration in the endogenous loci by PCR (Supplementary Figure 4).

We confirmed by timepoint protein harvests across the *P. falciparum* blood stage lifecycle and western blotting that HA-tagged PfCZIF1 (~100 kDa) is indeed most abundant in schizonts (Figure 2a), and the same is observed for HA-tagged PfCZIF2 (~70 kDa) (Figure 2c). Obtaining a signal for each protein by western blot was a technical challenge given their low expression, requiring several rounds of optimisation at the levels of cell culture, sample preparation, primary and secondary antibody titration, to reliably detect and quantify. PfCZIF1 was previously reported to be largely undetectable in trophozoites, consistent with our data in late trophozoites (24-32 h.p.i.) (Daubenberger *et al.* 2003) though lower levels are expressed in early trophozoites (12-18 h.p.i.) (Figure 2a). We speculate perhaps that while each protein is most highly expressed at schizonts, a substantial amount may be carried into the next invasion cycle up to the point of trophozoite development, and then rapidly declining in late trophozoites until expression rises to its highest level at schizogony.

Simultaneously with these timepoint harvests, parasites were fixed for IFA and imaged by confocal microscopy to determine the localisation of each protein across the blood stage lifecycle. Previous IFAs reported that PfCZIF1 localised broadly across the schizont but with a slightly polarised localisation in free merozoites using MAbs which targeted against the first 139 N-terminal amino acids, a region that spans all three C3H1 ZnF domains (Daubenberger *et al.* 2003). Given that this MAb was designed to target an epitope that encompasses several C3H1 ZnF domains, there remains the possibility that it is cross-reactive with other C3H1

ZnFs, including PfCZIF2. Likewise, given the claim that this MAb inhibits growth, it may have bound C3H1 ZnFs which are expressed at other lifecycle stages. Therefore, we approached localisation using our HA-tag approach to ensure target specificity towards PfCZIF1 and PfCZIF2.

Consistent with our earlier detection issues, obtaining immunofluorescence localisation data for HA-tagged PfCZIF1 and PfCZIF2 proved difficult given that each protein is lowly expressed. Several commercially available antibodies to probe for HA-tagged PfCZIF1 were trialled. In order to bolster target-specific signal, we optimised our experiments with biotin-conjugated anti-HA primary antibodies and a streptavidin-conjugated AlexaFluor488 as a secondary probe to boost the fluorescence signal without increasing noise. We were then able to consistently detect HA-tagged PfCZIF1 as distinct puncta in rings and early trophozoites, with some evidence of staining even in late trophozoites. In schizonts, the most notable signals remained diffuse puncta, with no clear evidence of co-localisation with MSP1 on the merozoite surface. At all developmental stages, a small number of PfCZIF1 foci appeared to localise near to, but not overlapping with, the dense granule (in merozoites)/parasitophorous vacuole membrane (PVM) marker EXP2 in rings, trophozoites and schizonts, PfCZIF1 tended to lie internal to EXP2 PVM staining, suggesting that PfCZIF1 resides within the parasite membrane. In schizonts, PfCZIF1 foci often resided close to EXP2 containing dense granules.

We observed a similar localisation pattern for PfCZIF2. At rings, early and late trophozoites, PfCZIF2 puncta appear to localise near to, but under, the PVM indicated by EXP2 (Figure 2d). Similarly, in schizonts the signal accumulates in a distinct location for each merozoite and appears to condense with newly synthesised EXP2 as it is being packaged into the dense granules. However, at no stage does PfCZIF2 completely co-localise with EXP2 (Figure 2d). Likewise, PfCZIF2 does not appear to localise to the merozoite surface at any lifecycle stage. Control experiments in wild-type parasites suggest that these signals are specific to HA-tagged protein for both PfCZIF1 and PfCZIF2 (Supplementary Figure 5).

To determine whether these proteins localised to other membranous compartments in merozoites within the schizont, we attempted co-localisation using

anti-RON4 (merozoite rhoptry/apical tip), anti-ERC (endoplasmic reticulum) and anti-ERD2 (Golgi). No co-localising puncta were observed for these markers against HA-tagged PfCZIF1 or PfCZIF2 (Supplementary Figure 6a, 6b). These data suggest that HA-tagged PfCZIF1 and PfCZIF2 localise to two different areas of the parasite during blood stage development - in puncta underneath the parasite plasma membrane during ring and trophozoite stages, and near dense granules in merozoites.

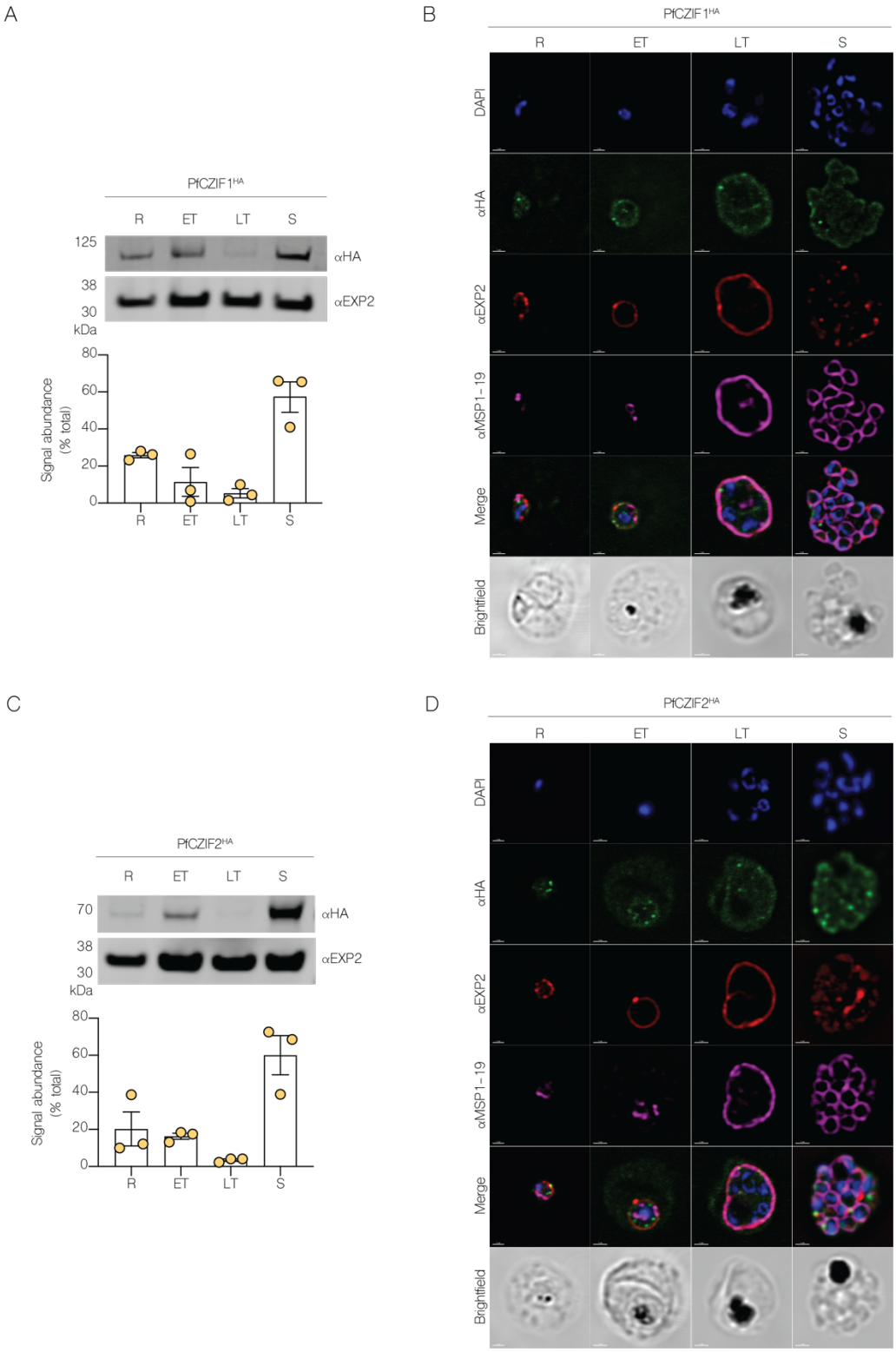

Figure 2. PfCZIF1 and PfCZIF2 are highly expressed in schizonts and localise in distinct puncta at different stages of development.

Parasite cultures were saponin harvested at various hours post-invasion (h.p.i.) at rings (R, 0-6 h.p.i.), early trophozoites (ET, 12-18 h.p.i), late trophozoites (LT, 24-

32 h.p.i.) and schizonts (S, 40-44 hrs h.p.i. with E64 treatment) to determine the protein expression profile for each of (a) PfCZIF1 and (c) PfCZIF2 in asexual stages by Western blot using anti-HA antibodies. Blot was probed with anti-EXP2 as a loading control as it is expressed at equal levels throughout the blood stage lifecycle. n = 3 biological replicates, error bars = SEM, data presented as a % total of the sum of all signals across rings, early trophozoites, late trophozoites and schizonts. Concurrent with protein harvests, parasites were fixed for IFA of HA-tagged (b) PfCZIF1 and (d) PfCZIF2 at the same time points and imaged by confocal microscopy. Blue = DAPI, green = anti-HA (AlexaFluor488), red = anti-EXP2 (AlexaFluor 555), magenta = anti-MSP1-19 (AlexaFluor 694). Images representative of n = 3 biological replicates.

PfCZIF1 and PfCZIF2 associate with a membrane but remain susceptible to proteinase K cleavage

As PfCZIF1 and PfCZIF2 are predicted to harbour C3H1 ZnF domains and have no predicted transmembrane domains (Supplementary Figure 7) or signal peptides (Supplementary Figure 8), the most likely localisation of these proteins would be free in the cytosol where they can interact with mRNA, consistent with the role of C3H1 ZnFs in other systems (Hall 2005). However, as schizont-expressed proteins and with PfCZIF1 reported to be exposed to antibodies on the merozoite surface, an alternate hypothesis was that they may localise to invasion organelles and be secreted during RBC entry.

To determine whether PfCZIF1 and PfCZIF2 were associated with a membrane in schizonts, we performed protein solubility assays to fractionate HA-tagged PfCZIF1 and PfCZIF2 from the cytosol or a membrane depending on the solubilising strength of a given reagent (Figure 3c). Schizont PfCZIF1 was previously reported to be soluble in sodium carbonate, consistent in this study and an identical result was achieved for PfCZIF2. Sodium carbonate interrupts weak peripheral membrane interactions, suggesting that it may bind a membrane indirectly via protein-protein or protein-lipid mechanisms (Fujiki *et al.* 1982). To determine a possible mode of binding, we later predicted using GPS-Lipid (Xie *et*

al. 2016) that both PfCZIF1 and PfCZIF2 possess putative S-palmitoylation sites at their N-termini (Supplementary Figure 9).

Given we found that the membrane associated PfCZIF1 and PfCZIF2 regularly localised near to the dense granule protein EXP2 in schizonts, we performed proteinase K protection assays to investigate whether these ZnF proteins may reside within a membrane bound organelle such as the dense granule. Sequential membrane solubilisation followed by proteinase K digestion showed that both HA-tagged PfCZIF1and HA-tagged PfCZIF2 are both susceptible to proteinase K cleavage after permeabilization of the RBC and parasite plasma membrane with digitonin compared to the endoplasmic reticulum resident ERC control (Figure 3d). This suggests that PfCZIF1 and PfCZIF2 are not protected within a membrane-bound organelle in merozoites, such as the dense granules or rhoptries (Cabrera *et al.* 2012). Based on the localisation studies that suggest PfCZIF1 and PfCZIF2 reside within the bounds of the parasite plasma membrane, these results suggest that PfCZIF1 and PfCZIF2 are peripheral membrane associated and exposed to the parasite cytosol.

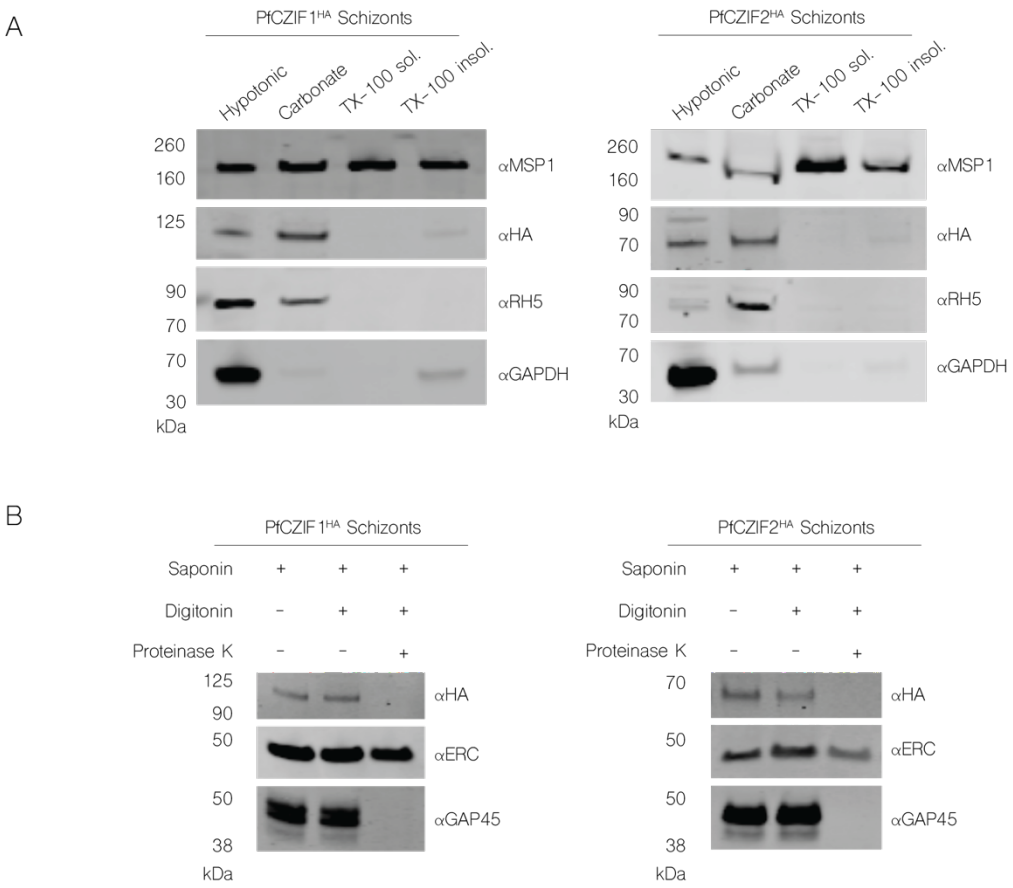

Figure 3. PfCZIF1 and PfCZIF2 are peripherally membrane-associated, cytosolically-exposed proteins.

(a) Protein solubility assays displayed that PfCZIF1 and PfCZIF2 are suggested to be peripherally associated to a membrane as they were mostly solubilised in sodium carbonate which disrupts weak protein-protein and protein-lipid interactions. Controls for a cytosolic (GAPDH), peripheral (RH5) and GPI-anchored (MSP1-19) protein were also probed. MSP1 also shows the presence of loaded protein in all wells. Example blots from n = 3 biological replicates. (b) Proteinase K protection assays revealed PfCZIF1 and PfCZIF2 to be cytosolically exposed proteins sensitive to proteinase K cleavage. ERC, localised to the endoplasmic reticulum lumen is protected whereas GAP45, localised to the inner membrane complex, is not. Example blots from n = 3 biological replicates.

PfCZIF1 and PfCZIF2 can be truncated but not deleted in tandem

To determine whether *Pfczif1* and *Pfczif2* were necessary for blood stage growth, we generated several gene-edited parasite lines to truncate each protein. First, we C-terminally truncated each of PfCZIF1 and PfCZIF2 such that they only expressed their N-terminal C3H1-ZnFs using selection linked integration-targeted gene disruption (SLI-TGD) to generate the mutant lines PfCZIF1$^{\Delta C\text{-term}}$ and PfCZIF2$^{\Delta C\text{-term}}$ (Figure 4a) (Spielmann *et al.* 2017). This truncation removed PfCZIF1's predicted pentapeptide tandem repeat and coiled-coil regions (Figure 4i). Each gene was disrupted successfully with PCR confirming only disrupted loci and lack of a wild-type amplicon (Figure 4b). To determine whether truncation of PfCZIF1 or PfCZIF2 affected parasite fitness, we measured the population expansion rate of cloned PfCZIF1$^{\Delta C\text{-term}}$ and PfCZIF2$^{\Delta C\text{-term}}$ parasites over 2 cycles and found no significant difference in growth compared to parental wildtype 3D7 (WT) (Figure 4c).

Using SLI-TGD we had established that the C-terminal regions of PfCZIF1 and PfCZIF2 are not essential for parasite growth, consistent with the suggested dispensability of *Pfczif1* and *Pfczif2* shown by random mutagenesis (Zhang *et al.* 2018). We also wished to validate if targeted truncation within the sequence encoding for the C3H1 ZnF domains was possible and thus we performed gene knockout in a way that removes two out of three C3H1 ZnFs from each protein using clustered regularly interspaced short palindromic repeats (CRISPR) Cas9 gene editing (Figure 4d). It is thought that at least two ZnF domains are required for C3H1 ZnF protein to function in an RNA binding capacity (Brown 2005). The most N-terminal C3H1 ZnF domain was left to serve as part of the short 5' flank for the repair plasmid integration. PCR confirmed that both PfCZIF1 and PfCZIF2 CRISPR-Cas9 knock-outs were successful, yielding the mutant lines PfCZIF1$^{C3H1\text{-}KO}$ and PfCZIF2$^{C3H1\text{-}KO}$ (Figure 4e). Population expansion of cloned PfCZIF1$^{C3H1\text{-}KO}$ and PfCZIF2$^{C3H1\text{-}KO}$ parasites over 2-cycles was measured and there was no reduction in growth compared to WT parasites (Figure 4f). Therefore, truncation of PfCZIF1 or PfCZIF2 individually is not deleterious to parasite growth. However, since both PfCZIF1 and PfCZIF2 have similar C3H1 ZnFs structures and both have

peak expression at schizogony, we hypothesised that the loss of one may be compensated for by the remaining function of the other.

To explore whether PfCZIF1 and PfCZIF2 could compensate for each other when one of these proteins was knocked-out, we generated mutants using a combination of SLI-TGD and CRISPR-Cas9 gene editing. We successfully generated the mutant lines PfCZIF1$^{\Delta C\text{-}term}$::PfCZIF2$^{C3H1\text{-}KO}$ and PfCZIF2$^{\Delta C\text{-}term}$::PfCZIF1$^{C3H1\text{-}KO}$, confirming truncations by PCR (Figure 4g) and assayed them over 2 cycles of growth. No difference in growth relative to wildtype was observed for PfCZIF1$^{\Delta C\text{-}term}$::PfCZIF2$^{C3H1\text{-}KO}$. From this experiment we conclude that if PfCZIF1 and PfCZIF2 have an important role in blood stage growth, then the N-terminal region of PfCZIF1 containing the three C3H1 ZnF domains is enough to compensate for the loss of all but the most N-terminal C3H1 ZnF domain in PfCZIF2. We observed an interesting contrast in the reverse situation with a growth defect for PfCZIF2$^{\Delta C\text{-}term}$::PfCZIF1$^{C3H1\text{-}KO}$. This suggests that the N-terminal region of PfCZIF2 containing the three C3H1-ZnF domains is insufficient to compensate for the loss of all but the most N-terminal C3H1-ZnF domain in PfCZIF1. This result suggested that PfCZIF1 and PfCZIF2 do have important roles in blood stage parasite growth, but it is likely the loss of one can compensate for the loss of the other. To confirm that having at least one of PfCZIF1 or PfCZIF2 is important for blood stage parasite growth, we attempted to produce a CRISPR-Cas9 double-knockout of PfCZIF2$^{C3H1\text{-}KO}$::PfCZIF1$^{C3H1\text{-}KO}$ in tandem that would truncate both proteins down to only a single C3H1 ZnF domain each. This attempt to knock-out the function of both genes failed, supporting that at least one of PfCZIF1 or PfCZIF2 is required for parasite growth. A schematic of our truncation strategies are illustrated in Figure 4j and Figure 4i for PfCZIF1 and PfCZIF2 respectively.

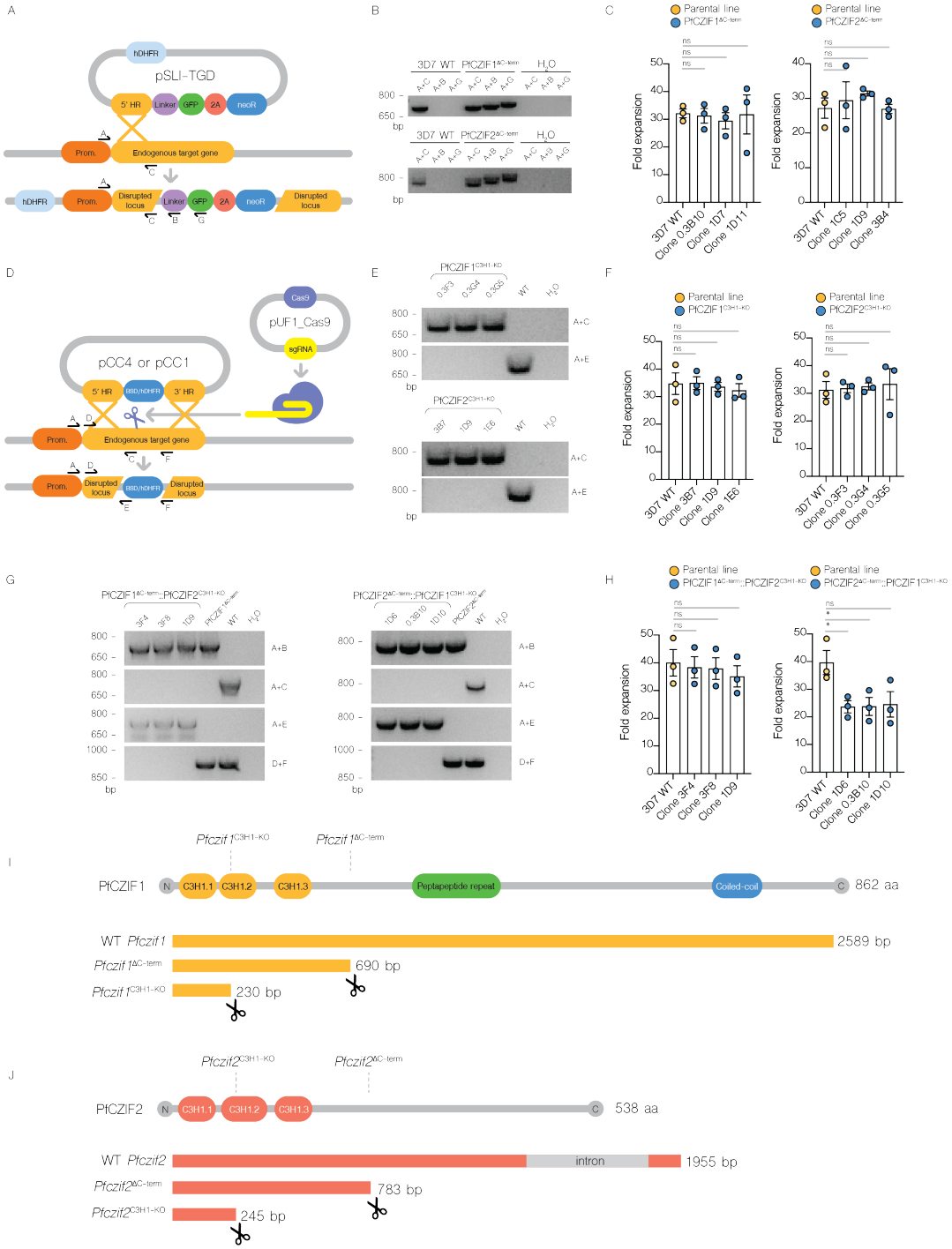

Figure 4. *Pfczif1* and *Pfczif2* are individually dispensable, but at least one functioning protein is required for parasite growth. (a) Schematic of the selection linked integration-targeted gene disruption (SLI-TGD) system used for C-terminal truncation to generate PfCZIF1$^{\Delta C\text{-term}}$ and PfCZIF2$^{\Delta C\text{-term}}$. A region homologous to the 5' end of the target gene amplified is cloned into pSLI-TGD, preceding a green fluorescent protein (GFP) reporter, a T2A skip peptide, and neomycin resistance cassette (NeoR). Post-transfection, parasites resistant to

WR99210 with the human dihydrofolate reductase (hDHFR) cassette were selected to enrich for populations with episomal plasmids. Integration was enriched by selecting for parasites resistant to geneticin (G418) with NeoR. NeoR is not expressed until the construct is integrated via single-crossover, where it is then able to be transcribed by the endogenous promoter of the target gene. (b) Confirmation of construct integration by PCR, using primers shown in (a). (c) 2 cycle growth over 120 hours assayed between parental (WT) and each of PfCZIF1$^{\Delta C\text{-term}}$ and PfCZIF2$^{\Delta C\text{-term}}$ clonal lines (clone names indicated above gels). ns = p-value > 0.05, error bars = SEM, unpaired two-tailed t-test, n = 3 biological replicates. (d) Schematic of the clustered regularly interspaced palindromic repeats (CRISPR)-Cas9 gene knockout system. Homology flanks corresponding to the 5' and 3' ends of either gene were cloned into a vector flanking a blasticidin resistance (BSD) or hDHFR cassette respectively to form a repair template. This template was then restriction digested to generate a linear repair template consisting only of the homology flanks and drug resistance cassette. A pUF1_Cas9 plasmid containing the single guide RNA (sgRNA) sequence and Cas9 was also introduced to induce a double-stranded break in the gene of interest to prompt homology-directed repair with the supplied template. (e) Confirmation of construct integration by PCR, using primers shown in (d). (f) 2 cycle growth over 120 hours assayed between parental (WT) and each of PfCZIF1$^{C3H1\text{-}KO}$ and PfCZIF2$^{C3H1\text{-}KO}$ clonal lines (clone names indicated above gels). ns = p-value > 0.05, error bars = SEM, unpaired two-tailed t-test, n = 3 biological replicates. (g) Double-transfectant lines for PfCZIF1$^{\Delta C\text{-term}}$::PfCZIF2$^{C3H1\text{-}KO}$ and PfCZIF2$^{\Delta C\text{-term}}$::PfCZIF1$^{C3H1\text{-}KO}$ were successfully generated and integration confirmed by PCR using primers shown in (a) and (d). (h) 2 cycle growth over 120 hours assayed between parental (WT) and each of PfCZIF1$^{\Delta C\text{-term}}$::PfCZIF2$^{C3H1\text{-}KO}$ and PfCZIF2$^{\Delta C\text{-term}}$::PfCZIF1$^{C3H1\text{-}KO}$ clonal lines. * = *p*-value < 0.05, ns = *p*-value > 0.05, error bars = SEM, unpaired two-tailed t-test, n = 3 biological replicates. Schematics of (i) PfCZIF1 and (j) PfCZIF2 gene truncations representing the portion of protein which continues to be expressed in the aforementioned gene-edited parasite lines. The dashed lines correspond to the portion of protein truncated towards the C-terminus.

The transcriptome at schizogony for C-terminal truncation of PfCZIF1 and PfCZIF2

Since C3H1 ZnFs are typically nucleic acid binding proteins, we hypothesised that PfCZIF1 and PfCZIF2 may have a transcriptional regulatory function. To investigate this, we harvested RNA from synchronous 3D7 wildtype, PfCZIF1$^{\Delta C\text{-}term}$ and PfCZIF2$^{\Delta C\text{-}term}$ mature schizonts and performed RNAseq differential expression analysis to observe global changes in the transcriptome with truncation of these proteins.

To perform differential expression analysis, we first visualised the level of variation between RNAseq libraries of biological replicates of RNA harvests by multidimensional scaling (MDS) in limma/voom in R (Supplementary Figure 11a, 11b) (Ritchie *et al.* 2015, Law *et al.* 2014). The level of dimensional separation between parental wildtype (WT) and mutant lines implies dissimilarities between lines. To determine whether this was representative of differential gene expression, we performed our analysis on the parental WT, PfCZIF1$^{\Delta C\text{-}term}$ and PfCZIF2$^{\Delta C\text{-}term}$ transcriptomic data against a Pf3D7 reference genome to pinpoint which genes were being upregulated or downregulated in a particular mutant (Figure 5a, 5b) The significance threshold for differential expression required a log fold change >2 and a false discovery rate (FDR) p-value of <0.05. Additionally, *var*, *stevor* and *rifin* genes were excluded from this analysis due to their known intrinsic differential expression even between samples of the same parasite origin (Tarr *et al.* 2018). Results showed that overall, there was minimal differential expression between WT and either PfCZIF1$^{\Delta C\text{-}term}$ (Figure 5a) or PfCZIF2$^{\Delta C\text{-}term}$ (Figure 5b). In PfCZIF1$^{\Delta C\text{-}term}$ schizonts, we observed that Pf3D7_1240800 was upregulated with no genes downregulated. Pf3D7_1240800 is annotated as Plasmodium RNA of Unknown Function 6 (RUF6), a non-coding RNA (ncRNA) thought to be involved in *var* gene regulation (Chakrabarti *et al.* 2007, Barcons-Simon *et al.* 2020). It is possible that this result is a false representation which was unfiltered from our analyses.

In PfCZIF2$^{\Delta C\text{-}term}$, there were more significant hits with four genes upregulated and five genes downregulated. Genes upregulated in PfCZIF2$^{\Delta C\text{-}term}$

schizonts included Pf3D7_0201500 (hyp9), Pf3D7_0201900 (EMP3), Pf3D7_0202000 (KAHRP) and Pf3D7_0202100 (LSAP2). We were concerned that the increased transcript levels of consecutive genes on chromosome 2 may represent a chromosomal deletion in our wildtype parasites compared to PfCZIF2$^{\Delta C\text{-term}}$ parasites, however equivalent transcript levels of neighbouring loci verified that this was not the case (from Pf3D7_0200800 to Pf3D7_0203000) (Supplementary Figure 12a). For downregulated genes in PfCZIF2$^{\Delta C\text{-term}}$ schizonts, we identified Pf3D7_0401900 (acyl-CoA synthetase), Pf3D7_0424800 (PHISTb), Pf3D7_0424900 (PHISTa), Pf3D7_0801100 (28S ribosomal RNA) and Pf3D7_1478000 (PHISTa). Given that Pf3D7_0424800 and Pf3D7_0424900 are adjacent genes, we scanned across Chromosome 4 (from Pf3D7_0424500 to Pf3D7_0425200) and confirmed that no chromosomal deletions in neighbouring loci were biasing our results (Supplementary Figure 12b).

Loss of PfCZIF2 leads to altered PfKAHRP expression

We observed by RNAseq that C-terminal truncation of PfCZIF2 resulted in a significant upregulation of knob-associated histidine rich protein (KAHRP, Pf3D7_0202000) transcript in schizonts. We therefore proceeded to investigate whether this was consistent for protein expression at schizont stages. Since KAHRP is normally expressed at early ring stages (Otto *et al.* 2010) and the protein is then exported to the RBC surface where it takes part in forming knob-like structures on the RBC surface from late ring stages onwards (Culvenor *et al.* 1987, Pologe *et al.* 1987), we also checked protein expression levels of KAHRP at ring and trophozoite stages as well as across other stages of the blood stage lifecycle. To quantify this, we analysed parental 3D7 wildtype (WT), PfCZIF2$^{\Delta C\text{-term}}$, and PfCZIF1$^{\Delta C\text{-term}}$ parasite lysates of synchronous schizonts (40-44 hrs), early rings (0-6 hrs) and trophozoite (20-24 hrs) stages by western blot, with loading normalised against parasite aldolase. We observed an average increase in KAHRP expression for PfCZIF2$^{\Delta C\text{-term}}$ parasites of 43% in schizonts (Figure 5c), 156% in rings (Figure 5d), and 144% in trophozoites (Figure 5e) when compared to WT parasite expression levels. When comparing PfCZIF2$^{\Delta C\text{-term}}$ with PfCZIF1 parasites$^{\Delta C\text{-term}}$, statistical significance was achieved for rings and trophozoites. As such, PfCZIF1$^{\Delta C\text{-term}}$

parasites did not show an increase in KAHRP expression for any lifecycle stage, consistent with the RNAseq results.

We then performed identical harvests in PfCZIF2$^{C3H1\text{-}KO}$ parasites where we observed a similar result with an average KAHRP expression increase of 74% in schizonts (Figure 5f), no observed increase in rings (Figure 5g), and an increase of 125% in trophozoites (Figure 5h) in comparison to WT expression. When comparing PfCZIF2$^{C3H1\text{-}KO}$ with PfCZIF1$^{C3H1\text{-}KO}$ parasites, statistical significance was only achieved in schizonts. In PfCZIF1$^{C3H1\text{-}KO}$, similar baseline levels to wildtype parasites were observed across ring, trophozoite and schizont stages. Combined, these data indicate that PfCZIF2$^{\Delta C\text{-}term}$ parasites have increased transcription of the virulence factor KAHRP, with both the C-terminal (PfCZIF2$^{\Delta C\text{-}term}$) and near complete (PfCZIF2$^{C3H1\text{-}KO}$) truncation of PfCZIF2 leading to significantly increased levels of KAHRP across different stages of blood stage parasite development.

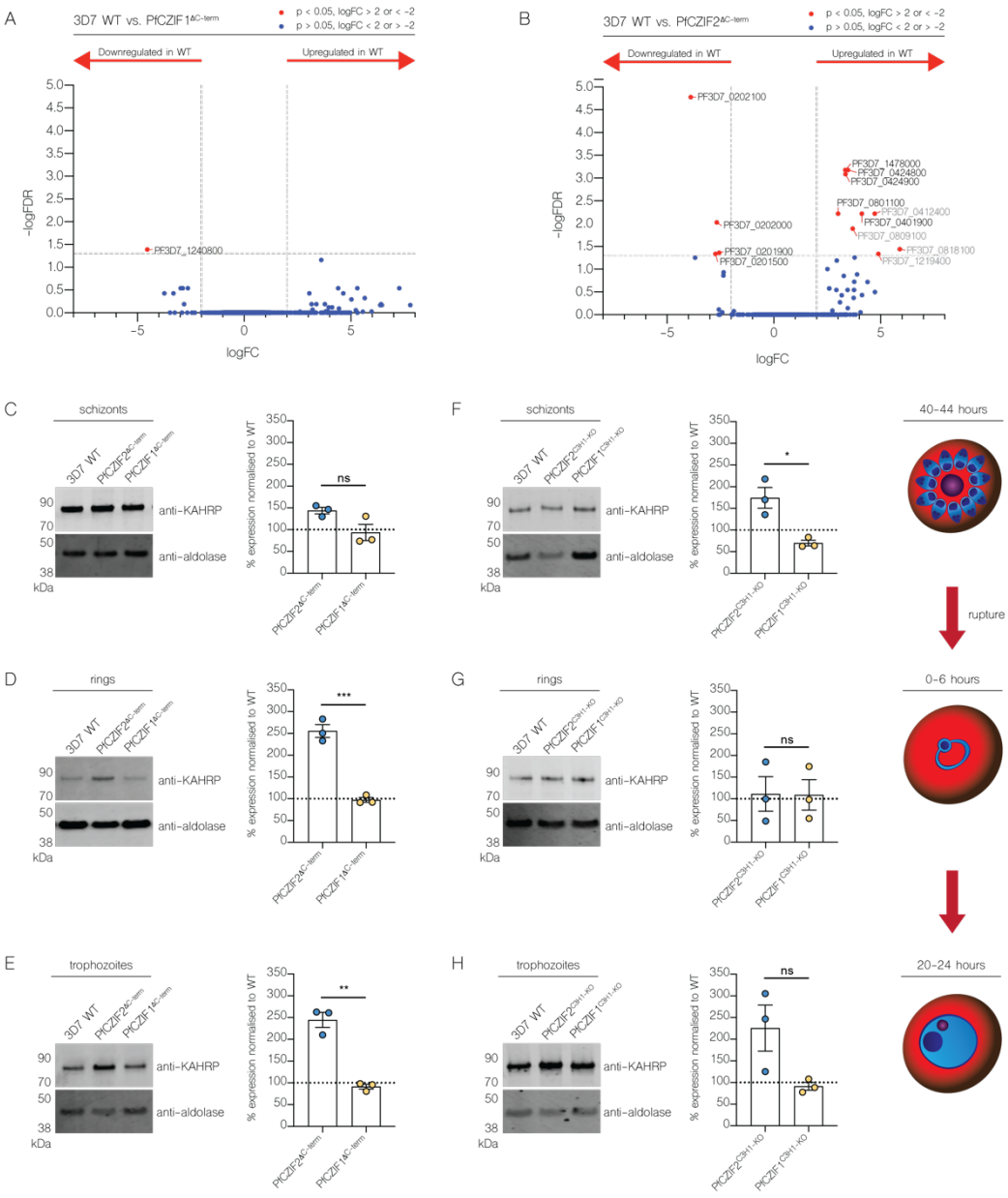

Figure 5: Transcriptional changes with PfCZIF1 and PfCZIF2 C-terminal truncations and changes in KAHRP protein levels with PfCZIF2 truncation. Volcano plots summarising RNAseq differential expression analyses between the parental Pf3D7 line (WT), which represents a transcriptome with baseline gene expression, and (a) PfCZIF1$^{\Delta C\text{-term}}$ schizonts and (b) PfCZIF2$^{\Delta C\text{-term}}$ schizonts. Downregulation in WT is synonymous with upregulation in a C-terminal mutant, and upregulation in WT is synonymous with downregulation in a C-terminal mutant. n = 3 biological replicates. Semi-quantitative western blots of synchronous (c) schizonts (d) rings and (e) trophozoites for parental WT, PfCZIF2$^{\Delta C\text{-term}}$ and PfCZIF1$^{\Delta C\text{-term}}$ parasites and relative expression of KAHRP protein against the

aldolase loading control. Aldolase was chosen as it is expressed equally for all conditions, and possesses comparable signal to KAHRP. n = 3, error bars = SEM. Dotted line indicates baseline WT expression. (f-h) An identical experiment was performed for (f) schizonts (g) rings and (h) trophozoites for PfCZIF2$^{C3H1\text{-}KO}$ and PfCZIF1$^{C3H1\text{-}KO}$ parasites with quantification. *P*-values: * = 0.0135, ** = 0.0011, *** = < 0.0005. n = 3, error bars = SEM. Dotted line indicates baseline WT expression.

Discussion

In this study, we characterised PfCZIF1 (Pf3D7_1468400) and identified a second C3H1 ZnF protein, PfCZIF2 (Pf3D7_0818100), that is expressed predominantly at schizont stages. Schizont specific expression is often associated with a role for a protein in merozoite development, schizont rupture or invasion of the host RBC. Indeed, a previous study linked PfCZIF1 (called D13) to a role in merozoite invasion from experiments utilising an MAb targeting its conserved N-terminus which was also reported to be inhibitory to blood stage parasite growth.

PfCZIF1 was previously shown to localise at one pole of the merozoite by IFA (Daubenberger *et al.* 2003). This localisation is highly atypical, as C3H1 ZnFs are usually known to directly bind to and regulate mRNA transcripts; a function that would appear likely to differ to any possible role on the merozoite surface. Immunofluorescence data obtained in this study for PfCZIF1 and PfCZIF2 suggest that they are unlikely to be on the merozoite surface at all. Using HA-tagged PfCZIF1 and PFCZIF2, we showed that these two proteins have peak expression at schizonts but can also be detected up until early trophozoites. In addition, they are likely cytosolically exposed and are peripherally bound to an intracellular membrane. Moreover, our IFAs indicate that both proteins lie in puncta underneath the parasite plasma membrane from rings to trophozoite stages, before localising to an area near the dense granule localised EXP2 in developing merozoites in schizonts. However, given that they do not completely co-localise with EXP2, it is possible they reside in a different compartment. The punctate patterns we observed were also markedly like the localisation of the RNA-binding proteins PfAlba1,

PfAlba2 and PfAlba4, which are speculated to occur in RNA storage/processing centres in the cytoplasm (Chene *et al.* 2012, Vembar *et al.* 2015). However experimental evidence of these compartments existing is currently lacking.

Why would we see a discrepancy between localisation achieved using a HA tagged protein in this study and localisations reported by Daubenberger *et al.* (Daubenberger *et al.* 2003)? The MAb used by Daubenberger *et al.* binds an epitope within the first 138 amino acids of the N-terminal region of PfCZIF1, a region with high amino acid sequence similarity to the C3H1 ZnF domains of PfCZIF2 (50.3%: PfCZIF1 aa1-126, PfCZIF2 aa1-161) and other C3H1 ZnF domain containing proteins, leaving open the possibility for cross-reactivity between proteins. While a band corresponding to PfCZIF2 at ~70 kDa by western blot was not reported by Daubenberger *et al.*, multiple bands of unmarked size (Daubenberger *et al.* Figure 2b, Figure 4a), particularly in maturing schizonts, were evident. This cross-reactivity could potentially also impact on growth inhibitory data and localisation by IFA. Investigation of phenotypes for the antibodies produced by Daubenberger *et al.* in our cell lines could be used to understand this discrepancy.

Our understanding of C3H1 ZnF domains in *P. falciparum* is currently in its infancy, with little functional inference available from other systems as the parasite lacks comparable homologues in model eukaryotes. Many studies reference the prototypical C3H1 ZnF tristetraprolin (TTP), where its most well-documented function is to induce the degradation of tumour necrosis factor alpha (TNF- α) mRNA transcripts by recruitment of deadenylases and decapping nucleases (Carballo *et al.* 1998, Sandler *et al.* 2011). Moreover, TTP is capable of protein-protein interactions, specifically requiring at least two intact C3H1 ZnFs to perform this function (Carman *et al.* 2004). There is therefore a precedent for C3H1 ZnFs to interact with proteins. Balancing this observation in *P. falciparum*, certain ZnF containing proteins have roles beyond nucleic acid binding, including ZnFs of the RING class (RNF5 and HRD1) and PHD class (PHD1, PHD2) which can form protein-protein interactions (Harbut *et al.* 2012, Chung *et al.* 2012, Voss *et al.* 2014). Of the few C3H1 ZnFs in *P. falciparum* characterised to date, none have been experimentally shown to perform protein-protein binding – and indeed only PfCZIF1 and PfCZIF2 appear specific to the schizont stage. The parasite possesses

27 genes predicted to express proteins with C3H1 ZnFs and of these, 13 were considered to be essential by random mutagenesis which do not include PfCZIF1 and PfCZIF2 (Zhang *et al.* 2018, Ngwa *et al.* 2021). Only three C3H1 ZnFs in *P. falciparum* have been investigated experimentally, including PfCZIF1 (Daubenberger *et al.* 2003). The remaining two include a predicted homologue of NGFI-A-binding protein 2 (NAB2) which binds DNA and RNA through an alternative PWI domain rather than its C3H1 ZnF domains, and YTH-domain like protein 1 (YTH1) which is involved in N^6-methyladenosine (m^6A) post-transcriptional modifications (Szymczyna et al. 2003, Baumgarten *et al.* 2019). Given the breadth of possible functions for C3H1 ZnFs, further investigation into whether PfCZIF1 and PfCZIF2 can interact with proteins using these domains would be of interest. This can be addressed by quantitative proteomics, including techniques such as dimerization inducible quantitative biotin identification (DiQ-BioID) which was recently adapted to *P. falciparum* (Birnbaum *et al.* 2020). DiQ-BioID is an efficient method to identify proteins in close proximity to PfCZIF1 and PfCZIF2, including likely interacting partners, with a direct interaction with these ZnFs requiring phenotypic validation for each likely interacting partner.

To probe the function of PfCZIF1 and PfCZIF2 in more detail, we truncated the proteins and assessed the impact of modification on parasite growth. We first assessed whether the C-terminus of PfCZIF1 and PfCZIF2, a region of low sequence conservation, have an important role in protein function and parasite growth by removing this region just prior to the end of the third ZnF. Removal of the 632 amino acids at the C-terminus of PfCZIF1 (PfCZIF1$^{\Delta C\text{-term}}$) indicated that the pentapeptide tandem repeat and the predicted coiled-coil region of PfCZIF1 are not essential. Notably, the coiled-coil region is absent in rodent malaria species including *P. yoelii* and *P. berghei*, suggesting that no loss of function is exhibited by this sequence, though is present in several primate malaria species including *P. vivax*, *P. ovale curtisi*, *P. ovale wallikeri*, *P. malariae*, *P. knowlesi* and *P. reichenowi*. Likewise, the exclusive presence of the pentapeptide tandem repeat in *P. falciparum*, *P. praefalciparum* and *P. reichenowi* suggests that these residues were not required in other species. Similarly, we identified removing the 277 amino acids at the C-terminus of PfCZIF2 in PfCZIF2$^{\Delta C\text{-term}}$ parasites was not deleterious.

We next assessed whether the C3H1 ZnF domains were required for parasite growth. We found that PfCZIF1 and PfCZIF2 can be truncated to remove two out of three C3H1 ZnFs but do not produce a growth defect in our single truncation lines PfCZIF1$^{C3H1\text{-}KO}$ and PfCZIF2$^{C3H1\text{-}KO}$. Typically, C3H1 ZnF proteins are thought to require at least two ZnFs for function (Carman *et al.* 2004, Brown 2005), so we expect that the loss of at least two domains would impact on function. We next tried CRISPR-Cas9 truncation down to a single C3H1 ZnF domain for one PfCZIF in a line that already had the other schizont expressed PfCZIF C-terminally truncated. Using this approach, we observed in PfCZIF2$^{\Delta C\text{-}term}$::PfCZIF1$^{C3H1\text{-}KO}$ parasites that there was a growth defect, indicating that the C-terminus of PfCZIF2 was important for parasite growth in the absence of a functional PfCZIF1. Somewhat surprisingly given the longer and more structurally diverse C-terminal region of PfCZIF1, the reverse was not true and PfCZIF1$^{\Delta C\text{-}term}$::PfCZIF2$^{C3H1\text{-}KO}$ grew normally. Given this result, we present this as the first piece of evidence to suggest a functionally dependent relationship between PfCZIF1 and PfCZIF2. This finding is supported by our inability to truncate both PfCZIF1 and PfCZIF2 down to a single C3H1 ZnF each in a doubly transfected line, despite repeated attempts, even though integration of each construct was readily achieved on its own. Therefore, it appears likely that both PfCZIF1 and PfCZIF2 are dispensable if the other protein remains and, in the case of PfCZIF1, PfCZIF2 remains intact. Generating and assessing the growth phenotype of a conditional knockout of PfCZIF2, in a PfCZIF1 knockout line, may shed more light on this functional relationship.

After ascertaining that schizont expressed PfCZIF1 and PfCZIF2 are dispensable if the other protein remains intact, we sought to investigate the effect of protein truncation on the parasite's transcriptome. We undertook RNAseq analysis on the C-terminal truncation mutants of PfCZIF1 and PfCZIF2 since these lines were available first. No clear change in parasite transcriptome for PfCZIF1$^{\Delta C\text{-}term}$ parasites was seen when compared to 3D7 parental WT parasites. For PfCZIF1$^{\Delta C\text{-}term}$ parasites, we saw a consistent upregulation of a series of proteins which are known to be exported into the parasite cytosol, most notably the knob associated histidine rich protein (KAHRP) which plays a key role in presentation of virulence proteins on the infected RBC surface. Upregulation of KAHRP at a

protein level in schizonts and trophozoites in the next cycle of parasite growth was confirmed by western blot for both PfCZIF2$^{\Delta C\text{-term}}$ and PfCZIF2$^{C3H1\text{-}KO}$ lines, supporting that regulation of KAHRP is impacted by independent partial and near complete truncation approaches. Given that KAHRP is most highly expressed during the development of the trophozoite at the point of knob formation and late host cell modification (Culvenor *et al.* 1987, Pologe *et al.* 1987), we speculate that PfCZIF2 may exercise its regulatory role on the transcripts of KAHRP and some other exported proteins in schizonts of the previous cycle. Although PfCZIF2 RNA expression peaks in schizonts, protein is expressed up until early trophozoites. Therefore, it is possible that PfCZIF2 may maintain a regulatory function on KAHRP and potentially other exported proteins until knob formation and the bulk of protein export is finished. On this note, two upregulated genes PfCZIF2$^{\Delta C\text{-term}}$ schizonts, which express proteins with *Plasmodium* export element (PEXEL) motifs ((Pf3D7_0201500 (hyp9), Pf3D7_0201900 (EMP3)), possess a similar expression profile to KAHRP and may be regulated by PfCZIF2 in a similar way. We hypothesise that once export of proteins and host-cell remodelling/virulence protein presentation is complete, PfCZIF2 may no longer be needed to help regulate transcripts of these proteins and expression of PfCZIF2 ramps down in late trophozoites prior to schizogony where it is re-expressed.

Direct investigation into the nucleic-acid binding capabilities of PfCZIF1 and PfCZIF2 has yet to be performed. If these C3H1 ZnFs perform their canonical function, it is plausible to hypothesise that they bind the 3' UTR of mRNA molecules at AU-rich sequences (Hudson *et al.* 2004, Wells *et al.* 2015) and for example, exhibit a post-transcriptional regulatory function. Approximately 1000 putative mRNA binding proteins (mRBPs) have been identified in *P. falciparum* across the lifecycle using cross-linking immunoprecipitation sequencing (CLIPseq), which comprise a 9.6% of the expressed proteome (Bunnik *et al.* 2016). Though other ZnFs were identified, neither PfCZIF1 nor PfCZIF2 were highlighted as RNA-binding or mRNA-binding hits. However, these studies were conducted using whole RNA bait from in asynchronous cultures containing trophozoites and schizonts, crosslinked to unknown proteins. Directly characterising PfCZIF1 and PfCZIF2's ability to bind RNA could instead be addressed best with a protein-bait

approach of CLIPseq (Ramanathan *et al.* 2019), to identify the corresponding unknown RNA sequence(s).

Together our studies have helped to inform our understanding of *Pfczif1* and *Pfczif2* function in asexual blood stages, highlighting their similar N-terminal C3H1 ZnFs domain structure, stage of expression patterns, putative localisation, potential redundant functionality and lack of evidence for a direct role in merozoite invasion of the host RBC. Determining the specialised biological roles of PfCZIF1 and PfCZIF2 will undoubtedly require functional studies on protein-protein and protein-nucleic acid interactions. This will provide the necessary clues for narrowing down which molecular niche they may be contributing to, whether they do have a role in merozoite invasion or whether their primary function is in RNA-binding and potential regulation of exported protein expression.

Methods

Protein structure prediction

Protein motifs were predicted using the ExPASY PROSITE web-based service using default settings, and ExPASY COILS (Swiss Institute for Bioinformatics). 3D secondary and tertiary protein structures simulated using the Phyre2 web-based service in both normal and intensive mode (Biotechnology and Biological Sciences Research Council). Transmembrane domains were predicted in TMHMM (Center for Biological Sequence analysis) using extensive output settings. Putative N-terminal signal peptides were predicted in SignalP-5.0 (Center for Biological Sequence Analysis) using long output settings for Eukarya. Lipid modifications were presented in GPS-Lipid (Xie *et al.* 2016) using default settings.

Identification of C3H1 ZnFs at schizogony

Pf3D7_0818100 (PfCZIF2) was identified using a nested strategy on PlasmoDB. Genes were text term-filtered for “zinc finger” in their annotation box or gene ontology (GO) terms. The output was then narrowed to annotations containing “C3H1” or “CCCH”. The resulting gene list was then further narrowed by only including genes with a defined

10-fold expression increase based on Transcripts Per Million abundance values (TPM) from trophozoites (24-32 hours) through to schizogony (40-48 hours) using an RNAseq data set from Otto *et al.* 2010.

Sequence alignments

Amino acid sequences for Pf3D7_1468400 and Pf3D7_0818100 and the genes encoding their respective equivalents in *P. falciparum* strains 7G8 (Pf7G8_140073500, Pf7G8_080023200), CD01 (PfCD01_140073600, PfCD01_080023700), Dd2 (PfDd2_140072700, PfDd2_080023300), FVO (PFFVO_05334, PFFVO_02121), GA01 (PfGA01_140073700, PfGA01_080021800), GB4 (PfGB4_140074300, PfGB4_080022900), GN01 (PfGN01_140073600, PfGN01_080023800), HB3 (PfHB3_140074000, PfHB3_080023600), IT (PfIT_140074700, PfIT_080023100), KE01 (PfKE01_140073100, PfKE01_080023700), KH01 (PfKH01_140073800, PfKH01_080023200), KH02 (PfKH02_140074000, PfKH02_080023700), MaliPS096 (PFMALIP_05529, PFMALIP_02139), IGH-CR14 (PFMG_04912, PFMG_04917), ML01 (PfML01_140074100, PfML01_080023700), NF135/5.C10 (PFNF135_05581, PFNF135_02241), SD01 (PfSD01_140071600, PfSD01_080023500), SN01 (PfSN01_140075500, PfSN01_080022700) and TG01 (PfTG01_140073600, PfTG01_080024000) as well as orthologous genes in *Plasmodium inui* (C922_00098, C922_02584), *Plasmodium berghei* (PBANKA_1331700, PBANKA_0712700), *Plasmodium cynomolgi* (PCYB_124660, PCYB_052360), *Plasmodium gallinaceum* (PGAL8A_00227800, PGAL8A_00111100), *Plasmodium knowlesi* (PKNH_1212800, PKNH_0501900), *Plasmodium malariae* (PmUG01_12048500, PmUG01_05032900), *Plasmodium ovale curtisi* (PocGH01_12046400, PocGH01_05022800), *Plasmodium praefalciparum* (PPRFG01_1469000, PPRFG01_0819600), *Plasmodium reichenowi* (PRCDC_1467600, PRCDC_0817400), *Plasmodium vivax* (PVX_117045, PVX_089510) and *Plasmodium yoelii* (PY02869, PY03958) were obtained from PlasmoDB. Pairwise and multiple sequence alignments were performed in Geneious 9.1.3 (Biomatters) with a global alignment with free end gaps using the Blosum62 cost matrix with the configuration: gap open penalty 12, gap extension penalty 3, refinement iterations 2.

Continuous blood stage parasite culture

P. falciparum 3D7 strain parasite cultures were maintained at 3% haematocrit of O^+ blood donated by the Red Cross Blood Service, Australia, in culture media composed of RPMI-HEPES (Sigma-Aldrich), 0.5% v/v Albumax (Gibco), 52 μM gentamycin (Gibco), 367 μM hypoxanthine (Sigma-Aldrich), 2 mM L-Glutamax (Gibco) and 2 mM sodium bicarbonate (Thermo Fisher Scientific), adjusted to a pH of 7.2-7.4. Culture media was 0.2 μm filter-sterilised before use. All cultures were stored in sealed acrylic boxes gassed with 1% O_2, 5% CO_2 and 94% N_2 (BOC Gases) and grown in 37°C incubators.

Plasmid construction and transfection

List of genetic constructs in this study: *Pfczif1*^{HA}, *Pfczif2*^{HA}, *Pfczif1*$^{\Delta C\text{-term}}$, *Pfczif2* $^{\Delta C\text{-term}}$, *Pfczif1*$^{C3H1\text{-}KO:BSD}$, *Pfczif2* $^{C3H1\text{-}KO:BSD}$, *Pfczif1*$^{C3H1\text{-}KO:hDHFR}$, *Pfczif2* $^{C3H1\text{-}KO:hDHFR}$, *Pfczif1*$^{pUF\text{-}Cas9}$, *Pfczif2* $^{pUF\text{-}Cas9}$. All homology flanks were amplified from Pf3D7 gDNA.

To append an HA-tag onto the C-terminus of PfCZIF1 and PfCZIF2, *Pfczif1*^{HA} and *Pfczif2*^{HA} transfection vectors were prepared from a pHA3 plasmid backbone. A 3' homology region of *Pfczif1* was amplified using the primers 5' GGT**AGATCT**GTGAGGATGCCA-TAGAAGAAG 3' and 5' GCT**GCAGACC**TTCTGATAAGAAAGAGAAAAAAGAC 3' by PCR and digested with BglII and PstI (sites in bold) to be cloned into pHA3. Similarly, a homology region *Pfczif2* was amplified using the primers 5' GGT**AGATCT**AGATCTTGATTTTATAAGAAATCTTAATGG 3' and 5' GGT**CTGCAGC**AATCATTTCTTTCATGTTGTAGTTC 3' were cloned into pHA3 in the same way.

To delete the C-terminal residues beyond the C3H1 ZnF domains of PfCZIF1 and PfCZIF2, *Pfczif1*$^{\Delta C\text{-term}}$ and *Pfczif2* $^{\Delta C\text{-term}}$ transfection vectors were prepared from the pSLI-TGD backbone. A 5' homology region of *Pfczif1* was amplified using the primers 5' GGT**GCGGCCGC**TAAGCCACACTTTTGAGTGAAGAAG 3' and 5' GGT**ACGCGT**AACAGCGTTTTTAGTCATATCATTC 3' by PCR and digested with NotI and MluI to be cloned into pSLI-TGD. Similarly, a homology region

Pfczif2 was amplified using the primers 5' GGT**GCGGCCGC**TAACGTGCACACCTTTACTTAGCG 3' and 5' GGT**ACGCGT**GTTCATCTTTTGTTCTTGTAATGTG 3' were cloned into pSLI-TGD in the same way.

To further delete two out of three C3H1 ZnF domains and the residues C-terminal of them in PfCZIF1 and PfCZIF2, *Pfczif1*$^{\text{C3H1-KO:BSD}}$, *Pfczif2* $^{\text{C3H1-KO:BSD}}$, *Pfczif1*$^{\text{C3H1-KO:hDHFR}}$ and *Pfczif2* $^{\text{C3H1-KO:hDHFR}}$ transfection vectors were prepared from an pCC4 (with a BSD resistance cassette) or pCC1 (with a hDHFR resistance cassette) backbone as a repair template for CRISPR-Cas9 gene editing. A 5' homology region of *Pfczif1* was amplified using the primers 5' GGT**ACTAGT**GTGTACACCTTGTGAGTACATAC 3' and 5' GGT**CTTAAG**GAACCATCTCCCCTTGTTTC 3', and a 3' homology region was amplified using the primers and 5' GG**TGAATTC**CGGTTTGTACTAATATAGATAATTTAG 3' and 5' GGT**CCATGG**TTCTGATAAGAAAGAGAAAAAAGAC 3'. Similarly for *Pfczif2*, a 5' homology region was amplified with 5' GGT**ACTAGT**TGCTTCATATTAGGGTAATTGG 3' and 5' GGT**CTTAAG**CTCTATATCTTCTTCGGTTTC 3', and a 3' homology region with 5' GG**TCCATGG**CTAAATCATTTCTTTCATGTTGTAG 3' and 5 'GGT**GAATTC**CTAGCAAAACAAGTAATAAATCAAG 3'. 5' homology flanks were digested with SpeI and AflII, while 3' homology flanks were digested with EcoRI and NcoI, before being cloned into pCC1 or pCC4. The region of plasmid spanning the repair templates were then linearised using SpeI and NcoI.

Guide sequences were designed on CHOPCHOP (Montague *et al.* 2014) and ordered as single-stranded oligonucleotides (5' AATGGCAACTTGTAAGTACC 3' for *Pfczif1* and 5' CATGTGAAAATGCCACACAA 3' for *Pfczif2*) and annealed together by InFusion cloning, before being cloned into a pUF-Cas9 backbone to form *Pfczif1*$^{\text{pUF-Cas9}}$, *Pfczif2* $^{\text{pUF-Cas9}}$.

To transfect in each construct of interest, 5% late schizontaemia *P. falciparum* 3D7 cultures were Percoll-purified and treated with 2 µM 4-[2-

(fluorophenyl)-5-(1-methylpiperidine-4-yl)-1H-pyrrol-3-yl] pyridine (Compound 1) for 4 hours to allow schizonts to fully develop their merozoites. Mature schizonts were then resuspended in cytomix (0.895% w/v KCl, 0.0017% w/v $CaCl_2$, 0.076% w/v ethylene glycol-bis(β-aminoethyl ether)-N,N,N',N-tetraacetic acid (EGTA), 0.102% w/v $MgCl_2$, 0.0871% w/v K_2HPO_4, 0.068% w/v KH_2PO_4, 0.708% w/v 4-2 4-(2-hydroxyethyl)-1-piperazineethanesulfonic acid (HEPES) containing 80 µg of the plasmid of interest (20 µg in the case of pUF-Cas9, alongside 60 µg of linearised template), and electroporated in a 0.2 cm cuvette (Bio-Rad) at 0.8 kV, capacitance 25 µF. Electroporated cells were placed into 1.5 mL tubes with 1 mL of culture media and shaken at 37 ºC for 20 min for merozoites to invade. Lines were drug selected using 4 nM WR99210 (Jacobus Pharmaceuticals) (*Pfczif1*^{HA}, *Pfczif2*^{HA}, *Pfczif1*$^{\Delta C\text{-term}}$, *Pfczif2*$^{\Delta C\text{-term}}$, *Pfczif1*$^{C3H1\text{-}KO:hDHFR}$, *Pfczif2*$^{C3H1\text{-}KO:hDHFR}$) or 5 µg/mL blasticidin-S-hydrochloride (Merck-Millipore) (*Pfczif1*$^{C3H1\text{-}KO:BSD}$, *Pfczif2*$^{C3H1\text{-}KO:BSD}$) for 3-4 weeks. Once cultures were growing for *Pfczif1*$^{\Delta C\text{-term}}$, *Pfczif2* $^{\Delta C\text{-term}}$ lines, 80 µg/mL geneticin (G418, Sigma-Aldrich) was added for an additional two weeks. Once lines were growing stably, and were PCR-confirmed to have incorporated the desired modification, clones were generated by limiting dilution.

Sample preparation and imaging by confocal microscopy

Parasite cultures at all stages were first washed in phosphate buffered saline (PBS), before being fixed in 4% v/v paraformaldehyde (PFA, Sigma-Aldrich), 0.0075% v/v glutaraldehyde (Electron Microscopy Sciences) pH 7.4 for 30 min with gentle agitation, then washed once in PBS. Fixed parasites were allowed to adhere to 0.01% poly-L-lysine-coated (Sigma-Aldrich) #1.5H high-precision coverslips (Carl Zeiss, Oberkochen, Germany) for 30 min, and permeabilised in 0.1% v/v Triton X-100 for 10 min. Cells were then blocked in 3% w/v bovine serum albumin (BSA, Sigma-Aldrich) diluted in PBS with 0.05% v/v Tween 20 (PBS-T). Primary antibodies, diluted in 1% w/v BSA PBS-T were added at the following concentrations: biotin-conjugated anti-HA 1/500 (Roche), mouse anti-EXP2 1/500, rabbit anti MSP1-19 1/1000, rabbit anti-ERD2 1/500, rabbit anti-RON4 1/500, rabbit anti-ERC 1/500, and left overnight at 4 ºC. Coverslips were then washed three times in PBS-T, and incubated with AlexaFluor secondary antibodies (Life Technologies) at the following concentrations: streptavidin 488 nm 1/500, mouse

555 nm 1/500, rabbit 647 nm 1/500, for one hour in the dark, then washed three times in PBS-T. Coverslips were ethanol dehydrated (70% v/v 3 min, 90% v/v 3 min, 100% v/v 3 min), air dried and mounted on glass slides with 20 μL Prolong® Gold antifade solution (refractive index 1.4) with 4', 6-diamidino-2-phenylindole dihydrochloride (DAPI, Thermofisher Scientific), allowing to cure overnight. Fully labelled samples were then imaged on an Olympus FV3000 confocal microscope using a 100 x MPLAPON oil objective, using the 405/488/561/633 nm lasers.

Saponin lysis and western blot

5-7% high parasitaemia synchronous cultures were resuspended in 0.15% w/v saponin (ThermoFisher Scientific), permitting lysis to occur for 10 mins on ice. Pellets were centrifuged at 16000 rcf, washed in 0.075% w/v saponin, and washed in PBS until the supernatant ran clear – all lysis reagents contained EDTA-free protease inhibitors (CØmplete, Roche). Saponin pellets then treated with DNase I (Qiagen) for 10 min at room temperature to remove DNA, before being resuspended in reducing sample buffer (0.125 M Tris-HCl pH 7, 20% v/v glycerol, 4% v/v SDS, 10% v/v β-mercaptoethanol (Sigma-Aldrich), 0.002% w/v bromophenol blue (Sigma-Aldrich), and centrifuged at 16000 g. Supernatants containing protein were separated by molecular weight on SDS-PAGE 4-12% Bis-Tris gels (Bolt, Invitrogen) at 110 V for 70 min, and transferred onto nitrocellulose membranes using the iBlot system (Invitrogen) at 20 V for 7 min. Membranes were washed in MilliQ H_2O before being blocked in 1% w/v skim milk with 0.05% v/v Tween 20 (Sigma-Aldrich) in PBS (1% milk PBS-T). Membranes were treated with relevant primary antibodies at the following concentrations diluted in 1% milk PBS-T: mouse anti-HA 12CA5 1/2500 (Sigma-Aldrich), rabbit anti-EXP2 1/10000, rabbit anti-ERC 1/10000, rabbit anti-GAP45 1/5000, rabbit anti-GAPDH 1/5000, mouse anti-RH5 1/5000, rabbit anti-MSP1-19 1/10000, and left overnight at 4 ^{o}C. Primary antibodies were washed off three times in PBS-T. Secondary antibodies, targeting relevant primary antibodies, included IRDye 800 goat anti-mouse and IRDye 680 goat anti-rabbit (LI-COR Biosciences) were added at 1/4000 in milk PBS-T, and permitted to incubate for 1 hour before being washed off three times in PBS-T, and once in PBS. Blots were then dried on Whatman filter paper and imaged

using an Odyssey Infrared Imaging System (LI-COR Biosciences). Semi-quantification of bands was performed in Image Studio Lite 2.5 (LI-COR Biosciences).

Protein solubility assay

Protein solubility assays were performed as previously described (Cabrera *et al.* 2012). Briefly, schizont saponin pellets were resuspended in 100 µL MilliQ H_2O, snap-frozen and freeze-thawed in dry ice four times before being passed through a 29-gauge needle 5 times. The pellet was centrifuged at 16000 g to collect the hypotonic supernatant. The remaining pellet was washed twice in MilliQ H_2O and once in PBS, then resuspended in 100 µL 0.1 M Na_2CO_3 for 30 min at 4 °C, before being centrifuged at 16000 g, and the carbonate-solubilised supernatant was collected. The remaining pellet was then washed again in MilliQ H_2O and PBS, and resuspended in 0.1% v/v Triton X-100 for 30 min at 4 °C, before being centrifuged at 16000 g followed by collection of the Triton X-100-solubilised supernatant. The final pellet was reserved, and washed twice in PBS. All fractions were then analysed by western blotting.

Proteinase K protection assay

A modified proteinase K protection assay was performed as previously described (Liffner *et al.* 2020). Briefly, high schizontaemia cultures were saponin lysed with all centrifugations at 440 rcf (to prevent parasite cell breakage) and split into three tubes. One tube was treated with SOTE (0.6 M sorbitol, 20 mM Tris HCl pH 7.5, 2 mM EDTA) centrifuged at 800 rcf, supernatant removed and the pellet was reserved. The second tube was treated as above, with a subsequent treatment of 0.02% w/v digitonin (Sigma-Aldrich) in SOTE and incubated for 10 min at 4 °C, centrifuged at 800 rcf for 20 min, supernatant removed, and the pellet reserved. The third tube was treated as combined above, followed with an additional treatment of 0.1 µg/µL Proteinase K (Sigma-Aldrich) in SOTE for 30 min at 4 °C and centrifuged at 16000 rcf for 10 min. Proteinase K was inactivated with 50 µL 100% v/v trichloroacetic acid (Sigma-Aldrich) for 3 min, followed by 500 µL 100% v/v acetone. All samples were washed in MilliQ H_2O twice before being analysed by western blotting.

Growth expansion assay and flow cytometry

To determine the rate of population expansion for a given transfected line, all clones and their parental wild-type line were tightly synchronised using a combination of sorbitol and heparin. The next day, synchronous 24-hour old trophozoites were adjusted to 0.15% parasitaemia and cultured in 96-well plates in technical triplicate at 1% haematocrit. Starting parasitaemia was verified and collected as a normalisation value on a Accuri™ C6 Plus (BD) flow cytometer and FlowJo Version 10 (Tree Star). Following two cycles (96 hours later), plates were analysed again by flow cytometry to obtain the final parasitaemia values. The rate of expansion was calculated as:

$$\text{Rate of expansion (fold change)} = \frac{average\ late\ stages\ (final\ \%)}{average\ late\ stages\ (set\text{-}up\ \%)}$$

Gating strategies for flow cytometry are included in Supplementary Figure 10.

Total RNA extraction for next generation sequencing (NGS)

Synchronous schizonts (3% parasitaemia: *Pfczif1*$^{\Delta C\text{-term}}$, *Pfczif2*$^{\Delta C\text{-term}}$, and parental wild-type) were resuspended in 10 x pellet volume of TRIzol® (Invitrogen), incubated at 37 ºC for 5 min, then resuspended in 2 x pellet volume of chloroform (Invitrogen) followed by a 3 min incubation at room temperature. The mixture was then centrifuged at 12000 rcf for 30 min to collect the aqueous supernatant containing total RNA, into new RNase-free tubes. The supernatant was then combined with an equal volume of 70% ethanol (diluted in PCR-grade H_2O) before being processed using a PureLink™ RNA mini kit (Qiagen) according to manufacturer's protocols. The purified RNA was incubated with 2 µL DNase I (Qiagen) at 1500 units/10 µL in 100 µL PCR-grade H_2O, and re-processed through the PureLink™ RNA mini kit in as described in the manufacturer's protocol for DNase-treatment.

Purified RNA samples were shipped frozen on dry ice to the Murdoch Children's Research Institute Victorian Clinical Genetics Services (MCRI-VCGS).

Total RNA libraries were prepared using the TruSeq Stranded Total RNA with Ribo-Zero Globin kit (Illumina) to enrich for non-host RBC RNA before being sequenced an a Novaseq platform with the following configuration: 2 x 150 base paired reads for 13,000,000 reads.

Differential expression analysis

Analyses were performed on the University of Adelaide Phoenix High Performance Computing (HPC) service, and personal computers. FASTQ files were first checked in FastQC 0.11.4 to verify the quality of the sequencing run. Once verified, an indexed genome was generated using version 46 of the PlasmoDB *P. falciparum* 3D7 genome in STAR 2.5.3. Reads were then aligned to the indexed genome in STAR 2.5.3a using SAMtools 1.3.1 to generate BAM output files. To check the alignments, BAM files were displayed in the Integrative Genomics Viewer (IGV, Broad Institute).

Differential expression analysis was performed using limma/voom in R Studio and Reads Per Kilobase of Transcript (RPKM) values were calculated for each gene. Given the overrepresentation of differentially expressed genes belonging to the *var*, *rifin* and *stevor* gene families, the analysis was performed using a modified reference genome which excludes these families (Tarr *et al.* 2018). A resulting fold change and false-discovery rate (FDR) p-value relative to a control transcriptome (parental wild-type) was then quantified. Data was exported from R-Studio and volcano plots were generated in Prism 9 (GraphPad), with a significance cut off threshold of logFDR < 0.05, logFC > 2.

Acknowledgements

We thank Prof Alan Cowman for providing RON4, RH5 GAP45 antibodies, Dr Paul Gilson for MSP1-19 and EXP2 antibodies, Dr Matt Dixon for ERD2, GAPDH and ERC antibodies. For the SLI-TGD vector, we thank Dr. Tobias Spielmann. We thank the Australian Red Cross Blood Bank for providing human red blood cells for parasite culture.

We thank Adelaide Microscopy (University of Adelaide) for providing support and access to microscopy facilities.

This work was supported by funding from the NHMRC (Project Grant APP1143974, DW), University of Adelaide Beacon Fellowship and Hospital Research Foundation Fellowship (DW), Australian Government Research Training Program Scholarship (JB).

Author contributions

Study design and planning J.M.B., P. G., M.D., D.W.W. Performed experiments and generated reagents J.M.B., G.K.H., D.W.W. Data analysis J.M.B., L.Y., M.A. Manuscript writing J.M.B., D.W.W. This manuscript was drafted with the input of all authors.

Competing interests

The authors declare no conflicts of interest.

Supplementary information

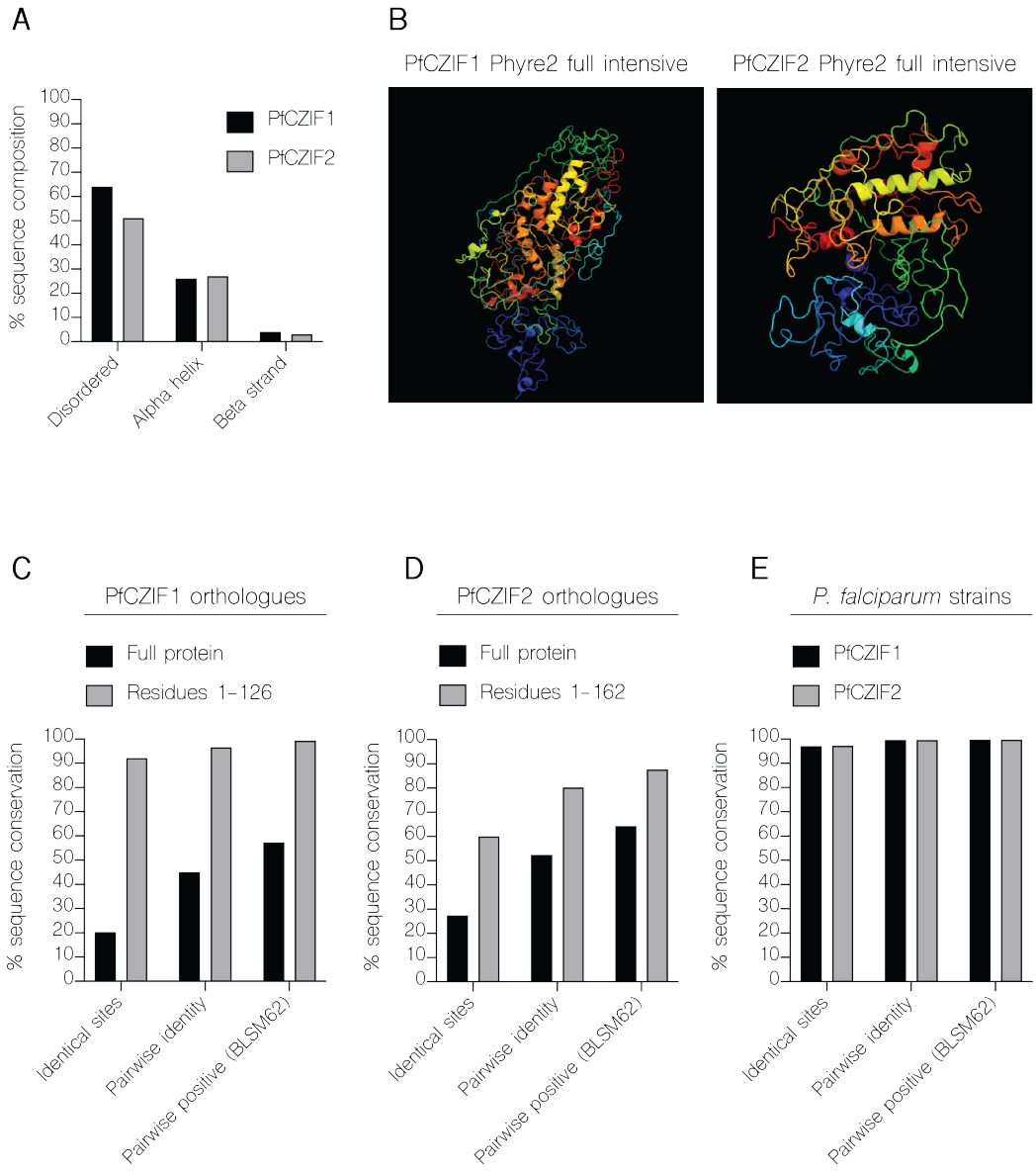

Supplementary Figure 1. **PfCZIF1 and PfCZIF2 are intrinsically disordered, conserved proteins. (a)** Excerpt of a Phyre2 intensive mode report for predicting secondary protein structure. Graph summarises the percentage proportion of PfCZIF1 and PfCZIF2's amino acid sequences predicted as disordered, forming alpha helices, or forming beta strands, **(b)** with a corresponding full-length protein model. Red = N-terminus, transitioning to blue = C-terminus. **(c-e)** Summary of pairwise alignment statistics. Identical sites refer to identical conserved amino acids, while pairwise identity is also inclusive of amino acids of chemical similarity which are predicted to not alter protein structure. Calculated in Geneious for:

(c) Syntenic orthologues of PfCZIF1 in *P. berghei* (PBANKA_1331700), *P. cynomolgi* (PCYB_124660), *P. gallinaceum* (PGAL8A_00227800), *P. inui* (C922_00098) *P. knowlesi* (PKNH_1213800), *P. malariae* (PmUG01_12048500), *P. ovale curtisi* (PocGH01_12046400), *P. praefalciparum* (PPRFG01_1469000), *P. reichenowi* (PRCDC_1467600), *P. vivax* (PVX_117045) and *P. yoelii* (PY02869). Visual representation of alignment shown in Supplementary Figure 2.

(d) Syntenic orthologues of PfCZIF2 in *P. berghei* (PBANKA_0712700), *P. cynomolgi* (PCYB_052360), *P. gallinaceum* (PGAL8A_00111100), *P. inui* (C922_02584), *P. knowlesi* (PKNH_0501900), *P. malariae* (PmUG01_05032900), *P. ovale curtisi* (PocGH01_05022800), *P. praefalciparum* (PPRFG01_0819600), *P. reichenowi* (PRCDC_0817400), *P. vivax* (PVX_089510) and *P. yoelii* (PY03958). Visual representation of alignment shown in Supplementary Figure 3.

(e) The equivalents of PfCZIF1 and PfCZIF2 in *P. falciparum* strains 7G8 (Pf7G8_140073500, Pf7G8_080023200), CD01 (PfCD01_140073600, PfCD01_080023700), Dd2 (PfDd2_140072700, PfDd2_080023300), FVO (PFFVO_05334, PFFVO_02121), GA01 (PfGA01_140073700, PfGA01_080021800), GB4 (PfGB4_140074300, PfGB4_080022900), GN01 (PfGN01_140073600, PfGN01_080023800), HB3 (PfHB3_140074000, PfHB3_080023600), IT (PfIT_140074700, PfIT_080023100), KE01 (PfKE01_140073100, PfKE01_080023700), KH01 (PfKH01_140073800, PfKH01_080023200), KH02 (PfKH02_140074000, PfKH02_080023700), MaliPS096 (PFMALIP_05529, PFMALIP_02139), IGH-CR14 (PFMG_04912, PFMG_04917), ML01 (PfML01_140074100, PfML01_080023700), NF135/5.C10 (PFNF135_05581, PFNF135_02241), SD01 (PfSD01_140071600, PfSD01_080023500), and SN01 (PfSN01_140075500, PfSN01_080022700) and TG01 (PfTG01_140073600, PfTG01_080024000) respectively.

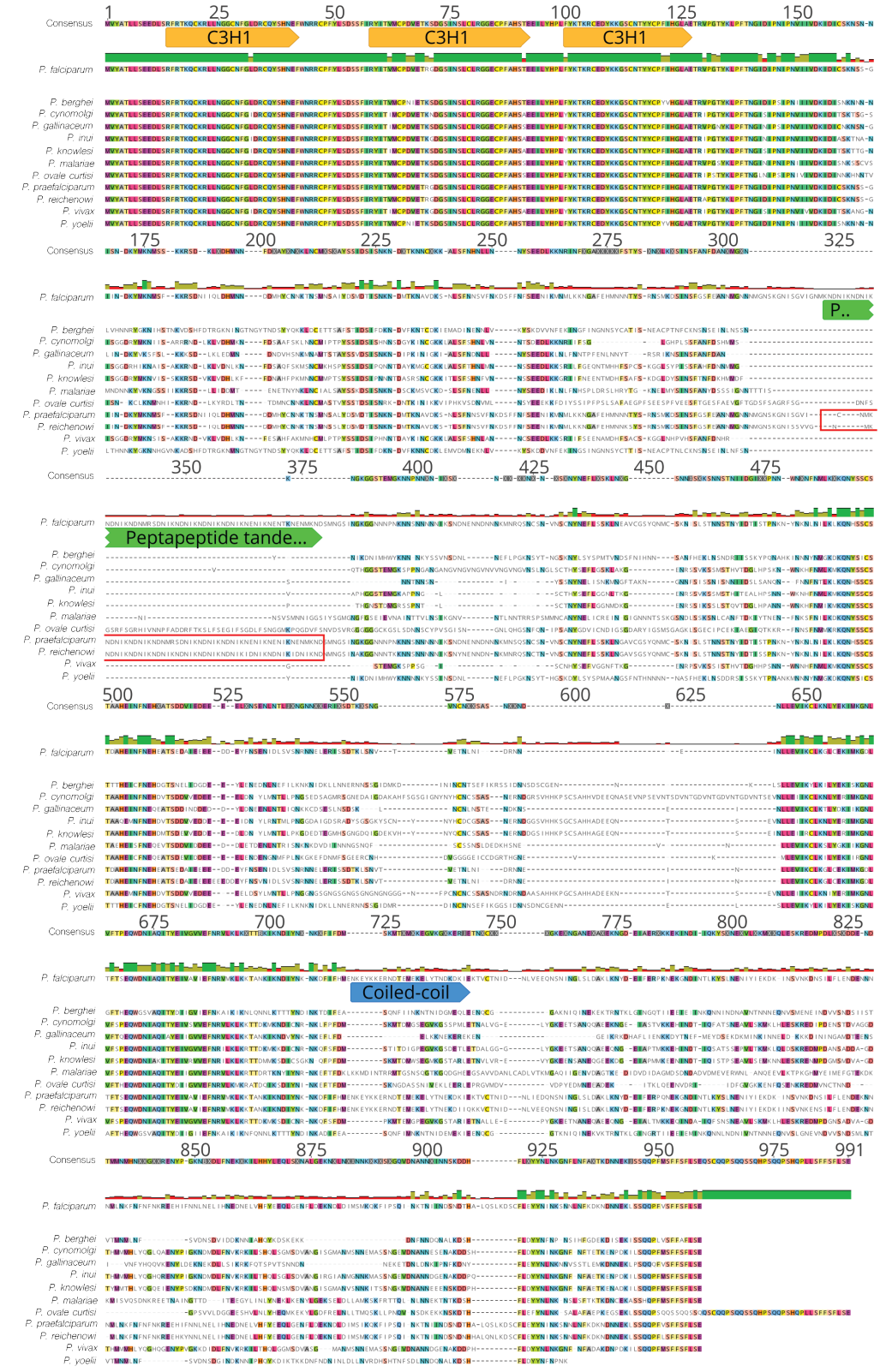

Supplementary Figure 2. Pairwise alignment of PfCZIF1 (Pf3D7_1467400) with its syntenic orthologues across *Plasmodium* spp, highlighting the location of specific domains. Outlined in red is the presence of the pentapeptide tandem repeat, exclusive to *P. falciparum*, *P. praefalciparum* and *P. reichenowi.*

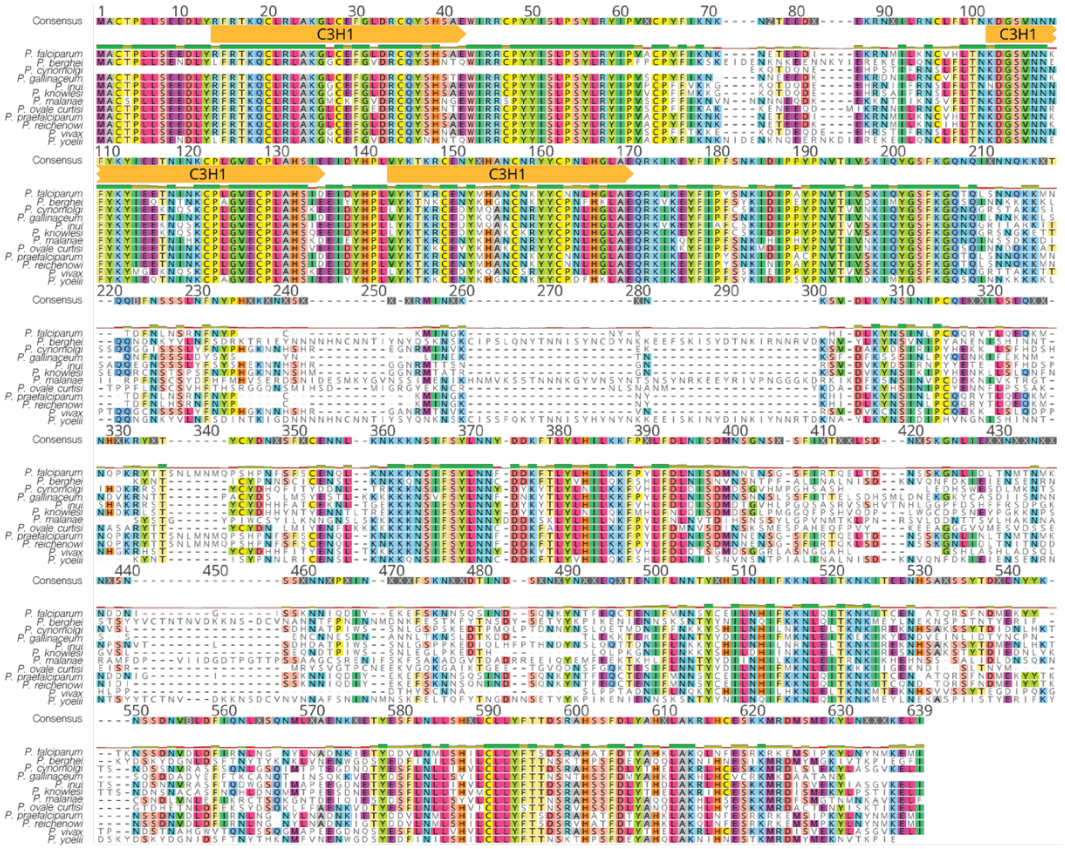

Supplementary Figure 3. Pairwise alignment of PfCZIF2 (Pf3D7_0818100) with its syntenic orthologues across *Plasmodium* spp., highlighting the location of specific domains.

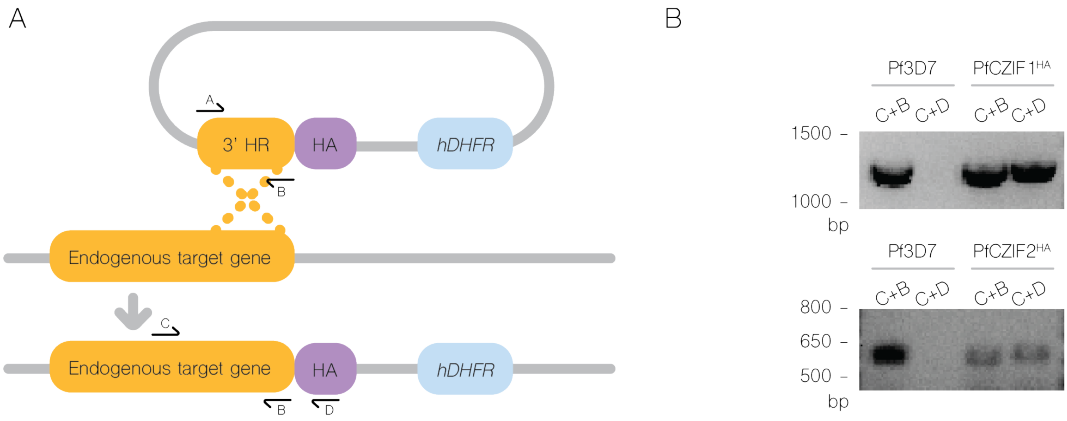

Supplementary Figure 4. Generation of HA-tagged PfCZIF1 and PfCZIF2. (a) Schematic of the pHA3 plasmid used to generate endogenously HA-tagged PfCZIF1 and PfCZIF2 by single-crossover homologous recombination. A 3' homology flank for each gene was amplified using primers A and B and subcloned into pHA3. (b) Successful integration of the HA tag was confirmed by PCR and gel electrophoresis, with the specificities of each primer pair illustrated in (a).

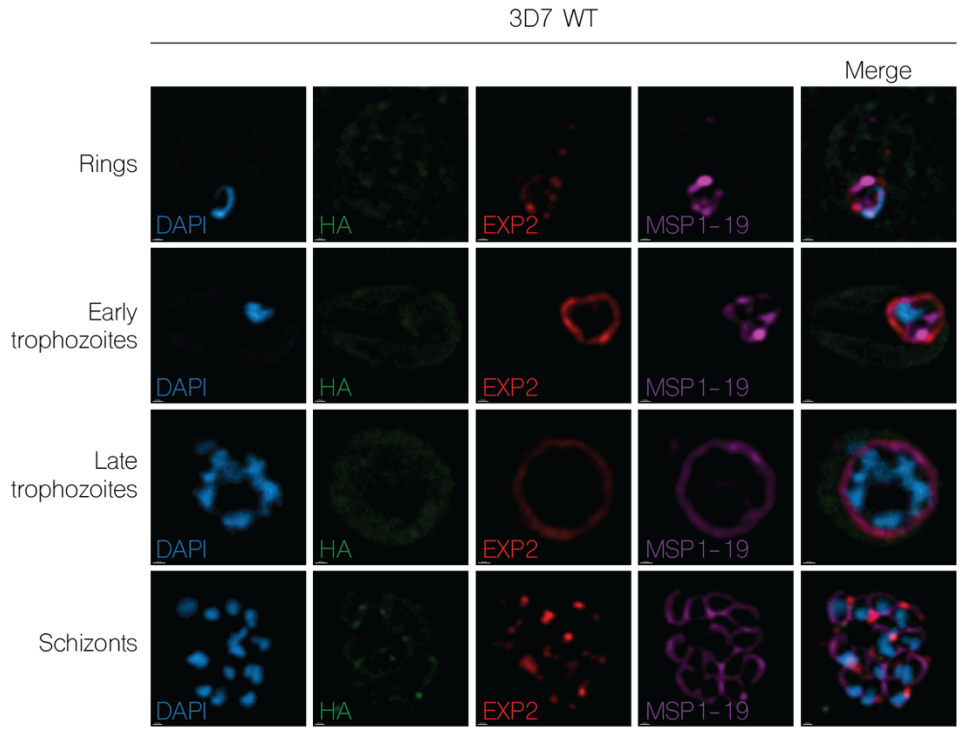

Supplementary Figure 5. Control IFA experiments in 3D7 WT parasites, which do not express a HA-tagged protein, show that sample preparation with biotin-conjugated anti-HA antibodies and a streptavidin-conjugated AlexaFluor 488 do not generate distinct fluorescent puncta across rings, early trophozoites, late trophozoites and mature schizonts.

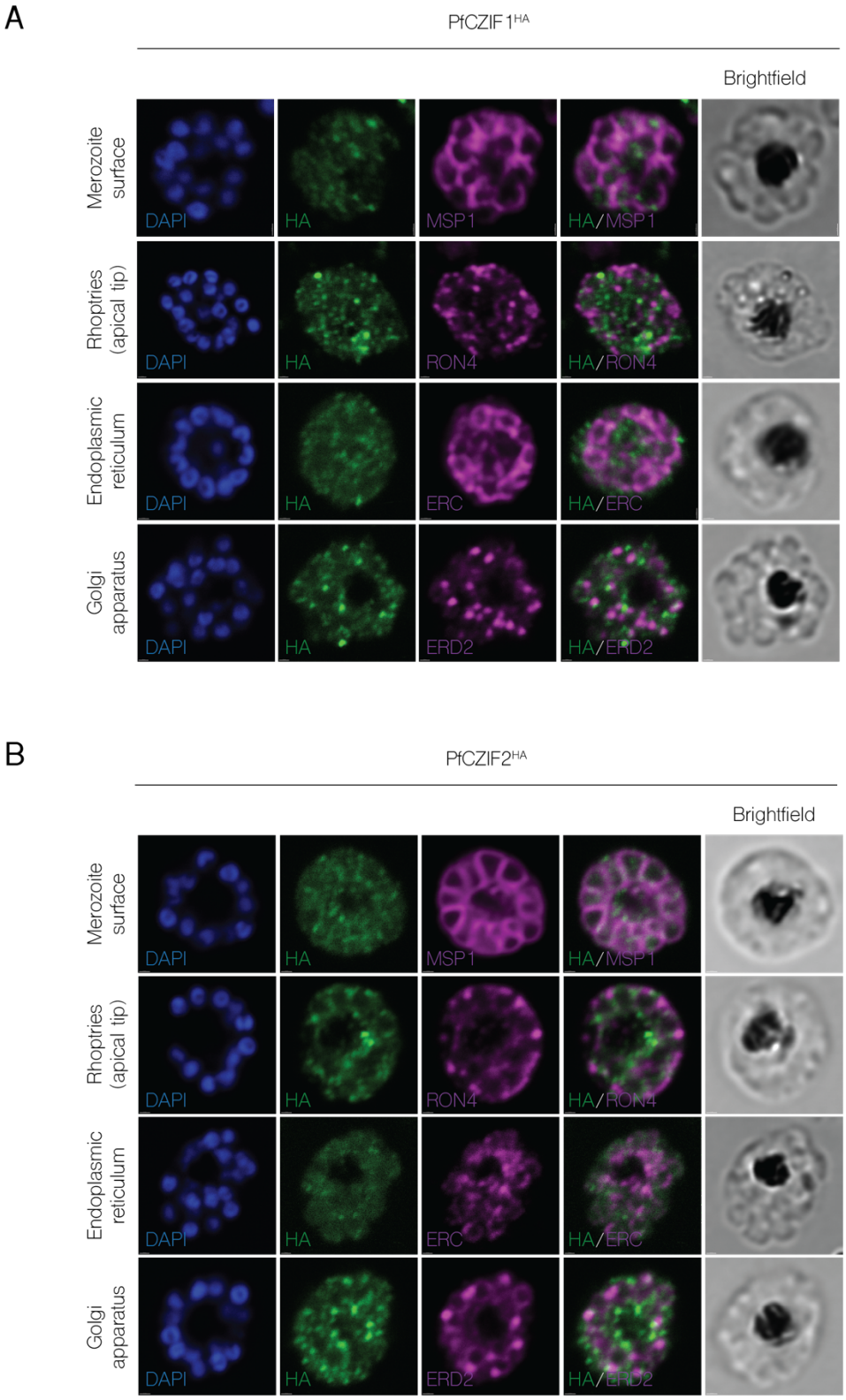

Supplementary Figure 6. **(a)** HA-tagged PfCZIF1 and **(b)** PfCZIF2 (visualised with AlexaFluor488) do not co-localise with other tested markers (visualised with AlexaFluor647) in schizonts. Markers include antibodies against the rhoptry neck (anti-RON4), endoplasmic reticulum (anti-ERC), and the Golgi apparatus (anti-ERD2). Nucleus is stained with DAPI.

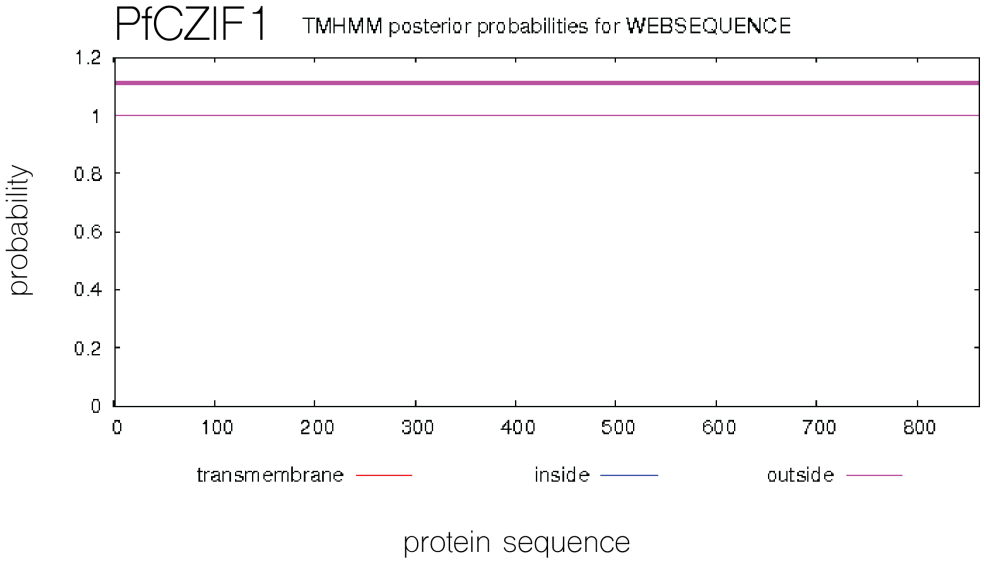

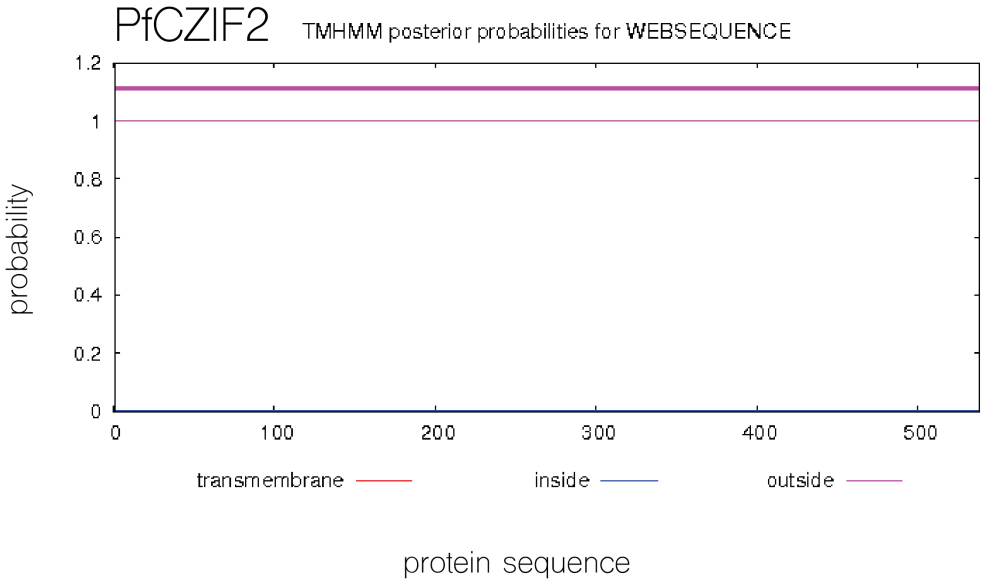

Supplementary Figure 7. PfCZIF1 and PfCZIF2 are not predicted to have transmembrane helices. Calculated for the full amino acid sequences for each protein in TMHMM (DTU Bioinformatics, Center for Biological Sequence Analysis) using extensive output settings.

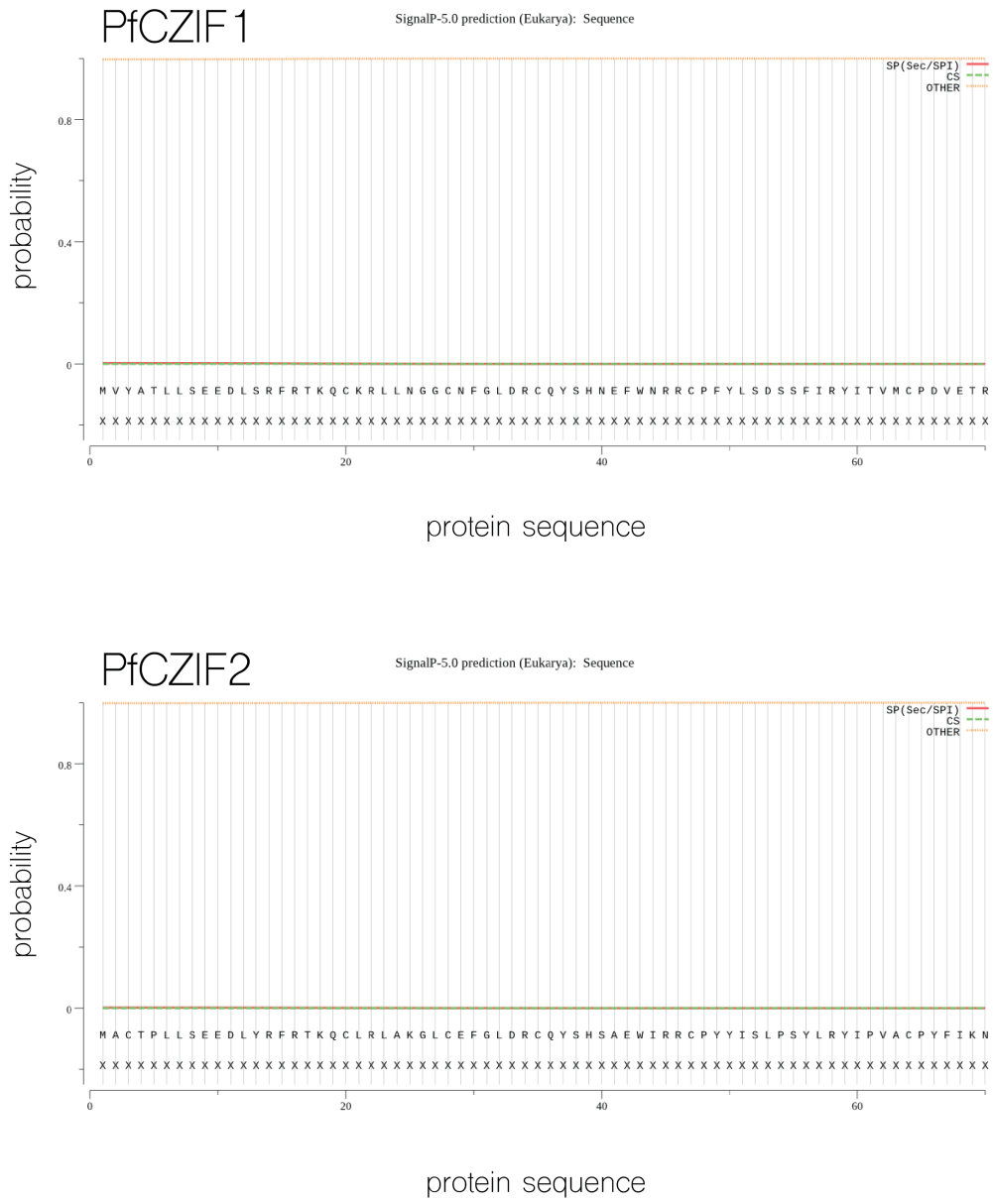

Supplementary Figure 8. PfCZIF1 and PfCZIF2 are not predicted to have an N-terminal signal peptide sequence. Calculated for the full amino acid sequences for each protein in TMHMM (DTU Bioinformatics, Center for Biological Sequence Analysis) using long output settings for Eukarya.

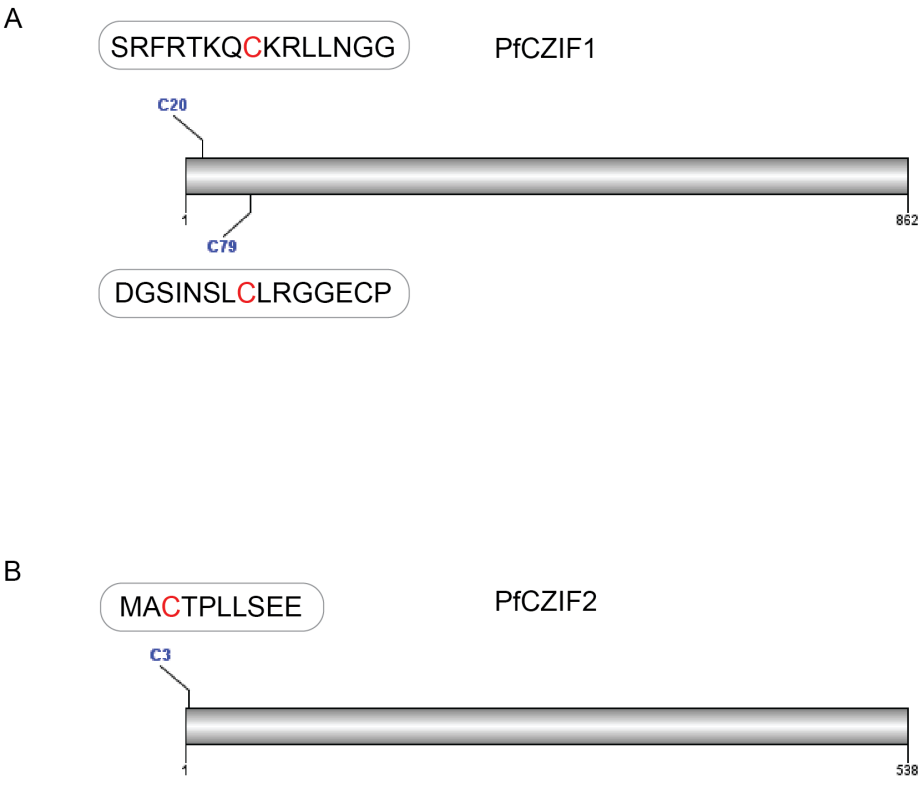

Supplementary Figure 9. PfCZIF1 and PfCZIF2 are predicted with S-palmitoylation sites at cysteine residues within their N-termini. Determined in GPS-Lipid (Xie *et al.* 2016) for the full amino acid sequences using default settings.

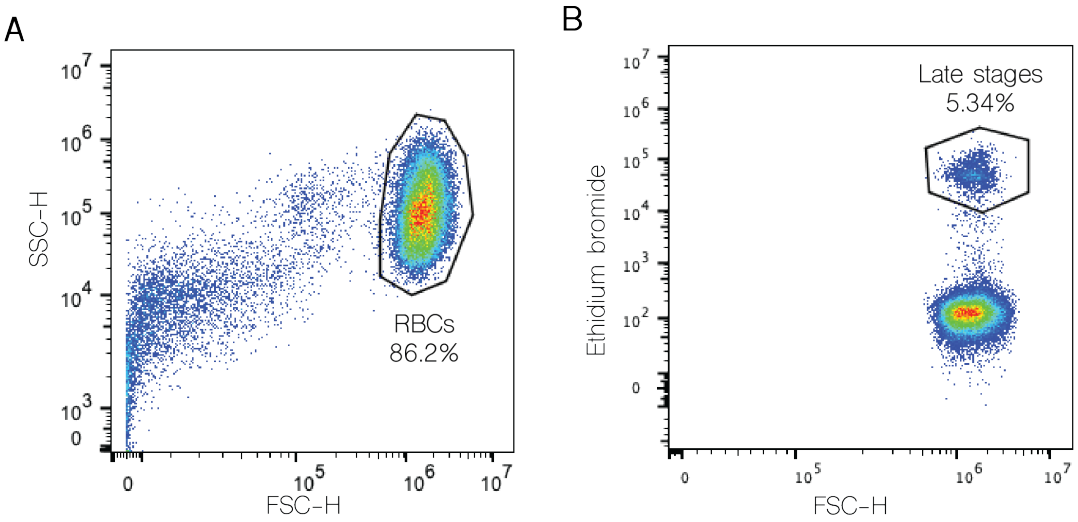

Supplementary Figure 10. Representative flow plots showing our gating strategies for flow cytometry analysis. **(a)** Gating for red blood cells (RBCs) (FSCH-H vs. SSC-H0 and **(b)** late-stage parasites (FSC-H vs. PE-H (EtBr)) which include trophozoites and schizonts. Plots were exported from FlowJo Version 10.

A

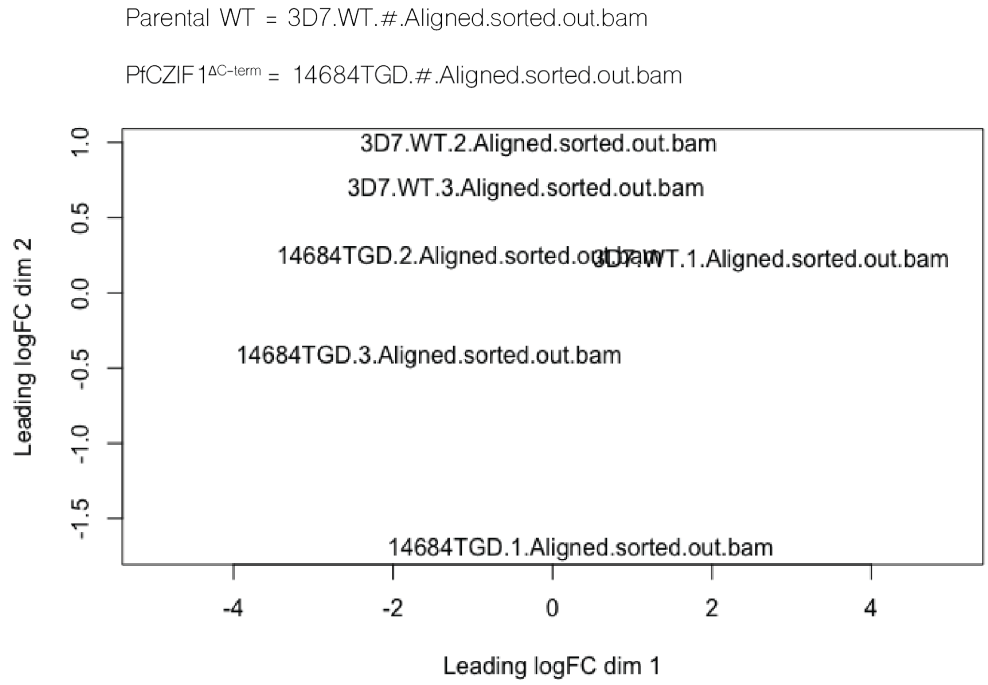

B

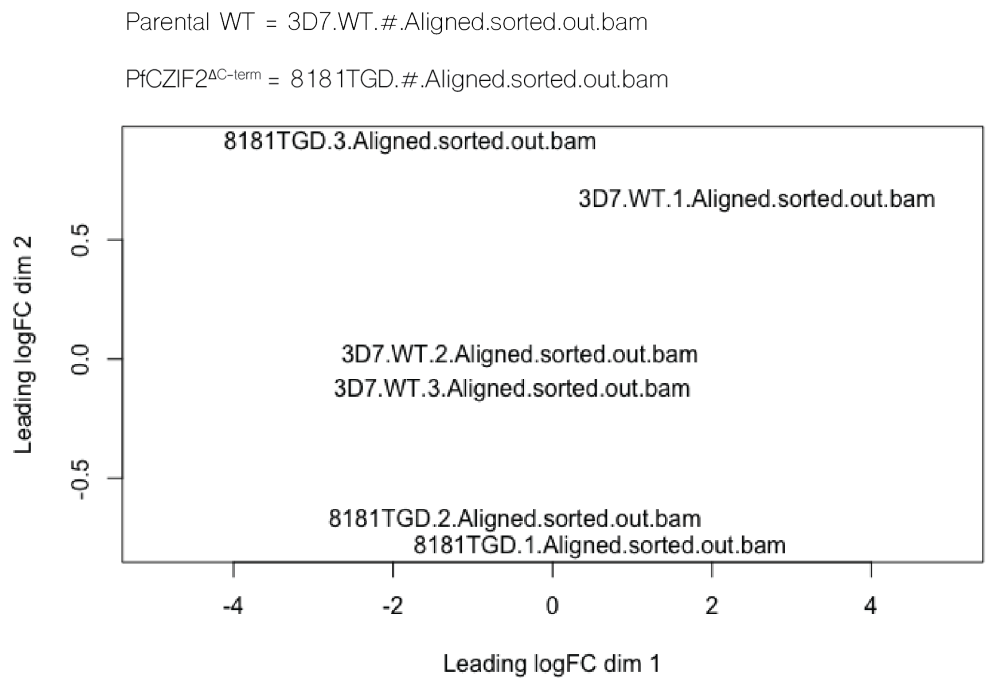

Supplementary Figure 11. Multidimensional scaling (MDS) plots reveal the level of library variation between the global transcriptomes of three biological replicates of parental WT compared to **(a)** PfCZIF1$^{\Delta C\text{-term}}$ **(b)** and PfCZIF2$^{\Delta C\text{-term}}$. The position of data refers to the position of the first letter of the data file name.

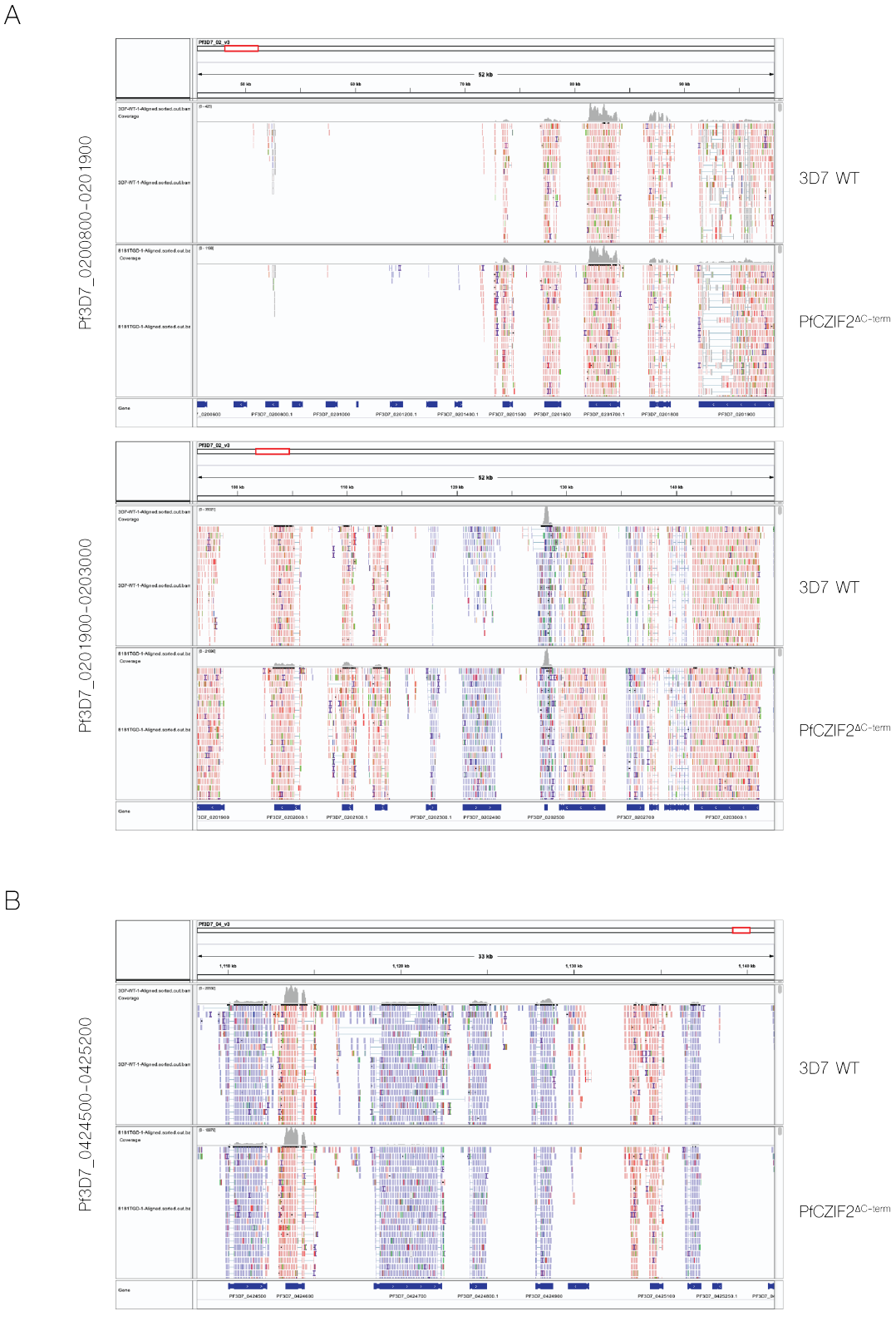

Supplementary Figure 12. No chromosomal deletions were detected at specific loci for **(a)** Chromosome 2 and **(b)** Chromosome 4 in parental WT vs. PfCZIF2$^{\Delta C\text{-}term}$ parasites. Alignment was obtained using the Integrative Genome Viewer (IGV, Broad Institute) using .bam files against a reference *P. falciparum* genome

(PlasmoDB Version 46). Alignment shows biological replicate 1 for each of the parental WT and PfCZIF2$^{\Delta C\text{-term}}$ and is representative of three biological replicates.

Chapter 4

Final discussion

Final discussion

Preface

The overarching aim of this thesis was to identify novel schizont or merozoite-expressed proteins and, within the scope of invasion-related themes, characterise their molecular function in blood stage *P. falciparum* parasites. To summarise, in Chapter 2 I made a major contribution to the investigation of the function and phylogenetic origins of PfCERLI2 as a duplicated gene product of its homologue PfCERLI1, with an emphasis on rhoptry biology. In contrast, in Chapter 3 I presented my insights on the interplay between the proteins PfCZIF1 and PfCZIF2 and their contributions to blood stage growth, while finding no link between these two proteins and invasion. Given that the proteins investigated in each chapter differ, this discussion will be split into two sections to highlight topics which build on concepts addressed in the individual chapter manuscripts. Here I will provide my analysis on study direction, pointing out key implications, means of alleviating experimental shortcomings, and summarising future directions.

Comparing structural features and localisation

PfCERLI1 was first characterised as a novel protein that is essential for blood stage growth and merozoite invasion which localises to the cytosolic face of the rhoptry bulb membrane. Moreover, PfCERLI1 possesses predicted structural features that could potentially facilitate membrane targeting (Suarez *et al.* 2019, Liffner *et al.* 2020). Our studies have shown that *Pfcerli2* arose from a gene duplication event of *Pfcerli1*, and as a result PfCERLI2 possesses several structural features akin to that of its paralogue. Most notably, both proteins possess a highly conserved Pro-His-Iso-Ser (PHIS) motif flanked by semi-conserved residues that is also found in three other proteins in *P. falciparum*. These include the cytosolic superoxide dismutase (PfFeSOD) which mitigates cellular damage caused by haemoglobin digestion-derived oxidative stress, caseinolytic protease (PfClpR) which is a chaperone protein involved in cellular homeostasis, and the ring-infected erythrocyte surface antigens (PfRESAs) which are a family of proteins involved in host cell remodelling (El Bakkouri *et al.* 2010, Boucher *et al.* 2006, Marti *et al.* 2004). The function of the PHIS motif has not been determined for any protein to date, but it is likely that the first proline, which is 100% conserved for all PHIS-containing proteins, is vital for its function. Likewise, the remaining residues possess high levels of conservation across PHIS-containing orthologues in Apicomplexans. However as the PHIS motif is contained within the intrinsically disordered regions of the protein, no meaningful secondary structure can be predicted surrounding this motif. Site-directed mutagenesis studies using techniques such as CRISPR-Cas9 to target the PHIS motif are likely needed to reveal whether this part of the protein is required for PfCERLI1 and PfCERLI2 function.

Both proteins possess a C2 domain, a domain class known to be involved in membrane targeting through a calcium-dependent process. Ca^{2+} ions, which are thought to be stored within the parasite itself as well as accessed from the host during invasion, are key for triggering the secretion of apical organellar proteins (de Oliveira *et al.* 2021). Similarly, calcium levels through the C2 domain may govern the localisation of proteins to the rhoptries, and thus the C2 domain may be

key for PfCERLI1 and PfCERLI2 for attaching to lipids. This mode of attachment has been shown by the double C2 domain (PfDOC2) protein, a protein kinase involved in microneme secretion that is associated to membranes in a calcium-dependent manner (Farrell *et al.* 2012, Jean *et al.* 2014). Experimental verification of whether the C2 domain is needed for localisation can be accomplished by targeted deletion of this motif using CRISPR-Cas9 or dimerizable Cre (DiCre). As an additional point of interest, Ca^{2+} levels are heavily modulated in response to potassium (K^+) concentration, where if K^+ is low then Ca^{2+} is increased accordingly (de Oliveira *et al.* 2021). This phenomenon elicits a response from PfACβ, another known C-RIP of the rhoptries, which activates protein kinase A (PfPKA) which phosphorylates PfCERLI1 and PfCERLI2. Moreover, we identified the catalytic subunit of PfPKA (PfPKAc) as an interactor for both proteins by DiQ-BioID. Interplay between PfACβ, phosphorylation by PfPKA, PfCERLI1 and PfCERLI2 may underpin a novel mechanism involving the C2 domain and membrane targeting.

The key structural difference between the proteins is in their C-terminal domains, where PfCERLI1 possesses a predicted Pleckstrin homology (PH) domain, whereas PfCERLI2 harbours a decapeptide tandem repeat (DTR). PH domains are known to target phospholipids on membranes, as well as recruit proteins to the Golgi – the organelle with which rhoptry biogenesis begins (Singh *et al.* 2021, Falkenburger *et al.* 2010, Dubremetz *et al.* 2007, Counihan *et al.* 2013). Our functional analysis suggests that PfCERLI2's DTR follows a region with similarities to a PH domain, but that has likely lost this function given the inclusion of structure disrupting inserts of PfCERLI2 compared to other Apicomplexan CERLI2s. The DTR itself appears to have evolved as an extension to the protein in *Laveranian* parasites – a subgenus of *Plasmodium,* which includes *P. billcollinsi, P. billbrayi*, *P. falciparum*, *P. gaboni*, *P. adleri*, *P. blacklocki* and *P. reichenowi* (Rayner *et al.* 2011). Both the PH and DTR of each protein appear to be essential in our SLI-TGD knockout models, which is intriguing given that PfCERLI2's DTR favours variability and is under positive selection, where the total repeat region can vary from 10 (Pf7G8) to 20 (PfCD01) units. Moreover, PCR amplification of the 3' exons of PfCERLI2 in PfDd2 parasites (as PfMAg-1), was reported to produce multiple banding patterns, which they owed to differences in repeat copy number (Gao *et al.* 2009). Therefore, constantly changing this region does not appear to

have an adverse impact on PfCERLI2 function. This does however suggest that PfCERLI2 requires at least 10 units in its DTR for function based on existing strains. The function of DTRs as a class remains extremely poorly characterised, though one sample from the mussel species *Mytilus californianus* and *Mytilus edulis* revealed a protein possessing a DTR of 75 repeat units, mussel foot protein 1 (Mfp-1), which it uses as an adhesin to cling to rocks. However as Mfp-1's DTR possesses completely different residues to PfCERLI2, it is unlikely to share a function based on being a DTR alone (Das *et al.* 2015).

PfCERLI2 as a vaccine candidate

Prior to our studies, PfCERLI2 was proposed as a viable vaccine candidate as it was thought to localise to the cell surface, could be targeted by inhibitory antibodies, and was predominantly expressed in schizonts and merozoites (Gao *et al.* 2009, Zenonos *et al.* 2014, Otto *et al.* 2010). Moreover, its low expression profile is akin to that of leading merozoite vaccine candidates such as RH5 (Drew & Beeson *et al.* 2015). Furthermore, PfCERLI2 exhibits low levels of sequence polymorphism which favours it as a non-variable immunogen, with the exception of its DTR. On that note, though serological studies have identified the presence of PfCERLI2-targeting antibodies, it remains unknown if they are protective or cross-reactive (Dent *et al.* 2015). We show extensively in our study using both super-resolution microscopy and biochemical localisation techniques that PfCERLI2 localises exclusively to the cytosolic face of the rhoptry bulb in schizonts and therefore is unlikely to be targeted by protective antibodies. Likewise, we could not detect PfCERLI2 in culture supernatants in Western blot experiments, removing the possibility of it being a secreted antigen. Studies conducted by Suarez *et al.* have similarly shown that the *T. gondii* orthologue TgRASP2, localises to a similar equivalent space on rhoptry neck and bulb, suggesting conservation of protein localisation across the phylum. The localisation of PfCERLI2 and several of its structural features are shared with its paralogue PfCERLI1 (Liffner *et al.* 2020). The unique position of these proteins on the surface of the rhoptry bulb highlights them as intracellular components of the rhoptry machinery and novel C-RIPs.

The roles of PfCERLI2 with insights from PfCERLI1

We have determined that *Pfcerli2* is resistant to genetic ablation and is therefore essential for parasite blood stage growth, similar to its paralogue *Pfcerli1*. To pinpoint its role, we have used glucosamine-inducible knockdowns of PfCERLI2 to show that it is specifically involved in merozoite invasion. Moreover given that PfCERLI2 is found on the cytosolic face of the rhoptry bulb, it is most likely to function and contribute to specific rhoptry-related processes during invasion. However as the knockdown phenotypes of PfCERLI1 and PfCERLI2 do not completely match, it is unlikely that they maintain identical roles.

We first observed in culture that PfCERLI2 knockdown led to fewer merozoite invasion events, though this was not caused by a change in merozoite number per schizont, making it unlikely that this protein influences schizogony at the point of cytokinesis. Indeed, a similar phenotype was observed during PfCERLI1 knockdown (Liffner *et al.* 2020). Notably, many PfCERLI2 knockdown merozoites appeared bound to the merozoite surface, suggesting a defect at the formation of the tight junction (TJ). We have demonstrated using quantitative microscopy that bound PfCERLI2 knockdown parasites do not traverse as far into the TJ and result in a similar phenotype to that of cytochalasin D-treated parasites. Thus, we hypothesise that PfCERLI2's role in invasion is at or before formation of the TJ. As PfCERLI2 knockdown does not affect rhoptry neck antigen secretion in the case of PfRON4 and PfRH4, invasion is likely to proceed normally up to the point these proteins are utilised and the TJ could form. Interestingly, a defect in rhoptry neck secretion was observed for PfCERLI1 knockdown, highlighting a key difference between the paralogues and potentially explaining why PfCERLI1 knockdown parasites failed to bind strongly to the RBC surface.

We have also shown that knockdown of PfCERLI2 inhibits proteolytic processing of the luminal bulb protein PfRAP1, though this is likely through an indirect mechanism. This is because PfRAP1 is known to be directly processed by plasmepsin IX (PfPMIX) and subtilisin 1 (PfSUB1) in the rhoptry lumen, the former of which when knocked down produces a similar phenotype which permits merozoites to egress but then fail to invade (Nasamu *et al.* 2017, Nasamu *et al.* 2020, Silmon de Monerri *et al.* 2011). It is possible that the rhoptry morphology

defect caused by PfCERLI2 knockdown impedes upon PfPMIX's function, thereby inhibiting its ability to proteolytically process PfRAP1 downstream. If this is the case, there is no need for a direct interaction between PfCERLI2 and PfPMIX, and indeed we did not identify PfPMIX or PfSUB1 as interactors by DiQ-BioID. Interestingly, knockdown of PfCERLI1 exhibits an identical PfRAP1 processing defect phenotype despite not impacting rhoptry morphology (Liffner *et al.* 2020). However, given PfCERLI1 knockdown affects rhoptry antigen distribution, it may also similarly affect normal PfPMIX activity.

Localisation of PfCERLI2

The *T. gondii* orthologues TgRASP1 and TgRASP2 were reported to be involved in coordinating membrane fusion between the tip of the rhoptry neck to the PPM to form a channel for tachyzoite antigen secretion. Intriguingly, neither protein is essential in *T. gondii* as opposed to PfCERLI1 and PfCERLI2, suggesting that there are redundant or alternative mechanisms for rhoptry-PPM fusion in *T. gondii*. However, given the differences in rhoptry size and numbers between tachyzoites and merozoites, the different rhoptry physiologies may be governed by different proteins (Suarez *et al.* 2019).

There is a discrepancy between the localisation of PfCERLI1 between Suarez *et al.* and Liffner *et al*. where the former suggests it to be on the rhoptry neck in egressed merozoites, while the latter suggests it to be on the bulb of merozoites still contained in schizonts (Suarez *et al.* 2019, Liffner *et al.* 2020). One possibility is that PfCERLI1 translocates on the cytosolic face of the rhoptry membrane between the bulb and neck during invasion. This has yet to be investigated, and will likely require further quantitative super-resolution imaging analyses. To this end, it is of interest to determine whether PfCERLI2 also possesses a differential localisation between schizonts and merozoites. This investigation is hampered by the fact that PfCERLI2 is extremely difficult to detect experimentally by fixed cell IFA upon complete maturation of the schizont for unknown reasons. In our attempts to understand why, we have explored the possibility that PfCERLI2 could be proteolytically cleaved in mature schizonts to remove its HA-tag though no cleavage products were detected by Western blot. We alternatively suggest that PfCERLI2, in its native conformation, may be resistant to

antibody labelling in fixed cells due to epitope masking at the end of its DTR. Therefore, remaining questions could be addressed using live fluorescent tags. Indeed, we were able to visualise GFP-tagged PfCERLI2 in live mature schizonts in our lines for DiQ-BioID. Live cell analysis of lines expressing GFP-tagged PfCERLI2, given the proper super-resolution capabilities, may determine whether the protein translocates while also serving as a tool for investigating protein dynamics during the invasion process.

Insights from the interactomes of PfCERLI1 and PfCERLI2 for further investigation

Our DiQ-BioID results for PfCERLI1 and PfCERLI2 do not currently suggest that the two interact in *P. falciparum*, however it remains possible that the two complex indirectly with other unidentified intermediate proteins. We did attempt an alternative pull-down method through immunoprecipitation of native protein in solubilised cells using HA-tagged PfCERLI1 and PfCERLI2. However, we experienced several difficulties in solubilising HA-tagged protein, likely due to a strong membrane association, and did not proceed further with this protocol. Nevertheless from our existing DiQ-BioID data, we have successfully shown that the two proteins share a possible common interactor in the multi-transmembrane domain containing protein PfROP14. The function of PfROP14 is currently unknown, however it has been shown to localise to the rhoptries in schizonts and is often positioned posterior to PfRON4 in the rhoptry neck (Zuccala *et al.* 2012). Therefore, PfROP14 may be a rhoptry bulb protein and furthermore a plausible C-RIP candidate.

We identified Pf3D7_0934800 (cAMP-dependent protein kinase catalytic subunit of protein kinase A, PfPKAc) as an interactor of PfCERLI1. PfPKAc is an essential kinase involved in numerous cellular processes including blood stage growth and merozoite invasion (Wurtz *et al.* 2009, Wilde *et al.* 2019). Moreover, phosphoproteomic studies have shown that its substrates include both PfCERLI1, PfCERLI2 and PfROP14 (Patel *et al.* 2019). Of most interest is PfPKA's role as a downstream effector for the cAMP-signalling pathway during invasion, requiring activation by cAMP second messenger molecules produced by PfACβ to perform phosphorylation. PfACβ, a C-RIP which is the sole generator of cAMP in blood

stage parasites, supplies cAMP for PfPKA en route to phosphorylating PfCERLI1, PfCERLI2 and other substrates (Patel *et al.* 2019). However, it remains unknown as to how phosphorylation affects these proteins mechanistically. Investigating the essentiality of phosphorylation sites on PfCERLI1 and PfCERLI2, which can be studied using targeted mutagenesis and CRISPR-Cas9, is of future interest.

The top interactor for PfCERLI1 was identified to be PhIL1a interacting candidate 1 (PfPIC1), which is a putative IMC protein. This opens up the possibility that there may be direct interactions between the rhoptry and IMC, possibly during early biogenesis of the nascent rhoptries from the Golgi or once the respective organelles are formed. Capturing this interaction is possible within the eight hour biotinylation period of our DiQ-BioID, as rhoptry biogenesis begins at early schizogony (Liffner *et al.* 2021). The precise timing of the formation of the nascent rhoptry though has yet to be elucidated. This relationship between the rhoptries and IMC is similarly observed in TgRASP2's interaction with TgFormin1, which is involved in actin polymerisation, where its *P. falciparum* orthologue PfFormin1 has been determined as essential and localises between the rhoptries and IMC (Suarez *et al.* 2019, Baum *et al.* 2008). Based on that evidence, it may be suggested that a similar mechanism to actin polymerisation plays a role in rhoptry biogenesis. Indeed, the precise mechanisms controlling movement of the rhoptries towards the apical tip is a missing puzzle piece in the current model for rhoptry biogenesis. Based on several of our DiQ-BioID hits, a mechanism for organellar movement may be facilitated by spindle or vesicle transport proteins. To this end, we identified spindle assembly abnormal protein 6 (Pf3D7_0607600) as an interactor for PfCERLI2, and a hypothetical vacuolar transport chaperone (Pf3D7_1230200) as a PfCERLI1 interactor for follow-up investigation.

A structural scaffold which tethers the rhoptries to the apical tip is another missing puzzle piece in merozoites, which is fulfilled by the conoid and apical annuli in *T. gondii* tachyzoites, and proteins such as TgDHHC7 and TgARO (Koreny *et al.* 2021, Beck *et al.* 2013). The potential role of ARO as a mediator of rhoptry tethering in *Plasmodium* spp., though not proven for PfARO, is interesting given its distance from the IMC and PPM as a C-RIP located on the bulb of *Plasmodium* rhoptries. A CERLI2 interacting protein broadly associated with

tethering of the rhoptries to the PPM in *T. gondii* is the methyltransferase PfAAMT. TgAAMT localises to the apical annuli/conoid in intracellular tachyzoites – a unique cytoskeletal structure originally thought to be absent in *P. falciparum* merozoites (Engelberg *et al.* 2020). Recent work has shown the existence of tubulin networks in *P. falciparum* that are reminiscent of the conoid (Bertiaux *et al.* 2021). Most interestingly, PfAAMT has been shown as a potential interactor of photosensitized INA-labelled protein 1 (PfPhIL1a) and may therefore interact with the IMC (Wichers *et al.* 2021). Wichers *et al.* have identified it as an IMC-interacting protein, while we have identified it as a potential rhoptry bulb-interacting protein through its interaction with CERLI2. Although the function of PfARO and PfAAMT have not been determined to date, one possibility is that these proteins may perform a role in tethering of the rhoptries that involves interactions with the IMC during biogenesis of these organelles or once formed.

Several conserved proteins of unknown function with peak expression at schizonts (Otto *et al.* 2010) were identified in our DiQ-BioID of PfCERLI1. Namely, we identified and designated five CERLI1-interacting candidates (C1C): Pf3D7_1133200 (PfC1C1), Pf3D7_1019600 (PfC1C2), Pf3D7_0310900 (PfC1C3), Pf3D7_1325900 (PfC1C4) and Pf3D7_1206300 (PfC1C5). Of these, only PfC1C3 has been shown to be refractory to deletion by saturation mutagenesis in *P. falciparum* and is likely essential for growth (Zhang *et al.* 2018). Interestingly, PfC1C1 was reported to bind PfCERLI2 in yeast-2-hybrid studies but not PfCERLI1 (LaCount *et al.* 2005). Functional characterisation of these candidates as a starting point will likely shed light on their interactions with PfCERLI1 in schizonts and during merozoite invasion.

Future directions using new techniques to study PfCERLI1 and PfCERLI2

Though to this point I have highlighted some of our key findings, there remains much yet unexplored for each of PfCERLI1 and PfCERLI2 which new techniques or approaches may address.

Observe dynamics during rhoptry fusion and invasion by live cell microscopy

We do not know whether PfCERLI1 and PfCERLI2 participate directly in invasion at the merozoite-RBC interface or in rhoptry fusion. The possibility of a

direct role at the interface is implied by the discrepancy between the localization for PfCERLI1 as either a bulb or neck antigens in schizonts and merozoites respectively (Liffner *et al.* 2020, Suarez *et al.* 2019), where the neck is in closer proximity to the RBC. Likewise, the cause for having a role in rhoptry fusion is supported by their cytosolically-exposed localisations. These potential for PfCERLI1 to translocate from the rhoptry bulb to the neck during merozoite invasion could be explored by live cell microscopy using GFP tagged lines developed in this study.

We have shown that endogenous tagging of PfCERLI1 and PfCERLI2 with large fluorescent tags such as GFP is feasible, allowing us to visualise each protein in live cells. By further modifying these lines with a corresponding C-RIP of interest with another fluorescent tag, this would allow us to directly compare C-RIP behaviours as well as serve as reference points for co-localisation. In mature schizonts arrested with an egress inhibitor, PfCERLI1 and PfCERLI2 should be visible as a double-donut structure in mature rhoptries. Upon removal of inhibitor and allowing egress of merozoites, we can visualize how this double-donut structure changes during the process of invasion to observe bulb fusion. Alternatively, if we observe a shift of signal from bulb to neck, this may suggest protein translocation and provide a precedent for these proteins to be involved in rhoptry-PPM fusion.

Identifying a unique rhoptry membrane scaffold for C-RIPs by expansion microscopy

Little is known about the ways proteins are scaffolded in the rhoptries, let alone on the surface of the rhoptry membrane. Within resolution limits of our microscopy platforms, we have only scratched the surface regarding the localization of PfCERLI1 and PfCERLI2 appearing as double-donuts of the rhoptry bulb. As we have not investigated colocalisation between PfCERLI1 and PfCERLI2, and have shown that the two do not interact in our DiQ-BioID dataset, there remains the possibility that the two are spatially separated. Super-resolution imaging of both proteins simultaneously using double-tagged lines, or using raised anti-PfCERLI1 and anti-PfCERLI2 antibodies, may detail differences in protein distribution on the surface of the rhoptry bulb. To visualise the finer architecture

and protein distribution, we can employ ultrastructure expansion microscopy (U-ExM). U-ExM is a technique which can enlarge cells and membrane-bound organelles in direct proportion to their original shape by isotropic expansion. This technique permits us to generate artificially enlarged parasite material for IFA using existing microscopy platforms available to our laboratory. U-ExM has recently been adapted in *T. gondii* which could detail the structures of the subpellicular microtubules and conoid of tachyzoites, and has been adapted in *P. falciparum* merozoites for examining the tubulin network of the cytoskeleton (Tosetti *et al.* 2020, Bertiaux *et al.* 2021). We believe this technique can be adapted to specifically examine rhoptry proteins.

Determining the crystal structure and the interface for protein-protein interactions

Elucidating the crystal structure of PfCERLI1 and PfCERLI2 would reveal whether these proteins share conserved secondary and tertiary structures, given that they have several domains in common. While certainly a crystal structure would be of benefit, we foresee that crystallising PfCERLI1 and PfCERLI2 will be difficult given that it is intrinsically disordered in all residues outside of the C2 and PH domains. While it has been shown that C2 and PH domains can be crystallised in isolation, this approach will not inform whether these domains interact with the remainder of the protein which in turn might alter their fold (Liu *et al.* 2006, Prashek *et al.* 2013). It remains that only experimental optimization can determine whether PfCERLI1 and PfCERLI2 crystals can be made, or whether purified protein can be analysed using alternative means not requiring crystals. Assuming crystals can be made and that this study is pursued, PfCERLI1 and PfCERLI2's structure can be determined using conventional techniques used in malaria so far such as small-angle X-ray scattering (SAXS), cryo-electron microscopy (cryo-EM) and X-ray crystallography (Gangnard *et al.* 2015, Li *et al.* 2016, Geiger *et al.* 2020). Alternatively, it may be possible to crystallise entire complexes with a stable quaternary structure (Wong *et al.* 2019). Exploring whether a crystal structure of PfCERLI1 or PfCERLI2 in complex with a confirmed interacting partner may provide a means of stabilising these proteins.

Targeting for therapeutics

Merozoite invasion of the host RBC is a unique bottleneck event which the parasite must overcome to survive and multiply. Indeed, invasion inhibitors as antimalarials have been a topic of interest in the field, with modes of action that can target each distinct phase of invasion identified to date (Burns *et al.* 2019). Given the essential function of PfCERLI1 and PfCERLI2 during invasion and high levels of conservation, they are potentially suitable as antimalarial drug targets which are less likely to develop mutations that confer resistance.

The design of specific inhibitors against PfCERLI1 and PfCERLI2 will undoubtedly require structure-based design which will first require a solved crystal structure for each protein, or structures of the complexes they form. At this point, we do not know exactly which of the possible interactions we have identified in PfCERLI1 or PfCERLI2 are real or are most essential to merozoite invasion. We do know, however, that loss of function for either of these proteins leads to altered rhoptry function which is indirectly linked to the loss of PfRAP1 proteolytic cleavage through PfPMIX (Liffner *et al.* 2020, Favuzza *et al.* 2020, Nasamu *et al.* 2017). Inhibitors for PfPMIX have been developed and were shown to inhibit merozoite invasion, demonstrating the utility of targeting a protein that is directly, or in PfCERLI1 and PfCERLI2's case indirectly, required for correct PfRAP1 processing (Ciana *et al.* 2013). Therefore, an inhibitor for PfCERLI1 and PfCERLI2 may allow us to target mechanisms preceding, but essential for, PfPMIX processing of PfRAP1.

Summary and conclusions

Understanding that *Pfcerli2* arose from a gene duplication of *Pfcerli1* has given much insight on their peculiar similarities in localisation and roles during merozoite invasion. To date, few proteins like PfCERLI1 and PfCERLI2 on the cytosolic face of the rhoptry bulb have been studied, and hence formed a precedent for the identification of novel C-RIPs. Our proteomics analyses, which aimed to uncover the protein binding partners of PfCERLI1 and PfCERLI2, serves as the first stepping stone for rationally identifying new C-RIPs and potentially uncovering novel interactions between the rhoptries with other cellular compartments. To conclude, PfCERLI1 and PfCERLI2 are essential proteins

involved in merozoite invasion with potential roles in several aspects of rhoptry biology.

In the following section, I present a discussion on two zinc finger domain containing proteins which have been explored in a separate aspect of *P. falciparum* growth and invasion.

PfCZIF1 and PfCZIF2

PfCZIF1 and PfCZIF2 are implied to function at schizogony

Based on transcriptomic data, we first presented an interest in characterising PfCZIF1, which was previously reported as a schizont-expressed protein targetable by growth inhibitory antibodies, and its possible role during merozoite invasion (Daubenberger *et al.* 2003). Therefore, there was a rationale for identifying proteins that were similar to PfCZIF1 that fulfilled similar criteria in order to study them in unison. Through bioinformatic searches, we identified PfCZIF2 as a potential homologue of PfCZIF1, where both proteins were structurally similar with conserved C3H1 ZnF domains, and had peak transcript expression at late schizonts in *P. falciparum* (Otto *et al.* 2010, Bunnik *et al.* 2013). This highlighted to us that they may have a role specific to schizonts, and could reveal a novel function of C3H1 ZnFs at this point in the lifecycle. Indeed, our hypotheses were formed from the fact that *Plasmodium* parasites exert high temporal control over gene expression, such that they have regulate expression of appropriate molecular machinery at the appropriate time (Toenhake *et al.* 2018). As two putative schizont-expressed proteins, our initial hypothesis was that both were essential for growth. However, as we discovered that each individual protein was dispensable, we no longer possessed a strong rationale for investigating their roles in invasion in isolation. We focussed our study instead to identify the existence of interplay between the two proteins in the context of late blood stage biology.

Functional interplay between PfCZIF1 and PfCZIF2

Truncating two out of three C3H1 ZnF domains in each of PfCZIF1 and PfCZIF2 in separate parasite lines did not cause a growth defect. As such, we considered whether these proteins were simply not essential, or performed a

functionally redundant role. Redundant proteins are ubiquitous across the *P. falciparum* proteome, especially for those involved in invasion and immune evasion (Wright & Rayner 2014). Given that PfCZIF1 and PfCZIF2 were the sole C3H1 ZnFs with peak expression at schizogony, we also considered the possibility that these proteins compensated for each other. We proceeded to produce a range of double transgenic parasite lines, which revealed two interesting outcomes. First, deleting all residues beyond the C3H1 ZnF in PfCZIF1 combined with truncating two out of three C3H1 ZnF domains and all residues C-terminal of them in PfCZIF2, resulted in no growth defect. Interestingly, when we attempted the *vice versa* modification, this returned with a parasite line that had a detectable fitness defect over two cycles of growth. Given that parasites appear unaffected by the loss of PfCZIF2's C3H1 ZnF domains but show a growth defect in the case of PfCZIF1 C3H1 ZnF domain loss, it appears to suggest the latter is of greater physiological importance. Importantly, the growth defect with PfCZIF1 C3H1 ZnF domain loss was only noticeable with the removal of PfCZIF2's C-terminal residues. This suggests that the C3H1 domains of PfCZIF2 alone can partially, but not fully, compensate for loss of PfCZIF1 function. We attempted to truncate the C3H1 ZnF domains for both PfCZIF1 and PfCZIF2 in a single parasite but failed, suggesting to us that indeed at least one of these proteins is required for blood stage parasite survival. Taken together, this evidence suggests that PfCZIF1 and PfCZIF2 have a level of functional redundancy, with PfCZIF1 likely the most important for *in vitro* growth of 3D7. Investigating functional interplay could be achieved in future studies by generating a double knockout/knockdown parasite line, with knockdown techniques including the glucosamine-inducible *glm*S ribozyme or the dimerisable Cre recombinase (DiCre). Potential interaction between the two proteins could also be investigated in the same manner addressed for PfCERLI1 and PfCERLI2 (Chapter 2) via DiQ-BioID.

C-terminal deletion affects key transcripts

Our RNAseq differential expression analysis revealed that expressing PfCZIF1 without its C-terminal residues causes little perturbation to the schizont transcriptome, causing only an upregulation of a non-coding RNA (ncRNA) RNA of Unknown Function 6 (PfRUF6), specifically encoded at the Pf3D7_1240800 loci on Chromosome 12, though identical products can be encoded by duplicated genes.

We have considered that RUF6 is possibly a false positive that was not excluded in our filter, given its known links to *var* and *rifin* genes (Chakrabarti *et al.* 2007, Barcons-Simon *et al.* 2020). However, given that C3H1 ZnFs may bind RNA, we did not exclude it entirely. PfRUF6 expression is known to be regulated by RNA exosome-associated RNase 6 (PfRrp6), which in turn is involved in epigenetic mechanisms of gene silencing (Fan *et al.* 2020). Though a potentially interesting link, we did not observe any change in Rrp6 expression in our data set to reflect a relationship with PfCZIF1.

We observed a distinct change in the transcriptome for C-terminal deletion mutants of PfCZIF2. Namely, several exported proteins including *Plasmodium* helical interspersed subtelomeric (PfPHIST) proteins, and knob-associated histidine rich protein (PfKAHRP) were differentially expressed. This result is intriguing and provides a precedent for PfCZIF2 to perform its role during protein export. The functions of PfPHIST proteins are highly diverse ranging from host cell remodelling, gametocytogenesis, alterations to cell rigidity as well as virulence-specific functions (Warncke *et al.* 2016). Upregulation of PfKAHRP has previously been observed in *in vitro* models of heat shock and increased cytoadhesion (reviewed in Daniyan *et al.* 2019), though we did not observe any heat shock proteins (PfHSPs) with respect to PfCZIF2. Nevertheless, upregulation of PfKAHRP transcripts in our PfCZIF2 C-terminal deletion mutants appears to be consistent with an increase in PfKAHRP protein, and the latter is also true in transfectants where two out of three C3H1 ZnFs are deleted. Overall this supports that PfCZIF2 may have a role in regulating PfKAHRP expression as shown across schizonts of multiple transfected lines. Moreover, this increase in protein expression was also observed in rings and trophozoites for both lines. One hypothesis is that PfCZIF2 silences or inhibits PfKAHRP expression in schizonts, where if it is lost, PfKAHRP is expressed earlier than normal. Indeed, the formation of knobs, is typically associated with host cell modification, virulence and immune evasion mechanisms which are deployed by the parasite at earlier points in the lifecycle including ring stages. Therefore, PfCZIF2 may serve to prevent unnecessary transcription of proteins like PfKAHRP at unnecessarily high levels in schizonts when it is not needed for virulence. However knob architecture does remain on the infected RBC at mature schizonts, including evidence of PfKAHRP

which is a likely remnant of being expressed and exported earlier in the lifecycle, rather than originating from newly synthesised protein (Looker *et al.* 2008, Deroost *et al.* 2016, Subramani *et al.* 2015, Watermeyer *et al.* 2016). Put together, we highlight the possibility of transcriptional mechanisms controlling PfKAHRP expression which involve PfCZIF2.

PfCZIF1 and PfCZIF2 localise to distinct intracellular spaces in blood stage parasites

Both PfCZIF1 and PfCZIF2 possess high sequence conservation and minimal polymorphisms between *P. falciparum* strains, suggesting that they are not under immune pressure. PfCZIF1 was initially said to be targetable by specific MAbs to inhibit growth *in vitro* (Daubenberger *et al.* 2003). This result, in combination with their preliminary IFA data, inferred that PfCZIF1 must be surface-exposed in order to be accessible to antibodies, and was therefore highlighted as a potential vaccine candidate. To determine its localisation more precisely, we used transgenic parasite lines which endogenously appended a HA-tag on PfCZIF1 as well as on PfCZIF2 for co-localisation studies by IFA. C-terminal HA-tagging of either protein did not appear to be deleterious, but interestingly neither protein could be successfully tagged with larger tags including GFP, which barred us from investigating localisation in live cells (data not shown). Moreover, our attempts to localise these proteins was heavily hampered by their extremely low protein expression, and therefore they could not be reliably visualised using standard IFA protocols. Nevertheless, we managed to reproducibly obtain their localisation using a biotin-conjugated anti-HA antibody and a streptavidin-conjugated AlexaFluor for bolstering fluorescent signal in fixed cells. During the earlier stages of blood stage development, both proteins are presented as distinct puncta in rings and trophozoites, concentrated around the cytosolic perimeter of the parasite, but do not co-localise with the PVM or PPM. In mature schizonts containing fully developed merozoites, neither PfCZIF1 nor PfCZIF2 co-localise with MSP1 on the merozoite surface. This evidence contrasts greatly with what was originally reported for PfCZIF1, and suggests that neither it nor PfCZIF2 are viable merozoite vaccine candidates if not exposed to the surface. Instead, both proteins appear to be internal and cytosolic-facing. We further showed that neither protein is likely encased in a membranous organelle by a proteinase K protection

assay and differential solubilisation suggested they may be attached peripherally to a membrane. Evidence for membrane attachment is supported by predictions of lipidation in PfCZIF1 and PfCZIF2. Using GPS-Lipid (Xie *et al.* 2016), we predicted S-palmitoylation sites at cysteines within their N-termini for both proteins. Interestingly in PfCZIF1, these cysteines match to two conserved consensus residues of the middle C3H1 ZnF domain. In contrast for PfCZIF2, a single cysteine at the start of the N-terminus, which is not part of the C3H1 ZnF domain, was predicted as S-palmitoylated. It is unknown whether lipidation of these consensus residues has any bearing on protein folding or function. Nevertheless, S-palmitoylation highlights one possible mechanism for membrane anchoring.

A "canonical" localisation for C3H1 ZnFs of *P. falciparum*

C3H1 ZnFs are thought to be RNA-binding motifs in prototypic eukaryotic models, with the most well-studied being tristetraprolin (TTP) which binds TNF-alpha mRNA to induce degradation by recruitment of deadenylases in the cytosol (Carballo *et al.* 1998). An orthologue of TTP has not been identified in *P. falciparum* - which possesses 27 predicted C3H1 ZnFs and the majority have no known function, or have instead been annotated with a putative function based on bioinformatic analyses (Reddy *et al.* 2015, Ngwa *et al.* 2021).

To date, experimental data from non-malaria homologues has been used to infer the function of five C3H1 ZnFs, not including PfCZIF1, all of which remain inconclusively localised. These five include putative splicing factor U2AF 1 (PfU2AF1), a predicted homologue of NGFI-A-binding protein 2 (PfNAB2), Pf3D7_0525000, Pf3D7_0906600, and YTH domain-like protein (PfYTH.1) (Reddy *et al.* 2015, Tuteja & Mehta 2010, Bunnik *et al.* 2016, Baumgarten *et al.* 2019, Stevens *et al.* 2018). Only PfNAB2 is inferred to have nuclear localisation based on its high homology with human HsZC3H14 and its a PW1-type nucleic acid binding domain (Szymczyna *et al.* 2003). Due to the presence of two nucleic acid binding domains, it is unclear whether its putative nuclear localisation is owed to its C3H1 ZnF or PW1 domain. Nevertheless, we do not observe a nuclear localisation for PfCZIF1 and PfCZIF2, and thus a canonical localisation for C3H1 ZnFs in *P. falciparum* cannot be inferred from existing proteins. For the remaining

C3H1 ZnFs, they are strongly implied to possess RNA-binding functions, based on bioinformatic annotations, which likely occur in the cytosol (Ngwa *et al.* 2021).

Insights from RNA-binding proteins as references for localisation

The localisation of several RBPs in *P. falciparum* appear to indicate that they localise either to the nucleus or broadly across the cytosol. It is unlikely for PfCZIF1 and PfCZIF2 to be freely cytosolically localised, as they did not extract strongly in the hypotonic fraction of our solubility assays. However, this does not rule out the possibility of binding cytosolically-exposed membranes. Studies have suggested the existence of a hypothetical subcellular spaces called RNA processing or storage centres, where RBPs including PfAlba, PfAlba2 and PfAlba4 are reported to be located (Chene *et al.* 2012, Vembar *et al.* 2015). RNA processing centres appear as perinuclear or cytosolic foci (Chene *et al.* 2012), the latter being reminiscent of the signals we observed for PfCZIF1 and PfCZIF2. It is unknown whether these centres possess membranes akin to vesicles, though no electron microscopy study to date has confirmed their existence. An additional hypothetical organellar space termed a cytosolic granule has also been suggested in studies of transcription in gametocytes, which are said to house the conserved CAF1/CCR4/NOT complex – a set of RBPs important for a myriad of post-transcriptional regulatory roles (Hart *et al.* 2019, Balagopal & Parker 2009). Whether these granules exists in blood stages remains to be investigated, however CCR4 has been noted as important for schizont egress and merozoite invasion, potentially operating from a similar subcellular space (Balu *et al.* 2011). If PfCZIF1 or PfCZIF2 were to localise to RNA processing centres or cytosolic granules, this would in turn suggest that these compartments are not free cytosolic entities and may be membrane-associated.

Determining the precise localisation of PfCZIF1 and PfCZIF2 will likely require access to antibodies or multi-tagged lines directed to a broader range of organellar spaces including RNA processing centers and cytosolic granules of high post-transcriptional regulatory activity. Co-localisation between PfCZIF1 or PfCZIF2 with other RBPs found in these niches may provide further insights as to the molecular niche these proteins occupy. Given the focus of my work was on blood stage invasion, we did not further investigate whether PfCZIF1 or PfCZIF2

localised to any of these reported membrane associated, cytosolic, transcription sites.

Insights for future directions

This study focused on determining the function of PfCZIF1 and PfCZIF2 in merozoite invasion, a potential role for PfCZIF1 reported from another study. As a result, we did not examine PfCZIF1 and PfCZIF2 from the perspectives of other lifecycle stages, or their potential for RNA-related functions as a primary focus. The following provides topic recommendations for investigating these proteins for future studies.

Investigation of protein function in other lifecycle stages

Outside of the blood stage, *Pfczif1* and *Pfczif2* are reported to be highly expressed in ookinetes, and remain moderately expressed in oocyst and salivary gland-derived sporozoites (Lopez-Barragan *et al.* 2011, Gomez-Diaz *et al.* 2017, Lindner *et al.* 2019). Ookinete expression is interesting, given that it is a precursor cell for the formation of the oocyst where sporogony occurs by asexual replication – considered a functional counterpart of schizogony for the mosquito stages. Incidentally, PfCZIF1 and PfCZIF2 appear to be most expressed at points in the lifecycle preceding mass replication events, hypothesising a potential role for regulating these processes. The remaining timepoint for mass replication is during merosome development in hepatic stages, though transcriptomic data studies for this have not been performed given the difficulty of isolating hepatic schizonts (Roth *et al.* 2018). I would hypothesize then that, given that hepatic schizonts generate the largest number of daughter cells in the magnitude of thousands (Prudencio *et al.* 2006), that PfCZIF1 and PfCZIF2 may be present and potentially functioning at this timepoint.

Assessing RNA binding capabilities

It would be interesting to determine whether disrupting the C3H1 ZnFs influences RNA binding, but this would first require evidence that PfCZIF1 and PfCZIF2 indeed bind RNA. Bioinformatic surveys have identified *in silico* that RBPs in *P. falciparum* comprise 3.5% of all genes, where 90% of all RBPs primarily fall into six classes including: RNA recognition motifs, DEAD/H-box

RNA helicases, K homology, zinc finger, or belong to the Puf and Alba protein families (Reddy *et al.* 2015). Of the zinc finger class, *P. falciparum* expresses C2H2, C3H1, RING and PHD type ZnFs (Ngwa *et al.* 2021). C3H1 ZnFs are prototypically RNA-binding proteins, and as such we would expect PfCZIF1 and PfCZIF2 to function as RBPs. However, PfCZIF1 and PfCZIF2 have not been identified as experimentally verified RBPs by crosslinking immunoprecipitation sequencing (CLIPseq) (Bunnik *et al.* 2016). This study suggested that approximately 1000 proteins, which comprises roughly a fifth of the whole proteome, are capable of RNA binding which forms a conflict with only 3.5% of the genome being annotated as RBPs. This discrepancy is likely due to transient or indirect interactions between proteins and RNA and the nature of CLIPseq, which can capture transient or closely proximal protein-RNA interactions in the cytosol, which are then crosslinked during sample preparation (Bunnik *et al.* 2016). Therefore, it is surprising that PfCZIF1 and PfCZIF2 were not identified as RBPs or RBP-interacting proteins despite the staggering overrepresentation of RBPs across the whole proteome (Bunnik *et al.* 2016). Unfortunately, techniques for further investigating RNA-protein interactions with a protein of interest are reliant on identifying the sequence where an RBP binds, such as RNA electrophoretic mobility shift assays (RNA-EMSA) (Fillebeen *et al* 2014). Given that there is no known nucleic sequence which binds PfCZIF1 or PfCZIF2, these proteins may not be RBPs. However, global CLIPseq studies like those performed by Bunnik *et al.* often provide greater RBP representation for highly expressed proteins, with false negatives possibly arising from the low RNA-RBP complex concentrations for particular candidates (Ramanathan *et al.* 2019). Both PfCZIF1 and PfCZIF2 are extremely lowly expressed and will likely require protein overexpression to mitigate this barrier. Our repeated attempts to episomally overexpress PfCZIF1 and PfCZIF2 however were not successful (data not shown). One possible pathway forward is to perform CLIPseq with purified PfCZIF1 and PfCZIF2 as the sole bait proteins in a *P. falciparum* RNA mixture. An alternative is to investigate whether these proteins bind DNA using chromatin immunoprecipitation sequencing (CHIPseq) (Toenhake *et al.* 2018), though C3H1 ZnFs have never been shown in any system to bind DNA.

Suggesting that PfCZIF1 and PfCZIF2 possess atypical C3H1 ZnF domains

In model eukaryotes, C3H1 ZnFs as a domain class have been studied to a much lesser extent than other ZnFs, with the C2H2 type being most prominent. There are 57 known C3H1 ZnFs in the human proteome, most of which have never been characterised (Hajikhezri *et al.* 2020). Therefore, it remains poorly studied whether C3H1 ZnFs possess a non-prototypic function outside of RNA binding. Certainly, some proteins even possess multiple ZnF classes, of which there are 30 types identified, where potential interplay between the different ZnF domain classes has never been elucidated (Cassandri *et al.* 2017). Classifications for ZnF proteins continue to evolve, with deviations from the standard classes. We showed that PfCZIF2 differs from PfCZIF1 at its middle positioned C3H1 ZnF domain due to an inserted sequence which separates the first conserved cysteine from the remainder of the conserved residues by 37 amino acids. This deviation from canonical structure suggests a change in folding mechanism and final structure, which we then attempted to model in Phyre2 to reveal the loss of an alpha-helix. As such, this domain may not maintain a typical C3H1 ZnF fold, but this would need to be confirmed using different methods. PfCZIF1 on the other hand, maintains an obvious C3H1 ZnF-like signature.

RNA degradation capabilities

If we assume that PfCZIF1 and PfCZIF2 are indeed C3H1 ZnFs with an RNA-binding function, one pathway for future investigations would be investigating the molecular mechanisms of transcript degradation. Rationale for this is the assumption that the canonical function of C3H1 ZnFs are mediators of mRNA turnover. As previously alluded to, TTP is the prototypic C3H1 ZnF in eukaryotes which functions by binding AU-rich elements (AREs) in the 3' UTR, serving as a platform for recruitment of deadenylases and decapping nucleases to the mRNA molecule (Carballo *et al.* 1998, Sandler *et al.* 2011). As such, TTP has remained the model for studies where a C3H1 ZnF has been identified. *P. falciparum* possesses the most AT-rich genome of the human infecting malaria species (with *P. gallinaceum* and related avian malarias being highest outside of humans) (Gardner *et al.* 2002, Videvall 2018), and naturally many transcripts are abundant with intragenic AREs even outside of the UTRs. Hypothetically, *P. falciparum* may

have evolved mechanisms which target AREs as a mode of post-transcriptional regulation. One such mechanism may indeed be the inclusion of C3H1 ZnFs in the proteome, of which there are 27 annotated in the *P. falciparum* genome (Ngwa *et al.* 2021), with the two most highly expressed at schizogony being PfCZIF1 and PfCZIF2. It would be interesting to assess whether PfCZIF1 and PfCZIF2 possess, for example, ribonuclease activity or act as a molecular hub akin to TTP for recruitment of other proteins. Though ribonuclease activity is difficult to assess without first identifying a putative binding RNA, identification of protein binding partners using proteomic methods, may shed light on these proteins acting as a hub. If PfCZIF1 and PfCZIF2 were to recruit deadenylases, one anticipated result would be an interaction with the deadenylase PfCAF1, which is the predicted *Plasmodium* orthologue of CAF1 in the combined CAF1/CCR4/NOT complex of model eukaryotes involved in post-transcriptional regulation. Interestingly, CAF1 in model eukaryotes is also known to bind TTP, and are both required to target mRNA for degradation (Sandler *et al.* 2011). PfCAF1 however has not been experimentally shown to have deadenylase activity, but intriguingly is involved in regulating egress and invasion-specific transcripts, namely for PfSUB1 and PfEBA-175 in schizonts (Balu *et al.* 2011). Put together, perhaps PfCZIF1 or PfCZIF2 fulfil a TTP-like function in *P. falciparum*.

Studying RNA surveillance mechanisms

It is known that several RNA surveillance mechanisms are absent in *Plasmodium* due to a lack of orthologues of relevant enzymatic machinery, including those involved in RNA interference (RNAi). As such, several RBPs involved in this process including Argonaute 2 and DICER in the RNA-induced silencing complex (RISC) do not have known orthologues in *Plasmodium* despite this system being functional in related Apicomplexans including *T. gondii* (Baum *et al.* 2009, Kolev *et al.* 2011). Nevertheless, artificial RNAi can indeed operate in *Plasmodium*, as shown in transgenic lines of *P. berghei* expressing mammalian Argonaute 2, suggesting that there are other proteins that can potentially fulfil the functions of the remaining RISC machinery, though this has never been explored in *P. falciparum* (Hentzschel *et al.* 2020). Therefore, *Plasmodium* parasites can be made RNAi-competent. Given that both Argonaute 2 and C3H1 ZnFs canonically

bind the 3' UTR of mRNAs, and that both are involved in transcript degradation, proteins including PfCZIF1 and PfCZIF2 may be in proximity for an interaction (Muller *et al.* 2020).

Another potential pathway to explore specifically for *P. falciparum* are novel RBPs involved in RNA surveillance pathways prior to or during translation which could process AT-rich transcripts. Typically, the presence of long stretches of AREs, poly-A or poly-U intergenic repeats are normally negative regulators of gene expression as these destabilise RNA polymerases, as well as increase the propensity for frameshifts and stalling during translation for most eukaryotes. Stalled transcripts are typically targeted for degradation by the No Go Decay (NGD) pathway, which involves recruitment of endoribonucleases, of which themselves are RBPs, to the ribosome (Navickas *et al.* 2020). It has been shown that *P. falciparum* is exceptional to this paradigm, where possessing AU-rich transcripts does not result in increased stalling as the parasite has evolved a highly degenerate NGD pathway (Pavlovic Djuranovic *et al.* 2020). Deciphering whether *Plasmodium* parasites possess their own novel RNA surveillance mechanisms that are unique to or reminiscent of those found in mammalian systems would be an interesting contribution to the field. Inevitably, this will require extensive studies of many candidate RBPs.

Summary and conclusions

PfCZIF1 and PfCZIF2 are peculiar schizont-expressed proteins, where in isolation each of them do not appear essential for the parasite. However, we have shown that both are linked and in tandem possess an important function. We believe that PfCZIF1, contrary to prior studies, is not suitable as a vaccine candidate given that is found in the parasite interior along with PfCZIF2, and is likely to exert their functions outside of schizont and merozoite-specific themes. Instead, these proteins warrant an investigation that is focussed on their C3H1 ZnF domains and a possible role in RNA regulation of exported proteins in blood stage parasites. To conclude, we have presented an initial overview characterisation of PfCZIF2, and an extended characterisation of PfCZIF1 in the malaria parasite *P. falciparum.*

Final conclusions

The body of work presented in this PhD thesis has provided the essential framework for studies of novel C-RIPs as well as C3H1 ZnF proteins of *P. falciparum* schizonts.

Our investigation of PfCERLI2, with reference to its paralogue PfCERLI1, have revealed its essential function during merozoite invasion and its links to rhoptry organelle biogenesis. Moreover, through our proteomics studies, we have elucidated new candidate proteins that are likely to bind PfCERLI1 or PfCERLI2 and suggests novel molecular interactions occurring at the cytosolic surface of the rhoptry bulbs. These studies will undoubtedly lead to further molecular discoveries regarding the functions of the PfCERLIs for rhoptry function.

Our characterisation of PfCZIF1 and PfCZIF2 highlights two novel proteins that are expressed at schizogony, but do not have a role in merozoite invasion. We have determined and validated that neither are viable as vaccine candidates, which informs the field to investigate these proteins in a different light – namely for roles involving mRNA transcript regulation, or their functions in other lifecycle stages.

Put together, this thesis has explored two distinct aspects of *P. falciparum* blood stage biology that hold relevance in the field. It is in our confidence that each study has provided the needed foundations for continued interest in these proteins.

Chapter 5

Materials and methods

Materials and methods

Preface

The methods presented in this chapter are a comprehensive overview of experimental protocols briefly summarised in the methods sections of Chapters 2 and 3. Methods performed exclusively by collaborators are not featured.

Materials and methods

Continuous parasite culture

P. falciparum 3D7 strain parasite cultures were cultured in class II biosafety cabinets (Gelman Sciences Australia, AES Environmental) in 5 mL petri dishes, 10 mL petri dishes, 30 mL petri dishes or 175 cm^2 filtered culture flasks (Corning). Cultures were maintained at 3% haematocrit ($(\frac{volume\ of\ packed\ RBCs}{volume\ of\ culture\ media}) \times 100$) of O positive blood donated by the Red Cross Blood Service, Australia, in culture media composed of RPMI-HEPES (Sigma-Aldrich), 0.5% v/v Albumax (Gibco), 52 μM gentamycin (Gibco), 367 μM hypoxanthine (Sigma-Aldrich), 2 mM L-Glutamax (Gibco) and 2 mM sodium bicarbonate (Thermo Fisher Scientific), adjusted to a pH of 7.2-7.4. Culture media was 0.2 μm filter-sterilised before use. All cultures were stored in sealed acrylic boxes gassed with 1% O_2, 5% CO_2 and 94% N_2 (BOC Gases) and grown in 37°C incubators.

Maintaining culture parasitaemia

Achieving 3% haematocrit for general culture was estimated using 35-40 μL droplets of fresh blood dispensed from a transfer pipette, or more accurately using a micropipette. The percentage parasitaemia of a given culture was determined from thin blood film smears of approximately 1-2 μL parasitized RBCs on glass microscopy slides (Paul Marienfield GmbH & Co., Lauda-Königshofen). Smears were fixed onto slides with 100% methanol and then transferred for staining in 10% v/v Giemsa's azur eosin methylene blue solution (Merck Millipore), which stains for nucleic acids, for 2-3 minutes in order to differentiate parasites from RBCs. Staining time was extended to improve the visibility of small ring-stage parasites. Cell counting under a light microscope was used to determine percentage parasitaemia, where parasitaemia at or exceeding 5-7% trophozoites must be reduced to maintain the viability of the parasites. This is owed to the fact that as the parasites progress further into their life cycle, they rupture from the host RBC to yield a six-fold increase, leading to rapid depletion of media, build-up of metabolic waste and subsequent parasite death. Parasitaemia was reduced by removing a desired portion of parasitised and unparasitised RBCs from the dish (termed "subbing"), and then re-achieving 3% haematocrit through addition of uninfected

RBCs to the amount removed, and 'fed' with culture medium. Observing the percentage parasitaemia of cultures was routinely practised, where the choice to achieve high or low parasitaemia was based on how the parasites were to be used in later experiments.

Cryopreservation and thawing of parasite cultures

Cultures of ring-stage parasites at 4% or higher parasitaemia were deemed suitable to freeze as back-up *P. falciparum* lines. Cultures were centrifuged at 550 rcf for 5 min, supernatant removed and resuspended in sterile glycerolyte 57 solution (45% v/v 6.165 M glycerol, 1.6% v/v sodium lactate, 0.0517% v/v NaH_2PO_4, 0.1242% v/v Na_2HPO_4, adjusted to a pH of 6.8). The amount of glycerolyte 57 used was twice the volume of the culture pellet – often 1-1.5 mL. 1/5 of this volume was added dropwise slowly with a transfer pipette to the pellet, resuspended and allowed to settle for 2 min. The remaining 4/5 was added in the same manner, resuspended and transferred to a cryotube (Nalgene). Cryopreserved cultures were stored in a -80^{o}C freezer or liquid nitrogen until required. For thawing, cryotubes were wiped with 70% ethanol to minimize chances of contamination and allowed to thaw at room temperature. Thawed cultures were transferred to a fresh tube and washed with 3.5% NaCl where the amount of NaCl was twice that of the volume of cryopreserved culture – often 1.5-2 mL. 1/4 of this solution was added dropwise to the culture and resuspended in the manner described above, cultures spun at 550 rcf for 5 min, supernatant removed, washed with the same amount of a 50/50 mixture of 3.5% NaCl once again removing supernatant. Washed cultures were re-plated into 10 mL dishes adjusted to 3% haematocrit.

Synchronising parasite cultures

To perform experiments requiring parasites at a specific point in the intraerythrocytic lifecycle, *P. falciparum* cultures were synchronized using the following methods.

Heparin treatment

Heparin is an anticoagulant capable of inhibiting merozoite invasion of the RBC, therefore preventing the subsequent invasion cycle. Newly egressed merozoites will die in the presence of heparin as they are unable to reinvade. This method is used to obtain young ring-stage parasites from cultures which are high in late schizonts by inhibiting invasion. Heparin (Pfizer) was added at a concentration of 20 IU/mL to parasite cultures and incubated, often overnight, until schizonts were estimated to have formed. Once schizonts had formed, the culture medium was discarded and replenished to remove the drug. Cultures were then re-incubated for the duration of time estimated for schizont rupture, allowing egressed merozoites to synchronously invade uninfected RBCs. Heparin would be re-applied once successfully-invaded ring stages were observed in culture.

Sorbitol treatment

Trophozoites at 20 hours or further into their lifecycles express transporters for the new permeability pathway (NPP), which remodels the RBC membrane for nutrient intake (Ginsburg *et al.* 1983). We manipulated this phenomenon to permit sorbitol to enter parasitized cells, causing an osmotic imbalance in older parasites which lyses them. This method is therefore used to enrich for ring-stage and early trophozoite parasites. Asynchronous cultures containing ring stages were centrifuged at 550 rcf for 5 min, supernatant removed and resuspended in 37^{o}C warmed 5% D-sorbitol (Sigma-Aldrich) at a volume estimated to be three times that of the culture pellet. Treated cultures were then incubated at 37^{o}C for 5 min, spun at 550 rcf for 5 min, supernatant removed, washed and centrifuged twice in culture media to remove residual sorbitol, then returned to culture supplemented with uninfected RBCs to 3% haematocrit.

Gelatin selection

At approximately midway through the intraerythrocytic lifecycle, parasites export an adhesive protein ‘knob’ PfEMP1 to the RBC membrane surface. These knobs are capable of adsorbing to gelatin to enrich for late-stage parasites and for parasites with minimal chromosomal deletions near the telomeric ends which can reduce expression of knobs (Waterkeyn *et al.* 2000). Asynchronous cultures were

centrifuged at 550 rcf for 5 min, supernatant removed, and resuspended in 5 mL of 37ºC warmed filter-sterilized 1% w/v gelatin in RPMI. Cells were left to separate into different phases by gravity for 45 min in 37ºC. Late-stage parasites were held in the supernatant. The supernatant was transferred to a 10 mL tube, spun at 550 rcf for 5 min, and supernatant removed. The pellet now contained late-stage parasites. The pellet was washed with 5 mL culture media and spun twice to remove residual gelatin, then returned to culture supplemented with uninfected RBCs to 3% haematocrit.

Percoll gradient

The size and density of the parasites increase as they progress through the intraerythrocytic lifecycle. Using the Percoll gradient separation method, we are able to purify for any desired lifecycle stage of parasite, though most efficiently for late stages. 70% Percoll diluted in PBS was warmed at 37ºC. Approximately 6 mL 70% Percoll in a 15 mL tube is required for purification of up to 30 mL cultures. A high parasitaemia Pf3D7 culture was spun down at 550 rcf for 5 min, supernatant removed and resuspended in 2 mL RPMI-HEPES or PBS. Using a transfer pipette, droplets of the 2 mL culture suspension was added on top of warm Percoll, running liquid down the side of the tube, avoiding resuspension into the Percoll layer. The culture was centrifuged at 1455 rcf for 10 min with low acceleration and brake. After centrifugation, the top aqueous layer was discarded, and a thick dark band containing late stages was collected in a new tube. This dark band was washed twice with 10 mL RPMI-HEPES (if returning to culture) or PBS (if used for harvesting pure parasites) by centrifuging at 550 rcf for 5 min. Parasites resuspended in RPMI-HEPES were returned to culture, supplemented with RBCs to 3% haematocrit.

Purification of merozoites using E64

E64 is a cysteine protease inhibitor capable of preventing schizont rupture through an unknown mechanism (Blackman 2008). Drug treatment using E64 concentrates the number of developing merozoites by preventing the subsequent invasion cycle. Synchronous late-stage trophozoite and schizont parasite cultures were treated for 6 hours with E64 (Sigma-Aldrich), spun down at 850 rcf for 10 min, supernatant removed, with the pellet re-suspended in 1.5 mL culture media.

This suspension containing enriched schizonts was passaged through a syringe with a 1.2 μm filter (Sartorius Stedum Biotechnology), forcing rupture of large schizonts, permitting only purified merozoites which were sufficiently small to be collected in the flow-through. Purified merozoites could then be prepared for immunofluorescence assays (IFAs) or relevant growth assays.

Protein motif identification

Protein motifs in the genes Pf3D7_1468400 and Pf3D7_0818100 were predicted using the ExPASY PROSITE web-based service using default settings (Swiss Institute for Bioinformatics) to determine that each protein contained three N-terminal C3H1-type zinc-finger domains. 3D secondary and tertiary protein structures for these domains were then simulated using the Phyre2 web-based service (Biotechnology and Biological Sciences Research Council) and Iterative Threading Assembly Refinement (I-TASSER, University of Michigan). The coiled coil motif in Pf3D7_1468400 was predicted using ExPASY COILS using default settings while the central peptapeptide repeat motif was previously identified (Daubenberger *et al.* 2003). The presence of putative transmembrane domains were predicted in TMHMM (Center for Biological Sequence analysis) using extensive output settings. Likewise, any putative N-terminal signal peptides were predicted in SignalP-5.0 (Center for Biological Sequence Analysis) using long output settings for Eukarya.

Identification of schizont-specific C3H1 zinc finger proteins

Pf3D7_1468400 and Pf3D7_0818100 were chosen as functionally comparable genes based on a nested search strategy on PlasmoDB. Genes were first filtered across the entire *P. falciparum* 3D7 genome for the text term "zinc finger" which searches for gene ontology (GO) terms across all annotations before being subject to a second filter searching for the text term "C3H1" or the synonymous motif name "CCCH" – resulting in 25 C3H1-type zinc finger-encoding genes. These 25 were then enriched for genes with non-uniform peak transcriptional expression at schizogony using a blood stage expression exclusion filter. Briefly, the RNA-seq transcriptional profiles of (Otto *et al.* 2010) were applied to the 25 gene set to select genes with a ten-fold increase in expression from trophozoite stage (defined as 24-32 hours) to schizogony (defined as 40-48 hours), which resulted in the identification of Pf3D7_1468400 and Pf3D7_0818100.

Cross-strain homologous/interspecies orthologous peptide alignment

Amino acid sequences for Pf3D7_1468400 and Pf3D7_0818100 and the genes encoding their respective equivalents in *P. falciparum* strains 7G8 (Pf7G8_140073500, Pf7G8_080023200), CD01 (PfCD01_140073600, PfCD01_080023700), Dd2 (PfDd2_140072700, PfDd2_080023300), FVO (PFFVO_05334, PFFVO_02121), GA01 (PfGA01_140073700, PfGA01_080021800), GB4 (PfGB4_140074300, PfGB4_080022900), GN01 (PfGN01_140073600, PfGN01_080023800), HB3 (PfHB3_140074000, PfHB3_080023600), IT (PfIT_140074700, PfIT_080023100), KE01 (PfKE01_140073100, PfKE01_080023700), KH01 (PfKH01_140073800, PfKH01_080023200), KH02 (PfKH02_140074000, PfKH02_080023700), MaliPS096 (PFMALIP_05529, PFMALIP_02139), IGH-CR14 (PFMG_04912, PFMG_04917), ML01 (PfML01_140074100, PfML01_080023700), NF135/5.C10 (PFNF135_05581, PFNF135_02241), SD01 (PfSD01_140071600, PfSD01_080023500), SN01 (PfSN01_140075500, PfSN01_080022700) and TG01 (PfTG01_140073600, PfTG01_080024000) as well as orthologous genes in *Plasmodium inui* (C922_00098, C922_02584), *Plasmodium berghei* (PBANKA_1331700, PBANKA_0712700), *Plasmodium cynomolgi* (PCYB_124660, PCYB_052360), *Plasmodium gallinaceum* (PGAL8A_00227800, PGAL8A_00111100), *Plasmodium knowlesi* (PKNH_1212800, PKNH_0501900), *Plasmodium malariae* (PmUG01_12048500, PmUG01_05032900), *Plasmodium ovale curtisi* (PocGH01_12046400, PocGH01_05022800), *Plasmodium praefalciparum* (PPRFG01_1469000, PPRFG01_0819600), *Plasmodium reichenowi* (PRCDC_1467600, PRCDC_0817400), *Plasmodium vivax* (PVX_117045, PVX_089510) and *Plasmodium yoelii* (PY02869, PY03958) were obtained from PlasmoDB. Pairwise and multiple sequence alignments were performed in Geneious 9.1.3 (Biomatters) with a global alignment with free end gaps using the Blosum62 cost matrix with the configuration: gap open penalty 12, gap extension penalty 3, refinement iterations 2.

Plasmid generation

A list of base, unmodified plasmid constructs used in this study are available in the Appendix.

PCR amplification of DNA inserts

DNA inserts of interest were PCR amplified in a 200 µL reaction tubes containing Phusion® High-Fidelity PCR Master Mix with HF Buffer (herein referred to as Phusion Flash, New England Biolabs), *P. falciparum* 3D7 strain gDNA, PCR-grade water and suitable primer pairs in an Eppendorf Mastercycler® Nexus. For diagnostic PCRs, 10 µL reactions were composed of: 5 µL Phusion Flash, 0.2 µL of each primer at 10 mM, 3.6 µL H_2O and 1 µL DNA. For collecting high quantities of inserts, 50 µL reactions were composed of: 25 µL Phusion Flash, 1 µL of each primer at 10 mM, 22 µL H_2O and 1 µL DNA. The following cycling profile was used: 2 min 95°C, 30 × (30 s, 95 °C; 30 s, Tm *°C (*primer melting temperature (Tm) varies according to primer pair, noted in Appendix); 10 min, 72 °C), 10°C until collected. PCR products were analysed on 1% agarose gels formulated with 1 TAE buffer and 1/10000 RedSafe (Intron Biotechnology), compared alongside a 1 kb DNA ladder (Invitrogen) at 110 V for 60 min, and viewed using a Gel Doc Molecular Imager (Bio Rad**)** The remainder of the PCR products were purified using a QIAquick® PCR Purification Kit (Qiagen).

Restriction digest of inserts and plasmid backbones

1 µg of purified PCR product was incubated with 5 µL Buffer 3.1 or Cutsmart and 1 µL of each appropriate restriction enzyme (New England Biolabs) with PCR-grade water topped up to 50 µL for 2+ hours at 37 °C, before PCR purification of the cut inserts. To generate the relevant plasmid backbone, vectors were also digested with the above reaction conditions, run on 1% low-melt agarose (Promega) gels at 110 V for 60 min, where the appropriate band was collected by gel extraction using a UV light and the PureLink™ Quick Gel Extraction Kit (Invitrogen) according to manufacturer's instructions.

Plasmid ligation

Inserts and vectors were ligated together using the T4 DNA ligase (New England Biolabs) according to the manufacturer's recommended reaction conditions. Briefly, using the New England Biolabs ligation calculator (https://nebiocalculator.neb.com/#!/ligation) to determine optimal ligation parameters, 3:1 and 5:1 insert to vector ratios (according to mass in ng) were combined together with 1 μL DNA ligase and 2 μL T4 DNA ligase buffer topped up to 20 μL in PCR-grade water. The ligation was allowed to proceed at room temperature for 1 hour before being heat-inactivated at 65 ºC for 20 min. The ligation mixture was then ethanol-precipitated in 1 μL glycogen (stock 20 mg/ml), 2 μL 3M sodium acetate pH 5.5 and 2x ligation volume (~44 μL) of ice-cold 100% ethanol and placed in -20 ºC for 1 hour. The mixture was then centrifuged at 16000 rcf for 10 min, supernatant removed and washed in 200 μL 70% ethanol, centrifuged at 16000 rcf for 5 min, supernatant removed and air-dried for 5 min. Dried DNA precipitate was then resuspended in 10 μL PCR-grade water.

InFusion cloning for CRISPR/Cas9 gene editing

20 base pair guide sequences were designed on CHOPCHOP version 3 (Montague *et al.* 2014) using the *P. falciparum* 3D7 genome targeting Pf3D7_1468400 and Pf3D7_0818100. Two high-ranking guide sequences, excluding the protospacer adjacent motif (PAM), were then exported to Geneious 9.1.3 (Biomatters) and ordered as separate complementary oligonucleotides flanked by two 15 base pair homology regions to the backbone construct to be subcloned into. Complementary oligonucleotides were then annealed into double-stranded DNA inserts by incubating 10 μL of each oligonucleotide with 2.2 μL NEB2 buffer (New England Biolabs) at 95 ºC for 10 min on a heat block. The entire heat block was then transferred to a large container of ice and allowed to cool gradually to permit annealing. The final guide inserts were then diluted to 0.5 μM in cold elution buffer (Qiagen). Meanwhile, 1 μg of guide backbone plasmid (Appendix) was digested with BtgZI as described earlier for restriction digests at 60 ºC for 3 hours before being heat-inactivated at 80 ºC for 20 min and cleaned up using a QIAquick® PCR Purification Kit (Qiagen). To subclone the guide sequences into

the guide backbone, InFusion cloning was performed. Guide backbone (50 ng) was mixed with 1 μL of guide insert, 2 μL PCR-grade H_2O and 1 μL InFusion enzyme mix (Takara) and incubated at 50 °C for 15 min. The completed product mixture (5 μL) was then transformed into 50 μL XL-10 Gold *Escherichia coli* or Stellar Competent *E. coli*.

Transformation of competent cells

Purified ligation product (25 ng) was transformed into 50 μL XL-10 gold *E. coli* competent cells (Agilent Technologies). Cells and product were left on ice for 30 min, heat-shocked at 42°C for 90 sec, replaced on ice for 2 min then added to 800 μL super optimal broth with catabolite repressor (SOC, containing glucose) media and incubated for 2 hours at 37°C while shaking at 250 rpm. Transformed bacteria (200 μL) were spread onto suitable antibiotic-treated agar plates (specific to the antibiotic resistance conferred by our constructs) and incubated at 37°C overnight. The next day, positive colonies were boiled in 100 μL H_2O to extract DNA, and successful integration of our desired inserts was confirmed by PCR and gel electrophoresis.

Broth cultures and DNA extraction by miniprep/midiprep

The same positive colonies were used to prepare minipreps using the QIAprep® Spin Miniprep Kit. Briefly, positive colonies were inoculated into 5 mL LB media containing antibiotic in tubes with cracked lids to permit aeration (for minipreps) or 250 mL LB media containing antibiotic in baffled flasks and incubated at 37 °C overnight. The next day, DNA was extracted via the QIAprep Spin Miniprep Kit (Qiagen) or the PureLink™ HiPure Plasmid Midiprep Kit (Invitrogen) as per manufacturer's instructions.

Preparing samples for Sanger sequencing

Samples were prepared for Sanger sequencing in 1.5 mL tubes containing 1000 ng pure plasmid, 1 μL of a desired primer at 10 mM, topped up to 12 μL in PCR-grade water. Samples were transported at room temperature to the Australian Genome Research Facility (AGRF) for Sanger sequencing. Completed sequencing

files were analysed using the Geneious software package and aligned to a reference of interest.

Transfection and maintenance of transfected lines

Protocols for the transfection of *P. falciparum* was based on established protocols (Wu *et al.* 1995, Deitsch *et al.* 2001) and advice from Tony Triglia of the Walter and Eliza Hall Institute of Medical Research (WEHI). The process is as follows.

Ethanol precipitation of DNA

To prepare sterile DNA for transfection, 80 μg of purified plasmid DNA was precipitated in twice the volume of sterile 100% ethanol and 3M sterile sodium acetate to 10% of the final volume, to be left on ice or in -20ºC for 30 minutes. DNA was then centrifuged for 5 minutes at 12000 rcf, supernatant removed, washed in 1.5 mL sterile 100% ethanol, and left either 3+ hours or overnight in -20ºC. When ready for transfection, supernatant was removed, and the DNA pellet was allowed to air-dry for 2 minutes. The pellet was then resuspended in 20 μL sterile 1x Tris-EDTA (TE) to dissolve DNA.

For parasite lines generated by CRISPR/Cas9, 60 μg of repair template plasmid was restriction enzyme digested to linearise a region containing a set of homology flanks, and was ethanol precipitated as described above. In a separate tube, 20 μg of guide plasmid which expresses the Cas9 endonuclease and guide sequence, was also ethanol precipitated, and combined with the linear repair template prior to transfection.

Transfection by red blood cell loading

Uninfected RBCs were centrifuged at 440 rcf for 1 min, washed in culture media and then washed in cytomix (0.895% w/v KCl, 0.0017% w/v $CaCl_2$, 0.076% w/v ethylene glycol-bis(β-aminoethyl ether)-N,N,N',N-tetraacetic acid (EGTA), 0.102% w/v $MgCl_2$, 0.0871% w/v K_2HPO_4, 0.068% w/v KH_2PO_4, 0.708% w/v 4-2 4-(2-hydroxyethyl)-1-piperazineethanesulfonic acid (HEPES)). Washed RBCs

were then resuspended in cytomix containing 200 µg of the plasmid of interest and kept on ice for 30 min. The combined RBCs and DNA were transferred to a 0.2 cm cuvette (Bio-Rad) to be electroporated (Bio-Rad) at 0.31 kV with a capacitance of 960 uF. The resulting time constant was estimated to be around 14 ms. Electroporated RBCs were rinsed from the cuvette with culture media, centrifuged at 440 rcf for 1 min, and washed twice before being introduced to 3-5% parasitaemia cultures of gelatin-purified schizont stage parasites in 10 mL dishes. Upon schizont rupture, merozoites will invade the DNA-loaded RBCs and actively take up the construct of interest. No drug selection was added for cultures on the same day as transfection.

Transfection by schizont loading

In order to directly introduce genetic constructs directly into the parasite to maximise the efficiency of transfection, electroporation by schizont loading was performed. Schizont parasitaemia cultures (3-5% parasitaemia, 40-44 hours post invasion) were Percoll-purified and replaced in culture media treated with 2 µM 4-[2-(fluorophenyl)-5-(1-methylpiperidine-4-yl)-1H-pyrrol-3-yl] pyridine (Compound 1, C1) for 2 hr in order to allow schizonts to fully develop their merozoites but arrest egress. Once developed, cultures were then centrifuged at 440 rcf for 5 min and washed in culture media to remove C1 before being transferred to 1.5 mL tubes and shaken at 37 ^{o}C for 20 min. After shaking, schizonts were resuspended in cytomix containing 80 µg of the plasmid of interest, and electroporated in the same manner described above with altered electroporation parameters: 0.8 kV, capacitance 25 uF, expected time constant of 1 ms. Electroporated parasites were placed into 1.5 mL tubes with culture media and 200 µL uninfected RBCs and shaken at 37 ^{o}C for 20 min to encourage merozoites to invade before being placed back into culture in 5 mL dishes. No drug selection was added for cultures on the same day as transfection.

Continuous culture of transfectants under WR and BSD

Post-transfection drug selection was used to enrich for parasites expressing the appropriate resistance cassette either episomally or integrally from a construct of interest. One of two drugs were used: 5 nM WR99210 or 5 µg/mL blasticidin-S-

hydrochloride. WR99210 is an inhibitor for the *P. falciparum* dihydrofolate reductase (*DHFR*), which is required for DNA synthesis. Selectable resistance can be conferred by expressing the human DHFR (*hDHFR*) gene in a construct of interest. In contrast, blasticidin-S-hydrochloride is a nucleoside antibiotic originating from *Streptomyces griseochromogenes* and is capable of inhibiting protein synthesis. Blasticidin-S-hydrochloride resistance is conferred by expression of blasticidin deaminase (*BSD*). Both aforementioned processes are essential for survival. In the case of red blood cell loaded transfections, for the first 10 days transfectants were given regular media changes with drug added. Days 2-5 typically reveal swollen dying trophozoite stages with fragmented haemozoin. After Day 10, cultures were fed and drugged every two days, and a supplement of fresh red blood cells added at Days 15 and 21. Upon seeing ring-stage parasites, cultures were permitted to grow to a parasitaemia of 3-5% and cryopreserved. For single-crossover transfections, rings were grown back to initiate drug cycling – a technique used to select against parasites carrying episomal plasmids and to enrich for single-crossover integrants. Cultures were cycled on and off drug for two weeks, where each two week interval is considered as one cycle. At least three drug cycles were performed to obtain highly integrated populations of parasites. Parasites were cryopreserved at the end of each cycle as backups. For schizont loaded transfectants, the aforementioned process was fast-tracked with cryopreservable ring stages becoming ready in less than two weeks. WR must be kept on cultures expressing a single-crossover construct to prevent looping out and reversion to wild-type. The same applies as well as for episomally expressed constructs to maintain the plasmid.

Continuous culture of CRISPR/Cas9-based transfectants

For double-crossover lines generated using CRISPR/Cas9 gene editing, when transfectants began to grow stably, they were negatively selected with 1 μM 5-fluorocytosine (5FC) to remove any non-linearised repair templates for 1 week. This is to eliminate any episomal expression of positive selection cassettes, including *hDHFR* and *BSD*. Lines episomally expressing the *Saccharomyces cerevisiae* cytosine deaminase-uridylphosphoribosyltransferase fusion gene (ScCDUP) are killed in the presence of 5FC (Reininger *et al.* 2012).

Continuous culture of SLI-TGD-based transfectants

For transfectants carrying a construct harbouring the selection-linked integration (SLI) system, transfectants were selected using WR99210 against *hDHFR* as aforementioned. However, resistance at this point may be conferred by episomal expression of *hDHFR*, rather than by stable integration into the genome. To ensure only integrants are selected, SLI plasmids are designed with a silent neomycin resistance cassette (*NeoR*). *NeoR* cannot be expressed episomally as it does not possess a promoter, and must be integrated into a gene of interest to borrow its promoter for activation. WR99210-resistant parasites harbouring a SLI plasmid were treated to a two week drug treatment with 80 μg/mL of the neomycin analogue G418 disulfate salt (geneticin, herein referred to as G418) until the cultures had stably integrated the construct to become resistant. G418 must be kept on the cultures to prevent looping out of single-crossover constructs and reversion to wild-type.

Single cell cloning by limiting dilution

For non-episomal transfectants after successful drug selection, parasite cultures exist in a heterogeneous mix of wild type and genetically-modified cells. To enrich for a homogeneous clonal population of only modified cells, parasites were cloned by limiting dilution in 96-well U-bottom plates (Corning) (Rosario 1981). Heterogeneous transfectant cultures were first centrifuged at 550 rcf, supernatant removed and the parasites resuspended to 4% haematocrit in culture media. This suspension was then diluted 1/4000 in culture media to thoroughly dilute the culture. Depending on the starting parasitaemia of the culture (obtainable by counting smears), a small aliquot of diluted suspension was added to a calculated amount 2% haematocrit mixture of uninfected RBCs in media (referred here as V_{dil}).

$$V_{dil}\ (\text{mL}) = \frac{culture\ parasitaemia \times 10\ mL}{4}$$

To adjust for 3, 1 or 0.3 parasites per well (ppw), 75 μL/25 μL/2.5 μL of diluted suspension was added to the calculated V_{dil} of uninfected RBCs. The mixture was thoroughly mixed, then plated 100 μL per well in 96-well plates. Plates were incubated for one week at 37°C before being fed with new media and

supplemented with drug for continued positive selection of integrants. The plated parasites were fed and drugged once every 2 days (for up to 4 days). A duplicate plate was then created by seeding 20 μL of each well into an identically structured 96-well plate. This duplicate is used for analysis by flow cytometry to determine which wells contained viable parasites. Wells with lower parasitaemias (ranging from 0.1 to 0.5) were deemed to be more likely clonal populations which had propagated from a single parasite. Wells with parasitaemias >1% were avoided. Three clones from three chosen wells were then transferred from the original 96-well plate and expanded in 10 mL dishes supplemented with media, drug and uninfected RBCs to 3% haematocrit. Parasites were then further screened by PCR to confirm successful integration and by western blot analysis for proteins of interest corresponding to the transfected line.

Saponin lysis

Saponin lysis is a technique which lyses the membrane of both the infected and uninfected RBC, leaving only intact parasites for use in DNA extraction and protein harvests. Specifically for protein harvests, all lysis reagents were formulated with CØmplete EDTA-free protease inhibitor cocktail tablet (Roche) to minimise protein degradation. To lyse cells, cultures at high parasitaemia were centrifuged at 550 rcf for 5 min, supernatant removed, then thoroughly resuspended in twice the pellet volume of 0.15% w/v saponin (Sigma-Aldrich) and placed on ice for 10 min to allow the reaction to proceed. Lysed RBCs were then centrifuged at 16000 rcf, supernatant removed and the pellet washed in 1 mL of 0.075% w/v saponin to lyse leftover RBCs. Pellets were washed in 1x PBS until a clear supernatant was achieved. Supernatant was removed and saponin pellets were stored at -80 ^{o}C.

Extracting DNA from saponin pellets

DNA was extracted from saponin pellets using the Wizard® Genomic DNA Purification Kit (Promega) or the PureLink™ Genomic DNA Mini Kit (Invitrogen) as per manufacturer's instructions for pellet sizes estimated to be ≤ 300 μL. Purified DNA was used as a template to PCR amplify sequences of interest to confirm successful transfections.

Western blot analysis

Western blot analysis is a versatile output for a variety of protein-based assays. Changes in the parasite's proteome, invadome or secretome at any defined point in the erythrocytic lifecycle could be examined both qualitatively and semi-quantitatively provided the appropriate antibodies were available for probing the proteins of interest. For the studies presented in this thesis, this technique was primarily used for investigating the potency of the *glm*S protein knockdown system for relative protein quantification and the resulting impact on other proteins involved in RBC invasion. Material for analysis was sourced from saponin harvests, which contains a mix of both protein and DNA. To remove parasite DNA which interferes with Western blot gel loading, saponin pellets were DNase I treated (Qiagen) for 5 min at room temperature before being resuspended in reducing sample buffer (0.125 M Tris-HCl pH 7, 20% v/v glycerol, 4% v/v SDS, 10% v/v β-mercaptoethanol (Sigma-Aldrich), 0.002% w/v bromophenol blue (Sigma-Aldrich)). Lysate proteins were separated by size on SDS-PAGE 4-12% Bis-tris Gels (Bolt, Invitrogen) in a Novex™ BOLT™ mini gel tank (Thermofisher) in 1× 2-(N-morpholino)ethanesulfonic acid (MES) buffer at 110 V for 80 min then transferred onto a nitrocellulose membrane (iBlot, Invitrogen) at 20 V for 7 min. Membranes were blocked in 1% w/v skim milk 0.05% v/v Tween20 (Sigma-Aldrich) in 1x PBS (hereby referred to as mPBS-T) for 1 hr at room temperature. Primary and secondary antibodies (listed in the Appendix) were diluted in mPBS-T and incubated on the membranes for 1 hr each at room temperature while rocking. Primary antibodies were washed three times in 0.05% v/v PBS-Tween20 (hereby referred to as PBS-T), while secondary antibodies were washed twice in PBS-T and once in PBS. Completed blots were dried on filter paper (Whatman) and visualised on the Odyssey Infrared Imaging System (LI-COR Biosciences). All band quantification and image adjustment were performed in Image Studio Lite 5.2.5 (LI-COR Biosciences).

Proteinase K protection assay

To determine whether a protein of interest was cytosolically exposed or compartmentalised in an organelle, a proteinase K protection assay modified from a previous study was performed (Cabrera *et al.* 2012). Three 10 mL aliquots of high

schizontaemia cultures were centrifuged at 440 rcf for 5 min, supernatant removed and lysed in 0.15% w/v saponin as described above. One set of schizonts were treated in SOTE (0.6 M sorbitol, 20 mM Tris HCl pH 7.5, 2 mM EDTA) alone and centrifuged at 800 rcf for 30 min before being washed in SOTE again. The second set of schizonts were treated as described above, with an additional treatment in SOTE with 0.02% w/v digitonin (Sigma-Aldrich) and was left incubating for 10 min at 4 °C before being centrifuged gently at 800 rcf for 20 min to ensure the sample pelleted without damaging organellar membranes. The third set of schizonts were treated with saponin and then digitonin, followed with a final treatment of 0.1 μg/μL Proteinase K (Sigma-Aldrich) in SOTE for 30 min at 4 °C and centrifuged at 16000 rcf for 10 min. Proteinase K was inactivated with 50 μL 100% v/v trichloroacetic acid (Sigma-Aldrich). All samples were resuspended in 500 μL acetone to ensure full Proteinase K deactivation, centrifuged at 16000 rcf for 5 min then washed twice in 500 μL MilliQ H_2O. The final pellets were used for Western blot analysis of a protein of interest's sensitivity to Proteinase K.

Protein solubility assays

To biochemically determine whether a protein of interest was membrane-associated and by what mechanism of association, a protein solubility assay was performed as previously described (Cabrera *et al.* 2012). High schizontaemia culture was saponin-lysed as described above, resuspended in 100 μL MilliQ H_2O, snap-frozen and freeze-thawed in dry ice four times, passed through a 29 gauge needle 5 times to disrupt parasite membranes, centrifuged at 16000 rcf for 10 min before reserving the water-soluble fraction containing cytosolic proteins. The remaining pellet was washed twice in MilliQ H_2O and once in PBS before being resuspended in 100 μL 0.1 M Na_2CO_3 for 30 min at 4 °C, then centrifuged before reserving the carbonate-soluble fraction containing peripherally-associated proteins. The pellet was washed in the same manner above before being resuspended in 0.1% v/v Triton X-100 for 30 min at 4 °C, centrifuged and the final supernatant reserved containing integral proteins. The remaining pellet was washed twice in PBS and was used to represent Triton X-100-insoluble proteins. All fractions were analysed by Western blot to determine a protein of interest's membrane solubility profile.

Introduction to IFA

Immunofluorescence assays (IFAs) were used as a technique to analyse and determine the subcellular localisation of a protein of interest. This thesis presents a qualitative assessment of protein localisation and quantitative analysis of several datasets.

Schizont fixation in paraformaldehyde and glutaraldehyde

High schizontaemia cultures were treated with E64 or C1 as described above, then centrifuged at 550 rcf, supernatant decanted and washed once in 1× PBS to remove residual culture media which has auto-fluorescent properties. Pellets were then mixed in five times the volume of 4% v/v paraformaldehyde (PFA, Sigma-Aldrich), 0.0075% v/v glutaraldehyde (Electron Microscopy Sciences) pH 7.4 fixative (herein collectively referred to as cell fixative) diluted in 1× PBS and gently rocked (~60 rpm) for 30 min. The fixed cells were centrifuged again at 550 rcf, fixative removed and the pellet washed in 0.2 μm filter-sterilised 1× PBS (herein referred to as PBS_{FS}).

Preparing coverslips

All liquid reagents used for IFA preparation were filter-sterilised using a 0.2 μm filter (Minisart) to eliminate dust or contaminating bacteria which have auto-fluorescent properties. #1.5H high-precision coverslips (Carl Zeiss, Oberkochen, Germany) were soaked in methanol, placed in 6-well plates (Corning), airdried, coated in 0.01% v/v poly-L-lysine (brand) for 30 min at room temperature then washed in MilliQ H_2O. Fixed cells (200 μL) adjusted to 1% haematocrit in PBS_{FS} were then laid on top at room temperature for 30 min, with non-adherent cells being gently aspirated off. Cells were permeabilised with 0.1% v/v Triton X-100 for 10 minutes then incubated in 3% bovine serum albumin (BSA, Sigma-Aldrich) in PBS-T for 1 hr. Primary antibodies (concentrations in Appendix) were diluted in 1% w/v BSA in PBS-T and applied to the coverslips overnight at 4°C. The next day, coverslips were washed three times in PBS-T for 5 min each rocking, before being incubated with Alexa Fluor-conjugated secondary antibodies at a concentration of 1/500 in 1% w/v BSA PBS-T (a combination of any of: mouse or chicken 488 nm,

mouse 555 nm (for the Olympus FV3000) or 594 nm (for the Zeiss LSM800), rabbit 647 nm, Life Technologies) for 1 hour in the dark at room temperature. Coverslips were again washed three times in PBS-T before being post-fixed in cell fixative for 10 min to fix primary-secondary antibody complexes and to promote the stability of the fluorophores over time in storage. Fixative was aspirated off, washed in PBS_{FS} then dehydrated in ethanol (70% v/v 3 min, 90% v/v 3 min, 100% v/v 3 min), air dried and then mounted on glass slides with 20 µL Prolong® Gold antifade solution (refractive index 1.4) (Thermofisher Scientific) with 4', 6-diamidino-2-phenylindole dihydrochloride (DAPI, Thermofisher Scientific). The mountant was allowed to cure overnight in the dark and coverslips were analysed on an Olympus FV3000 confocal microscope or a Zeiss LSM800 Airyscan super-resolution microscope.

Olympus FV3000 confocal microscope settings

The following settings are a representative configuration for the FV3000 across multiple experiments, as re-optimisation is required at the beginning of every experiment due to slight variation.

$Channel_{target}$	Laser %	HV	Gain	Offset
405_{DAPI}	1.0	565	1000	3
$488_{Pf3D7\_1468400HA}$	2.0	625	1000	3
$488_{Pf3D7\_0818100HA}$	3.0	600	1000	3
$488_{Pf3D7\_0210600HA}$	1.0	600	1000	3
$488_{Pf3D7\_0405200HA}$	2.0	675	1000	3
555_{RAP1}	1.0	500	1000	3
555_{RH5}	2.0	450	1000	3
555_{AMA1}	2.0	650	1000	3
$647_{MSP1\text{-}19}$	1.0	410	1000	3
647_{RON4}	1.0	530	1000	3
647_{ERC}	1.0	545	1000	3
647_{ERD2}	1.0	480	1000	3
647_{EXP2}	1.0	350	1000	3

647_{GAP45}	1.0	450	1000	3
647_{GAPDH}	1.0	450	1000	3

Zeiss LSM800 Airyscan super-resolution microscope settings

The following settings are a representative configuration for the LSM800 across multiple experiments, as re-optimisation was often required at the beginning of every experiment due to slight variations in samples.

$Channel_{target}$	Laser %	HV	Gain	Offset
405_{DAPI}	0.4	850	1.5 x	3
$488_{Pf3D7\_0405200HA}$	1.0	850	1.5 x	3
488_{AMA1}	1.5	750	1.5 x	3
594_{RAP1}	0.5	700	1.5 x	3
$647_{MSP1\text{-}19}$	0.5	500	1.5 x	3
647_{RON4}	0.5	750	1.5 x	3

Quantification of colocalisation

Colocalisation statistics were calculated in IMARIS (Bitplane) over three biological replicates by defining a region of interest between an unknown signal (i.e. HA-tagged PfCERLI2) and the signal of a corresponding organelle marker. Threshold values were then set for each marker to distinguish between background and genuine signal, and this value would be used universally across all images within the same biological replicate to subtract background. Colocalisation was quantified by Pearsons' correlation coefficients.

Glucosamine-sensitivity protein knockdown growth assay

To investigate potential growth defects resulting from protein knockdown from genes endogenously modified with the *glm*S system, relevant *glm*S parasite cultures were synchronised to ring-stages using sorbitol lysis (Lambros & Vanderberg 1979) and adjusted to 1% parasitaemia at 1% haematocrit in 96 well U-bottom plates (Corning). Briefly, 45 μL of adjusted culture was then suspended in 5 μL of a 10x stock of D-(+)-glucosamine hydrochloride at varying concentrations between 50 mM-0.39 mM (hereby referred to as GlcN, Sigma-Aldrich) or media to a final volume of 50 μL to produce 1 in 10 dilutions between 5 mM-0.039 mM. Parasites were incubated at 37ºC as per standard culture conditions for 72 hours (termed a 1 cycle assay). Alternatively, parasites were set up at 0.1% parasitaemia in 1% haematocrit for 120 hours (termed a 2 cycle assay) to investigate potential delayed growth effects of protein knockdown. Completed assays were then stained in 10 μg/mL ethidium bromide (Bio-Rad) in 1x PBS and the final parasitaemia was assessed using the BD Accuri™ C6 Plus flow cytometer (Late stage parasites: FSC-H high; PE-H (EtBr) high population). All flow cytometry files were analysed using FlowJo Version 10 (Tree Star).

Merozoite protein knockdown invasion assay

To directly assess merozoite invasion, GlcN-treated glmS modified lines with an episomally-expressed cytosolic GFP were set up at 1% ring stages at 1% haematocrit as described above, and grown until new ring stages had formed 48 hours post assay setup. Cytosolic GFP is required to quantify newly invaded ring stages by flow cytometry as opposed to other lifecycle stages. Assays were analysed by flow cytometry, with the newly invaded ring stages identified as a FITC-H high, PE-H low population with gating and analysis undertaken on FlowJo.

Morphological assessment of parasite development

To observe whether protein knockdown of a protein of interest had an impact on merozoite quantity per schizont or merozoite morphology, relevant *glm*S parasites were treated with or without 2.5 mM GlcN at ring stages until they matured into 40-44 hr old schizonts. To ensure full merozoite development,

schizonts were arrested with E64 for 4 hrs to prevent rupture and then smeared as a thin blood film. Smears were stained in Giemsa as described above and then the number of merozoites per schizont were counted by light microscopy (n = 20 individual schizonts). Qualitative assessment of schizont morphology was also assessed. To count free merozoites, *glm*S modified lines with an episomally-expressed cytosolic GFP were treated with +/- 2.5 mM GlcN, grown to schizonts and were permitted to incubate until rupture and for merozoites quantified by flow cytometry as a FSC-H low, PE-H High populations before analysis by FlowJo software.

Schizont rupture assay

To observe whether protein knockdown of a protein of interest affected schizont rupture and merozoite egress, synchronous relevant *glm*S ring stages of relevant *glm*S parasite lines were treated in duplicate with or without 2.5 mM GlcN in 96-well U bottom plates as described above. Parasites were permitted to grow into schizonts prior to rupture and the parasitaemia was recorded by flow cytometry. Plates were then incubated for an additional 6 hrs to allow for schizont rupture followed by a second round of parasitaemia measurement by flow cytometry. To calculate the percentage of schizont rupture within this time window, the following equation was used:

$$\% \text{ schizont rupture} = \left(\frac{post-rupture\ schizontaemia}{pre-rupture\ schizontaemia}\right) \times 100$$

Bound merozoite assay by light microscopy

To determine whether protein knockdown inhibited merozoite invasion prior to, or following, tight junction formation, ring-stage parasites were either treated with 2.5 mM GLCN or left untreated and incubated until schizont rupture. Following schizont rupture, Giemsa-stained smears were made of these cultures without washing or removing the culture medium, blinded and counted to determine the number of bound merozoites and newly invaded rings in each treatment. For each treatment >1000 RBCs were counted per replicate.

Bound merozoite assay and invasion scoring by confocal microscopy

To determine whether PfCERLI2 protein knockdown inhibited invasion, prior, at or following tight junction formation, uninfected RBCs were stained in 1 mM CellTrace™ Far Red (Invitrogen) to allow for fluorescent visualisation and downstream 3D modelling of the RBC. Stained RBCs at 6% haematocrit were treated with 1 mM cytochalasin D (ThermoFisher Scientific) or left untreated, then distributed as 75 µL aliquots in a 96 well plate. Ring-stages at 4-5% parasitaemia were treated with 2.5 mM GLCN or left untreated, incubated until young schizonts had formed at the point of chromatin segregation, Percoll-purified, then treated with E64 for 4 hours. Viable merozoites were purified as described previously with modifications (Riglar *et al.* 2011). Percoll-purified schizonts were resuspended in 2 mL culture media excluding Albumax and passed through a 1.2 mm Minisart® Syringe Filter, and 75 µL of flowthrough was immediately added to wells containing CellTrace-stained, cytochalasin D-treated or untreated RBCs, now at a final haematocrit of 3%. The plate was shaken at 300 rpm at 37 ºC for 2 minutes to allow for a short invasion window, then cells fixed in a fixative (of final concentration 4% w/v paraformaldehyde (PFA, Sigma-Aldrich), 0.0075% v/v glutaraldehyde (Electron Microscopy Sciences), pH 7.4). Samples were prepared for confocal microscopy as described earlier. Labels included anti-AMA1 (mouse 1/500), anti-MSP1-19 (rabbit 1/1000) and DAPI. Slides were blinded shortly after sample preparation, and Z-stacks of 20 merozoites were taken per treatment group on an LSM800 (Zeiss) in Airyscan mode. Invasion was scored under three tiers: 1-attached, 2-partially invaded, 3-invaded, which could be determined by whether the merozoite appeared on the surface of, partway through the interface of, or enveloped inside the CellTrace fluorescent label respectively. The diameter of AMA1 of each merozoite was measured in Imaris (Bitplane). Samples were unblinded after AMA1 diameter measurements were performed and differences in AMA1 diameter for invading merozoites of PfCERLI2 knock-down and wildtype parasites quantified. Measurements for merozoites with an invasion score = 3 (fully entered the RBC) were excluded from the data as the tight junction ratchets behind the merozoite upon completion of invasion, potentially becoming smaller, misrepresenting the correlation between invasion progression and diameter size.

Knockout expansion rate assay

This assay is used to determine the expansion rate between blood stage cycles to compare wild-type and selection-linked integration targeted gene disruption (SLI-TGD) knockout lines of interest by flow cytometry. All SLI-TGD lines must be selected on G418 for two weeks prior as the drug must be removed during the assay. All clones of a given knockout line and a wild-type parental line containing ring stages were sorbitol treated, returned to culture and grownfor 24 hours at 37°C. Once trophozoites had formed, parasitaemias were assessed by flow cytometry. Parasitaemias were then adjusted to either 1% (1 cycle growth format) or 0.15% (2 cycle growth format) and once again checked by flow cytometry, and these values were recorded as the baseline parasitaemia for the assay for normalisation. Adjusted parasites were then grown in 96-well plates in technical triplicate for each line or clone and allowed to grow for 48 hours (1 cycle growth format) or 96 hours (2 cycle growth format) for analysis at trophozoite stage by flow cytometry. Once the final parasitaemias were quantified in FlowJo Version 10, the rate of expansion was calculated as:

$$\text{Rate of expansion (fold change)} = \frac{average\ late\ stages\ (final\ \%)}{average\ late\ stages\ (set{-}up\ \%)}$$

Introduction to RNA-seq

RNA sequencing (RNA-seq) is a technique used to investigate broad changes in the transcriptome – mRNA expression patterns, at a defined point in time for a population of cells using next-generation sequencing (NGS) of RNA followed by bioinformatic analyses. Specifically, this technique was used to study the changes in transcriptomic profile of SLI-TGD gene knockout parasite lines compared to their parental wild-type line at the point of schizogony approximately 40-44 hours into the erythrocytic lifecycle. The aim was to determine whether a given C3H1 zinc finger protein gene knockout conferred changes in expression of other genes. In doing so would provide insights into the potential function of the C3H1 zinc finger protein and its putative relationship with other proteins.

RNA extraction of erythrocytic stages

The following utilised RNase free tips, tubes and PCR-grade water to minimise RNA degradation and ensure the integrity of samples for NGS. Polypropylene tubes must be used as they are compatible with several corrosive chemicals used during RNA extraction. High parasitaemia synchronous 40-44 schizont SLI-TGD and parental wild-type cultures were centrifuged at 550 rcf and the supernatant decanted. Cells were then immediately resuspended in 10 pellet volumes of TRIzol® (Invitrogen) and incubated at 37 ºC for 5 min before being frozen at -80 ºC for storage. Samples were thawed when required and then resuspended in 1/5 TRIzol® volume of chloroform (Invitrogen), incubated for 3 min at room temperature before being centrifuged at 12000 rcf for 30 min at 4 ºC. After centrifugation, only the aqueous supernatant containing RNA was carefully aliquoted into new tubes and the organic phase pellets were discarded. An equal supernatant volume of 70% ethanol made with PCR-grade water was mixed with the RNA supernatants and inverted twice to mix. The aqueous ethanol mixture was then processed using an PureLink™ RNA mini kit (Qiagen) with modifications to the manufacturer's protocol (advice from Prof. Mike Duffy, Bio21 Institute, The University of Melbourne). To summarise the modified kit protocol, the ethanol mixture was passed through an RNeasy mini column, 700 µL at a time, and spun at 8000 rcf for 30 seconds, flowthrough discarded. This was followed by 700 µL of Buffer RW1, spun at 8000 rcf for 30 sec, flowthrough discarded, then 500 µL Buffer RPE, spun at 8000 rcf for 30 sec, flowthrough discarded. An additional 500 µL Buffer RPE was added, spun at 8000 rcf for 2 min, flowthrough discarded. Columns were then centrifuged at 16000 rcf for 1 min to dry the membrane, then the collection tube was replaced with a new one. RNA was eluted in 50 µL PCR-grade water, left to equilibrate for 2 min, spun at 16000 rcf for 1 min. To remove contaminant gDNA from the RNA samples, the resulting elute was treated with 2 µL DNase I (Qiagen) at 1500 units/10 µL and topped up the mixture to 100 µL in PCR-grade water. Samples were incubated for 10 min at RT. 350 µL Buffer RLT was added, and samples were mixed by inversion, followed by 250 µL of 100% ethanol and mixed by pipetting. The resulting mixture was then passed through an RNeasy column in the manner described above, and eluted once again in 50 µL PCR-grade water. RNA concentration and integrity were assessed using a Nanodrop (**brand**), expecting a 260/280 and 260/230 ratio teetering around ~2. Samples were parafilmed and stored at -80 ºC.

Next-generation sequencing

Purified RNA samples were shipped frozen on dry ice to the Murdoch Children's Research Institute Victorian Clinical Genetics Services (MCRI-VCGS). Total RNA libraries were prepared using the TruSeq Stranded Total RNA with Ribo-Zero Globin kit (Illumina) to enrich for non-host RBC RNA before being sequenced an a Novaseq platform with the following configuration: 2 × 150 base paired reads for 13,000,000 reads (as per advice from Dr. Lee Yeoh, Bio21 Institute, The University of Melbourne).

Differential expression analysis using bash and R

The bioinformatic pipeline for RNAseq differential gene expression analysis required the use of two programming languages: GNU Bash (herein referred to as Bash) and R. All Bash-based analyses were performed on the University of Adelaide Phoenix High Performance Computing (HPC) service. All R-based analyses were performed on an integrated development environment (IDE) graphical user interface (GUI) via RStudio Desktop 1.1.463.

Bash analysis pipeline

R1 and R2 (complementary reads) sequencing files in the compressed format fastq.gz were uploaded to Phoenix in the working directory /fast/users/a1687185/1481RNAseqproject and kept in organised directories made using ngsSkeleton (GitHub, University of Adelaide Bioinformatics Hub). FASTQ files were subject to a quality check using FastQC 0.11.4 to identify overrepresented sequences and to assess the quality of the sequencing run. Files for the *P. falciparum* 3D7 genome version 46 were uploaded as a FASTA format and in general feature format (GFF) from PlasmoDB to Phoenix and were used to generate an indexed genome using STAR 2.5.3a using a Simple Linux Utility for Resource Management (SLURM) job request with parameters: *time* ≤ 100 hr, *memory* = 64 GB, *cores* = 12, *runThreadN* 10, *sjdbGTFfeatureExon* exon, *sjdbGTFtagExonParentTranscript* Parent, *sjdbOverhang* 150, *genomeSAindexNbases* 11. A functional script can be found in the Appendix. The value for the parameter *sjdbOverhang* was obtained from the largest read found in the

FastQC report minus 1. The parameter *genomeSAindexNbases* defines the length in base pairs for the pre-indexing string and was calculated as:

$log_2\left(\frac{genomelength}{2}\right) - 1$, where *genomelength* = 23,723,408 base pairs calculated from a character count of the *P. falciparum* 3D7 version 46 genome FASTA file.

FASTQ files were then mapped to the reference indexed genome using STAR 2.5.3a and SAMtools 1.3.1 using a SLURM job request with parameters: *time* = 100 hr, *memory* = 64 GB, *cores* = 12, *runThreadN* 12, *alignIntronMin* 5, *alignIntronMax* 3000, *outSAMtype* BAM Unsorted. The values for the parameters *alignIntronMin* and *alignIntronMax* were set based on the approximate shortest and longest known introns in the *P. falciparum* genome. A functional script can be found in the Appendix. Once completed, Binary Alignment Map (BAM) files were created which contained alignments of the R1 and R2 reads to the reference genome. In order to visualise the alignments, BAM files were converted to a Binary Alignment Index (BAI) format using the SAMtools index program in SAMtools 1.9. Both BAM and BAI files were downloaded and analysed in Integrative Genomics Viewer (IGV) (Broad Institute) to visualise the completed alignments.

R analysis pipeline

An R Markdown (RMD) *limma/voom* script based on the Walter and Eliza Hall Institute (WEHI) Bioconductor R pipeline, initially modified by Dr. Lee Yeoh (Bio21 Institute, The University of Melbourne) and Dr. Mark Armstrong (Bioinformatics Hub, The University of Adelaide), was further modified in RStudio Desktop 1.1.463. The biocLite.R packages *Rsubread*, *edgeR*, *limma*, *statmod* (required for differential analysis and statistics, Bioconductor) as well as the organiser package *here* (required for reading file path directories, GitHub) was installed. In order to allow RStudio to read GFF file formats, the PlasmoDB *P. falciparum* 3D7 genome version 46 was modified in Phoenix using the *sed* function to change the 9th tab-delimited field from *ID=* to *gene_id=* to produce the modified PlasmoDB-46_Pfalciparum3D7_new.gff file. Paths to data files were defined using a tab-delimited file bam_paths.txt assigning the *CellType* to the first field (which assigns a name to your sample), and the *BamFile* path to the second field to locate and import the BAM files. An example of a bam_paths.txt

file can be found in the Appendix. Once the GFF and BAM files had been loaded, *Rsubread* was run on three biological replicates of two different *CellType* groups (i.e. comparing three replicates of wild-types to a mutant line). Once completed, a Reads Per Kilobase of Transcript (RPKM) value was calculated for every gene to be used for differential analysis. Only genes with >10 reads per million reads in at least 2 biological replicates were filtered for differential analysis. Samples were quality-checked using *voom* to check the success of the filter. A sample cluster was then performed to identify if the biological replicates had broadly similar transcriptomes to each other using multi-dimensional scaling (i.e. to show whether wild-type transcript libraries are clearly separated from mutant transcript libraries). Samples were then fit to a linear model to assess differential expression using the eBayes moderated t-statistic to list the top ten most differentially expressed genes between two *CellTypes* and displayed on a volcano plot. All output was saved as tab-delimited .txt files, or .csv files. A full RMD including annotated comments. In order to perform a modified analysis which excludes large polymorphic gene families (i.e. *var*, *rifin* and *stevor* families), a filtered Gene Transfer Format (GTF) file from (Tarr *et al.* 2018) was used in place of PlasmoDB-46_Pfalciparum3D7_new.gff with the same subsequent analyses.

Rhoptry and microneme ligand secretion assay

Secretion assays were modified from a previous protocol (Absalon *et al.* 2016). This assay assesses whether particular merozoite invasion ligands (of the micronemes, rhoptry neck and bulb) undergoes a correlative secretion defect when a corresponding protein of interest is knocked down. This was testable by cleaving the invasion receptors of new host red blood cells with proteolytic enzymes, preventing merozoite invasion but permitting secretion of invasion ligands into the culture supernatant to be analysed. Briefly, sorbitol-treated synchronous *glm*S modified ring stages at 5-6% parasitaemia were centrifuged at 550 rcf and set up in 6 well plates (Corning) at 8% haematocrit in 3 mL of media. An identical plate with wild type parasites was also prepared as a control. Each well was treated with 2.5 mM GlcN and incubated overnight as per standard culture. On the next day, the grown trophozoite cultures were centrifuged at 550 rcf, placed in 1.5 mL tubes and enzyme treated (23.5 units/mL neuraminidase, 1 mg/mL trypsin, 1 mg/mL chymotrypsin in incomplete RPMI-HEPES, warmed at 37 ^{o}C) for 45 min at 37^{o}C, inverting tubes every 15 minutes to mix, to cleave off RBC surface

receptors. Enzymes were decanted and stored at 4 ºC for reuse and the pellet washed twice in culture media before being returned to culture re-supplemented with +/- 2.5 mM GlcN. Schizonts were permitted to develop and rupture, and merozoites were prevented from invading the next day. Culture supernatants (secreted protein fraction) were collected and the pellets (unsecreted protein fraction) were subject to saponin lysis. Samples were then analysed by Western blot as previously described, loading no more than 10 µL into each well to prevent overloading of albumin in supernatant samples. The same protocol was used for identifying changes in protein cleavage during invasion.

Introduction to DiQ-BioID

Dimerization induced quantitative proximity-dependent biotin identification (DiQ-BioID) was a recently developed method for identifying putative protein binding partners for a bait protein of interest in *P. falciparum* blood stage cultures (Birnbaum *et al.* 2020). To perform DiQ-BioID, a gene of interest which expresses the bait protein must be C-terminally tagged at the endogenous locus with an FK binding protein (FKBP) and a GFP reporter. This was performed using the SLI system (Birnbaum *et al.* 2017, Spielmann *et al.* 2017). To this line, a second episomal construct expressing the BirA biotinylator which is C-terminally tagged with the FKBP-rapamycin-binding protein domain (FRB) and a mCherry reporter is transfected in. Parasite lines must express both halves of the system. When rapalog is added to culture, this allows BirA to be recruited to the bait protein by facilitating the dimerization of FKBP and FRB which can be observed microscopically with the co-localisation of GFP and mCherry. Additionally, in the presence of excess biotin, BirA covalently attaches biotin to proteins in its proximity, including the bait protein and any of its surrounding protein partners. Biotinylated proteins can then be purified using streptavidin-based immunoprecipitation, and candidates for the bait protein's interactome are identified by mass spectrometry.

Preparation of biotin-labelled material for DiQ-BioID

30 mL cultures of 36 hour old early schizonts of a parasite line with an endogenously FKBP-tagged bait protein (i.e. PfCERLI1$^{FKBP-GFP}$) expressing an episomal biotinylator (i.e. BirA), were treated with 150 µM biotin (Sigma-Aldrich) and with or without rapalog A/C heterodimerizer (AP21967, Takara) for 8 hours total.

Simultaneous treatments were performed in a control line expressing only the biotinylator. At 4 hours into treatment, E64 was added and cultures incubated for the final 4 hours until mature segmented schizonts had formed. Prior to harvest, co-localisation of bait protein with BirA was confirmed by widefield microscopy of live cells, and a small aliquot of culture was fixed with PFA/glutaraldehyde for validating correct biotinylation at a site of interest by IFA. The remaining culture was centrifuged at 550 rcf, and washed twice in PBS to remove excess biotin and albumin. Parasites were harvested by saponin lysis, as described in detail earlier. This was repeated for 3-5 biological replicates for the test and control lines. Once all replicates had been harvested, purification of biotinylated targets by immunoprecipitation was performed over three days.

On day 1, each lysate was resuspended in 1.5 mL lysis buffer (50 mM Tris-HCl pH 7.5, 500 nM NaCl, 1% Triton X-100, 1 mM dithiothreitol (DTT), 1 mM phenylmethylsulfonyl fluoride (PMSF) with CØmplete EDTA-free protease inhibitor cocktail tablet (Roche)) and homogenised by sonication for 30 seconds three times with a minute in-between sonications for samples to cool on ice. Samples were centrifuged at 16000 g to 10 min at 4 ºC to separate the pellet and supernatant. While waiting, 50 µL slurries of magnetic streptavidin beads (Pierce) were washed twice in 500 µL lysis buffer, magnetized to a rack for 3 min and supernatant removed. Lysate supernatant (1.5 mL) was then incubated with beads at 4 ºC O/N to enrich for biotinylated proteins. A dummy sample without parasite material was also prepared, to be used as a blanking control for peptide quantification on day 3.

On day 2, beads were magnetized for 3 min, and flowthrough was discarded (a small amount kept for validation). Beads were washed three times in 1 mL lysis buffer, rotating at room temperature for 5 min. Beads were magnetized for 3 min, supernatant discarded and then washed six times in 1 mL 50 mM ammonium bicarbonate (Sigma-Aldrich). Beads were magnetized for 3 min, supernatant discarded, then finally resuspended in 200 µL ammonium bicarbonate containing 1 µg equivalent of sequencing-grade trypsin (Promega) to be incubated O/N at 37 ºC with gentle shaking to thoroughly coat the beads.

On day 3, an additional 0.5 μg of sequencing-grade trypsin was added to each bead-lysate slurry, and incubated for 4 hours at 37 ºC, gently shaking. After incubation, beads were magnetized and supernatant containing peptides, termed the elute, were transferred to a fresh tube. To collect any residual peptides from the beads, the beads were washed twice in 150 μL ddH_2O, magnetized for 3 min and rinses were pooled with the elute. To eliminate any residual beads in the elute, peptides were centrifuged at 16000 g for 10 min at 4 ºC, and the supernatant was transferred to another fresh tube (leaving about 30 μL at the bottom in order not to take up any residual beads). The final elute, containing pure peptides, was then acidified to 0.5% v/v formic acid (Thermofisher) in order to inactivate trypsin. Peptide concentration was measured by Nanodrop by using the dummy sample as a blanking control, where an average of three consecutive measurements was taken. Samples were then parafilmed to prevent evaporation, and stored at 4º C until ready for shipment.

Chapter 6

Bibliography

Bibliography

ABIODUN, G. J., MAHARAJ, R., WITBOOI, P. & OKOSUN, K. O. 2016. Modelling the influence of temperature and rainfall on the population dynamics of Anopheles arabiensis. *Malar J,* 15**,** 364.

ABSALON, S., ROBBINS, J. A. & DVORIN, J. D. 2016. An essential malaria protein defines the architecture of blood-stage and transmission-stage parasites. *Nat Commun,* 7**,** 11449.

AHLBORG, N., HADDAD, D., SIDDIQUE, A. B., ROUSSILHON, C., ROGIER, C., TRAPE, J. F., TROYE-BLOMBERG, M. & BERZINS, K. 2002. Antibody responses to the repetitive Plasmodium falciparum antigen Pf332 in humans naturally primed to the parasite. *Clin Exp Immunol,* 129**,** 318-25.

ALEXANDER, D. L., MITAL, J., WARD, G. E., BRADLEY, P. & BOOTHROYD, J. C. 2005. Identification of the moving junction complex of Toxoplasma gondii: a collaboration between distinct secretory organelles. *PLoS Pathog,* 1**,** e17.

ARCHER, N. M., PETERSEN, N., CLARK, M. A., BUCKEE, C. O., CHILDS, L. M. & DURAISINGH, M. T. 2018. Resistance to Plasmodium falciparum in sickle cell trait erythrocytes is driven by oxygen-dependent growth inhibition. *Proc Natl Acad Sci U S A,* 115**,** 7350-7355.

AURRECOECHEA, C., BARRETO, A., BASENKO, E. Y., BRESTELLI, J., BRUNK, B. P., CADE, S., CROUCH, K., DOHERTY, R., FALKE, D., FISCHER, S., GAJRIA, B., HARB, O. S., HEIGES, M., HERTZ-FOWLER, C., HU, S., IODICE, J., KISSINGER, J. C., LAWRENCE, C., LI, W., PINNEY, D. F., PULMAN, J. A., ROOS, D. S., SHANMUGASUNDRAM, A., SILVA-FRANCO, F., STEINBISS, S. A.-O. H. O. O., STOECKERT, C. J., JR., SPRUILL, D., WANG, H., WARRENFELTZ, S. & ZHENG, J. 2016. EuPathDB: the eukaryotic pathogen genomics database resource. *Nucleic Acids Research*, 45**,** D581-591.

AURRECOECHEA, C., BRESTELLI J FAU - BRUNK, B. P., BRUNK BP FAU - DOMMER, J., DOMMER J FAU - FISCHER, S., FISCHER S FAU - GAJRIA, B., GAJRIA B FAU - GAO, X., GAO X FAU - GINGLE, A., GINGLE A FAU - GRANT, G., GRANT G FAU - HARB, O. S., HARB OS FAU - HEIGES, M., HEIGES M FAU - INNAMORATO, F., INNAMORATO F FAU - IODICE, J., IODICE J FAU - KISSINGER, J. C., KISSINGER JC FAU - KRAEMER, E.,

KRAEMER E FAU - LI, W., LI W FAU - MILLER, J. A., MILLER JA FAU - NAYAK, V., NAYAK V FAU - PENNINGTON, C., PENNINGTON C FAU - PINNEY, D. F., PINNEY DF FAU - ROOS, D. S., ROOS DS FAU - ROSS, C., ROSS C FAU - STOECKERT, C. J., JR., STOECKERT CJ JR FAU - TREATMAN, C., TREATMAN C FAU - WANG, H. & WANG, H. 2008. PlasmoDB: a functional genomic database for malaria parasites. *Nucleic Acids Research*, 37**,** D539-543.

AYIMBA, E., HEGEWALD, J., SEGBENA, A. Y., GANTIN, R. G., LECHNER, C. J., AGOSSSOU, A., BANLA, M. & SOBOSLAY, P. T. 2011. Proinflammatory and regulatory cytokines and chemokines in infants with uncomplicated and severe Plasmodium falciparum malaria. *Clin Exp Immunol,* 166**,** 218-26.

BALAGOPAL, V. & PARKER, R. 2009. Polysomes, P bodies and stress granules: states and fates of eukaryotic mRNAs. *Curr Opin Cell Biol,* 21**,** 403-8.

BALDI, D. L., ANDREWS, K. T., WALLER, R. F., ROOS, D. S., HOWARD, R. F., CRABB, B. S. & COWMAN, A. F. 2000. RAP1 controls rhoptry targeting of RAP2 in the malaria parasite Plasmodium falciparum. *EMBO J,* 19**,** 2435-43.

BALDWIN, M. R., LI, X., HANADA, T., LIU, S. C. & CHISHTI, A. H. 2015. Merozoite surface protein 1 recognition of host glycophorin A mediates malaria parasite invasion of red blood cells. *Blood,* 125**,** 2704-11.

BALU, B., MAHER, S. P., PANCE, A., CHAUHAN, C., NAUMOV, A. V., ANDREWS, R. M., ELLIS, P. D., KHAN, S. M., LIN, J. W., JANSE, C. J., RAYNER, J. C. & ADAMS, J. H. 2011. CCR4-associated factor 1 coordinates the expression of Plasmodium falciparum egress and invasion proteins. *Eukaryot Cell,* 10**,** 1257-63.

BANNISTER, L. H., HOPKINS, J. M., DLUZEWSKI, A. R., MARGOS, G., WILLIAMS, I. T., BLACKMAN, M. J., KOCKEN, C. H., THOMAS, A. W. & MITCHELL, G. H. 2003. Plasmodium falciparum apical membrane antigen 1 (PfAMA-1) is translocated within micronemes along subpellicular microtubules during merozoite development. *J Cell Sci,* 116**,** 3825-34.

BANNISTER, L. H., HOPKINS, J. M., FOWLER, R. E., KRISHNA, S. & MITCHELL, G. H. 2000. Ultrastructure of rhoptry development in Plasmodium falciparum erythrocytic schizonts. *Parasitology,* 121 (Pt 3)**,** 273-87.

BANNISTER, L. H., MITCHELL, G. H., BUTCHER, G. A. & DENNIS, E. D. 1986. Lamellar membranes associated with rhoptries in erythrocytic merozoites of

Plasmodium knowlesi: a clue to the mechanism of invasion. *Parasitology,* 92 (Pt 2)**,** 291-303.

BARCONS-SIMON, A., CORDON-OBRAS, C., GUIZETTI, J., BRYANT, J. M. & SCHERF, A. 2020. CRISPR Interference of a Clonally Variant GC-Rich Noncoding RNA Family Leads to General Repression of var Genes in Plasmodium falciparum. *mBio,* 11.

BARCUS, M. J., HIEN, T. T., WHITE, N. J., LARAS, K., FARRAR, J., SCHWARTZ, I. K., CORWIN, A. & BAIRD, J. K. 2002. Short report: hepatitis b infection and severe Plasmodium falciparum malaria in Vietnamese adults. *Am J Trop Med Hyg,* 66**,** 140-2.

BARNES, K. I., DURRHEIM, D. N., LITTLE, F., JACKSON, A., MEHTA, U., ALLEN, E., DLAMINI, S. S., TSOKA, J., BREDENKAMP, B., MTHEMBU, D. J., WHITE, N. J. & SHARP, B. L. 2005. Effect of artemether-lumefantrine policy and improved vector control on malaria burden in KwaZulu-Natal, South Africa. *PLoS Med,* 2**,** e330.

BARTOLONI, A. & ZAMMARCHI, L. 2012. Clinical aspects of uncomplicated and severe malaria. *Mediterr J Hematol Infect Dis,* 4**,** e2012026.

BAUM, J., PAPENFUSS, A. T., MAIR, G. R., JANSE, C. J., VLACHOU, D., WATERS, A. P., COWMAN, A. F., CRABB, B. S. & DE KONING-WARD, T. F. 2009. Molecular genetics and comparative genomics reveal RNAi is not functional in malaria parasites. *Nucleic Acids Res,* 37**,** 3788-98.

BAUM, J., RICHARD, D., HEALER, J., RUG, M., KRNAJSKI, Z., GILBERGER, T.-W., GREEN, J. L., HOLDER, A. A. & COWMAN, A. F. 2006. A Conserved Molecular Motor Drives Cell Invasion and Gliding Motility across Malaria Life Cycle Stages and Other Apicomplexan Parasites. *Journal of Biological Chemistry,* 281**,** 5197-5208.

BAUM, J., TONKIN, C. J., PAUL, A. S., RUG, M., SMITH, B. J., GOULD, S. B., RICHARD, D., POLLARD, T. D. & COWMAN, A. F. 2008. A malaria parasite formin regulates actin polymerization and localizes to the parasite-erythrocyte moving junction during invasion. *Cell Host Microbe,* 3**,** 188-98.

BAUMGARTEN, S., BRYANT, J. M., SINHA, A., REYSER, T., PREISER, P. R., DEDON, P. C. & SCHERF, A. 2019. Transcriptome-wide dynamics of extensive m(6)A mRNA methylation during Plasmodium falciparum blood-stage development. *Nat Microbiol,* 4**,** 2246-2259.

BECK, J. R., FUNG, C., STRAUB, K. W., COPPENS, I., VASHISHT, A. A., WOHLSCHLEGEL, J. A. & BRADLEY, P. J. 2013. A Toxoplasma palmitoyl acyl transferase and the palmitoylated armadillo repeat protein TgARO govern apical rhoptry tethering and reveal a critical role for the rhoptries in host cell invasion but not egress. *PLoS Pathog,* 9**,** e1003162.

BEESON, J. G., DREW, D. R., BOYLE, M. J., FENG, G., FOWKES, F. J. & RICHARDS, J. S. 2016. Merozoite surface proteins in red blood cell invasion, immunity and vaccines against malaria. *FEMS Microbiol Rev,* 40**,** 343-72.

BEESON, J. G., ROGERSON, S. J., COOKE, B. M., REEDER, J. C., CHAI, W., LAWSON, A. M., MOLYNEUX, M. E. & BROWN, G. V. 2000. Adhesion of Plasmodium falciparum-infected erythrocytes to hyaluronic acid in placental malaria. *Nat Med,* 6**,** 86-90.

BERTIAUX, E., BALESTRA, A. C., BOURNONVILLE, L., LOUVEL, V., MACO, B., SOLDATI-FAVRE, D., BROCHET, M., GUICHARD, P. & HAMEL, V. 2021. Expansion microscopy provides new insights into the cytoskeleton of malaria parasites including the conservation of a conoid. *PLoS Biol,* 19**,** e3001020.

BERTSCHI, N. L., TOENHAKE, C. G., ZOU, A., NIEDERWIESER, I., HENDERSON, R., MOES, S., JENOE, P., PARKINSON, J., BARTFAI, R. & VOSS, T. S. 2017. Malaria parasites possess a telomere repeat-binding protein that shares ancestry with transcription factor IIIA. *Nat Microbiol,* 2**,** 17033.

BEUTLER, E. 2008. Glucose-6-phosphate dehydrogenase deficiency: a historical perspective. *Blood,* 111**,** 16-24.

BHATT, S., WEISS, D. J., CAMERON, E., BISANZIO, D., MAPPIN, B., DALRYMPLE, U., BATTLE, K., MOYES, C. L., HENRY, A., ECKHOFF, P. A., WENGER, E. A., BRIET, O., PENNY, M. A., SMITH, T. A., BENNETT, A., YUKICH, J., EISELE, T. P., GRIFFIN, J. T., FERGUS, C. A., LYNCH, M., LINDGREN, F., COHEN, J. M., MURRAY, C. L. J., SMITH, D. L., HAY, S. I., CIBULSKIS, R. E. & GETHING, P. W. 2015. The effect of malaria control on Plasmodium falciparum in Africa between 2000 and 2015. *Nature,* 526**,** 207-211.

BIRNBAUM, J., FLEMMING, S., REICHARD, N., SOARES, A. B., MESÉN-RAMÍREZ, P., JONSCHER, E., BERGMANN, B. & SPIELMANN, T. 2017. A genetic system to study *Plasmodium falciparum* protein function. *Nature Methods,* 14**,** 450.

BIRNBAUM, J., SCHARF, S., SCHMIDT, S., JONSCHER, E., HOEIJMAKERS, W. A. M., FLEMMING, S., TOENHAKE, C. G., SCHMITT, M., SABITZKI, R., BERGMANN, B., FRÖHLKE, U., MESÉN-RAMÍREZ, P., SOARES, A. B., HERRMANN, H., BÁRTFAI, R. & SPIELMANN, T. 2020. A Kelch13-defined endocytosis pathway mediates artemisinin resistance in malaria parasites. *Science,* 367**,** 51-59.

BIRRELL, G. W., CHALLIS, M. P., DE PAOLI, A., ANDERSON, D., DEVINE, S. M., HEFFERNAN, G. D., JACOBUS, D. P., EDSTEIN, M. D., SIDDIQUI, G. & CREEK, D. J. 2020. Multi-omic Characterization of the Mode of Action of a Potent New Antimalarial Compound, JPC-3210, Against *Plasmodium falciparum*. *Mol Cell Proteomics,* 19**,** 308-325.

BLACKMAN, M. J. 2008. Malarial proteases and host cell egress: an 'emerging' cascade. *Cell Microbiol,* 10**,** 1925-34.

BLACKMAN, M. J., FUJIOKA, H., STAFFORD, W. H., SAJID, M., CLOUGH, B., FLECK, S. L., AIKAWA, M., GRAINGER, M. & HACKETT, F. 1998. A subtilisin-like protein in secretory organelles of Plasmodium falciparum merozoites. *J Biol Chem,* 273**,** 23398-409.

BOOTHROYD, J. C. & DUBREMETZ, J. F. 2008. Kiss and spit: the dual roles of Toxoplasma rhoptries. *Nat Rev Microbiol,* 6**,** 79-88.

BOUCHER, I. W., BRZOZOWSKI, A. M., BRANNIGAN, J. A., SCHNICK, C., SMITH, D. J., KYES, S. A. & WILKINSON, A. J. 2006. The crystal structure of superoxide dismutase from Plasmodium falciparum. *BMC Struct Biol,* 6**,** 20.

BOYLE, M. J., RICHARDS, J. S., GILSON, P. R., CHAI, W. & BEESON, J. G. 2010a. Interactions with heparin-like molecules during erythrocyte invasion by Plasmodium falciparum merozoites. *Blood,* 115**,** 4559-68.

BOYLE, M. J., WILSON, D. W., RICHARDS, J. S., RIGLAR, D. T., TETTEH, K. K. A., CONWAY, D. J., RALPH, S. A., BAUM, J. & BEESON, J. G. 2010b. Isolation of viable *Plasmodium falciparum* merozoites to define erythrocyte invasion events and advance vaccine and drug development. *Proceedings of the National Academy of Sciences,* 107**,** 14378-14383.

BRASIL, P., ZALIS, M. G., DE PINA-COSTA, A., SIQUEIRA, A. M., JÚNIOR, C. B., SILVA, S., AREAS, A. L. L., PELAJO-MACHADO, M., DE ALVARENGA, D. A. M., DA SILVA SANTELLI, A. C. F., ALBUQUERQUE, H. G., CRAVO, P., SANTOS DE ABREU, F. V., PETERKA, C. L., ZANINI, G. M., SUÁREZ

MUTIS, M. C., PISSINATTI, A., LOURENÇO-DE-OLIVEIRA, R., DE BRITO, C. F. A., DE FÁTIMA FERREIRA-DA-CRUZ, M., CULLETON, R. & DANIEL-RIBEIRO, C. T. 2017. Outbreak of human malaria caused by Plasmodium simium in the Atlantic Forest in Rio de Janeiro: a molecular epidemiological investigation. *The Lancet Global Health,* 5**,** e1038-e1046.

BROWN, R. S. 2005. Zinc finger proteins: getting a grip on RNA. *Curr Opin Struct Biol,* 15**,** 94-8.

BULL, P. C. & ABDI, A. I. 2016. The role of PfEMP1 as targets of naturally acquired immunity to childhood malaria: prospects for a vaccine. *Parasitology,* 143**,** 171-86.

BULLEN, H. E., CHARNAUD, S. C., KALANON, M., RIGLAR, D. T., DEKIWADIA, C., KANGWANRANGSAN, N., TORII, M., TSUBOI, T., BAUM, J., RALPH, S. A., COWMAN, A. F., DE KONING-WARD, T. F., CRABB, B. S. & GILSON, P. R. 2012. Biosynthesis, localization, and macromolecular arrangement of the Plasmodium falciparum translocon of exported proteins (PTEX). *J Biol Chem,* 287**,** 7871-84.

BUNNIK, E. M., BATUGEDARA, G., SARAF, A., PRUDHOMME, J., FLORENS, L. & LE ROCH, K. G. 2016. The mRNA-bound proteome of the human malaria parasite Plasmodium falciparum. *Genome Biol,* 17**,** 147.

BUNNIK, E. M., CHUNG, D. W., HAMILTON, M., PONTS, N., SARAF, A., PRUDHOMME, J., FLORENS, L. & LE ROCH, K. G. 2013. Polysome profiling reveals translational control of gene expression in the human malaria parasite Plasmodium falciparum. *Genome Biol,* 14**,** R128.

BURNS, A. L., DANS, M. G., BALBIN, J. M., DE KONING-WARD, T. F., GILSON, P. R., BEESON, J. G., BOYLE, M. J. & WILSON, D. W. 2019. Targeting malaria parasite invasion of red blood cells as an antimalarial strategy. *FEMS Microbiol Rev,* 43**,** 223-238.

BUSHELL, E., GOMES, A. R., SANDERSON, T., ANAR, B., GIRLING, G., HERD, C., METCALF, T., MODRZYNSKA, K., SCHWACH, F., MARTIN, R. E., MATHER, M. W., MCFADDEN, G. I., PARTS, L., RUTLEDGE, G. G., VAIDYA, A. B., WENGELNIK, K., RAYNER, J. C. & BILLKER, O. 2017. Functional Profiling of a Plasmodium Genome Reveals an Abundance of Essential Genes. *Cell,* 170**,** 260-272.e8.

BUSTAMANTE, L. Y., BARTHOLDSON, S. J., CROSNIER, C., CAMPOS, M. G., WANAGURU, M., NGUON, C., KWIATKOWSKI, D. P., WRIGHT, G. J. & RAYNER, J. C. 2013. A full-length recombinant Plasmodium falciparum PfRH5 protein induces inhibitory antibodies that are effective across common PfRH5 genetic variants. *Vaccine,* 31**,** 373-9.

CABRERA, A., HERRMANN, S., WARSZTA, D., SANTOS, J. M., JOHN PETER, A. T., KONO, M., DEBROUVER, S., JACOBS, T., SPIELMANN, T., UNGERMANN, C., SOLDATI-FAVRE, D. & GILBERGER, T. W. 2012. Dissection of minimal sequence requirements for rhoptry membrane targeting in the malaria parasite. *Traffic,* 13**,** 1335-50.

CALIS, J. C., PHIRI, K. S., FARAGHER, E. B., BRABIN, B. J., BATES, I., CUEVAS, L. E., DE HAAN, R. J., PHIRI, A. I., MALANGE, P., KHOKA, M., HULSHOF, P. J., VAN LIESHOUT, L., BELD, M. G., TEO, Y. Y., ROCKETT, K. A., RICHARDSON, A., KWIATKOWSKI, D. P., MOLYNEUX, M. E. & VAN HENSBROEK, M. B. 2008. Severe anemia in Malawian children. *N Engl J Med,* 358**,** 888-99.

CARBALLO, E., LAI, W. S. & BLACKSHEAR, P. J. 1998. Feedback inhibition of macrophage tumor necrosis factor-alpha production by tristetraprolin. *Science,* 281**,** 1001-1005.

CARMAN, J. A. & NADLER, S. G. 2004. Direct association of tristetraprolin with the nucleoporin CAN/Nup214. *Biochem Biophys Res Commun,* 315**,** 445-9.

CARROLL, D. 2011. Genome engineering with zinc-finger nucleases. *Genetics,* 188**,** 773-82.

CARTER, R. & MENDIS, K. N. 2002. Evolutionary and historical aspects of the burden of malaria. *Clin Microbiol Rev,* 15**,** 564-94.

CASANOVA, J. L. 2015. Human genetic basis of interindividual variability in the course of infection. *Proc Natl Acad Sci U S A,* 112**,** E7118-27.

CASSANDRI, M., SMIRNOV, A., NOVELLI, F., PITOLLI, C., AGOSTINI, M., MALEWICZ, M., MELINO, G. & RASCHELLA, G. 2017. Zinc-finger proteins in health and disease. *Cell Death Discov,* 3**,** 17071.

CHAKRABARTI, K., PEARSON, M., GRATE, L., STERNE-WEILER, T., DEANS, J., DONOHUE, J. P. & ARES, M., JR. 2007. Structural RNAs of known and unknown function identified in malaria parasites by comparative genomics and RNA analysis. *RNA,* 13**,** 1923-39.

CHANG, K. H., TAM, M. & STEVENSON, M. M. 2004. Inappropriately low reticulocytosis in severe malarial anemia correlates with suppression in the development of late erythroid precursors. *Blood,* 103**,** 3727-35.

CHASEN, N. M., ASADY, B., LEMGRUBER, L., VOMMARO, R. C., KISSINGER, J. C., COPPENS, I. & MORENO, S. N. J. 2017. A Glycosylphosphatidylinositol-Anchored Carbonic Anhydrase-Related Protein of Toxoplasma gondii Is Important for Rhoptry Biogenesis and Virulence. *mSphere,* 2.

CHAUMEAU, V., FUSTEC, B., NAY HSEL, S., MONTAZEAU, C., NAW NYO, S., METAANE, S., SAWASDICHAI, S., KITTIPHANAKUN, P., PHATHARAKOKORDBUN, P., KWANSOMBOON, N., ANDOLINA, C., CERQUEIRA, D., CHAREONVIRIYAPHAP, T., NOSTEN, F. H. & CORBEL, V. 2018. Entomological determinants of malaria transmission in Kayin state, Eastern Myanmar: A 24-month longitudinal study in four villages. *Wellcome Open Res,* 3**,** 109.

CHEN, L., LOPATICKI, S., RIGLAR, D. T., DEKIWADIA, C., UBOLDI, A. D., THAM, W. H., O'NEILL, M. T., RICHARD, D., BAUM, J., RALPH, S. A. & COWMAN, A. F. 2011. An EGF-like protein forms a complex with PfRh5 and is required for invasion of human erythrocytes by Plasmodium falciparum. *PLoS Pathog,* 7**,** e1002199.

CHENE, A., VEMBAR, S. S., RIVIERE, L., LOPEZ-RUBIO, J. J., CLAES, A., SIEGEL, T. N., SAKAMOTO, H., SCHEIDIG-BENATAR, C., HERNANDEZ-RIVAS, R. & SCHERF, A. 2012. PfAlbas constitute a new eukaryotic DNA/RNA-binding protein family in malaria parasites. *Nucleic Acids Res,* 40**,** 3066-77.

CHENG, Q., JONES, G., LIU, E. X., KIDSON, C. & SAUL, A. 1991. Identification of a common *Plasmodium* epitope (CPE) recognised by a pan-specific inhibitory monoclonal antibody. *Mol Biochem Parasitol,* 49**,** 73-82.

CHUNG, D. W., PONTS, N., PRUDHOMME, J., RODRIGUES, E. M. & LE ROCH, K. G. 2012. Characterization of the ubiquitylating components of the human malaria parasite's protein degradation pathway. *PLoS One,* 7**,** e43477.

CIANA, C. L., SIEGRIST, R., AISSAOUI, H., MARX, L., RACINE, S., MEYER, S., BINKERT, C., DE KANTER, R., FISCHLI, C., WITTLIN, S. & BOSS, C. 2013. Novel in vivo active anti-malarials based on a hydroxy-ethyl-amine scaffold. *Bioorg Med Chem Lett,* 23**,** 658-62.

COHEN, S., MC, G. I. & CARRINGTON, S. 1961. Gamma-globulin and acquired immunity to human malaria. *Nature,* 192**,** 733-7.

COLEMAN, B. I., SAHA, S., SATO, S., ENGELBERG, K., FERGUSON, D. J. P., COPPENS, I., LODOEN, M. B. & GUBBELS, M. J. 2018. A Member of the Ferlin Calcium Sensor Family Is Essential for Toxoplasma gondii Rhoptry Secretion. *mBio,* 9.

COLEY, A. M., PARISI, K., MASCIANTONIO, R., HOECK, J., CASEY, J. L., MURPHY, V. J., HARRIS, K. S., BATCHELOR, A. H., ANDERS, R. F. & FOLEY, M. 2006. The most polymorphic residue on *Plasmodium falciparum* apical membrane antigen 1 determines binding of an invasion-inhibitory antibody. *Infection and immunity,* 74**,** 2628-2636.

COLLINS, C. R., HACKETT, F., HOWELL, S. A., SNIJDERS, A. P., RUSSELL, M. R., COLLINSON, L. M. & BLACKMAN, M. J. 2020. The malaria parasite sheddase SUB2 governs host red blood cell membrane sealing at invasion. *Elife,* 9.

CORBALAN-GARCIA, S. & GÓMEZ-FERNÁNDEZ, J. C. 2014. Signaling through C2 domains: More than one lipid target. *Biochimica et Biophysica Acta (BBA) - Biomembranes,* 1838**,** 1536-1547.

COUNIHAN, N. A., CHISHOLM, S. A., BULLEN, H. E., SRIVASTAVA, A., SANDERS, P. R., JONSDOTTIR, T. K., WEISS, G. E., GHOSH, S., CRABB, B. S., CREEK, D. J., GILSON, P. R. & DE KONING-WARD, T. F. 2017. Plasmodium falciparum parasites deploy RhopH2 into the host erythrocyte to obtain nutrients, grow and replicate. *Elife,* 6.

COUNIHAN, N. A., KALANON, M., COPPEL, R. L. & DE KONING-WARD, T. F. 2013. *Plasmodium* rhoptry proteins: why order is important. *Trends in Parasitology,* 29**,** 228-236.

COWMAN, A. F., BERRY, D. & BAUM, J. 2012. The cellular and molecular basis for malaria parasite invasion of the human red blood cell. *J Cell Biol,* 198**,** 961-71.

COWMAN, A. F. & CRABB, B. S. 2006. Invasion of red blood cells by malaria parasites. *Cell,* 124**,** 755-66.

COWMAN, A. F., HEALER, J., MARAPANA, D. & MARSH, K. 2016. Malaria: Biology and Disease. *Cell,* 167**,** 610-624.

COWMAN, A. F., TONKIN, C. J., THAM, W. H. & DURAISINGH, M. T. 2017. The Molecular Basis of Erythrocyte Invasion by Malaria Parasites. *Cell Host Microbe,* 22**,** 232-245.

CULVENOR, J. G., DAY, K. P. & ANDERS, R. F. 1991. Plasmodium falciparum ring-infected erythrocyte surface antigen is released from merozoite dense granules after erythrocyte invasion. *Infect Immun,* 59**,** 1183-7.

CULVENOR, J. G., LANGFORD, C. J., CREWTHER, P. E., SAINT, R. B., COPPEL, R., L, KEMP, D. J., ANDERS, R. F. & BROWN, G. V. 1987. Plasmodium falciparum: Identification and localization of a knob protein antigen expressed by a cDNA clone. *Experimental Parasitology,* 63**,** 58-67.

CUNNINGHAM, J., JONES, S., GATTON, M. L., BARNWELL, J. W., CHENG, Q., CHIODINI, P. L., GLENN, J., INCARDONA, S., KOSACK, C., LUCHAVEZ, J., MENARD, D., NHEM, S., OYIBO, W., REES-CHANNER, R. R., GONZALEZ, I. & BELL, D. 2019. A review of the WHO malaria rapid diagnostic test product testing programme (2008-2018): performance, procurement and policy. *Malar J,* 18**,** 387.

DAS, S., HERTRICH, N., PERRIN, A. J., WITHERS-MARTINEZ, C., COLLINS, C. R., JONES, M. L., WATERMEYER, J. M., FOBES, E. T., MARTIN, S. R., SAIBIL, H. R., WRIGHT, G. J., TREECK, M., EPP, C. & BLACKMAN, M. J. 2015. Processing of Plasmodium falciparum Merozoite Surface Protein MSP1 Activates a Spectrin-Binding Function Enabling Parasite Egress from RBCs. *Cell Host Microbe,* 18**,** 433-44.

DAS, S., MARTINEZ RODRIGUEZ, N. R., WEI, W., WAITE, J. H. & ISRAELACHVILI, J. N. 2015. Peptide Length and Dopa Determine Iron-Mediated Cohesion of Mussel Foot Proteins. *Adv Funct Mater,* 25**,** 5840-5847.

DAUBENBERGER, C. A., DIAZ, D., CURCIC, M., MUELLER, M. S., SPIELMANN, T., CERTA, U., LIPP, J. & PLUSCHKE, G. 2003. Identification and characterization of a conserved, stage-specific gene product of Plasmodium falciparum recognized by parasite growth inhibitory antibodies. *Infect Immun,* 71**,** 2173-2181.

DAY, N. P., PHU, N. H., MAI, N. T., CHAU, T. T., LOC, P. P., CHUONG, L. V., SINH, D. X., HOLLOWAY, P., HIEN, T. T. & WHITE, N. J. 2000. The pathophysiologic and prognostic significance of acidosis in severe adult malaria. *Crit Care Med,* 28**,** 1833-40.

DE OLIVEIRA, L. S., ALBORGHETTI, M. R., CARNEIRO, R. G., BASTOS, I. M. D., AMINO, R., GRELLIER, P. & CHARNEAU, S. 2021. Calcium in the Backstage of Malaria Parasite Biology. *Front Cell Infect Microbiol,* 11**,** 708834.

DEITSCH, K., DRISKILL, C. & WELLEMS, T. 2001. Transformation of malaria parasites by the spontaneous uptake and expression of DNA from human erythrocytes. *Nucleic acids research,* 29**,** 850-853.

DENT, A. E., NAKAJIMA, R., LIANG, L., BAUM, E., MOORMANN, A. M., SUMBA, P. O., VULULE, J., BABINEAU, D., RANDALL, A., DAVIES, D. H., FELGNER, P. L. & KAZURA, J. W. 2015. Plasmodium falciparum Protein Microarray Antibody Profiles Correlate With Protection From Symptomatic Malaria in Kenya. *J Infect Dis,* 212**,** 1429-38.

DEPONTE, M., HOPPE, H. C., LEE, M. C., MAIER, A. G., RICHARD, D., RUG, M., SPIELMANN, T. & PRZYBORSKI, J. M. 2012. Wherever I may roam: protein and membrane trafficking in P. falciparum-infected red blood cells. *Mol Biochem Parasitol,* 186**,** 95-116.

DEROOST, K., PHAM, T. T., OPDENAKKER, G. & VAN DEN STEEN, P. E. 2016. The immunological balance between host and parasite in malaria. *FEMS Microbiol Rev,* 40**,** 208-57.

DESAI, M., TER KUILE, F. O., NOSTEN, F., MCGREADY, R., ASAMOA, K., BRABIN, B. & NEWMAN, R. D. 2007. Epidemiology and burden of malaria in pregnancy. *Lancet Infect Dis,* 7**,** 93-104.

DESHAIES, R. J. & JOAZEIRO, C. A. 2009. RING domain E3 ubiquitin ligases. *Annu Rev Biochem,* 78**,** 399-434.

DICKO, A., DIEMERT, D. J., SAGARA, I., SOGOBA, M., NIAMBELE, M. B., ASSADOU, M. H., GUINDO, O., KAMATE, B., BABY, M., SISSOKO, M., MALKIN, E. M., FAY, M. P., THERA, M. A., MIURA, K., DOLO, A., DIALLO, D. A., MULLEN, G. E., LONG, C. A., SAUL, A., DOUMBO, O. & MILLER, L. H. 2007. Impact of a Plasmodium falciparum AMA1 vaccine on antibody responses in adult Malians. *PLoS One,* 2**,** e1045.

DICKO, A., SAGARA, I., ELLIS, R. D., MIURA, K., GUINDO, O., KAMATE, B., SOGOBA, M., NIAMBELE, M. B., SISSOKO, M., BABY, M., DOLO, A., MULLEN, G. E., FAY, M. P., PIERCE, M., DIALLO, D. A., SAUL, A., MILLER, L. H. & DOUMBO, O. K. 2008. Phase 1 study of a combination AMA1 blood stage malaria vaccine in Malian children. *PLoS One,* 3**,** e1563.

DIEZ-SILVA, M., PARK, Y., HUANG, S., BOW, H., MERCEREAU-PUIJALON, O., DEPLAINE, G., LAVAZEC, C., PERROT, S., BONNEFOY, S., FELD, M. S., HAN, J., DAO, M. & SURESH, S. 2012. Pf155/RESA protein influences the

dynamic microcirculatory behavior of ring-stage Plasmodium falciparum infected red blood cells. *Sci Rep,* 2**,** 614.

DOOLAN, D. L., DOBANO, C. & BAIRD, J. K. 2009. Acquired immunity to malaria. *Clin Microbiol Rev,* 22**,** 13-36.

DOUGLAS, A. D., WILLIAMS, A. R., ILLINGWORTH, J. J., KAMUYU, G., BISWAS, S., GOODMAN, A. L., WYLLIE, D. H., CROSNIER, C., MIURA, K., WRIGHT, G. J., LONG, C. A., OSIER, F. H., MARSH, K., TURNER, A. V., HILL, A. V. & DRAPER, S. J. 2011. The blood-stage malaria antigen PfRH5 is susceptible to vaccine-inducible cross-strain neutralizing antibody. *Nat Commun,* 2**,** 601.

DREW, D. R. & BEESON, J. G. 2015. PfRH5 as a candidate vaccine for Plasmodium falciparum malaria. *Trends Parasitol,* 31**,** 87-8.

DUBOIS, D. J. & SOLDATI-FAVRE, D. 2019. Biogenesis and secretion of micronemes in Toxoplasma gondii. *Cell Microbiol,* 21**,** e13018.

DUBREMETZ, J. F. 2007. Rhoptries are major players in Toxoplasma gondii invasion and host cell interaction. *Cell Microbiol,* 9**,** 841-8.

DUFFY, M. F., TANG, J., SUMARDY, F., NGUYEN, H. H., SELVARAJAH, S. A., JOSLING, G. A., DAY, K. P., PETTER, M. & BROWN, G. V. 2017. Activation and clustering of a Plasmodium falciparum var gene are affected by subtelomeric sequences. *FEBS J,* 284**,** 237-257.

DURAISINGH, M. T., MAIER, A. G., TRIGLIA, T. & COWMAN, A. F. 2003. Erythrocyte-binding antigen 175 mediates invasion in Plasmodium falciparum utilizing sialic acid-dependent and -independent pathways. *Proc Natl Acad Sci U S A,* 100**,** 4796-801.

EBRAHIMZADEH, Z., MUKHERJEE, A., CROCHETIÈRE, M.-È., SERGERIE, A., AMIAR, S., THOMPSON, L. A., GAGNON, D., GAUMOND, D., STAHELIN, R. V., DACKS, J. B. & RICHARD, D. 2019. A pan-apicomplexan phosphoinositide-binding protein acts in malarial microneme exocytosis. *EMBO reports,* 20**,** e47102.

EDGAR, R. C. 2004. MUSCLE: multiple sequence alignment with high accuracy and high throughput. *Nucleic Acids Research,* 32**,** 1792-1797.

EL BAKKOURI, M., POW, A., MULICHAK, A., CHEUNG, K. L., ARTZ, J. D., AMANI, M., FELL, S., DE KONING-WARD, T. F., GOODMAN, C. D., MCFADDEN, G. I., ORTEGA, J., HUI, R. & HOURY, W. A. 2010. The Clp

chaperones and proteases of the human malaria parasite Plasmodium falciparum. *J Mol Biol,* 404**,** 456-77.

ELSWORTH, B., MATTHEWS, K., NIE, C. Q., KALANON, M., CHARNAUD, S. C., SANDERS, P. R., CHISHOLM, S. A., COUNIHAN, N. A., SHAW, P. J., PINO, P., CHAN, J. A., AZEVEDO, M. F., ROGERSON, S. J., BEESON, J. G., CRABB, B. S., GILSON, P. R. & DE KONING-WARD, T. F. 2014. PTEX is an essential nexus for protein export in malaria parasites. *Nature,* 511**,** 587-91.

ENGELBERG, K., CHEN, C.-T., BECHTEL, T., GUZMÁN, V. S., DROZDA, A. A., CHAVAN, S., WEERAPANA, E. & GUBBELS, M.-J. 2019.

ENGELBERG, K., CHEN, C. T., BECHTEL, T., SANCHEZ GUZMAN, V., DROZDA, A. A., CHAVAN, S., WEERAPANA, E. & GUBBELS, M. J. 2020. The apical annuli of Toxoplasma gondii are composed of coiled-coil and signalling proteins embedded in the inner membrane complex sutures. *Cell Microbiol,* 22**,** e13112.

FALKENBURGER, B. H., JENSEN, J. B., DICKSON, E. J., SUH, B. C. & HILLE, B. 2010. Phosphoinositides: lipid regulators of membrane proteins. *J Physiol,* 588**,** 3179-85.

FAN, Y., SHEN, S., WEI, G., TANG, J., ZHAO, Y., WANG, F., HE, X., GUO, G., SHANG, X., YU, X., MA, Z., HE, X., LIU, M., ZHU, Q., LE, Z., WEI, G., CAO, J., JIANG, C. & ZHANG, Q. 2020. Rrp6 Regulates Heterochromatic Gene Silencing via ncRNA RUF6 Decay in Malaria Parasites. *mBio,* 11.

FARRELL, A., THIRUGNANAM, S., LORESTANI, A., DVORIN, J. D., EIDELL, K. P., FERGUSON, D. J., ANDERSON-WHITE, B. R., DURAISINGH, M. T., MARTH, G. T. & GUBBELS, M. J. 2012. A DOC2 protein identified by mutational profiling is essential for apicomplexan parasite exocytosis. *Science,* 335**,** 218-21.

FAVUZZA, P., DE LERA RUIZ, M., THOMPSON, J. K., TRIGLIA, T., NGO, A., STEEL, R. W. J., VAVREK, M., CHRISTENSEN, J., HEALER, J., BOYCE, C., GUO, Z., HU, M., KHAN, T., MURGOLO, N., ZHAO, L., PENINGTON, J. S., REAKSUDSAN, K., JARMAN, K., DIETRICH, M. H., RICHARDSON, L., GUO, K.-Y., LOPATICKI, S., THAM, W.-H., ROTTMANN, M., PAPENFUSS, T., ROBBINS, J. A., BODDEY, J. A., SLEEBS, B. E., SABROUX, H. J., MCCAULEY, J. A., OLSEN, D. B. & COWMAN, A. F. 2020. Dual Plasmepsin-Targeting Antimalarial Agents Disrupt Multiple Stages of the Malaria Parasite Life Cycle. *Cell Host & Microbe*.

FILLEBEEN, C., WILKINSON, N. & PANTOPOULOS, K. 2014. Electrophoretic mobility shift assay (EMSA) for the study of RNA-protein interactions: the IRE/IRP example. *J Vis Exp*.

FRENAL, K., TAY, C. L., MUELLER, C., BUSHELL, E. S., JIA, Y., GRAINDORGE, A., BILLKER, O., RAYNER, J. C. & SOLDATI-FAVRE, D. 2013. Global analysis of apicomplexan protein S-acyl transferases reveals an enzyme essential for invasion. *Traffic,* 14**,** 895-911.

FRIED, M. & DUFFY, P. E. 1996. Adherence of Plasmodium falciparum to chondroitin sulfate A in the human placenta. *Science,* 272**,** 1502-4.

FU, M. & BLACKSHEAR, P. J. 2017. RNA-binding proteins in immune regulation: a focus on CCCH zinc finger proteins. *Nat Rev Immunol,* 17**,** 130-143.

FUJIKI, Y., HUBBARD, A. L., FOWLER, S. & LAZAROW, P. B. 1982. Isolation of Intracellular membranes by Means of Sodium Carbonate Treatment: Application to Endoplasmic Reticulum. *The Journal of Cell Biology,* 93**,** 97-102.

GANGNARD, S., LEWIT-BENTLEY, A., DECHAVANNE, S., SRIVASTAVA, A., AMIRAT, F., BENTLEY, G. A. & GAMAIN, B. 2015. Structure of the DBL3X-DBL4epsilon region of the VAR2CSA placental malaria vaccine candidate: insight into DBL domain interactions. *Sci Rep,* 5**,** 14868.

GAO, X., GUNALAN, K., YAP, S. S. & PREISER, P. R. 2013. Triggers of key calcium signals during erythrocyte invasion by Plasmodium falciparum. *Nat Commun,* 4**,** 2862.

GAO, Y. H., LI, H. L., LU, Y., GAO, F. M., LIN, Y. H., ZHOU, H. C., ZHANG, L. H. & WANG, H. 2009. Identification of a vaccine candidate antigen, PfMAg-1, from *Plasmodium falciparum* with monoclonal antibody M26-32. *Parasitol Res,* 105**,** 1723-32.

GARDNER, M. J., HALL, N., FUNG, E., WHITE, O., BERRIMAN, M., HYMAN, R. W., CARLTON, J. M., PAIN, A., NELSON, K. E., BOWMAN, S., PAULSEN, I. T., JAMES, K., EISEN, J. A., RUTHERFORD, K., SALZBERG, S. L., CRAIG, A., KYES, S., CHAN, M. S., NENE, V., SHALLOM, S. J., SUH, B., PETERSON, J., ANGIUOLI, S., PERTEA, M., ALLEN, J., SELENGUT, J., HAFT, D., MATHER, M. W., VAIDYA, A. B., MARTIN, D. M., FAIRLAMB, A. H., FRAUNHOLZ, M. J., ROOS, D. S., RALPH, S. A., MCFADDEN, G. I., CUMMINGS, L. M., SUBRAMANIAN, G. M., MUNGALL, C., VENTER, J. C., CARUCCI, D. J., HOFFMAN, S. L., NEWBOLD, C., DAVIS, R. W., FRASER,

C. M. & BARRELL, B. 2002. Genome sequence of the human malaria parasite Plasmodium falciparum. *Nature,* 419**,** 498-511.

GASTEIGER, E., GATTIKER, A., HOOGLAND, C., IVANYI, I., APPEL, R. D. & BAIROCH, A. 2003. ExPASy: The proteomics server for in-depth protein knowledge and analysis. *Nucleic Acids Res,* 31**,** 3784-8.

GATTON, M. L., CHAUDHRY, A., GLENN, J., WILSON, S., AH, Y., KONG, A., ORD, R. L., REES-CHANNER, R. R., CHIODINI, P., INCARDONA, S., CHENG, Q., AIDOO, M. & CUNNINGHAM, J. 2020. Impact of Plasmodium falciparum gene deletions on malaria rapid diagnostic test performance. *Malar J,* 19**,** 392.

GAUR, D., MAYER, D. C. & MILLER, L. H. 2004. Parasite ligand-host receptor interactions during invasion of erythrocytes by Plasmodium merozoites. *Int J Parasitol,* 34**,** 1413-29.

GEIGER, M., BROWN, C., WICHERS, J. S., STRAUSS, J., LILL, A., THUENAUER, R., LIFFNER, B., WILCKE, L., LEMCKE, S., HEINCKE, D., PAZICKY, S., BACHMANN, A., LÖW, C., WILSON, D. W., FILARSKY, M., BURDA, P.-C., ZHANG, K., JUNOP, M. & GILBERGER, T. W. 2019. Structural Insights Into PfARO and Characterization of its Interaction With PfAIP. *Journal of Molecular Biology*.

GILSON, P. R. & CRABB, B. S. 2009. Morphology and kinetics of the three distinct phases of red blood cell invasion by Plasmodium falciparum merozoites. *Int J Parasitol,* 39**,** 91-6.

GILSON, P. R., NEBL, T., VUKCEVIC, D., MORITZ, R. L., SARGEANT, T., SPEED, T. P., SCHOFIELD, L. & CRABB, B. S. 2006. Identification and stoichiometry of glycosylphosphatidylinositol-anchored membrane proteins of the human malaria parasite Plasmodium falciparum. *Mol Cell Proteomics,* 5**,** 1286-99.

GINSBURG, H. & KRUGLIAK, M. 1983. Uptake of L-tryptophan by erythrocytes infected with malaria parasites (Plasmodium falciparum). *Biochim Biophys Acta,* 729**,** 97-103.

GLUSHAKOVA, S., YIN, D., LI, T. & ZIMMERBERG, J. 2005. Membrane transformation during malaria parasite release from human red blood cells. *Curr Biol,* 15**,** 1645-50.

GOEL, V. K., LI, X., CHEN, H., LIU, S. C., CHISHTI, A. H. & OH, S. S. 2003. Band 3 is a host receptor binding merozoite surface protein 1 during the Plasmodium falciparum invasion of erythrocytes. *Proc Natl Acad Sci U S A,* 100**,** 5164-9.

GOMEZ-DIAZ, E., YERBANGA, R. S., LEFEVRE, T., COHUET, A., ROWLEY, M. J., OUEDRAOGO, J. B. & CORCES, V. G. 2017. Epigenetic regulation of Plasmodium falciparum clonally variant gene expression during development in Anopheles gambiae. *Sci Rep,* 7**,** 40655.

GRIGNARD, L., SHAH, S., CHUA, T. H., WILLIAM, T., DRAKELEY, C. J. & FORNACE, K. M. 2019. Natural Human Infections With Plasmodium cynomolgi and Other Malaria Species in an Elimination Setting in Sabah, Malaysia. *J Infect Dis,* 220**,** 1946-1949.

GRÜRING, C., HEIBER, A., KRUSE, F., FLEMMING, S., FRANCI, G., COLOMBO, SARA F., FASANA, E., SCHOELER, H., BORGESE, N., STUNNENBERG, HENDRIK G., PRZYBORSKI, JUDE M., GILBERGER, T.-W. & SPIELMANN, T. 2012. Uncovering Common Principles in Protein Export of Malaria Parasites. *Cell Host & Microbe,* 12**,** 717-729.

GUILLOTTE, M., NATO, F., JUILLERAT, A., HESSEL, A., MARCHAND, F., LEWIT-BENTLEY, A., BENTLEY, G. A., VIGAN-WOMAS, I. & MERCEREAU-PUIJALON, O. 2016. Functional analysis of monoclonal antibodies against the Plasmodium falciparum PfEMP1-VarO adhesin. *Malar J,* 15**,** 28.

HAJIKHEZRI, Z., DARWEESH, M., AKUSJARVI, G. & PUNGA, T. 2020. Role of CCCH-Type Zinc Finger Proteins in Human Adenovirus Infections. *Viruses,* 12.

HALL, T. M. 2005. Multiple modes of RNA recognition by zinc finger proteins. *Curr Opin Struct Biol,* 15**,** 367-73.

HANSSEN, E., DEKIWADIA, C., RIGLAR, D. T., RUG, M., LEMGRUBER, L., COWMAN, A. F., CYRKLAFF, M., KUDRYASHEV, M., FRISCHKNECHT, F., BAUM, J. & RALPH, S. A. 2013. Electron tomography of *Plasmodium falciparum* merozoites reveals core cellular events that underpin erythrocyte invasion. *Cellular Microbiology,* 15**,** 1457-1472.

HARBUT, M. B., PATEL, B. A., YEUNG, B. K., MCNAMARA, C. W., BRIGHT, A. T., BALLARD, J., SUPEK, F., GOLDE, T. E., WINZELER, E. A., DIAGANA, T. T. & GREENBAUM, D. C. 2012. Targeting the ERAD pathway via inhibition

of signal peptide peptidase for antiparasitic therapeutic design. *Proc Natl Acad Sci U S A,* 109**,** 21486-91.

HARBUT, M. B., PATEL, B. A., YEUNG, B. K., MCNAMARA, C. W., BRIGHT, A. T., BALLARD, J., SUPEK, F., GOLDE, T. E., WINZELER, E. A., DIAGANA, T. T. & GREENBAUM, D. C. 2012. Targeting the ERAD pathway via inhibition of signal peptide peptidase for antiparasitic therapeutic design. *Proc Natl Acad Sci U S A,* 109**,** 21486-91.

HART, K. J., OBERSTALLER, J., WALKER, M. P., MINNS, A. M., KENNEDY, M. F., PADYKULA, I., ADAMS, J. H. & LINDNER, S. E. 2019. Plasmodium male gametocyte development and transmission are critically regulated by the two putative deadenylases of the CAF1/CCR4/NOT complex. *PLoS Pathog,* 15**,** e1007164.

HARTMEYER, G. N., STENSVOLD, C. R., FABRICIUS, T., MARMOLIN, E. S., HOEGH, S. V., NIELSEN, H. V., KEMP, M. & VESTERGAARD, L. S. 2019. Plasmodium cynomolgi as Cause of Malaria in Tourist to Southeast Asia, 2018. *Emerg Infect Dis,* 25**,** 1936-1939.

HEASLIP, A. T., NISHI, M., STEIN, B. & HU, K. 2011. The motility of a human parasite, Toxoplasma gondii, is regulated by a novel lysine methyltransferase. *PLoS Pathog,* 7**,** e1002201.

HEIDE, J., VAUGHAN, K. C., SETTE, A., JACOBS, T. & SCHULZE ZUR WIESCH, J. 2019 Comprehensive Review of Human *Plasmodium falciparum*-specific CD8+ T Cell Epitopes, *Front. Immunol*, 10**,** 397.

HENTZSCHEL, F., MITESSER, V., FRASCHKA, S. A., KRZIKALLA, D., CARRILLO, E. H., BERKHOUT, B., BARTFAI, R., MUELLER, A. K. & GRIMM, D. 2020. Gene knockdown in malaria parasites via non-canonical RNAi. *Nucleic Acids Res,* 48**,** e2.

HOEIJMAKERS, W. A. M., MIAO, J., SCHMIDT, S., TOENHAKE, C. G., SHRESTHA, S., VENHUIZEN, J., HENDERSON, R., BIRNBAUM, J., GHIDELLI-DISSE, S., DREWES, G., CUI, L., STUNNENBERG, H. G., SPIELMANN, T. & BARTFAI, R. 2019. Epigenetic reader complexes of the human malaria parasite, Plasmodium falciparum. *Nucleic Acids Res,* 47**,** 11574-11588.

HOFFMAN, S. L., GOH, L. M., LUKE, T. C., SCHNEIDER, I., LE, T. P., DOOLAN, D. L., SACCI, J., DE LA VEGA, P., DOWLER, M., PAUL, C., GORDON, D. M.,

STOUTE, J. A., CHURCH, L. W., SEDEGAH, M., HEPPNER, D. G., BALLOU, W. R. & RICHIE, T. L. 2002. Protection of humans against malaria by immunization with radiation-attenuated Plasmodium falciparum sporozoites. *J Infect Dis,* 185**,** 1155-64.

HOLDER, A. A., MOHD RIDZUAN, M. A. & GREEN, J. L. 2012. Calcium dependent protein kinase 1 and calcium fluxes in the malaria parasite. *Microbes Infect,* 14**,** 825-30.

HOWARD, R. F., NARUM, D. L., BLACKMAN, M. & THURMAN, J. 1998. Analysis of the processing of *Plasmodium falciparum* rhoptry-associated protein 1 and localization of Pr86 to schizont rhoptries and p67 to free merozoites. *Molecular and Biochemical Parasitology,* 92**,** 111-122.

HUDSON, B. P., MARTINEZ-YAMOUT, M. A., DYSON, H. J. & WRIGHT, P. E. 2004. Recognition of the mRNA AU-rich element by the zinc finger domain of TIS11d. *Nat Struct Mol Biol,* 11**,** 257-64.

IDRO, R., MARSH, K., JOHN, C. C. & NEWTON, C. R. 2010. Cerebral malaria: mechanisms of brain injury and strategies for improved neurocognitive outcome. *Pediatr Res,* 68**,** 267-74.

INNAN, H. & KONDRASHOV, F. 2010. The evolution of gene duplications: classifying and distinguishing between models. *Nature Reviews Genetics,* 11**,** 97-108.

JACOT, D., DAHER, W. & SOLDATI-FAVRE, D. 2013. Toxoplasma gondii myosin F, an essential motor for centrosomes positioning and apicoplast inheritance. *EMBO J,* 32**,** 1702-16.

JAKEMAN, G. N., SAUL, A., HOGARTH, W. L. & COLLINS, W. E. 1999. Anaemia of acute malaria infections in non-immune patients primarily results from destruction of uninfected erythrocytes. *Parasitology,* 119 (Pt 2)**,** 127-33.

JAKKA, S. R., VEENA, S., ATMAKURI, R. M. & EISENHUT, M. 2006. Characteristic abnormalities in cerebrospinal fluid biochemistry in children with cerebral malaria compared to viral encephalitis. *Cerebrospinal Fluid Res,* 3**,** 8.

JANSE, C. J. & WATERS, A. P. 2007. The exoneme helps malaria parasites to break out of blood cells. *Cell,* 131**,** 1036-8.

JEAN, S., ZAPATA-JENKS, M. A., FARLEY, J. M., TRACY, E. & MAYER, D. C. 2014. Plasmodium falciparum double C2 domain protein, PfDOC2, binds to calcium when associated with membranes. *Exp Parasitol,* 144**,** 91-5.

JMOL. *Jmol: an open-source Java viewer for chemical structures in 3D* [Online]. Available: http://www.jmol.org [Accessed 2019].

JOHNSON, B. A. & KALRA, M. G. 2012. Prevention of malaria in travelers. *Am Fam Physician,* 85**,** 973-7.

JUKES, T. H. & CANTOR, C. R. 1969. Evolution of Protein Molecules. *In:* MUNRO, H. N. (ed.) *Mammalian Protein Metabolism.* New York: Academic Press.

KANTELE, A. & JOKIRANTA, T. S. 2011. Review of cases with the emerging fifth human malaria parasite, Plasmodium knowlesi. *Clin Infect Dis,* 52**,** 1356-62.

KARASOV, A. O., BOOTHROYD, J. C. & ARRIZABALAGA, G. 2005. Identification and disruption of a rhoptry-localized homologue of sodium hydrogen exchangers in Toxoplasma gondii. *Int J Parasitol,* 35**,** 285-91.

KAUTH, C. W., WOEHLBIER, U., KERN, M., MEKONNEN, Z., LUTZ, R., MUCKE, N., LANGOWSKI, J. & BUJARD, H. 2006. Interactions between merozoite surface proteins 1, 6, and 7 of the malaria parasite Plasmodium falciparum. *J Biol Chem,* 281**,** 31517-27.

KELLEY, L. A., MEZULIS, S., YATES, C. M., WASS, M. N. & STERNBERG, M. J. 2015. The Phyre2 web portal for protein modeling, prediction and analysis. *Nat Protoc,* 10**,** 845-58.

KHAMMANEE, T., SAWANGJAROEN, N., BUNCHERD, H., TUN, A. W. & THANAPONGPICHAT, S. 2019. Molecular Surveillance of Pfkelch13 and Pfmdr1 Mutations in Plasmodium falciparum Isolates from Southern Thailand. *Korean J Parasitol,* 57**,** 369-377.

KOLEV, N. G., TSCHUDI, C. & ULLU, E. 2011. RNA interference in protozoan parasites: achievements and challenges. *Eukaryot Cell,* 10**,** 1156-63.

KORENY, L., ZEESHAN, M., BARYLYUK, K., TROMER, E. C., VAN HOOFF, J. J. E., BRADY, D., KE, H., CHELAGHMA, S., FERGUSON, D. J. P., EME, L., TEWARI, R. & WALLER, R. F. 2021. Molecular characterization of the conoid complex in Toxoplasma reveals its conservation in all apicomplexans, including Plasmodium species. *PLoS Biol,* 19**,** e3001081.

KREMER, J. R., MASTRONARDE, D. N. & MCINTOSH, J. R. 1996. Computer Visualization of Three-Dimensional Image Data Using IMOD. *Journal of Structural Biology,* 116**,** 71-76.

LACOUNT, D. J., VIGNALI, M., CHETTIER, R., PHANSALKAR, A., BELL, R., HESSELBERTH, J. R., SCHOENFELD, L. W., OTA, I., SAHASRABUDHE, S.,

KURSCHNER, C., FIELDS, S. & HUGHES, R. E. 2005. A protein interaction network of the malaria parasite Plasmodium falciparum. *Nature,* 438**,** 103-7.

LAI, W. S., STUMPO, D. J. & BLACKSHEAR, P. J. 1990. Rapid insulin-stimulated accumulation of an mRNA encoding a proline-rich protein. *Journal of Biological Chemistry,* 265**,** 16556-16563.

LAMBROS, C. & VANDERBERG, J. P. 1979. Synchronization of Plasmodium falciparum erythrocytic stages in culture. *J Parasitol,* 65**,** 418-20.

LANGHORNE, J., NDUNGU, F. M., SPONAAS, A. M. & MARSH, K. 2008. Immunity to malaria: more questions than answers. *Nat Immunol,* 9**,** 725-32.

LAURENS, M. B. 2020. RTS,S/AS01 vaccine (Mosquirix): an overview. *Hum Vaccin Immunother,* 16**,** 480-489.

LAW, C. W., CHEN, Y., SHI, W. & SMYTH, G. K. 2014. voom: Precision weights unlock linear model analysis tools for RNA-seq read counts. *Genome Biol,* 15**,** R29.

LE, S. Q. & GASCUEL, O. 2008. An Improved General Amino Acid Replacement Matrix. *Molecular Biology and Evolution,* 25**,** 1307-1320.

LEK, A., EVESSON, F. J., SUTTON, R. B., NORTH, K. N. & COOPER, S. T. 2012. Ferlins: regulators of vesicle fusion for auditory neurotransmission, receptor trafficking and membrane repair. *Traffic,* 13**,** 185-94.

LEMGRUBER, L., LUPETTI, P., DE SOUZA, W. & VOMMARO, R. C. 2011. New details on the fine structure of the rhoptry of Toxoplasma gondii. *Microsc Res Tech,* 74**,** 812-8.

LI, H., BOGYO, M. & DA FONSECA, P. C. 2016. The cryo-EM structure of the Plasmodium falciparum 20S proteasome and its use in the fight against malaria. *FEBS J,* 283**,** 4238-4243.

LIBERLES, D. A. 2001. Evaluation of Methods for Determination of a Reconstructed History of Gene Sequence Evolution. *Molecular Biology and Evolution,* 18**,** 2040-2047.

LIFFNER, B., BALBIN, J. M., WICHERS, J. S., GILBERGER, T. W. & WILSON, D. W. 2021. The Ins and Outs of Plasmodium Rhoptries, Focusing on the Cytosolic Side. *Trends Parasitol,* 37**,** 638-650.

LIFFNER, B., FRÖLICH, S., HEINEMANN, G. K., LIU, B., RALPH, S. A., DIXON, M. W. A., GILBERGER, T.-W. & WILSON, D. W. 2020. PfCERLI1 is a

conserved rhoptry associated protein essential for *Plasmodium falciparum* merozoite invasion of erythrocytes. *Nature Communications,* 11**,** 1411.

LINDNER, S. E., SWEARINGEN, K. E., SHEARS, M. J., WALKER, M. P., VRANA, E. N., HART, K. J., MINNS, A. M., SINNIS, P., MORITZ, R. L. & KAPPE, S. H. I. 2019. Transcriptomics and proteomics reveal two waves of translational repression during the maturation of malaria parasite sporozoites. *Nat Commun,* 10**,** 4964.

LIU, L., SONG, X., HE, D., KOMMA, C., KITA, A., VIRBASIUS, J. V., HUANG, G., BELLAMY, H. D., MIKI, K., CZECH, M. P. & ZHOU, G. W. 2006. Crystal structure of the C2 domain of class II phosphatidylinositide 3-kinase C2alpha. *J Biol Chem,* 281**,** 4254-60.

LOOKER, O., BLANCH, A. J., LIU, B., NUNEZ-IGLESIAS, J., MCMILLAN, P. J., TILLEY, L. & DIXON, M. W. A. 2019. The knob protein KAHRP assembles into a ring-shaped structure that underpins virulence complex assembly. *PLoS Pathog,* 15**,** e1007761.

LOPATICKI, S., MAIER, A. G., THOMPSON, J., WILSON, D. W., THAM, W.-H., TRIGLIA, T., GOUT, A., SPEED, T. P., BEESON, J. G., HEALER, J. & COWMAN, A. F. 2011. Reticulocyte and Erythrocyte Binding-Like Proteins Function Cooperatively in Invasion of Human Erythrocytes by Malaria Parasites. *Infection and Immunity,* 79**,** 1107.

LOPEZ-BARRAGAN, M. J., LEMIEUX, J., QUINONES, M., WILLIAMSON, K. C., MOLINA-CRUZ, A., CUI, K., BARILLAS-MURY, C., ZHAO, K. & SU, X. Z. 2011. Directional gene expression and antisense transcripts in sexual and asexual stages of Plasmodium falciparum. *BMC Genomics,* 12**,** 587.

MAEDA, K. & AKIRA, S. 2017. Regulation of mRNA stability by CCCH-type zinc-finger proteins in immune cells. *Int Immunol,* 29**,** 149-155.

MAGUIRE, G. P., HANDOJO, T., PAIN, M. C., KENANGALEM, E., PRICE, R. N., TJITRA, E. & ANSTEY, N. M. 2005. Lung injury in uncomplicated and severe falciparum malaria: a longitudinal study in papua, Indonesia. *J Infect Dis,* 192**,** 1966-74.

MAIER, A. G., MATUSCHEWSKI, K., ZHANG, M. & RUG, M. 2019. Plasmodium falciparum. *Trends Parasitol,* 35**,** 481-482.

MARSH, K., FORSTER, D., WARUIRU, C., MWANGI, I., WINSTANLEY, M., MARSH, V., NEWTON, C., WINSTANLEY, P., WARN, P., PESHU, N. & ET

AL. 1995. Indicators of life-threatening malaria in African children. *N Engl J Med,* 332**,** 1399-404.

MARTI, M., GOOD, R. T., RUG, M., KNUEPFER, E. & COWMAN, A. F. 2004. Targeting malaria virulence and remodeling proteins to the host erythrocyte. *Science,* 306**,** 1930-3.

MARTINEZ-DE LA PUENTE, J., SANTIAGO-ALARCON, D., PALINAUSKAS, V. & BENSCH, S. 2021. Plasmodium relictum. *Trends Parasitol,* 37**,** 355-356.

MATUSCHEWSKI, K. 2006. Getting infectious: formation and maturation of Plasmodium sporozoites in the Anopheles vector. *Cell Microbiol,* 8**,** 1547-56.

MBANEFO, E. C., AHMED, A. M., TITOUNA, A., ELMARAEZY, A., TRANG, N. T., PHUOC LONG, N., HOANG ANH, N., DIEM NGHI, T., THE HUNG, B., VAN HIEU, M., KY ANH, N., HUY, N. T. & HIRAYAMA, K. 2017. Association of glucose-6-phosphate dehydrogenase deficiency and malaria: a systematic review and meta-analysis. *Sci Rep,* 7**,** 45963.

MENENDEZ, C., ORDI, J., ISMAIL, M. R., VENTURA, P. J., APONTE, J. J., KAHIGWA, E., FONT, F. & ALONSO, P. L. 2000. The impact of placental malaria on gestational age and birth weight. *J Infect Dis,* 181**,** 1740-5.

MERCIER, C., ADJOGBLE, K. D., DAUBENER, W. & DELAUW, M. F. 2005. Dense granules: are they key organelles to help understand the parasitophorous vacuole of all apicomplexa parasites? *Int J Parasitol,* 35**,** 829-49.

MILALI, M. P., SIKULU-LORD, M. T. & GOVELLA, N. J. 2017. Bites before and after bedtime can carry a high risk of human malaria infection. *Malar J,* 16**,** 91.

MONTAGUE, T. G., CRUZ, J. M., GAGNON, J. A., CHURCH, G. M. & VALEN, E. 2014. CHOPCHOP: a CRISPR/Cas9 and TALEN web tool for genome editing. *Nucleic Acids Res,* 42**,** W401-7.

MOON, R. W., HALL, J., RANGKUTI, F., HO, Y. S., ALMOND, N., MITCHELL, G. H., PAIN, A., HOLDER, A. A. & BLACKMAN, M. J. 2013. Adaptation of the genetically tractable malaria pathogen *Plasmodium knowlesi* to continuous culture in human erythrocytes. *Proceedings of the National Academy of Sciences of the United States of America,* 110**,** 531-536.

MUELLER, C., KLAGES, N., JACOT, D., SANTOS, J. M., CABRERA, A., GILBERGER, T. W., DUBREMETZ, J. F. & SOLDATI-FAVRE, D. 2013. The Toxoplasma protein ARO mediates the apical positioning of rhoptry organelles, a prerequisite for host cell invasion. *Cell Host Microbe,* 13**,** 289-301.

MUELLER, C., SAMOO, A., HAMMOUDI, P. M., KLAGES, N., KALLIO, J. P., KURSULA, I. & SOLDATI-FAVRE, D. 2016. Structural and functional dissection of Toxoplasma gondii armadillo repeats only protein. *J Cell Sci,* 129**,** 1031-45.

MUELLER, I., ZIMMERMAN, P. A. & REEDER, J. C. 2007. Plasmodium malariae and Plasmodium ovale--the "bashful" malaria parasites. *Trends Parasitol,* 23**,** 278-83.

MULLER, M., FAZI, F. & CIAUDO, C. 2019. Argonaute Proteins: From Structure to Function in Development and Pathological Cell Fate Determination. *Front Cell Dev Biol,* 7**,** 360.

NAEEM, M. A., AHMED, S. & KHAN, S. A. 2018. Detection of asymptomatic carriers of malaria in Kohat district of Pakistan. *Malar J,* 17**,** 44.

NAING, C., WHITTAKER, M. A., NYUNT WAI, V. & MAK, J. W. 2014. Is Plasmodium vivax malaria a severe malaria?: a systematic review and meta-analysis. *PLoS Negl Trop Dis,* 8**,** e3071.

NASAMU, A. S., GLUSHAKOVA, S., RUSSO, I., VAUPEL, B., OKSMAN, A., KIM, A. S., FREMONT, D. H., TOLIA, N., BECK, J. R., MEYERS, M. J., NILES, J. C., ZIMMERBERG, J. & GOLDBERG, D. E. 2017. Plasmepsins IX and X are essential and druggable mediators of malaria parasite egress and invasion. *Science,* 358**,** 518.

NASAMU, A. S., POLINO, A. J., ISTVAN, E. S. & GOLDBERG, D. E. 2020. Malaria parasite plasmepsins: More than just plain old degradative pepsins. *J Biol Chem,* 295**,** 8425-8441.

NAVICKAS, A., CHAMOIS, S., SAINT-FORT, R., HENRI, J., TORCHET, C. & BENARD, L. 2020. No-Go Decay mRNA cleavage in the ribosome exit tunnel produces 5'-OH ends phosphorylated by Trl1. *Nat Commun,* 11**,** 122.

NGUANSANGIAM, S., DAY, N. P., HIEN, T. T., MAI, N. T., CHAISRI, U., RIGANTI, M., DONDORP, A. M., LEE, S. J., PHU, N. H., TURNER, G. D., WHITE, N. J., FERGUSON, D. J. & PONGPONRATN, E. 2007. A quantitative ultrastructural study of renal pathology in fatal Plasmodium falciparum malaria. *Trop Med Int Health,* 12**,** 1037-50.

NGWA, C. J., FARRUKH, A. & PRADEL, G. 2021. Zinc finger proteins of Plasmodium falciparum. *Cell Microbiol***,** e13387.

NGWA, C. J., KIESOW, M. J., PAPST, O., ORCHARD, L. M., FILARSKY, M., ROSINSKI, A. N., VOSS, T. S., LLINAS, M. & PRADEL, G. 2017.

Transcriptional Profiling Defines Histone Acetylation as a Regulator of Gene Expression during Human-to-Mosquito Transmission of the Malaria Parasite Plasmodium falciparum. *Front Cell Infect Microbiol,* 7**,** 320.

NORMARK, J., NILSSON, D., RIBACKE, U., WINTER, G., MOLL, K., WHEELOCK, C. E., BAYARUGABA, J., KIRONDE, F., EGWANG, T. G., CHEN, Q., ANDERSSON, B. & WAHLGREN, M. 2007. PfEMP1-DBL1alpha amino acid motifs in severe disease states of Plasmodium falciparum malaria. *Proc Natl Acad Sci U S A,* 104**,** 15835-40.

NOSTEN, F. & WHITE, N. J. 2007. Artemisinin-based combination treatment of falciparum malaria. *Am J Trop Med Hyg,* 77**,** 181-92.

O'DONNELL, R. A., SAUL, A., COWMAN, A. F. & CRABB, B. S. 2000. Functional conservation of the malaria vaccine antigen MSP-119across distantly related *Plasmodium* species. *Nat Med,* 6**,** 91-5.

OTTO, T. D., WILINSKI, D., ASSEFA, S., KEANE, T. M., SARRY, L. R., BOHME, U., LEMIEUX, J., BARRELL, B., PAIN, A., BERRIMAN, M., NEWBOLD, C. & LLINAS, M. 2010. New insights into the blood-stage transcriptome of Plasmodium falciparum using RNA-Seq. *Mol Microbiol,* 76**,** 12-24.

PARADIS, E. & SCHLIEP, K. 2019. ape 5.0: an environment for modern phylogenetics and evolutionary analyses in R. *Bioinformatics,* 35**,** 526-528.

PATEL, A., PERRIN, A. J., FLYNN, H. R., BISSON, C., WITHERS-MARTINEZ, C., TREECK, M., FLUECK, C., NICASTRO, G., MARTIN, S. R., RAMOS, A., GILBERGER, T. W., SNIJDERS, A. P., BLACKMAN, M. J. & BAKER, D. A. 2019. Cyclic AMP signalling controls key components of malaria parasite host cell invasion machinery. *PLoS Biol,* 17**,** e3000264.

PAVLOVIC DJURANOVIC, S., ERATH, J., ANDREWS, R. J., BAYGUINOV, P. O., CHUNG, J. J., CHALKER, D. L., FITZPATRICK, J. A., MOSS, W. N., SZCZESNY, P. & DJURANOVIC, S. 2020. Plasmodium falciparum translational machinery condones polyadenosine repeats. *Elife,* 9.

PEI, X., GUO, X., COPPEL, R., BHATTACHARJEE, S., HALDAR, K., GRATZER, W., MOHANDAS, N. & AN, X. 2007. The ring-infected erythrocyte surface antigen (RESA) of Plasmodium falciparum stabilizes spectrin tetramers and suppresses further invasion. *Blood,* 110**,** 1036-42.

PICARD, B. & WEGNEZ, M. 1979. Isolation of a 7S particle from Xenopus laevis oocytes: a 5S RNA-protein complex. *Proc Natl Acad Sci U S A,* 76**,** 241-5.

PINKEVYCH, M., PETRAVIC, J., CHELIMO, K., KAZURA, J. W., MOORMANN, A. M. & DAVENPORT, M. P. 2012. The dynamics of naturally acquired immunity to Plasmodium falciparum infection. *PLoS Comput Biol,* 8**,** e1002729.

PINO, P., CALDELARI, R., MUKHERJEE, B., VAHOKOSKI, J., KLAGES, N., MACO, B., COLLINS, C. R., BLACKMAN, M. J., KURSULA, I., HEUSSLER, V., BROCHET, M. & SOLDATI-FAVRE, D. 2017. A multistage antimalarial targets the plasmepsins IX and X essential for invasion and egress. *Science,* 358**,** 522-528.

POLOGE, L. G., PAVLOVEC, A., SHIO, H. & RAVETCH, J. V. 1987. Primary structure and subcellular localization of the knobassociated histidine-rich protein of Plasmodium falciparum. *Proc Natl Acad Sci U S A.,* 84**,** 7139-7143.

PONGPONRATN, E., TURNER, G. D., DAY, N. P., PHU, N. H., SIMPSON, J. A., STEPNIEWSKA, K., MAI, N. T., VIRIYAVEJAKUL, P., LOOAREESUWAN, S., HIEN, T. T., FERGUSON, D. J. & WHITE, N. J. 2003. An ultrastructural study of the brain in fatal Plasmodium falciparum malaria. *Am J Trop Med Hyg,* 69**,** 345-59.

PRASHEK, J., TRUONG, T. & YAO, X. 2013. Crystal structure of the pleckstrin homology domain from the ceramide transfer protein: implications for conformational change upon ligand binding. *PLoS One,* 8**,** e79590.

PRICE, R. N., SIMPSON, J. A., NOSTEN, F., LUXEMBURGER, C., HKIRJAROEN, L., TER KUILE, F., CHONGSUPHAJAISIDDHI, T. & WHITE, N. J. 2001. Factors contributing to anemia after uncomplicated falciparum malaria. *Am J Trop Med Hyg,* 65**,** 614-22.

PRUDENCIO, M., RODRIGUEZ, A. & MOTA, M. M. 2006. The silent path to thousands of merozoites: the Plasmodium liver stage. *Nat Rev Microbiol,* 4**,** 849-56.

R_CORE_TEAM. 2020. *R: A language and environment for statistical computing* [Online]. Vienna, Austria: R Foundation for Statistical Computing. Available: www.R-project.org/ [Accessed 25th March 2020].

RAMANATHAN, M., PORTER, D. F. & KHAVARI, P. A. 2019. Methods to study RNA-protein interactions. *Nat Methods,* 16**,** 225-234.

RAYNER, J. C., LIU, W., PEETERS, M., SHARP, P. M. & HAHN, B. H. 2011. A plethora of Plasmodium species in wild apes: a source of human infection? *Trends Parasitol,* 27**,** 222-9.

REDDY, B. P., SHRESTHA, S., HART, K. J., LIANG, X., KEMIREMBE, K., CUI, L. & LINDNER, S. E. 2015. A bioinformatic survey of RNA-binding proteins in Plasmodium. *BMC Genomics,* 16**,** 890.

REININGER, L., GARCIA, M., TOMLINS, A., MULLER, S. & DOERIG, C. 2012. The Plasmodium falciparum, Nima-related kinase Pfnek-4: a marker for asexual parasites committed to sexual differentiation. *Malar J,* 11**,** 250.

REYNOLDS, C. R., ISLAM, S. A. & STERNBERG, M. J. E. 2018. EzMol: A Web Server Wizard for the Rapid Visualization and Image Production of Protein and Nucleic Acid Structures. *Journal of Molecular Biology,* 430**,** 2244-2248.

RICHARD, D., MACRAILD, C. A., RIGLAR, D. T., CHAN, J.-A., FOLEY, M., BAUM, J., RALPH, S. A., NORTON, R. S. & COWMAN, A. F. 2010. Interaction between *Plasmodium falciparum* Apical Membrane Antigen 1 and the Rhoptry Neck Protein Complex Defines a Key Step in the Erythrocyte Invasion Process of Malaria Parasites. *Journal of Biological Chemistry,* 285**,** 14815-14822.

RICHARDS, J. S., ARUMUGAM, T. U., REILING, L., HEALER, J., HODDER, A. N., FOWKES, F. J., CROSS, N., LANGER, C., TAKEO, S., UBOLDI, A. D., THOMPSON, J. K., GILSON, P. R., COPPEL, R. L., SIBA, P. M., KING, C. L., TORII, M., CHITNIS, C. E., NARUM, D. L., MUELLER, I., CRABB, B. S., COWMAN, A. F., TSUBOI, T. & BEESON, J. G. 2013. Identification and prioritization of merozoite antigens as targets of protective human immunity to Plasmodium falciparum malaria for vaccine and biomarker development. *J Immunol,* 191**,** 795-809.

RIECKMANN, K. H. 2006. The chequered history of malaria control: are new and better tools the ultimate answer? *Ann Trop Med Parasitol,* 100**,** 647-62.

RIECKMANN, K. H., CARSON, P. E., BEAUDOIN, R. L., CASSELLS, J. S. & SELL, K. W. 1974. Letter: Sporozoite induced immunity in man against an Ethiopian strain of Plasmodium falciparum. *Trans R Soc Trop Med Hyg,* 68**,** 258-9.

RIGLAR, D. T., RICHARD, D., WILSON, D. W., BOYLE, M. J., DEKIWADIA, C., TURNBULL, L., ANGRISANO, F., MARAPANA, D. S., ROGERS, K. L., WHITCHURCH, C. B., BEESON, J. G., COWMAN, A. F., RALPH, S. A. & BAUM, J. 2011. Super-resolution dissection of coordinated events during malaria parasite invasion of the human erythrocyte. *Cell Host Microbe,* 9**,** 9-20.

RITCHIE, M. E., PHIPSON, B., WU, D., HU, Y., LAW, C. W., SHI, W. & SMYTH, G. K. 2015. limma powers differential expression analyses for RNA-sequencing and microarray studies. *Nucleic Acids Res,* 43**,** e47.

RIVADENEIRA, E. M., WASSERMAN, M. & ESPINAL, C. T. 1983. Separation and concentration of schizonts of *Plasmodium falciparum* by Percoll gradients. *J Protozool,* 30**,** 367-70.

ROGERSON, S. J., CHAIYAROJ, S. C., NG, K., REEDER, J. C. & BROWN, G. V. 1995. Chondroitin sulfate A is a cell surface receptor for Plasmodium falciparum-infected erythrocytes. *J Exp Med,* 182**,** 15-20.

ROSARIO, V. 1981. Cloning of naturally occurring mixed infections of malaria parasites. *Science*. 212**,** 4498, 1037-8.

ROTH, A., MAHER, S. P., CONWAY, A. J., UBALEE, R., CHAUMEAU, V., ANDOLINA, C., KABA, S. A., VANTAUX, A., BAKOWSKI, M. A., THOMSON-LUQUE, R., ADAPA, S. R., SINGH, N., BARNES, S. J., COOPER, C. A., ROUILLIER, M., MCNAMARA, C. W., MIKOLAJCZAK, S. A., SATHER, N., WITKOWSKI, B., CAMPO, B., KAPPE, S. H. I., LANAR, D. E., NOSTEN, F., DAVIDSON, S., JIANG, R. H. Y., KYLE, D. E. & ADAMS, J. H. 2018. A comprehensive model for assessment of liver stage therapies targeting Plasmodium vivax and Plasmodium falciparum. *Nat Commun,* 9**,** 1837.

RTS, S. C. T. P. 2015. Efficacy and safety of RTS,S/AS01 malaria vaccine with or without a booster dose in infants and children in Africa: final results of a phase 3, individually randomised, controlled trial. *The Lancet,* 386**,** 31-45.

SACHANONTA, N., CHOTIVANICH, K., CHAISRI, U., TURNER, G. D., FERGUSON, D. J., DAY, N. P. & PONGPONRATN, E. 2011. Ultrastructural and real-time microscopic changes in P. falciparum-infected red blood cells following treatment with antimalarial drugs. *Ultrastruct Pathol,* 35**,** 214-25.

SAGARA, I., DICKO, A., ELLIS, R. D., FAY, M. P., DIAWARA, S. I., ASSADOU, M. H., SISSOKO, M. S., KONE, M., DIALLO, A. I., SAYE, R., GUINDO, M. A., KANTE, O., NIAMBELE, M. B., MIURA, K., MULLEN, G. E., PIERCE, M., MARTIN, L. B., DOLO, A., DIALLO, D. A., DOUMBO, O. K., MILLER, L. H. & SAUL, A. 2009. A randomized controlled phase 2 trial of the blood stage AMA1-C1/Alhydrogel malaria vaccine in children in Mali. *Vaccine,* 27**,** 3090-8.

SALANTI, A., STAALSOE, T., LAVSTSEN, T., JENSEN, A. T., SOWA, M. P., ARNOT, D. E., HVIID, L. & THEANDER, T. G. 2003. Selective upregulation of

a single distinctly structured var gene in chondroitin sulphate A-adhering Plasmodium falciparum involved in pregnancy-associated malaria. *Mol Microbiol,* 49**,** 179-91.

SALAZAR, E., BANK, E. M., RAMSEY, N., HESS, K. C., DEITSCH, K. W., LEVIN, L. R. & BUCK, J. 2012. Characterization of Plasmodium falciparum adenylyl cyclase-beta and its role in erythrocytic stage parasites. *PLoS One,* 7**,** e39769.

SANDLER, H., KRETH, J., TIMMERS, H. T. & STOECKLIN, G. 2011. Not1 mediates recruitment of the deadenylase Caf1 to mRNAs targeted for degradation by tristetraprolin. *Nucleic Acids Res,* 39**,** 4373-86.

SASI, P., BURNS, S. P., WARUIRU, C., ENGLISH, M., HOBSON, C. L., KING, C. G., MOSOBO, M., BEECH, J. S., ILES, R. A., BOUCHER, B. J. & COHEN, R. D. 2007. Metabolic acidosis and other determinants of hemoglobin-oxygen dissociation in severe childhood Plasmodium falciparum malaria. *Am J Trop Med Hyg,* 77**,** 256-60.

SCHLIEP, K. P. 2010. phangorn: phylogenetic analysis in R. *Bioinformatics,* 27**,** 592-593.

SCHOFIELD, L., BUSHELL, G. R., COOPER, J. A., SAUL, A. J., UPCROFT, J. A. & KIDSON, C. 1986. A rhoptry antigen of *Plasmodium falciparum* contains conserved and variable epitopes recognized by inhibitory monoclonal antibodies. *Molecular and Biochemical Parasitology,* 18**,** 183-195.

SCHOFIELD, L., VILLAQUIRAN, J., FERREIRA, A., SCHELLEKENS, H., NUSSENZWEIG, R. & NUSSENZWEIG, V. 1987. Gamma interferon, CD8+ T cells and antibodies required for immunity to malaria sporozoites. *Nature,* 330**,** 664-6.

SHERLING, E. S., PERRIN, A. J., KNUEPFER, E., RUSSELL, M. R. G., COLLINSON, L. M., MILLER, L. H. & BLACKMAN, M. J. 2019. The Plasmodium falciparum rhoptry bulb protein RAMA plays an essential role in rhoptry neck morphogenesis and host red blood cell invasion. *PLoS Pathog,* 15**,** e1008049.

SHULMAN, C. E., MARSHALL, T., DORMAN, E. K., BULMER, J. N., CUTTS, F., PESHU, N. & MARSH, K. 2001. Malaria in pregnancy: adverse effects on haemoglobin levels and birthweight in primigravidae and multigravidae. *Trop Med Int Health,* 6**,** 770-8.

SIDDIQUI, G., SRIVASTAVA, A., RUSSELL, A. S. & CREEK, D. J. 2017. Multi-omics Based Identification of Specific Biochemical Changes Associated With PfKelch13-Mutant Artemisinin-Resistant *Plasmodium falciparum*. *J Infect Dis,* 215**,** 1435-1444.

SIGRIST, C. J. A., CERUTTI, L., HULO, N., GATTIKIER, A., FALQUET, L., PAGNI, M., BAIROCH, A. & BUCHER, P. 2002. PROSITE: A documented database using patterns and profiles as motif descriptors. *Briefings in Bioinformatics,* 3**,** 265-274.

SILMON DE MONERRI, N. C., FLYNN, H. R., CAMPOS, M. G., HACKETT, F., KOUSSIS, K., WITHERS-MARTINEZ, C., SKEHEL, J. M. & BLACKMAN, M. J. 2011. Global identification of multiple substrates for *Plasmodium falciparum* SUB1, an essential malarial processing protease. *Infection and immunity,* 79**,** 1086-1097.

SILTBERG, J. & LIBERLES, D. A. 2002. A simple covarion-based approach to analyse nucleotide substitution rates. *Journal of Evolutionary Biology,* 15**,** 588-594.

SINGH, N., REYES-ORDONEZ, A., COMPAGNONE, M. A., MORENO, J. F., LESLIE, B. J., HA, T. & CHEN, J. 2021. Redefining the specificity of phosphoinositide-binding by human PH domain-containing proteins. *Nat Commun,* 12**,** 4339.

SINGH, S., ALAM, M. M., PAL-BHOWMICK, I., BRZOSTOWSKI, J. A. & CHITNIS, C. E. 2010. Distinct external signals trigger sequential release of apical organelles during erythrocyte invasion by malaria parasites. *PLoS Pathog,* 6**,** e1000746.

SINGH, S., PLASSMEYER, M., GAUR, D. & MILLER, L. H. 2007. Mononeme: a new secretory organelle in Plasmodium falciparum merozoites identified by localization of rhomboid-1 protease. *Proc Natl Acad Sci U S A,* 104**,** 20043-8.

SPIELMANN, T., BIRNBAUM, J., FLEMMING, S., REICHARD, N., BLANCKE SOARES, A., MESÉN-RAMÍREZ, P., JONSCHER, E., BERGMANN, B. & SPIELMANN, T. 2017. Selection linked integration (SLI) for endogenous gene tagging and knock sideways in Plasmodium falciparum parasites. *Protocol Exchange*.

SRINIVASAN, P., YASGAR, A., LUCI, D. K., BEATTY, W. L., HU, X., ANDERSEN, J., NARUM, D. L., MOCH, J. K., SUN, H., HAYNES, J. D., MALONEY, D. J., JADHAV, A., SIMEONOV, A. & MILLER, L. H. 2013. Disrupting malaria

parasite AMA1-RON2 interaction with a small molecule prevents erythrocyte invasion. *Nat Commun,* 4**,** 2261.

STEVENS, A. T., HOWE, D. K. & HUNT, A. G. 2018. Characterization of mRNA polyadenylation in the apicomplexa. *PLoS One,* 13**,** e0203317.

SUAREZ, C., LENTINI, G., RAMASWAMY, R., MAYNADIER, M., AQUILINI, E., BERRY-STERKERS, L., CIPRIANO, M., CHEN, A. L., BRADLEY, P., STRIEPEN, B., BOULANGER, M. J. & LEBRUN, M. 2019. A lipid-binding protein mediates rhoptry discharge and invasion in *Plasmodium falciparum* and *Toxoplasma gondii* parasites. *Nature Communications,* 10**,** 4041.

SUBRAMANI, R., QUADT, K., JEPPESEN, A. E., HEMPEL, C., PETERSEN, J. E., HASSENKAM, T., HVIID, L. & BARFOD, L. 2015. Plasmodium falciparum-infected erythrocyte knob density is linked to the PfEMP1 variant expressed. *mBio,* 6**,** e01456-15.

SUPURAN, C. T. 2008. Carbonic anhydrases: novel therapeutic applications for inhibitors and activators. *Nat Rev Drug Discov,* 7**,** 168-81.

SZYMCZYNA, B. R., BOWMAN, J., MCCRACKEN, S., PINEDA-LUCENA, A., LU, Y., COX, B., LAMBERMON, M., GRAVELEY, B. R., ARROWSMITH, C. H. & BLENCOWE, B. J. 2003. Structure and function of the PWI motif: a novel nucleic acid-binding domain that facilitates pre-mRNA processing. *Genes Dev,* 17**,** 461-75.

TABACZAR, S., CZOGALLA, A., PODKALICKA, J., BIERNATOWSKA, A. & SIKORSKI, A. F. 2017. Protein palmitoylation: Palmitoyltransferases and their specificity. *Exp Biol Med (Maywood),* 242**,** 1150-1157.

TARR, S. J., DIAZ-INGELMO, O., STEWART, L. B., HOCKING, S. E., MURRAY, L., DUFFY, C. W., OTTO, T. D., CHAPPELL, L., RAYNER, J. C., AWANDARE, G. A. & CONWAY, D. J. 2018. Schizont transcriptome variation among clinical isolates and laboratory-adapted clones of the malaria parasite Plasmodium falciparum. *BMC Genomics,* 19**,** 894.

TAYLOR, G. A., CARBALLO, E., LEE, D. M., LAI, W. S., THOMPSON, M. J., PATEL, D. D., SCHENKMAN, D. I., GILKESON, G. S., BROXMEYER, H. E., HAYNES, B. F. & BLACKSHEAR, P. J. 1996. A pathogenetic role for TNF alpha in the syndrome of cachexia, arthritis, and autoimmunity resulting from tristetraprolin (TTP) deficiency. *Immunity,* 4**,** 445-54.

TAYLOR, H. M., MCROBERT, L., GRAINGER, M., SICARD, A., DLUZEWSKI, A. R., HOPP, C. S., HOLDER, A. A. & BAKER, D. A. 2010. The Malaria Parasite Cyclic GMP-Dependent Protein Kinase Plays a Central Role in Blood-Stage Schizogony. *Eukaryotic Cell,* 9**,** 37.

THAM, W.-H., WILSON, D. W., LOPATICKI, S., SCHMIDT, C. Q., TETTEH-QUARCOO, P. B., BARLOW, P. N., RICHARD, D., CORBIN, J. E., BEESON, J. G. & COWMAN, A. F. 2010. Complement receptor 1 is the host erythrocyte receptor for *Plasmodium falciparum* PfRh4 invasion ligand. *Proceedings of the National Academy of Sciences,* 107**,** 17327.

THEVENAZ, P., RUTTIMANN, U. E. & UNSER, M. 1998. A pyramid approach to subpixel registration based on intensity. *IEEE Trans Image Process,* 7**,** 27-41.

THIAM, L. G., ANIWEH, Y., QUANSAH, E. B., DONKOR, J. K., GWIRA, T. M., KUSI, K. A., NIANG, M. & AWANDARE, G. A. 2020. Cell trace far-red is a suitable erythrocyte dye for multi-color *Plasmodium falciparum* invasion phenotyping assays. *Experimental Biology and Medicine,* 245**,** 11-20.

TILLEY, L., STRAIMER, J., GNADIG, N. F., RALPH, S. A. & FIDOCK, D. A. 2016. Artemisinin Action and Resistance in Plasmodium falciparum. *Trends Parasitol,* 32**,** 682-696.

TOENHAKE, C. G., FRASCHKA, S. A., VIJAYABASKAR, M. S., WESTHEAD, D. R., VAN HEERINGEN, S. J. & BARTFAI, R. 2018. Chromatin Accessibility-Based Characterization of the Gene Regulatory Network Underlying Plasmodium falciparum Blood-Stage Development. *Cell Host Microbe,* 23**,** 557-569 e9.

TONKIN, M. L., ROQUES, M., LAMARQUE, M. H., PUGNIERE, M., DOUGUET, D., CRAWFORD, J., LEBRUN, M. & BOULANGER, M. J. 2011. Host cell invasion by apicomplexan parasites: insights from the co-structure of AMA1 with a RON2 peptide. *Science,* 333**,** 463-7.

TOSETTI, N., DOS SANTOS PACHECO, N., BERTIAUX, E., MACO, B., BOURNONVILLE, L., HAMEL, V., GUICHARD, P. & SOLDATI-FAVRE, D. 2020. Essential function of the alveolin network in the subpellicular microtubules and conoid assembly in Toxoplasma gondii. *Elife,* 9.

TRAGER, W. & JENSEN, J. B. 1976. Human malaria parasites in continuous culture. *Science,* 193**,** 673.

TUTEJA, R. & MEHTA, J. 2010. A genomic glance at the components of the mRNA export machinery in Plasmodium falciparum. *Commun Integr Biol.,* 3**,** 318-326.

VARNAITĖ, R. & MACNEILL, S. A. 2016. Meet the neighbors: Mapping local protein interactomes by proximity-dependent labeling with BioID. *Proteomics,* 16**,** 2503-2518.

VEMBAR, S. S., MACPHERSON, C. R., SISMEIRO, O., COPPEE, J. Y. & SCHERF, A. 2015. The PfAlba1 RNA-binding protein is an important regulator of translational timing in Plasmodium falciparum blood stages. *Genome Biol,* 16**,** 212.

VIDEVALL, E. 2018. Plasmodium parasites of birds have the most AT-rich genes of eukaryotes. *Microb Genom,* 4.

VIRIYAVEJAKUL, P., KHACHONSAKSUMET, V. & PUNSAWAD, C. 2014. Liver changes in severe Plasmodium falciparum malaria: histopathology, apoptosis and nuclear factor kappa B expression. *Malar J,* 13**,** 106.

VOLZ, J. C., YAP, A., SISQUELLA, X., THOMPSON, J. K., LIM, N. T., WHITEHEAD, L. W., CHEN, L., LAMPE, M., THAM, W. H., WILSON, D., NEBL, T., MARAPANA, D., TRIGLIA, T., WONG, W., ROGERS, K. L. & COWMAN, A. F. 2016. Essential Role of the PfRh5/PfRipr/CyRPA Complex during Plasmodium falciparum Invasion of Erythrocytes. *Cell Host Microbe,* 20**,** 60-71.

VOSS, T. S., BOZDECH, Z. & BARTFAI, R. 2014. Epigenetic memory takes center stage in the survival strategy of malaria parasites. *Curr Opin Microbiol,* 20**,** 88-95.

WARNCKE, J. D., VAKONAKIS, I. & BECK, H. P. 2016. Plasmodium Helical Interspersed Subtelomeric (PHIST) Proteins, at the Center of Host Cell Remodeling. *Microbiol Mol Biol Rev,* 80**,** 905-27.

WATERKEYN, J. G., WICKHAM, M. E., DAVERN, K. M., COOKE, B. M., COPPEL, R. L., REEDER, J. C., CULVENOR, J. G., WALLER, R. F. & COWMAN, A. F. 2000. Targeted mutagenesis of Plasmodium falciparum erythrocyte membrane protein 3 (PfEMP3) disrupts cytoadherence of malaria-infected red blood cells. *EMBO J,* 19**,** 2813-23.

WATERMEYER, J. M., HALE, V. L., HACKETT, F., CLARE, D. K., CUTTS, E. E., VAKONAKIS, I., FLECK, R. A., BLACKMAN, M. J. & SAIBIL, H. R. 2016. A spiral scaffold underlies cytoadherent knobs in Plasmodium falciparum-infected erythrocytes. *Blood,* 127**,** 343-51.

WEISS, G. E., CRABB, B. S. & GILSON, P. R. 2016. Overlaying Molecular and Temporal Aspects of Malaria Parasite Invasion. *Trends Parasitol,* 32**,** 284-295.

WEISS, G. E., GILSON, P. R., TAECHALERTPAISARN, T., THAM, W.-H., DE JONG, N. W. M., HARVEY, K. L., FOWKES, F. J. I., BARLOW, P. N., RAYNER, J. C., WRIGHT, G. J., COWMAN, A. F. & CRABB, B. S. 2015. Revealing the Sequence and Resulting Cellular Morphology of Receptor-Ligand Interactions during *Plasmodium falciparum* Invasion of Erythrocytes. *PLOS Pathogens,* 11**,** e1004670.

WELLS, M. L., WASHINGTON, O. L., HICKS, S. N., NOBILE, C. J., HARTOONI, N., WILSON, G. M., ZUCCONI, B. E., HUANG, W., LI, L., FARGO, D. C. & BLACKSHEAR, P. J. 2015. Post-transcriptional regulation of transcript abundance by a conserved member of the tristetraprolin family in Candida albicans. *Mol Microbiol,* 95**,** 1036-53.

WHITE, N. J. 2018. Anaemia and malaria. *Malar J,* 17**,** 371.

WHITE, N. J., PUKRITTAYAKAMEE, S., HIEN, T. T., FAIZ, M. A., MOKUOLU, O. A. & DONDORP, A. M. 2014. Malaria. *The Lancet,* 383**,** 723-735.

WICHERS, J. S., WUNDERLICH, J., HEINCKE, D., PAZICKY, S., STRAUSS, J., SCHMITT, M., KIMMEL, J., WILCKE, L., SCHARF, S., VON THIEN, H., BURDA, P. C., SPIELMANN, T., LOW, C., FILARSKY, M., BACHMANN, A. & GILBERGER, T. W. 2021. Identification of novel inner membrane complex and apical annuli proteins of the malaria parasite Plasmodium falciparum. *Cell Microbiol,* 23**,** e13341.

WICKHAM, M. E., CULVENOR, J. G. & COWMAN, A. F. 2003. Selective inhibition of a two-step egress of malaria parasites from the host erythrocyte. *J Biol Chem,* 278**,** 37658-63.

WILDE, M. L., TRIGLIA, T., MARAPANA, D., THOMPSON, J. K., KOUZMITCHEV, A. A., BULLEN, H. E., GILSON, P. R., COWMAN, A. F. & TONKIN, C. J. 2019. Protein Kinase A Is Essential for Invasion of Plasmodium falciparum into Human Erythrocytes. *mBio,* 10.

WILSON, D. W., CRABB, B. S. & BEESON, J. G. 2010. Development of fluorescent *Plasmodium falciparum* for *in vitro* growth inhibition assays. *Malaria Journal,* 9**,** 152.

WILSON, D. W., LANGER, C., GOODMAN, C. D., MCFADDEN, G. I. & BEESON, J. G. 2013. Defining the timing of action of antimalarial drugs against *Plasmodium falciparum*. *Antimicrobial agents and chemotherapy,* 57**,** 1455-1467.

WIRTH, C. C. & PRADEL, G. 2012. Molecular mechanisms of host cell egress by malaria parasites. *Int J Med Microbiol,* 302**,** 172-8.

WONG, W., HUANG, R., MENANT, S., HONG, C., SANDOW, J. J., BIRKINSHAW, R. W., HEALER, J., HODDER, A. N., KANJEE, U., TONKIN, C. J., HECKMANN, D., SOROKA, V., SOGAARD, T. M. M., JORGENSEN, T., DURAISINGH, M. T., CZABOTAR, P. E., DE JONGH, W. A., THAM, W. H., WEBB, A. I., YU, Z. & COWMAN, A. F. 2019. Structure of Plasmodium falciparum Rh5-CyRPA-Ripr invasion complex. *Nature,* 565**,** 118-121.

WOO, Y. H., ANSARI, H., OTTO, T. D., KLINGER, C. M., KOLISKO, M., MICHÁLEK, J., SAXENA, A., SHANMUGAM, D., TAYYROV, A., VELUCHAMY, A., ALI, S., BERNAL, A., DEL CAMPO, J., CIHLÁŘ, J., FLEGONTOV, P., GORNIK, S. G., HAJDUŠKOVÁ, E., HORÁK, A., JANOUŠKOVEC, J., KATRIS, N. J., MAST, F. D., MIRANDA-SAAVEDRA, D., MOURIER, T., NAEEM, R., NAIR, M., PANIGRAHI, A. K., RAWLINGS, N. D., PADRON-REGALADO, E., RAMAPRASAD, A., SAMAD, N., TOMČALA, A., WILKES, J., NEAFSEY, D. E., DOERIG, C., BOWLER, C., KEELING, P. J., ROOS, D. S., DACKS, J. B., TEMPLETON, T. J., WALLER, R. F., LUKEŠ, J., OBORNÍK, M. & PAIN, A. 2015. Chromerid genomes reveal the evolutionary path from photosynthetic algae to obligate intracellular parasites. *eLife,* 4**,** e06974.

WORLD_HEALTH_ORGANIZATION. 2000. *World malaria report 2000* [Online]. Geneva: World Health Organization. Available: www.who.int/malaria/publications/world-malaria-report-2000/en/ [Accessed August 4th 2021].

WORLD_HEALTH_ORGANIZATION. 2019. *World malaria report 2019* [Online]. Geneva: World Health Organization. Available: www.who.int/malaria/publications/world-malaria-report-2019/en/ [Accessed August 4th 2021].

WORLD_HEALTH_ORGANIZATION. 2020. *World malaria report 2020* [Online]. Geneva: World Health Organization. Available: www.who.int/publications/i/item/9789240015791 [Accessed August 4th 2021].

WRIGHT, G. J. & RAYNER, J. C. 2014. Plasmodium falciparum erythrocyte invasion: combining function with immune evasion. *PLoS Pathog,* 10**,** e1003943.

WU, Y., SIFRI, C. D., LEI, H. H., SU, X. Z. & WELLEMS, T. E. 1995. Transfection of Plasmodium falciparum within human red blood cells. *Proc Natl Acad Sci U S A,* 92**,** 973-7.

WURTZ, N., PASTORINO, B., ALMERAS, L., BRIOLANT, S., VILLARD, C. & PARZY, D. 2009. Expression and biochemical characterization of the Plasmodium falciparum protein kinase A catalytic subunit. *Parasitol Res,* 104**,** 1299-305.

XIE, Y., ZHENG, Y., LI, H., LUO, X., HE, Z., CAO, S., SHI, Y., ZHAO, Q., XUE, Y., ZUO, Z. & REN, J. 2016. GPS-Lipid: a robust tool for the prediction of multiple lipid modification sites. *Sci Rep,* 6**,** 28249.

YAO, Z., ZHANG, M., KOBAYASHI, H., SAKAHARA, H., NAKADA, H., YAMASHINA, I. & KONISHI, J. 1995. Improved targeting of radiolabeled streptavidin in tumors pretargeted with biotinylated monoclonal antibodies through an avidin chase. *J Nucl Med,* 36**,** 837-41.

YEO, T. W., LAMPAH, D. A., TJITRA, E., GITAWATI, R., KENANGALEM, E., PIERA, K., GRANGER, D. L., LOPANSRI, B. K., WEINBERG, J. B., PRICE, R. N., DUFFULL, S. B., CELERMAJER, D. S. & ANSTEY, N. M. 2009. Relationship of cell-free hemoglobin to impaired endothelial nitric oxide bioavailability and perfusion in severe falciparum malaria. *J Infect Dis,* 200**,** 1522-9.

YEOH, S., O'DONNELL, R. A., KOUSSIS, K., DLUZEWSKI, A. R., ANSELL, K. H., OSBORNE, S. A., HACKETT, F., WITHERS-MARTINEZ, C., MITCHELL, G. H., BANNISTER, L. H., BRYANS, J. S., KETTLEBOROUGH, C. A. & BLACKMAN, M. J. 2007. Subcellular discharge of a serine protease mediates release of invasive malaria parasites from host erythrocytes. *Cell,* 131**,** 1072-83.

ZENONOS, Z. A., RAYNER, J. C. & WRIGHT, G. J. 2014. Towards a comprehensive Plasmodium falciparum merozoite cell surface and secreted recombinant protein library. *Malar J,* 13**,** 93.

ZHANG, M., WANG, C., OTTO, T. D., OBERSTALLER, J., LIAO, X., ADAPA, S. R., UDENZE, K., BRONNER, I. F., CASANDRA, D., MAYHO, M., BROWN, J., LI, S., SWANSON, J., RAYNER, J. C., JIANG, R. H. Y. & ADAMS, J. H. 2018.

Uncovering the essential genes of the human malaria parasite Plasmodium falciparum by saturation mutagenesis. *Science,* 360.

ZHANG, W., XU, C., BIAN, C., TEMPEL, W., CROMBET, L., MACKENZIE, F., MIN, J., LIU, Z. & QI, C. 2011. Crystal structure of the Cys2His2-type zinc finger domain of human DPF2. *Biochem Biophys Res Commun,* 413**,** 58-61.

ZOUGBEDE, S., MILLER, F., RAVASSARD, P., REBOLLO, A., CICERON, L., COURAUD, P. O., MAZIER, D. & MORENO, A. 2011. Metabolic acidosis induced by Plasmodium falciparum intraerythrocytic stages alters blood-brain barrier integrity. *J Cereb Blood Flow Metab,* 31**,** 514-26.

ZUCCALA, E. S., GOUT, A. M., DEKIWADIA, C., MARAPANA, D. S., ANGRISANO, F., TURNBULL, L., RIGLAR, D. T., ROGERS, K. L., WHITCHURCH, C. B., RALPH, S. A., SPEED, T. P. & BAUM, J. 2012. Subcompartmentalisation of Proteins in the Rhoptries Correlates with Ordered Events of Erythrocyte Invasion by the Blood Stage Malaria Parasite. *PLOS ONE,* 7**,** e46160.

Appendices

Appendix I: Molecular cloning

Annealing temperatures (Tm) detailed in (round brackets), expressed in degrees Celsius. Restriction enzyme sites in **bold**. Restriction enzymes detailed in [square brackets].

Table 1: Constructs and primers for flanks in Chapter 2

Final construct	Forward primer	Reverse primer
pPfCERLI 2^{HAGlmS}	GGT**AGATCT**GAAGGAATCTTTT GGAGATGAGC (57.5) [BglII]	GGT**CTGCAGC**TATATTTTGTATGG TATTTTCTAATTGTGC (53.8) [PstI]
pSLI-TGD:PfCE RLI2	GGT**GCGGCCGC**TCCACATATA AGTGATTTCGAGCC (58.7) [NotI]	GGT**ACGCGT**CCTTGCACACTTCTT GTCC (56.4) [MluI]
pSLI-2xFKBP-GFP:PfCE RLI1	GGT**GCGGCCGC**CATATCAAAT TTGGTTCTTGAAG (52.4) [NotI]	GGT**CCTAGG**ATCACTATAGTTGTA CATATTTTTGC (54.3) [AvrII]
pSLI-2xFKBP-GFP:PfCE RLI2	GGT**GCGGCCGG**AAGGAATCTT TTGGAGATGAGC [NotI]	GGT**CCTAGG**TATATTTTGTATGGT ATTTTCTAATTGTGC [AvrII]

Table 2: Primers for integration/expression screening in Chapter 2

Primer	Sequence
PfCERLI2 3' Int F	GCCATTACAATTTTCACAAACGACC (60.1)
HA screen R	CATCATAGGGATAGCCAGCG (57.7)
glmS screen R	GAAATCCTTACGGCTGTGATCTG (59.4)
PfCERLI1 3' SLI Int F	CAAAGAAACGGACCTTAGCACAAC (60.8)
PfCERLI2 3' SLI Int F	GCCATTACAATTTTCACAAACGACC (60.1)

SLI GFP screen R	CCATTAACATCACCATCTAATTC (53.3)
mCherry F	CAAGGGCGAGGAGGATAAC (57.3)
mCherry R	GTACAGCTCGTCCATGCC (57.9)

Table 3: Constructs and primers for flanks for Chapter 3

Final construct	Forward primer	Reverse primer
pHA3:PfCZIF1	GGT**AGATCT**GTGAGGATGCCATAGAAGAAG (55.8) [BglII]	GCT**GCAGACC**TTCTGATAAGAAAGAGAAAAAAGAC (53.8) [PstI]
pHA3:PfCZIF2	GGT**AGATCT**AGATCTTGATTTTATAAGAAATCTTAATGG (55.4) [BglII]	GGT**CTGCAGC**AATCATTTCTTTCATGTTGTAGTTC (54.6) [PstI]
pSLI-TGD:PfCZIF1	GGT**GCGGCCGC**TAAGCCACACTTTTGAGTGAAGAAG (58) [NotI]	GGT**ACGCGT**AACAGCGTTTTTAGTCATATCATTC (56.2) [MluI]
pSLI-TGD:PfCZIF2	GGT**GCGGCCGC**TAACGTGCACACCTTTACTTAGCG (54.3) [NotI]	GGT**ACGCGT**GTTCATCTTTTGTTCTTGTAATGTG (55.4) [MluI]
pCC1:PfCZIF1	Flank 1: GGT**ACTAGT**GTGTACACCTTGTGAGTACATAC (55.3) [SpeI] Flank 2: GG**TGAATTC**CGGTTTGTACTAATATAGATAATTTAG (52.4) [EcoRI]	Flank 1: GGT**CTTAAG**GAACCATCTCCCCTTGTTTC (54.4) [AflII] Flank 2: GGT**CCATGG**TTCTGATAAGAAAGAGAAAAAAGAC (53.8) [NcoI]
pCC4:PfCZIF1	Identical as above.	Identical as above.
pCC1:PfCZIF2	Flank 1: GGT**ACTAGT**TGCTTCATATTAGGGTAATTGG (52.1) [SpeI] Flank 2: GGT**TCCATGG**CTAAATCATTTCTTTCATGTTGTAG (54.3) [EcoRI]	Flank 1: GGT**CTTAAG**CTCTATATCTTCTTCGGTTTC (53.1) [AflII] Flank 2: GGT**GAATTC**CTAGCAAAACAAGTAATAAATCAAG (54.6) [NcoI]
pCC4:PfCZIF2	Identical as above.	Identical as above.

pUFCas9: PfCZIF1 Guide R10	TTGGCTGAGACGAGAGTCCC	GGGACTCTCGTCTCAGCCAA
pUFCas9: PfCZIF1 Guide R11	AATGGCAACTTGTAAGTACC	GGTACTTACAAGTTGCCATT
pUFCas9: PfCZIF2 Guide R1	CATGTGAAAATGCCACACAA	CATGTGAAAATGCCACACAA
pUFCas9: PfCZIF2 Guide R2	AGTATAGTCATAGTGCGGAA	TTCCGCACTATGACTATACT
pSLI-2xFKBP-GFP:PfCZIF1	GGT**GCGGCCGC**GTGAGGATGCCATAGAAGAAG (55.8) [NotI]	GGT**CCTAGG**TTCTGATAAGAAAGAGAAAAAA (53.8) [AvrII]
pSLI-2xFKBP-GFP:PfCZIF2	GGT**GCGGCCGC**AGATCTTGATTTTATAAGAAATCTTAATGG (55.4) [NotI]	GGT**CCTAGG**AATCATTTCTTTCATGTTGTAGTTC (54.6) [AvrII]
pArl1a:PfCZIF1	GGT**GGTACC**ATGGTTTATGCCACACTTTTG (55.3) [KpnI]	GGT**CCTAGG**TTCTGATAAGAAAGAGAAAAAAGAC (53.8) [AvrII]
pArl1a:PfCZIF2	GGT**GGTACC**ATGGCGTGCACACC (55.6) [KpnI]	GGT**CCTAGG**AATCATTTCTTTCATGTTGTAGTTC (52.3) [AvrII]

Table 4: Primers for integration/expression screening for Chapter 3

Primer	Sequence
PfCZIF1 3' Int F	CAGAATCATTCAAGTTGTAGTAC (53.3)
PfCZIF2 3' Int F	CCACACAAAGGTCTTTCAATG (55.6)
HA screen R	CATCATAGGGATAGCCAGCG (57.7)
glmS screen R	GAAATCCTTACGGCTGTGATCTG (59.4)
PfCZIF1 TGD Int F	GTGTACACCTTGTGAGTACAT (55.3)
PfCZIF2 TGD Int F	GTCGCCACGTATAAGACTG (55.6)

SLI linker screen R	CTCATCGTACGTCTACCTGC (57.6)
SLI GFP screen R	CCATTAACATCACCATCTAATTC (53.3)
BSD screen R	GATTGTAGCCGTTGCTCTTTC (57.6)

Base plasmids

A

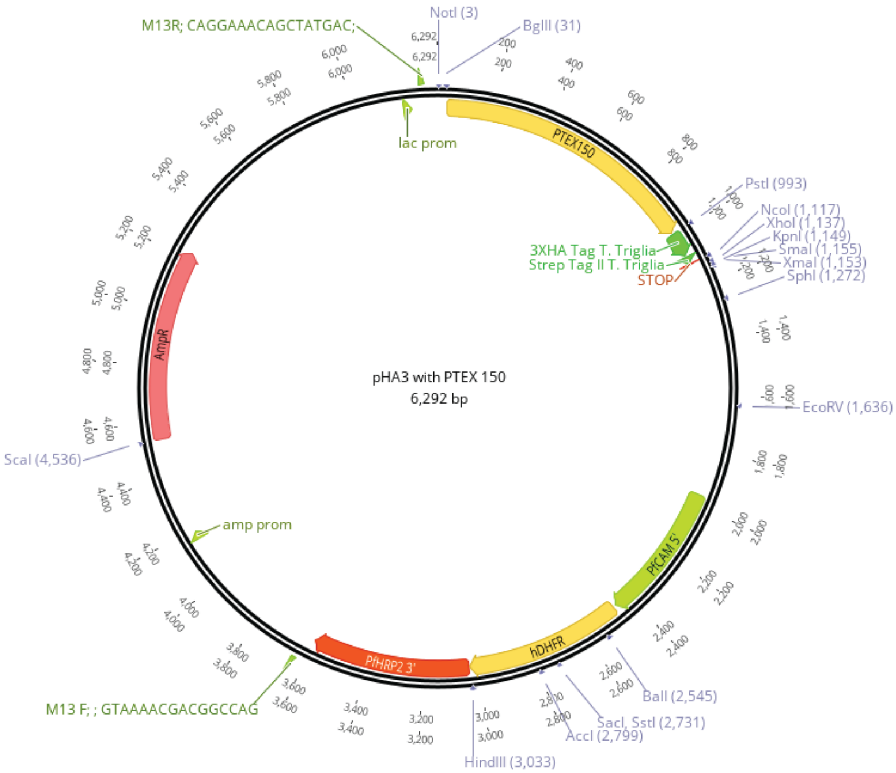

B

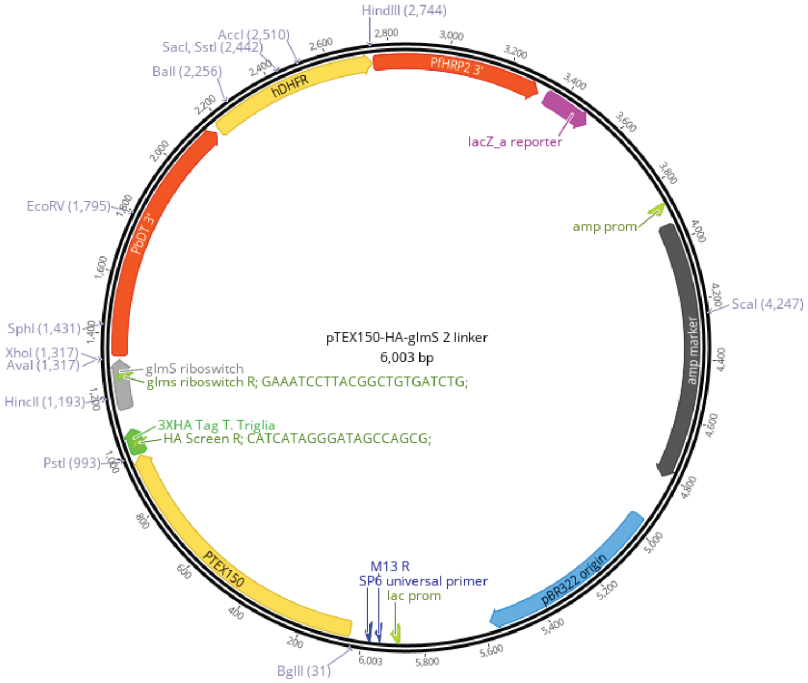

Figure 1. Restriction map of constructs for endogenous HA-tagging.

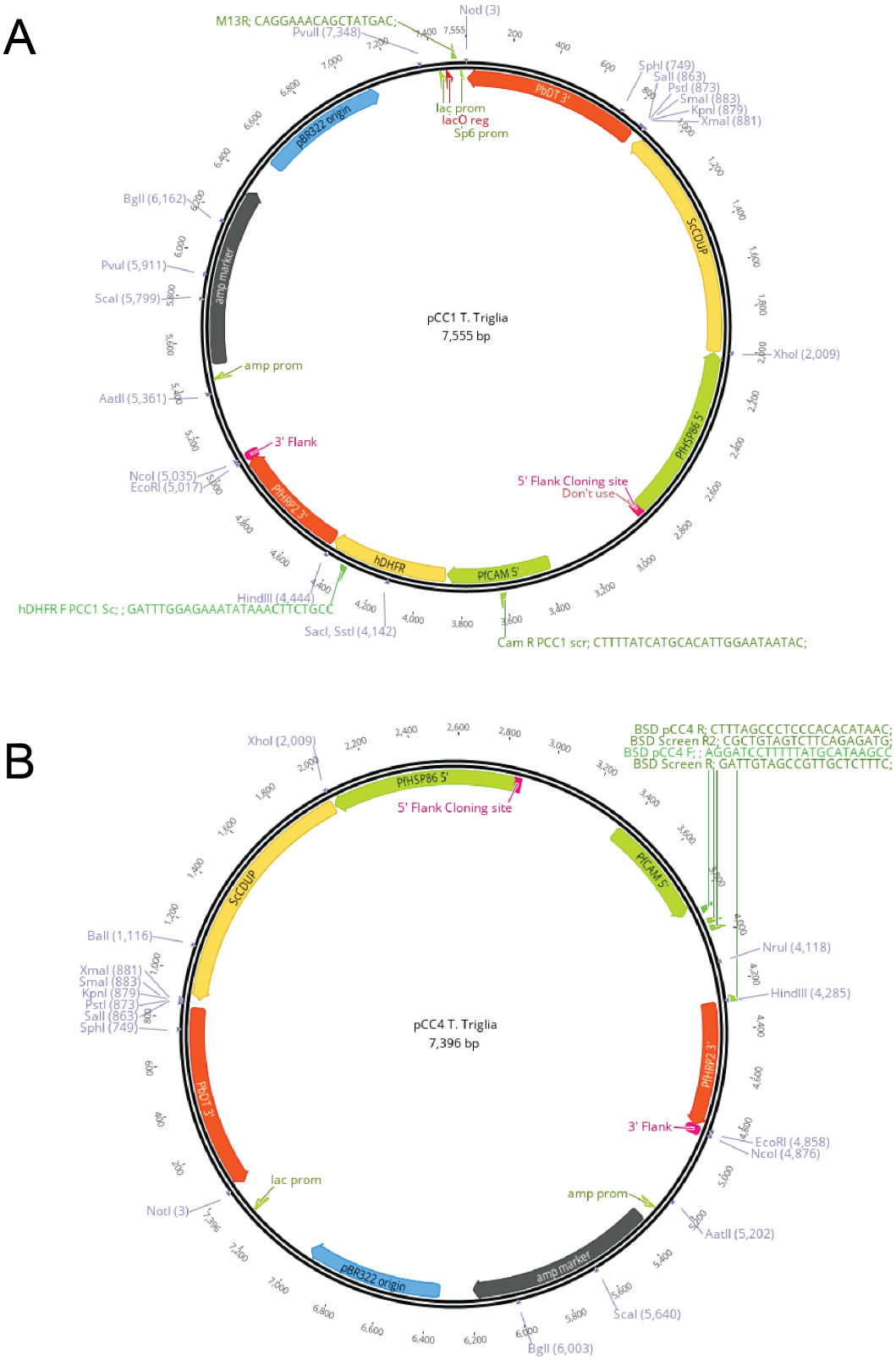

Figure 2. Restriction map of constructs used as repair templates for CRISPR-Cas9.

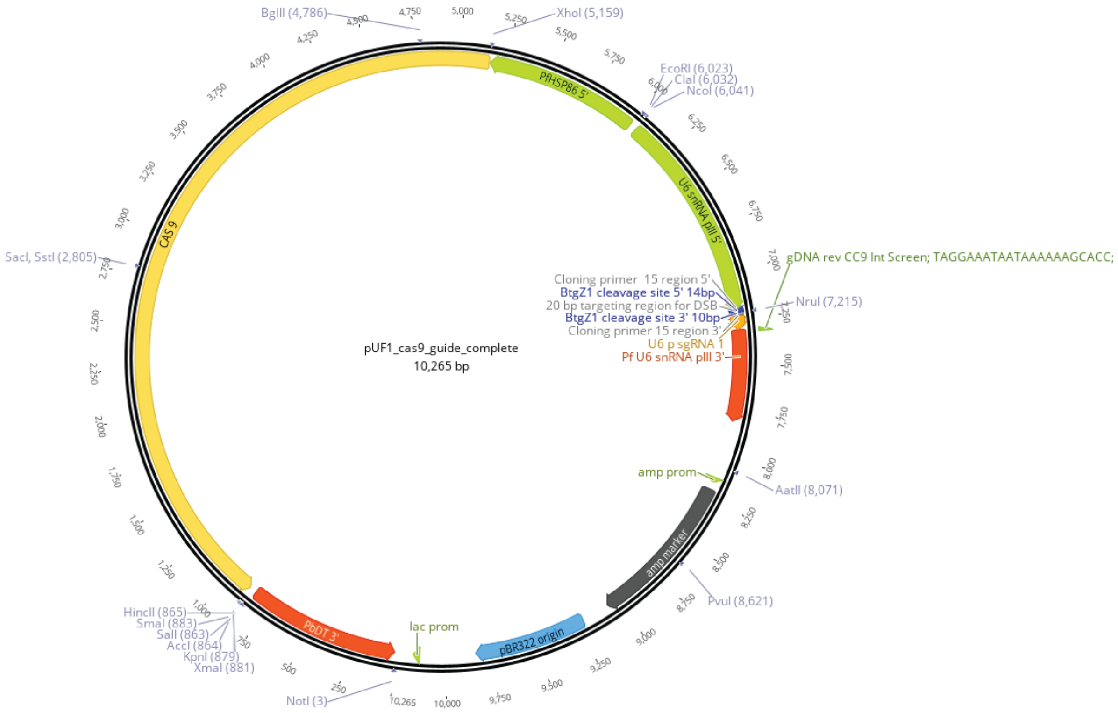

Figure 3. Restriction map of guide construct for CRISPR-Cas9 gene editing.

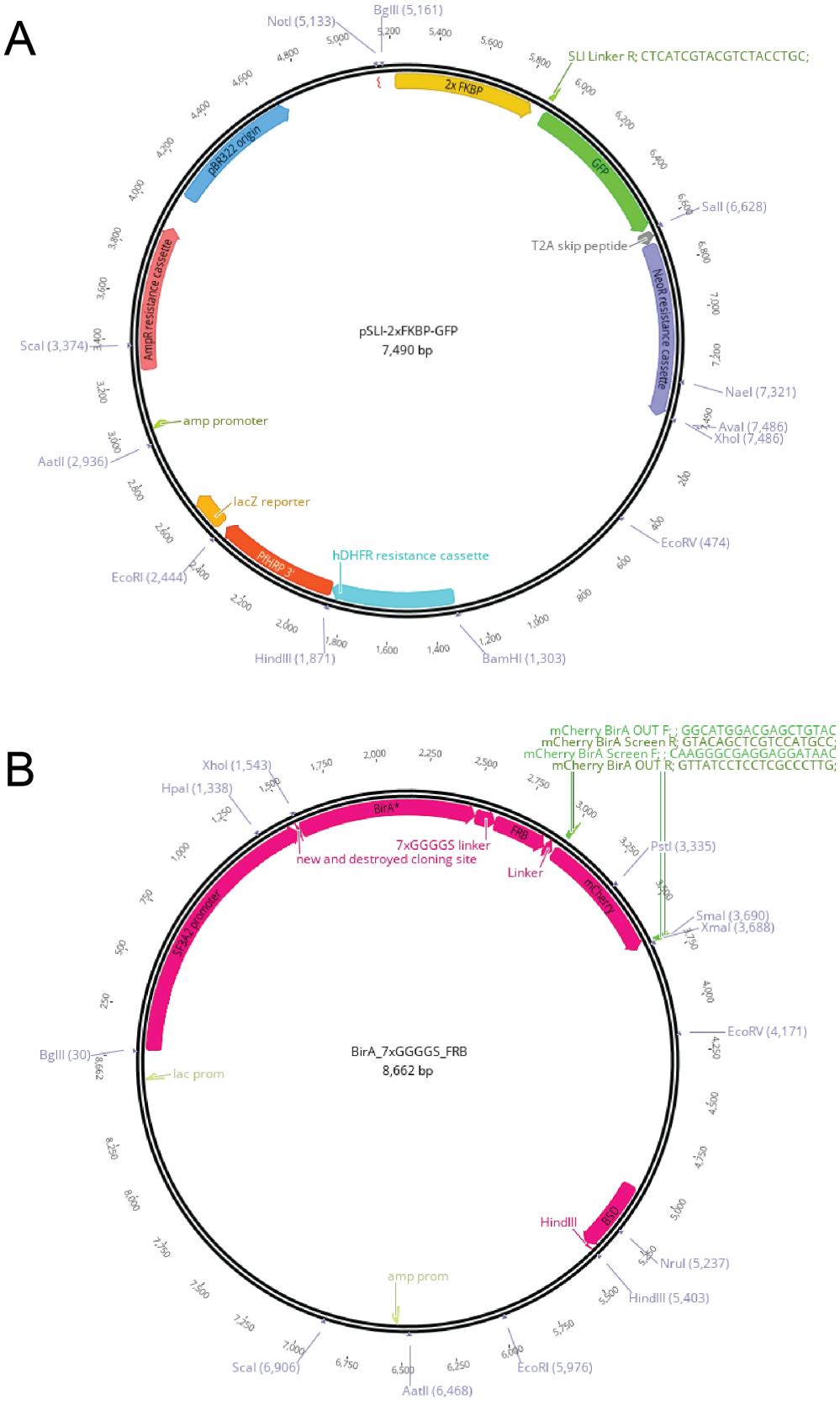

Figure 4. Restriction map of constructs for DiQ-BioID.

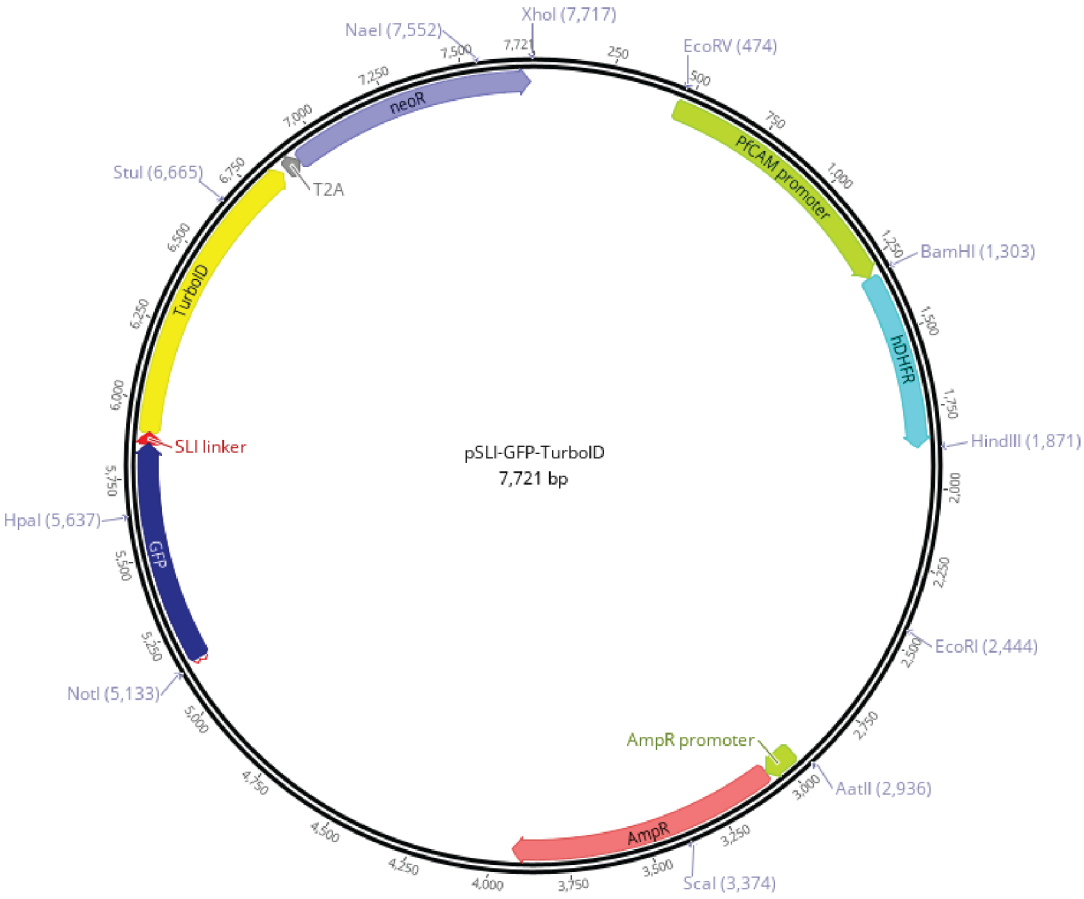

Figure 5. Restriction map of construct for TurboID.

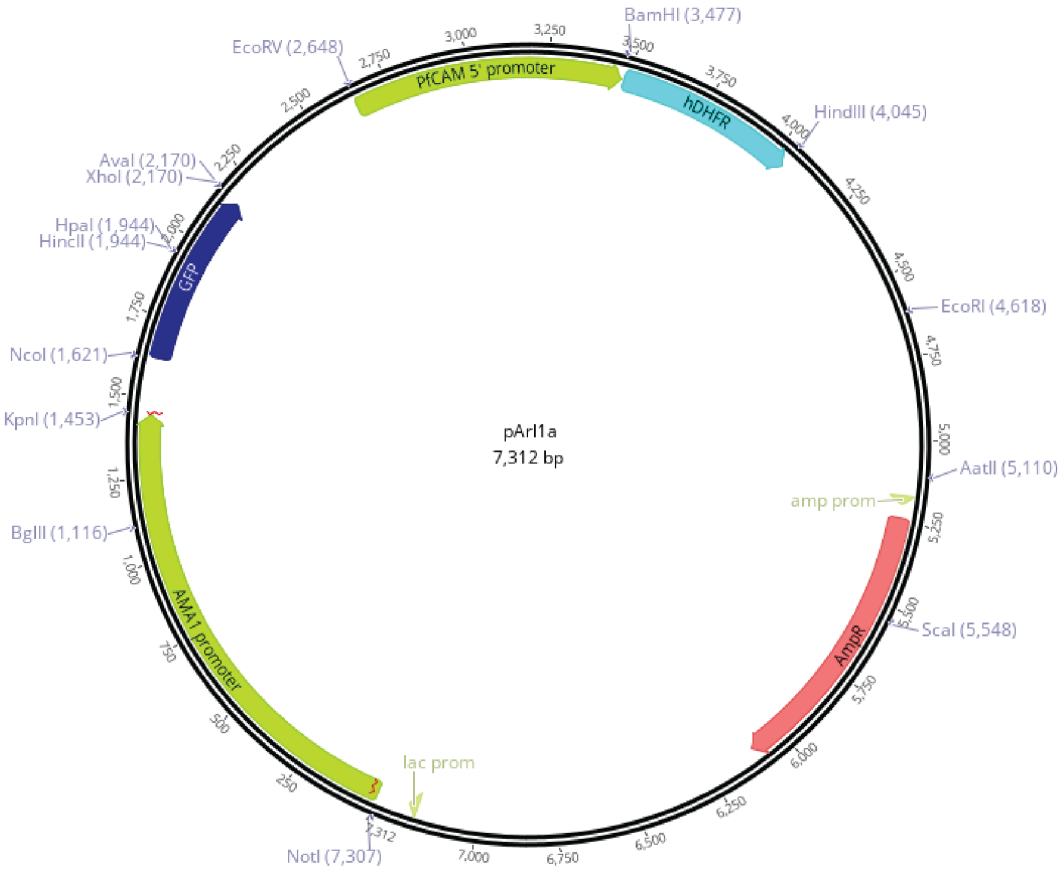

Figure 6. Restriction map of construct for episomal protein overexpression in schizonts.

Appendix II: RNAseq

The following includes script examples in *bash (Linux)* and *R* for processing files for RNAseq and differential expression analysis.

Chapter 3: Genome indexing

```
 GNU nano 2.3.1                          File: 1481run_star_index

#!/bin/bash
#parameters for SLURM
#SBATCH --time=0-1:00:00

# Multiple-core job for XXX CPUs
#SBATCH --nodes=1 --ntasks=1 --cpus-per-task=4 --mem=16384 # in MB

#SBATCH --output slurm-%j.o --error slurm-%j.e --mail-user=a1687185@adelaide.edu.au
install -m444 "$0" "$(pwd)/slurm-${SLURM_JOB_ID}_${SLURM_JOB_NAME}"
set -o noclobber
set -e

module load STAR/2.7.0d-foss-2016b

STAR --runMode genomeGenerate --runThreadN 4 --genomeDir /fast/users/a1687185/1481RNAseqproject/ngsSkeleton/genome/star_index --genomeFastaFiles /fast/
users/a1687185/1481RNAseqproject/ngsSkeleton/genome/PlasmoDB-46_Pfalciparum3D7_Genome.fasta --sjdbGTFfile /fast/users/a1687185/1481RNAseqproject/ngsSke
leton/genome/PlasmoDB-46_Pfalciparum3D7.gff --sjdbOverhang 150 --genomeSAindexNbases 11
```

Chapter 3: Binary Alignment Map (BAM) file generation

```
a1687185 — a1687185@l03:/fast/users/a1687185/1481RNAseqproject/ngsSkeleton/slurm — ssh a1687185@p...
 GNU nano 2.3.1                  File: 1481run_star_map2

#!/bin/bash
#SBATCH -p batch
#SBATCH -N 1
#SBATCH -n 8
#SBATCH --time=1-00:00:00
#SBATCH --mem=16GB
#SBATCH -o /fast/users/a1687185/1481RNAseqproject/ngsSkeleton/slurm/%x_%j.out
#SBATCH -e /fast/users/a1687185/1481RNAseqproject/ngsSkeleton/slurm/%x_%j.err
#SBATCH --mail-type=END
#SBATCH --mail-type=FAIL
#SBATCH --mail-user=juan.balbin@adelaide.edu.au

##Params
REFS=/fast/users/a1687185/1481RNAseqproject/ngsSkeleton/genome/star_index
FASTDATA=/fast/users/a1687185/1481RNAseqproject/ngsSkeleton/0_rawData/fastq
ALIGNDATA=/fast/users/a1687185/1481RNAseqproject/ngsSkeleton/2_alignedData/star_output
CORES=6

## Modules
module load STAR/2.5.3a-foss-2016b

## Aligning, filtering and sorting
for R1 in ${FASTDATA}/*_R1.fastq.gz
  do


  R2=${R1%_R1.fastq.gz}_R2.fastq.gz
  BNAME=$(basename ${R1%_R1.fastq.gz})
  echo -e "STAR will align:\t${R1}\n\t${R2}"

    STAR \
        --runThreadN ${CORES} \
        --genomeDir ${REFS} \
        --readFilesIn ${R1} ${R2} \
        --readFilesCommand gunzip -c \
        --outFileNamePrefix ${ALIGNDATA}/bams/${BNAME} \
        --outSAMtype BAM SortedByCoordinate

  done


^G Get Help   ^O WriteOut   ^R Read File   ^Y Prev Page   ^K Cut Text   ^C Cur Pos
^X Exit       ^J Justify    ^W Where Is    ^V Next Page   ^U UnCut Text ^T To Spell
```

Chapter 3: BAM paths for *limma*

bam_paths

```
CellType BamFile
WT       a1687185/Desktop/RNAseq_data/1481bam_filesintronlimited/3D7_WT-1-Aligned.sorted.out.bam
Pf3D7_1468400KO  a1687185/Desktop/RNAseq_data/1481bam_filesintronlimited/14684TGD-1-Aligned.sorted.out.bam
WT       a1687185/Desktop/RNAseq_data/1481bam_filesintronlimited/3D7-WT-2-Aligned.sorted.out.bam
Pf3D7_1468400KO  a1687185/Desktop/RNAseq_data/1481bam_filesintronlimited/14684TGD-2-Aligned.sorted.out.bam
WT       a1687185/Desktop/RNAseq_data/1481bam_filesintronlimited/3D7-WT-3-Aligned.sorted.out.bam
Pf3D7_1468400KO  a1687185/Desktop/RNAseq_data/1481bam_filesintronlimited/14684TGD-3-Aligned.sorted.out.bam
```

Chapter 3: *limma/voom* for differential expression analysis

Installation

Do once.

```{r install packages, eval=FALSE}
# source("http://www.bioconductor.org/biocLite.R")
# biocLite("Rsubread")
# biocLite("edgeR")
# biocLite("limma")
# biocLite("statmod")
# update.packages()
```

```{r load previous}
load("limma.RData")
```

Load libraries

```{r load libraries}
library(Rsubread)
library(limma)
library(edgeR)
library(here)
```

Define paths

You need to tell R the paths to the gff and the `bam_list`, which is a tab-delimited file specifying the paths to the bam files as follows:

```
CellType  BamFile
A RNA_14_STAR_NewOption_D4_M+G+Aligned_sorted.bam
B RNA_15_STAR_NewOption_D4_M+G-Aligned_sorted.bam
```

Limma/Voom will do DE between two types of sample, which is specified in the first column. Multiple replicates will have the same `CellType`. Don't actually call them A and B, but give them sane names (e.g. `female` or whatever).

Tell R the paths to the gff file and the bam_list as above. The GTF file used here is from Tarr et al. BMC Genomics (2018)

```{r define paths}
# gff_file="3D7_v12_exons_mod.gtf"
# all_bam_list="bam_list"
# gff_file="Pb_test.gtf"
# all_bam_list="bam_list_test"
gff_file=here("data/genome/GTF_VarRifStev_filtered_out.gtf")
all_bam_list=here("data/bam_paths.txt")
```

Import bam data into R

```{r load bam files}
all_targets <- readTargets(file=all_bam_list)
all_celltype <- factor(all_targets$CellType)
all_design <- model.matrix(~all_celltype)
```

In the following step, we need to look at (isStrandSpecific) and (PE orientation). The easiest way is to just see how many reads align for each setting, e.g.

strandSpecific=2 "reversely stranded"
RNA_14_STAR_NewOption_D4_M+G+Aligned_sorted.bam: 80.8%
RNA_15_STAR_NewOption_D4_M+G-Aligned_sorted.bam: 73.7%

strandSpecific=1 "stranded"
assigned fragments:
RNA_14_STAR_NewOption_D4_M+G+Aligned_sorted.bam: 7.8%
RNA_15_STAR_NewOption_D4_M+G-Aligned_sorted.bam: 7.2%

strandSpecific=0 "no"
RNA_14_STAR_NewOption_D4_M+G+Aligned_sorted.bam: 88.4%
RNA_15_STAR_NewOption_D4_M+G-Aligned_sorted.bam: 80.7%

So for your bam files, it looks like `2` is for sense and `1` is for antisense. In the following code block, you should only use one command at a time. If you want to change it, uncomment the line that you want to use.

```{r featurecounts, cache=TRUE}
all_fcounts <- featureCounts(files=all_targets$BamFile,annot.ext=gff_file,isGTFAnnotationFile=TRUE,nthreads=8,isPairedEnd=TRUE,strandSpecific=2)
#all_fcounts <- featureCounts(files=all_targets$BamFile,annot.ext=gff_file,isGTFAnnotationFile=TRUE,nthreads=8,isPairedEnd=TRUE,strandSpecific=1)
#all_fcounts <- featureCounts(files=all_targets$BamFile,annot.ext=gff_file,isGTFAnnotationFile=TRUE,nthreads=8,isPairedEnd=TRUE,strandSpecific=0)
```

```
        ==========     _____ _    _ ____  _____  ______          _____
        =====         / ____| |  | |  _ \|  __ \|  ____|   /\   |  __ \
          =====      | (___ | |  | | |_) | |__) | |__     /  \  | |  | |
            ====      \___ \| |  | |  _ <|  _  /|  __|   / /\ \ | |  | |
              ====    ____) | |__| | |_) | | \ \| |____ / ____ \| |__| |
        ==========   |_____/ \____/|____/|_|  \_\______/_/    \_\_____/
       Rsubread 2.0.1

//========================== featureCounts setting ===========================\\
||                                                                            ||
||             Input files : 6 BAM files                                      ||
||                           o 3D7-WT-1-Aligned.sorted.out.bam                ||
||                           o 8181TGD-1-Aligned.sorted.out.bam               ||
||                           o 3D7-WT-2-Aligned.sorted.out.bam                ||
||                           o 8181TGD-2-Aligned.sorted.out.bam               ||
||                           o 3D7-WT-3-Aligned.sorted.out.bam                ||
||                           o 8181TGD-3-Aligned.sorted.out.bam               ||
||                                                                            ||
||              Annotation : GTF_VarRifStev_filtered_out.gtf (GTF)            ||
||      Dir for temp files : .                                                ||
||                 Threads : 8                                                ||
||                   Level : meta-feature level                               ||
||             Paired-end : yes                                               ||
||      Multimapping reads : counted                                          ||
|| Multi-overlapping reads : not counted                                      ||
||   Min overlapping bases : 1                                                ||
||                                                                            ||
||          Chimeric reads : counted                                          ||
||        Both ends mapped : not required                                     ||
||                                                                            ||
\\============================================================================//
```

```{r featurecounts no dup, cache=TRUE}
# all_fcounts <- featureCounts(files=all_targets$BamFile,annot.ext=gff_file,isGTFAnnotationFile=TRUE,nthreads=8,isPairedEnd=TRUE,strandSpecific=2,ignoreDup=TRUE)
```

Write out RPKM

```{r write RPKM}
x <- DGEList(counts=all_fcounts$counts, genes=all_fcounts$annotation[,c("GeneID","Length")])
x_rpkm <- rpkm(x,x$genes$Length)

write.csv(x_rpkm,file="all_rpkm")
```

Here follows DE analysis

```{r filter reads}
#all_isexpr <- rowSums(cpm(all_fcounts$counts) > 3) >= 3
all_isexpr <- rowSums(cpm(all_fcounts$counts) > 3) >= 1
#all_isexpr <- rowSums(cpm(all_fcounts$counts) > 0) >= 0
all_x <- all_fcounts$counts[all_isexpr,]
```

Normalization. Perform voom normalization:

```{r normalisation}
all_y <- voom(all_x,all_design,plot=TRUE)
```

Normalization. Perform voom normalization:

```{r normalisation}
all_y <- voom(all_x,all_design,plot=TRUE)
```

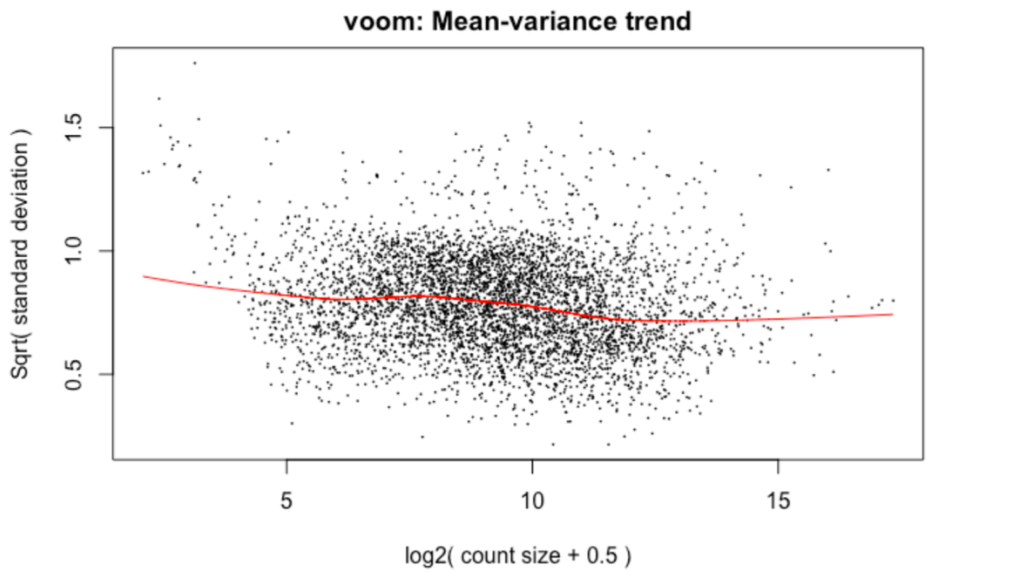

"Sample clustering. The following multi-dimensional scaling plot shows that sample A libraries are clearly separated from sample B libraries."

```{r clustering}
plotMDS(all_y,xlim=c(-5,5))
```

"Sample clustering. The following multi-dimensional scaling plot shows that sample A libraries are clearly separated from sample B libraries."

```{r clustering}
plotMDS(all_y,xlim=c(-5,5))
```

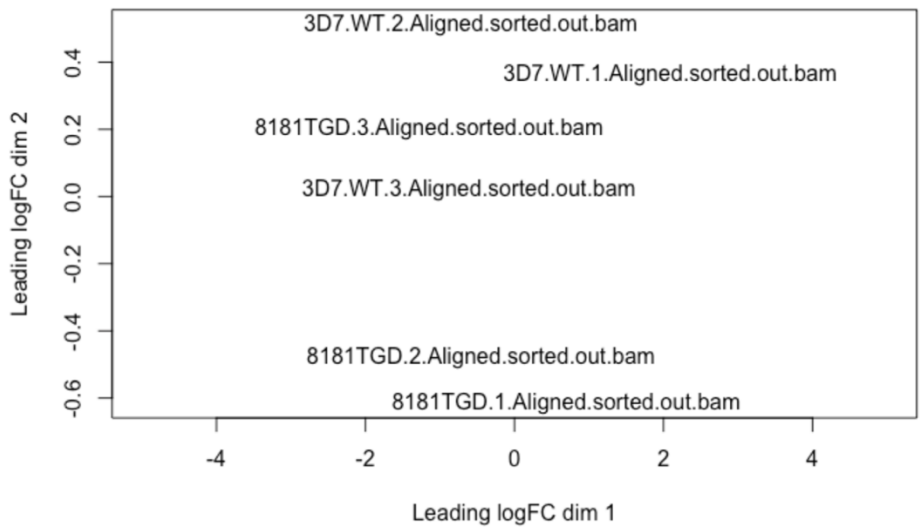


```{r DE analysis}
topTable(all_fit,coef=2)

volcanoplot(all_fit,coef=2)
```

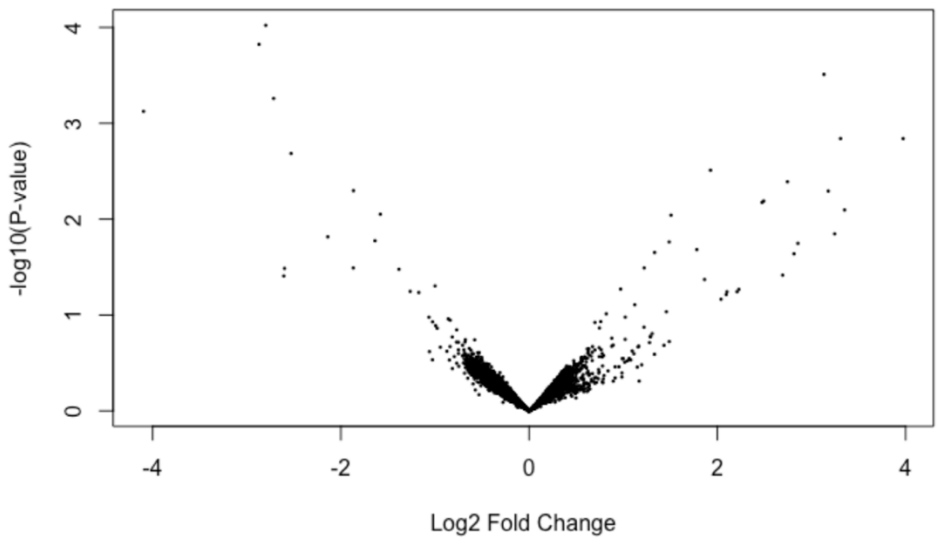

```
topTable(wt_rg_fit,coef=2,number=Inf,p.value=0.5)

topTable(a_fit,coef=2,number=Inf,p.value=1.01)
nrow(topTable(a_fit,coef=2,number=Inf,p.value=1.01))
nrow(topTable(r_fit,coef=2,number=Inf,p.value=1.01))
nrow(topTable(g_fit,coef=2,number=Inf,p.value=1.01))


a: extreme outlier -> 9.5 log(FC)
r: outlier -> 7.5 log(FC)
g: outlier -> 9 log(FC)


```{r export DE analysis}
write.csv(topTable(all_fit,coef=2,number=Inf,p.value=0.05),file="limma_out_all.sig")
```

```{r export DE analysis nodup}
write.csv(topTable(wt_rg_fit,coef=2,number=Inf,p.value=0.05),file="limma_out_wt_rg_nodup")
```
in both analyses (KO_vs_WT and by sex), makes no difference with nodup.

I also tried making p.value=1 and it's identical
```{r export full DE analysis}
write.csv(topTable(all_fit,coef=2,number=Inf,p.value=2),file="limma_out_all.full")
```
```

Appendix III: Targeting malaria parasite invasion of red blood cells as an antimalarial strategy

(co-authored review)

FEMS Microbiology Reviews, fuz005, 43, 2019, 223–238

doi: 10.1093/femsre/fuz005
Advance Access Publication Date: 11 February 2019
Review article

REVIEW ARTICLE

Targeting malaria parasite invasion of red blood cells as an antimalarial strategy

Amy L. Burns[1], Madeline G. Dans[2,3,†], Juan M. Balbin[1,†], Tania F. de Koning-Ward[3], Paul R. Gilson[2], James G. Beeson[2,4,5], Michelle J. Boyle[2,6] and Danny W. Wilson[1,2,*]

[1]Research Centre for Infectious Diseases, School of Biological Sciences, University of Adelaide, Adelaide, Australia 5005, [2]Burnet Institute, Melbourne, Victoria, Australia 3004, [3]Deakin University, School of Medicine, Waurn Ponds, Victoria, Australia 3216, [4]Central Clinical School and Department of Microbiology, Monash University 3004, [5]Department of Medicine, University of Melbourne, Australia 3052 and [6]QIMR Berghofer Medical Research Institute, Herston, Queensland, Australia 4006

*Corresponding author: Danny Wilson. Research Centre for Infectious Diseases, School of Biological Sciences, The University of Adelaide, Australia 5005. E-mail: danny.wilson@adelaide.edu.au

One sentence summary: Malaria invasion of red blood cells is an essential step in parasite replication and this review discusses targets and drug chemotypes being developed to stop invasion and growth.

†These authors contributed equally.

Editor: Christiaan van Ooij

ABSTRACT

Plasmodium spp. parasites that cause malaria disease remain a significant global-health burden. With the spread of parasites resistant to artemisinin combination therapies in Southeast Asia, there is a growing need to develop new antimalarials with novel targets. Invasion of the red blood cell by *Plasmodium* merozoites is essential for parasite survival and proliferation, thus representing an attractive target for therapeutic development. Red blood cell invasion requires a co-ordinated series of protein/protein interactions, protease cleavage events, intracellular signals, organelle release and engagement of an actin-myosin motor, which provide many potential targets for drug development. As these steps occur in the bloodstream, they are directly susceptible and exposed to drugs. A number of invasion inhibitors against a diverse range of parasite proteins involved in these different processes of invasion have been identified, with several showing potential to be optimised for improved drug-like properties. In this review, we discuss red blood cell invasion as a drug target and highlight a number of approaches for developing antimalarials with invasion inhibitory activity to use in future combination therapies.

Keywords: malaria; merozoites; invasion; antimalarial(s); *P. falciparum*; *P. vivax*

INTRODUCTION

Malaria is a mosquito borne disease caused by parasites of the genus *Plasmodium*. The majority of the ~445 000 malaria related deaths in 2016 were caused by *P. falciparum* and occurred in sub-Saharan Africa (Murray *et al.* 2014; WHO 2017). In addition, *P. vivax*, *P. malariae*, *P. ovale* (comprised of two different subspecies; *P. ovale curtisi* and *P. ovale wallikeri* (Sutherland

Received: 8 December 2018; **Accepted:** 11 February 2019

et al. 2010)) and two zoonotic species, *P. knowlesi* and *P. simium* (Singh *et al.* 2004; Brasil *et al.* 2017), are recognised as significant contributors to global malaria disease burden. While intervention against *Anopheles* mosquito vectors and the success of artemisinin-based combination therapies have contributed to marked decreases in disease burden since the year 2000, there is growing concern regarding the spread of *P. falciparum* strains throughout Southeast Asia which are resistant to artemisinin-based drugs and their partner drugs utilized in combination therapies (Dondorp *et al.* 2009; Ariey *et al.* 2014; Ashley *et al.* 2014; Tun *et al.* 2015; Das *et al.* 2018). Resistance to other clinically used antimalarials, such as chloroquine and sulfadoxine-pyrimethamine, is also widespread globally (Plowe *et al.* 1997; Trape *et al.* 1998; Mehlotra *et al.* 2001). Thus, there is an urgent need to bring to market new antimalarials with novel mechanisms of action which are active against all drug-resistant strains, effective against all human pathogenic *Plasmodium* spp. and can clear parasitemia rapidly for improved clinical outcomes (Burrows *et al.* 2017). Targeting multiple lifecycle stages would improve the effectiveness of combination therapies across endemic areas and help slow the development of drug resistance.

Human infections begin with the bite of a mosquito vector and release of malaria sporozoites, with the sporozoite then traveling to the liver and invading hepatocytes (reviewed in Aly, Vaughan and Kappe 2009). After rapid multiplication of liver stage parasites, the mature hepatic schizont ruptures and releases red blood cell (RBC) invading merozoites into the blood stream. In the case of *P. falciparum*, after merozoite invasion of a RBC a 48 hour cycle of growth, multiplication, RBC rupture and release of 16–32 new merozoites ensues (reviewed in White *et al.* 2014). The number of merozoites produced per cycle of growth and the length of the blood stage lifecycle varies between human malaria species. A small portion of blood stage parasites (<1%) differentiate into sexual stage gametocytes, which are transmitted to *Anopheles* vectors during blood meal feeding (reviewed in Liu, Miao and Cui 2011).

As all malaria pathology is caused by blood stage parasites, and this is when infection is diagnosed and clinical symptoms occur, antimalarials used for treatment of clinical disease or clearance of parasitemia predominantly target this stage of the lifecycle. One emerging strategy to kill blood stage parasites is to target merozoite invasion of the RBC with antimalarials. RBC invasion is an extracellular step in the blood stage lifecycle which is essential for parasite proliferation. A model for the sequential process of invasion, from late stage merozoite development, priming of invasion ligands, merozoite release from the schizont (Fig. 1), through RBC contact and invasion (Fig. 2), is described: briefly (i) merozoites attach to the RBC, (ii) the apical tip of the egg-shaped merozoite contacts the RBC, (iii) invasion ligands from organelles situated at the apical tip (the rhoptry and micronemes) are secreted upon calcium signals and an irreversible interaction known as the tight junction is formed, (iv) the actin-myosin invasion motor engages, protease cleavage events are triggered as the RBC membrane is pulled around the parasite to form the parasitophorous vacuole and (v) the invasion pore is fused behind the invaded parasite (Dvorak *et al.* 1975; Gilson and Crabb 2009; Weiss *et al.* 2015). An important consideration in terms of drug-development is that RBC invasion requires a series of co-ordinated and often irreversible events to occur in sequence, with even small perturbations of this complex process likely to limit parasite survival *in vivo*.

RBC invasion is the essential first step in the disease causing blood stage of the lifecycle and the extracellular merozoite is exposed directly to the bloodstream. Vaccine development targeting merozoite invasion is well advanced with vaccines against merozoite surface protein 1 (MSP1, Phase 2b; Genton *et al.* 2003; Ogutu *et al.* 2009), MSP2 (Phase 2b; Genton *et al.* 2003), apical membrane antigen 1 (AMA1, Phase 2b; Thera *et al.* 2011), reticulocyte binding homologue 5 (Rh5, Phase 1a; Payne *et al.* 2017), erythrocyte binding antigen (EBA-175, Phase 1a; Koram *et al.* 2016) and others reaching clinical trials, but with limited efficacy demonstrated to date (reviewed in Draper *et al.* 2015; Beeson *et al.* 2016). However, many essential proteins and protein/protein interactions required for invasion are unique to malaria parasites and are highly conserved between isolates, making them strong targets for antimalarial development. Given this, there are several broad approaches that could be used therapeutically to block merozoite invasion. The importance of key parasite-parasite and parasite-RBC protein interactions on the merozoite surface highlights the possibility of blocking protein-protein interactions directly; potentially by targeting RBC receptor(s). In addition, protease cleavage events, calcium signalling, the action of the invasion motor and structural changes are also key processes in RBC invasion which could be targeted by drugs. Importantly, a drug that blocks a merozoite's ability to invade immediately and permanently ends the parasite's lifecycle, with this cidal activity potentially having benefits in terms of reducing the risk of tolerance leading to resistance and removing the parasites ability to transition to mosquito transmissible gametocytes. However, it has only been in recent years that protocols have been developed to test invasion-inhibitory compounds against *P. falciparum* merozoites directly *in vitro*), with the availability of these techniques now allowing improved screening and characterisation of new invasion-inhibitory chemotypes.

This review will give an overview on compounds that inhibit invasion, either through inhibition of an upstream invasion priming event in the developing schizont (Fig. 1) or during the merozoite invasion process (Fig. 2), that have shown potential to be developed into antimalarial drugs. Targeting RBC invasion has been established as a proof-of-concept through the demonstration of potent inhibitory activity of numerous compounds *in vitro* (summarised in Supplementary Table S1) and through several *in vivo* studies using animal models (Xiao *et al.* 1996; Zenonos *et al.* 2015; Nasamu *et al.* 2017; Pino *et al.* 2017). Numerous chemical starting points and targets have been identified that could be the basis for the development of potent inhibitors for therapeutic use, as described below. We compare this concept to the clinical use of inhibitors which block HIV entry into host cells (Barre-Sinoussi *et al.* 1983; Gallo *et al.* 1983) to demonstrate that RBC invasion is a viable therapeutic target. In addition, we consider studies from the related apicomplexan parasite *Toxoplasma gondii*, for which a number of optimisable inhibitors have been developed against targets analogous to proteins in malaria parasites. As resistance to frontline artemisinin-based combination therapies continues to spread (Dondorp *et al.* 2009; Ariey *et al.* 2014; Ashley *et al.* 2014), this review is a timely reminder that malaria invasion of RBCs provides an 'Achilles heel' within the parasite's lifecycle that is of increasing interest for antimalarial development.

VIRAL ENTRY INHIBITORS AS A MODEL FOR DEVELOPMENT OF RBC INVASION-INHIBITORY ANTIMALARIALS

Viruses are highly successful and widespread lifeforms that require establishment of an infection inside a host cell in order

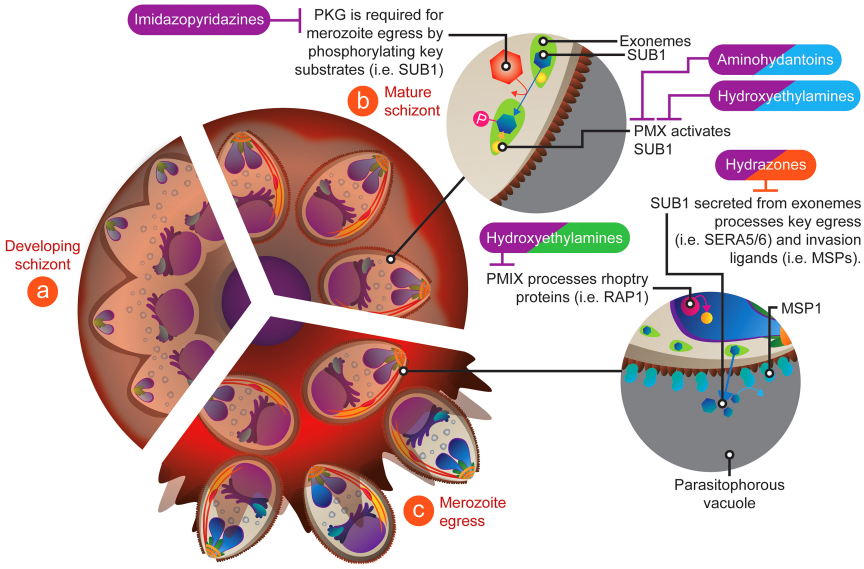

Figure 1. Druggable targets during merozoite development where inhibitors block downstream invasion of the RBC. **(a)** Late stage merozoite development showing partial formation of merozoite membranes and invasion organelles. **(b)** Merozoite formation is completed in mature schizonts. The PVM becomes permeable and PfPKG is activated, leading to activation and discharge of subtilisin-like protease 1 (PfSUB1) from the exonemes. The protease Plasmepsin X (PMX) also resides in the exonemes and is required to process PfSUB1 into an active form. **(c)** Cleavage of PfSUB1 by exoneme resident Plasmepsin X leads to activation of the egress regulating papain-like proteases SERA5 and SERA6, with loss of SERA 5/6 activity preventing merozoite egress from schizonts. Release and activation of PfSUB1 also leads to the cleavage of a number of merozoite invasion ligands including MSP1, MSP6, MSP7, AMA1, with the rhoptry antigen RAP1 processed by Plasmepsin IX (PMIX). Whilst these ligands are largely not required until merozoite contact with the RBC and invasion commences (see Fig. 2), inhibition of these cleavage events around schizont egress is associated with loss of invasion. Inhibitors have been labelled using a dual-colour system that allows their activity against merozoite development/egress (this figure) and their latter effects against invasion (Fig. 2) to be highlighted for inhibitors of: PMIX (purple/green), PMX (purple/blue), PfSUB1 (purple/orange).

to replicate. As a consequence, the essential step of viral entry into the host cell has been targeted by peptide/protein mimics and small molecule entry inhibitors for a diverse range of viruses including HIV (Kilby *et al.* 1998; Dorr *et al.* 2005), orthomyxoviruses (Malakhov *et al.* 2006), flaviviruses (Wang *et al.* 2009), paramyxoviruses (Lambert *et al.* 1996; Rapaport *et al.* 1995), filoviruses (Watanabe *et al.* 2000) and coronaviruses (Bosch *et al.* 2003). The three-step process of viral entry, consisting of attachment, co-receptor binding, and fusion, precedes release of the viral genome into the host's cytoplasm where new virions are assembled before budding and release of the virions from the cell.

HIV entry into memory CD4 + T-lymphocytes (Klatzmann *et al.* 1984; Ho *et al.* 1995) is reliant on a very small number of viral-protein/host-protein interactions and protease cleavage events. Similar to malaria RBC invasion, HIV cell-entry is orchestrated by a multi-step process and is completed within a fraction of the total viral generation time (defined as time between virion release, infection of a new host cell and generation of daughter viral particles (excluding viral latency), estimated between 48 and 63 hours (2.0–2.6 days) (Dixit *et al.* 2004; Murray, Kelleher and Cooper 2011; Puller, Neher and Albert 2017)). Host cell entry begins with virion attachment, binding to the host's co-receptor and entry; with inhibitors, both clinically approved and in development, identified to target each step (reviewed in Kuritzkes 2009; Henrich and Kuritzkes 2013). Maraviroc, the first licenced chemokine receptor antagonist and first host targeting antiretroviral drug, specifically inhibits entry of HIV isolates by binding to the host cell receptor, C-C chemokine receptor type 5 (CCR5), one of two chemokine receptors that HIV viruses use for entry into the cell (Dorr *et al.* 2005; Wood and Armour 2005). Maraviroc specifically inhibits the entry of CCR5-tropic (R5) viruses and is routinely used in second-line antiretroviral combination therapies against R5 HIV viruses (reviewed in Perry 2010).

After binding of the host cell receptors CCR5 or CXCR4 (CXC chemokine receptor type 4), a conformational change occurs within the virion membrane which exposes the heptad repeat domains on viral envelope glycoprotein gp41 (heptad repeat 1 (HR1) and HR2) (reviewed in Klasse 2012). Enfuvirtide, the first antiretroviral fusion-inhibitor approved for HIV treatment, is a 36-amino acid synthetic peptide that mimics the HR2 region of gp41 that binds to HR1, preventing the formation of the six-helix gp41 bundle that is critical for viral fusion and entry (Kilby *et al.* 1998). Enfuvirtide is typically active against HIV-1 isolates that are resistant to other classes of antiretroviral drugs and is reserved for second-line combination therapies of advanced stage HIV infections (Kitchen *et al.* 2008).

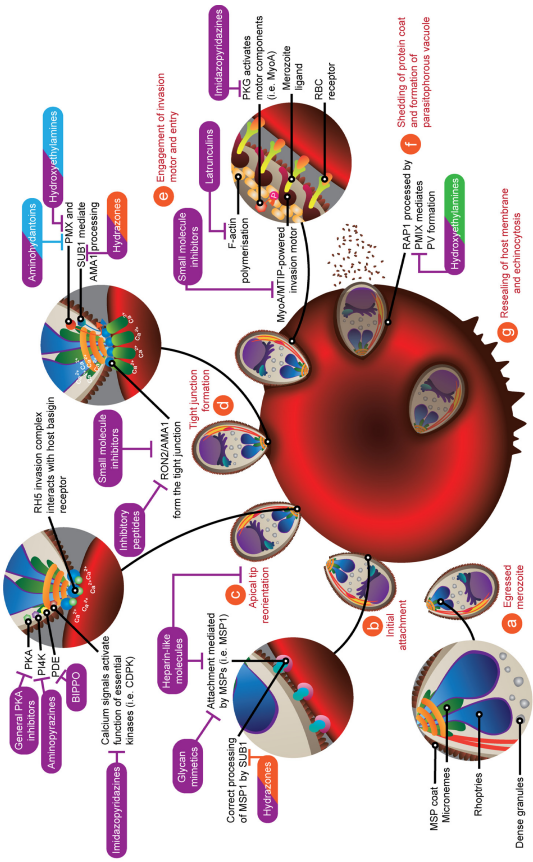

Figure 2. Malaria merozoite invasion of the RBC and invasion inhibitors. (**a**) Merozoites are released into the blood stream after rupture of schizonts (mature blood stage parasites), ready to invade new RBCs. (**b**) Initial attachment requires low-affinity interactions between the surface coat of MSPs, and host receptors on the surface of the RBC. (**c**) Merozoites reorientate such that the apical tip binds to the surface of the RBC and invasion ligands are secreted from the apical tip organelles, the rhoptries and microneme. The rhoptry antigen PfRH5 binds to its RBC receptor basigin in a key early interaction required for merozoite invasion. (**d**) An irreversible tight-junction is formed when the microneme-secreted protein AMA1 binds to the rhoptry neck protein complex that is embedded on the RBC membrane. (**e**) Entry of the parasite is powered by an actin-myosin motor that pulls the RBC around the invading merozoite while (**f**) the surface coat of MSPs is simultaneously shed. Calcium signalling and phosphorylation by kinases are thought to play a key role in controlling the sequence of events required for invasion during this period. The vacuole membrane fuses behind the invading parasite forming a parasitophorous vacuole. (**g**) Shortly after internalization, a large proportion of RBCs temporarily distort in a process known as echinocytosis. It has been postulated that echinocytosis is caused by rhoptry secretion and rapid entry of Ca^{2+} discharged from the rhoptries into the RBC during invasion, but a more recent explanation suggests that it is incorporation of parasite rhoptry contents into the RBC membrane which leads to RBC membrane ruffling (Dvorak *et al.* 1975; Gilson and Crabb 2009). Examples of drug inhibitors which act at certain stages of the invasion process are labelled in purple. Labels with two colours indicate the inhibitor also has activity around merozoite egress (see Fig. 1).

Although the cellular targets and kinetics of HIV entry into CD4 + T-lymphocytes differ to the requirements of *Plasmodium* invasion into RBCs, these examples of clinically used HIV entry inhibitors for treatment of disease provide an informative comparison for considering the development of antimalarial drugs that target RBC invasion.

PLASMODIUM INVASION INHIBITORS AND PROSPECTS FOR DEVELOPMENT

The majority of current antimalarials target the blood stage of the lifecycle and work through various targets such as; (i) the parasites intracellular food vacuole (chloroquine, artemisinin)(Fidock *et al.* 2000; Klonis *et al.* 2011), (ii) DNA replication (pyrimethamine)(Cowman *et al.* 1988), (iii) mitochondrion function (atovaquone (Fry and Pudney 1992) and proguanil (Dickerman *et al.* 2016)) or, (iv) the apicoplast, the parasite's remnant plastid organelle (doxycycline, azithromycin, clindamycin) (Dahl and Rosenthal 2007; Goodman, Su and McFadden 2007). Currently, no clinically used antimalarial has activity against RBC invasion (Wilson *et al.* 2013), except azithromycin when used at higher concentrations (Wilson *et al.* 2015).

In vitro live-cell filming of *P. falciparum* has shown that RBC invasion, from formation of the tight junction to completion of RBC entry, generally takes less than 1 min (Gilson and Crabb 2009). However, the time taken for a merozoite to commence invasion after egress from a schizont is variable, with one study finding that it took 10 min for 80% of invasion events to be completed *in vitro*. Depending on the drug target, key processes required for RBC invasion could be susceptible to an antimalarial during merozoite development and schizont egress (Fig. 1a–c) or during the process of invasion itself (Fig. 2a–g). To be clinically useful, invasion-inhibitory drugs would need to have a long half-life so that the drug can be maintained in the blood at a high enough level to inhibit invasion as it occurs. A drug with a very short half-life (i.e. artesunate has a half-life of < 30 minutes; Dondorp *et al.* 2009) would not be suitable. Of interest, the half-life of the HIV entry inhibitor maraviroc is ~16 hours (Perry 2010). The myriad of essential and unique targets required to work in a coordinated fashion to enable the rapid process of invasion, combined with the sensitivity of the invasion process to perturbation, provides a promising avenue for new antimalarial development. In this review, we highlight several essential processes targeted in invasion-inhibitory drug development (Figs 1 and 2) and outline some of the compounds that have been tested to date (Supplementary Table S1).

Inhibition of MSPs and RBC receptors using glycan derivatives

Heparin like molecules as invasion inhibitors

Heparin, a member of the glycosaminoglycan family, is a known inhibitor of RBC invasion (Butcher, Parish and Cowden 1988; Boyle *et al.* 2017). A diversity of other sulfated carbohydrates and heparin-like-molecules (HLMs) have also been identified to inhibit invasion of *P. falciparum* merozoites, including curdlan sulfate (Havlik, Rovelli and Kaneko 1994; Evans *et al.* 1998), polyvinyl-sulfonate sodium salt (Kisilevsky *et al.* 2002), suramin (Fleck *et al.* 2003), carrageenans (Adams *et al.* 2005), sulfated cyclodextrins (Crandall *et al.* 2007), fucosylated chondroitin sulfate (Bastos *et al.* 2014), K5 polysaccharides (Boyle *et al.* 2010), inulin sulfate, xylan sulfate, tragacanth sulfate and scleroglucan sulfate (Boyle *et al.* 2017). Furthermore, HLM invasion-inhibitory activity has also been reported for the zoonotic malaria parasite *P. knowlesi* (Lyth *et al.* 2018) and *P. berghei* (Xiao *et al.* 1996), indicating that pan-species invasion inhibition of human malaria parasites is achievable with these molecules. Although precise mechanisms of action for sulfated carbohydrates in inhibiting invasion are not fully understood, HLMs have been reported to inhibit the earliest step in invasion, initial RBC attachment, and to bind MSP1 (Boyle *et al.* 2010), as well as to rhoptry and microneme proteins involved in reorientation and signalling steps of invasion (Fig. 2a-c) (Baum *et al.* 2009; Kobayashi *et al.* 2010; Kobayashi *et al.* 2013). Therefore, it is likely that these compounds target multiple essential ligands in the invasion process, thus reducing the potential for developing drug resistance. Indeed, attempts to generate heparin resistant parasite strains *in vitro* have been unsuccessful (Boyle *et al.* 2010). Although limited studies have been performed to evaluate the activity of HLMs *in vivo*, there is data from animal models (Xiao *et al.* 1996) and human clinical trials supporting their potential development (Havlik *et al.* 2005; Leitgeb *et al.* 2017).

Heparin has been historically used as an adjunct treatment for disseminated intravascular coagulation that can occur in severe malaria (Smitskamp and Wolthuis 1971; Munir *et al.* 1980; Rampengan 1991), but its use was stopped because its anticoagulative properties led to an increased risk of bleeding. Recently, heparins with periodate oxidation of non-sulfated uronic acid residues that greatly reduced anticoagulation activity of heparin (Pisano *et al.* 2005) were shown to be highly inhibitory to RBC invasion (Boyle *et al.* 2017). Similar HLMs have been tested for inhibition of lung cancer growth in mice with no anticoagulation activity reported across a range of tissue (Yu *et al.* 2010). Of further promise, curdlan sulfate (Boyle *et al.* 2010) has a 10-fold reduced anticoagulative activity and testing in a small human trial suggested that treatment reduced malaria disease severity (Havlik *et al.* 2005). A recent phase I clinical trial of the non-anticoagulant HLM sevuparin, a negatively charged polysaccharide manufactured from heparin, limited parasite replication by blocking invasion (Leitgeb *et al.* 2017). HLMs such as sevuparin also disrupt pathogenic mediators such as rosetting and sequestration of infected RBCs, (Udomsangpetch *et al.* 1989; Carlson *et al.* 1992; Rowe *et al.* 1994; Barragan *et al.* 1999; Vogt *et al.* 2006; Kyriacou *et al.* 2007; Skidmore *et al.* 2008; Bastos *et al.* 2014; Saiwaew *et al.* 2017), potentially enabling HLMs to provide dual protective mechanisms of action against severe malaria. Current HLMs that have been identified with antimalarial activity have relatively low potency (Boyle *et al.* 2017) and they have also been reported to have relatively short half-lives when used clinically (i.e. heparin < 1 hour (Perry, Herron and King 1974), sevuparin ~1 hour (Leitgeb *et al.* 2017), curdlan sulfate ~2–3 hours (Gordon *et al.* 1994)). However, the clinically used HLM fondaparinux has a longer half-life (17–21 hours)(Donat *et al.* 2002). Work on improving oral availability of heparin derivatives (reviewed in Neves *et al.* 2016), as well as prolonging HLM drug activity and potency (Hoffart *et al.* 2006; Boyle *et al.* 2017) are ongoing and offer an avenue for HLMs to be developed as antimalarials with invasion-inhibitory activity.

Targeting MSP 1 using glycan mimetics

Initial interactions between the merozoite and the RBC membrane are low affinity, reversible and can occur irrespective of the parasite's orientation. These interactions are mediated by glycosylphosphatidyl inositol (GPI) anchored proteins present on the merozoite's surface (Holder *et al.* 1992; Gilson *et al.* 2006). MSP1 is the most abundant GPI anchored protein on the merozoite surface (Gilson *et al.* 2006) and the proteolytic cleavage of MSP1 to

83 kDa, 30 kDa, 38 kDa and 42 kDa fragments is essential for RBC invasion (Blackman and Holder 1992). The N-terminal MSP1–83 fragment binds to the RBC receptor glycophorin A and the C-terminal MSP1–42 fragment has a role in binding to band-3 on the RBC surface. (Baldwin *et al.* 2015).

The 19 kDa C-terminal cysteine rich epidermal growth factor (EGF)-like domain of MSP-1 is formed after secondary cleavage of MSP1–42 and this essential proteolytic event has been investigated as a potential vaccine and drug target (Goel *et al.* 2003). Testing of EGF domain inhibitors with anticancer properties against MSP1–19 identified a small-molecule glycan mimetic, 2-butyl-5-chloro-3-(4-nitro-benzyl)-3H-imidazole-4-carbaldehyde (NIC), as a specific inhibitor of MSP1–19 function and parasite invasion (Fig. 2b, c) (Chandramohanadas *et al.* 2014). The invasion-inhibitory activity of NIC was confirmed using live filming of invasion and through the use of purified merozoites. NIC not only inhibited the growth of *P. falciparum* isolates, it also inhibited *P. falciparum* expressing *P. chabaudi* rodent malaria MSP1–19 and *P. vivax* field isolates, with IC_{50}s ~20 μM; indicating the pan-species potential of these molecules against malaria parasite invasion. The authors highlight the possibility of targeting the EGF domain of MSP1–19 using small molecule glycans that are being developed as anti-cancer agents (Fig. 2b) (Sugahara *et al.* 2012), but to date no examples of this have been published and further development of this strategy would be required before clinical applications could be assessed. A potential advantage of developing inhibitors that target MSPs, such as HLMs and glycan mimetics, is that they can target merozoites throughout their extracellular phase; post release from schizonts through to resealing of the parasitophorous vacuole membrane.

Small molecule inhibitors of the tight junction that forms between AMA 1 and the RON protein complex

After binding to the RBC and apical re-orientation, the invading merozoite releases proteins residing within specialised apical secretory organelles, the micronemes and rhoptries, to establish an irreversible zone of attachment called the tight junction (Aikawa *et al.* 1978; Bannister and Mitchell 1989). This tight junction is formed as a result of AMA1 (secreted from the micronemes) binding to the RBC bound rhoptry neck (RON) 2/4/5 (secreted from the rhoptries) protein complex (Alexander *et al.* 2006; Collins *et al.* 2009; Richard *et al.* 2010; Tonkin *et al.* 2011), with a known high affinity interaction demonstrated between AMA1 and RON2 (Srinivasan *et al.* 2011; Tonkin *et al.* 2011). The essential interaction between AMA1 and RON2 has been targeted by vaccine induced antibodies (Hodder, Crewther and Anders 2001; Kennedy *et al.* 2002), inhibitory peptides (Harris *et al.* 2005) and drug development (reviewed in Devine *et al.* 2017) (Fig. 2d). A phase 2b vaccine trial of children in Mali demonstrated high anti-AMA1 antibody titres and protection against clinical malaria caused by parasites harbouring vaccine-like alleles after 6 months, but there was minimal efficacy against clinical malaria overall, highlighting the difficulties with targeting a polymorphic antigen such as AMA1 (Thera *et al.* 2011). However, recent studies report substantial conservation of AMA1 function between species, providing evidence that generating cross-species inhibitory activity may be possible (Drew *et al.* 2018).

Several invasion-inhibitory peptides that target AMA1/RON2 binding have been developed. The 20-amino acid R1 peptide, identified from a random phage display library (Harris *et al.* 2005), exhibits high binding affinity for the 3D7 parasite line AMA1/RON2 complex (KD_{50} ~0.2 μM) (Harris *et al.* 2005). RON2L mimics a conserved peptide region of RON2 and competes with native RON2 for the hydrophobic binding pocket of AMA1, blocking formation of the tight junction and inhibiting RBC invasion (Srinivasan *et al.* 2011). Making use of the high binding affinity of peptides that block AMA1/RON2 interactions, a RON2L(peptide)/AMA1 binding inhibition assay was used to screen 21 733 small-molecule inhibitors for activity against AMA1/RON2 (Srinivasan *et al.* 2013), with three hits suggested to directly inhibit RBC invasion. Modification of the lead compound, NCHC00015280 (a pyrrolopyrimidine; IC_{50} 30 μM), yielded two analogues that showed a three (9.8 μM) and five (6 μM) fold improvement in invasion inhibition (Srinivasan *et al.* 2013). However, subsequent studies failed to show binding of these compounds to AMA1 with an affinity commensurate with their reported growth inhibitory activity (Devine *et al.* 2014; Pihan *et al.* 2015), leading Devine *et al.* (2014) to conclude that these compounds inhibited invasion through an AMA1/RON2 independent manner. Nevertheless, the essential role of the AMA1/RON2 complex for invasion, the availability of complete protein structures for *in silico* screening and optimisation makes inhibitors of AMA1/RON2 complex function an attractive target for further development.

The actin-myosin invasion motor as an invasion-inhibitory target

After formation of the tight junction, the actin-myosin motor is engaged and the RBC membrane is pulled around the merozoite via treadmilling of short actin filaments (F-actin) which are pulled unidirectionally. Invasion is powered by a myosin motor complex embedded in the merozoite's pellicle (inner membrane complex; Fig. 2e) (Soldati, Foth and Cowman 2004) (reviewed in Tardieux and Baum 2016). Given the importance and complexity of the actin-myosin motor, a number of targets have been investigated for antimalarial development.

Inhibitors of actin dynamics as invasion-inhibitory drugs

A number of natural agents, such as cytochalasins (a fungal alkaloid) and latrunculins (from marine sponges) have been reported to disrupt actin polymerisation dynamics and ultimately arrest RBC invasion (Fig. 2e) (Miller *et al.* 1979; Cooper 1987; Johnson *et al.* 2016). Latrunculins bind to actin's monomeric form (G-actin) near the Adenosine Triphosphate (ATP) binding site and prevent polymerisation to filamentous actin (F-actin). A recent study identified key amino acid differences between human and *Plasmodium* spp. actin within the ATP binding pocket and sought to synthesise truncated latrunculin B analogues with improved activity against *P. falciparum* malaria and reduced toxicity against mammalian cells (Johnson *et al.* 2016). Truncated latrunculin analogues achieved a 6-fold improved potency against *in vitro* parasite growth (to 7 μM) and 17-fold higher selectivity over mammalian cell cytotoxicity (Johnson *et al.* 2016). To address whether these analogues had activity directly against parasite invasion, the authors used *T. gondii* invasion inhibition assays since this related apicomplexan parasite shares an identical amino acid sequence around the actin ATP binding pocket as *P. falciparum* (Johnson *et al.* 2016). Lead latrunculin analogues showed a >5-fold improvement in invasion-inhibitory activity against *T. gondii* (to 16 μM), indicating that latrunculin analogues target parasite actin during invasion and that activity against apicomplexan parasites is likely to be conserved (Johnson *et al.*

2016). But the high IC_{50}s of these compounds against both parasites highlights that further development is needed.

Inhibitors of the myosin A/MTIP complex

Myosin A (MyoA) is the F-actin bound motor that powers apicomplexan gliding motility during invasion (Meissner, Schluter and Soldati 2002)(Fig. 2e). The ATP-powered protomotive movement of MyoA is dependent on a conserved complex between MyoA's C-terminal domain and the conserved N-terminal domain of MyoA tail interacting protein (MTIP, called myosin light chain 1 (MLC1) in *T. gondii*) (Bosch *et al.* 2006, 2007). Not only is the interaction between MyoA and MTIP essential for parasite invasion of the RBC, but structural characterisation has also identified distinct differences between *Plasmodium* spp. and human homologs, thus presenting a viable target for drug development (Bosch *et al.* 2006).

Modelling of the interaction between MTIP and a growth inhibitory 15-amino acid C-terminal MyoA peptide (Bosch *et al.* 2006) was used to identify small molecule MTIP/MyoA binding inhibitors in a library of 300 000 compounds (Kortagere 2010). A pyrazole-urea based compound (C416) demonstrated the best growth inhibitory activity (IC_{50} of 0.145 μM) (Kortagere 2010) and further structure-based screening identified several analogues with improved activity over the original peptide (C2–1 IC_{50} 0.047 μM; C3–21 IC_{50} 0.385 μM). C3–21 was investigated further and was found to inhibit gliding motility of mosquito stage sporozoites, a marker assay for actin-myosin based motor function that is shared between sporozoites and RBC invading merozoites (Kortagere 2010). Comparative analysis identified that some compounds inhibited growth of both *P. falciparum* and *T. gondii*, thus suggesting a conserved target between the two divergent parasites. However, many analogues also showed variation in efficacy between *P. falciparum* and *T. gondii*, suggesting structural differences between the MyoA/MTIP interaction can be sufficient to reduce efficacy against different apicomplexan parasites (Kortagere 2010; Kortagere *et al.* 2011).

Another high-throughput screen of 12,160 non-cytotoxic compounds against *T. gondii* tachyzoite host cell invasion identified 21 compounds that inhibited parasite motility (Carey *et al.* 2004). One of these hits, tachyplegin A, was found to covalently bind to TgMLC1 (MTIP in *Plasmodium* spp.) and the resulting post-translational modifications caused loss of MyoA function and inability to drive the invasion motor (Carey *et al.* 2004; Heaslip 2010; Leung *et al.* 2014). These studies have identified a diverse range of chemical scaffolds that inhibit function of the MTIP/MyoA driven invasion motor, a conserved complex that is essential for RBC invasion of apicomplexan parasites.

Inhibitors of protease cleavage events required for RBC invasion

Invasion requires a co-ordinated series of proteolytic cleavage events to enable the correct function of essential proteins. The essential role of serine proteases in schizont rupture and RBC invasion have seen them become a significant target of invasion inhibitor drug development (reviewed in O'Donnell and Blackman 2005). The *P. falciparum* subtilisin proteases PfSUB1 (Blackman *et al.* 1998; Yeoh *et al.* 2007) and PfSUB2 are bacterial-like enzymes that have received significant interest because of the key role they play in the essential processing of proteins required for RBC invasion (Figs. 1 and 2) (Supplementary Table S1). PfSUB1 has been shown to cleave MSPs (MSP1, MSP6 and MSP7), invasion ligands released from the micronemes (AMA1) and rhoptry (RAP1) (Yeoh *et al.* 2007; Koussis *et al.* 2009; Silmon de Monerri *et al.* 2011) and is involved in priming the proteolytic cascade that leads to schizont rupture and merozoite egress (Fig. 1c)(Yeoh *et al.* 2007). Comparison of the stage-specific efficacy of the PfSUB1 inhibitor MRT12113 indicates that the IC_{50} against *P. falciparum in vitro* invasion inhibition (~25 μM) was lower than that for schizont rupture inhibition (~180 μM) (Yeoh *et al.* 2007), highlighting the potential sensitivity of the invasion process to chemical inhibition compared to other stages of blood stage development. Interestingly, a follow-up study identified that even partial inhibition of MSP1 processing at invasion inhibitory concentrations of MRT12113 was associated with invasion inhibition, indicating the sensitivity of the invasion process to chemical inhibition (Koussis *et al.* 2009). More recent studies have begun to optimise inhibitors of PfSUB1 from a range of chemical scaffolds (Gemma *et al.* 2012; Bouillon *et al.* 2013; Giovani *et al.* 2014; Kher *et al.* 2014). *Plasmodium* spp. SUB1 are highly conserved and trials using recombinant proteins suggest that 'pan-species' inhibitors can be developed that target the SUB1 of multiple species (Withers-Martinez *et al.* 2012). Indeed, an *in silico* screen using a 3D homology model of PvSUB1 led to the discovery of Cpd2, a compound that inhibits the activity of both recombinant PvSUB1 and PfSUB1 (Bouillon *et al.* 2013). Furthermore, Cpd2 had an *in vitro* IC_{50} of 0.37 μM against *P. falciparum* parasites and inhibited growth of *P. berghei* rodent malaria parasites in a dose-dependent manner, highlighting the pan-species potential of SUB1 inhibitors (Bouillon *et al.* 2013).

Recently its been demonstrated that the aspartic proteases Plasmepsin IX and X (Nasamu *et al.* 2017; Pino *et al.* 2017) have key roles in RBC invasion (Fig. 2d, f) and invasion/egress (Fig. 1b, c), respectively. Plasmepsin IX is located in the rhoptry organelle in merozoites and loss of this protease causes aberrant rhoptry formation and prevents cleavage of key invasion ligands (Nasamu *et al.* 2017; Pino *et al.* 2017). Plasmepsin X is located in merozoite exonemes (secreted from the merozoite prior to rupture) and is involved in activating SUB1 (essential for invasion and schizont rupture), as well as directly processing ligands excreted from the microneme (Nasamu *et al.* 2017; Pino *et al.* 2017). The activity of Plasmepsin IX and X was effectively inhibited by the hydroxylethylamine aspartic protease inhibitor 49c (Ciana *et al.* 2013) at low nanomolar concentrations, providing evidence that both essential proteases can be targeted by one drug (Pino *et al.* 2017). Furthermore, 49c was effective in a *P. berghei* rodent model of malaria against multiple life-cycle stages, including liver stage parasites and gametocytes (Pino *et al.* 2017). Recombinant Plasmepsin X was found to be inhibited by the orally bioavailable aminohydantoins (Meyers *et al.* 2014; Nasamu *et al.* 2017). Further investigation revealed the aminohydantoins inhibited *P. falciparum* growth *in vitro* at submicromolar concentrations and growth of *P. chabaudi* rodent malaria parasites *in vivo*, providing a second starting point for drug development against Plasmepsin X (Meyers *et al.* 2014; Nasamu *et al.* 2017). Since 49c is a potent inhibitor of Plasmepsin IX (rhoptry biogenesis and invasion ligand processing) and both 49c/aminohydantoins inhibit Plasmepsin X function (activation of the egress/invasion priming PfSUB1, invasion ligand processing), both chemical starting points offer activity against merozoite egress and invasion (Nasamu *et al.* 2017; Pino *et al.* 2017).

Inhibitors of malaria merozoite intracellular signalling

The targeting of cellular signal transduction pathways has successfully been used to treat non-infectious diseases such as cancer and autoimmune diseases (Aggarwal *et al.* 2007; Croce

et al. 2016; Marciano and Holland 2017) and is now of increasing interest for antimalarial development. One leading drug target involved in signalling during RBC invasion is calcium dependent protein kinase 1 (CDPK1), a parasite kinase not present in the human host (Harper and Harmon 2005) that has key roles in microneme secretion, activation of the actin-myosin motor and other processes required for RBC invasion (Fig. 2b-e) (Green et al. 2008; Bansal et al. 2013; Bansal et al. 2018). PfCDPK1 has been targeted in several high throughput screens (HTS) of compound libraries (Green et al. 2008; Kato et al. 2008; Lemercier et al. 2009; Chapman et al. 2013; Ansell et al. 2014; Chapman et al. 2014). 2,6,9 trisubstituted purines such as purfalcamine inhibited *P. falciparum* parasite growth (IC_{50} of 230 nM) as well as host cell invasion of related *T. gondii* tachyzoites, consistent with a CDPK in *T. gondii* having a key role in invasion (Kato et al. 2008; Lourido et al. 2010; Kumar et al. 2017). However, purfalcamine was unsuccessful in clearing *P. yoelii* rodent malaria parasites *in vivo*, possibly due to poor pharmacokinetics and reduced efficacy against PyCDPK1 (Kato et al. 2008). A second screen identified 3,6-disubstituted imidazopyridazines as compounds of interest, with modification of early leads reducing the growth inhibitory IC_{50} to < 100 nM and providing superior pharmacokinetics to the initial hit compounds (Chapman et al. 2013; Chapman et al. 2014). However, *in vivo* efficacy against *P. berghei* rodent malaria parasites was again limited (Chapman et al. 2013; Chapman et al. 2014). Further investigation revealed that a number of optimised imidazopyridazine PfCDPK1 inhibitors were more likely to be targeting *P. falciparum* cGMP dependent protein kinase G (PfPKG; Green et al. 2015). Based on conflicting evidence for whether PfCDPK1 is essential for blood stage parasite growth, the limited efficacy *in vivo* and variable specificity of inhibitors, it has been suggested that PfCDPK1 may not be suitable for blood stage drug development (Green et al. 2015; Bansal et al. 2018)(reviewed in Cabrera et al. 2018).

PfPKG has also been a focus for antimalarial development since it is expressed in multiple stages of the lifecycle and has different activation properties to mammalian kinases (McRobert et al. 2008; Alam et al. 2015; Govindasamy et al. 2016). Inhibitors of PfPKG are potent inhibitors of merozoite egress from the developed schizont and are being developed as antimalarials (Taylor et al. 2010). Studies have also identified that inhibition of PfPKG blocks invasion of mechanically released merozoites, with speculation that this invasion-inhibitory activity is due to preventing discharge of the invasion priming protease PfSUB1 (Fig. 1b, c) and interfering with phosphorylation of proteins thought to have a role in invasion including PfCDPK1 and invasion motor components (Fig. 2b-e) (Collins et al. 2013; Alam et al. 2015; Das et al. 2015). Recently, a highly potent series of compounds were developed based on an imidazopyridine inhibitor of PKG used for treatment of the apicomplexan parasite *Eimeria tenalla* in chickens. The most active of these, ML10, had an IC_{50} of 2 nM against *P. falciparum* parasite growth *in vitro*. ML10 was also highly efficacious in a *P. chabaudi* rodent model of malaria, with twice daily doses of 100 mg/kg for 4 days reducing parasitemia to undetectable levels in a *P. falciparum* humanized mouse model of malaria (a promising outcome for development of a PKG inhibitor for inclusion in combination therapies.

Development of inhibitors against cAMP-dependent protein kinase A (PKA), which has key roles in microneme secretion (Dawn et al. 2014), phosphorylation of the functional domain of AMA1 (Leykauf, 2010) and activation of the actin-myosin motor (Lasonder et al. 2012), has been less successful. General inhibitors of PKA, such as H89 and KT5720, and its messenger molecule cAMP have been used as biological tools to block PfPKA and to study its function, but these compounds have low potency (IC_{50} typically > 1 μM) (Syin et al. 2001; Beraldo et al. 2005; Leykauf et al. 2010; Salazar et al. 2012) and we are currently unaware of any compounds that have been optimized for activity against PfPKA and cAMP (Buskes et al. 2016; Cabrera et al. 2018).

An alternative strategy to inhibit invasion is to target 3',5'-cyclic nucleotide phosphodiesterases (PDEs) which regulate degradation of cAMP and cGMP into AMP and GMP, respectively. Increased cAMP and cGMP leads to activation of PKA and PKG, respectively, making PDEs significant regulators of signalling during egress and invasion (Fig. 2c) (Collins et al. 2013; Baker et al. 2017). Screening of human PDE inhibitors identified zaprinast (growth inhibitory IC_{50} of 35 μM) (Yuasa et al. 2005) and a pyrazolopyrimidinone, termed BIPPO, (growth IC_{50} of 0.4 μM) (Howard et al. 2015) as having activity against PfPDEα, an isoform that specifically inhibits cGMP. Since PfPDEα has been demonstrated to be dispensable to blood stage parasite growth (Wentzinger et al. 2008) and treatment with BIPPO causes activation of cAMP (PfPDEβ) and cGMP (PfPDEα) dependent pathways, it has been suggested that BIPPO may inhibit multiple PfPDE isoforms due to conservation in active sites (Wentzinger et al. 2008; Howard et al. 2015). Modelling suggests that there are key similarities between human, *Plasmodium* and *Toxoplasma* PDE orthologues that would support this cross-reactivity (Howard et al. 2015). Indeed, BIPPO retains activity against isoforms of human PDEs, including PDE9 (IC_{50} = 30 nM), and selectivity for *Plasmodium* PDEs would need to be greatly improved before this PDE inhibitor could be developed as an antimalarial (Howard et al. 2015).

Although a number of kinases with key roles in RBC invasion have been identified, the development of effective inhibitors against these signalling molecules is still a work in progress with improvements in specificity and potency required for many early leads. However, the feasibility of targeting signalling effector molecules can be demonstrated by recent efforts to develop inhibitors against phosphatidylinositol 4-kinase (PI4K), a key enzyme in protein trafficking required across multiple lifecycle stages, including merozoite development (McNamara et al. 2013). This has led to the 2-aminopyrazine compound UCT943 being taken forward into pre-clinical development (Brunschwig et al. 2018).

Invasion inhibitory starting points originating from diverse or focussed drug libraries

HTS of small molecule or compound libraries have been used extensively to identify growth inhibitory compounds of the asexual blood stages of *P. falciparum* malaria. However, relatively few screens have been directly designed to identify inhibitors of RBC invasion. Medicines for Malaria Venture (MMV) released a 400-compound library in 2011, termed the Malaria Box, which contains a diverse set of compounds that display antimalarial properties (Spangenberg et al. 2013). Subramanian et al. (2018) recently screened the Malaria Box for activity against *P. falciparum* blood stage egress and merozoite invasion inhibitors (Subramanian et al. 2018) and identified 11 out of 26 hits that inhibited the schizont to ring stage transition at an IC_{50} of <500 nM. Upon microscopic examination of blood smears, MMV665878 and MMV006429 treated schizonts ruptured normally, but free merozoites were found attached to RBCs and few successful invasion events were evident, a phenotype typical of invasion inhibitors (Weiss et al. 2015). Further testing

revealed that MMV665878 and MMV006429 were potent invasion inhibitors with up to 50% of invasion events inhibited at concentrations down to 300 nM in assays using purified merozoites (Subramanian *et al.* 2018). Of the 26 compounds identified in this screen, 10 of them have been characterised as inhibitors of PfATP4, a sodium efflux pump on the parasite plasma membrane, indicating either PfATP4 is involved in egress and invasion, or that the compounds have targets additional to PfATP4 (Lehane *et al.* 2014; Subramanian *et al.* 2018).

Screens of the related Apicomplexan parasite *T. gondii* have opened up new starting points for invasion-inhibitory drug development against apicomplexan parasites. *T. gondii in vitro* motility and invasion assays were used as secondary screens against a library of 527 putative kinase inhibitors (Kamau *et al.* 2012). Of the 14 lead compounds with growth inhibitory or enhancing affects, compounds C5 (IC_{50} 1.82 μM) and C1 (IC_{50} 1.36 μM) were found to irreversibly inhibit motility or motility and invasion, respectively. A second study using a fluorescence microscopy based assay screened 1222 covalent inhibitors directly for inhibition of *T. gondii* tachyzoite attachment and invasion, identifying 5 invasion-inhibitory compounds. The leading compound, WRR-086, demonstrated low micromolar (IC_{50} of 5.7 μM) invasion-inhibitory activity. Biochemical and genetic analysis identified a homologue of human DJ-1 (TgDJ-1) as the target of WRR-086, with inhibition of TgDJ-1 linked to loss of microneme secretion and failure to invade (Hall *et al.* 2011). Screening compounds for their invasion-inhibitory activity is providing starting points for the development of drugs with novel mechanisms of action and uncovering new insights into invasion biology of apicomplexan parasites.

The clinically used antibiotic azithromycin as an inhibitor of RBC invasion

The majority of compounds identified that have invasion-inhibitory activity against malaria parasites have no record of clinical use. Recent identification of the invasion-inhibitory activity of the antibiotic azithromycin (Wilson *et al.* 2015) marks one of the few clinically used compounds that have been shown to inhibit *Plasmodium* spp. invasion of RBCs. Macrolide antibiotics are known to target the malaria parasite's remnant plastid (the apicoplast) 70S bacteria-like ribosomal complex (Sidhu *et al.* 2007; Goodman *et al.* 2013). Inhibition of the apicoplast ribosome prevents replication of this essential organelle, resulting in the loss of isoprenoid pyrophosphate (IPP) precursor synthesis and parasite death a full two cycles of growth post treatment (termed delayed death) (Dahl and Rosenthal 2007; Goodman, Su and McFadden 2007). Despite the limitations of a slow killing antimalarial for treatment of disease, azithromycin's safe clinical profile and long half-life (>50 hours) has led to the antibiotic being trialled as a partner drug in artemisinin combination therapies (Cook *et al.* 2006; Sykes *et al.* 2009).

Recently it was found that azithromycin could rapidly inhibit RBC invasion *in vitro* (IC_{50}, 10 μM, in ethanol), which is independent of apicoplast-targeted delayed death (IC_{50}, 0.04 μM, in ethanol) activity (Wilson *et al.* 2015). Although the speed of azithromycin's invasion-inhibitory activity for an otherwise slow acting drug provides a new avenue to develop the drug as an antimalarial, the requirement for a 250-fold higher concentration of azithromycin needed to inhibit invasion currently prevents clinical use of this drug as an invasion inhibitor. However, of note is the identification of several analogues that show >5-fold improvement in invasion-inhibitory activity (Wilson *et al.* 2015, Burns *et al.* Unpublished Data), indicating that improved invasion-inhibitory potency is achievable. Importantly, the most invasion-inhibitory azithromycin analogues also exhibit improved activity against short-term blood stage parasite development and retain activity against the apicoplast, suggesting that azithromycin can be developed to have both fast acting (RBC invasion inhibition and short-term parasite growth inhibition) and apicoplast-targeting delayed death properties (Wilson *et al.* 2015, Burns *et al.* Unpublished Data). Given azithromycin's history of safety, proven activity, long half-life (>50 hours), availability of modified analogues and ease of modification, the identification of azithromycin's invasion-inhibitory activity opens up an attractive starting point to develop an invasion-inhibitory antimalarial with dual-mechanisms of action.

INVASION INHIBITORS IN COMBINATION THERAPIES

A focus of antimalarial development for treatment of clinical disease is on single-dose drug combinations that act broadly across blood-stage development to quickly kill parasites (Burrows *et al.* 2017). As a standalone drug, it is unrealistic to expect an antimalarial which only targets invasion will eliminate all parasites within a matter of hours. However, such a drug could be of benefit in a combination therapy and, as demonstrated in this review, many invasion inhibitors have activity against other lifecycle stages. Combination therapies that have two (or more) safe and efficacious drugs with different mechanisms of action have significant potential advantages, including reducing the risk of developing drug resistance (Hastings 2011). Importantly, the reported mechanisms of action for invasion inhibitors developed to date are not involved in the mechanisms of action of existing antimalarials, limiting the likelihood of cross-resistance.

Evidence from rodent models of malaria suggest that antimalarial monotherapy using drugs that target intracellular parasite growth may not prevent all parasites from progressing through to the next cycle (Khoury *et al.* 2017). Failure to rapidly inhibit blood stage replication may increase the risk of selecting for drug resistance and lead to higher numbers of mosquito transmissible gametocytes posttreatment, thereby contributing to transmission. Targeting invasion directly, the first step in blood stage parasite growth, in a combination therapy would immediately stop progression of parasites into the next cycle of growth, thus limiting opportunities for drug resistance to develop and reducing the number of new gametocytes.

Combining a drug that targets intracellular parasite development (timing of action of current antimalarials) with one that inhibits RBC invasion (extracellular) has intrinsic appeal as targeting these two developmental stages could facilitate rapid clearance of disease causing blood stage parasites and increase drug efficacy. Evidence from monotherapy drug efficacy studies of severe malaria patients suggests that rapid parasite clearance after treatment results in reduced mortality (Dondorp *et al.* 2005). Complicating the speed of parasite clearance, studies have highlighted that a number of clinically used antimalarials have reduced efficacy as malaria parasites transition from mature schizonts, through invasion and into newly established ring stage infections (Painter, Morrisey and Vaidya 2010; Wilson *et al.* 2013; Dogovski *et al.* 2015; Khoury *et al.* 2017). Since each surviving *P. falciparum* schizont is capable of releasing 16–32 new RBC

invading merozoites, providing additional cover through a drug combination that includes a potent invasion inhibitor has the potential to fast-track parasite clearance.

Since *P. falciparum* invasion occurs roughly every 48 hours, this raises the question as to whether clinical treatment with a drug that has a short half-life risks being ineffective across one growth cycle if administered temporally distant from the next period of rupture and invasion. Studies evaluating circulating and sequestered populations of parasites in infected subjects have generally found a wide developmental age range for parasite populations at the time of sampling; predominantly young parasites in peripheral blood and mostly mature stages for parasites sequestered in capillaries (but younger parasites can also be at high levels) in cerebral malaria, non-cerebral malaria and placental malaria cases (MacPherson *et al.* 1985; Oo *et al.* 1987; Silamut *et al.* 1999; Beeson *et al.* 2002; Pongponratn *et al.* 2003). These studies indicate that there is limited parasite synchronicity *in vivo* and it is likely that invasion inhibitors will encounter invading merozoites soon after administration and regularly across the next 48 hours.

In terms of ideal drug properties, invasion inhibitors should have: (i) a half-life that allows the drug to be maintained at effective concentrations with a dosing regimen no more frequent than daily, and (ii) an effective concentration well below that of each dose, allowing inhibitory concentrations of drug to be available over a time period equivalent to many cycles of parasite invasion and growth. As demonstrated by the clinical use of the HIV entry inhibitor maraviroc (half-life ~16 hours; Perry 2010), maintaining drug concentrations to inhibit pathogen host cell entry over several replication cycles is clinically achievable. In terms of clinically used compounds with invasion-inhibitory antimalarial activity, the half-life is known for azithromycin (>50 hours) and several HLMs (Heparin < 1 hour, sevuparin ~1 hour, curdlan sulfate ~2–3 hours and fondaparinux 17–21 hours), and the half-life will need to be a consideration for any invasion inhibitors with higher potency.

Drug resistance models suggest that the increased selective window (when drug levels fall below the minimal inhibitory concentration) of long-lasting drugs can potentially increase drug resistance selection pressure posttreatment (Stepniewska and White 2008; Kay and Hastings 2015). In contrast, drugs with a short half-life, such as the artemisinins, have a much shorter selective window and are considered less likely to select for resistance due to minimal parasite exposure to sub-inhibitory concentrations (Stepniewska and White 2008); but more frequent dosing is required to maintain treatment efficacy. Therefore, there are several important considerations in selecting ideal drug combinations with the potential impacts on clinical efficacy, reducing the risk of drug resistance and reducing transmission all needing to be assessed for combination therapies that include an invasion inhibitor. Despite the potential benefits of having an invasion-inhibitory drug in antimalarial combination therapies, the therapeutic efficacy of a drug combination featuring both an invasion inhibitor and an intracellular blood stage growth inhibitor *in vitro* or *in vivo* has yet to be assessed directly. Thus, future studies will need to assess the potential synergies of using an invasion inhibitor in a combination therapy as well as model the therapeutic and resistance-proofing benefits of doing so.

CONCLUSION

Targeting RBC invasion is a promising antimalarial drug development strategy because: (i) extracellular parasites are exposed directly to drugs in the bloodstream, (ii) most parasite proteins required for invasion lack human equivalents, offering possibilities for selective inhibition and (iii) blocking invasion immediately stops multiplication of disease causing blood stage parasites. Inhibition of host cell entry is a validated strategy for HIV combination therapies (Kilby *et al.* 1998; Dorr *et al.* 2005) and the predicted viral generation time of HIV (≥48 hours; Dixit *et al.* 2004; Murray, Kelleher and Cooper 2011; Puller, Neher and Albert 2017) is similar to the blood stage lifecycle of *P. falciparum*. Therefore, the clinical use of HIV entry inhibitors provides a proof-of-concept that inhibitors of RBC invasion can have a role in antimalarial combination therapies.

The targets of invasion-inhibitory antimalarials under development are mostly essential, conserved and non-redundant (i.e. Yeoh *et al.* 2007; Boyle *et al.* 2010; Kortagere 2010; Wilson *et al.* 2015; Pino *et al.* 2017). The conservation evident in key, drug targetable, invasion machinery between malaria isolates, different *Plasmodium* spp. and different lifecycle stages (i.e. sporozoite invasion) is leading to the development of pan-invasion inhibitors. Therapeutic inhibition of invasion is likely to have profound effects on parasite viability since the merozoite has a short half-life and failure to invade immediately ends parasite growth and multiplication. This would mitigate the risk that parasites develop drug tolerance and persist as is the case for artemisinin resistance. Merozoite invasion may be more sensitive to treatment than other intracellular RBC stages, as demonstrated by a lower IC_{50} for invasion inhibition (~25 μM) than achieved for rupture inhibition (~180 μM) for the PfSUB1 inhibitor MRT121113 (Yeoh *et al.* 2007). Therefore, improving a drug's activity against the process of merozoite invasion could have a significant impact on parasite clearance and clinical effectiveness. To date, a number of diverse chemotypes with different targets have been identified to inhibit RBC invasion (Supplementary Table S1), but there is tremendous scope to develop new inhibitors of this essential step in parasite growth for use in combination therapies. The search for new invasion-inhibitory targets is helped by the availability of published mature schizont stage proteomic and phosphoproteomic resources (www.plasmodb.org) that highlight potential merozoite specific therapeutic targets for assessment (Solyakov *et al.* 2011; Lasonder *et al.* 2015). Encouragingly, the development of specific assays to quantify the invasion-inhibitory activity of compounds (Wilson *et al.* 2013; Wilson *et al.* 2015; Weiss, Crabb and Gilson 2016) has led to the identification of new chemical scaffolds that inhibit invasion.

Although several compounds with invasion-inhibitory activity have achieved promising levels of potency *in vitro* and *in vivo* (Gemma *et al.* 2012; Bouillon *et al.* 2013; Giovani *et al.* 2014; Kher *et al.* 2014; Meyers *et al.* 2014; Nasamu *et al.* 2017; Pino *et al.* 2017), an important way forward for invasion inhibitor development is to optimise additional compounds with activity in the low nanomolar range to fast-track further development options. Another future research priority is the evaluation of invasion-inhibitory compounds in combination with currently used and new emerging therapeutics that target intraerythrocytic parasite development, including artemisinin. Such studies would better define the properties and timing of action of drugs to be used in optimal combinations. While proof-of-concept for invasion inhibitors has been demonstrated in animal models, further *in vivo* studies are needed to better define the therapeutic potential of the different inhibitor classes alone and in combination. Incorporation of mathematical modelling, as is increasingly being used in drug evaluation and clinical trials, to assess

the ideal properties of invasion inhibitors in combination therapies *in vivo* would be particularly valuable for informing development priorities.

Combining an invasion inhibitor with artemisinin or a similar drug that acts broadly across malaria's blood stages would provide complete drug coverage across this disease causing stage of the lifecycle. Despite the potential to identify potent, specific and broad acting antimalarials targeting invasion, the discovery and development of drugs that act against this essential and exposed step in blood stage replication has been limited. The recent identification of numerous promising drug leads and targets, combined with improved merozoite purification methods and screening strategies, has revealed promising new avenues for the development of next-generation therapeutics for malaria.

SUPPLEMENTARY DATA

Supplementary data are available at *FEMSRE* online

Authorship contributions

DWW, MJB, TdKW, PRG and JGB conceived the idea of this review; ALB, MGD MJB, JMB and DWW conducted the literature review and wrote the manuscript. JMB created the figures. All authors contributed to the design, content and editing of this manuscript.

ACKNOWLEDGMENT

JGB is a member of the NHMRC Australian Centre for Research Excellence in Malaria Elimination.

FUNDING

DW received funding from the NHMRC (Fellowship APP1035715, Project Grant APP1143974) and University of Adelaide Beacon Fellowship. MJB received funding from NHMRC (Career Development Fellowship APP1141632 and Project Grant APP112656), and JGB (1077636) and TdKW (1136300) were supported by NHMRC Senior Research Fellowships. ALB, MGD and JMB recieved support from ARC postgraduate scholarships.

Conflict of interest. None declared.

REFERENCES

Adams Y, Smith SL, Schwartz-Albiez R *et al.* Carrageenans inhibit the *in vitro* growth of *Plasmodium falciparum* and cytoadhesion to CD36. *Parasitol Res* 2005;**97**:290–4.

Aggarwal BB, Sethi G, Baladandayuthapani V *et al.* Targeting cell signaling pathways for drug discovery: an old lock needs a new key. *J Cell Biochem* 2007;**102**:580–92.

Aikawa M, Miller LH, Johnson J *et al.* Erythrocyte entry by malarial parasites. A moving junction between erythrocyte and parasite. *J Cell Biol* 1978;**77**:72–82.

Alam MM, Solyakov L, Bottrill AR *et al.* Phosphoproteomics reveals malaria parasite Protein Kinase G as a signalling hub regulating egress and invasion. *Nat Commun* 2015;**6**:7285.

Alexander DL, Arastu-Kapur S, Dubremetz JF *et al. Plasmodium falciparum* AMA1 binds a rhoptry neck protein homologous to TgRON4, a component of the moving junction in *Toxoplasma gondii*. *Eukaryot Cell* 2006;**5**:1169–73.

Aly ASI, Vaughan AM, Kappe SHI. Malaria parasite development in the mosquito and infection of the mammalian host. *Annu Rev Microbiol* 2009;**63**:195–221.

Ansell KH, Jones HM, Whalley D *et al.* Biochemical and antiparasitic properties of inhibitors of the *Plasmodium falciparum* calcium-dependent protein kinase PfCDPK1. *Antimicrob Agents Chemother* 2014;**58**:6032–43.

Ariey F, Witkowski B, Amaratunga C *et al.* A molecular marker of artemisinin-resistant *Plasmodium falciparum* malaria. *Nature* 2014;**505**:50–5.

Ashley E, Dhorda M, Fairhurst R *et al.* Spread of artemisinin resistance in *Plasmodium falciparum* malaria. *N Engl J Med* 2014;**371**:411–23.

Baker DA, Drought LG, Flueck C *et al.* Cyclic nucleotide signalling in malaria parasites. *Open Biol* 2017;**7**:170213.

Baker DA, Stewart LB, Large JM *et al.* A potent series targeting the malarial cGMP-dependent protein kinase clears infection and blocks transmission. *Nat Commun* 2017;**8**:430.

Baldwin MR, Li X, Hanada T *et al.* Merozoite surface protein 1 recognition of host glycophorin A mediates malaria parasite invasion of red blood cells. *Blood* 2015;**125**:2704–11.

Bannister LH, Mitchell GH. The fine structure of secretion by *Plasmodium knowlesi* merozoites during red cell invasion. *J Protozool* 1989;**36**:362–7.

Bansal A, Molina-Cruz A, Brzostowski J *et al.* PfCDPK1 is critical for malaria parasite gametogenesis and mosquito infection. *Proc Natl Acad Sci USA* 2018;**115**:774–9.

Bansal A, Singh S, More KR *et al.* Characterization of *Plasmodium falciparum* calcium-dependent protein kinase 1 (PfCDPK1) and its role in microneme secretion during erythrocyte invasion. *J Biol Chem* 2013;**288**:1590–602.

Barragan A, Spillmann D, Kremsner PG *et al. Plasmodium falciparum*: molecular background to strain-specific rosette disruption by glycosaminoglycans and sulfated glycoconjugates. *Exp Parasitol* 1999;**91**:133–43.

Barre-Sinoussi F, Chermann JC, Rey F *et al.* Isolation of a T-lymphotropic retrovirus from a patient at risk for acquired immune deficiency syndrome (AIDS). *Science* 1983;**220**:868–71.

Bastos MF, Albrecht L, Kozlowski EO *et al.* Fucosylated chondroitin sulfate inhibits *Plasmodium falciparum* cytoadhesion and merozoite invasion. *Antimicrob Agents Chemother* 2014;**58**:1862–71.

Baum J, Chen L, Healer J *et al.* Reticulocyte-binding protein homologue 5 - an essential adhesin involved in invasion of human erythrocytes by *Plasmodium falciparum*. *Int J Parasitol* 2009;**39**:371–80.

Beeson JG, Amin N, Kanjala M *et al.* Selective accumulation of mature asexual stages of *Plasmodium falciparum*-infected erythrocytes in the placenta. *Infect Immun* 2002;**70**:5412–5.

Beeson JG, Drew DR, Boyle MJ *et al.* Merozoite surface proteins in red blood cell invasion, immunity and vaccines against malaria. *FEMS Microbiol Rev* 2016;**40**:343–72.

Beraldo FH, Almeida FM, da Silva AM *et al.* Cyclic AMP and calcium interplay as second messengers in melatonin-dependent regulation of *Plasmodium falciparum* cell cycle. *J Cell Biol* 2005;**170**:551–7.

Blackman MJ, Fujioka H, Stafford WH *et al.* A subtilisin-like protein in secretory organelles of *Plasmodium falciparum* merozoites. *J Biol Chem* 1998;**273**:23398–409.

Blackman MJ, Holder AA Secondary processing of the *Plasmodium falciparum* merozoite surface protein-1 (MSP1) by a calcium-dependent membrane-bound serine protease:

shedding of MSP133 as a noncovalently associated complex with other fragments of the MSP1. *Mol Biochem Parasitol* 1992;**50**:307–15.
Bosch BJ, van der Zee R, de Haan CAet al. The coronavirus spike protein is a class I virus fusion protein: structural and functional characterization of the fusion core complex. *J. Virol.* 2003;**77**:8801–1112885899
Bosch J, Turley S, Daly TM *et al.* Structure of the MTIP-MyoA complex, a key component of the malaria parasite invasion motor. *Proc Natl Acad Sci USA* 2006;**103**:4852–7.
Bosch J, Turley S, Roach CM *et al.* The closed MTIP-myosin A-tail complex from the malaria parasite invasion machinery. *J Mol Biol* 2007;**372**:77–88.
Bouillon A, Giganti D, Benedet C *et al.* In Silico screening on the three-dimensional model of the *Plasmodium vivax* SUB1 protease leads to the validation of a novel anti-parasite compound. *J Biol Chem* 2013;**288**:18561–73.
Boyle MJ, Richards JS, Gilson PR *et al.* Interactions with heparin-like molecules during erythrocyte invasion by *Plasmodium falciparum* merozoites. *Blood* 2010;**115**:4559–68.
Boyle MJ, Skidmore M, Dickerman B *et al.* Identification of heparin modifications and polysaccharide inhibitors of *Plasmodium falciparum* merozoite invasion that have potential for novel drug development. *Antimicrob Agents Chemother* 2017;**61**:e00709–17.
Boyle MJ, Wilson DW, Richards JS *et al.* Isolation of viable *Plasmodium falciparum* merozoites to define erythrocyte invasion events and advance vaccine and drug development. *Proc Natl Acad Sci USA* 2010;**107**:14378–83.
Brasil P, Zalis MG, de Pina-Costa A *et al.* Outbreak of human malaria caused by *Plasmodium simium* in the Atlantic Forest in Rio de Janeiro: A molecular epidemiological investigation. *Lancet Glob Health* 2017;**5**:e1038–46.
Brunschwig C, Lawrence N, Taylor D *et al.* UCT943, a Next-generation *Plasmodium falciparum* PI4K inhibitor preclinical candidate for the treatment of malaria. *Antimicrob Agents Chemother* 2018;**62**:e00012–18.
Burrows JN, Duparc S, Gutteridge WE *et al.* New developments in anti-malarial target candidate and product profiles. *Malar J* 2017;**16**:26.
Buskes MJ, Harvey KL, Richards BJ *et al.* Antimalarial activity of novel 4-cyano-3-methylisoquinoline inhibitors against *Plasmodium falciparum*: design, synthesis and biological evaluation. *Org Biomol Chem* 2016;**14**:4617–39.
Butcher GA, Parish CR, Cowden WB. Inhibition of growth *in vitro* of *Plasmodium falciparum* by complex polysaccharides. *Trans R Soc Trop Med Hyg* 1988;**82**:558–9.
Cabrera DG, Horatscheck A, Wilson CR *et al.* Plasmodial kinase inhibitors: license to cure? *J Med Chem* 2018;**61**:8061–77.
Carey KL, Westwood NJ, Mitchison TJ *et al.* A small-molecule approach to studying invasive mechanisms of *Toxoplasma gondii*. *Proc Natl Acad Sci USA* 2004;**101**:7433–8.
Carlson J, Ekre HP, Helmby H *et al.* Disruption of *Plasmodium falciparum* erythrocyte rosettes by standard heparin and heparin devoid of anticoagulant activity. *Am J Trop Med Hyg* 1992;**46**:595–602.
Chandramohanadas R, Basappa, Russell B *et al.* Small molecule targeting malaria merozoite surface protein-1 (MSP-1) prevents host invasion of divergent plasmodial species. *J Infect Dis* 2014;**210**:1616–26.
Chapman TM, Osborne SA, Bouloc N *et al.* Substituted imidazopyridazines are potent and selective inhibitors of *Plasmodium falciparum* calcium-dependent protein kinase 1 (PfCDPK1). *Bioorg Med Chem Lett* 2013;**23**:3064–9.
Chapman TM, Osborne SA, Wallace C *et al.* Optimization of an imidazopyridazine series of inhibitors of *Plasmodium falciparum* calcium-dependent protein kinase 1 (PfCDPK1). *J Med Chem* 2014;**57**:3570–87.
Ciana CL, Siegrist R, Aissaoui H *et al.* Novel *in vivo* active antimalarials based on a hydroxy-ethyl-amine scaffold. *Bioorg Med Chem Lett* 2013;**23**:658–62.
Collins CR, Hackett F, Strath M *et al.* Malaria parasite cGMP-dependent protein kinase regulates blood stage merozoite secretory organelle discharge and egress. *PLoS Pathog* 2013;**9**:e1003344.
Collins CR, Withers-Martinez C, Hackett F *et al.* An inhibitory antibody blocks interactions between components of the malarial invasion machinery. *PLoS Pathog* 2009;**5**:e1000273.
Cook JA, Randinitis EJ, Bramson CR *et al.* Lack of a pharmacokinetic interaction between azithromycin and chloroquine. *Am J Trop Med Hyg* 2006;**74**:407–12.
Cooper J. Effects of cytochalasin and phalloidin on actin. *J Cell Biol* 1987;**105**:1473–8.
Cowman AF, Morry MJ, Biggs BA *et al.* Amino acid changes linked to pyrimethamine resistance in the dihydrofolate reductase-thymidylate synthase gene of *Plasmodium falciparum*. *Proc Natl Acad Sci USA* 1988;**85**:9109–13.
Crandall IE, Szarek WA, Vlahakis JZ *et al.* Sulfated cyclodextrins inhibit the entry of *Plasmodium* into red blood cells. Implications for malarial therapy. *Biochem Pharmacol* 2007;**73**:632–42.
Croce CM, Zhang K, Wei YQ. Announcing signal transduction and targeted therapy. *Signal Transduct Target Ther* 2016;**1**:15006.
Dahl EL, Rosenthal PJ. Multiple antibiotics exert delayed effects against the *Plasmodium falciparum* apicoplast. *Antimicrob Agents Chemother* 2007;**51**:3485–90.
Das S, Hertrich N, Perrin AJ *et al.* Processing of *Plasmodium falciparum* Merozoite surface protein MSP1 activates a spectrin-binding function enabling parasite egress from RBCs. *Cell Host Microbe* 2015;**18**:433–44.
Das S, Saha B, Hati AK *et al.* Evidence of artemisinin-resistant *Plasmodium falciparum* malaria in eastern India. *N Engl J Med* 2018;**379**:1962–4.
Dawn A, Singh S, More KR *et al.* The central role of cAMP in regulating *Plasmodium falciparum* merozoite invasion of human erythrocytes. *PLoS Pathog* 2014;**10**:e1004520.
Devine SM, Lim SS, Chandrashekaran IR *et al.* A critical evaluation of pyrrolo[2,3-d]pyrimidine-4-amines as *Plasmodium falciparum* apical membrane antigen 1 (AMA1) inhibitors. *MedChemComm* 2014;**5**:1500–6.
Devine SM, MacRaild CA, Norton RS *et al.* Antimalarial drug discovery targeting apical membrane antigen 1. *Medchemcomm* 2017;**8**:13–20.
Dickerman BK, Elsworth B, Cobbold SA *et al.* Identification of inhibitors that dually target the new permeability pathway and dihydroorotate dehydrogenase in the blood stage of *Plasmodium falciparum*. *Sci Rep* 2016;**6**:37502.
Dixit NM, Markowitz M, Ho DD *et al.* Estimates of intracellular delay and average drug efficacy from viral load data of HIV-infected individuals under antiretroviral therapy. *Antivir Ther* 2004;**9**:237–46.
Dogovski C, Xie SC, Burgio G *et al.* Targeting the cell stress response of *Plasmodium falciparum* to overcome artemisinin resistance. *PLoS Biol* 2015;**13**:e1002132.
Donat F, Duret JP, Santoni A *et al.* The pharmacokinetics of fondaparinux sodium in healthy volunteers. *Clin Pharmacokinet* 2002;**41**(Suppl 2):1–9.

Dondorp A, Nosten F, Stepniewska K *et al.* Artesunate versus quinine for treatment of severe *falciparum* malaria: A randomised trial. *Lancet* 2005;**366**:717–25.

Dondorp AM, Nosten F, Yi P *et al.* Artemisinin resistance in *Plasmodium falciparum* malaria. *N Engl J Med* 2009;**361**:455–67.

Dorr P, Westby M, Dobbs S *et al.* Maraviroc (UK-427,857), a potent, orally bioavailable, and selective small-molecule inhibitor of chemokine receptor CCR5 with broad-spectrum anti-human immunodeficiency virus type 1 activity. *Antimicrob Agents Chemother* 2005;**49**:4721–32.

Draper SJ, Angov E, Horii T *et al.* Recent advances in recombinant protein-based malaria vaccines. *Vaccine* 2015;**33**:7433–43.

Drew DR, Sanders PR, Weiss G *et al.* Functional Conservation of the AMA1 host-cell invasion ligand between *P. falciparum* and *P. vivax*: A novel platform to accelerate vaccine and drug development. *J Infect Dis* 2018;**217**:498–507.

Dvorak JA, Miller LH, Whitehouse WC *et al.* Invasion of erythrocytes by malaria merozoites. *Science* 1975;**187**:748–50.

Evans SG, Morrison D, Kaneko Y *et al.* The effect of curdlan sulphate on development *in vitro* of *Plasmodium falciparum*. *Trans R Soc Trop Med Hyg* 1998;**92**:87–89.

Fidock DA, Nomura T, Talley AK *et al.* Mutations in the *P. falciparum* digestive vacuole transmembrane protein PfCRT and evidence for their role in chloroquine resistance. *Mol Cell* 2000;**6**:861–71.

Fleck SL, Birdsall B, Babon J *et al.* Suramin and suramin analogues inhibit merozoite surface protein-1 secondary processing and erythrocyte invasion by the malaria parasite *Plasmodium falciparum*. *J Biol Chem* 2003;**278**:47670–7.

Fry M, Pudney M. Site of action of the antimalarial hydroxynaphthoquinone, 2-[trans-4-(4'-chlorophenyl) cyclohexyl]-3-hydroxy-1,4-naphthoquinone (566C80). *Biochem Pharmacol* 1992;**43**:1545–53.

Gallo RC, Sarin PS, Gelmann EP *et al.* Isolation of human T-cell leukemia virus in acquired immune deficiency syndrome (AIDS). *Science* 1983;**220**:865–7.

Gemma S, Giovani S, Brindisi M *et al.* Quinolylhydrazones as novel inhibitors of *Plasmodium falciparum* serine protease PfSUB1. *Bioorg Med Chem Lett* 2012;**22**:5317–21.

Genton B, Al-Yaman F, Betuela I *et al.* Safety and immunogenicity of a three-component blood-stage malaria vaccine (MSP1, MSP2, RESA) against *Plasmodium falciparum* in Papua New Guinean children. *Vaccine* 2003;**22**:30–41.

Gilson PR, Crabb BS. Morphology and kinetics of the three distinct phases of red blood cell invasion by *Plasmodium falciparum* merozoites. *Int J Parasitol* 2009;**39**:91–96.

Gilson PR, Nebl T, Vukcevic D *et al.* Identification and stoichiometry of glycosylphosphatidylinositol-anchored membrane proteins of the human malaria parasite *Plasmodium falciparum*. *Mol Cell Proteomics* 2006;**5**:1286–99.

Giovani S, Penzo M, Brogi S *et al.* Rational design of the first difluorostatone-based PfSUB1 inhibitors. *Bioorg Med Chem Lett* 2014;**24**:3582–6.

Goel VK, Li X, Chen H *et al.* Band 3 is a host receptor binding merozoite surface protein 1 during the *Plasmodium falciparum* invasion of erythrocytes. *Proc Natl Acad Sci USA* 2003;**100**:5164–9.

Goodman CD, Su V, McFadden GI. The effects of anti-bacterials on the malaria parasite *Plasmodium falciparum*. *Mol Biochem Parasitol* 2007;**152**:181–91.

Goodman CD, Useglio M, Peiru S *et al.* Chemobiosynthesis of new antimalarial macrolides. *Antimicrob Agents Chemother* 2013;**57**:907–13.

Gordon M, Guralnik M, Kaneko Y *et al.* A phase I study of curdlan sulfate–an HIV inhibitor. Tolerance, pharmacokinetics and effects on coagulation and on CD4 lymphocytes. *J Med* 1994;**25**:163–80.

Govindasamy K, Jebiwott S, Jaijyan DK *et al.* Invasion of hepatocytes by *Plasmodium* sporozoites requires cGMP-dependent protein kinase and calcium dependent protein kinase 4. *Mol Microbiol* 2016;**102**:349–63.

Green JL, Moon RW, Whalley D *et al.* Imidazopyridazine Inhibitors of *Plasmodium falciparum* Calcium-Dependent Protein Kinase 1 also target cyclic GMP-dependent protein kinase and heat shock protein 90 to kill the parasite at different stages of intracellular development. *Antimicrob Agents Chemother* 2015;**60**:1464–75.

Green JL, Rees-Channer RR, Howell SA *et al.* The motor complex of *Plasmodium falciparum*: Phosphorylation by a calcium-dependent protein kinase. *J Biol Chem* 2008;**283**:30980–9.

Hall CI, Reese ML, Weerapana E *et al.* Chemical genetic screen identifies *Toxoplasma* DJ-1 as a regulator of parasite secretion, attachment, and invasion. *Proc Natl Acad Sci USA* 2011;**108**:10568–73.

Harper JF, Harmon A. Plants, symbiosis and parasites: A calcium signalling connection. *Nat Rev Mol Cell Biol* 2005;**6**:555–66.

Harris KS, Casey JL, Coley AM *et al.* Binding hot spot for invasion inhibitory molecules on *Plasmodium falciparum* apical membrane antigen 1. *Infect Immun* 2005;**73**:6981–9.

Harris PK, Yeoh S, Dluzewski AR *et al.* Molecular identification of a malaria merozoite surface sheddase. *PLoS Pathog* 2005;**1**:241–51.

Hastings I. How artemisinin-containing combination therapies slow the spread of antimalarial drug resistance. *Trends Parasitol* 2011;**27**:67–72.

Havlik I, Looareesuwan S, Vannaphan S *et al.* Curdlan sulphate in human severe/cerebral *Plasmodium falciparum* malaria. *Trans R Soc Trop Med Hyg* 2005;**99**:333–40.

Havlik I, Rovelli S, Kaneko Y. The effect of curdlan sulphate on *in vitro* growth of *Plasmodium falciparum*. *Trans R Soc Trop Med Hyg* 1994;**88**:686–7.

Heaslip AT. A Small-Molecule inhibitor of *T. gondii* motility induces the posttranslational modification of Myosin Light Chain-1 and Inhibits Myosin motor activity. *PLoS Pathog* 2010;**6**:e1000720.

Henrich TJ, Kuritzkes DR. HIV-1 entry inhibitors: Recent development and clinical use. *Curr Opin Virol* 2013;**3**:51–7.

Ho DD, Neumann AU, Perelson ASet. Rapid turnover of plasma virions and CD4 lymphocytes in HIV-1 infection. *Nature* 1995;**373**:123–6.

Hodder AN, Crewther PE, Anders RF. Specificity of the protective antibody response to apical membrane antigen 1. *Infect Immun* 2001;**69**:3286–94.

Hoffart V, Lamprecht A, Maincent P *et al.* Oral bioavailability of a low molecular weight heparin using a polymeric delivery system. *J Control Release* 2006;**113**:38–42.

Holder AA, Blackman MJ, Burghaus PA *et al.* A malaria merozoite surface protein (MSP1)-structure, processing and function. *Mem Inst Oswaldo Cruz* 1992;**87**(Suppl 3):37–42.

Howard BL, Harvey KL, Stewart RJ *et al.* Identification of potent phosphodiesterase inhibitors that demonstrate cyclic nucleotide-dependent functions in apicomplexan parasites. *ACS Chem Biol* 2015;**10**:1145–54.

Johnson S, Rahmani R, Drew DR *et al.* Truncated latrunculins as actin inhibitors targeting *Plasmodium falciparum* motility and host cell invasion. *J Med Chem* 2016;**59**:10994–1005.

Appendix IV: The Ins and Outs of *Plasmodium* Rhoptries, Focusing on the Cytosolic Side

(co-authored review)

CellPress

Trends in Parasitology

Review

The Ins and Outs of *Plasmodium* Rhoptries, Focusing on the Cytosolic Side

Benjamin Liffner,[1] Juan Miguel Balbin,[1] Jan Stephan Wichers,[2,3] Tim-Wolf Gilberger,[2,3,4] and Danny W. Wilson[1,5,*]

Parasites of the genus *Plasmodium* cause human and animal malaria, leading to significant health and economic impacts. A key aspect of the complex life cycle of *Plasmodium* parasites is the invasion of the parasite into its host cell, which is mediated by secretory organelles. The largest of these organelles, the rhoptry, undergoes rapid and profound physiological changes when it secretes its contents during merozoite and sporozoite invasion of the host erythrocyte and hepatocyte, respectively. Here we discuss recent advancements in our understanding of the dynamic rhoptry biology during the parasite's invasive stages, with a focus on the roles of cytosolically exposed rhoptry-interacting proteins (C-RIPs). We explore potential similarities between the molecular mechanisms driving merozoite and sporozoite rhoptry function.

Highlights

Plasmodium parasites secrete proteins from their rhoptries during host cell invasion.

Rhoptries undergo significant physiological changes during invasion, and these differ significantly between the rhoptries of merozoites and sporozoites.

Rhoptry secretion requires fusion between rhoptry pairs and between the rhoptries and parasite plasma membrane.

Proteins on the cytosolic face of the rhoptries likely coordinate many of the poorly explored aspects of rhoptry biology, including rhoptry biogenesis, morphology, and secretion.

Invasive Stages of the *Plasmodium* Life Cycle

Plasmodium spp. malaria parasites cause >400 000 deaths each year, mainly in children under 5 years of age [1]. The *Plasmodium* life cycle features four stages in which the parasite invades host cells. The first occurs when parasites in the ookinete stage invade the midgut of a mosquito (reviewed in [2]). The second, when sporozoite-stage parasites invade the salivary gland of a mosquito (reviewed in [3]). The third, after an infected mosquito bites a vertebrate host, the sporozoite invades and establishes an infection inside a hepatocyte (reviewed in [4]). The fourth follows multiplication and release of merozoites into the blood stream from the infected hepatocyte, with these merozoites going on to invade and multiply inside red blood cells (RBCs) during the disease-causing blood stage (reviewed in [5]). Evidence to date suggests that malaria parasite invasion of the mosquito salivary glands, hepatocytes, and RBCs is facilitated by similar invasion machinery. One key piece of this shared invasion machinery, the rhoptries, undergoes dynamic changes in structure during invasion that are likely required for secretion of essential invasion ligands from the rhoptry lumen. Notably, ookinetes are the only invasive stage that lack rhoptries, likely because they do not form a **parasitophorous vacuole** (**PV**; see Glossary) [2]. Here we present recent findings on rhoptry biology, with a focus on the **cytosolically exposed rhoptry-interacting proteins** (**C-RIPs**) and their roles in orchestrating the rhoptries' unique biology during merozoite and sporozoite invasion of host cells (Box 1), insights that may help to identify new therapeutic targets.

Rhoptries in Parasite Invasive Stages

Rhoptries are the largest of the secretory organelles that are present in the invasive stages of most apicomplexan parasites; however, their number, morphology, and contents vary greatly both between apicomplexan organisms and life cycle stages (reviewed in [6]). In *Plasmodium*, rhoptries are possessed by both sporozoites and merozoites, where they form *de novo* during **sporogony** and **schizogony** [7,8], but they are notably absent in ookinetes, even though ookinetes are invasive [9]. For both sporozoites and merozoites, rhoptries are club-shaped organelles that are segregated into neck and bulb portions, with the neck closer to the apical

[1]Research Centre for Infectious Diseases, School of Biological Sciences, University of Adelaide, Adelaide 5005, Australia
[2]Centre for Structural Systems Biology, 22607, Hamburg, Germany
[3]Bernhard Nocht Institute for Tropical Medicine, 20359 Hamburg, Germany
[4]Biology Department, University of Hamburg, 20146 Hamburg, Germany
[5]Burnet Institute, 85 Commercial Road, Melbourne 3004, Victoria, Australia

*Correspondence: Danny.wilson@adelaide.edu.au (D.W. Wilson).

Box 1. *Plasmodium* Merozoites and Sporozoites in Action

The Merozoite

The most well understood invasion event of *Plasmodium* spp. parasites is the invasion of RBCs by merozoites. Merozoites recognise RBCs and initiate an early, weak attachment before reorienting themselves such that their apical tip contacts the RBC membrane [5,25]. Following RBC recognition, proteins are secreted from the apical organelles of the merozoite and form an irreversible tight junction between the merozoite and RBC [66,67]. Utilising an actin–myosin-based motor complex, the merozoite then pulls the RBC membrane around itself [68,69], forming a parasitophorous vacuole that it will develop inside (merozoite invasion reviewed in [5]). For *P. falciparum* – the cause of most human malaria deaths and the parasite species referred to in this review unless stated otherwise – the parasite grows and replicates over the next 48hrs to form a schizont containing 16–32 new daughter merozoites [70]. To release the daughter merozoites to invade new RBCs, schizonts first rupture their PVM, followed by the RBC membrane [71].

The Sporozoite

Sporozoites develop inside oocysts that form in the mosquito midgut [72]. Once mature, the oocyst ruptures and releases sporozoites into the haemolymph of the mosquito, where they migrate to salivary glands [3]. Sporozoites then attach to the basal lamina of the salivary gland and move into the space between the basal lamina and salivary gland basal epithelial cell membrane [3,73]. From this position, the sporozoite invades the basal epithelial cell, forming a short-lived parasitophorous vacuole that is shed prior to invasion through the apical membrane into the secretory cavity, forming a new parasitophorous vacuole [3,73]. This second parasitophorous vacuole is also shed, and the sporozoites migrate to the salivary gland duct where they reside until the mosquito's next blood meal [3,74] (sporozoite salivary gland invasion reviewed in [3]). When the infected mosquito takes its next blood meal, it injects sporozoites subcutaneously that migrate to the liver via the circulatory system [75]. Here, sporozoites can cross the liver sinusoidal barrier, through a process known as cell traversal, where the sporozoite forms a transient vacuole; this is destroyed by parasite-derived proteins before the sporozoite exits the other side of the cell [76–78]. Once the sporozoite reaches a hepatocyte it undergoes a productive invasion event where it forms a parasitophorous vacuole and differentiates to form a hepatic schizont, which then ruptures to release thousands of merozoites into the blood stream [79] (sporozoite invasion and secretory organelles reviewed in [76]).

tip of the parasite [10]. Merozoites contain two rhoptries, while sporozoites are reported to contain two or more rhoptries that are longer and narrower than merozoite rhoptries [10,11]. In *Toxoplasma gondii*, a related apicomplexan parasite, the host-cell-invading tachyzoites have around ten long and thin rhoptries with up to two of these structures thought to secrete their contents independently [12]. To date, 45 proteins have been experimentally localised to the rhoptries of merozoites and 11 have been localised to the rhoptries of sporozoites (Figure 1). For some *Plasmodium* rhoptry-localised proteins, our understanding of their possible function is in part inferred from findings in *T. gondii*. Although we present some evidence from *T. gondii* in this review, differences in rhoptry physiology and rhoptry-associated protein localisation have been previously reported between *Plasmodium* spp. and *T. gondii* [13–15]. Therefore, these comparisons are provided as a guide and further studies are needed to fully characterise the functions of rhoptry-associated proteins between apicomplexan parasites with different host cell ranges and physiology.

Rhoptry Biogenesis

At the beginning of oocyst development [8], and following merozoite invasion [10], *Plasmodium* parasites lack rhoptries and so undertake *de novo* rhoptry biogenesis (reviewed in [7]). Rhoptries form from Golgi-derived vesicles during the trophozoite stage of blood-stage parasites [16], but it is currently unclear what the trigger for rhoptry biogenesis is. Rhoptry-resident proteins are typically trafficked to the nascent rhoptry through the classical secretory pathway, as most identified rhoptry proteins contain a signal peptide [7,17,18]. Additionally, it has been shown that inhibition of the classical secretory pathway prevents rhoptry biogenesis [18,19]. Recently, rhoptry apical membrane antigen (RAMA) and Sortilin have been shown to be involved in rhoptry biogenesis by trafficking other rhoptry proteins to both the rhoptry bulb and neck [20–22], with disruption of RAMA leading to the formation of rhoptries with a dysmorphic neck region [22]. During nascent rhoptry development, the organelle does not have its typical bulb and neck distinction, and it is

Glossary

Adenylate cyclases (AC): a family of enzymes that catalyse the conversion of ATP to cyclic AMP.
Carbonic anhydrases: a family of pH-responsive enzymes that reversibly catalyse the interconversion of carbon dioxide and water to bicarbonate and hydrogen ions.
Cytosolically exposed rhoptry-interacting protein (C-RIP): any protein that is found either on the cytosolic side of the rhoptry membrane exclusively or spans the rhoptry membrane and is exposed to both the rhoptry lumen and cell cytoplasm.
Cytosolically exposed rhoptry-leaflet-interacting protein (CERLI): a family of proteins, on the cytosolic face of the rhoptries, that are involved in rhoptry secretion and structure.
DHHC: a protein domain, named after its conserved amino acid sequence, which has the enzymatic function of adding palmitoyl modifications to other proteins, which typically coordinates their localisation.
Inducible knockout: the inducible removal of a protein of interest from an organism upon the addition of a particular stimulus, typically through induced gene excision. Inducible knockouts can be used to study the function of genes whose removal would lead to death, and as such are similar to a knockout system.
Knockdown: use of a genetic system to inducibly decrease the expression of either a gene or protein of interest. Knockdown systems can be used to study the effect of partial loss of the function of a gene or protein on an organism.
Knockout: use of a genetic system to irreversibly remove a gene of interest from an organism. Knockouts can be used to study the effect of complete loss of the function of a gene on an organism. Irreversible knockouts cannot be used on genes that are essential to survival of the organism, as their knockout would lead to death.
Oocyst-derived sporozoites: sporozoites that have been extracted from oocysts in the mosquito midgut. These sporozoites are primed to invade the mosquito salivary gland.
Parasite plasma membrane (PPM): the lipid bilayer that surrounds the merozoite.

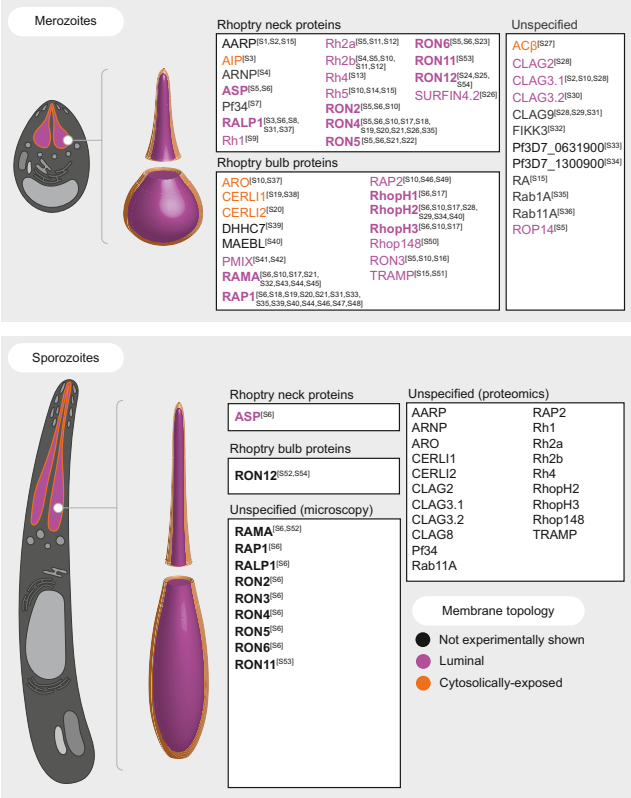

Figure 1. Rhoptry Proteins of *Plasmodium* Merozoites and Sporozoites. Summary of all proteins that have been experimentally localised to the rhoptries of either merozoites or sporozoites, in *Plasmodium* using microscopy-based techniques. Proteins are categorised as either rhoptry neck, rhoptry bulb, or unspecified, where the protein either localises across the entirety of the rhoptry or has not been mapped to a subcompartment of the rhoptries. Proteins are further categorised by their membrane topology, with proteins in purple residing in the rhoptry lumen, those in orange exposed to the parasite cytosol, and those in black not determined experimentally. Rhoptry topology classification is inferred either from experimental evidence, such as proteinase K protection assay, or circumstantial evidence, such as secretion from the rhoptries. Only a small number of proteins have been experimentally localised to the rhoptries of sporozoites using microscopy. Therefore, this diagram includes probable sporozoite rhoptry proteins, which possess a merozoite rhoptry localisation and have been identified in sporozoites by proteomics in one of the following studies [81–83]. Merozoite proteins in bold have been localised in both *Plasmodium falciparum* and the rodent-infecting parasite *Plasmodium berghei* except for RON11, which has been localised only in *P. berghei*. Sporozoite proteins in bold have been localised in only the rodent-infecting parasites *P. berghei* or *Plasmodium yoelii*. Each

(Figure legend continued at the bottom of the next page.)

Parasitophorous vacuole membrane (PVM): the lipid bilayer that contains the parasitophorous vacuole.
Parasitophorous vacuole (PV): a vacuole, derived partially from the host cell, that the parasite forms during host cell invasion.
Salivary gland-derived sporozoites: sporozoites that have been extracted from the salivary gland of mosquitoes. These sporozoites are primed to invade their vertebrate hosts.
Schizogony: the process of merozoite development that occurs inside schizonts.
Schizont: the stage of the *Plasmodium* life cycle that contains newly formed daughter merozoites.
Sporogony: the process of sporozoite formation inside oocysts of the mosquito midgut.
Tight junction: a complex of proteins, secreted from the parasite, that form an irreversible interaction with the host cell during invasion.

thought that rhoptry bulb biogenesis occurs first, with rhoptry neck biogenesis occurring later [16]. To date, rhoptry biogenesis has not been studied in detail in sporozoites.

Rhoptry Structure

In merozoites from fully mature **schizonts**, rhoptries exist as two club-shaped organelles that have distinct bulb and neck regions [10,16]. Rhoptries of *Plasmodium falciparum* merozoites are typically around 500 nm in length (neck to bulb), 200 nm wide at the bulb, and comprise between 2% and 7% of the total merozoite volume [10]. Despite their morphological differences, it is currently unclear how antigens localise specifically to the neck or bulb, as no membrane separates them [10,23]. Typically, rhoptry neck proteins facilitate recognition of and early interactions with the host cell, such as *P. falciparum* reticulocyte-binding protein homologue 5 (RH5) binding to its RBC receptor basigin [24] and the rhoptry neck (RON) complex (RON2, 4, and 5) that is involved in establishing an irreversible **tight junction** between the merozoite and RBC [24–28]. Conversely, the rhoptry bulb proteins [such as rhoptry-associated protein 1 (RAP1)] are typically secreted directly into the host cell cytosol and facilitate the later processes of invasion, such as establishing and modifying the nascent **parasitophorous vacuole membrane** (**PVM**) and host cell [26,29,30].

Rhoptry Physiology during Merozoite Invasion

Following schizont rupture, the rhoptry neck fuses with the **parasite plasma membrane** (**PPM**) to enable the secretion of rhoptry neck proteins [10,31] (Figure 2). It is currently unclear what proteins mediate fusion between the rhoptry neck and PPM, but it has been suggested that it may involve snap receptor (SNARE) or SNARE-like proteins as they perform similar functions in other systems [30]. After fusing with the PPM, the two rhoptries also begin to fuse together starting at the neck (Figure 2), a process likely to coincide with secretion of neck antigens required for early steps of invasion, including formation of the tight junction that cements the apical tip of the merozoite to the RBC membrane. Once the rhoptry necks have fused together and with the PPM, the rhoptries temporarily exist with two bulbs but only a single neck [10] (Figure 2). As the merozoite begins actively invading the RBC, the two bulbs fuse together and the merozoite steadily secretes rhoptry bulb proteins and lipids [32] into the RBC that are used in the formation of the PVM as the single rhoptry decreases in overall size [10] (Figure 2).

Once the merozoite has completed invasion, the single fused rhoptry maintains its bulb and neck differentiation [10] (Figure 2). This observation has led to the suggestion that the structure of the rhoptries may be supported by either an internal or external scaffold [10]. The composition of this scaffold, however, is yet to be elucidated. Additionally, rhoptries are absent in early ring-stage parasites [33], suggesting that the rhoptries are rapidly disassembled following merozoite invasion, a process which has yet to be explored experimentally.

The Potential for Interaction between Merozoite Rhoptries and Micronemes

Micronemes are Golgi-derived secretory vesicles that, like rhoptries, secrete proteins involved with host cell invasion, although there are no proteins known to localise to both the rhoptries and micronemes in *Plasmodium* [34,35]. Early studies of merozoite physiology by electron microscopy observed fusion between micronemes and the rhoptry neck [36,37], leading to

protein is labelled with a numbered reference where it was localised to the rhoptries. A full list of these references can be found in Table S1 in the supplemental information online. Abbreviations: AARP, Apical asparagine rich protein; AC, Adenylate cyclase; AIP, ARO-interacting protein; ARNP, Apical rhoptry neck protein; ARO, armadillo repeats only; ASP, Apical sushi protein; CERLI, cytosolically exposed rhoptry-leaflet-interacting protein; CLAG, Cytoadherence-linked asexual gene; MAEBL, Membrane-associated erythrocyte binding-like protein; PMIX, Plasmepsin IX; RA, Rhoptry antigen; RALP, rhoptry-associated leucine zipper-like protein; RAMA, rhoptry apical membrane antigen; RAP, Rhoptry associated protein; Rab, Ras-associated binding protein; Rh, reticulocyte binding protein homologue; RON, rhoptry neck; ROP, Rhoptry protein; SURFIN, Surface associated interspersed protein; TRAMP, Thrombospondin-related apical membrane protein.

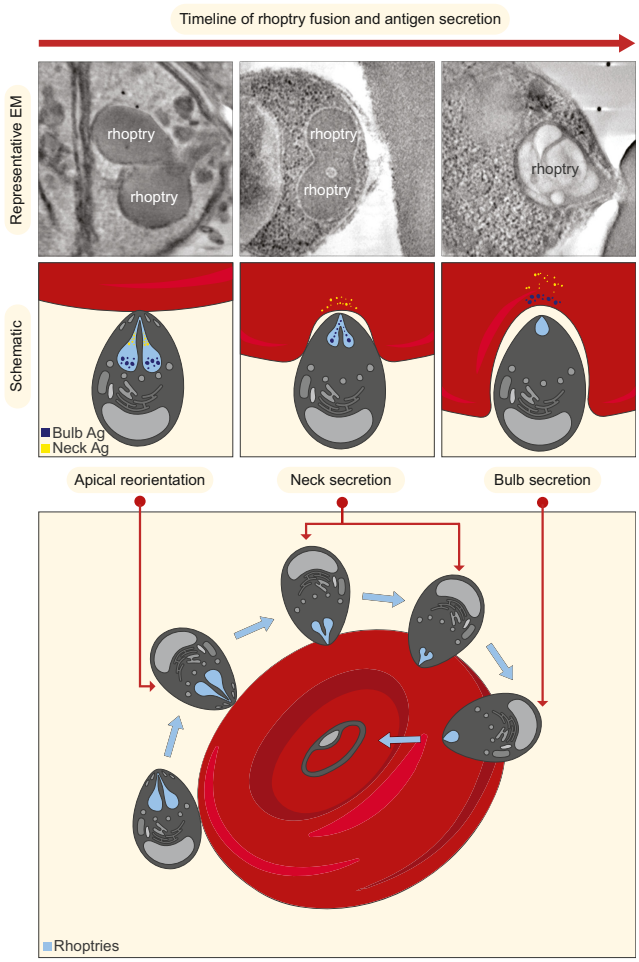

Figure 2. Rhoptry Physiology during Merozoite Invasion. Prior to the release of merozoites from schizonts, they contain two separate rhoptries. Following schizont rupture, the merozoite contacts the red blood cell (RBC) and forms an initial weak attachment before reorienting itself so that the apical tip of the merozoite comes into contact with the RBC membrane. While

(Figure legend continued at the bottom of the next page.)

the suggestions that microneme contents could be secreted via the rhoptry pore and that microneme/rhoptry invasion ligands are mixed early during invasion. However, the most detailed physiological study of merozoite invasion to date showed no evidence of fusion between the micronemes and the rhoptry neck by electron microscopy, even with multiple different fixation techniques [10]. As merozoite invasion is a rapid process, this study could not entirely conclude that the micronemes do not fuse with the rhoptry neck [10]. The authors did, however, observe micronemes in the merozoite following the completion of invasion [10], suggesting that if fusion does occur, it does not occur en masse prior to invasion. This observation is supported by similar EM studies in *T. gondii*, which have not observed fusion between the micronemes and rhoptries [38,39]. Additionally, *T. gondii* treated with the potent rhoptry secretion inhibitor 4-bromophenacyl bromide (4-BPB) has been shown to have functional microneme secretion [40], further suggesting that microneme secretion does not occur via the rhoptries. Although 4-BPB inhibits *P. falciparum* growth *in vitro*, whether micronemes are secreted with this treatment has not been tested [41]. One potential reason for the discrepancy between these studies is that the early EM studies that observed rhoptry–microneme fusion were performed on *Plasmodium cathemerium* [36], an avian malaria parasite, while those performed more recently were with *P. falciparum* [10], opening up the possibility that potential differences exist between the microneme secretion mechanisms of these two parasites. While it cannot currently be concluded whether or not the rhoptries and micronemes fuse in merozoites, ookinetes possess micronemes but not rhoptries [9]. Therefore, even if micronemes do fuse with the rhoptries of merozoites, it is not a requirement for microneme secretion in other life cycle stages.

Rhoptry Physiology in Sporozoites

Rhoptries of merozoites and sporozoites differ in both shape and number, likely reflecting the differences in host cell tropism between the two. While most merozoite rhoptry proteins that have been studied in sporozoites also localise to the rhoptries, and the rhoptries perform similar functions in both stages, there are key differences between both the physiology and molecular biology of sporozoites and merozoites. As in merozoites [16], sporozoite rhoptries are formed *de novo* from the Golgi during their development inside oocysts [11]. However, it is thought that sporozoites have two or more rhoptries [42–44] and these rhoptries are far longer and narrower (approximately 4 μm × 100 nm in *Plasmodium berghei*) [11] than those of merozoites (600 nm × 300 nm in *Plasmodium yoelii*) [42]. Additionally, sporozoite rhoptry necks and bulbs are not as easily discernible as in merozoites, as the tapered neck region forms a much smaller proportion of the whole organelle [11].

Rhoptries of merozoites are involved in the invasion of only a single type of host cell, the RBC [5], while rhoptries of sporozoites are important for both salivary gland and hepatocyte invasion [3,45], leading to potentially different physiology in each invasive stage. Following RBC invasion, the rhoptries of merozoites are rapidly disassembled and cannot be observed by electron microscopy in early ring-stage parasites [33]. By contrast, sporozoite rhoptries remain intact after invasion of the salivary gland [43] and are disassembled only after hepatocyte invasion. It has

this is occurring, the two rhoptries of the merozoite fuse together at their necks. Additionally, the rhoptries also fuse to the parasite's plasma membrane, which allows for the secretion of rhoptry neck contents. Following the secretion of the rhoptry neck contents, the merozoite establishes an irreversible tight junction between itself and the RBC. After the formation of the tight junction, the merozoite begins secreting the contents of the rhoptry bulb into the RBC cytosol. As this occurs, the two rhoptries continue their fusion with each other, fusing from the neck towards the bulb as invasion progresses. At the completion of invasion the merozoite contains only a single rhoptry, which is approximately 75% smaller than at the beginning of invasion [25]. Representative electron micrographs depicting rhoptry fusion have been reproduced with permission [10]. Within minutes of successful RBC invasion, the merozoite rapidly forms a ring-stage parasite. Between the completion of invasion and formation of the ring-stage parasite, the rhoptries are no longer visible and it is speculated that they are disassembled.

been observed that rhoptries of merozoites decrease in volume approximately 75% following rhoptry secretion [10]. While it has not been studied in detail, early comparisons between **oocyst-derived sporozoites** and **salivary gland-derived sporozoites** noted that the rhoptries of salivary gland-derived sporozoites were much less pronounced [43], suggesting that the volume of these organelles may also decrease after salivary gland invasion. During merozoite invasion of the RBC, it is known that the rhoptry neck fuses with the PPM prior to secretion of rhoptry contents and formation of the irreversible tight junction [10,32]. Therefore, rhoptry fusion to the PPM is likely only required once for invasion to proceed and this fusion event is unlikely to be transient. Conversely, sporozoite rhoptries must secrete their contents during invasion of both salivary glands and hepatocytes. Therefore, it is likely that either not all rhoptries in the oocyst-derived sporozoite fuse with the PPM during salivary gland invasion, leaving some rhoptries for hepatocyte invasion, or a rhoptry fission mechanism exists to disassociate the rhoptry neck and PPM, thus allowing invasion of a second cell type. Moreover, during merozoite invasion, the two rhoptries fuse together to form a single fully fused rhoptry at invasion completion [10,32]. If this were to occur during both sporozoite invasion events, oocyst-derived sporozoites should contain more rhoptries than those in the salivary glands. This model fits with evidence suggesting that sporozoites have two or more rhoptries [42–44], but further evidence is needed to confirm at which stage the parasite has two or more rhoptries and whether sporozoite rhoptry fusion does occur during salivary gland and/or hepatocyte invasion.

C-RIPs as Key Mediators of Rhoptry Biology

To date, studies of rhoptry proteins have primarily focussed on proteins that are secreted from the rhoptry, principally due to their interest as vaccine candidates. By contrast, very few studies have characterised proteins that coordinate rhoptry biogenesis, structure, fusion, secretion, or disassembly. Much of this currently poorly explored biology involves dynamic interactions either between the two individual rhoptries, or between the rhoptries and other parts of the cell, such as the PPM for rhoptry secretion. In these processes, the luminal secreted rhoptry proteins are unlikely to drive or coordinate these dynamic interactions. By contrast, proteins that either localise to the cytosolic surface of the rhoptries, or span the rhoptry membrane, hereafter referred to as C-RIPs, are well placed to mediate interactions between individual rhoptries and between the rhoptries and other parts of the cell. Therefore, C-RIPs are in the right place at the right time to have key roles in rhoptry biogenesis, fusion between the rhoptries, fusion with the PPM, force generation for rhoptry secretion, rhoptry disassembly, and overall rhoptry architecture. Despite their likely importance in many key processes during host cell invasion, only ten C-RIPs have been identified across all Apicomplexa (Table 1). So far, characterised C-RIPs have been shown to have roles in rhoptry secretion [13,46], rhoptry architecture [47,48], and rhoptry biogenesis [49–52]. Additionally, **knockdown** or **inducible knockout** of nine out of ten known C-RIPs is deleterious to parasite growth (Table 1), suggesting important functions for these proteins.

CERLI1

Cytosolically exposed rhoptry-leaflet-interacting protein 1 (**CERLI1**), also known as rhoptry apical surface protein 1 (RASP1) in *T. gondii*, has been shown to be essential for *P. falciparum* invasion and to localise to the cytosolic face of the rhoptries [13,30]. Knockdown, or induced knockout, of CERLI1 has been shown to inhibit processing of rhoptry antigens, alter rhoptry antigen distribution, and inhibit secretion of both rhoptry neck and bulb proteins [13,30]. The observation that CERLI1 knockdown leads to inhibition of rhoptry secretion led to speculation that CERLI1 may be involved in the fusion between the rhoptry neck and PPM that is required for rhoptry secretion [30]. A more recent study indicates that *P. falciparum* CERLI1 localises exclusively to the rhoptry bulb in mature schizonts [13], likely precluding a role in the rhoptry neck to PPM fusion if this localisation holds true throughout merozoite invasion. Therefore,

Table 1. Summary of Cytosolically Exposed or Membrane-associated Nonsecreted Rhoptry Proteins in *P. falciparum*[a,b]

Full name	Short name	EuPathDB ID	EuPathDB annotation	Functional domains?	Localisation	Essential?[c]	KD/KO phenotype?	Refs
Cytosolically exposed rhoptry leaflet interacting protein 1	CERLI1	Pf3D7_0210600	CERLI1	C2, PH	Cytosolic face of rhoptry bulb	**Yes**	Rhoptry secretion defect	[13,30]
Cytosolically exposed rhoptry leaflet interacting protein 2	CERLI2	Pf3D7_0405200	ag-1 blood-stage membrane protein homologue	C2	Cytosolic face of rhoptry bulb	**Yes**	Rhoptry morphology defect	[48]
Armadillo repeats only	ARO	Pf3D7_0414900	Armadillo-domain-containing rhoptry protein	Armadillo repeats	Cytosolic face of rhoptry bulb	Yes	Aberrant rhoptry positioning[d]	[51,80]
ARO-interacting protein	AIP	Pf3D7_1136700	Armadillo-interacting protein	N/A	Cytosolic face of rhoptry neck	Yes	Invasion defect	[14,52]
Adenylate cyclase beta	ACβ	Pf3D7_0802600	Adenylyl cyclase beta	Adenylate cyclase	Cytosolic face of rhoptries	Yes	Invasion defect	[52,56,57]
Myosin F	MyoF	Pf3D7_1329100	Myosin F, putative	Myosin motor, WD40 repeats	Cytoplasm and cytoplasmic face of rhoptries[d]	No	Aberrant rhoptry positioning[d]	[50]
Ferlin 2	Fer2	Pf3D7_1455600	Ferlin, putative	C2	Cytoplasmic face of IMC and rhoptries[d]	Yes	Rhoptry secretion defect[d]	[46]
Sodium/hydrogen exchanger	NHE	Pf3D7_1303500	Sodium/hydrogen exchanger	Na^+/H^+ exchanger	Rhoptries[d]	No	None observed[d]	[84]
Carbonic anhydrase 1	CA1	Pf3D7_1140000	Carbonic anhydrase	Carbonic anhydrase 2a	Rhoptry bulb[d]	Yes	Rhoptry biogenesis defect[d]	[47]
Palmitoyltransferase DHHC7	DHHC7	Pf3D7_0528400	Palmitoyltransferase DHHC7	DHHC palmitoyltransferase	Rhoptries	Yes	Aberrant rhoptry positioning[d]	[49,59]

[a]All proteins summarised here are present in *P. falciparum* and have been shown experimentally to localise either to the cytosolic face of the rhoptry membrane or possess a rhoptry localisation but not be secreted from the rhoptries.
[b]EuPathDB gene IDs, annotation, and domain prediction were obtained from EuPathDB and PlasmoDB [64,85]. Essentiality for the asexual stages of *P. falciparum* was inferred from a previous saturation mutagenesis study [65].
[c]Where essentiality is listed in bold, attempts to knock out that gene have failed in the corresponding reference.
[d]For some proteins, the localisation or knockdown (KD)/knockout (KO) rhoptry phenotype has been determined only for the *Toxoplasma gondii* homologue of the protein listed in this table.

while CERLI1 has been unequivocally shown to be a key facilitator for rhoptry secretion, it is currently unclear what the function of this protein is at a molecular level.

CERLI2

CERLI2, also known as rhoptry apical surface protein 2 (RASP2) in *T. gondii*, is a paralogue of CERLI1 [48]. Bioinformatic and phylogenetic analyses of CERLI1 and CERLI2 across Apicomplexa revealed that *cerli2* likely arose through gene duplication of *cerli1* in early apicomplexans [48]. Like CERLI1, CERLI2 is also essential for merozoite invasion and has been

shown to localise to the cytosolic face of the rhoptry bulb [48]. Interestingly, the homologues of CERLI1 and CERLI2 in *T. gondii* have been shown to interact [30], suggesting that the functions of these two proteins may be linked. Like CERLI1, knockdown of CERLI2 inhibits rhoptry antigen processing and distribution [48]. Unlike CERLI1, however, knockdown of CERLI2 did not lead to a measurable defect in the secretion of rhoptry neck antigens [48]. Serial block-face-scanning electron microscopy (SBF-SEM) showed that, in CERLI2 knockdown merozoites, the rhoptries are much larger and aberrantly elongated, indicating that loss of CERLI2 protein expression may impact on correct rhoptry biogenesis [48]. As rhoptry neck secretion was not altered following CERLI2 knockdown, it was suggested that CERLI2 knockdown leads to rhoptry structural changes that inhibit rhoptry functions downstream of rhoptry neck secretion, such as fusion between the rhoptries and/or rhoptry bulb secretion [48]; but this is yet to be experimentally assessed.

Adenylate Cyclase Beta (ACβ)

P. falciparum encodes two known **adenylate cyclases** (AC), also known as adenylyl cyclases, Acα, and ACβ (reviewed in [53]). These enzymes are classified by their ability to catalyse the conversion of ATP to cAMP, a molecule that has many important functions in intracellular signalling (reviewed in [54]). Of the two adenylate cyclases in *P. falciparum*, only ACβ is expressed in the blood stage of the life cycle, with ACα expressed in the sexual and exoerythrocytic stages of the parasite life cycle [53,55,56]. Curiously, **knockout** of *ACα* in *P. berghei* showed an inhibition of exocytosis of the sporozoite surface protein thrombospondin-related anonymous protein (TRAP) [55], but its influence on rhoptry secretion and localisation in sporozoites has not been determined. Unsurprisingly, as the sole producer of cAMP during the blood stage, ACβ is essential for blood-stage growth [57]. ACβ has been shown to localise to the cytosolic face of the rhoptries, and its inducible knockout inhibits merozoite invasion [57]. Inducible knockout of ACβ did not influence secretion of rhoptry neck antigens [57], but it was not assessed whether the secretion of rhoptry bulb antigens were affected. Phosphoproteomics revealed that inducible knockout of ACβ led to the hypophosphorylation of many key rhoptry proteins, including ARO, RON2, AIP, and CERLI1 [57]. These data suggest that ACβ may be involved in signalling across multiple key rhoptry proteins required for correct rhoptry function.

ACβ is thought to be bicarbonate-responsive, due to its homology to human soluble adenylate cyclase and marked pH dependence [56]. Intracellular bicarbonate levels are typically regulated by **carbonic anhydrases**, which catalyse the conversion of carbon dioxide and water into bicarbonate and hydrogen ions (reviewed in [58]). Interestingly, a recent study characterised a carbonic anhydrase in *T. gondii* which has a homologue in *P. falciparum* (Pf3D7_1140000) and showed that it was glycosylphosphatidylinositol (GPI) anchored to the cytosolic face of the rhoptry bulb membrane [47]. Additionally, this study showed that knockout of this *T. gondii* carbonic anhydrase led to inhibition of tachyzoite invasion and a defect in rhoptry biogenesis [47]. While the precise functions of either ACβ or the rhoptry-resident carbonic anhydrase during apicomplexan parasite invasion has yet to be defined, unravelling the molecular mechanisms of and interplay between these proteins may shed light on the regulation of many key rhoptry processes.

C-RIPs with an Apparent Role in Rhoptry Biogenesis

Five of the ten characterised C-RIPs – armadillo repeats only (ARO) [51,52], ARO-interacting protein (AIP) [14], carbonic anhydrase 1 (CA1) [47], myosin F (MyoF) [50], and palmitoyltransferase **DHHC7** [49,59] – are likely to have a role in rhoptry biogenesis. In *T. gondii*, knockdown or inducible knockout of all of these C-RIPs, except AIP, results in a phenotype where the rhoptries fail to be anchored to the apical tip of the parasite [47,49–51]. In *P. falciparum*, ARO [14,51] coordinates the rhoptry localisation of AIP [14], and knockdown of AIP is inhibitory to merozoite invasion; but it remains to be determined whether this is due to a rhoptry biogenesis defect.

While the absence of four of these proteins in *T. gondii* converges on the same aberrant rhoptry mislocalisation phenotype, known interactions between these proteins open up the possibility that this occurs through a shared, rather than separate, mechanism. TgARO's rhoptry localisation is dependent upon palmitoylation by TgDHHC7 [49], and TgARO is known to interact with TgMyoF and TgACβ [51]. Given the bicarbonate sensitivity of PfACβ [56] and the involvement of PfACβ in the phosphorylation of PfARO and PfAIP [57], it is possible that the pH changes caused by CA1 may regulate ACβ and in turn the functions of ARO and its interacting partners AIP and MyoF. Ultimately, whether loss of one of these proteins disrupts a wider protein network involving the others, resulting in a similar defect in rhoptry biogenesis, remains to be elucidated in *T. gondii* and is yet to be explored in detail for *Plasmodium* spp. Further, whether any or all of these proteins also have a role in rhoptry biology at the point of invasion may be masked with current inducible protein-depletion techniques highlighting aberrant rhoptry biogenesis, and new techniques may be needed to elucidate their function during invasion going forward.

Ferlin 2

Ferlins are a group of calcium-responsive C2-domain-containing proteins that have been shown to play important roles in vesicle and membrane fusion events (reviewed in [60]). A recent study in *T. gondii* identified three putative Ferlins, with two (TgFER1 and TgFER2) having identifiable homologues in *P. falciparum* [46]. PbFER1, also known as Ferlin-like protein (PbFLP), has been shown to be essential for RBC membrane and PVM rupture during *P. berghei* gamete egress and is expressed in schizonts [61]. Additionally, depletion of PbFLP caused life-cycle arrest in *P. berghei* gametocytes [61], although it is currently unclear if it has an important function during merozoite or sporozoite invasion. In intracellular *T. gondii* tachyzoites, TgFER2 was shown to primarily lie along the cytosolic face of the inner-membrane complex with a minor accumulation along the rhoptry membrane [46]. In extracellular tachyzoites, however, TgFER2 concentrated to the cytosolic face of the rhoptry neck [46]. Inducible knockdown of TgFER2 resulted in an inhibition of tachyzoite invasion, which was shown to be due to an inhibition of rhoptry secretion [6]. It is mechanistically unclear how FER2 is involved in rhoptry secretion but given the canonical role of Ferlins in membrane fusion events and its localisation, future studies should investigate whether FER2 is involved the fusion between the rhoptry neck and PPM.

Concluding Remarks

Our understanding of *Plasmodium* spp. rhoptry physiology, in both merozoites and sporozoites, is still heavily reliant on two-dimensional EM studies that were carried out many decades ago [8,11,16,32,36,37,43,62]. More recently, however, emerging technologies such as SBF-SEM have allowed for a high-resolution three-dimensional snapshot into the rhoptry physiology in merozoites [10]. Despite this, much is still to be learned about the physiology of rhoptries during host cell invasion, particularly for sporozoites (see Outstanding Questions). At a protein level, only recently was the first functional analysis of *Plasmodium* spp. C-RIPs carried out, with all C-RIPs studied to date shown to have important functions in rhoptry biology [13,14,30,48,57]. Studies in *T. gondii* have implicated additional C-RIPs, including Ferlin 2 [46], as having important roles in rhoptry biology. Additionally, a recent study identified over 100 proteins predicted to localise to the rhoptries of *T. gondii* [63]. Thirty of these proteins have identifiable homologues in *P. falciparum* [64], around half are predicted to be essential for *P. falciparum* blood-stage growth [65], and 12 currently have no functional annotation (see Table S2 in the supplemental information online). Therefore, it is likely that this group of proteins contains novel C-RIPs that also have key roles in rhoptry biology. Future exploration of C-RIP functions will be facilitated by application of emerging quantitative imaging and proteomic techniques that will begin to unravel the complex protein–protein interactions coordinating rhoptry biogenesis, structure, fusion, secretion, and disassembly during both merozoite and sporozoite host-cell invasion.

Outstanding Questions

How extensively does rhoptry physiology differ between merozoite and sporozoite invasion? What selective pressures may have accounted for these differences evolutionarily?

Is there a protein, or set of proteins, that act as the master regulator for the initiation of rhoptry secretion? Is this regulator shared by all parasites that possess rhoptries, and does this highlight rhoptry secretion as a potential pan-Apicomplexa drug target?

Very few rhoptry proteins have had their structure resolved. How can emerging techniques, such as cryo-EM, enhance structure elucidation in the future? How would this influence the attractiveness of rhoptry proteins as drug targets?

What is the full breadth of functions fulfilled by C-RIPs? Many of these proteins are either expressed in life-cycle stages that lack rhoptries (such as gametocytes and ookinetes) or are conserved in nonparasitic ancestors of the Apicomplexa. What functions do they serve in the absence of rhoptries?

How are rhoptries disassembled postinvasion, how rapidly does this disassembly occur, and how does it differ between merozoites and sporozoites?

What governs the number of rhoptries possessed by each sporozoite? Are only a subset of rhoptries used in each of the two sporozoite invasion events, or do sporozoite rhoptries undergo a fission event to detach them from the PPM after secretion?

How does the rhoptry maintain its structure? Is it supported by an internal or external scaffold and if so, what is this scaffold comprised of? It is currently unclear how proteins might localise specifically to either the rhoptry neck or bulb; how could this be influenced or governed by a scaffold that dictates rhoptry structure?

What similar biological systems, or processes, may provide insight into key rhoptry functions? What processes do rhoptry fusion, secretion, and disassembly most closely mirror from other biological systems?

Acknowledgments

We thank Professors E. Hanssen, J. Baum, S. Ralph, and colleagues for permission to use the electron microscopy tomograms of merozoite rhoptry architecture changes during invasion. This work was supported by funding from the Hospital Research Foundation (Fellowship to D.W.), DAAD/Universities Australia joint research co-operation scheme (T.G., D.W., B.L., J.B., J.W.), Australian Government Research Training Program Scholarship (B.L., J.B.), South Australian Commonwealth Scholarship (B.L.) and DFG BA5213/3-1 (J.W.).

Declaration of Interests

The authors declare no competing interests.

Supplemental Information

Supplemental information associated with this article can be found online at https://doi.org/10.1016/j.pt.2021.03.006.

References

1. World Health Organization (2020) *World Malaria Report 2020*, WHO
2. Vinetz, J.M. (2005) *Plasmodium* ookinete invasion of the mosquito midgut. In *Malaria: Drugs, Disease and Post-genomic Biology* (Compans, R.W. *et al.*, eds), pp. 357–382, Springer
3. Ghosh, A.K. and Jacobs-Lorena, M. (2009) *Plasmodium* sporozoite invasion of the mosquito salivary gland. *Curr. Opin. Microbiol.* 12, 394–400
4. Vaughan, A.M. and Kappe, S.H.I. (2017) Malaria parasite liver infection and exoerythrocytic biology. *Cold Spring Harbor Perspec. Med.* 7, a025486
5. Cowman, A.F. *et al.* (2017) The molecular basis of erythrocyte invasion by malaria parasites. *Cell Host Microbe* 22, 232–245
6. Gubbels, M.-J. and Duraisingh, M.T. (2012) Evolution of apicomplexan secretory organelles. *Int. J. Parasitol.* 42, 1071–1081
7. Counihan, N.A. *et al.* (2013) *Plasmodium* rhoptry proteins: why order is important. *Trends Parasitol.* 29, 228–236
8. Sinden, R.E. and Strong, K. (1978) An ultrastructural study of the sporogonic development of *Plasmodium falciparum* in *Anopheles gambiae*. *Trans. R. Soc. Trop. Med. Hyg.* 72, 477–491
9. Patra, K.P. and Vinetz, J.M. (2012) New ultrastructural analysis of the invasive apparatus of the *Plasmodium* ookinete. *Am. J. Trop. Med. Hyg.* 87, 412–417
10. Hanssen, E. *et al.* (2013) Electron tomography of *Plasmodium falciparum* merozoites reveals core cellular events that underpin erythrocyte invasion. *Cell. Microbiol.* 15, 1457–1472
11. Schrevel, J. *et al.* (2008) Vesicle trafficking during sporozoite development in *Plasmodium berghei*: ultrastructural evidence for a novel trafficking mechanism. *Parasitology* 135, 1–12
12. Boothroyd, J.C. and Dubremetz, J.-F. (2008) Kiss and spit: the dual roles of *Toxoplasma* rhoptries. *Nat. Rev. Microbiol.* 6, 79–88
13. Liffner, B. *et al.* (2020) PfCERLI1 is a conserved rhoptry associated protein essential for *Plasmodium falciparum* merozoite invasion of erythrocytes. *Nat. Commun.* 11, 1411
14. Geiger, M. *et al.* (2020) Structural insights into PfARO and characterization of its interaction with PfAIP. *J. Mol. Biol.* 432, 878–896
15. Bertiaux, E. *et al.* (2021) Expansion microscopy provides new insights into the cytoskeleton of malaria parasites including the conservation of a conoid. *PLoS Biol.* 19, e3001020
16. Bannister, L.H. *et al.* (2000) Ultrastructure of rhoptry development in *Plasmodium falciparum* erythrocytic schizonts. *Parasitology* 121, 273–287
17. Deponte, M. *et al.* (2012) Wherever I may roam: Protein and membrane trafficking in *P. falciparum*-infected red blood cells. *Mol. Biochem. Parasitol.* 186, 95–116
18. Howard, R.F. and Schmidt, C.M. (1995) The secretory pathway of *Plasmodium falciparum* regulates transport of p82/RAP-1 to the rhoptries. *Mol. Biochem. Parasitol.* 74, 43–54
19. Ghoneim, M.A. (2013) Trafficking of *Plasmodium falciparum* chimeric rhoptry protein with Brefeldin A. *Folia Parasitol.* 60, 75–78
20. Hallée, S. *et al.* (2018) Evidence that the *Plasmodium falciparum* protein sortilin potentially acts as an escorter for the trafficking of the rhoptry-associated membrane antigen to the rhoptries. *mSphere* 3, e00551-17
21. Hallée, S. *et al.* (2018) The malaria parasite *Plasmodium falciparum* sortilin is essential for merozoite formation and apical complex biogenesis. *Cell. Microbiol.* 20, e12844
22. Sherling, E.S. *et al.* (2019) The *Plasmodium falciparum* rhoptry bulb protein RAMA plays an essential role in rhoptry neck morphogenesis and host red blood cell invasion. *PLoS Pathog.* 15, e1008049
23. Zuccala, E.S. *et al.* (2012) Subcompartmentalisation of proteins in the rhoptries correlates with ordered events of erythrocyte invasion by the blood stage malaria parasite. *PLoS One* 7, e46160
24. Volz, J.C. *et al.* (2016) Essential role of the PfRh5/PfRipr/CyRPA complex during *Plasmodium falciparum* invasion of erythrocytes. *Cell Host Microbe* 20, 60–71
25. Weiss, G.E. *et al.* (2015) Revealing the sequence and resulting cellular morphology of receptor-ligand interactions during *Plasmodium falciparum* invasion of erythrocytes. *PLoS Pathog.* 11, e1004670
26. Riglar, D.T. *et al.* (2011) Super-resolution dissection of coordinated events during malaria parasite invasion of the human erythrocyte. *Cell Host Microbe* 9, 9–20
27. Tham, W.-H. *et al.* (2012) Erythrocyte and reticulocyte binding-like proteins of *Plasmodium falciparum*. *Trends Parasitol.* 28, 23–30
28. Tham, W.-H. *et al.* (2015) *Plasmodium falciparum* adhesins play an essential role in signalling and activation of invasion into human erythrocytes. *PLoS Pathog.* 11, e1005343
29. Counihan, N.A. *et al.* (2017) *Plasmodium falciparum* parasites deploy RhopH2 into the host erythrocyte to obtain nutrients, grow and replicate. *eLife* 6, e23217
30. Suarez, C. *et al.* (2019) A lipid-binding protein mediates rhoptry discharge and invasion in *Plasmodium falciparum* and *Toxoplasma gondii* parasites. *Nat. Commun.* 10, 4041
31. Aikawa, M. *et al.* (1978) Erythrocyte entry by malarial parasites. A moving junction between erythrocyte and parasite. *J. Cell Biol.* 77, 72–82
32. Bannister, L.H. *et al.* (1986) Lamellar membranes associated with rhoptries in erythrocytic merozoites of *Plasmodium knowlesi*: a clue to the mechanism of invasion. *Parasitology* 92, 291–303
33. Sachanonta, N. *et al.* (2011) Ultrastructural and real-time microscopic changes in *P. falciparum*-infected red blood cells following treatment with antimalarial drugs. *Ultrastruct. Pathol.* 35, 214–225
34. Carruthers, V.B. and Tomley, F.M. (2008) Microneme proteins in apicomplexans. In *Molecular Mechanisms of Parasite Invasion: Subcellular Biochemistry* (Burleigh, B.A. and Soldati-Favre, D., eds), pp. 33–45, Springer

35. Dubois, D.J. and Soldati-Favre, D. (2019) Biogenesis and secretion of micronemes in *Toxoplasma gondii*. *Cell. Microbiol.* 21, e13018
36. Aikawa, M. (1966) The fine structure of the erythrocytic stages of three avian malarial parasites, *Plasmodium Fallax*, *P. Lophurae*, and *P. Cathemerium*. *Am. J. Trop. Med. Hyg.* 15, 449–471
37. Scholtyseck, E. and Mehlhorn, H. (1970) Ultrastructural study of characteristic organelles (paired organelles, micronemes, micropores) of sporozoa and related organisms. *Z. Parasitenkd.* 34, 97–127
38. Lemgruber, L. *et al.* (2011) New details on the fine structure of the rhoptry of *Toxoplasma gondii*. *Microsc. Res. Tech.* 74, 812–818
39. Paredes-Santos, T.C. *et al.* (2012) Dynamics and 3D organization of secretory organelles of *Toxoplasma gondii*. *J. Struct. Biol.* 177, 420–430
40. Ravindran, S. *et al.* (2009) 4-Bromophenacyl bromide specifically inhibits rhoptry secretion during *Toxoplasma* invasion. *PLoS One* 4, e8143
41. Flammersfeld, A. *et al.* (2020) A patatin-like phospholipase functions during gametocyte induction in the malaria parasite *Plasmodium falciparum*. *Cell. Microbiol.* 22, e13146
42. Sam-Yellowe, T. (2014) Rhoptries and other merozoite organelles involved in invasion. In *Encyclopedia of Malaria* (Hommel, M. and Kremsner, P.G., eds), pp. 1–11, Springer
43. Sinden, R.E. and Garnham, P.C.C. (1973) A comparative study on the ultrastructure of *Plasmodium* sporozoites within the oocyst and salivary glands, with particular reference to the incidence of the micropore. *Trans. R. Soc. Trop. Med. Hyg.* 67, 631–637
44. Tokunaga, N. *et al.* (2019) Expression and localization profiles of rhoptry proteins in *Plasmodium berghei* sporozoites. *Front. Cell. Infect. Microbiol.* 9, 316
45. Sinnis, P. and Coppi, A. (2007) A long and winding road: the *Plasmodium* sporozoite's journey in the mammalian host. *Parasitol. Int.* 56, 171–178
46. Coleman, B.I. *et al.* (2018) A member of the ferlin calcium sensor family is essential for *Toxoplasma gondii* rhoptry secretion. *mBio* 9, e01510-18
47. Chasen, N.M. *et al.* (2017) A glycosylphosphatidylinositol-anchored carbonic anhydrase-related protein of *Toxoplasma gondii* is important for rhoptry biogenesis and virulence. *mSphere* 2, e00027-17
48. Liffner, B. *et al.* (2020) *Pfcerli2*, a duplicated gene in the malaria parasite *Plasmodium falciparum* essential for invasion of erythrocytes as revealed by phylogenetic and cell biological analysis. *bioRxiv* Published online November 27, 2020. https://doi.org/10.1101/2020.11.26.400549
49. Beck, J.R. *et al.* (2013) A *Toxoplasma* palmitoyl acyl transferase and the palmitoylated armadillo repeat protein TgARO govern apical rhoptry tethering and reveal a critical role for the rhoptries in host cell invasion but not egress. *PLoS Pathog.* 9, e1003162
50. Jacot, D. *et al.* (2013) *Toxoplasma gondii* myosin F, an essential motor for centrosomes positioning and apicoplast inheritance. *EMBO J.* 32, 1702–1716
51. Mueller, C. *et al.* (2013) The *Toxoplasma* protein ARO mediates the apical positioning of rhoptry organelles, a prerequisite for host cell invasion. *Cell Host Microbe* 13, 289–301
52. Mueller, C. *et al.* (2016) Structural and functional dissection of *Toxoplasma gondii* armadillo repeats only protein. *J. Cell Sci.* 129, 1031
53. Baker, D. (2004) Adenylyl and guanylyl cyclases from the malaria parasite *Plasmodium falciparum*. *IUBMB Life* 56, 535–540
54. Hanoune, J. and Defer, N. (2001) Regulation and role of adenylyl cyclase isoforms. *Annu. Rev. Pharmacol. Toxicol.* 41, 145–174
55. Ono, T. *et al.* (2008) Adenylyl cyclase α and cAMP signaling mediate *Plasmodium* sporozoite apical regulated exocytosis and hepatocyte infection. *PLoS Pathog.* 4, e1000008
56. Salazar, E. *et al.* (2012) Characterization of *Plasmodium falciparum* adenylyl cyclase-β and its role in erythrocytic stage parasites. *PLoS One* 7, e39769
57. Patel, A. *et al.* (2019) Cyclic AMP signalling controls key components of malaria parasite host cell invasion machinery. *PLoS Biol.* 17, e3000264
58. Supuran, C.T. (2008) Carbonic anhydrases: novel therapeutic applications for inhibitors and activators. *Nat. Rev. Drug Discov.* 7, 168–181
59. Frénal, K. *et al.* (2013) Global analysis of apicomplexan protein S-acyl transferases reveals an enzyme essential for invasion. *Traffic* 14, 895–911
60. Lek, A. *et al.* (2012) Ferlins: regulators of vesicle fusion for auditory neurotransmission, receptor trafficking and membrane repair. *Traffic* 13, 185–194
61. Obrova, K. *et al.* (2019) Transmission of the malaria parasite requires ferlin for gamete egress from the red blood cell. *Cell. Microbiol.* 21, e12999
62. Stewart, M.J. *et al.* (1985) Rhoptry secretion of membranous whorls by *Plasmodium berghei* sporozoites. *J. Protozool.* 32, 280–283
63. Barylyuk, K. *et al.* (2020) A comprehensive subcellular atlas of the *Toxoplasma* proteome via hyperLOPIT provides spatial context for protein functions. *Cell Host Microbe* 28, 752–766.e9
64. Aurrecoechea, C. *et al.* (2008) PlasmoDB: a functional genomic database for malaria parasites. *Nucleic Acids Res.* 37, D539–D543
65. Zhang, M. *et al.* (2018) Uncovering the essential genes of the human malaria parasite *Plasmodium falciparum* by saturation mutagenesis. *Science* 360, eaap7847
66. Vulliez-Le Normand, B. *et al.* (2012) Structural and functional insights into the malaria parasite moving junction complex. *PLoS Pathog.* 8, e1002755
67. Richard, D. *et al.* (2010) Interaction between *Plasmodium falciparum* apical membrane antigen 1 and the rhoptry neck protein complex defines a key step in the erythrocyte invasion process of malaria parasites. *J. Biol. Chem.* 285, 14815–14822
68. Baum, J. *et al.* (2006) A conserved molecular motor drives cell invasion and gliding motility across malaria life cycle stages and other apicomplexan parasites. *J. Biol. Chem.* 281, 5197–5208
69. Keeley, A. and Soldati, D. (2004) The glideosome: a molecular machine powering motility and host-cell invasion by Apicomplexa. *Trends Cell Biol.* 14, 528–532
70. Cowman, A.F. *et al.* (2016) Malaria: biology and disease. *Cell* 167, 610–624
71. Hale, V.L. *et al.* (2017) Parasitophorous vacuole poration precedes its rupture and rapid host erythrocyte cytoskeleton collapse in *Plasmodium falciparum* egress. *Proc. Natl. Acad. Sci. U. S. A.* 114, 3439–3444
72. Beier, J.C. (1998) Malaria parasite development in mosquitoes. *Annu. Rev. Entomol.* 43, 519–543
73. Sterling, C.R. *et al.* (1973) The passage of *Plasmodium berghei* sporozoites through the salivary glands of *Anopheles stephensi*: an electron microscope study. *J. Parasitol.* 59, 593–605
74. Pimenta, P.F. *et al.* (1994) The journey of malaria sporozoites in the mosquito salivary gland. *J. Eukaryot. Microbiol.* 41, 608–624
75. Sidjanski, S. and Vanderberg, J.P. (1997) Delayed migration of *Plasmodium* sporozoites from the mosquito bite site to the blood. *Am. J. Trop. Med. Hyg.* 57, 426–429
76. Arredondo, S.A. *et al.* (2021) Secretory organelle function in the *Plasmodium* sporozoite. *Trends Parasitol.* 37, 651–663
77. Tavares, J. *et al.* (2013) Role of host cell traversal by the malaria sporozoite during liver infection. *J. Exp. Med.* 210, 905–915
78. Ishino, T. *et al.* (2005) A *Plasmodium* sporozoite protein with a membrane attack complex domain is required for breaching the liver sinusoidal cell layer prior to hepatocyte infection. *Cell. Microbiol.* 7, 199–208
79. Baer, K. *et al.* (2007) Release of hepatic *Plasmodium yoelii* merozoites into the pulmonary microvasculature. *PLoS Pathog.* 3, e171
80. Cabrera, A. *et al.* (2012) Dissection of minimal sequence requirements for rhoptry membrane targeting in the malaria parasite. *Traffic* 13, 1335–1350
81. Swearingen, K.E. *et al.* (2017) Proteogenomic analysis of the total and surface-exposed proteomes of *Plasmodium vivax* salivary gland sporozoites. *PLoS Negl. Trop. Dis.* 11, e0005791
82. Lindner, S.E. *et al.* (2019) Transcriptomics and proteomics reveal two waves of translational repression during the maturation of malaria parasite sporozoites. *Nat. Commun.* 10, 4964

83. Hamada, S. *et al.* (2021) In-depth proteomic analysis of *Plasmodium berghei* sporozoites using trapped ion mobility spectrometry with parallel accumulation-serial fragmentation. *Proteomics* 21, e2000305
84. Karasov, A.O. *et al.* (2005) Identification and disruption of a rhoptry-localized homologue of sodium hydrogen exchangers in *Toxoplasma gondii*. *Int. J. Parasitol.* 35, 285–291
85. Aurrecoechea, C. *et al.* (2017) EuPathDB: the eukaryotic pathogen genomics database resource. *Nucleic Acids Res.* 45, D581–D591